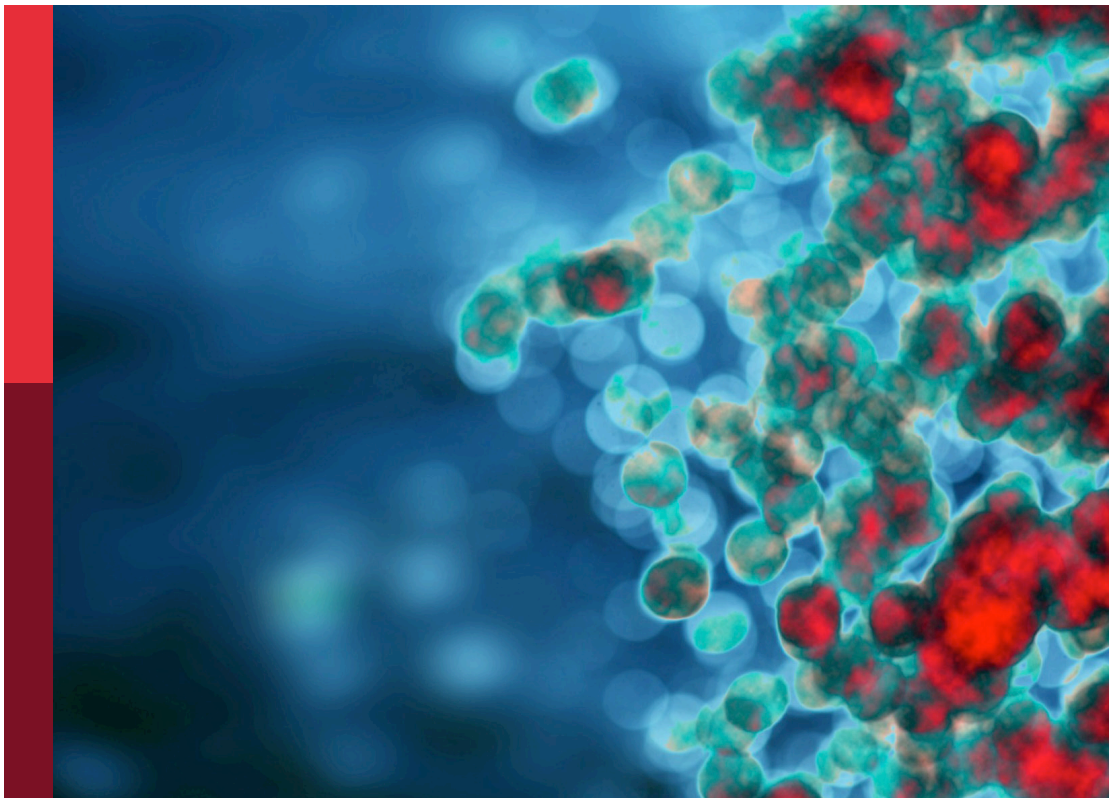
frontiers | Research Topics

Immunotherapy and small molecule inhibitors as combinational cancer therapeutics

Edited by
Mohd Wajid Ali Khan, Shariq Qayyum, Saravanan Rajendrasozhan, Subhash Kumar Tripathi and Mohammad Azhar Aziz

Published in
Frontiers in Immunology
Frontiers in Oncology



FRONTIERS EBOOK COPYRIGHT STATEMENT

The copyright in the text of individual articles in this ebook is the property of their respective authors or their respective institutions or funders. The copyright in graphics and images within each article may be subject to copyright of other parties. In both cases this is subject to a license granted to Frontiers.

The compilation of articles constituting this ebook is the property of Frontiers.

Each article within this ebook, and the ebook itself, are published under the most recent version of the Creative Commons CC-BY licence. The version current at the date of publication of this ebook is CC-BY 4.0. If the CC-BY licence is updated, the licence granted by Frontiers is automatically updated to the new version.

When exercising any right under the CC-BY licence, Frontiers must be attributed as the original publisher of the article or ebook, as applicable.

Authors have the responsibility of ensuring that any graphics or other materials which are the property of others may be included in the CC-BY licence, but this should be checked before relying on the CC-BY licence to reproduce those materials. Any copyright notices relating to those materials must be complied with.

Copyright and source acknowledgement notices may not be removed and must be displayed in any copy, derivative work or partial copy which includes the elements in question.

All copyright, and all rights therein, are protected by national and international copyright laws. The above represents a summary only. For further information please read Frontiers' Conditions for Website Use and Copyright Statement, and the applicable CC-BY licence.

ISSN 1664-8714
ISBN 978-2-8325-3417-5
DOI 10.3389/978-2-8325-3417-5

About Frontiers

Frontiers is more than just an open access publisher of scholarly articles: it is a pioneering approach to the world of academia, radically improving the way scholarly research is managed. The grand vision of Frontiers is a world where all people have an equal opportunity to seek, share and generate knowledge. Frontiers provides immediate and permanent online open access to all its publications, but this alone is not enough to realize our grand goals.

Frontiers journal series

The Frontiers journal series is a multi-tier and interdisciplinary set of open-access, online journals, promising a paradigm shift from the current review, selection and dissemination processes in academic publishing. All Frontiers journals are driven by researchers for researchers; therefore, they constitute a service to the scholarly community. At the same time, the *Frontiers journal series* operates on a revolutionary invention, the tiered publishing system, initially addressing specific communities of scholars, and gradually climbing up to broader public understanding, thus serving the interests of the lay society, too.

Dedication to quality

Each Frontiers article is a landmark of the highest quality, thanks to genuinely collaborative interactions between authors and review editors, who include some of the world's best academicians. Research must be certified by peers before entering a stream of knowledge that may eventually reach the public - and shape society; therefore, Frontiers only applies the most rigorous and unbiased reviews. Frontiers revolutionizes research publishing by freely delivering the most outstanding research, evaluated with no bias from both the academic and social point of view. By applying the most advanced information technologies, Frontiers is catapulting scholarly publishing into a new generation.

What are Frontiers Research Topics?

Frontiers Research Topics are very popular trademarks of the *Frontiers journals series*: they are collections of at least ten articles, all centered on a particular subject. With their unique mix of varied contributions from Original Research to Review Articles, Frontiers Research Topics unify the most influential researchers, the latest key findings and historical advances in a hot research area.

Find out more on how to host your own Frontiers Research Topic or contribute to one as an author by contacting the Frontiers editorial office: frontiersin.org/about/contact

Immunotherapy and small molecule inhibitors as combinational cancer therapeutics

Topic editors

Mohd Wajid Ali Khan — University of Hail, Saudi Arabia
Shariq Qayyum — Brigham and Women's Hospital, Harvard Medical School, United States
Saravanan Rajendrasozhan — University of Hail, Saudi Arabia
Subhash Kumar Tripathi — Seattle Children's Research Institute, United States
Mohammad Azhar Aziz — Aligarh Muslim University, India

Citation

Khan, M. W. A., Qayyum, S., Rajendrasozhan, S., Tripathi, S. K., Aziz, M. A., eds. (2023). *Immunotherapy and small molecule inhibitors as combinational cancer therapeutics*. Lausanne: Frontiers Media SA. doi: 10.3389/978-2-8325-3417-5

Table of contents

05 Editorial: Immunotherapy and small molecule inhibitors as combinational cancer therapeutics
Mohd Wajid Ali Khan, Mohammad Azhar Aziz and Saravanan Rajendrasozhan

07 Immunotherapy or targeted therapy as the first-line strategies for unresectable hepatocellular carcinoma: A network meta-analysis and cost-effectiveness analysis
Kun Liu, Youwen Zhu and Hong Zhu

18 Cancel cancer: The immunotherapeutic potential of CD200/CD200R blockade
Deborah Choe and Dongwon Choi

28 Cyclooxygenase-2-Prostaglandin E2 pathway: A key player in tumor-associated immune cells
Kaipeng Jin, Chao Qian, Jinti Lin and Bing Liu

38 Treatment of extranodal NK/T-cell lymphoma: From past to future
Zheng Yan, Shuna Yao, Zhizhong Wang, Wenping Zhou, Zhihua Yao and Yanyan Liu

58 Knockout of ENO1 leads to metabolism reprogramming and tumor retardation in pancreatic cancer
Qingru Song, Kai Zhang, Tianjiao Sun, Congcong Xu, Wei Zhao and Zhiqian Zhang

68 Identification of a glutamine metabolism reprogramming signature for predicting prognosis, immunotherapy efficacy, and drug candidates in bladder cancer
Yan Xu, Zhixiu Xia, Xiaoyu Sun, Baojun Wei, Yang Fu, Du Shi and Yuyan Zhu

86 Neoadjuvant immunotherapy for colorectal cancer: Right regimens, right patients, right directions?
Jiahao Zhu, Jie Lian, Benjie Xu, Xiangyi Pang, Shengjun Ji, Yutian Zhao and Haibo Lu

105 Adrenergic receptor signaling regulates the CD40-receptor mediated anti-tumor immunity
Akansha Singh and Ashish Ranjan

116 Directional preference for glioblastoma cancer cell membrane encapsulated nanoparticle population: A probabilistic approach for cancer therapeutics
Saif Khan, Mohd Wajid Ali Khan, Subuhi Sherwani, Sultan Alouffi, Mohammad Jahoor Alam, Khalid Al-Motair and Shahper Khan

127 Dysregulation of systemic soluble immune checkpoints in early breast cancer is attenuated following administration of neoadjuvant chemotherapy and is associated with recovery of CD27, CD28, CD40, CD80, ICOS and GITR and substantially increased levels of PD-L1, LAG-3 and TIM-3
Bernardo L. Rapoport, Helen C. Steel, Carol A. Benn, Simon Nayler, Teresa Smit, Liezl Heyman, Annette J. Theron, Nomsa Hlatshwayo, Luyanda L.I. Kwofie, Pieter W.A. Meyer and Ronald Anderson

139 Case report: Complete response of an anaplastic thyroid carcinoma patient with *NRAS* Q61R/*BRAF* D594N mutations to the triplet of dabrafenib, trametinib and PD-1 antibody
Lin Gui, Yiming Zhu, Xiaomo Li, Xiaohui He, Tonghui Ma, Yi Cai and Shaoyan Liu

145 LCL161 enhances expansion and survival of engineered anti-tumor T cells but is restricted by death signaling
Arya Afsahi, Christopher M. Silvestri, Allyson E. Moore, Carly F. Graham, Kaylyn Bacchiochi, Martine St-Jean, Christopher L. Baker, Robert G. Korneluk, Shawn T. Beug, Eric C. LaCasse and Jonathan L. Bramson

162 UXT at the crossroads of cell death, immunity and neurodegenerative diseases
Pengzhe Han, Shaojian Mo, Zhengwang Wang, Jiale Xu, Xifeng Fu and Yanzhang Tian

177 Cost-effectiveness analysis of serplulimab plus chemotherapy in the first-line treatment for PD-L1-positive esophageal squamous cell carcinoma in China
Shixian Liu, Nana Jiang, Lei Dou and Shunping Li

187 Cost-effectiveness of sacituzumab govitecan in hormone receptor-positive/human epidermal growth factor receptor 2-negative metastatic breast cancer
Demin Shi, Yan Li, Xueyan Liang and Lingyuan Chen

196 Afatinib combined with anti-PD1 enhances immunotherapy of hepatocellular carcinoma *via* ERBB2/STAT3/PD-L1 signaling
Chao Yu, Xinyi Zhang, Min Wang, Gaoxin Xu, Siqi Zhao, Yongheng Feng, Chao Pan, Weijun Yang, Jin Zhou, Longcheng Shang and Yong Ma

207 Targeting macrophage Syk enhances responses to immune checkpoint blockade and radiotherapy in high-risk neuroblastoma
Deepak Rohila, In Hwan Park, Timothy V. Pham, Riley Jones, Elisabette Tapia, Kevin X. Liu, Pablo Tamayo, Alice Yu, Andrew B. Sharabi and Shweta Joshi

224 Inhibitors of the CD73-adenosinergic checkpoint as promising combinatory agents for conventional and advanced cancer immunotherapy
Zoya Kurago, Gang Guo, Huidong Shi, Roni J. Bollag, Michael W. Groves, J. Kenneth Byrd and Yan Cui

frontiers | Frontiers in Immunology

TYPE Editorial
PUBLISHED 22 August 2023
DOI 10.3389/fimmu.2023.1270182

Check for updates

OPEN ACCESS

EDITED AND REVIEWED BY
Emanuela Ricciotti,
University of Pennsylvania, United States

*CORRESPONDENCE
Mohd Wajid Ali Khan
wajidkhan11@gmail.com
Mohammad Azhar Aziz
azharbiotech@yahoo.com

RECEIVED 31 July 2023
ACCEPTED 07 August 2023
PUBLISHED 22 August 2023

CITATION
Khan MWA, Aziz MA and Rajendrasozhan S (2023) Editorial: Immunotherapy and small molecule inhibitors as combinational cancer therapeutics.
Front. Immunol. 14:1270182.
doi: 10.3389/fimmu.2023.1270182

COPYRIGHT
© 2023 Khan, Aziz and Rajendrasozhan. This is an open-access article distributed under the terms of the Creative Commons Attribution License (CC BY). The use, distribution or reproduction in other forums is permitted, provided the original author(s) and the copyright owner(s) are credited and that the original publication in this journal is cited, in accordance with accepted academic practice. No use, distribution or reproduction is permitted which does not comply with these terms.

Editorial: Immunotherapy and small molecule inhibitors as combinational cancer therapeutics

Mohd Wajid Ali Khan[1,2]*, Mohammad Azhar Aziz[3]* and Saravanan Rajendrasozhan[1]

[1]Department of Chemistry, College of Science, University of Ha'il, Ha'il, Saudi Arabia, [2]Medical and Diagnostic Research Centre, University of Ha'il, Ha'il, Saudi Arabia, [3]Interdisciplinary Nanotechnology Center, Zakir Husain College of Engineering and Technology, Aligarh Muslim University, Aligarh, India

KEYWORDS

immunotherapy, cancer therapeutics, immune check point, small molecules, PD1 (programmed cell death protein 1)

Editorial on the Research Topic
Immunotherapy and small molecule inhibitors as combinational cancer therapeutics

Cancer is a multidimensional chronic disease, with various factors contributing to its progression. The immune system plays a crucial role in identifying and eliminating tumor cells. However, aggressive cancers and advanced stages can pose challenges in treatment due to poor cancer cell targeting. To overcome this, research focus has shifted to developing novel small molecules which can further enhance immune system function, increasing the efficacy of cancer immunotherapies, and offering promising therapeutic options for different cancer types.

Cancer immunotherapy based on checkpoint inhibitors, aims to restore the normal defense of the body, to counter cancer cells. Programmed cell death protein 1/programmed death–ligand 1 (PD1/PDL1) check point inhibitors are already in clinical use. There are ongoing efforts to identify several other checkpoints that tumor cells exploit to mask and restrict the immune response. One of these checkpoints reviewed in this Research Topic is the CD200/CD200R pathway (Choe et al.). Authors introduced and reviewed the mechanism of CD200 checkpoint inhibition by tumor cells. Targeting of CD200/CD200R pathway would lead to antitumor activity within its environment. In another paper, evidence is provided to support the use of the drug Afatinib as a combination therapy in hepatocellular carcinoma along with PD1 inhibitors (Yu et al.). Another case report demonstrated the beneficial use of PD1 inhibitor along with two other drugs in a patient with BRAF and NRAS mutations (Gui et al.).

Cancer metabolism has been explored as a precision based therapeutic target. In this Research Topic, the role of Afatinib has been explained in terms of its link in D-Glutamine and D-Glutamic acid metabolism. Separately, another study took up the task to delineate the role of ENO1 in pancreatic cancer (PC) (Song et al.). The α-enolase (ENO1) is one of the key enzymes in the glycolytic pathway used by cancer cells for energy generation

(Warburg effect). Overexpression of this gene has been associated with increased tumorigenesis in PC. The indispensable role of ENO1 in PC was proved by employing the knockout strategy. Thus, it can serve as a potential drug target to shut off glycolysis in cancer cells. However, the plasticity of cancer cells remains a concern and must be addressed when employing such approaches.

Abnormal glutamine metabolism has also been identified as a key factor in bladder cancer progression. The necessity to assess the prognosis and therapeutic efficacy of bladder cancer treatments based on an analysis of glutamine metabolism related genes is vital. The Cancer Genome Atlas was used to identify glutamine metabolism-related genes as prognostic markers, and established a novel Glutamine Metabolism Immunity Index (GMII) based on univariate and multivariate COX regression analyses. Candidate small-molecule drugs targeting the GMII core target proteins were identified based on molecular docking analysis. The GMII consisting of eight independent prognostic genes was established using molecular docking analysis as an excellent discriminating tool for predicting the survival of patients with bladder cancer. These results showed 12 potential small-molecule drugs that could bind to three of the GMII core target proteins (Xu et al.).

Cyclooxygenases-2 (COX-2) and Prostaglandin E2 (PGE2), which are important in chronic inflammatory diseases, can increase tumor incidence and promote tumor growth and metastasis. The COX-2-PGE2 pathway promotes tumor immune evasion by regulating myeloid-derived suppressor cells, lymphocytes (CD8+ T cells, CD4+ T cells and natural killer cells), and antigen presenting cells (macrophages and dendritic cells). Based on conventional treatment, the addition of COX-2 inhibitors or EP antagonists may boost immunotherapy response in anti-tumor immune escape scenarios (Jin et al.).

Drug repurposing is one of the ideas that is underexplored in cancer therapy. With the availability of computational infrastructure and artificial intelligence based algorithms, it has never been so feasible to test various drugs and their combinations in different types and stages of cancer. The key to personalized medicine also lies in our ability to identify the right target in the right patient. The most challenging aspect of the targeted delivery of anti-cancer agents is achieving selective recognition of cancer cells. Recently, homotypic binding and specific protein-receptor interactions have emerged as the preferred method for delivering anti-cancer drugs. To effectively use cancer cell membrane encapsulated nanoparticles (CCMEN) as a delivery strategy, accurately predicting their selective targeting efficiency is of utmost importance. Eleven high-priority glioblastoma cell surface antigens were selected for probabilistic modeling based on relevance, expression levels availability, and crystal structure information from literature and databases. A new term, Breakeven point (BEP), was introduced as a characteristic of typical cancer cell membrane encapsulated delivery agents. The model's predictions closely matched the experimentally observed values within a range of ±7% for both experimental test culture types. The probabilistic model efficiently predicts the directional preference of nanoparticle-coated cancer cell membranes (GCC membrane) for glioblastoma. It can be easily adapted for other cancer types involving CCMEN as delivery agents for potential immunotherapy, offering greater specificity in future cancer treatment development (Khan et al.).

Tumors with limited immune cell infiltration and immune activity may be due to restricting anti-CD40 agonistic antibody (αCD40) immune activation by releasing certain tumor antigens. Dendritic cells (DC) can be activated through αCD40 and stimulate antigen presentation, concomitantly activating cytotoxic CD8 cells. Authors found that activation of β-2 adrenergic receptor (β2AR) initiates the signaling of CD40 in DCs through direct inhibition of IkBa phosphorylation and indirect upregulating of phosphorylated-cAMP response element binding protein (pCREB). The alteration in the CD40 pathways was observed when a pan β-Blocker 'propranolol', was introduced, causing better tumor regression, enhanced influx of effector T cells, as well as decreasing the number of regulatory T cells as compared to monotherapy (Singh et al.).

Several studies focused on novel cancer immunotherapies to boost anti-tumor immunity, including adoptive cell-based therapies. Various immune cells and molecules are targeted to enhance tumor-specific T cell responses. Precision and personalized therapeutic approaches are a promising route for further innovation in immuno-oncology needed for treatment of aggressive cancers. Combinational therapies show promise, but extensive pre-clinical evaluation and testing is vital before clinical development and adoption.

Author contributions

MK: Conceptualization, Supervision, Writing – original draft, Writing – review & editing. MA: Conceptualization, Writing – original draft, Writing – review & editing. SR: Writing – review & editing.

Conflict of interest

The authors declare that the research was conducted in the absence of any commercial or financial relationships that could be construed as a potential conflict of interest.

The authors declared that they were an editorial board member of Frontiers, at the time of submission. This had no impact on the peer review process and the final decision

Publisher's note

All claims expressed in this article are solely those of the authors and do not necessarily represent those of their affiliated organizations, or those of the publisher, the editors and the reviewers. Any product that may be evaluated in this article, or claim that may be made by its manufacturer, is not guaranteed or endorsed by the publisher.

frontiers | Frontiers in Immunology

TYPE Original Research
PUBLISHED 11 January 2023
DOI 10.3389/fimmu.2022.1103055

Check for updates

OPEN ACCESS

EDITED BY
Mohammad Azhar Aziz,
Aligarh Muslim University, India

REVIEWED BY
Mohammad A. AL-Mterin,
University of Nizwa, Oman
Yinying Lu,
Fifth Medical Center of the PLA General Hospital, China

*CORRESPONDENCE
Hong Zhu
zhuhong0719@126.com

†These authors have contributed equally to this work

SPECIALTY SECTION
This article was submitted to Cancer Immunity and Immunotherapy, a section of the journal Frontiers in Immunology

RECEIVED 19 November 2022
ACCEPTED 27 December 2022
PUBLISHED 11 January 2023

CITATION
Liu K, Zhu Y and Zhu H (2023) Immunotherapy or targeted therapy as the first-line strategies for unresectable hepatocellular carcinoma: A network meta-analysis and cost-effectiveness analysis. *Front. Immunol.* 13:1103055. doi: 10.3389/fimmu.2022.1103055

COPYRIGHT
© 2023 Liu, Zhu and Zhu. This is an open-access article distributed under the terms of the Creative Commons Attribution License (CC BY). The use, distribution or reproduction in other forums is permitted, provided the original author(s) and the copyright owner(s) are credited and that the original publication in this journal is cited, in accordance with accepted academic practice. No use, distribution or reproduction is permitted which does not comply with these terms.

Immunotherapy or targeted therapy as the first-line strategies for unresectable hepatocellular carcinoma: A network meta-analysis and cost-effectiveness analysis

Kun Liu[1†], Youwen Zhu[1†] and Hong Zhu[1,2*]

[1]Department of Oncology, Xiangya Hospital, Central South University, Changsha, Hunan, China, [2]National Clinical Research Center for Geriatric Disorders, Xiangya Hospital, Central South University, Changsha, Hunan, China

Introduction: The existence of many phase III randomized controlled trials (RCTs) of first-line treatment for unresectable hepatocellular carcinoma (HCC) puzzle doctors and patients in choosing the most effective treatment strategies. We aimed to assess the efficacy, safety, and cost-effectiveness of immunotherapy or targeted therapy as the first-line strategy for unresectable HCC.

Methods: The included clinical trials were retrieved from PubMed, Embase, the Cochrane library, and Web of Science databases, in which immunotherapy or targeted therapy was regarded as the first-line treatment for unresectable HCC, published in English between January 1, 2010, and September 20, 2022. We conducted a network meta-analysis (NMA) and cost-effectiveness analysis (CEA) from the Chinese payer's perspective. Overall survival (OS), progression-free survival (PFS), the ranks of different treatments using P-score, and adverse events (AEs) were evaluated by NMA. Total costs, life-years (LYs), quality-adjusted life-years (QALYs), and incremental cost-benefit ratio (ICER) were estimated from 15-year Markov models developed by CEA.

Results: We identified 2,825 records, including 11,796 patients, from 15 RCTs. The NMA revealed that sintilimab plus a bevacizumab biosimilar (HR, 0.57; 95% CI, 0.43 to 0.75; P = 0.96) and camrelizumab plus rivoceranib (HR, 0.56; 95% CI, 0.41 to 0.66; P = 0.94) could lead to great improvements in OS and PFS compared with sorafenib-related survival. The CEA indicated that tislelizumab increased by 0.220 QALYs (0.312 LYs) and decreased by $1,938 compared with sorafenib, which yielded ICERs of -$8,809/QALY (-$2,612/LY). Sensitivity analysis showed that the model was stable.

Conclusion: Sintilimab plus a bevacizumab biosimilar and camrelizumab plus rivoceranib significantly prolonged OS and PFS, respectively. Further considering the pharmacoeconomics factors, tislelizumab is the most cost-effective first-line treatment strategy for unresectable HCC in China.

KEYWORDS

unresectable hepatocellular carcinoma, immunotherapy, targeted therapy, network meta-analysis, cost-effectiveness analysis

1 Introduction

Primary liver cancer, including hepatocellular carcinoma (HCC), intrahepatic cholangiocarcinoma and other rare types, was the sixth most commonly diagnosed cancer and the third leading cause of cancer death globally in 2020. Approximately 906,000 new cases of liver cancer were reported globally, out of which 830,000 had a fatal outcome (1). Based on previous data, it is estimated that primary liver cancer will be the fourth most commonly diagnosed cancer and the third leading cause of cancer death in 2022 in China, with 431,383 new cases and 302,327 deaths (2). Although there is a wide variety of treatment methods for primary liver cancer, their efficacy is still unsatisfactory due to the difficulty in early diagnosis, as most patients are diagnosed at the advanced stage of the illness. Currently, some therapeutic approaches include surgery, transarterial chemoembolization, hepatic arterial infusion chemotherapy, radiotherapy, targeted therapy, and immunotherapy (3). However, their efficacy of them is not so desirable. Therefore, it is necessary to recommend the most effective treatment for clinicians and patients to choose.

For patients struggling with unresectable HCC, cancer treatment strategies like targeted therapy and immunotherapy are proven to be effective. In the past decade, numerous immunotherapy drugs and targeted therapy drugs have been gradually tried to apply to the first-line treatment of unresectable HCC, such as brivanib, sunitinib, linifanib, sorafenib, sorafenib plus doxorubicin, sorafenib plus erlotinib, lenvatinib, nivolumab, donafenib, and atezolizumab plus bevacizumab (4–12). Currently, the first-line recommended drugs include sorafenib, lenvatinib, atezolizumab plus bevacizumab, durvalumab, and nivolumab (13). Some regimens have been reported in clinical trials for first-line treatment, like sintilimab plus a bevacizumab biosimilar, cabozantinib plus atezolizumab, tislelizumab, and camrelizumab, durvalumab, pembrolizumab plus lenvatinib (14–19). Additionally, some researchers conducted a comparison of the efficacy of several of them. Liu W et al. found that sintilimab plus a bevacizumab biosimilar was the most effective treatment (20). In addition, another paper demonstrated that atezolizumab plus bevacizumab and sintilimab plus a bevacizumab biosimilar were comparable in efficacy (21). These studies have also become data references for clinical medication.

Following the European Society of Medical Oncology (ESMO) congress, the latest progress of first-line treatment regimens for HCC was updated in 2022, some of which have yielded breakthrough achievements. In the RATIONALE-301 trial, tislelizumab, compared with sorafenib, showed a non-inferiority efficacy in prolonging median overall survival (mOS) [15.9 vs 13.1 months; Hazard ratio (HR), 0.85; 95% confidence interval (CI), 0.712 to 1.019; P = 0.0398] (16). In the SHR-1210-III-310 trial, camrelizumab plus rivoceranib significantly prolonged mOS (22.1 vs 15.2 months; R, 0.62; 95% CI, 0.49 to 0.80; P < 0.0001) and mPFS (5.6 vs 3.7 months; HR, 0.52; 95% CI, 0.41 to 0.65; P < 0.0001) compared with sorafenib (17). In addition, lenvatinib plus pembrolizumab prolonged mOS (21.2 vs 19.0 months; HR, 0.840; 95% CI, 0.708 to 0.997; P = 0.0227) and mPFS (8.2 vs 8.1 months; HR, 0.834; 95% CI, 0.712 to 0.978) compared with lenvatinib alone but did not reach the significance threshold in the LEAP-002 study (19).

Considering that the previous research did not include these regimens comprehensively to compare efficacy indirectly, we conducted this network meta-analysis. However, due to the high morbidity and mortality of primary liver cancer in the Chinese population and most patients diagnosed as an advanced stage at the initial visit, the country and society are facing a huge burden of medical and health care. What's more, a growing number of novel drugs with expensive cost showed satisfactory efficacy. Therefore, we also performed a cost-effectiveness analysis to evaluate which regimen can balance clinical benefits and medical cost better from Chinese payers' perspectives.

2 Methods

2.1 Network meta-analysis

We performed this work according to the PRISMA statement, including a PRISMA NMA checklist (Supplementary Table 1).

2.1.1 Study selection and assessment of bias risks

We searched PubMed, Embase, the Cochrane library, and Web of Science for English-language publications from January 1, 2010, to September 20, 2022, with the search terms "nivolumab", "pembrolizumab", "atezolizumab", "camrelizumab", "durvalumab", "tislelizumab", "PD-1", "PD-L1", "immunotherapy", "sorafenib", "sunitinib", "linifanib", "lenvatinib", "donafenib", "bevacizumab", "targeted therapy", "molecular targeted therapy", "unresectable hepatocellular carcinoma", and "clinical trial" (Supplementary Table 2).

We also retrieved abstracts from the conferences of the European Society of Medical Oncology (ESMO) and the American Society of Clinical Oncology (ASCO). The chosen literature for the conduction of this study should abide by the following inclusion criteria: (1) phase III RCTs for unresectable hepatocellular carcinoma; (2) included immunotherapy or targeted therapy treatment arm instead of locoregional therapy as the first-line treatment; (3) the endpoint included OS and PFS. The exclusion criteria are as follows: (1) a number of patients in the experimental group <10; (2) detailed reports of adverse effects were not available; (3) not published in English. Two independent reviewers (K.L. and Y.W.Z.) screened these studies to exclude repeated articles and those articles not meet the inclusion criteria and extracted relevant data. In the case of disagreement between the two reviewers, we invited a third independent reviewer (H.Z.) for evaluation. We selected the most updated report when there are several reports from the same clinical trial. When we find potentially included abstracts, we first determine whether they meet the inclusion criteria based on their content. In addition, we will contact researchers or the marketing department of the corresponding medical company to obtain detailed data to make the final decision. The bias risk assessment for these clinical trials was performed according to the Cochrane Collaboration guideline (22).

2.1.2 Statistical analysis

The HRs and its 95% CI for OS and PFS of various treatment schemes were obtained using the R software (version 4.1.1, available: http://www.rproject.org) along with the package of "netmeta". Since there is little data to evaluate the heterogeneity between clinical trials, we established a fixed-effect model. In addition, we compared indirectly the safety of different regimens and calculated the odds ratio (OR) and its 95% CI of all grade adverse events (AEs) and ≥ 3-grade AEs. Finally, we used P-score to rank the efficacy and safety of each regimen.

2.2 Cost-effectiveness analysis

We performed this work according to the Consolidated Health Economic Evaluation Reporting Standards (CHEERS) checklist (Supplementary Table 3), while this analysis did not involve human subjects or animal study.

2.1.1 Patients and treatments

The patients have received the first-line treatment of various regimens. In the case of progressed disease (PD) or intolerable AEs, patients received regorafenib recommended by the National Comprehensive Cancer Network (NCCN®) guidelines and the Chinese Society of Clinical Oncology (CSCO) guidelines as subsequent therapy (13, 23, 24). On the other hand, the remaining patients received the best supportive care (BSC) until death, and those who reached death received terminal care. The specific use of different drugs is detailed in Supplementary Table 4. According to these RCTs and the published articles, we assumed that patients were 65 kg in weight, and 164 cm in height with a body surface area of 1.72 m^2 (25, 26) (Table 1).

2.2.2 Model structure

To evaluate the cost-effectiveness of the different first-line regimens of patients with unresectable HCC, we constructed a Markov model with a length of 6 weeks and three health states (PFS, progressive disease (PD), and death) (Supplementary Figure 1) using TreeAge Pro 2020 (TreeAge Software, Williamstown, MA, https://www.treeage.com) and the the time horizon was 15 years. The costs and effects were discounted at a rate of 3% per year (34). The outputs we measured included the total cost, life-years (LYs), quality-adjusted LYs (QALYs), and incremental cost-effectiveness ratios (ICERs). The willingness-to-pay (WTP) was $37,653 per QALY in China (25).

2.2.3 Utility estimates

We collected data from the OS and PFS curves from included RCTs using GetData Graph Digitizer (version 2.26; http://www.getdata-graph-digitizer.com/index.php), whereas the Weibull distribution was chosen as the best-fitting parameter model. This selection was made among well-known models such as log-logistic, Gompertz, Weibull, exponential, and log-normal distribution according to Akaike's information criterion (AIC) and Bayesian information criterion (BIC) (Supplementary Figure 2 and Table 5) (36). As for sorafenib, we reconstructed the survival curves according to the survival data reported by each clinical trial. We got two parameters, shape (γ) and scale (λ), using R software (25). We used previously published utilities of 0.76 and 0.68 as the mean health utility value for the PFS and the PD state, respectively (27). We also consider the disutility values of grade 3/4 AEs in our analysis (28).

2.2.4 Cost inputs

Direct medical costs were taken solely into account from the Chinese payers' perspective, including costs of drugs, AEs management (grade 3 or higher AEs with an incidence rate higher than 5%) (27, 29–34), BSC, terminal care, follow-up, and monitoring (30, 35). The drug price and part of the cost of AEs management are from Xiangya Hospital of Central South University. The remaining costs were derived from previously published literature (Table 1). All costs are exchanged into US dollars at the rate of *$1 = ¥6.8917*.

2.2.5 Sensitivity analyses

We performed one-way sensitivity analysis and probabilistic sensitivity analysis to evaluate the uncertainty of the model results. One-way sensitivity analysis was conducted within a variance of 20% from their baseline values according to varied values of a certain parameter. We also performed a probabilistic sensitivity analysis to assess the probability of effectiveness of the treatment regimens through 10000 Monte Carlo repetitions.

3 Results

3.1 Network meta-analysis

The current NMA was conducted upon 15 phase III RCTs in which 2,825 records were screened and 11,796 patients were enrolled (Supplementary Figure 3). The model diagram of the NMA is shown

10.3389/fimmu.2022.1103055

TABLE 1 Model Parameters: Clinical and Cost data.

Parameters	Baseline value	Range		Reference	Distribution
		Minimum	Maximum		
Clinical data					
Weibull survival model of sorafenib					
OS	Scale= 0.05419, Shape= 1.060795	–	–	(27)	–
PFS	Scale= 0.21713, Shape= 0.81887	-	-	(27)	-
HRs of other regimens versus sorafenib	See the results of network meta-analysis				–
Proportion (%) of receiving active second-line treatment					
Brivanib	0.210	0.168	0.252	(4)	Beta
Donafenib	0.372	0.298	0.446	(11)	Beta
Durvalumab	0.432	0.346	0.518	(18)	Beta
Lenvatinib	0.330	0.264	0.396	(9)	Beta
Linifanib	0.363	0.290	0.436	(6)	Beta
Nivolumab	0.380	0.304	0.456	(10)	Beta
Sorafenib	0.398	0.318	0.478	(4–12, 14–19)	Beta
Sunitinib	0.766	0.613	0.919	(5)	Beta
Tislelizumab	0.485	0.388	0.582	(16)	Beta
Atezolizumab plus bevacizumab	0.360	0.288	0.432	(12)	Beta
Cabozantinib plus atezolizumab	0.200	0.160	0.240	(15)	Beta
Camrelizumab plus rivoceranib	0.397	0.318	0.476	(17)	Beta
Pembrolizumab plus lenvatinib	0.441	0.353	0.529	(19)	Beta
Sintilimab plus IBI305	0.290	0.232	0.348	(14)	Beta
Sorafenib plus erlotinib	0.450	0.360	0.540	(8)	Beta
Sorafenib plus doxorubicin	0.728	0.582	0.874	(7)	Beta
Risk of main AEs in lenvatinib group					
Risk of decreased appetite	0.046	0.037	0.055	(9)	Beta
Risk of AST increased	0.050	0.040	0.060	(9)	Beta
Risk of thrombocytopenia	0.055	0.044	0.066	(9)	Beta
Risk of proteinuria	0.057	0.046	0.068	(9)	Beta
Risk of decreased weight	0.076	0.061	0.091	(9)	Beta
Risk of hypertension	0.233	0.186	0.280	(9)	Beta
Risk of main AEs in tislelizumab group					
Risk of AST increase	0.059	0.047	0.071	(16)	Beta
Risk of main AEs in orther group	See the results of randomized controlled trials			(4–8, 10–12, 14, 15, 17–19)	Beta
Utility					
PFS	0.760	0.608	0.912	(27)	Beta
PD	0.680	0.544	0.60	(27)	Beta
Disutility due to AEs (grade ≥3)	0.160	0.128	0.192	(28)	Beta
Cost data (US, $)					
Drug cost, $/per cycle					

(Continued)

TABLE 1 Continued

Parameters	Baseline value	Range		Reference	Distribution
		Minimum	Maximum		
Brivanib	10,769	8,615	12,923	Local Charge	Gamma
Donafenib	2,204	1,763	2,645	Local Charge	Gamma
Durvalumab	2,625	2,100	3,150	Local Charge	Gamma
Lenvatinib	1,975	1,580	2,370	Local Charge	Gamma
Linifanib	7,601	6,081	9,121	Local Charge	Gamma
Nivolumab	2,515	2,012	3,018	Local Charge	Gamma
Sorafenib	2,422	1,938	2,906	Local Charge	Gamma
Sunitinib	1,312	1,050	1,574	Local Charge	Gamma
Tislelizumab	842	674	1010	Local Charge	Gamma
Atezolizumab plus bevacizumab	6,624	5,299	7,945	Local Charge	Gamma
Cabozantinib plus atezolizumab	6,330	5,064	7,596	Local Charge	Gamma
Camrelizumab plus rivoceranib	1,832	1,466	2,198	Local Charge	Gamma
Pembrolizumab plus lenvatinib	3,275	2,620	3,930	Local Charge	Gamma
Sintilimab plus IBI305	3,819	3,055	4,583	Local Charge	Gamma
Sorafenib plus erlotinib	2,974	2,379	3,569	Local Charge	Gamma
Sorafenib plus doxorubicin	2,490	1,992	2,988	Local Charge	Gamma
Regorafenib	3,154	2,523	3,785	Local Charge	Gamma
Cost of AEs					
Brivanib	74	59	89	(29–32)	Gamma
Donafenib	4	3	5	(29, 31)	Gamma
Durvalumab	5	4	6	(30)	Gamma
Lenvatinib	42	34	50	(29–32)	Gamma
Linifanib	96	77	115	(29–32)	Gamma
Nivolumab	6	5	7	(30)	Gamma
Sorafenib	13	10	16	(29–31)	Gamma
Sunitinib	157	126	188	(29–33)	Gamma
Tislelizumab	6	5	7	(30)	Gamma
Atezolizumab plus bevacizumab	9	7	11	(29, 30)	Gamma
Cabozantinib plus atezolizumab	22	18	26	(29–31)	Gamma
Camrelizumab plus rivoceranib	117	94	140	(29–33)	Gamma
Pembrolizumab plus lenvatinib	26	21	31	(29–31)	Gamma
Sintilimab plus IBI305	49	39	59	(29–32)	Gamma
Sorafenib plus erlotinib	154	123	185	(27, 29, 30, 33)	Gamma
Sorafenib plus doxorubicin	81	65	97	(29, 31–34)	Gamma
Follow-up and monitoring per cycle	228	182	274	(35)	Gamma
Best supportive care per cycle	423	338	508	(30)	Gamma
Terminal care per patient	2,035	1,628	2,442	(35)	Gamma
Body weight (kilogram)	65	52	78	(25, 26)	Normal
Body surface area (meters^2)	1.72	1.38	2.06	(25, 26)	Normal

(Continued)

TABLE 1 Continued

Parameters	Baseline value	Range		Reference	Distribution
		Minimum	Maximum		
Discount rate	0.03	0	0.05	(34)	Uniform

OS, overall survival; PFS, progression-free survival; IBI305, bevacizumab biosimilar; AEs, adverse events; AST, aspartate aminotransferase; NA, not applicable.

in Supplementary Figure 4. These trials involved regimens brivanib (N = 577), donafenib (N = 328), durvalumab (N = 389), lenvatinib (N = 877), linifanib (N = 514), nivolumab (N = 371), sunitinib (N = 530), tislelizumab (N = 342), atezolizumab plus bevacizumab (N = 336), cabozantinib plus atezolizumab (N = 432), camrelizumab plus rivoceranib (N = 272), durvalumab plus tremelimumab (N = 393), pembrolizumab plus lenvatinib (N = 395), sintilimab plus a bevacizumab biosimilar (N = 381), sorafenib plus doxorubicin (N = 180), sorafenib plus erlotinib (N = 358), and sorafenib (N = 4,925) (Supplementary Table 6). The risk of bias is shown in Supplementary Table 7. From the indirect comparisons of the NMA, sintilimab plus a bevacizumab biosimilar (HR, 0.57; 95% CI, 0.43 to 0.75 or 1.75; 1.33 to 2.32; P-score = 0.96) and camrelizumab plus rivoceranib (HR, 0.56; 95% CI, 0.41 to 0.66 or 1.92; 1.53 to 2.42; P-score = 0.94) could lead to great improvements in OS and PFS compared with the sorafenib-related survival (Figures 1 and 2). The HRs for OS and PFS of active treatment compared with the sorafenib treatment are shown in Figures 1 and 2. The forest plot revealed that tislelizumab had a lower likelihood of all-grade (OR, 0.14; 95% CI, 0.07 to 0.25; P-score = 0.05) and grade 3 or higher AEs (0.25; 0.18 to 0.35; P-score = 0.05) than those of sorafenib, respectively (Supplementary Figure 5).

3.2 Cost-effectiveness analysis

3.2.1 Base-case analysis

A Markov model was composed of 11,403 participants with a 15-year time horizon, in which the durvalumab plus tremelimumab group was excluded. The total costs and QALYs (LYs) of brivanib, sunitinib, linifanib, sorafenib plus doxorubicin, sorafenib plus erlotinib, lenvatinib, cabozantinib plus atezolizumab, durvalumab, tislelizumab, nivolumab, donafenib, pembrolizumab plus lenvatinib, camrelizumab plus rivoceranib, atezolizumab plus bevacizumab, sintilimab plus a bevacizumab biosimilar, and sorafenib were $64,723 and 0.374 (0.524), $26,922 and 0.945 (1.379), $59,860 and 1.379 (1.681), $38,052 and 1.186 (1.717), $35,787 and 1.297 (1.888), $28,080 and 1.367 (1.942), $56,396 and 1.410 (1.994), $33,972 and 1.498 (2.128), $26,808 and 1.509 (2.149), $32,703 and 1.515 (2.148), $31,063 and 1.535 (2.180), $44,731 and 1.594 (2.260), $40,307 and 1.795 (2.603), $73,457 and 1.870 (2.646), $56,259 and 2.076 (2.950), and $28,746 and 1.289 (1.837), which yielded ICERs of -$39,319 (-$27,401), $5,302 ($3,983), -$250,919 (-$199,449), -$83,838 (-$77,550), $138,059 ($880,125), -$3,680 (-$6,343), $228,512 ($176,115), $25,005 ($17,959), -$8,809 (-$2,612), $17,509 ($12,724), $9,419 ($6,755), $52,410 ($37,790), $22,848 ($15,093), $76,955

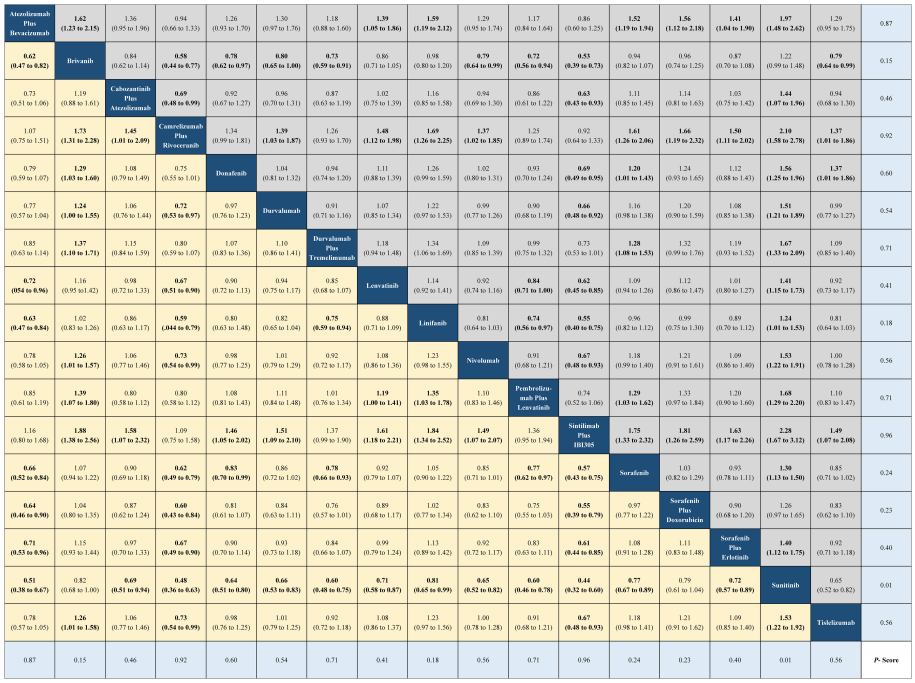


FIGURE 1
Network meta-analysis for overall survival.

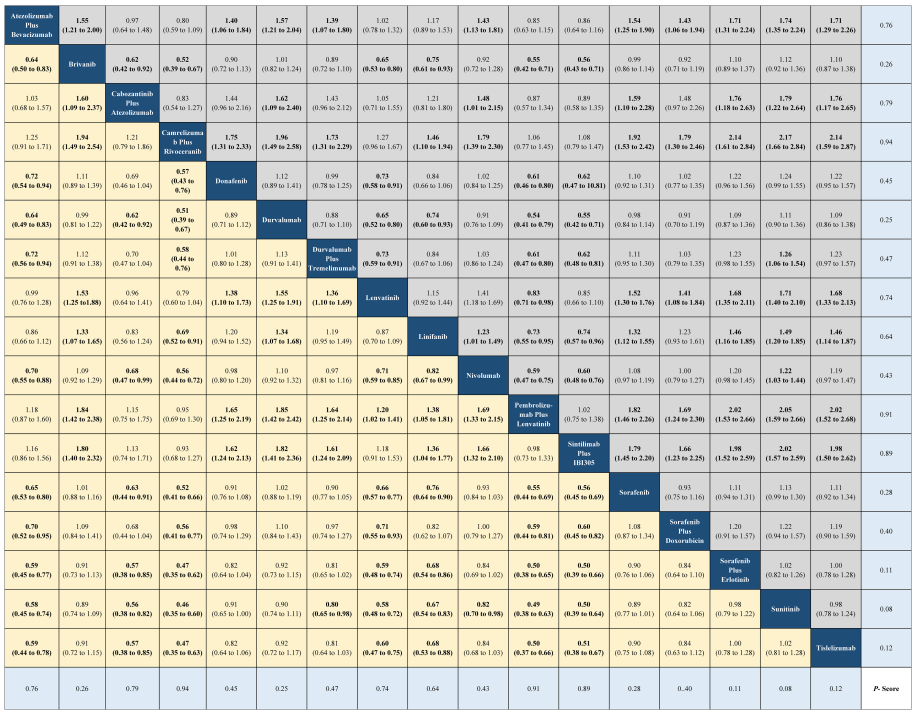


FIGURE 2
Network meta-analysis for progression-free survival.

($55,267), and $34,959 ($24,675) per QALY (LY) gained than sorafenib, respectively (Table 2). Our results demonstrate that tislelizumab or lenvatinib versus sorafenib as first-line systematic treatment were dominant. Further pairwise comparative analysis, treatment with tislelizumab produced an additional 0.142 QALYs (0.207 LYs) and a cost reduction of $1,272 compared with lenvatinib, resulting in an ICER of -$8,958/QALY (-6,145/LY). A comparison of ICER's pairwise treatment strategies is shown in Supplementary Table 8. In summary, tislelizumab was cost-effective as the first-line strategy for unresectable HCC in China.

3.2.2 Sensitivity analysis

The results of one-way sensitivity showed that HRs of OS of the tislelizumab versus sorafenib when comparing tislelizumab and sorafenib, followed by the cost of sorafenib, regorafenib, and tislelizumab. When comparing lenvatinib and sorafenib, HRs of OS of the lenvatinib versus sorafenib, followed by the costs of lenvatinib, sorafenib and regorafenib (Figure 3). In the probabilistic sensitivity analysis, the acceptability curve showed that for different WTP values, the most cost-effective solutions are also different (Figure 4). For example, tislelizumab is a better choice when it is less than the WTP threshold of $37,653/QALY in China. When the WTP value is between $37,653/QALY and $80,000/QALY, camrelizumab plus rivoceranib is the better choice. When WTP is greater than $80,000/QALY, sintilimab plus a bevacizumab biosimilar is a better choice (Figure 4). The scatter plot showed that the probability of tislelizumab, lenvatinib, donafenib, nivolumab, camrelizumab plus rivoceranib, durvalumab, sintilimab plus a bevacizumab biosimilar, pembrolizumab plus lenvatinib, sorafenib plus erlotinib, sunitinib, atezolizumab plus bevacizumab, brivanib, linifanib, sorafenib plus doxorubicin, cabozantinib plus atezolizumab therapies being cost-effective were 96.7%, 86.3%, 84.5%, 82.4%, 75.4%, 73.6%, 60.0%, 24.0%, 0.3%, 1.6%, 0.9%, 0%, 0%, 0%, and 0% compared with sorafenib at a WTP threshold of $37,653/QALY, respectively (Supplementary Figure 6).

4 Discussion

At present, the morbidity and mortality of primary liver cancer, especially HCC, are very high in the world, and most patients are in the advanced stage. Among all regions of the world, the highest incidence of HCC has been observed in Asia, and China has recorded many cases (37). Furthermore, Chinese patients with unresectable HCC face substantial financial pressure due to medical expenses. From 2012 to 2014, the expenditures of an HCC patient were ¥55,529 ($8,057) in 13 Chinese provinces on average, which included ¥4,592 ($666) of non-medical and the rest ¥50,937 ($7,391) of medical expenditures (38). Due to the poor prognosis and medical care burden of unresectable HCC, numerous clinical trials are conducted to explore an effective treatment option (16, 17, 19, 37). For the moment, there are a large quantity of novel drugs for unresectable HCC to choose, such as brivanib, sunitinib, linifanib, sorafenib plus doxorubicin, sorafenib plus erlotinib, lenvatinib, cabozantinib plus atezolizumab, durvalumab, tislelizumab, nivolumab, donafenib, pembrolizumab plus lenvatinib, camrelizumab plus rivoceranib, atezolizumab plus bevacizumab, sintilimab plus a bevacizumab biosimilar, and sorafenib. Although these therapeutic strategies are effective for treating unresectable HCC, the high cost of these drugs

TABLE 2 Baseline results.

Strategy	LYs	QALYs	Total cost $	ICER $/LY[a]	ICER $/QALY[a]
Brivanib	0.524	0.374	64,723	Dominated[b]	Dominated
Sunitinib	1.379	0.945	26,922	3,983	5,302
Linifanib	1.681	1.165	59,860	Dominated	Dominated
Sorafenib plus Doxorubicin	1.717	1.186	38,052	Dominated	Dominated
Sorafenib	1.837	1.289	28,746	–	–
Sorafenib plus Erlotinib	1.888	1.297	35,787	138,059	880,125
Lenvatinib	1.942	1.367	28,080	Dominant[c]	Dominant
Cabozantinib plus Atezolizumab	1.994	1.410	56,396	176,115	228,512
Durvalumab	2.128	1.498	33,972	17,959	25,005
Tislelizumab	2.149	1.509	26,808	Dominant	Dominant
Nivolumab	2.148	1.515	32,703	12,724	17,509
Donafenib	2.180	1.535	31,063	6,755	9,419
Pembrolizumab plus Lenvatinib	2.260	1.594	44,731	37,790	52,410
Camrelizumab plus Rivoceranib	2.603	1.795	40,307	15,093	22,848
Atezolizumab plus Bevacizumab	2.646	1.870	73,457	55,267	76,955
Sintilimab plus IBI305	2.950	2.076	56,259	24,675	34,959

[a] Compared to sorafenib.
[b] Other strategies showed lower effectiveness and high cost, as compared with the sorafenib (Dominated).
[C] Other strategies showed higher effectiveness and lower cost, as compared with the sorafenib (Dominant).
ICER, incremental cost-effectiveness ratio; LY, life-year; QALY, quality-adjusted life-year; IBI305, bevacizumab biosimilar.

places a heavy burden on social health resources and patients. In addition, there is a lack of head-to-head clinical trials of 16 treatment strategies to show which one is better, and fewer studies to consider its overall cost-effectiveness. Therefore, we performed the first well-rounded network meta-analysis and cost-effectiveness analysis of first-line systemic regiments for unresectable HCC to facilitate treatment strategies for patients and clinicians.

Additionally, there is a lack of head-to-head clinical trials to determine which one was the best choice. Even more, only a few studies discussed the overall cost-effectiveness of each strategy separately. Therefore, this was the first well-rounded NMA and cost-effectiveness analysis evaluating the first-line systematic regimens for unresectable HCC to facilitate treatment strategies for both patients and clinicians.

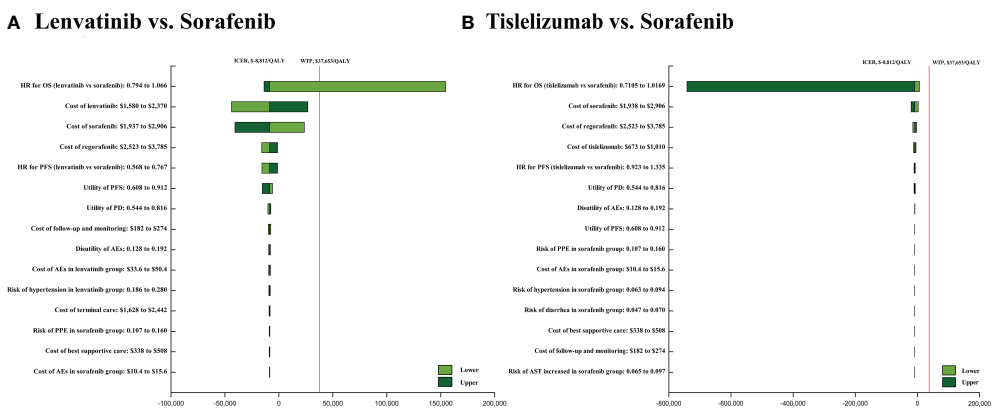


FIGURE 3
The one-way sensitivity analyses of lenvatinib vs sorafenib **(A)**, tislelizumab vs. sorafenib **(B)**. PFS, progression-free survival; PD, disease progressed; AEs, adverse events.

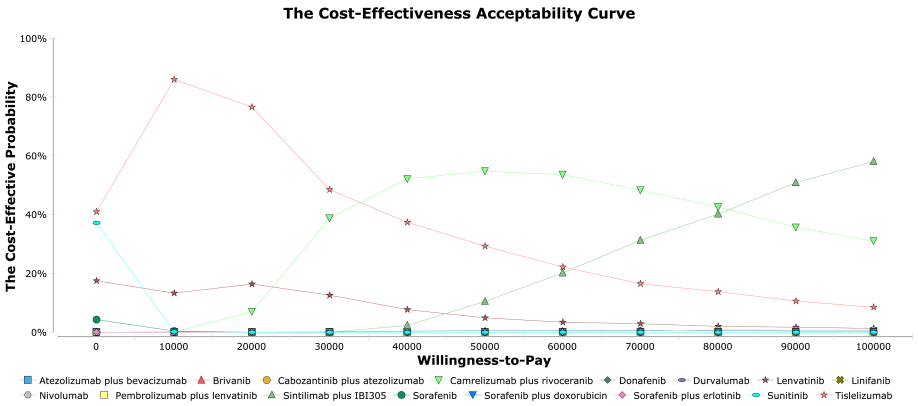


FIGURE 4
The cost-effectiveness acceptability curves.

The last ten years have shown that many novel drugs have been approved to treat irresectable liver cancer. Sorafenib was the first approved molecularly-targeted drug and was regarded as a standard in improving the prognosis of patients struggling with unresectable HCC. In this study, we also uniformly selected sorafenib as a control. However, our findings differed slightly from those of published research (21). Network meta-analysis results revealed that sintilimab plus a bevacizumab biosimilar showed the best effectiveness in prolonging OS, followed by camrelizumab plus rivoceranib and atezolizumab plus bevacizumab. On the other hand, camrelizumab plus rivoceranib ranked the first in prolonging PFS, followed by pembrolizumab plus lenvatinib and sintilimab plus a bevacizumab biosimilar. The anti-angiogenesis effect of immunotherapy combined with targeted therapy is obvious, which highlights the characteristics and advantages of immunotherapy, and gradually changes the existing clinical standard and treatment mode of unresectable HCC. However, all grade and grade 3 or higher AEs in camrelizumab plus rivoceranib group is much higher than other groups. The grade 3 or higher AEs in camrelizumab plus rivoceranib group included hypertension, hepatic insufficiency, palmar-plantar erythro-dysesthesia, and so on, most of which are related to TKI (17). Meanwhile, all grade and grade 3 or higher AEs in the immunotherapy alone group are much lower than other group, such as durvalumab, tislelizumab, and nivolumab. The latter indicated the possibility of immunotherapy being a new trend in curing patients with unresectable HCC. In conclusion, NMA provides strong evidence for the efficacy of immunotherapy in combination with targeted therapy as the first-line treatment for unresectable HCC. Our estimates of survival suggest that the efficacy of immunotherapy plus targeted therapy is better than others. Although immunotherapy remains the most favorable safety, the increased efficacy of combination therapy comes at the cost of a high risk of toxicity, which often results in permanent discontinuation. Therefore, doctors and patients need to consider both efficacy and safety when selecting treatment options according to the patient's condition in clinical practice.

It is a cost-based innovative treatment strategy that we need to take into consideration in China, an economic powerhouse. The baseline results of the cost-effectiveness analysis indicated that tislelizumab and lenvatinib increased by 0.220 and 0.078 QALYs and decreased by $1,938 and $666 compared with sorafenib, respectively. What's more, tislelizumab increased by 0.142 QALYs and decreased by $1,272 compared with lenvatinib. The treatment of and sintilimab plus a bevacizumab biosimilar, atezolizumab plus bevacizumab, and camrelizumab plus rivoceranib are related to better efficacy in all first-line strategy, producing 2.076, 1.870, and 1.795 QALYs respectively, which are accordance with the results of NMA. However, considering the medical expenditure of all treatment strategies, tislelizumab is the dominant cost-effective strategies as the first-line treatment for unresectable HCC. The main reasons were: first, considering the affordability of Chinese patients, the price of tislelizumab negotiated with the government is the lowest among all first-line treatment. Second, the costs of dealing with AEs were the least due to the low incidence of grade 3 or higher AEs. Third, patients receiving BSC, who are intolerant to standard treatment strategies for unresectable HCC, accounted for a relatively small percentage.

Our cost-effectiveness analysis is sensitive to the relative efficacy of the first-line treatment for unresectable HCC. The analysis suggested that the economic outcome of lenvatinib became more favorable in patients with lower HR of OS compared with sorafenib and worse in patients with higher HR. However, regardless of whether the HR of OS was higher or lower in tislelizumab group compared with sorafenib, the economic outcome was favorable. This finding is similar to previously published researches, in which the HR of OS is the most influential factor (28, 30, 39–42). Changes in WTP values also affect economic outcomes. Tislelizumab was the most cost-effective treatment option at a WTP threshold of $37,653 per QALY, whereas camrelizumab plus rivoceranib was a preferable option at a WTP threshold of $37,653 to $80,000 per QALY and sintilimab plus a bevacizumab biosimilar was an affordable option at a WTP threshold of higher than $80,000 per QALY. Due to China's vast territory and abundant resources, GDP per capita varies greatly. We also calculated WTP values for different regions of China. For example, The WTP values of Beijing, Shanghai, Jiangsu, Guangdong, Hubei, Neimenggu, Anhui, Hunan, Jiangxi, Guizhou, Guangxi, Heilongjiang and Gansu were $80,053/QALY, $75,656/QALY, $59,768/QALY, $42,964/QALY, $37,698/QALY, $37,132/QALY, $30,646/QALY, $30,167/QALY, $28,513/QALY, $22,114/QALY, $21,740/QALY, $20,329/QALY and $17,804/QALY, respectively (43). Surprisingly, tislelizumab is the best strategy of

choice in underdeveloped and relatively developed regions of China. In most developed regions, camrelizumab plus rivoceranib is regarded as the best choice. Only in Beijing, sintilimab plus a bevacizumab biosimilar is an optional choice. Therefore, the different economic factors of different regions should be taken into account when approving novel medicines for clinical use. Currently, the drugs used in the first-line treatment of liver cancer have certain clinical benefits and may be used on a large scale, but their economic toxicity still exists. Economic toxicity can bankrupt patients with high treatment costs, cause cancer patients to stop treatment, and even lead to poor patient outcomes in China (34). In the CSCO guidelines version 2022, sorafenib, lenvatinib, donafenib, sintilimab plus a bevacizumab biosimilar, and camrelizumab plus rivoceranib are recommended first-line strategies, with a wide range of costs (23). Thus, our results can be used to find a reasonable balance between the price of new drugs and their clinical efficacy, inform national regulatory agencies when making healthcare decisions, and make a significant contribution to adequately address economic toxicity.

There are some limitations in our study. Firstly, when using the network meta-analysis method to compare first-line treatment regimens indirectly, we assumed that the included studies did not differ in patient characteristics and summarized the chemotherapy groups, and selected a fixed-effect model. However, it is a difference that we cannot eliminate. For instance, the ORIENT-32 trial recruited participants from the Chinese population and the IMbrave150 trial and LEAP-002 trial recruited globally. Secondly, considering that there were multiple survival curves of sorafenib, we pooled and reconstructed the survival curves according to the original survival data of the sorafenib group in each clinical trial. Thirdly, we inferred the long-term survival benefit in terms of the short-term survival data of each experiment, which will change with the change of long-term follow-up. This is an inevitable limitation in our model. Therefore, it is necessary to verify and evaluate the concordance of these health outcomes in a model with real-world data. In addition, we only considered the occurrence of more than 5% of grade 3 or higher adverse events, which may underestimate the cost of adverse events. Nevertheless, the cost and disutility of AEs were not the significant factors influencing the results

5 Conclusion

Briefly, sintilimab plus a bevacizumab biosimilar and camrelizumab plus rivoceranib showed the best efficacy in prolonging OS and PFS compared with sorafenib, respectively. What's more, we found that tislelizumab is the most cost-effective first-line treatment strategy for unresectable HCC in China at the WTP of $37,653 QALY. In economically developed areas of China, camrelizumab plus rivoceranib is also a recommended cost-effective treatment strategy. The results could help clinicians select the most appropriate drugs for their patients and set reimbursement policies.

Data availability statement

The original contributions presented in the study are included in the article/Supplementary Material. Further inquiries can be directed to the corresponding author.

Ethics statement

This article is based on previously conducted studies and does not contain any new studies with human participants or animals performed by any of the authors, it does not require the approval of the independent ethics committee.

Author contributions

KL, YZ, and HZ designed the experiment. YZ, and KL performed the experiments. YZ and KL analyzed the data. HZ contributed analysis tools and funding. YZ, KL, and HZ wrote the manuscript. KL and YZ contributed equally. All authors contributed to the article and approved the submitted version.

Funding

This work was supported by the Clinical Research Project of Xiangya Hospital (grant number, 2016L06 to HZ).

Conflict of interest

The authors declare that the research was conducted in the absence of any commercial or financial relationships that could be construed as a potential conflict of interest.

Publisher's note

All claims expressed in this article are solely those of the authors and do not necessarily represent those of their affiliated organizations, or those of the publisher, the editors and the reviewers. Any product that may be evaluated in this article, or claim that may be made by its manufacturer, is not guaranteed or endorsed by the publisher.

Supplementary material

The Supplementary Material for this article can be found online at: https://www.frontiersin.org/articles/10.3389/fimmu.2022.1103055/full#supplementary-material

References

1. Sung H, Ferlay J, Siegel RL, Laversanne M, Soerjomataram I, Jemal A, et al. Global cancer statistics 2020: GLOBOCAN estimates of incidence and mortality worldwide for 36 cancers in 185 countries. *CA Cancer J Clin* (2021) 71:209–49. doi: 10.3322/caac.21660

2. Xia C, Dong X, Li H, Cao M, Sun D, He S, et al. Cancer statistics in China and united states, 2022: profiles, trends, and determinants. *Chin Med J (Engl)* (2022) 135:584–90. doi: 10.1097/CM9.0000000000002108

3. Liu Z, Liu X, Liang J, Liu Y, Hou X, Zhang M, et al. Immunotherapy for hepatocellular carcinoma: Current status and future prospects. *Front Immunol* (2021) 12:765101. doi: 10.3389/fimmu.2021.765101

4. Johnson PJ, Qin S, Park JW, Poon RT, Raoul JL, Philip PA, et al. Brivanib versus sorafenib as first-line therapy in patients with unresectable, advanced hepatocellular carcinoma: results from the randomized phase III BRISK-FL study. *J Clin Oncol* (2013) 31:3517–24. doi: 10.1200/JCO.2012.48.4410

5. Cheng AL, Kang YK, Lin DY, Park JW, Kudo M, Qin S, et al. Sunitinib versus sorafenib in advanced hepatocellular cancer: results of a randomized phase III trial. *J Clin Oncol* (2013) 31:4067–75. doi: 10.1200/JCO.2012.45.8372

6. Cainap C, Qin S, Huang WT, Chung IJ, Pan H, Cheng Y, et al. Linifanib versus sorafenib in patients with advanced hepatocellular carcinoma: results of a randomized phase III trial. *J Clin Oncol* (2015) 33:172–9. doi: 10.1200/JCO.2013.54.3298

7. Abou-Alfa GK, Shi Q, Knox JJ, Kaubisch A, Niedzwiecki D, Posey J, et al. Assessment of treatment with sorafenib plus doxorubicin vs sorafenib alone in patients with advanced hepatocellular carcinoma: Phase 3 CALGB 80802 randomized clinical trial. *JAMA Oncol* (2019) 5:1582–8. doi: 10.1001/jamaoncol.2019.2792

8. Zhu AX, Rosmorduc O, Evans TR, Ross PJ, Santoro A, Carrilho FJ, et al. SEARCH: a phase III, randomized, double-blind, placebo-controlled trial of sorafenib plus erlotinib in patients with advanced hepatocellular carcinoma. *J Clin Oncol* (2015) 33:559–66. doi: 10.1200/JCO.2013.53.7746

9. Kudo M, Finn RS, Qin S, Han KH, Ikeda K, Piscaglia F, et al. Lenvatinib versus sorafenib in first-line treatment of patients with unresectable hepatocellular carcinoma: a randomised phase 3 non-inferiority trial. *Lancet* (2018) 391:1163–73. doi: 10.1016/S0140-6736(18)30207-1

10. Yau T, Park JW, Finn RS, Cheng AL, Mathurin P, Edeline J, et al. Nivolumab versus sorafenib in advanced hepatocellular carcinoma (CheckMate 459): a randomised, multicentre, open-label, phase 3 trial. *Lancet Oncol* (2022) 23:77–90. doi: 10.1016/S1470-2045(21)00604-5

11. Qin S, Bi F, Gu S, Bai Y, Chen Z, Wang Z, et al. Donafenib versus sorafenib in first-line treatment of unresectable or metastatic hepatocellular carcinoma: A randomized, open-label, parallel-controlled phase II-III trial. *J Clin Oncol* (2021) 39:3002–11. doi: 10.1200/JCO.21.00163

12. Cheng AL, Qin S, Ikeda M, Galle PR, Ducreux M, Kim TY, et al. Updated efficacy and safety data from IMbrave150: Atezolizumab plus bevacizumab vs. sorafenib for unresectable hepatocellular carcinoma. *J Hepatol* (2022) 76:862–73. doi: 10.1016/j.jhep.2021.11.030

13. *National comprehensive cancer network clinical practice guidelines in oncology (NCCN guidelines): Hepatobiliary cancers, version 2.2022* . Available at: https://www.nccn.org/professionals/physician_gls/pdf/hepatobiliary.pdf (Accessed July 15, 2022).

14. Ren Z, Xu J, Bai Y, Xu A, Cang S, Du C, et al. Sintilimab plus a bevacizumab biosimilar (IBI305) versus sorafenib in unresectable hepatocellular carcinoma (ORIENT-32): a randomised, open-label, phase 2-3 study. *Lancet Oncol* (2021) 22:977–90. doi: 10.1016/S1470-2045(21)00252-7

15. Kelley RK, Rimassa L, Cheng AL, Kaseb A, Qin S, Zhu AX, et al. Cabozantinib plus atezolizumab versus sorafenib for advanced hepatocellular carcinoma (COSMIC-312): a multicentre, open-label, randomised, phase 3 trial. *Lancet Oncol* (2022) 23:995–1008. doi: 10.1016/S1470-2045(22)00326-6

16. Qin S, Kudo M, Meyer T, Finn RS, Vogel A, Bai Y, et al. LBA36 final analysis of RATIONALE-301: Randomized, phase III study of tislelizumab versus sorafenib as first-line treatment for unresectable hepatocellular carcinoma. *Ann Oncol* (2022) 33:S1402–S3. doi: 10.1016/j.annonc.2022.08.033

17. Qin S, Chan LS, Gu S, Bai Y, Ren Z, Lin X, et al. LBA35 camrelizumab (C) plus rivoceranib (R) vs. sorafenib (S) as first-line therapy for unresectable hepatocellular carcinoma (uHCC): A randomized, phase III trial. *Ann Oncol* (2022) 33:S1401–S2. doi: 10.1016/j.annonc.2022.08.032

18. Abou-Alfa GK, Chan SL, Kudo M, Lau G, Kelley RK, Furuse J, et al. Phase 3 randomized, open-label, multicenter study of tremelimumab (T) and durvalumab (D) as first-line therapy in patients (pts) with unresectable hepatocellular carcinoma (uHCC): HIMALAYA. *J Clin Oncol* (2022) 40:379–. doi: 10.1200/JCO.2022.40.4_suppl.379

19. Finn RS, Kudo M, Merle P, Meyer T, Qin S, Ikeda M, et al. LBA34 primary results from the phase III LEAP-002 study: Lenvatinib plus pembrolizumab versus lenvatinib as first-line (1L) therapy for advanced hepatocellular carcinoma (aHCC). *Ann Oncol* (2022) 33:S1401. doi: 10.1016/j.annonc.2022.08.031

20. Liu W, Quan B, Lu S, Tang B, Li M, Chen R, et al. First-line systemic treatment strategies for unresectable hepatocellular carcinoma: A systematic review and network meta-analysis of randomized clinical trials. *Front Oncol* (2021) 11:771045. doi: 10.3389/fonc.2021.771045

21. Fulgenzi CAM, D'Alessio A, Airoldi C, Scotti L, Demirtas CO, Gennari A, et al. Comparative efficacy of novel combination strategies for unresectable hepatocellular carcinoma: A network metanalysis of phase III trials. *Eur J Cancer.* (2022) 174:57–67. doi: 10.1016/j.ejca.2022.06.058

22. Cumpston M, Li T, Page MJ, Chandler J, Welch VA, Higgins JP, et al. Updated guidance for trusted systematic reviews: a new edition of the cochrane handbook for systematic reviews of interventions. *Cochrane Database Syst Rev* (2019) 10:Ed000142. doi: 10.1002/14651858.ED000142

23. Available at: http://www.csco.org.cn/cn/index.aspx (Accessed 2022).

24. Available at: http://www.nhc.gov.cn/ (Accessed 2022).

25. Zhu Y, Liu K, Wang K, Peng L. Vascular endothelial growth factor receptor inhibitors in Chinese patients with advanced radioactive iodine-refractory differentiated thyroid cancer: A network meta-analysis and cost-effectiveness analysis. *Front Endocrinol (Lausanne).* (2022) 13:909333. doi: 10.3389/fendo.2022.909333

26. Zhu Y, Liu K, Ding D, Wang K, Liu X, Tan X. Chemo-immunotherapy regimes for recurrent or metastatic nasopharyngeal carcinoma: A network meta-analysis and cost-effectiveness analysis. *Front Pharmacol* (2022) 13:858207. doi: 10.3389/fphar.2022.858207

27. Liao W, Huang J, Hutton D, Zhu G, Wu Q, Wen F, et al. Cost-effectiveness analysis of cabozantinib as second-line therapy in advanced hepatocellular carcinoma. *Liver Int* (2019) 39:2408–16. doi: 10.1111/liv.14257

28. Li L, Yang S, Chen Y, Tian L, He Y, Wu B, et al. Immune checkpoint inhibitors plus an anti-VEGF antibody as the first-line treatment for unresectable hepatocellular carcinoma: A network meta-analysis and cost-effectiveness analysis. *Front Pharmacol* (2022) 13:891008. doi: 10.3389/fphar.2022.891008

29. Cai H, Zhang L, Li N, Zheng B, Liu M. Lenvatinib versus sorafenib for unresectable hepatocellular carcinoma: a cost-effectiveness analysis. *J Comp Eff Res* (2020) 9:553–62. doi: 10.2217/cer-2020-0041

30. Zhao M, Pan X, Yin Y, Hu H, Wei J, Bai Z, et al. Cost-effectiveness analysis of five systemic treatments for unresectable hepatocellular carcinoma in China: An economic evaluation based on network meta-analysis. *Front Public Health* (2022) 10:869960. doi: 10.3389/fpubh.2022.869960

31. Meng R, Zhang X, Zhou T, Luo M, Qiu Y. Cost-effectiveness analysis of donafenib versus lenvatinib for first-line treatment of unresectable or metastatic hepatocellular carcinoma. *Expert Rev Pharmacoecon Outcomes Res* (2022) 22:1079–86. doi: 10.1080/14737167.2022.2079498

32. Zhou T, Cao Y, Wang X, Yang L, Wang Z, Ma A, et al. Economic evaluation of sintilimab plus bevacizumab versus sorafenib as a first-line treatment for unresectable hepatocellular carcinoma. *Adv Ther* (2022) 39:2165–77. doi: 10.1007/s12325-022-02079-4

33. Li M, Lin S, Wilson L, Huang P, Wang H, Lai S, et al. Cost-effectiveness analysis of hepatic arterial infusion of FOLFOX combined sorafenib for advanced hepatocellular carcinoma with portal vein invasion. *Front Oncol* (2021) 11:562135. doi: 10.3389/fonc.2021.562135

34. Zhu Y, Liu K, Ding D, Zhou Y, Peng L. Pembrolizumab plus chemotherapy as first-line treatment for advanced esophageal cancer: A cost-effectiveness analysis. *Adv Ther* (2022) 39:2614–29. doi: 10.1007/s12325-022-02101-9

35. Guan H, Wang C, Zhao Z, Han S. Cost-effectiveness of donafenib as first-line treatment of unresectable hepatocellular carcinoma in China. *Adv Ther* (2022) 39:3334–46. doi: 10.1007/s12325-022-02185-3

36. Latimer NR. Survival analysis for economic evaluations alongside clinical trials–extrapolation with patient-level data: inconsistencies, limitations, and a practical guide. *Med Decis Making.* (2013) 33:743–54. doi: 10.1177/0272989X12472398

37. Sayiner M, Golabi P, Younossi ZM. Disease burden of hepatocellular carcinoma: A global perspective. *Dig Dis Sci* (2019) 64:910–7. doi: 10.1007/s10620-019-05537-2

38. Zou H, Li M, Lei Q, Luo Z, Xue Y, Yao D, et al. Economic burden and quality of life of hepatocellular carcinoma in greater China: A systematic review. *Front Public Health* (2022) 10:801981. doi: 10.3389/fpubh.2022.801981

39. Chiang CL, Chan SK, Lee SF, Wong IO, Choi HC. Cost-effectiveness of pembrolizumab as a second-line therapy for hepatocellular carcinoma. *JAMA Netw Open* (2021) 4:e2033761. doi: 10.1001/jamanetworkopen.2020.33761

40. Su D, Wu B, Shi L. Cost-effectiveness of atezolizumab plus bevacizumab vs sorafenib as first-line treatment of unresectable hepatocellular carcinoma. *JAMA Netw Open* (2021) 4:e210037. doi: 10.1001/jamanetworkopen.2021.0037

41. Chiang CL, Chan SK, Lee SF, Choi HC. First-line atezolizumab plus bevacizumab versus sorafenib in hepatocellular carcinoma: A cost-effectiveness analysis. *Cancers (Basel).* (2021) 13:931. doi: 10.3390/cancers13050931

42. Hou Y, Wu B. Atezolizumab plus bevacizumab versus sorafenib as first-line treatment for unresectable hepatocellular carcinoma: a cost-effectiveness analysis. *Cancer Commun (Lond).* (2020) 40:743–5. doi: 10.1002/cac2.12110

43. *Wangyi*. Available at: https://www.163.com/dy/article/HEBAKHK80553CGLS.html (Accessed September, 2022).

frontiers | Frontiers in Oncology

TYPE Review
PUBLISHED 23 January 2023
DOI 10.3389/fonc.2023.1088038

Check for updates

OPEN ACCESS

EDITED BY
Mohd Wajid Ali Khan,
University of Hail, Saudi Arabia

REVIEWED BY
Jules Russick,
Karolinska Institutet (KI), Sweden
Munir Akkaya,
The Ohio State University, United States

*CORRESPONDENCE
Dongwon Choi
dongwcho@usc.edu

SPECIALTY SECTION
This article was submitted to Cancer Molecular Targets and Therapeutics, a section of the journal Frontiers in Oncology

RECEIVED 02 November 2022
ACCEPTED 11 January 2023
PUBLISHED 23 January 2023

CITATION
Choe D and Choi D (2023) Cancel cancer: The immunotherapeutic potential of CD200/CD200R blockade. *Front. Oncol.* 13:1088038. doi: 10.3389/fonc.2023.1088038

COPYRIGHT
© 2023 Choe and Choi. This is an open-access article distributed under the terms of the Creative Commons Attribution License (CC BY). The use, distribution or reproduction in other forums is permitted, provided the original author(s) and the copyright owner(s) are credited and that the original publication in this journal is cited, in accordance with accepted academic practice. No use, distribution or reproduction is permitted which does not comply with these terms.

Cancel cancer: The immunotherapeutic potential of CD200/CD200R blockade

Deborah Choe and Dongwon Choi*

Department of Surgery, Norris Comprehensive Cancer Center, Keck School of Medicine of USC, University of Southern California, Los Angeles, CA, United States

Immune checkpoint molecules function to inhibit and regulate immune response pathways to prevent hyperactive immune activity from damaging healthy tissues. In cancer patients, targeting these key molecules may serve as a valuable therapeutic mechanism to bolster immune function and restore the body's natural defenses against tumors. CD200, an immune checkpoint molecule, is a surface glycoprotein that is widely but not ubiquitously expressed throughout the body. By interacting with its inhibitory receptor CD200R, CD200 suppresses immune cell activity within the tumor microenvironment, creating conditions that foster tumor growth. Targeting the CD200/CD200R pathway, either through the use of monoclonal antibodies or peptide inhibitors, has shown to be effective in boosting anti-tumor immune activity. This review will explore CD200 and the protein's expression and role within the tumor microenvironment, blood endothelial cells, and lymph nodes. This paper will also discuss the advantages and challenges of current strategies used to target CD200 and briefly summarize relevant preclinical/clinical studies investigating the immunotherapeutic efficacy of CD200/CD200R blockade.

KEYWORDS

CD200, CD200R, immunotherapy, immune-checkpoint, tumor microenvironment, lymphatics

1 Introduction

The development and growth of a tumor are influenced by multiple factors in its surroundings, such as the activation of pro-metastatic pathways (1), the angiogenesis of tumor-nourishing blood vessels (2), and the presence of tumor-related inflammation (3), including the activity of tumor-specific T cells (4). The induction of these pro-tumorigenic events is modulated by specific cells known as tumor-associated myeloid cells (TAMCs) (5). Members of TAMCs include myeloid-derived suppressor cells (MDSCs), tumor-associated macrophages (TAMs) (6), and dendritic cells (DCs) (7). MDSCs, which are immature myeloid cells that are highly numbered in various tumors, are capable of downregulating anti-tumor immune activity *via* the release of different chemicals and factors (8). They include reactive oxygen species (ROS), nitric oxide (NO) synthase, arginase 1, and anti-inflammatory cytokines (8). Targeting the pathways that involve these select groups of cells may be valuable for exploring potential immunotherapy against cancers (7). One major

player in the regulation of TAMCs and subsequently the growth of a tumor is CD200 (6), an immunomodulatory protein that binds to the CD200R receptor and downregulates immune cell activity (9).

Alternatively known as OX2, CD200 is a 41-47 kDa, highly conserved glycoprotein (10) that is widely expressed on a variety of cell types, including follicular DCs, B cells, T cells, thymocytes, endothelial cells, placental epithelial cells, kidney cells, and neuronal cells (11). By interacting with its inhibitory receptor CD200R, CD200 modulates immune cell activity by inhibiting proinflammatory cytokine secretion, enhancing anti-inflammatory cytokine secretion (12), and promoting both regulatory T cell (Treg) induction (13) and MDSC production (14). Likewise, the CD200/CD200R interaction suppresses the activities of both natural killer (NK) cells (15) and basophils (16). More specifically regarding NK cells, evidence from some cancer studies strongly suggests that CD200 activity directly suppresses the cytotoxic mechanisms of NK cells and their ability to produce interferon-gamma (IFN-γ) (15). Other cancer studies demonstrate the additional ability of the CD200/CD200R pathway to promote the apoptosis of NK cells (17).

The broad expression of CD200 is advantageous, as the body can regulate the protein's levels accordingly and regionally manage immune activity and inflammation in specific areas (18). Although the effects of CD200/CD200R may decrease inflammation, it can also, unfortunately, suppress the body's natural ability to combat tumors (19, 20),. This has been supported by previous studies which have discovered that high levels of CD200 were expressed on an array of cancer cells, including but not limited to various leukemias (21), malignant melanoma (22), and several neuroendocrine cancers (23). Furthermore, the gene encoding the CD200 protein has been acquired by various viruses, including the Kaposi's sarcoma-associated herpesvirus (KSHV) (24) and rat cytomegalovirus (RCMV) (25), which allows these pathogens to favorably suppress their hosts' antiviral immune mechanisms. Exploring the evolutionary advantage of viral CD200 orthologs, the expression and role of CD200 in different biological settings, and previous studies investigating CD200-averse immunotherapy may help us better understand CD200/CD200R's candidacy as a safe and suitable target for cancer therapy.

2 CD200 and CD200R

Human CD200 is a transmembrane glycoprotein composed of 278 amino acids that is encoded by a gene on chromosome 3 (17) (26). CD200 belongs to the immunoglobulin superfamily (IgSF) of proteins (27). IgSF proteins distinctively possess at least one immunoglobulin (Ig)-like domain that is structurally composed of two antiparallel β-sheets held together by a disulfide bone (28). CD200 possesses two extracellular Ig-like domains, one transmembrane domain (18), and a 19-amino acid cytoplasmic region (29). This short intracellular "tail" does not contain any relevant motifs involved in signaling pathways (29).

Linked to the CD200 gene is the gene for CD200R, which is composed of 348 amino acids (26). CD200R is also an IgSF protein and possesses two extracellular Ig-like domains (18, 29). However, unlike CD200, CD200R has phosphorylatable tyrosine motifs present in its 67-amino acid cytoplasmic region, reflecting the receptor's ability to participate in intracellular signaling (30). The last residue of the three tyrosine residues in this cytoplasmic region is part of an NPxY motif (31). In contrast with CD200's broad expression, CD200R's expression is limited to the surfaces of myeloid cells, including DCs, macrophages, and mast cells (32), as well as specific lymphoid cells (B cells and select T cells) (33). CD200R is especially highly expressed on the surfaces of neutrophils, macrophages (32), and basophils (16).

CD200 binds to CD200R with an equilibrium dissociation constant (K_D) of approximately 0.5 μM at 37°C (32). This binding is facilitated by the proteins' similar structures, resembling interactions that are involved in immunological synapses (18). Both being IgSF proteins, CD200 and CD200R interact through their shared NH_2-terminal Ig-like domains (18, 27). Once CD200 binds, the third tyrosine residue associated with the NPxY motif within CD200R's cytoplasmic tail becomes phosphorylated (31, 34). This results in the subsequent phosphorylation of tyrosine kinase 1 (DOK-1) and tyrosine kinase 2 (DOK-2), which are adaptor proteins (34). P hosphorylation of DOK-1 and DOK-2 leads to the binding of SHIP to DOK-1 and the recruitment of RasGAP, which negatively regulates the MAPK/ERK signaling pathway (34). A visual representation of the intracellular events that lead to RasGAP recruitment have been depicted in Figure 1. These events ultimately result in the inhibition of proinflammatory cytokine release and immune cell activation, such as the suppression of mast cell degranulation (34).

2.1 Soluble CD200

In addition to the form expressed on cellular surfaces, there are soluble forms of CD200 (known as sCD200) that are present in serum. A previous study investigating chronic lymphocytic leukemia (CLL) found that upregulated sCD200, and not the surface-expressed form of the immune checkpoint molecule, was correlated with worse tumor prognosis in patients with CLL (35). In addition, the engraftment of CLL cells from patients to immunocompromised mice was more successful in animals that had also received sCD200 plasma transfusions (35). In response to this study's findings on sCD200, a separate group of researchers investigating glioblastoma multiforme (GBM) analyzed patients' tumor sera and compared sCD200 levels among different types of brain tumors (14). They found that patients with GBM had significantly higher levels of sCD200 in sera compared to patients with ependymoma (14). Moreover, increased sCD200 levels were correlated with poor tumor prognoses in patients with GBM, ependymoma, and medulloblastoma. Additionally, investigators found that sCD200 was significantly associated with the expansion of MDSCs in patients with GBM (14). They suspected that sCD200 originating from tumors in the brain are able to travel to cervical lymph nodes *via* the cerebral spinal fluid and further suppress immune activity (14). The findings from both the CLL and GBM studies suggest that a soluble form of CD200 may further enhance immunosuppression and the development of select cancers.

2.2 CD200RL

Furthermore, CD200R is classified as a "paired receptor," which means that the inhibiting receptor is associated with at least one other

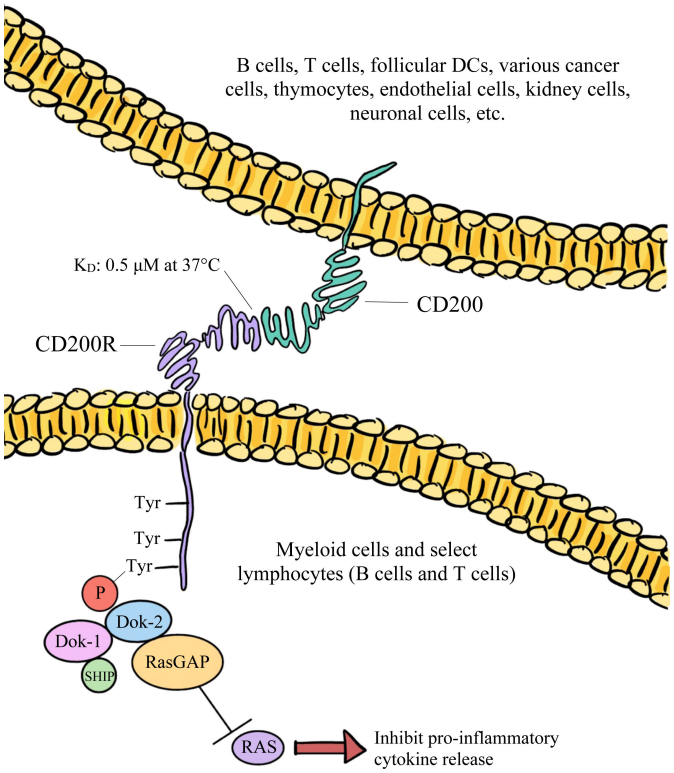


FIGURE 1
The broadly expressed CD200 glycoprotein predominantly interacts with its CD200R receptor and downregulates both the function and activation of immune cells *via* the inhibition of RAS signaling.

activating receptor (32, 36). It is thought that activating receptors arose from inhibiting receptors due to a gene duplication event (37). The activating sibling receptor for CD200R is known as CD200RL (for "CD200R-like") (32). Humans only possess one form of CD200RL (known as CD200R1L), while mice can possess up to four different forms of the receptor (known as mCD200RLa, -b, -c, and -d) (32, 37). Despite sharing considerable sequence homology with CD200R (32), CD200R1L receptors do not bind to CD200 (38). Moreover, unlike in CD200R, the cytoplasmic regions present in CD200R1L are shorter and do not contain any signaling motifs (37). Rather, the transmembrane portions of activating receptors have charged amino acid residues that interact with adaptor proteins to deliver activating signals *via* YxxM or tyrosine-based activation motifs (37). Some studies suggest that CD200R1L may be linked to an increased risk for parasitic infections and skin conditions, including atopic dermatitis as well as psoriasis (37). Unfortunately, compared to CD200R, there are fewer studies exploring CD200RL and the receptor's exact signaling mechanism and significance are not completely understood.

However, a study published in 2021 may represent a step forward in uncovering some of this information. Flow cytometry, Western blot, and qPCR analyses found that CD200R1L is expressed on human neutrophils in peripheral blood (37). Monoclonal antibody crosslinking of CD200R1L resulted in both significant production of ROS and interleukin-8 (IL-8), a chemotactic cytokine for neutrophils (37). These findings indicate that the activating receptors may serve a functional role on the surfaces of primary neutrophils in humans (37). Furthermore, sequence phylogeny suggests that the gene duplication event generating CD200RL likely occurred independently and multiple times among distantly related species and that the receptor has been conserved throughout evolution, indicating its biological importance in immunoregulation (37). Likewise, the faster mutation rate associated with the activating receptor relative to the inhibiting receptor led investigators to speculate that pathogenic pressure may have played a critical role in driving these mutations (37). This observation is consistent with CD200R1L-induced ROS production and the activating receptor's anti-pathogenic role among neutrophils (37). Additionally, this data supports the "counterbalance theory" of paired receptors, which states that activating receptors may have evolved in hosts in response to pathogens that bind to inhibiting receptors (39). These activating receptors would thus serve a protective role by essentially "counterbalancing" the immunosuppressive signals triggered by pathogens capable of binding to inhibiting receptors (39).

2.3 Viral CD200 orthologs

Given CD200/CD200R's ability to suppress immune activity, it is not surprising that the CD200-encoding gene has been acquired by a number of viruses, including the Shope (rabbit) fibroma virus (40), Yaba monkey tumor virus (41), human herpesvirus-6 (42), human herpesvirus-7 (16), and human herpesvirus-8 (43). From an evolutionary perspective, the acquisition of the gene for CD200 by many of these viruses is considered to have taken place independently among the various viral families according to their unique mechanisms of pathogenesis (24).

KSHV, also known as human herpesvirus-8, is a member of the *Gammaherpesviridae* subfamily (24) and the virus is necessary for the development of Kaposi sarcoma (KS) (44), a cancerous inflammatory cytokine disease (45) that is spread primarily *via* saliva (46). Unfortunately, in most cases, the cancer is not immediately detectable in the body as it develops after a period of latency following viral infection (47). KS commonly develops in HIV patients, suggesting that KS tumorigenesis may be enhanced under conditions of immunosuppression (48).

The KSHV ortholog of CD200, known as viral OX2 (vOX2), is a 55 kDa protein that is encoded by the virus's K14 open reading frame (43). RNA analysis has shown that transcription of the viral gene is activated during KSHV's replicative state, which is the lytic cycle (24). The vOX2 protein is found on the surfaces of cells infected with KSHV (43), which can range from B cells and DCs to epithelial cells and endothelial cells (48). The gene for vOX2 has approximately 40% sequence similarity with the human gene for CD200 (24). Although this level of sequence similarity is relatively low, vOX2 surprisingly shares key residues with CD200 in its binding site for CD200R (18). The viral ortholog also interacts with CD200R with a nearly identical binding affinity as that of CD200/CD200R (24). Through its binding to CD200R, vOX2 can effectively target host immune cells and inhibit anti-viral activity directed against the pathogen (49). For example, by binding to host CD200R, vOX2 can downregulate the activities of T cells (49), macrophages (24), neutrophils (50), and basophils (16). More specifically, vOX2 has been found to decrease the synthesis of the proinflammatory cytokines tumor necrosis factor-alpha (TNF-α) and IFN-γ from macrophages and T cells, respectively (49). The viral protein has also been shown to decrease the mobilization of CD107a (49), a marker for NK cell activity (49, 51).

Likewise, the CD200 ortholog for RCMV is known as the e127 protein and it binds to rat CD200R with a nearly identical affinity as the host ligand, despite only sharing 56% amino acid sequence similarity (25). Like vOX2, e127 has been shown to be expressed on the surfaces of infected cells (25). However, compared to viral orthologs, researchers suspect that the suppressive effects of e127 on host immune activity are more muted (25). Although both vOX2 and e127 successfully bind to host CD200R, the viral orthologs are not able to bind to respective CD200RL receptors (52). With the "counterbalance theory" in mind, researchers speculate that over time viruses capable of binding both inhibiting and activating host receptors eventually evolved to lose the ability to bind to activating receptors, which served as an evolutionary advantage for the pathogens (52).

Interestingly, one virus that is thought to have evolved further to ultimately lose its ability to interact with CD200R is the myxoma virus (MV). MV belongs to the *Chordopoxvirinae* subfamily and the virus's natural hosts are rabbits (53). One study demonstrated that the lack of expression of the virus's M141R protein in infected rabbits was associated with significant increases in the number of activated macrophages and NO production (53). These findings combined with analysis of sequence homology led investigators to strongly suspect that the M141R protein is an ortholog of CD200 (53). However, in another study, although M141 expression was also linked to downregulated immune activity and suppressed NO production, these effects could not be specifically attributed to mechanisms involving CD200R (54). Furthermore, compared to herpesvirus orthologs, it was found that the genetic and structural differences between poxvirus orthologs and their host CD200 proteins were more substantial (54). For example, poxvirus orthologs generally share lower sequence similarity with host CD200 compared to herpesvirus orthologs (54). Poxvirus orthologs also possess only one Ig-like domain rather than two (54). Overall, investigators concluded that M141 does not bind host CD200R and that the viral protein most likely exerts its immunosuppressive effects through a different signaling pathway (54). As a result, they also suggested that the CD200-similar sequences present in poxviruses most likely were acquired non-independently and thus evolved further among other poxvirus family members possessing such sequences (54).

2.4 CD200's expression and role in the tumor microenvironment

High levels of CD200 have been found to be expressed on various types of human cancer cells, including hairy cell leukemia (55), acute myeloid leukemia (56), malignant melanoma (22), CLL (21), multiple myeloma (21), testicular cancer (21), renal carcinoma (21), colon carcinoma (21), and GBM (57). Moreover, CD200 overexpression is correlated with poor prognosis among some of these cancers, suggesting that high levels of CD200 may facilitate tumorigenesis (21, 58–60). This observation can be explained by CD200's primarily inhibitory role in the tumor microenvironment (TME) and the mechanisms through which the protein suppresses immune cell function and activation. In addition to tumor cells within the TME (21), CD200 is also predominantly found on T cells (30) and the endothelial cells lining tumor-nourishing blood vessels (61). In the TME, the soluble forms of CD200 are also present and can interact with CD200Rs (62), which are primarily found on TAMCs (including TAMs, TADCs, and MDSCs) (63). The binding of CD200 to CD200R results in increased induction of $CD4^+CD25^+Foxp3^+$ Tregs, which act to negatively regulate immune responses (13). In addition to decreasing the activities of basophils (16) and NK cells (15), CD200/CD200R inhibits the release of TNF-α from activated macrophages expressing CD200R, suppressing the further activation of other macrophages (24). In macrophages, CD200/CD200R also upregulates the production of transforming growth factor-beta (TGF-β), an anti-inflammatory cytokine (64). The CD200/CD200R axis also decreases the release of interleukin-2 (IL-2) and IFN-γ, which are Th1-type proinflammatory cytokines, and increases the release of interleukin-10 (IL-10) and interleukin-4 (IL-4), which are Th2-type anti-inflammatory cytokines (12). Furthermore, this pathway increases the production of MDSCs (14). A visual representation of some of the various effects of CD200/CD200R on immune cell activity within the TME has been depicted in Figure 2. Therefore, the interactions between CD200 and CD200R in the TME negatively modulate levels of immune activity, ultimately fostering an environment that favors tumor development, growth, and spread (30).

One group of investigators examined the interaction between CD200 and MDSCs within the TME of pancreatic ductal adenocarcinoma (PDAC) (8). The researchers chose to study PDAC because the immunosuppression associated with the disease oftentimes makes the cancer resistant to immunotherapy (8). Immunofluorescence staining revealed that CD200 was highly expressed on tumor epithelial

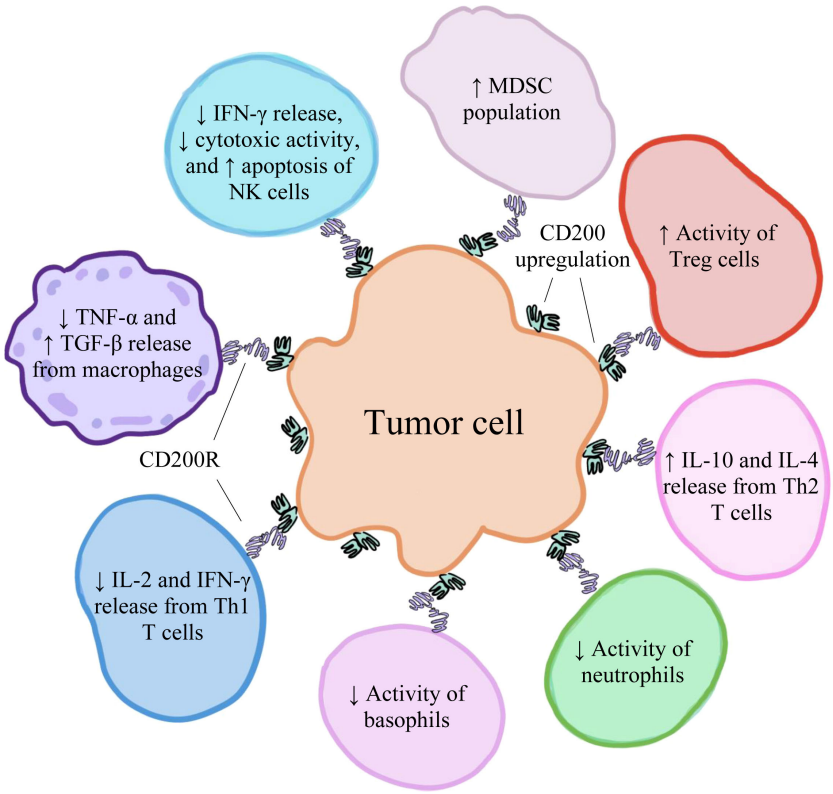


FIGURE 2
The upregulation of CD200 on various human cancer cells has an immunosuppressive effect on immune cells within the tumor microenvironment, creating conditions that favor tumor development, growth, and spread.

cells and on stromal cells within the PDAC TME (8). In addition, RNA from PDAC stromal cells was characterized as having significantly upregulated levels of CD200 compared to control RNA from normal pancreatic fibroblasts (8). Moreover, the researchers investigated CD200 expression on MDSCs in both cancer patients and healthy patients. Not only was there a higher number of MDSCs in cancer patients than in healthy patients but also a larger percentage of MDSCs expressing CD200R (8). The researchers wanted to further investigate the processes through which CD200 is able to regulate the population of MDSCs. Using single-cell RNA sequencing, they were able to isolate genes and downstream pathways, including those involved in interferon and cytokine signaling, that were highly upregulated in MDSCs expressing CD200R (8). Given these findings, the researchers suspected that by stimulating the expansion of the MDSC population, CD200 upregulation in the TME of PDAC potentially allows tumor cells to resist immunotherapy (8).

Another group of investigators examined the interactions between CD200 and NK cells within the TME of basal cell carcinoma (BCC) (17). They attributed the absence of NK cells in the BCC TME to sCD200, which is released from tumor cells *via* ectodomain shedding (17). The investigators demonstrated that CD200 downregulates NK cells' anti-tumor activity by suppressing their activation, degranulation, and release of both cytokines and chemokines (17). More specifically, upon binding to CD200R on NK cells, sCD200 inhibits the MAPK/ERK pathway, suppressing tumor cell killing *via* the inhibition of IFN-γ release and promoting NK cell apoptosis *via* upregulated production of pro-apoptotic genes, including Fas, Fas ligand, and FADD (17). To demonstrate that CD200/CD200R negatively interferes with the MAPK/ERK pathway, the investigators cultured NK cells in the presence of CD200 (17). They observed a 4-fold decrease in both phosphorylated ERK 1 and ERK 2 in NK cells expressing CD200R but not in NK cells lacking CD200R (17). Furthermore, the researchers cultured mice neuronal cells expressing CD200R with human CD200 (17). They observed a decrease in phosphorylated ERK 1 and ERK 2 relative to overall ERK levels (17). To determine the mechanism through which CD200 promotes the apoptosis of NK cells, the investigators obtained NK cells from isolates of human peripheral blood mononuclear cells and introduced them to human CD200 (17). In the NK cells expressing CD200R, there was upregulated expression of Fas, Fas ligand, and FADD but not in the NK cells lacking CD200R (17). Overall, through these findings and those of additional experiments, this study effectively demonstrated that CD200 in the BCC TME suppresses NK cells' cytotoxic activity and induces NK cell apoptosis, which foster immunosuppressed conditions favoring tumor development (17).

2.5 CD200's expression and role in blood endothelial cells

The variable expression of CD200 in blood endothelial cells may further reveal the protein's specific role in the vascular endothelium. Endothelial cells that line different blood vessels vary in their function

and response to stress, including inflammation (65, 66). This is reflected by the cells' variable expression of molecules like CD200, which has been found in blood vessels located in the lung (65), spleen (65), kidney (11), and fallopian tube (67). In a study involving rats, immunohistochemistry staining revealed that CD200 was strongly expressed on endothelial cells lining arterioles, the majority of veins (including venules), and some types of capillaries (65). However, expression was low in endothelial cells lining large arteries and the central veins located in the liver (65). The investigators speculated that varying levels of CD200 in different vessels may be attributed to environmental factors, including the force of blood flow and stimulatory factors released by cells from surrounding tissues (65, 68).

In the same study, the investigators also found that an anti-CD200 antibody disturbed the adhesion of T cells to human endothelial cells *in vitro*, suggesting that the interactions between CD200 and CD200R may facilitate the attachment of immune cells to the vessel endothelium (65). These findings suggest that variable factors like inflammatory stress may influence blood endothelial expression of CD200, which allows endothelial cells to successfully adhere to immune cells and deliver anti-inflammatory signals (65).

Furthermore, CD200 expression in blood endothelial cells may highlight how the protein's presence can be strategically induced by certain metastasizing cancers. A study that investigated CD200 and CD200R expression in the TME of human squamous cell carcinoma (SCC) found that high levels of CD200 were expressed on endothelial cells lining the cancer's vasculature (61). Additionally, it was found that the supernatant derived from the SCC tumor effectively induced the expression of CD200 on human dermal blood endothelial cells *in vitro* (61). The endothelial cells lining the vessels that surround and nourish tumors play a key role in enabling tumor metastasis, because the tumor cells must first pass through the endothelium before they are able to reach the circulatory system (69). Likewise, these endothelial cells are also important in the combating of tumors, because immune cells must first successfully pass through the endothelium of tumor vessels before they can access the tumor (61). Given this data, the investigators believe that the SCC tumor cells may favorably suppress immune activity in local blood endothelial cells by upregulating CD200 expression in these endothelial cells, facilitating the tumor's entry into the circulatory system and, therefore, metastasis (61).

2.6 CD200's expression and role in lymphatics

Lymphatic expression of CD200 also exhibits a degree of regional specificity. More specifically, CD200's expression pattern among lymph node lymphatic endothelial cells (LECs) during inflammation may further highlight the protein's specific immunomodulatory role within the lymphatic system (70). In addition to regulating the entrance and exit of immune cells from lymph nodes, lymph node LECs also facilitate the various interactions that transpire among different immune cells (70, 71). The organization of lymph node LECs further increase the lymph node's efficiency in coordinating these interactions (70). For instance, within the lymph node subcapsular sinus (SCS), the space between the lymph node cortex and capsule, the LECs lining the sinus are further organized into ceiling and floor LECs (71). The SCS ceiling is the outward-facing wall of the sinus that is closest to the cortex, while the SCS floor is the inward-facing wall of the sinus that is closest to the parenchyma of the lymph node (71). These regional types of LECs uniquely respond to inflammation, which is further supported by their heterogeneous expression of molecules (70). In one murine study, inflammation that was similar to psoriasis was induced in mice ears by applying a cream containing imiquimod (70), a topical medicine used to treat genital warts and some skin cancers (72). Using single-cell RNA sequencing, investigators found that during skin inflammation, CD200 expression increased in SCS floor LECs of auricular lymph nodes (70). In normal skin, CD200 expression in LECs lining both the SCS ceiling and floor was variable (70). SCS resident macrophages and DCs, which are found in the floor endothelium (71), can be considered as the lymph node's first layer of immune defense encountered by the incoming afferent lymph (73). Therefore, investigators speculated that CD200 upregulation in SCS floor LECs during inflammation may represent the body's attempt to resolve inflammation at this protective frontline (70).

3 Targeting CD200/CD200R as immunotherapy

Considering CD200/CD200R's ability to downregulate immune activity and suppress the body's anti-tumor defenses, this cellular interaction has sparked researchers' interest as being a key target for immunotherapy. Two currently explored mechanisms used to block the CD200/CD200R pathway include anti-CD200 monoclonal antibodies (51) and peptide CD200 inhibitors (57).

3.1 Anti-CD200 monoclonal antibody

Like CD200, other key immune checkpoint molecules that suppress immune cell function include cytotoxic T-lymphocyte-associated protein 4 (CTLA-4), programmed cell death protein 1 (PD-1), and T cell immunoglobulin-3 (Tim-3) (74). Monoclonal antibodies against these regulatory proteins have been developed, and their safety and efficacy as novel immunotherapy have been or are currently being investigated in clinical trials (74, 75). Some of these therapeutic monoclonal antibodies, including ipilimumab (anti-CTLA-4) and nivolumab (anti-PD-1), have already been approved by the FDA (76). Likewise, a monoclonal antibody that targets CD200 and prevents the ligand from binding to CD200R may effectively block the protein's immunosuppressive signaling and restore the body's protective defenses against tumor growth (51).

One study found that introduction of a human anti-CD200 monoclonal antibody was able to successfully enhance immune responses against acute myeloid leukemia (AML) (51). It was previously found that AML individuals with high levels of CD200 expression had reduced NK cell (15) and T cell activities (77), suggesting that CD200 overexpression had inhibited immune responses directed against AML cells (78). Based on these observations, the investigators developed a fully human anti-CD200 monoclonal antibody (designated "TTI-CD200") to see if targeting CD200 could block the inhibitory signals transmitted to immune cells

(51). When K562 human leukemia cells expressing high levels of CD200 (high-CD200) were exposed to regular NK cells *in vitro*, CD107a levels decreased in comparison to K562 cells expressing low levels of CD200 (low-CD200), confirming that the suppression of NK cell activity was CD200-related (51). However, TTI-CD200 introduction successfully restored NK cell activity to similar levels observed in low-CD200 K562 cells (51). Additionally, when high-CD200 K562 cells were cultured with TTI-CD200, the secretion of IFN-γ from NK cells increased (51). Investigators further took high-CD200 and low-CD200 AML blast cells from patients and cultured them with autologous lymphocytes (51). They exposed these cells to either TTI-CD200 or an isotope (control) (51). Compared to high-CD200 blast cells treated with the isotope, high-CD200 blast cells treated with the antibody exhibited increased levels of CD107a (51). On the other hand, low-CD200 blast cells did not show an increase in CD107a, regardless of receiving either the antibody or isotope treatment (51). Taken together, these findings demonstrate that the anti-CD200 monoclonal antibody effectively enhanced the previously diminished immune activity against myeloid leukemia cells *in vitro*.

In a Phase I clinical trial (NCT00648739) sponsored by Alexion Pharmaceuticals, a group of investigators tested the efficacy, safety, pharmacodynamics, and pharmacokinetics of samalizumab, a recombinant humanized anti-CD200 monoclonal antibody, in treating tumors associated with CLL and multiple myeloma (MM) (79). In the study, 26 patients (23 with CLL and 3 with MM) were each assigned one of seven different doses of samalizumab ranging from 50 to 600 mg/m^2, which they planned to receive intravenously every 28 days (79). Only 21 of the 26 total patients ultimately received more than one treatment of samalizumab and were assessed at the end of the study (79). There was an observed dose-related reduction in the expression of CD200 on CLL cells following treatment (79). This decrease in expression was found to be longer-lasting in patients who received higher doses (300–500 mg/m^2) of samalizumab compared to those who received lower doses (50–200 mg/m^2) (79). Similarly, in both MM and CLL patients, there was a dose-related reduction in the presence of CD4$^+$ T cells expressing CD200 but not in other T cell types (79). The tumor burden or the total amount of tumor present in the body was decreased in 14 CLL patients, which represented 64% of the total CLL patients who were assessed (79). However, in all MM patients, their disease had progressed over the course of the study (79). The maximum tolerated dose was not determined and the severity of any reported adverse events related to samalizumab treatment was only mild to moderate (79). Although the clinical trial was discontinued by Alexion Pharmaceuticals due to administrative reasons, the preliminary findings from the study demonstrate the relative safety of samalizumab and its potential to reduce the tumor load associated with CLL (79).

3.2 Peptide CD200 inhibitor

Compared to therapeutic monoclonal antibodies, using peptide inhibitors as immunotherapy has more advantages. Peptides are associated with lower toxicity (80), higher stability, and greater efficiency (81). They can better infiltrate cancerous tissues due to their smaller size (82) and they have high target precision, which means there is less risk for potential side effects (80). Additionally, peptides can be easily synthesized (80), altered (81), and are less expensive to produce compared to antibodies, making them a more favorable approach to cancer therapy (82).

Developing a peptide ligand that can effectively bind to CD200's activating receptors may potentially block the inhibitory signals delivered by CD200/CD200R. It was previously found that tumor vascular endothelial cells in GBM had upregulated levels of CD200 expression (83). Through CD200 sequence analysis, investigators identified metalloprotease cleavage sites that, when cleaved, release peptides containing sequences compatible with CD200RL-binding (83). They were able to develop a peptide ligand (known as CD200AR-L) that could successfully bind to activating receptors, despite not fully understanding the exact mechanism of the synthetic ligand (83). However, one study may have identified the signaling pathway activated by CD200AR-L. Through *in vitro* studies, it was found that CD200AR-L stimulated immune activity by activating the DAP10 and DAP12 signaling pathways, which were transcriptionally upregulated in murine cells exposed to the peptide ligand (84). Additionally, investigators demonstrated *in vivo* that CD200AR-L downregulates the expression of CD200R1 in wild-type mice but not in mice lacking DAP10, which was found to be specifically involved in tumor growth regulation (84). Through stimulating these signaling pathways, the binding of CD200AR-L to activating receptors has been shown to increase cytokine secretion and boost anti-tumor defenses *via* the activation of antigen-presenting cells (APCs) (84). Overall, by interacting with activating receptors, CD200AR-L is able to block CD200's inhibitory signaling by stimulating both DAP10/12 and downregulating expression of CD200R1 (84).

A study investigating high-grade glioma in mice found that administering CD200AR-L in addition to tumor-derived vaccines improved the animals' immune response, which was originally diminished due to CD200 expression on cancer cells (57).

Both CD200R KO mice and wild-type mice received tumor-derived vaccines that contained either CD200AR-L or saline (control) (57). The two groups of mice that received vaccines containing CD200AR-L were found to have statistically significant increases in anti-tumor immune activity compared to those that received vaccines containing saline (57). Additionally, there was a significant increase in immune activity in wild-type mice that received the functional peptide ligand compared to those that received the ligand with its peptide sequence scrambled (57). The same group of investigators wanted to further assess CD200AR-L (20) and its effects in a study involving dogs diagnosed with spontaneous high-grade glioma (85). They found that, after tumor resection surgery, intradermal administration of canine CD200AR-L before tumor-lysate vaccination lengthened the dogs' lifespans compared to the historical control group of dogs that only received the vaccine (median survival times = 12.9 months vs. 6.83 months) (85). This significant increase in post-surgery survival time for dogs receiving CD200AR-L was attributed to reduced CD200 expression on T cells and APCs and, therefore, their increased activities within the glioma TME (85).

Given the successful outcomes of both the murine and canine preclinical studies, the investigators developed humanized variations of CD200AR-L (designated "hCD200AR-L") and tested their effects on human CD14$^+$ cells (20). They ultimately chose to move forward with the hP1A8 peptide variant in a clinical trial (20). The hP1A8 form was able to effectively bind to immuno-activating receptors on CD14$^+$ cells and upregulate immune activity by stimulating the activity of antigen-specific T cells, the maturation of DCs, and the production of proinflammatory cytokines (20). Furthermore, hP1A8 was associated with reduced CD200R expression, and it was also the analog of the most successful

peptide tested in the prior murine study (20). In an ongoing Phase I clinical trial (NCT04642937) sponsored by OX2 Therapeutics, hP1A8's therapeutic efficacy and appropriate dosage range are currently being studied (86). The peptide is being tested in conjunction with imiquimod and the GBM6-AD vaccine to treat GBM in 24 adult patients (86). The estimated date of study completion is November 2023 (86).

3.3 Risks and challenges of targeting CD200/CD200R

Despite efforts to investigate whether CD200-averse immunotherapy can be effectively applied to human patients, we must be mindful of existing limitations of the previously discussed CD200-targeting mechanisms. For instance, therapeutic peptides can have relatively short half-lives, low bioavailability, and the potential to be digested by enzymes present in the body (80). But, more importantly, there are other greater health risks that need to be acknowledged when considering CD200/CD200R blockade.

Because CD200 is expressed widely in the human body, targeting CD200/CD200R may have unintended consequences that can be especially harmful. For instance, targeting an immunomodulatory protein can impact the body's ability to regulate inflammation during and following various infections and injuries. One study demonstrated that mice lacking CD200 expression had greater activity of lung macrophages and were thus more susceptible to prolonged influenza infection and eventual death (87). However, when the mice were treated with a CD200R agonist, they did not develop inflammatory lung disease (87). Another murine study demonstrated that blocking CD200R expression in animals was associated with higher risk of infection following ischemic stroke, greater movement of white blood cells into the brain, and increased mortality (88). This study demonstrated that blocking CD200 from binding to its inhibiting receptor interferes with the body's ability to resolve inflammation stimulated by ischemic cerebral injury (88). Likewise, CD200 expression regulates levels of inflammation associated with various autoimmune diseases (19). The beneficial effects of CD200 were demonstrated in prior animal studies which found that the CD200/CD200R pathway lowered levels of inflammation and disease susceptibility in different autoimmune disease models, including those of arthritis and multiple sclerosis (89). Thus, it is possible that targeting the CD200/CD200R axis may lead to unintended hyperactive autoimmunity, which can significantly increase inflammation and damage otherwise healthy tissues (89). Furthermore, CD200 has shown to play a key role in the setting of transplants. CD200 expression is associated with a reduced likelihood of transplant rejection in mice (90). One study found that skin grafts from donor mice lacking either CD200 or CD200R1 had faster rates of graft rejection than those from control donor mice (91). Therefore, targeting CD200 may not be a viable option for patients receiving transplants.

4 Conclusion and future considerations

With all things considered, targeting CD200/CD200R has the potential to therapeutically bolster anti-tumor activity within the TME, surrounding blood vessels, and lymph nodes. However, further research and clinical studies are warranted to validate and reinforce CD200's safety, efficacy, and accessibility as a target for immunotherapy. Not only are there limitations to current strategies used to target CD200, but there are overall health risks and potentially serious consequences that can arise from targeting an immunoregulatory protein that is broadly expressed. More specifically, blocking the CD200/CD200R pathway may result in hyperactive inflammation that could exacerbate the symptoms of cancer patients receiving immunotherapy. Furthermore, CD200-targeted immunotherapy may have varying success among patients depending on the type of cancer and their stage of disease progression, as demonstrated by the preliminary results of the samalizumab clinical trial (79). Additionally, it is worthwhile investigating the efficacy of CD200-targeted immunotherapy in conjunction with other forms of immunotherapy and cancer treatments. Simultaneously blocking other immune checkpoint molecules, such as CTLA-4, PD-1, and Tim-3, in addition to CD200 may synergistically boost anti-tumor activity. On the other hand, the effects of CD200-targeted immunotherapy may not be as successful if other immunosuppressive treatments, such as radiation or chemotherapy, are simultaneously administered. Nevertheless, given the current knowledge on CD200/CD200R, with further research, CD200-averse treatment shows promising potential to become the next FDA-approved immunotherapeutic drug.

Author contributions

DChoe wrote the article and DChoi edited it. All authors contributed to the article and approved the submitted version.

Funding

This study was supported by the National Institutes of Health (R01CA250065).

Acknowledgments

I would like to thank the Keck School of Medicine of USC, Dr. Young-Kwon Hong, and the members of the Hong Lab for their support, kindness, and generosity.

Conflict of interest

The authors declare that the research was conducted in the absence of any commercial or financial relationships that could be construed as a potential conflict of interest.

Publisher's note

All claims expressed in this article are solely those of the authors and do not necessarily represent those of their affiliated organizations, or those of the publisher, the editors and the reviewers. Any product that may be evaluated in this article, or claim that may be made by its manufacturer, is not guaranteed or endorsed by the publisher.

References

1. Qian BZ, Pollard JW. Macrophage diversity enhances tumor progression and metastasis. *Cell* (2010) 141(1):39–51. doi: 10.1016/j.cell.2010.03.014

2. Weidner N, Semple JP, Welch WR, Folkman J. Tumor angiogenesis and metastasis–correlation in invasive breast carcinoma. *N Engl J Med* (1991) 324(1):1–8. doi: 10.1056/NEJM199101033240101

3. Mantovani A, Allavena P, Sica A, Balkwill F. Cancer-related inflammation. *Nature* (2008) 454(7203):436–44. doi: 10.1038/nature07205

4. Khazaie K, von Boehmer H. The impact of Cd4+Cd25+ treg on tumor specific Cd8+ T cell cytotoxicity and cancer. *Semin Cancer Biol* (2006) 16(2):124–36. doi: 10.1016/j.semcancer.2005.11.006

5. Murdoch C, Muthana M, Coffelt SB, Lewis CE. The role of myeloid cells in the promotion of tumour angiogenesis. *Nat Rev Cancer* (2008) 8(8):618–31. doi: 10.1038/nrc2444

6. Wang L, Liu JQ, Talebian F, El-Omrani HY, Khattabi M, Yu L, et al. Tumor expression of Cd200 inhibits il-10 production by tumor-associated myeloid cells and prevents tumor immune evasion of ctl therapy. *Eur J Immunol* (2010) 40(9):2569–79. doi: 10.1002/eji.201040472

7. Dou A, Fang J. Heterogeneous myeloid cells in tumors. *Cancers (Basel)* (2021) 13 (15):3772. doi: 10.3390/cancers13153772

8. Choueiry F, Torok M, Shakya R, Agrawal K, Deems A, Benner B, et al. Cd200 promotes immunosuppression in the pancreatic tumor microenvironment. *J Immunother Cancer* (2020) 8(1):e000189. doi: 10.1136/jitc-2019-000189

9. Barclay AN, Wright GJ, Brooke G, Brown MH. Cd200 and membrane protein interactions in the control of myeloid cells. *Trends Immunol* (2002) 23(6):285–90. doi: 10.1016/s1471-4906(02)02223-8

10. Barclay AN, Ward HA. Purification and chemical characterisation of membrane glycoproteins from rat thymocytes and brain, recognised by monoclonal antibody mrc ox 2. *Eur J Biochem* (1982) 129(2):447–58. doi: 10.1111/j.1432-1033.1982.tb07070.x

11. Wright GJ, Jones M, Puklavec MJ, Brown MH, Barclay AN. The unusual distribution of the Neuronal/Lymphoid cell surface Cd200 (Ox2) glycoprotein is conserved in humans. *Immunology* (2001) 102(2):173–9. doi: 10.1046/j.1365-2567.2001.01163.x

12. Gorczynski L, Chen Z, Hu J, Kai Y, Lei J, Ramakrishna V, et al. Evidence that an ox-2-Positive cell can inhibit the stimulation of type 1 cytokine production by bone marrow-derived B7-1 (and B7-2)-Positive dendritic cells. *J Immunol* (1999) 162(2):774–81. doi: 10.4049/jimmunol.162.2.774

13. Coles SJ, Hills RK, Wang EC, Burnett AK, Man S, Darley RL, et al. Increased Cd200 expression in acute myeloid leukemia is linked with an increased frequency of Foxp3+ regulatory T cells. *Leukemia* (2012) 26(9):2146–8. doi: 10.1038/leu.2012.75

14. Moertel CL, Xia J, LaRue R, Waldron NN, Andersen BM, Prins RM, et al. Cd200 in cns tumor-induced immunosuppression: The role for Cd200 pathway blockade in targeted immunotherapy. *J Immunother Cancer* (2014) 2(1):46. doi: 10.1186/s40425-014-0046-9

15. Coles SJ, Wang EC, Man S, Hills RK, Burnett AK, Tonks A, et al. Cd200 expression suppresses natural killer cell function and directly inhibits patient anti-tumor response in acute myeloid leukemia. *Leukemia* (2011) 25(5):792–9. doi: 10.1038/leu.2011.1

16. Shiratori I, Yamaguchi M, Suzukawa M, Yamamoto K, Lanier LL, Saito T, et al. Down-regulation of basophil function by human Cd200 and human herpesvirus-8 Cd200. *J Immunol* (2005) 175(7):4441–9. doi: 10.4049/jimmunol.175.7.4441

17. Morgan HJ, Rees E, Lanfredini S, Powell KA, Gore J, Gibbs A, et al. Cd200 ectodomain shedding into the tumor microenvironment leads to nk cell dysfunction and apoptosis. *J Clin Invest* (2022) 132(21):e150750 . doi: 10.1172/JCI150750

18. Hatherley D, Lea SM, Johnson S, Barclay AN. Structures of Cd200/Cd200 receptor family and implications for topology, regulation, and evolution. *Structure* (2013) 21 (5):820–32. doi: 10.1016/j.str.2013.03.008

19. Kotwica-Mojzych K, Jodlowska-Jedrych B, Mojzych M. Cd200:Cd200r interactions and their importance in immunoregulation. *Int J Mol Sci* (2021) 22 (4):1602. doi: 10.3390/ijms22041602

20. Xiong Z, Ampudia Mesias E, Pluhar GE, Rathe SK, Largaespada DA, Sham YY, et al. Cd200 checkpoint reversal: A novel approach to immunotherapy. *Clin Cancer Res* (2020) 26(1):232–41. doi: 10.1158/1078-0432.CCR-19-2234

21. Moreaux J, Veyrune JL, Reme T, De Vos J, Klein B. Cd200: A putative therapeutic target in cancer. *Biochem Biophys Res Commun* (2008) 366(1):117–22. doi: 10.1016/j.bbrc.2007.11.103

22. Petermann KB, Rozenberg GI, Zedek D, Groben P, McKinnon K, Buehler C, et al. Cd200 is induced by erk and is a potential therapeutic target in melanoma. *J Clin Invest* (2007) 117(12):3922–9. doi: 10.1172/JCI32163

23. Love JE, Thompson K, Kilgore MR, Westerhoff M, Murphy CE, Papanicolau-Sengos A, et al. Cd200 expression in neuroendocrine neoplasms. *Am J Clin Pathol* (2017) 148(3):236–42. doi: 10.1093/ajcp/aqx071

24. Foster-Cuevas M, Wright GJ, Puklavec MJ, Brown MH, Barclay AN. Human herpesvirus 8 K14 protein mimics Cd200 in down-regulating macrophage activation through Cd200 receptor. *J Virol* (2004) 78(14):7667–76. doi: 10.1128/JVI.78.14.7667-7676.2004

25. Foster-Cuevas M, Westerholt T, Ahmed M, Brown MH, Barclay AN, Voigt S. Cytomegalovirus E127 protein interacts with the inhibitory Cd200 receptor. *J Virol* (2011) 85(12):6055–9. doi: 10.1128/JVI.00064-11

26. Vieites JM, de la Torre R, Ortega MA, Montero T, Peco JM, Sanchez-Pozo A, et al. Characterization of human Cd200 glycoprotein receptor gene located on chromosome 3q12-13. *Gene* (2003) 311:99–104. doi: 10.1016/s0378-1119(03)00562-6

27. Clark MJ, Gagnon J, Williams AF, Barclay AN. Mrc ox-2 antigen: A Lymphoid/Neuronal membrane glycoprotein with a structure like a single immunoglobulin light chain. *EMBO J* (1985) 4(1):113–8. doi: 10.1002/j.1460-2075.1985.tb02324.x

28. Wai Wong C, Dye DE, Coombe DR. The role of immunoglobulin superfamily cell adhesion molecules in cancer metastasis. *Int J Cell Biol* (2012) 2012:340296. doi: 10.1155/2012/340296

29. Wright GJ, Puklavec MJ, Willis AC, Hoek RM, Sedgwick JD, Brown MH, et al. Lymphoid/Neuronal cell surface Ox2 glycoprotein recognizes a novel receptor on macrophages implicated in the control of their function. *Immunity* (2000) 13(2):233–42. doi: 10.1016/s1074-7613(00)00023-6

30. Liu JQ, Hu A, Zhu J, Yu J, Talebian F, Bai XF. Cd200-Cd200r pathway in the regulation of tumor immune microenvironment and immunotherapy. *Adv Exp Med Biol* (2020) 1223:155–65. doi: 10.1007/978-3-030-35582-1_8

31. Mihrshahi R, Barclay AN, Brown MH. Essential roles for Dok2 and rasgap in Cd200 receptor-mediated regulation of human myeloid cells. *J Immunol* (2009) 183 (8):4879–86. doi: 10.4049/jimmunol.0901531

32. Wright GJ, Cherwinski H, Foster-Cuevas M, Brooke G, Puklavec MJ, Bigler M, et al. Characterization of the Cd200 receptor family in mice and humans and their interactions with Cd200. *J Immunol* (2003) 171(6):3034–46. doi: 10.4049/jimmunol.171.6.3034

33. Abramiuk M, Grywalska E, Korona-Glowniak I, Niedzwiedzka-Rystwej P, Polak G, Kotarski J, et al. Cd200 and Cd200r expression on peripheral blood lymphocytes and serum Cd200 concentration as a new marker of endometriosis. *J Clin Med* (2020) 9 (9):3035 . doi: 10.3390/jcm9093035

34. Zhang S, Cherwinski H, Sedgwick JD, Phillips JH. Molecular mechanisms of Cd200 inhibition of mast cell activation. *J Immunol* (2004) 173(11):6786–93. doi: 10.4049/jimmunol.173.11.6786

35. Wong KK, Brenneman F, Chesney A, Spaner DE, Gorczynski RM. Soluble Cd200 is critical to engraft chronic lymphocytic leukemia cells in immunocompromised mice. *Cancer Res* (2012) 72(19):4931–43. doi: 10.1158/0008-5472.CAN-12-1390

36. Akkaya M, Barclay AN. Heterogeneity in the Cd200r paired receptor family. *Immunogenetics* (2010) 62(1):15–22. doi: 10.1007/s00251-009-0415-6

37. Pascoal Ramos MI, Kesmir C, Stok JE, Geerdink R, Satravelas N, Westerlaken GHA, et al. Cd200r1l is a functional evolutionary conserved activating receptor in human neutrophils. *J Leukoc Biol* (2022) 111(2):367–77. doi: 10.1002/JLB.2A0520-334R

38. Hatherley D, Cherwinski HM, Moshref M, Barclay AN. Recombinant Cd200 protein does not bind activating proteins closely related to Cd200 receptor. *J Immunol* (2005) 175(4):2469–74. doi: 10.4049/jimmunol.175.4.2469

39. Barclay AN, Hatherley D. The counterbalance theory for evolution and function of paired receptors. *Immunity* (2008) 29(5):675–8. doi: 10.1016/j.immuni.2008.10.004

40. Willer DO, McFadden G, Evans DH. The complete genome sequence of shope (Rabbit) fibroma virus. *Virology* (1999) 264(2):319–43. doi: 10.1006/viro.1999.0002

41. Kilpatrick DR, Rouhandeh H. Cloning and physical mapping of yaba monkey tumor virus DNA. *Virology* (1985) 143(2):399–406. doi: 10.1016/0042-6822(85)90380-0

42. Gompels UA, Nicholas J, Lawrence G, Jones M, Thomson BJ, Martin ME, et al. The DNA sequence of human herpesvirus-6: Structure, coding content, and genome evolution. *Virology* (1995) 209(1):29–51. doi: 10.1006/viro.1995.1228

43. Chung YH, Means RE, Choi JK, Lee BS, Jung JU. Kaposi's sarcoma-associated herpesvirus Ox2 glycoprotein activates myeloid-lineage cells to induce inflammatory cytokine production. *J Virol* (2002) 76(10):4688–98. doi: 10.1128/jvi.76.10.4688-4698.2002

44. Moses AV, Jarvis MA, Raggo C, Bell YC, Ruhl R, Luukkonen BG, et al. Kaposi's sarcoma-associated herpesvirus-induced upregulation of the c-kit proto-oncogene, as identified by gene expression profiling, is essential for the transformation of endothelial cells. *J Virol* (2002) 76(16):8383–99. doi: 10.1128/jvi.76.16.8383-8399.2002

45. Fiorelli V, Gendelman R, Samaniego F, Markham PD, Ensoli B. Cytokines from activated T cells induce normal endothelial cells to acquire the phenotypic and functional features of aids-kaposi's sarcoma spindle cells. *J Clin Invest* (1995) 95(4):1723–34. doi: 10.1172/JCI117849

46. Li Y, Zhong C, Liu D, Yu W, Chen W, Wang Y, et al. Evidence for kaposi sarcoma originating from mesenchymal stem cell through kshv-induced mesenchymal-to-Endothelial transition. *Cancer Res* (2018) 78(1):230–45. doi: 10.1158/0008-5472.CAN-17-1961

47. Grundhoff A, Ganem D. Inefficient establishment of kshv latency suggests an additional role for continued lytic replication in kaposi sarcoma pathogenesis. *J Clin Invest* (2004) 113(1):124–36. doi: 10.1172/JCI17803

48. Dittmer DP, Damania B. Kaposi sarcoma-associated herpesvirus: Immunobiology, oncogenesis, and therapy. *J Clin Invest* (2016) 126(9):3165–75. doi: 10.1172/JCI84418

49. Misstear K, Chanas SA, Rezaee SA, Colman R, Quinn LL, Long HM, et al. Suppression of antigen-specific T cell responses by the kaposi's sarcoma-associated herpesvirus viral Ox2 protein and its cellular orthologue, Cd200. *J Virol* (2012) 86 (11):6246–57. doi: 10.1128/JVI.07168-11

50. Rezaee SA, Gracie JA, McInnes IB, Blackbourn DJ. Inhibition of neutrophil function by the kaposi's sarcoma-associated herpesvirus Vox2 protein. *AIDS* (2005) 19 (16):1907–10. doi: 10.1097/01.aids.0000189849.75699.46

51. Rastogi N, Baker S, Man S, Uger RA, Wong M, Coles SJ, et al. Use of an anti-Cd200-Blocking antibody improves immune responses to aml in vitro and in vivo. *Br J Haematol* (2021) 193(1):155–9. doi: 10.1111/bjh.17125

52. Kwong LS, Akkaya M, Barclay AN, Hatherley D. Herpesvirus orthologues of Cd200 bind host Cd200r but not related activating receptors. *J Gen Virol* (2016) 97 (1):179–84. doi: 10.1099/jgv.0.000335

53. Cameron CM, Barrett JW, Liu L, Lucas AR, McFadden G. Myxoma virus M141r expresses a viral Cd200 (Vox-2) that is responsible for down-regulation of macrophage and T-cell activation in vivo. *J Virol* (2005) 79(10):6052–67. doi: 10.1128/JVI.79.10.6052-6067.2005

54. Akkaya M, Kwong LS, Akkaya E, Hatherley D, Barclay AN. Rabbit Cd200r binds host Cd200 but not Cd200-like proteins from poxviruses. *Virology* (2016) 488:1–8. doi: 10.1016/j.virol.2015.10.026

55. D'Arena G, De Feo V, Pietrantuono G, Seneca E, Mansueto G, Villani O, et al. Cd200 and chronic lymphocytic leukemia: Biological and clinical relevance. *Front Oncol* (2020) 10:584427. doi: 10.3389/fonc.2020.584427

56. Tonks A, Hills R, White P, Rosie B, Mills KI, Burnett AK, et al. Cd200 as a prognostic factor in acute myeloid leukaemia. *Leukemia* (2007) 21(3):566–8. doi: 10.1038/sj.leu.2404559

57. Xiong Z, Ampudia-Mesias E, Shaver R, Horbinski CM, Moertel CL, Olin MR. Tumor-derived vaccines containing Cd200 inhibit immune activation: Implications for immunotherapy. *Immunotherapy* (2016) 8(9):1059–71. doi: 10.2217/imt-2016-0033

58. Rexin P, Tauchert A, Hanze J, Heers H, Schmidt A, Hofmann R, et al. The immune checkpoint molecule Cd200 is associated with tumor grading and metastasis in bladder cancer. *Anticancer Res* (2018) 38(5):2749–54. doi: 10.21873/anticanres.12517

59. Gorczynski RM, Clark DA, Erin N, Khatri I. Role of Cd200 expression in regulation of metastasis of Emt6 tumor cells in mice. *Breast Cancer Res Treat* (2011) 130(1):49–60. doi: 10.1007/s10549-010-1259-3

60. D'Arena G, Vitale C, Coscia M, Lamorte D, Pietrantuono G, Perutelli F, et al. Cd200 baseline serum levels predict prognosis of chronic lymphocytic leukemia. *Cancers (Basel)* (2021) 13(16):4239. doi: 10.3390/cancers13164239

61. Belkin DA, Mitsui H, Wang CQ, Gonzalez J, Zhang S, Shah KR, et al. Cd200 upregulation in vascular endothelium surrounding cutaneous squamous cell carcinoma. *JAMA Dermatol* (2013) 149(2):178–86. doi: 10.1001/jamadermatol.2013.1609

62. Wong KK, Zhu F, Khatri I, Huo Q, Spaner DE, Gorczynski RM. Characterization of Cd200 ectodomain shedding. *PloS One* (2016) 11(4):e0152073. doi: 10.1371/journal.pone.0152073

63. Liu JQ, Talebian F, Wu L, Liu Z, Li MS, Wu L, et al. A critical role for Cd200r signaling in limiting the growth and metastasis of Cd200+ melanoma. *J Immunol* (2016) 197(4):1489–97. doi: 10.4049/jimmunol.1600052

64. Hayakawa K, Wang X, Lo EH. Cd200 increases alternatively activated macrophages through camp-response element binding protein - C/Ebp-beta signaling. *J Neurochem* (2016) 136(5):900–6. doi: 10.1111/jnc.13492

65. Ko YC, Chien HF, Jiang-Shieh YF, Chang CY, Pai MH, Huang JP, et al. Endothelial Cd200 is heterogeneously distributed, regulated and involved in immune cell-endothelium interactions. *J Anat* (2009) 214(1):183–95. doi: 10.1111/j.1469-7580.2008.00986.x

66. Aird WC. Phenotypic heterogeneity of the endothelium: I. *Structure Function Mechanisms Circ Res* (2007) 100(2):158–73. doi: 10.1161/01.RES.0000255691.76142.4a

67. Bukovsky A, Presl J, Zidovsky J, Mancal P. The localization of thy-1.1, mrc ox 2 and ia antigens in the rat ovary and fallopian tube. *Immunology* (1983) 48(3):587–96. https://www.ncbi.nlm.nih.gov/pubmed/6131030

68. Andersson M, Karlsson L, Svensson PA, Ulfhammer E, Ekman M, Jernas M, et al. Differential global gene expression response patterns of human endothelium exposed to shear stress and intraluminal pressure. *J Vasc Res* (2005) 42(5):441–52. doi: 10.1159/000087983

69. Mierke CT. Role of the endothelium during tumor cell metastasis: Is the endothelium a barrier or a promoter for cell invasion and metastasis? *J Biophys* (2008) 2008:183516. doi: 10.1155/2008/183516

70. Sibler E, He Y, Ducoli L, Keller N, Fujimoto N, Dieterich LC, et al. Single-cell transcriptional heterogeneity of lymphatic endothelial cells in normal and inflamed murine lymph nodes. *Cells* (2021) 10(6):1371. doi: 10.3390/cells10061371

71. Jalkanen S, Salmi M. Lymphatic endothelial cells of the lymph node. *Nat Rev Immunol* (2020) 20(9):566–78. doi: 10.1038/s41577-020-0281-x

72. Bubna AK. Imiquimod - its role in the treatment of cutaneous malignancies. *Indian J Pharmacol* (2015) 47(4):354–9. doi: 10.4103/0253-7613.161249

73. Louie DAP, Liao S. Lymph node subcapsular sinus macrophages as the frontline of lymphatic immune defense. *Front Immunol* (2019) 10:347. doi: 10.3389/fimmu.2019.00347

74. Tu L, Guan R, Yang H, Zhou Y, Hong W, Ma L, et al. Assessment of the expression of the immune checkpoint molecules pd-1, Ctla4, Tim-3 and lag-3 across different cancers in relation to treatment response, tumor-infiltrating immune cells and survival. *Int J Cancer* (2020) 147(2):423–39. doi: 10.1002/ijc.32785

75. Acharya N, Sabatos-Peyton C, Anderson AC. Tim-3 finds its place in the cancer immunotherapy landscape. *J Immunother Cancer* (2020) 8(1):e000911. doi: 10.1136/jitc-2020-000911

76. Vaddepally RK, Kharel P, Pandey R, Garje R, Chandra AB. Review of indications of fda-approved immune checkpoint inhibitors per nccn guidelines with the level of evidence. *Cancers (Basel)* (2020) 12(3):738 . doi: 10.3390/cancers12030738

77. Coles SJ, Hills RK, Wang EC, Burnett AK, Man S, Darley RL, et al. Expression of Cd200 on aml blasts directly suppresses memory T-cell function. *Leukemia* (2012) 26 (9):2148–51. doi: 10.1038/leu.2012.77

78. Coles SJ, Gilmour MN, Reid R, Knapper S, Burnett AK, Man S, et al. The immunosuppressive ligands pd-L1 and Cd200 are linked in aml T-cell immunosuppression: Identification of a new immunotherapeutic synapse. *Leukemia* (2015) 29(9):1952–4. doi: 10.1038/leu.2015.62

79. Mahadevan D, Lanasa MC, Farber C, Pandey M, Whelden M, Faas SJ, et al. Phase I study of samalizumab in chronic lymphocytic leukemia and multiple myeloma: Blockade of the immune checkpoint Cd200. *J Immunother Cancer* (2019) 7(1):227. doi: 10.1186/s40425-019-0710-1

80. Marqus S, Pirogova E, Piva TJ. Evaluation of the use of therapeutic peptides for cancer treatment. *J BioMed Sci* (2017) 24(1):21. doi: 10.1186/s12929-017-0328-x

81. Zhang L, Huang Y, Lindstrom AR, Lin TY, Lam KS, Li Y. Peptide-based materials for cancer immunotherapy. *Theranostics* (2019) 9(25):7807–25. doi: 10.7150/thno.37194

82. Sachdeva S, Joo H, Tsai J, Jasti B, Li X. A rational approach for creating peptides mimicking antibody binding. *Sci Rep* (2019) 9(1):997. doi: 10.1038/s41598-018-37201-6

83. Moertel C, Martinez-Puerta F, Pluhar GGE, Castro MG, Olin M. Cd200ar-l: Mechanism of action and preclinical and clinical insights for treating high-grade brain tumors. *Expert Opin Investig Drugs* (2022) 31(9):875–9. doi: 10.1080/13543784.2022.2108588

84. Ampudia-Mesias E, Puerta-Martinez F, Bridges M, Zellmer D, Janeiro A, Strokes M, et al. Cd200 immune-checkpoint peptide elicits an anti-glioma response through the Dap10 signaling pathway. *Neurotherapeutics* (2021) 18(3):1980–94. doi: 10.1007/s13311-021-01038-1

85. Olin MR, Ampudia-Mesias E, Pennell CA, Sarver A, Chen CC, Moertel CL, et al. Treatment combining Cd200 immune checkpoint inhibitor and tumor-lysate vaccination after surgery for pet dogs with high-grade glioma. *Cancers (Basel)* (2019) 11(2):137. doi: 10.3390/cancers11020137

86. ClinicalTrials.gov. *Study of Cd200 activation receptor ligand (Cd200ar-l) and allogeneic tumor lysate vaccine immunotherapy for recurrent glioblastoma* (2021). United States National Library of Medicine. Available at: https://clinicaltrials.gov/ct2/show/NCT04642937 (Accessed July 7, 2022).

87. Snelgrove RJ, Goulding J, Didierlaurent AM, Lyonga D, Vekaria S, Edwards L, et al. A critical function for Cd200 in lung immune homeostasis and the severity of influenza infection. *Nat Immunol* (2008) 9(9):1074–83. doi: 10.1038/ni.1637

88. Ritzel RM, Al Mamun A, Crapser J, Verma R, Patel AR, Knight BE, et al. Cd200-Cd200r1 inhibitory signaling prevents spontaneous bacterial infection and promotes resolution of neuroinflammation and recovery after stroke. *J Neuroinflamm* (2019) 16 (1):40. doi: 10.1186/s12974-019-1426-3

89. Hoek RM, Ruuls SR, Murphy CA, Wright GJ, Goddard R, Zurawski SM, et al. Down-regulation of the macrophage lineage through interaction with Ox2 (Cd200). *Science* (2000) 290(5497):1768–71. doi: 10.1126/science.290.5497.1768

90. Gorczynski RM, Cattral MS, Chen Z, Hu J, Lei J, Min WP, et al. An immunoadhesin incorporating the molecule ox-2 is a potent immunosuppressant that prolongs allo- and xenograft survival. *J Immunol* (1999) 163(3):1654–60. doi: 10.4049/jimmunol.163.3.1654

91. Yu K, Chen Z, Gorczynski R. Effect of Cd200 and Cd200r1 expression within tissue grafts on increased graft survival in allogeneic recipients. *Immunol Lett* (2013) 149(1-2):1–8. doi: 10.1016/j.imlet.2012.11.004

frontiers | Frontiers in Oncology

TYPE Review
PUBLISHED 27 January 2023
DOI 10.3389/fonc.2023.1099811

Check for updates

OPEN ACCESS

EDITED BY
Saravanan Rajendrasozhan,
University of Hail, Saudi Arabia

REVIEWED BY
Chiara Focaccetti,
Universitàdi Roma Tor Vergata,
Italy
Emanuela Ricciotti,
University of Pennsylvania, United States

*CORRESPONDENCE
Bing Liu
liubingzju@zju.edu.cn
Jinti Lin
11918336@zju.edu.cn

†These authors have contributed equally to this work

SPECIALTY SECTION
This article was submitted to Cancer Immunity and Immunotherapy, a section of the journal Frontiers in Oncology

RECEIVED 16 November 2022
ACCEPTED 12 January 2023
PUBLISHED 27 January 2023

CITATION
Jin K, Qian C, Lin J and Liu B (2023) Cyclooxygenase-2-Prostaglandin E2 pathway: A key player in tumor-associated immune cells.
Front. Oncol. 13:1099811.
doi: 10.3389/fonc.2023.1099811

COPYRIGHT
© 2023 Jin, Qian, Lin and Liu. This is an open-access article distributed under the terms of the Creative Commons Attribution License (CC BY). The use, distribution or reproduction in other forums is permitted, provided the original author(s) and the copyright owner(s) are credited and that the original publication in this journal is cited, in accordance with accepted academic practice. No use, distribution or reproduction is permitted which does not comply with these terms.

Cyclooxygenase-2-Prostaglandin E2 pathway: A key player in tumor-associated immune cells

Kaipeng Jin[1,2,3†], Chao Qian[1,2,3†], Jinti Lin[1,2,3*] and Bing Liu[1,2,3*]

[1]Department of Orthopedic Surgery, The Second Affiliated Hospital, Zhejiang University School of Medicine, Hangzhou, Zhejiang, China, [2]Orthopedics Research Institute of Zhejiang University, Hangzhou, Zhejiang, China, [3]Key Laboratory of Motor System Disease Research and Precision Therapy of Zhejiang Province, Hangzhou, Zhejiang, China

Cyclooxygenases-2 (COX-2) and Prostaglandin E2 (PGE2), which are important in chronic inflammatory diseases, can increase tumor incidence and promote tumor growth and metastasis. PGE2 binds to various prostaglandin E receptors to activate specific downstream signaling pathways such as PKA pathway, β-catenin pathway, NF-κB pathway and PI3K/AKT pathway, all of which play important roles in biological and pathological behavior. Nonsteroidal anti-inflammatory drugs (NSAIDs), which play as COX-2 inhibitors, and EP antagonists are important in anti-tumor immune evasion. The COX-2-PGE2 pathway promotes tumor immune evasion by regulating myeloid-derived suppressor cells, lymphocytes ($CD8^+$ T cells, $CD4^+$ T cells and natural killer cells), and antigen presenting cells (macrophages and dendritic cells). Based on conventional treatment, the addition of COX-2 inhibitors or EP antagonists may enhance immunotherapy response in anti-tumor immune escape. However, there are still a lot of challenges in cancer immunotherapy. In this review, we focus on how the COX-2-PGE2 pathway affects tumor-associated immune cells.

KEYWORDS

COX-2, PGE2, COX-2 inhibitors, EP, tumor immune escape

Introduction

Cyclooxygenases-2 (COX-2) and Prostaglandin E2 (PGE2) are important inflammatory factors, associated with survival, invasion, growth and immune escape of cancer cells. One of the "hallmarks" of cancer is chronic inflammatory disease, which often promotes tumorigenesis and tumor progression (1). For example, inflammatory bowel disease patients had a higher lifetime risk of colon cancer linked to colitis at a younger age than the general population, demonstrating that cancer is easily caused by chronic inflammation (2). Tumor-associated inflammation involves complex interactions between epithelial and mesenchymal cells and in some cases can lead to epigenetic alterations. More broadly, however, chronic inflammation can lead to the production of growth factors that support the development of emerging tumors and cause them to behave as "unhealable wounds" (3). Chronic inflammation can also promote tumor development by facilitating tumor immune escape and establishing an immunosuppressive microenvironment, both of which are cancer-

related characteristics. Tumor immune escape occurs through a variety of immunosuppressive mechanisms, such as dysfunctional antigen-presenting cells (APCs), tumor cell resistance to immune attack, decreased cytotoxicity of $CD8^+$ T cells and natural killer (NK) cells, induction of immunosuppressive cells such as myeloid-derived suppressor cells (MDSCs), transition of T helper (Th) cells from Th1 to Th2 and Th17, transition of macrophages from M1 to M2 (4).

Numerous studies have shown the importance of nonsteroidal anti-inflammatory drugs (NSAIDs) and EP receptor antagonists in reducing tumor incidence, metastasis and mortality. NSAIDs cause tumor regression and suppress tumor growth by inhibiting the COX-2-PGE2 signaling pathway in several ways: 1. activation of tumor epithelial cells; 2. inhibition of tumor epithelial cell survival and tumor immune surveillance; 3. establishment of tumor-supporting microenvironment; 4. alteration of DNA methylation mechanisms (2). However, the molecular mechanisms underlying the anti-tumor effects of NSAIDs and EP receptor antagonists have not yet been fully understood. More clinical trials and studies are required to explore this further.

In this review, we emphasize our current understanding of COX-2 and PGE2 regulation of tumor immunity. In addition, we are looking into how the COX-2-PGE2 pathway affects tumor-associated immune cells. Given the significance of this pathway in tumor immune escape, we will discuss how to target each component of this pathway as potential strategy for overcoming tumor immune escape while avoiding some serious adverse effects associated with the use of NSAIDs or COX-2 inhibitors.

Cyclooxygenase

Cyclooxygenases (COX) include COX-1 and COX-2, also known as prostaglandin G/H synthase-1 and -2, are membrane-bound enzymes that are mainly found on the nuclear membrane and luminal side of the endoplasmic reticulum (5). COX-1 is structurally expressed in many healthy tissues and provides steady-state levels of prostaglandins to perform "housekeeping functions". In contrast, COX-2 is an inducible isoform produced by prostaglandin-like substances that is typically absent or expressed at low levels in normal organs and tissues, but is overexpressed in many tumor and inflammatory tissues (6). In addition to inducing inflammation, COX-2 can also promote cell survival and proliferation. Therefore, COX-2 may be associated with tumorigenesis and development. Indeed, COX-2 has been found to be highly expressed in different tumors, including breast cancer (7), the melanoma (8), and colorectal cancer (2). Its levels are associated with the development, aggressiveness and prognosis of many tumor entities. Regular use of NSAIDs dramatically decreased the incidence of sporadic colorectal cancer as well as breast, lung, and prostate cancers, according to a new analysis that searched all epidemiological studies (case-control and cohort studies) conducted since 1980 (9). According to one study, genetically removing COX enzymes from mouse melanoma (BRAFV600E or NrasG12D), colorectal cancer (CT26) or breast cancer (4T1) cell lines resulted in dramatic tumor eradication (10). When metastases were assessed 2 weeks after surgical resection of the primary breast cancer tumor, fibroblast-targeted Ptgs2-deficient mice (Ptgs2DFb) were found to develop fewer metastases than WT mice (11). Patients with gastric cancer who have low staging and higher levels of COX-2 expression are at greater risk of dying from the disease. In addition, COX-2 has been identified as an independent prognostic factor for gastric cancer (12). According to the findings mentioned above, COX-2 is thought to be crucial for tumor growth.

COX-2-PGE2 signaling in tumor cells

COX enzymes convert arachidonic acid to the endogenous peroxidation intermediate PGH2, which is modified by prostaglandin synthase to produce five structurally related prostaglandins, including prostaglandin D2, prostaglandin E2, prostaglandin I2, prostaglandin F2α, and thromboxane A2. The two essential enzymes that catalyze the initial and concluding phases of this synthetic pathway are COX-2 and prostaglandin E2 synthase (PGES), including microsomal PGES (mPGES) and cytosolic PGES. In addition, PGE2 is converted to its inactive form, 15-keto-PGE2 (PGEM), which is then further metabolized to a stable terminal metabolite by the enzyme 15-hydroxyprostaglandin dehydrogenase (15-PGDH). High levels of PGEM increase the risk of gastric and colorectal cancers (13, 14), implying that PGEM may be a biomolecular marker for cancer risk prediction. Prostaglandins control cellular processes by attaching to G protein-coupled receptors on the cell surface. These cell surface receptors are named EP (EP1, EP2, EP3, EP4), DP (DP1, DP2), FP, IP, and TP. PGE2 transmits signals by binding to four receptors, EP1 through EP4 (15) (Figure 1). The expression of each EP receptor and the strength of each EP signal determine the PGE2 signal's final output. Each EP interacts with its unique G protein to activate particular downstream signaling pathways such as PKA pathway, β-catenin pathway, NF-κB pathway and PI3K/AKT pathway, which have various functions in biological and pathological behavior. Activated EP1 can upregulate the level of intracellular calcium ion concentrations; EP2 and EP4 receptors are associated with cAMP stimulation and PKA signaling through sequential activation of Gas and adenylyl cyclase; EP3 is responsible for downregulating cAMP levels and lead to different cellular responses through different G proteins (16, 17).

The most abundant prostaglandin, PGE2, is frequently linked to a poor prognosis in a number of human cancers, including colon, head and neck, lung, and breast cancers (6, 17, 18). In immunologically active hosts, the formation of tumors by mutant BRAFV600E mouse melanoma cells requires the synthesis of prostaglandin E2, which inhibits immunity and fosters tumor inflammation (10). It has been shown that mPGES1 expression increased in human melanoma, and that elevated expression of this protein are linked to reduced patient survival (19). The mPGES-1 gene deletion significantly reduced the risk of developing colon cancer and resulted in reduced multiplicity of distal colon tumors as well as tumor load in mice treated with azoxymethane (AOM) (20). In addition, in ApcMin/+ and AOM mice models, elevated endogenous PGE2, caused by 15-PGDH gene deletion, encouraged the development of colon cancer (21). Taken together, PGE2 is essential in the growth of cancers (Figure 2).

In addition, numerous evidence has shown that the COX-2-PGE2 pathway promotes tumor development. It has been shown that PGE2 promotes sporadic or colitis-associated colon carcinogenesis *via* EP1 and EP2 receptor in colon cancer cell lines (22). According to

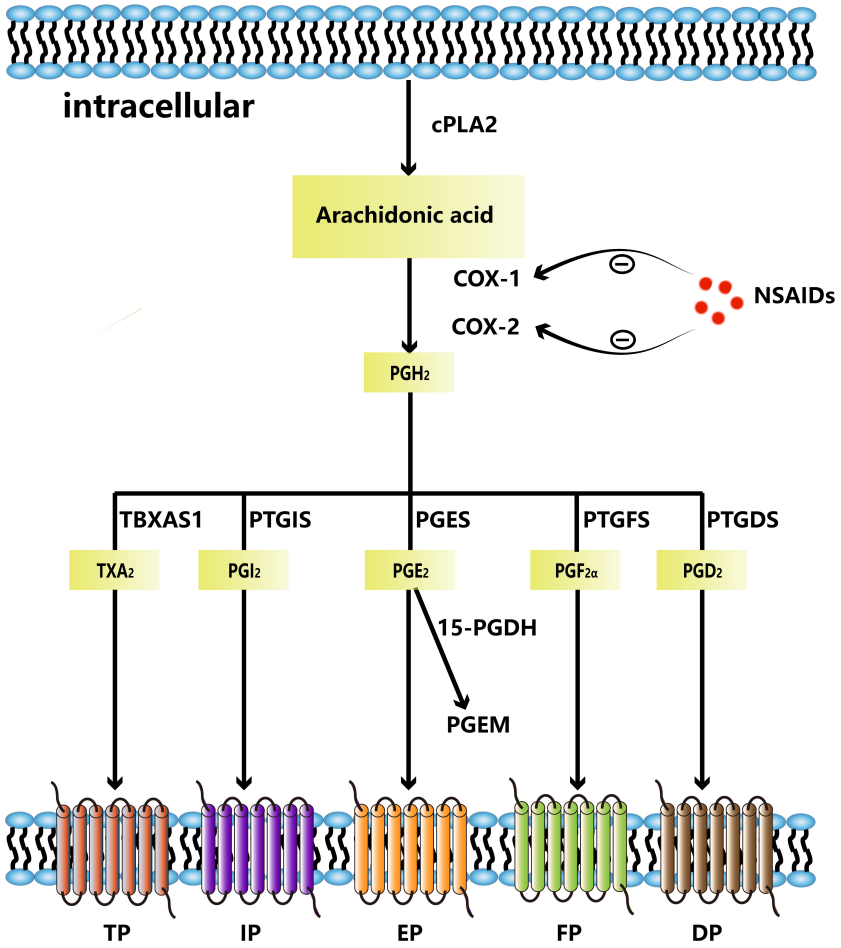


FIGURE 1
Arachidonic acid is metabolized to PGH_2 by COX-1 and COX-2. NSAIDs can inhibit COX-1 and COX-2. PGH_2 is metabolized to thromboxane A2(TXA_2)by TBXAS1, PGI_2 by PTGIS, PGE_2 by PGES, $PGF_{2\alpha}$ by PGES, PGD_2 by PTGDS, respectively. PGE_2 can be metabolized to PGEM by 15-PDGH. TXA_2 binds to TP, PGI_2 binds to IP, PGE_2 binds to EP, $PGF_{2\alpha}$ binds to FP and PGD_2 binds to DP.

research, numerous tumors are linked to EP1 receptor. For example, selective EP1 antagonist (ONO-8713) can significantly reduce the number of tumor cells in mouse with UVB-induced acute skin inflammation (23). PGE2 upregulates anti-apoptosis protein expression in hepatocellular carcinoma cells *via* EP1 receptors (24). While EP3 receptors were downregulated, EP1, EP2 and EP4 receptors were all highly increased in COX-2-driven mammary cancers. Downregulation of EP3 receptors suggests a possible protective role against mammary tumors. EP2 and EP4 receptor levels were reduced in the mammary glands of anti-inflammatory pain-treated mice, while EP1 and EP3 levels were not altered (25). According to Fujino et al, EP3 receptors could boost vascular endothelial growth factor receptor-1 signaling and encourage tumor cell metastasis (26). Therefore, it may be debatable how EP3 contributes to carcinogenesis, and more research is required. The role of the EP4 receptor in tumors appears to be more clearly defined than that of other EP receptors. EP4 is a high-affinity EP receptor, and it is considered to be a pro-cancer mediator in many different types of malignancies due to its high expression. In colorectal cancer, deletion of EP4 can attenuates the abnormal AOM-induced crypt (27, 28), and therefore EP4 receptor can be used for prostate cancer immunotherapy. For example, YY001, an antagonist of the EP4 receptor, inhibits prostate cancer growth by modulating the tumor microenvironment (TME), leading to significant tumor regression, long-term survival and long-lasting immune memory (29). Besides, in mouse model, EP4 knockdown suppressed metastasis of oral cancer cells in the lung (30). Collectively, these findings imply a critical function for the PGE2/EP4 signaling pathway in tumor development.

COX-2-PGE2 Pathway in Tumor Immunology

The COX-2-PGE2 pathway induces tumor immune evasion by regulating myeloid-derived suppressor cells (MDSCs), lymphocytes ($CD8^+$ T cells, $CD4^+$ T cells and natural killer cells), and antigen presenting cells (APCs). Understanding the mechanisms of the COX-2-PGE2 pathway may provide a solid foundation for developing new methods to overcome tumor immune escape (Figure 3).

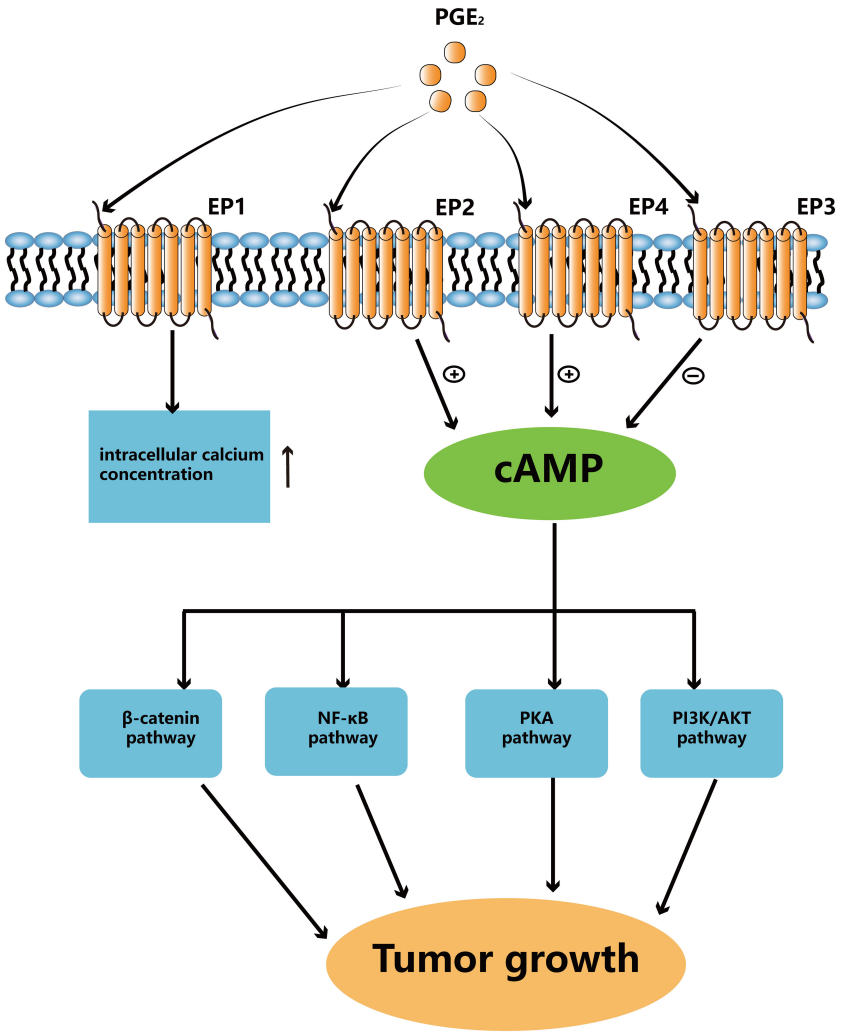


FIGURE 2
PGE_2 binds to different EPs to activate downstream signaling pathways. Activated EP1 can upregulate the level of intracellular calcium ion concentrations. EP2 and EP4 can upregulate cAMP levels to activate different pathways which can promote tumor growth. EP3 is responsible for downregulating cAMP levels.

Myeloid-derived suppressor cells

Granulocyte/polymorphonuclear stem cells and monocyte MDSCs, which come from the granulocyte or monocyte myeloid lineage, respectively, are the two main kinds of MDSCs found in both humans and animals. However, unlike mice, a tiny group of myeloid precursor cells known as "early MDSCs" have been found in humans. These cells have a potent immunosuppressive function and consist mainly of myeloid progenitor cells and precursor cells, accounting for less than 5% of the total number of MDSCs (31). MDSCs mediate immunosuppression by producing arginase and inducible nitric oxide synthase, and TGF-β, IL-10 and COX-2. These substances directly or indirectly enhance Treg activity (32), inhibit cytotoxic activity of NK cells (33), and promote the polarization of macrophages toward M2-like phenotype. They synergistically impair the tumoricidal properties of effector $CD8^+$ T cells, leading to tumor cell evasion of host antitumor immunity (34). MDSCs are significantly linked to a poor clinical course of cancer (35). In mice and patients, the clinical cancer stage and the amount of metastatic tumors are favorably linked with the blood levels of MDSCs (36) (Figure 4).

The EP4 antagonist YY001 promotes the proliferation and anti-cancer activities of T lymphocytes while inhibiting myeloid-derived suppressor cells' development, maturation, and immune-suppressive actions. Additionally, it alters the chemokine profile of tumor cells *in vitro* and *in vivo*, which decreases the amounts of MDSCs and T cells in the TME (29). *In vitro* experiments, PGE2 participated in MDSC-mediated immunosuppression by inducing arginase I expression through EP4 and inhibiting effector T cell activity (37). One study found that treatment of colorectal cancer mice with aspirin or EP antagonists significantly protected mice from tumor formation and reduced aggregation of MDSCs and expression of COX-2/Arg-1 (38). Thus, PGE2 inhibits MDSCs by blocking EP4 receptors, thereby promoting tumor immune evasion. The number of Gr1(+) CD11b(+) immature myeloid suppressor cells was considerably decreased by the celecoxib during the chemoprevention of 1,2-dimethylhydrazine diHCL-(1,2-DMH-) induced colon cancers in Swiss mice (39). The COX-2 pathway promotes glioma formation by directly supporting the phylogeny of MDSCs and their accumulation in TME, where MDSCs limit CTL infiltration (40). Taken together,

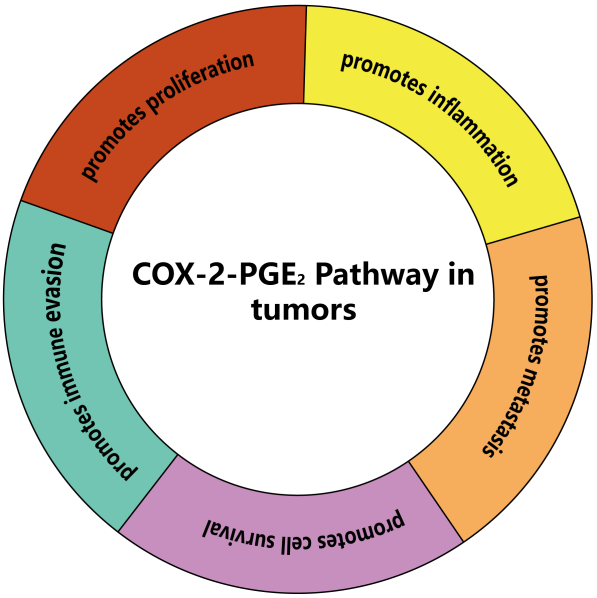


FIGURE 3
The main effects of COX-2-PGE2 pathway on tumors. COX-2-PGE2 pathway can promote proliferation, inflammation, metastasis, cell survival and immune evasion of tumors.

the COX-2-PGE2 signaling pathway promotes tumor immune evasion by inducing the accumulation of MDSCs cells, which in turn promotes tumor growth and development. However, the regulatory role of COX-2-PGE2 pathway on MDSCs *in vivo* has not been fully investigated.

Macrophages

Microglia, Kupffer cells, and Langerhans cells in the brain, liver, and epidermis are examples of tissue-specific macrophages. Macrophages possess the ability to remove apoptotic cells, cellular debris and pathogens (41). Similar to the Th1 and Th2 dichotomy, the distinction between M1 and M2 phenotypes supports the idea of macrophage phenotypic heterogeneity. When exposed to lipopolysaccharide and interferon-c, macrophages develop the M1 phenotype and exhibit anticancer properties. Macrophages become polarized to the M2 phenotype in response to Th2 cytokines which promote cell proliferation and tumor formation (42, 43). TAMs have an M2-like phenotype in the majority of cancers (44), which facilitates tumor-associated angiogenesis, promotes tumor cell invasion and migration, and inhibits immune surveillance to promote tumor metastasis (45). Clinical studies have shown that macrophages promote tumorigenesis. In a meta-analysis, more than 80% of studies indicated a link between high macrophage density and poor patient prognosis (46). In primary tumors, TAMs have been shown to inhibit $CD8^+$ T cell recruitment and anti-tumor immunity (47).

Previous studies have pointed out that the COX-2-PGE2 signaling pathway contributes significantly to the polarization of M1 to M2 and tumor immune escape. The majority of the COX-2 seen in both human and mouse intestinal cancers is known to come from TAMs. Celecoxib, a selective COX-2 inhibitor, shifted the TAM phenotype from M2 to M1 in a colorectal cancer animal model in accordance to the decrease in the number of polyps in ApcMin/1 mice (48). While inhibiting the growth of immune-stimulated M1 macrophages, PGE2-binding EP4 promoted development of immune-suppressed

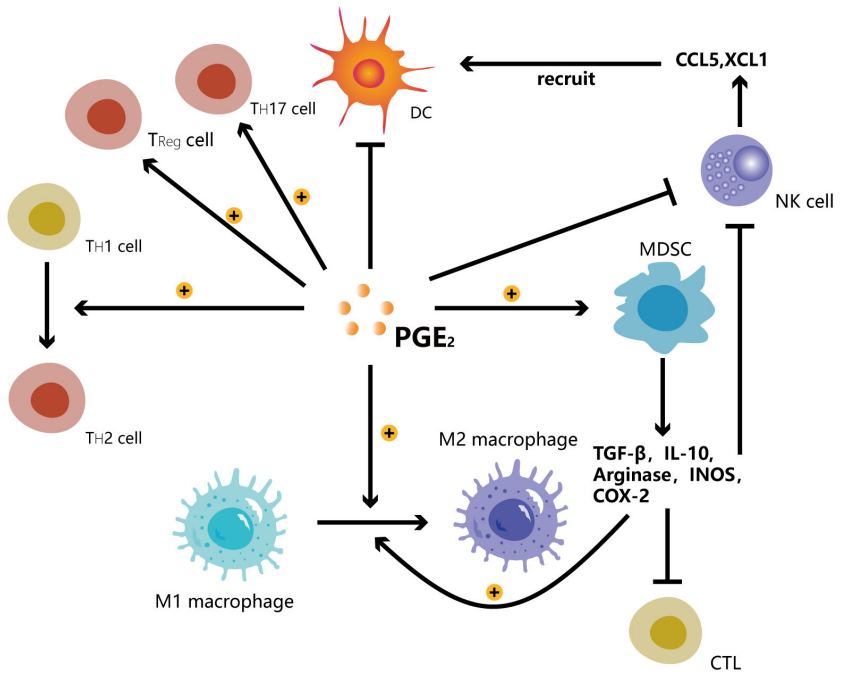


FIGURE 4
PGE_2 promotes the transition of T helper cells from TH1 to TH2 and the shift of macrophages from M1 to M2. PGE_2 induces the development of Treg cells, TH17 cells and MDSCs while inhibiting Dendritic cells, NK cells. MDSCs secrete TGF-β, IL-10, arginase, INOS, COX-2 to promote the shift of macrophages from M1 to M2 while inhibiting the functions of cytotoxic lymphocytes (CTL) and NK cells. NK cells can secrete CCL5 and XCL1 chemokines to recruit DCs.

M2 macrophages and MDSCs (49). Eruslanov et al. found that in the mouse colon cancer cell line CT26, overexpression of 15-PGDH shifted TAMs from M2-directed TAM to M1-directed macrophages (50). In the GC transgenic model, overexpression of COX-2 and mPGES-1 led to TAM recruitment in gastric tumors (51). These findings collectively imply that COX-2 and PGE2 stimulate tumor development *via* M2 TAMs. EP1 and EP3 receptors also play an important role in tumor growth. Targeting EP1 receptor can decrease F4/80 (+) macrophage infiltration and inhibit colon cancer growth (52). EP3 signaling in DCs induces a switch of macrophages from pro-inflammatory to pro-reparative phenotype (53).

NK Cells

As a part of innate immunity, NK cells play an important role in tumor immune surveillance and viral infection resistances. In addition to immediately identifying and eliminating tumor cells, NK cells secrete cytokines that promote CTL activation and growth. However, the functional response of NK cells is compromised in tumors (54). In all cancer types, patient survival was substantially correlated with high expression of NK marker genes (55). In cancerous environment, NK cells dysfunction is integral and inevitable, leading to not only the proliferation of tumor cells but also the formation of distant metastases (56). The abundance of peritumoral NK cells is also associated with high pathological complete response rates in neoadjuvant chemotherapy for large and locally advanced breast cancers (57). In the course of infection with chronic lymphocytic choriomeningitis virus, intrinsic NK cell signaling can inhibit the expansion of $CD8^+$ T cells, thereby promoting tumor immune evasion (58).

The COX-2-PGE2 pathway can enhance tumor immune evasion. PGE2 has been reported to inhibit cytotoxic effects and cytokine generation of NK cells in breast cancer as well as thyroid cancer through the EP4 signaling pathway (59, 60). In mouse tumors, NK cell-derived chemokines CCL5 and XCL1 promote the accumulation of dendritic cells (DCs). PGE2-producing tumors inhibit NK cell function, chemokine production, and DCs chemokine receptor expression to promote tumor immune escape (55). Breast tumor cells have been shown to express fewer MHC class I molecules when EP4 signaling is inhibited, which enhances the NK cells' capacity to fight the tumor (61).

Dendritic cells

DCs have a unique function in the induction and regulation of innate and acquired immune responses. To direct T cell responses, DCs in the TME collect, prepare, and present tumor-associated antigens on MHC molecules as well as supply co-stimulatory and soluble components (62). In humans, reduced DC numbers and activity affect the prognosis of colorectal cancer patients (63). When patients were stratified based on cDC1-related gene expression, higher cDC1 signaling in tumors was found to be positively correlated with survival (55). However, eight studies have come to the conflicting conclusion that tumor-associated DCs can be a predictor of progressive prognosis in colorectal cancer (64).

PGE2 plays an important role in the control of DCs behaviors include differentiating, producing cytokines, polarizing TH cells, migrating, and maturing (65). In addition, it has been found that inhibiting EP2 and EP4 receptors increases both MHC molecule expression and antigen uptake by lung dendritic cells (11). Tumor-derived prostaglandin analogs inhibited both the aggregation and activation of CD103+ DCs within the tumor, including their capacity to produce IL-12, as well as the expression of type I immune-related markers (10). Secretion of PGE2 may inhibit the capacity of DCs to activate $CD8^+$ T lymphocytes, thus promoting T cell exclusion from TME (41). Human DC surface HLA class II antigen expression levels are downregulated by IL-6 through the functions of COX-2, lysosomal protease, and arginase (66). Furthermore, an *in vitro* study demonstrated that NSAIDs prevent DCs from presenting MHC-restricted antigens (67). Taken together, the COX-2-PGE2 signaling pathway promotes tumor immune evasion by inhibiting DC cells.

$CD4^+$ T helper Cells

APCs activate naive $CD4^+$ T cells, which then initiate differentiation into various effector T cells during inflammatory and immunological responses to infections and cancer (68). Th1 cells, in general, control more aggressive responses by encouraging cytotoxic immune responses, whereas Th2 cells control less tissue-damaging immune responses (69, 70). As a result of resident tissue cells being stimulated to release chemokines by Th17-associated cytokines, neutrophils and macrophages are drawn to the sites of inflammation. In turn, the recruited cells generate more cytokines and protein hydrolases, exacerbating the immunological reaction (71, 72). TGF-β suppresses TH2-mediated cancer immunity. In a mouse model of breast cancer, induction of TGF-β receptor II gene deletion in $CD4^+$ T cells inhibited tumor growth (73). Higher levels of circulating $CD4^+$ T lymphocytes were linked to smaller tumor sizes in GC patients (74). Th17 cells were found in greater numbers in the peripheral blood and tumor tissue of patients with oral squamous cell carcinoma (66). In conclusion, the formation and progression of tumors are highly correlated with $CD4^+$ T cell activity.

COX-2 deficiency delays mammary carcinogenesis by enhancing type 1 immune responses in breast cancers (75). At high doses, PGE2 induces a shift from a Th1-dominant to a Th2-dominant immune response by downregulating Th1-induced activation of the IL-12 pathway (68). Additionally, PGE2 stimulates IL-23 production and prevents DCs from releasing IL-12 and IL-27, which increases the pathogenic inflammatory Th17 phenotype (76). Although the majority of published studies indicate that PGE2 boosts Th2-type responses, evidence shows that COX-2 has an inhibitory effect on Th2 immune responses. In contrast to Th1-mediated lung inflammation, Jaffar et al. demonstrated that specific inhibition of COX-2 *in vivo* decreases PGE2 production and causes a considerable rise in Th2-mediated lung inflammation (77). Some studies have shown that PGE2 can promote Th1 differentiation through the EP1 receptor (78). Thus, the results are contradictory and more research is required.

$CD8^+$ cytotoxic T cells

$CD8^+$ cytotoxic T cells, the primary killer cells of pathogens and tumor cells, are essential for the destruction of intracellular infections and malignant cells, and may provide long-term immune protection (79, 80). Exercise alters the metabolism of $CD8^+$ T cells, thereby enhancing their antitumor efficacy (81). In colorectal cancer, low tumor stage, negative nodal stage, longer overall survival, and an inflammatory immune phenotype were all substantially correlated with the density and proportion of proliferating $CD8^+$ cytotoxic T cells (82). These results suggest that $CD8^+$ T cells are capable of suppressing tumor growth.

In ErbB2 transgenic mice, COX-2 (MEC) KO breast cancer tumors contained more $CD8^+$ cytotoxic immune cells (CTL) (7). Some studies found that the amount of $CD8^+$ T cells and the percentage of functional $CD8^+$ T cells were considerably decreased in PTGS2 overexpression tumors (83). These findings suggest that activation of the COX2 enzymes can reduce tumor-infiltrating $CD8^+$ T cells. In addition, effector $CD8^+$ T cells in tumors are inhibited from killing tumors by tumor-producing, PGE2-activated immunosuppressive cells in TME *via* EP4 receptors (84). During chronic lymphocytic choroidal meningitis virus infection, EP2 and EP4 are upregulated on virus-specific CTL inhibiting CTL survival and function (85). Increased secretion of PGE2 by breast cancer cells also recruits Treg cells into the primary tumor, thereby increasing apoptosis of $CD8^+$ T cells and bone metastasis of cancer cells (86). PGE2 directly inhibits cytotoxic T cell activity and induces regulatory T cell function *in vitro* through upregulation of CD94 and NKG2A complexes (87). However, more evidence is needed to demonstrate whether the COX-2-PGE2 pathway promotes tumor immune evasion by suppressing $CD8^+$ T cells.

Potential strategies for cancer therapy

Immunotherapy has grown in popularity as a cancer treatment option in recent years. Given the importance of the COX-2-PGE2 pathway in carcinogenesis and progression, there is a clear opportunity for therapeutic intervention. NSAIDs are a class of drugs that primarily suppress COX enzyme activity, which also lowers prostaglandins production. The use of NSAIDs to inhibit tumor growth has been considered. Combination therapy with NSAIDs and anti-PD-1 monoclonal antibody induces tumor eradication faster than anti-PD-1 alone (10). In addition, an *in vivo* investigation revealed that NSAIDs improved anti-tumor responses and reversed the imbalance between Th1 and Th2 in the metastatic spread of colorectal cancer (88). Some studies have demonstrated that NSAIDs can reduce cancer-associated mortalities and lower cancer incidence (89). For this reason, the FDA has approved celecoxib, a selective COX-2 inhibitor, for the treatment of population with familial adenomatous polyposis who wish to avoid developing colorectal polyps. In experimental animals, specific COX-2 inhibitors can prevent the development of mammary tumors (90). However, due to the risk of adverse cardiovascular events, celecoxib, along with other NSAIDs (except from aspirin), should not be used for an extended period of time, particularly in patients with a history of atherosclerotic heart disease (91). Excessive bleeding is the most serious side effect of aspirin, and both the risk and mortality rate increase with age (92). One way to prevent these negative consequences is to target only downstream PGE2 signaling. Cell surface inhibitory receptors (such as PD-1) are centrally involved in T cell exhaustion (93). And PGE2 could be one of the inducers of PD-L1 expression (94). We suppose that COX2-PGE2 pathway may result in T cell exhaustion by inducing PD-L1 expression. Emerging data from multiple solid tumor mouse models indicates that EP4 antagonists and PD1/PD-L1 blockade are effective in inhibiting primary tumor growth (49, 95, 96). Therefore, it may be a new potential strategy to combine EP antagonists with PD1/PD-L1 blockade in treating T cell exhaustion. In addition, combination immunotherapy with chimeric antigen receptor T (CAR-T) cells and checkpoint blockade is thought to be the next immunotherapy frontier (97). For instance, combination PD-L1 blockade and CD19 CAR-T cell therapy resulted in better outcomes in patients with heavily B-ALL (98). PGE2 signaling can activate protein kinase A, and then inhibits T-cell receptor activation, which inhibits the antitumor effect of CAR-T cell therapy (99). Thus, we conclude that targeting EP receptors (such as EP2 and EP4) could represent a novel strategy for improving the efficacy of adoptive immunotherapy. Some clinical trials are ongoing to evaluate the efficacy of these inhibitors. A phase I trial showed that EP4 antagonist (E7046) was safe in patients with advanced malignancies (ClinicalTrials.gov, Number NCT02540291). 1 clinical trial is recruiting patients to evaluate whether a dual EP2/EP4 antagonist (TPST-1495) suppresses tumor growth (ClinicalTrials.gov, Number NCT04344795). Although there is abundant EP receptor expression in fibroblasts and inflammatory cells, the role of the COX-2-PGE2 signaling pathway in TME is not fully understood, and more studies are needed to demonstrate this.

Summary

In this review, we discuss the role of the COX-2-PGE2 pathway in tumor immune evasion regulation. The idea that efficient therapeutic approaches should involve eliminating tumor cells and suppressing tumor immune evasion is being supported by a growing body of evidence, such as the use of checkpoint inhibitors to target immunosuppressive cells and reactivate immunosuppressive effector T cells. The COX-2-PGE2 signaling pathway may assist tumors in evading immune systems by inducing tumor-associated immune cells aggregation, impaired APC activity, a switch from Th1 to Th2 and Th17 immune responses or by suppressing $CD8^+$ cytotoxic T cell and NK cell functions to promote tumor immune escape. In conclusion, the COX-2-PGE2 pathway not only is an effective target for tumor eradication, but it also suppresses tumor immune escape. Therefore, the addition of cyclooxygenase-2 inhibitors or EP antagonists to standard treatment may enhance the response of immunotherapy in anti-tumor immune escape.

Author contributions

KJ and CQ drafted the manuscript and revised the manuscript. JL and BL were in charge of the whole research conduction and paper writing. All authors contributed to the article and approved the submitted version.

Funding

This study was supported by grants from the National Natural Science Foundation of China (NO.81872181), and the Natural Science Foundation of Zhejiang Province (NO. LY21H160034).

Conflict of interest

The authors declare that the research was conducted in the absence of any commercial or financial relationships that could be construed as a potential conflict of interest.

Publisher's note

All claims expressed in this article are solely those of the authors and do not necessarily represent those of their affiliated organizations, or those of the publisher, the editors and the reviewers. Any product that may be evaluated in this article, or claim that may be made by its manufacturer, is not guaranteed or endorsed by the publisher.

References

1. Hou J, Karin M, Sun B. Targeting cancer-promoting inflammation - have anti-inflammatory therapies come of age? *Nat Rev Clin Oncol* (2021) 18(5):261–79. doi: 10.1038/s41571-020-00459-9

2. Wang D, DuBois RN. The role of anti-inflammatory drugs in colorectal cancer. *Annu Rev Med* (2013) 64:131–44. doi: 10.1146/annurev-med-112211-154330

3. Singh R, Mishra MK, Aggarwal H. Inflammation, immunity, and cancer. *Mediators Inflamm* (2017) 2017:6027305. doi: 10.1155/2017/6027305

4. Wang D, Cabalag CS, Clemons NJ, DuBois RN. Cyclooxygenases and prostaglandins in tumor immunology and microenvironment of gastrointestinal cancer. *Gastroenterology* (2021) 161(6):1813–29. doi: 10.1053/j.gastro.2021.09.059

5. Tong D, Liu Q, Wang LA, Xie Q, Pang J, Huang Y, et al. The roles of the COX2/PGE2/EP axis in therapeutic resistance. *Cancer Metastasis Rev* (2018) 37(2-3):355–68. doi: 10.1007/s10555-018-9752-y

6. Wang D, Dubois RN. Eicosanoids and cancer. *Nat Rev Cancer* (2010) 10(3):181–93. doi: 10.1038/nrc2809

7. Markosyan N, Chen EP, Evans RA, Ndong V, Vonderheide RH, Smyth EM. Mammary carcinoma cell derived cyclooxygenase 2 suppresses tumor immune surveillance by enhancing intratumoral immune checkpoint activity. *Breast Cancer Res* (2013) 15(5):R75. doi: 10.1186/bcr3469

8. Botti G, Fratangelo F, Cerrone M, Liguori G, Cantile M, Anniciello AM, et al. COX-2 expression positively correlates with PD-L1 expression in human melanoma cells. *J Transl Med* (2017) 15(1):46. doi: 10.1186/s12967-017-1150-7

9. Harris RE. Cyclooxygenase-2 (cox-2) blockade in the chemoprevention of cancers of the colon, breast, prostate, and lung. *Inflammopharmacology* (2009) 17(2):55–67. doi: 10.1007/s10787-009-8049-8

10. Zelenay S, van der Veen AG, Bottcher JP, Snelgrove KJ, Rogers N, Acton SE, et al. Cyclooxygenase-dependent tumor growth through evasion of immunity. *Cell* (2015) 162 (6):1257–70. doi: 10.1016/j.cell.2015.08.015

11. Gong Z, Li Q, Shi J, Wei J, Li P, Chang CH, et al. Lung fibroblasts facilitate pre-metastatic niche formation by remodeling the local immune microenvironment. *Immunity* (2022) 55(8):1483–500.e9. doi: 10.1016/j.immuni.2022.07.001

12. Mrena J, Wiksten JP, Thiel A, Kokkola A, Pohjola L, Lundin J, et al. Cyclooxygenase-2 is an independent prognostic factor in gastric cancer and its expression is regulated by the messenger RNA stability factor HuR. *Clin Cancer Res* (2005) 11(20):7362–8. doi: 10.1158/1078-0432.CCR-05-0764

13. Wang T, Cai H, Zheng W, Michel A, Pawlita M, Milne G, et al. A prospective study of urinary prostaglandin E2 metabolite, helicobacter pylori antibodies, and gastric cancer risk. *Clin Infect Dis* (2017) 64(10):1380–6. doi: 10.1093/cid/cix106

14. Johnson JC, Schmidt CR, Shrubsole MJ, Billheimer DD, Joshi PR, Morrow JD, et al. Urine PGE-m: A metabolite of prostaglandin E2 as a potential biomarker of advanced colorectal neoplasia. *Clin Gastroenterol Hepatol* (2006) 4(11):1358–65. doi: 10.1016/j.cgh.2006.07.015

15. Narumiya S, Sugimoto Y, Ushikubi F. Prostanoid receptors: structures, properties, and functions. *Physiol Rev* (1999) 79(4):1193–226. doi: 10.1152/physrev.1999.79.4.1193

16. Sugimoto Y, Narumiya S. Prostaglandin e receptors. *J Biol Chem* (2007) 282 (16):11613–7. doi: 10.1074/jbc.R600038200

17. Reader J, Holt D, Fulton A. Prostaglandin E2 EP receptors as therapeutic targets in breast cancer. *Cancer Metastasis Rev* (2011) 30(3-4):449–63. doi: 10.1007/s10555-011-9303-2

18. Hambek M, Baghi M, Wagenblast J, Schmitt J, Baumann H, Knecht R. Inverse correlation between serum PGE2 and T classification in head and neck cancer. *Head Neck.* (2007) 29(3):244–8. doi: 10.1002/hed.20503

19. Kim SH, Roszik J, Cho SN, Ogata D, Milton DR, Peng W, et al. The COX2 effector microsomal PGE2 synthase 1 is a regulator of immunosuppression in cutaneous melanoma. *Clin Cancer Res* (2019) 25(5):1650–63. doi: 10.1158/1078-0432.Ccr-18-1163

20. Nakanishi M, Menoret A, Tanaka T, Miyamoto S, Montrose DC, Vella AT, et al. Selective PGE(2) suppression inhibits colon carcinogenesis and modifies local mucosal immunity. *Cancer Prev Res (Phila)* (2011) 4(8):1198–208. doi: 10.1158/1940-6207.Capr-11-0188

21. Myung SJ, Rerko RM, Yan M, Platzer P, Guda K, Dotson A, et al. 15-hydroxyprostaglandin dehydrogenase is an in vivo suppressor of colon tumorigenesis. *Proc Natl Acad Sci USA* (2006) 103(32):12098–102. doi: 10.1073/pnas.0603235103

22. Schumacher Y, Aparicio T, Ourabah S, Baraille F, Martin A, Wind P, et al. Dysregulated CRTC1 activity is a novel component of PGE2 signaling that contributes to colon cancer growth. *Oncogene* (2016) 35(20):2602–14. doi: 10.1038/onc.2015.283

23. Tober KL, Wilgus TA, Kusewitt DF, Thomas-Ahner JM, Maruyama T, Oberyszyn TM. Importance of the EP(1) receptor in cutaneous UVB-induced inflammation and tumor development. *J Invest Dermatol* (2006) 126(1):205–11. doi: 10.1038/sj.jid.5700014

24. Bai XM, Jiang H, Ding JX, Peng T, Ma J, Wang YH, et al. Prostaglandin E2 upregulates survivin expression via the EP1 receptor in hepatocellular carcinoma cells. *Life Sci* (2010) 86(5-6):214–23. doi: 10.1016/j.lfs.2009.12.009

25. Chang SH, Liu CH, Conway R, Han DK, Nithipatikom K, Trifan OC, et al. Role of prostaglandin E2-dependent angiogenic switch in cyclooxygenase 2-induced breast cancer progression. *Proc Natl Acad Sci USA* (2004) 101(2):591–6. doi: 10.1073/pnas.2535911100

26. Fujino H, Toyomura K, Chen XB, Regan JW, Murayama T. Prostaglandin E_2 regulates cellular migration *via* induction of vascular endothelial growth factor receptor-1 in HCA-7 human colon cancer cells. *Biochem Pharmacol* (2011) 81(3):379–87. doi: 10.1016/j.bcp.2010.11.001

27. Watanabe K, Kawamori T, Nakatsugi S, Ohta T, Ohuchida S, Yamamoto H, et al. Role of the prostaglandin e receptor subtype EP1 in colon carcinogenesis. *Cancer Res* (1999) 59(20):5093–6.

28. Mutoh M, Watanabe K, Kitamura T, Shoji Y, Takahashi M, Kawamori T, et al. Involvement of prostaglandin e receptor subtype EP(4) in colon carcinogenesis. *Cancer Res* (2002) 62(1):28–32.

29. Peng S, Hu P, Xiao YT, Lu W, Guo D, Hu S, et al. Single-cell analysis reveals EP4 as a target for restoring T-cell infiltration and sensitizing prostate cancer to immunotherapy. *Clin Cancer Res* (2022) 28(3):552–67. doi: 10.1158/1078-0432.CCR-21-0299

30. Osawa K, Umemura M, Nakakaji R, Tanaka R, Islam RM, Nagasako A, et al. Prostaglandin E(2) receptor EP4 regulates cell migration through Orai1. *Cancer Sci* (2020) 111(1):160–74. doi: 10.1111/cas.14247

31. Bronte V, Brandau S, Chen SH, Colombo MP, Frey AB, Greten TF, et al. Recommendations for myeloid-derived suppressor cell nomenclature and characterization standards. *Nat Commun* (2016) 7:12150. doi: 10.1038/ncomms12150

32. Marvel D, Gabrilovich DI. Myeloid-derived suppressor cells in the tumor microenvironment: expect the unexpected. *J Clin Invest* (2015) 125(9):3356–64. doi: 10.1172/jci80005

33. Mao Y, Sarhan D, Steven A, Seliger B, Kiessling R, Lundqvist A. Inhibition of tumor-derived prostaglandin-e2 blocks the induction of myeloid-derived suppressor cells and recovers natural killer cell activity. *Clin Cancer Res* (2014) 20(15):4096–106. doi: 10.1158/1078-0432.Ccr-14-0635

34. Lindau D, Gielen P, Kroesen M, Wesseling P, Adema GJ. The immunosuppressive tumour network: Myeloid-derived suppressor cells, regulatory T cells and natural killer T cells. *Immunology* (2013) 138(2):105–15. doi: 10.1111/imm.12036

35. Veglia F, Sanseviero E, Gabrilovich DI. Myeloid-derived suppressor cells in the era of increasing myeloid cell diversity. *Nat Rev Immunol* (2021) 21(8):485–98. doi: 10.1038/s41577-020-00490-y

36. Diaz-Montero CM, Salem ML, Nishimura MI, Garrett-Mayer E, Cole DJ, Montero AJ. Increased circulating myeloid-derived suppressor cells correlate with clinical cancer stage, metastatic tumor burden, and doxorubicin-cyclophosphamide chemotherapy. *Cancer Immunol Immunother* (2009) 58(1):49–59. doi: 10.1007/s00262-008-0523-4

37. Rodriguez PC, Hernandez CP, Quiceno D, Dubinett SM, Zabaleta J, Ochoa JB, et al. Arginase I in myeloid suppressor cells is induced by COX-2 in lung carcinoma. *J Exp Med* (2005) 202(7):931–9. doi: 10.1084/jem.20050715

38. Yan G, Zhao H, Zhang Q, Zhou Y, Wu L, Lei J, et al. A RIPK3-PGE2 circuit mediates myeloid-derived suppressor cell-potentiated colorectal carcinogenesis. *Cancer Res* (2018) 78(19):5586–99. doi: 10.1158/0008-5472.CAN-17-3962

39. Talmadge JE, Hood KC, Zobel LC, Shafer LR, Coles M, Toth B. Chemoprevention by cyclooxygenase-2 inhibition reduces immature myeloid suppressor cell expansion. *Int Immunopharmacol.* (2007) 7(2):140–51. doi: 10.1016/j.intimp.2006.09.021

40. Fujita M, Kohanbash G, Fellows-Mayle W, Hamilton RL, Komohara Y, Decker SA, et al. COX-2 blockade suppresses gliomagenesis by inhibiting myeloid-derived suppressor cells. *Cancer Res* (2011) 71(7):2664–74. doi: 10.1158/0008-5472.Can-10-3055

41. Hansen M, Andersen MH. The role of dendritic cells in cancer. *Semin Immunopathol* (2017) 39(3):307–16. doi: 10.1007/s00281-016-0592-y

42. Mantovani A, Sica A, Sozzani S, Allavena P, Vecchi A, Locati M. The chemokine system in diverse forms of macrophage activation and polarization. *Trends Immunol* (2004) 25(12):677–86. doi: 10.1016/j.it.2004.09.015

43. Mosser DM, Edwards JP. Exploring the full spectrum of macrophage activation. *Nat Rev Immunol* (2008) 8(12):958–69. doi: 10.1038/nri2448

44. Mantovani A, Sozzani S, Locati M, Allavena P, Sica A. Macrophage polarization: tumor-associated macrophages as a paradigm for polarized M2 mononuclear phagocytes. *Trends Immunol* (2002) 23(11):549–55. doi: 10.1016/s1471-4906(02)02302-5

45. Qian BZ, Pollard JW. Macrophage diversity enhances tumor progression and metastasis. *Cell* (2010) 141(1):39–51. doi: 10.1016/j.cell.2010.03.014

46. Bingle L, Brown NJ, Lewis CE. The role of tumour-associated macrophages in tumour progression: Implications for new anticancer therapies. *J Pathol* (2002) 196 (3):254–65. doi: 10.1002/path.1027

47. DeNardo DG, Brennan DJ, Rexhepaj E, Ruffell B, Shiao SL, Madden SF, et al. Leukocyte complexity predicts breast cancer survival and functionally regulates response to chemotherapy. *Cancer Discov* (2011) 1(1):54–67. doi: 10.1158/2159-8274.Cd-10-0028

48. Nakanishi Y, Nakatsuji M, Seno H, Ishizu S, Akitake-Kawano R, Kanda K, et al. COX-2 inhibition alters the phenotype of tumor-associated macrophages from M2 to M1 in ApcMin/+ mouse polyps. *Carcinogenesis* (2011) 32(9):1333–9. doi: 10.1093/carcin/bgr128

49. Lu W, Yu W, He J, Liu W, Yang J, Lin X, et al. Reprogramming immunosuppressive myeloid cells facilitates immunotherapy for colorectal cancer. *EMBO Mol Med* (2021) 13(1):e12798. doi: 10.15252/emmm.202012798

50. Eruslanov E, Kaliberov S, Daurkin I, Kaliberova L, Buchsbaum D, Vieweg J, et al. Altered expression of 15-hydroxyprostaglandin dehydrogenase in tumor-infiltrated CD11b myeloid cells: a mechanism for immune evasion in cancer. *J Immunol* (2009) 182(12):7548–57. doi: 10.4049/jimmunol.0802358

51. Oshima H, Oshima M, Inaba K, Taketo MM. Hyperplastic gastric tumors induced by activated macrophages in COX-2/mPGES-1 transgenic mice. *EMBO J* (2004) 23 (7):1669–78. doi: 10.1038/sj.emboj.7600170

52. O'Callaghan G, Ryan A, Neary P, O'Mahony C, Shanahan F, Houston A. Targeting the EP1 receptor reduces fas ligand expression and increases the antitumor immune response in an *in vivo* model of colon cancer. *Int J Cancer* (2013) 133(4):825–34. doi: 10.1002/ijc.28076

53. Nakamoto S, Ito Y, Nishizawa N, Goto T, Kojo K, Kumamoto Y, et al. EP3 signaling in dendritic cells promotes liver repair by inducing IL-13-mediated macrophage differentiation in mice. *FASEB J* (2020) 34(4):5610–27. doi: 10.1096/fj.201901955R

54. O'Brien KL, Finlay DK. Immunometabolism and natural killer cell responses. *Nat Rev Immunol* (2019) 19(5):282–90. doi: 10.1038/s41577-019-0139-2

55. Böttcher JP, Bonavita E, Chakravarty P, Blees H, Cabeza-Cabrerizo M, Sammicheli S, et al. NK cells stimulate recruitment of cDC1 into the tumor microenvironment promoting cancer immune control. *Cell* (2018) 172(5):1022–37.e14. doi: 10.1016/j.cell.2018.01.004

56. Cerwenka A, Lanier LL. Natural killer cell memory in infection, inflammation and cancer. *Nat Rev Immunol* (2016) 16(2):112–23. doi: 10.1038/nri.2015.9

57. Verma C, Kaewkangsadan V, Eremin JM, Cowley GP, Ilyas M, El-Sheemy MA, et al. Natural killer (NK) cell profiles in blood and tumour in women with large and locally advanced breast cancer (LLABC) and their contribution to a pathological complete response (PCR) in the tumour following neoadjuvant chemotherapy (NAC): differential restoration of blood profiles by NAC and surgery. *J Transl Med* (2015) 13:180. doi: 10.1186/s12967-015-0535-8

58. Chen T, Zhang T, Liu C, Wang C, Ding S, Shao Z, et al. NK cells suppress CD8(+) T cell immunity *via* NKG2D in severe aplastic anemia. *Cell Immunol* (2019) 335:6–14. doi: 10.1016/j.cellimm.2018.10.004

59. Holt D, Ma X, Kundu N, Fulton A. Prostaglandin E(2) (PGE (2)) suppresses natural killer cell function primarily through the PGE(2) receptor EP4. *Cancer Immunol Immunother* (2011) 60(11):1577–86. doi: 10.1007/s00262-011-1064-9

60. Park A, Lee Y, Kim MS, Kang YJ, Park YJ, Jung H, et al. Prostaglandin E2 secreted by thyroid cancer cells contributes to immune escape through the suppression of natural killer (NK) cell cytotoxicity and NK cell differentiation. *Front Immunol* (2018) 9:1859. doi: 10.3389/fimmu.2018.01859

61. Kundu N, Ma X, Holt D, Goloubeva O, Ostrand-Rosenberg S, Fulton AM. Antagonism of the prostaglandin e receptor EP4 inhibits metastasis and enhances NK function. *Breast Cancer Res Treat* (2009) 117(2):235–42. doi: 10.1007/s10549-008-0180-5

62. Wculek SK, Cueto FJ, Mujal AM, Melero I, Krummel MF, Sancho D. Dendritic cells in cancer immunology and immunotherapy. *Nat Rev Immunol* (2020) 20(1):7–24. doi: 10.1038/s41577-019-0210-z

63. Della Porta M, Danova M, Rigolin GM, Brugnatelli S, Rovati B, Tronconi C, et al. Dendritic cells and vascular endothelial growth factor in colorectal cancer: Correlations with clinicobiological findings. *Oncology* (2005) 68(2-3):276–84. doi: 10.1159/000086784

64. Malietzis G, Lee GH, Jenkins JT, Bernardo D, Moorghen M, Knight SC, et al. Prognostic value of the tumour-infiltrating dendritic cells in colorectal cancer: A systematic review. *Cell Commun Adhes* (2015) 22(1):9–14. doi: 10.3109/15419061.2015.1036859

65. Jia XY, Chang Y, Sun XJ, Dai X, Wei W. The role of prostaglandin E2 receptor signaling of dendritic cells in rheumatoid arthritis. *Int Immunopharmacol* (2014) 23 (1):163–9. doi: 10.1016/j.intimp.2014.08.024

66. Kitamura H, Ohno Y, Toyoshima Y, Ohtake J, Homma S, Kawamura H, et al. Interleukin-6/STAT3 signaling as a promising target to improve the efficacy of cancer immunotherapy. *Cancer Sci* (2017) 108(10):1947–52. doi: 10.1111/cas.13332

67. Kim HJ, Lee YH, Im SA, Kim K, Lee CK. Cyclooxygenase inhibitors, aspirin and ibuprofen, inhibit MHC-restricted antigen presentation in dendritic cells. *Immune Netw* (2010) 10(3):92–8. doi: 10.4110/in.2010.10.3.92

68. Li H, Edin ML, Gruzdev A, Cheng J, Bradbury JA, Graves JP, et al. Regulation of T helper cell subsets by cyclooxygenases and their metabolites. *Prostaglandins Other Lipid Mediat* (2013) 104-105:74–83. doi: 10.1016/j.prostaglandins.2012.11.002

69. Bashyam H. Th1/Th2 cross-regulation and the discovery of IL-10. *J Exp Med* (2007) 204(2):237. doi: 10.1084/jem.2042fta

70. Endo T, Ogushi F, Sone S. LPS-dependent cyclooxygenase-2 induction in human monocytes is down-regulated by IL-13, but not by IFN-gamma. *J Immunol* (1996) 156 (6):2240–6. doi: 10.4049/jimmunol.156.6.2240

71. Peck A, Mellins ED. Plasticity of T-cell phenotype and function: the T helper type 17 example. *Immunology* (2010) 129(2):147–53. doi: 10.1111/j.1365-2567.2009.03189.x

72. Peck A, Mellins ED. Breaking old paradigms: Th17 cells in autoimmune arthritis. *Clin Immunol* (2009) 132(3):295–304. doi: 10.1016/j.clim.2009.03.522

73. Li S, Liu M, Do MH, Chou C, Stamatiades EG, Nixon BG, et al. Cancer immunotherapy via targeted TGF-β signalling blockade in T(H) cells. *Nature* (2020) 587(7832):121–5. doi: 10.1038/s41586-020-2850-3

74. Li F, Sun Y, Huang J, Xu W, Liu J, Yuan Z. CD4/CD8 + T cells, DC subsets, Foxp3, and IDO expression are predictive indictors of gastric cancer prognosis. *Cancer Med* (2019) 8(17):7330–44. doi: 10.1002/cam4.2596

75. Markosyan N, Chen EP, Ndong VN, Yao Y, Sterner CJ, Chodosh LA, et al. Deletion of cyclooxygenase 2 in mouse mammary epithelial cells delays breast cancer onset through augmentation of type 1 immune responses in tumors. *Carcinogenesis* (2011) 32(10):1441–9. doi: 10.1093/carcin/bgr134

76. Khayrullina T, Yen JH, Jing H, Ganea D. *In vitro* differentiation of dendritic cells in the presence of prostaglandin E2 alters the IL-12/IL-23 balance and promotes differentiation of Th17 cells. *J Immunol* (2008) 181(1):721–35. doi: 10.4049/jimmunol.181.1.721

77. Jaffar Z, Wan KS, Roberts K. A key role for prostaglandin I2 in limiting lung mucosal Th2, but not Th1, responses to inhaled allergen. *J Immunol* (2002) 169(10):5997–6004. doi: 10.4049/jimmunol.169.10.5997

78. Nagamachi M, Sakata D, Kabashima K, Furuyashiki T, Murata T, Segi-Nishida E, et al. Facilitation of Th1-mediated immune response by prostaglandin e receptor EP1. *J Exp Med* (2007) 204(12):2865–74. doi: 10.1084/jem.20070773

79. Raskov H, Orhan A, Christensen JP, Gogenur I. Cytotoxic CD8(+) T cells in cancer and cancer immunotherapy. *Br J Cancer.* (2021) 124(2):359–67. doi: 10.1038/s41416-020-01048-4

80. Reina-Campos M, Scharping NE, Goldrath AW. CD8(+) T cell metabolism in infection and cancer. *Nat Rev Immunol* (2021) 21(11):718–38. doi: 10.1038/s41577-021-00537-8

81. Rundqvist H, Veliça P, Barbieri L, Gameiro PA, Bargiela D, Gojkovic M, et al. Cytotoxic T-cells mediate exercise-induced reductions in tumor growth. *Elife* (2020) 9. doi: 10.7554/eLife.59996

82. Blessin NC, Li W, Mandelkow T, Jansen HL, Yang C, Raedler JB, et al. Prognostic role of proliferating CD8(+) cytotoxic tcells in human cancers. *Cell Oncol (Dordr)* (2021) 44(4):793–803. doi: 10.1007/s13402-021-00601-4

83. Pu D, Yin L, Huang L, Qin C, Zhou Y, Wu Q, et al. Cyclooxygenase-2 inhibitor: A potential combination strategy with immunotherapy in cancer. *Front Oncol* (2021) 11:637504. doi: 10.3389/fonc.2021.637504

84. Take Y, Koizumi S, Nagahisa A. Prostaglandin e receptor 4 antagonist in cancer immunotherapy: Mechanisms of action. *Front Immunol* (2020) 11:324. doi: 10.3389/fimmu.2020.00324

85. Chen JH, Perry CJ, Tsui YC, Staron MM, Parish IA, Dominguez CX, et al. Prostaglandin E2 and programmed cell death 1 signaling coordinately impair CTL function and survival during chronic viral infection. *Nat Med* (2015) 21(4):327–34. doi: 10.1038/nm.3831

86. Karavitis J, Hix LM, Shi YH, Schultz RF, Khazaie K, Zhang M. Regulation of COX2 expression in mouse mammary tumor cells controls bone metastasis and PGE2-induction

of regulatory T cell migration. *PloS One* (2012) 7(9):e46342. doi: 10.1371/journal.pone.0046342

87. Zeddou M, Greimers R, de Valensart N, Nayjib B, Tasken K, Boniver J, et al. Prostaglandin E2 induces the expression of functional inhibitory CD94/NKG2A receptors in human CD8+ T lymphocytes by a cAMP-dependent protein kinase a type I pathway. *Biochem Pharmacol* (2005) 70(5):714–24. doi: 10.1016/j.bcp.2005.05.015

88. Yao M, Kargman S, Lam EC, Kelly CR, Zheng Y, Luk P, et al. Inhibition of cyclooxygenase-2 by rofecoxib attenuates the growth and metastatic potential of colorectal carcinoma in mice. *Cancer Res* (2003) 63(3):586–92.

89. Rothwell PM, Price JF, Fowkes FG, Zanchetti A, Roncaglioni MC. Tognoni G, et al. short-term effects of daily aspirin on cancer incidence, mortality, and non-vascular death: Analysis of the time course of risks and benefits in 51 randomised controlled trials. *Lancet* (2012) 379(9826):1602–12. doi: 10.1016/s0140-6736(11)61720-0

90. Mazhar D, Ang R, Waxman J. COX inhibitors and breast cancer. *Br J Cancer* (2006) 94(3):346–50. doi: 10.1038/sj.bjc.6602942

91. Cuzick J, Otto F, Baron JA, Brown PH, Burn J, Greenwald P, et al. Aspirin and non-steroidal anti-inflammatory drugs for cancer prevention: An international consensus statement. *Lancet Oncol* (2009) 10(5):501–7. doi: 10.1016/s1470-2045(09)70035-x

92. Cuzick J, Thorat MA, Bosetti C, Brown PH, Burn J, Cook NR, et al. Estimates of benefits and harms of prophylactic use of aspirin in the general population. *Ann Oncol* (2015) 26(1):47–57. doi: 10.1093/annonc/mdu225

93. Wherry EJ. T Cell exhaustion. *Nat Immunol* (2011) 12(6):492–9. doi: 10.1038/ni.2035

94. Goto S, Konnai S, Hirano Y, Kohara J, Okagawa T, Maekawa N, et al. Upregulation of PD-L1 expression by prostaglandin E(2) and the enhancement of IFN-γ by anti-PD-L1 antibody combined with a COX-2 inhibitor in mycoplasma bovis infection. *Front Vet Sci* (2020) 7:12. doi: 10.3389/fvets.2020.00012

95. Sajiki Y, Konnai S, Cai Z, Takada K, Okagawa T, Maekawa N, et al. Enhanced immunotherapeutic efficacy of anti-PD-L1 antibody in combination with an EP4 antagonist. *Immunohorizons* (2020) 4(12):837–50. doi: 10.4049/immunohorizons.2000089

96. Wang Y, Cui L, Georgiev P, Singh L, Zheng Y, Yu Y, et al. Combination of EP(4) antagonist MF-766 and anti-PD-1 promotes anti-tumor efficacy by modulating both lymphocytes and myeloid cells. *Oncoimmunology* (2021) 10(1):1896643. doi: 10.1080/2162402x.2021.1896643

97. Sterner RC, Sterner RM. CAR-T cell therapy: Current limitations and potential strategies. *Blood Cancer J* (2021) 11(4):69. doi: 10.1038/s41408-021-00459-7

98. Li AM, Hucks GE, Dinofia AM, Seif AE, Teachey DT, Baniewicz D, et al. Checkpoint inhibitors augment CD19-directed chimeric antigen receptor (CAR) T cell therapy in relapsed b-cell acute lymphoblastic leukemia. *Blood* (2018) 132(Supplement 1):556–. doi: 10.1182/blood-2018-99-112572

99. Newick K, O'Brien S, Sun J, Kapoor V, Maceyko S, Lo A, et al. Augmentation of CAR T-cell trafficking and antitumor efficacy by blocking protein kinase a localization. *Cancer Immunol Res* (2016) 4(6):541–51. doi: 10.1158/2326-6066.Cir-15-0263

frontiers | Frontiers in Immunology

TYPE Review
PUBLISHED 07 February 2023
DOI 10.3389/fimmu.2023.1088685

Check for updates

OPEN ACCESS

EDITED BY
Mohammad Azhar Aziz,
Aligarh Muslim University, India

REVIEWED BY
Minoru Kanaya,
Aiiku Hospital, Japan
Jiajia Zhou,
University of Michigan, United States
Abdulaziz Alfahed,
Prince Sattam Bin Abdulaziz University, Saudi Arabia

*CORRESPONDENCE
Yanyan Liu
yyliu@zzu.edu.cn
Zhihua Yao
zlyyyaozhihua1260@zzu.edu.cn

SPECIALTY SECTION
This article was submitted to Cancer Immunity and Immunotherapy, a section of the journal Frontiers in Immunology

RECEIVED 03 November 2022
ACCEPTED 27 January 2023
PUBLISHED 07 February 2023

CITATION
Yan Z, Yao S, Wang Z, Zhou W, Yao Z and Liu Y (2023) Treatment of extranodal NK/T-cell lymphoma: From past to future. *Front. Immunol.* 14:1088685. doi: 10.3389/fimmu.2023.1088685

COPYRIGHT
© 2023 Yan, Yao, Wang, Zhou, Yao and Liu. This is an open-access article distributed under the terms of the Creative Commons Attribution License (CC BY). The use, distribution or reproduction in other forums is permitted, provided the original author(s) and the copyright owner(s) are credited and that the original publication in this journal is cited, in accordance with accepted academic practice. No use, distribution or reproduction is permitted which does not comply with these terms.

Treatment of extranodal NK/T-cell lymphoma: From past to future

Zheng Yan[1], Shuna Yao[1], Zhizhong Wang[2], Wenping Zhou[1], Zhihua Yao[1*] and Yanyan Liu[1*]

[1]Department of Internal Medicine, Affiliated Cancer Hospital of Zhengzhou University & Henan Cancer Hospital, Zhengzhou, Henan, China, [2]Department of Molecular Pathology, Affiliated Cancer Hospital of Zhengzhou University & Henan Cancer Hospital, Zhengzhou, Henan, China

Extranodal NK/T-cell lymphoma (ENKTCL) is the most common subtype of T/NK-cell lymphoma in Asia and Latin America, but very rare in North American and Europe. Patient survival has improved significantly over the past two decades. However, standard treatment has not yet been established, although dozens of prospective trials have been conducted. To help understand how the treatment of ENKTCL has evolved in the past and what trends lie ahead, we have comprehensively reviewed the treatment of this aggressive malignancy, with a particular focus on neglected or unanswered issues, such as the optimal staging method, the best partner of asparaginase (Asp), the individualized administration of Asp, the preferred sequence of CT and RT and so on. Overall, the 5-year overall survival (OS) of patients with Ann Arbor stage I/II disease increased from < 50% in the early 20th century to > 80% in recent years, and the median OS of patients with Ann Arbor stage III/IV disease increased from < 1 year to more than 3 years. The improvement in patient survival is largely attributable to advances in radiation technology and the introduction of Asp and anti-PD-1/PD-L1 immunotherapy into practice. Radiotherapy is essential for patients with early-stage disease, while Asp-based chemotherapy (CT) and PD-1/PD-L1 inhibitors significantly improved the prognosis of patients with advanced-stage disease. ENKTCL management is trending toward simpler regimens, less toxicity, and higher efficacy. Novel drugs, such as manufactured T cells, monoclonal antibodies, and small molecule inhibitors, are being intensively investigated. Based on the fact that ENKTCL is highly resistant to cytotoxic drugs except Asp, and aggressive CT leads to higher toxicity rather than better outcomes, we recommend it is unnecessary to expend additional resources to compare different combinations of Asp with cytotoxic agents. Instead, more efforts should be made to optimize the use of Asp and immunotherapy to maximize efficacy and minimize toxicity, explore ways to overcome resistance to Asp and immunotherapy, identify novel treatment targets, and define subpopulations who may benefit more from specific treatments.

KEYWORDS

extranodal NK/T-cell lymphoma, asparaginase, PD-1/PD-L1 inhibitor, immunotherapy, treatment, novel drug, review

1 Introduction

Extranodal NK/T-cell lymphoma (ENKTCL) is a unique hematological malignant entity characterized by universal extranodal involvement and invariable Epstein-Barr virus (EBV) infection. The disease has a distinctive ethnic and geographic distribution. It is more common in East Asia and Latin America, but remarkably rare in other regions. ENKTCL is the most common T/NK-cell lymphoma subtype in Asia and Latin America. According to the latest data reported by the International Cooperative Non-Hodgkin T-cell Lymphoma Prospective Registry study (ICT study), ENKTCL accounted for 28.6% of T/NK-cell lymphomas in Asia during 2016-2019 (1). Relatively, the frequency is as high as 40-50% in Mexico (2, 3) and 8% in Europe and the United States (4).

ENKTCL most commonly originates from the mucosa of nasal cavity and adjacent structures, namely the upper aerodigestive tract (UAT) including the nasopharynx, oropharynx, oral cavity, and hypopharynx, resulting in destructive facial lesions. Other organs and tissues, such as skin, bones, digestive tract, lungs, liver, and reproductive organs, may also be involved in a small number of newly diagnosed cases and a large number of relapsed/refractory (R/R) cases. At presentation, most cases (70-90%) have UAT involvement and Ann Arbor stage I/II disease (1, 5–7).

Survival of patients with ENKTCL has improved significantly over the past two decades, and there is a consensus that for early-stage disease, radiotherapy (RT) is essential; for advanced-stage disease, Asp-based chemotherapy (CT) is superior to Asp-absent CT. Despite better patient outcomes and dozens of prospective studies, standard treatment has not been established. The reason is that most of these clinical trials had small sample sizes and focused on the efficacy evaluation of Asp in combination with different CT regimens. Further, many important questions remain unanswered, such as what is the best way to stage the disease? How to select patients with early-stage disease who do not require CT? How to optimize the efficacy of Asp-based CT? Which drug works best in combination with Asp? What is the optimal order for RT and CT? How many courses of CT are required for patients with early-stage disease? How to identify patients more likely to benefit from personalized treatment?

To help understand how treatments for ENKTCL have evolved in the past and where they may go in the future, and to help conduct well-designed clinical trials to accelerate the establishment of standard care, we comprehensively reviewed progress in the treatment of this disease over the past two decades. In particular, we mainly focused on several neglected or unanswered issues in the treatment of ENKTCL, including the optimal staging method, the best partner of Asp, the individualized administration of Asp, the preferred sequence of CT and RT and so on. The pathologic and genetic features of this disease have recently been well reviewed by others (8–10). When analyzing the outcomes of patients treated with different approaches or modalities, we visualized the data using figures, as most data are from retrospective studies with small cohorts and heterogenous treatments, which are difficult to compare directly.

2 Milestones in ENKTCL recognition and treatment

The condition of progressive necrotizing granuloma of the nasal cavity was first described in 1897, causing rapid invasion of the nose and face (midline) (11, 12). The disease was named in early literature as “malignant granuloma of nose”, “progressive lethal granulomatous ulceration of the nose”, “lethal midline granuloma”, and “granuloma gangraenescens” based on clinical characteristics (13), or “polymorphic reticulosis” and “angiocentric lymphoma” based on pathological characteristics (14). In 1982, it was recognized as a type of T-cell lymphoma (15). The association of this disease with EBV was first reported in 1985 (16). In 1987, The disease was identified as originating from NK cells (17). The revised European-American Lymphoma (REAL) classification, published in 1994, first presented this disease as a distinct subtype of malignant lymphoma called “angiocentric lymphoma” (18). A workshop in the same year comparing T-cell lymphoma in Asian and Western countries concluded that nasal T-/NK cell lymphoma, also called angiocentric lymphoma, is a distinct clinicopathologic entity. The workshop proposed nasal T-/NK cell lymphoma for midline facial lesions and nasal-type T-/NK cell lymphoma for tumors in other anatomic sites (19). The 2001 WHO classification named this entity as “extranodal NK/T-cell lymphoma, nasal type” (20) and later, in the 5th edition of the WHO classification of haematolymphoid tumors in 2022, “extranodal NK/T-cell lymphoma, nasal type” was renamed “extranodal NK/T-cell lymphoma”.

Before the 1920s, surgery, antibiotics, and steroids had been used to treat ENKTCL, but all had failed. Durable responses were not observed until the use of RT (radium implantation in 1921 and X-rays in 1925) (12, 21, 22). Since then, RT has been increasingly used in practice. For CT, responses were anecdotally observed in patients treated with the antimetabolite methotrexate in 1964 (23). However, CT has been an adjuvant therapy for a long time due to its low response rate and rapid development of drug resistance. This state persisted until the introduction of L-asparaginase (L-Asp). The first case of L-Asp-induced complete response (CR) in refractory ENKTCL was reported in 1986 (24). In 2005, ENKTCL cells were found to be selectively sensitive to L-Asp (25), but long-term survivors were still rare in patients with advanced-stage disease until the introduction of programmed cell death protein 1 (PD-1) and its ligand (PD-L1) blockade immunotherapy in recent years. PD-1 blockade was reported to be highly active in relapsed/refractory (R/R) ENKTCL patients in 2017 (26) and later used to treat newly diagnosed early-stage disease in 2022 (27). The milestones in the recognition and treatment of ENKTCL are summarized in Figure 1.

3 Survival trend of patients with ENKTCL in the past two decades

ENKTCL is one of the tumors with the most dramatic change in survival over the past 20 years. The 5-year overall survival (OS) for

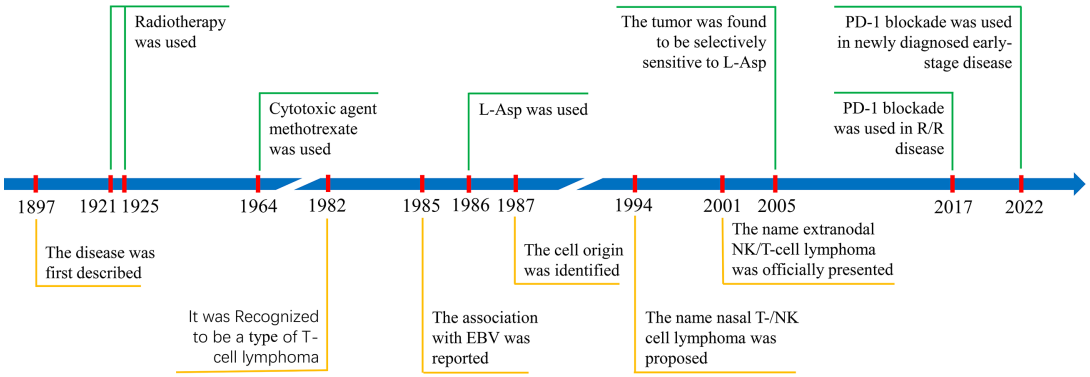


FIGURE 1
Milestones in the recognition (shown in yellow below the timeline) and treatment (shown in green above the timeline) of ENKTCL.

patients with Ann Arbor stage I/II disease has increased from < 50% in the early 2000s to > 80% in recent years. Survival data for early-stage disease published since 2000 are summarized in Figure 2. Here, we included only patients treated with RT or RT plus CT because RT is essential for early-stage disease. The improved survival can be attributed to several factors: the accumulation of knowledge about the biological behavior of the disease, accurate staging with modern photographic techniques, advances in RT techniques, and the introduction of Asp-based CT. Significant changes in survival were also seen in patients with advanced-stage disease. The median OS for advanced-stage disease has increased from a few months to more than 3 years. The better prognosis in advanced-stage disease is largely attributable to the introduction of Asp and PD-1/PD-L1 blockade immunotherapy. Data of advanced-stage disease published since 2000 are summarized in Figure 3.

4 The role of Asp in ENKTCL treatment

4.1 Asp is a game changer

ENKTCL is known to be resistant to conventional CT. In most reports, the CR rate in patients treated with anthracycline (Anth)-based CT was around 30% (29, 43, 46, 93). The resistance of ENKTCL to multiple cytotoxic drugs was initially attributed to the expression of P-glycoproteins (P-gp) on tumor cells (115). However, ENKTCL is also extremely resistant to P-gp independent agents such as methotrexate and cytarabine (25), and the response and survival of patients treated with P-gp independent agents are disappointing. In Anth-resistant ENKTCL patients treated with gemcitabine-based CT, the CR rate and median progression-free survival (PFS) were only 20% and 2.3 months, respectively (116). Further, in two prospective

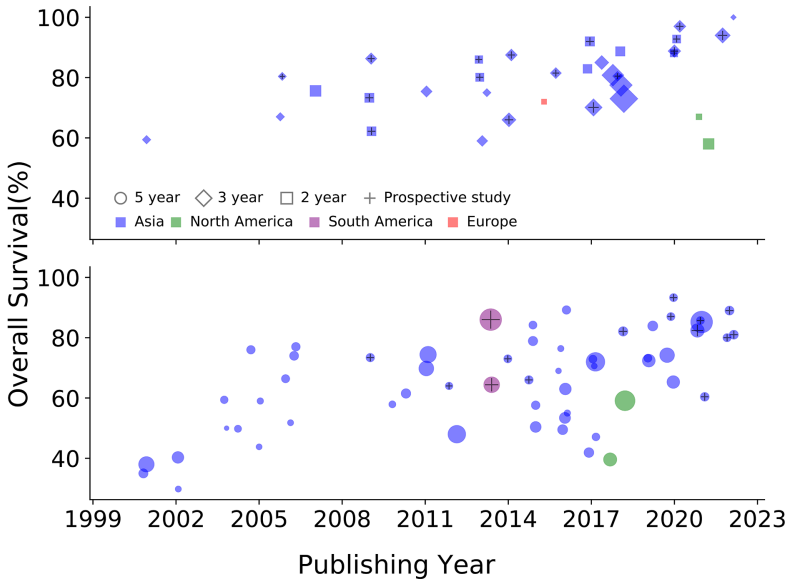


FIGURE 2
Survival trends of patients with Ann Arbor stage I/II ENKTCL over the past two decades. Only data from patients treated with RT or RT plus CT are included. The area of each marker in the figure indicates the sample size of the study. Data are cited from (27–97).

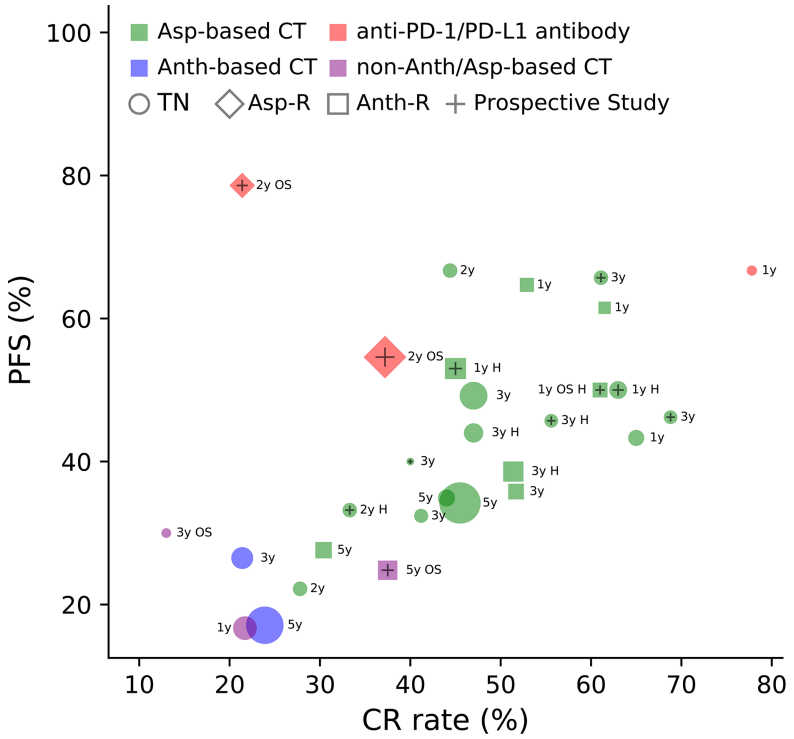


FIGURE 3
Complete response (CR) rate and progression-free survival (PFS) of patients with Ann Arbor stage III/IV or relapsed/refractory ENKTCL treated with different drug types. Asp, asparaginase; Asp-R, asparaginase-resistant; Anth, anthracycline; Anth-R, anthracycline-resistant; CT, chemotherapy; TN, treatment naïve; OS, overall survival (when PFS is not available, OS is displayed); y, year; H, hematopoietic stem cell transplantation. The area of each marker in the figure indicates the sample size of the study. Data are cited from (35, 68, 69, 72, 73, 82, 84, 94, 98–114).

studies, the CR rates in patients with stage III/IV or Anth-resistant disease treated with the IMEP regimen (ifosfamide, methotrexate, etoposide, and prednisone) were 8% and 32%, respectively (35, 99). The absolute efficacy of CT is clearly demonstrated in patients with advanced-stage disease (Figure 3). We can see that the efficacy of non-Anth/Asp-based CT is as poor as the efficacy of Anth-based CT.

However, CR rates with Asp-based CT range from 40% to 70% in most reports, both in early-stage or advanced-stage disease, and in treatment naive or Anth-resistant disease (Figure 3). A multicenter retrospective study from the China Lymphoma Collaborative Group analyzed data from 286 newly diagnosed advanced-stage ENKTCL cases and found that patients treated with Asp-containing CT had a significantly higher CR rate (45.5% *vs.* 23.9%, $P = 0.006$), 5-year PFS (34.2% *vs.* 17.1%, $P < 0.001$), and OS (45.3% *vs.* 27.8%, $P < 0.001$) than those treated with Asp-absent CT (110). The superiority of Asp-based CT over non-Asp-based CT is convincing enough through historical comparison, despite the lack of randomized controlled trials (Figure 3). This conclusion is also supported by systemic reviews and meta-analyses (117).

4.2 Anti-lymphoma mechanism of Asp

The excellent anti-ENKTCL activity of Asp is attributed to its unique anti-tumor mechanism and the natural weakness of ENKTCL cells. Asparagine is a non-essential amino acid that can be synthesized enzymatically from aspartic acid and ammonia in all normal cells of our body in the presence of asparagine synthetase (AsnS). L-Asp, in contrast to AsnS, is an enzyme that selectively hydrolyzes the extracellular amino acid L-asparagine to L-aspartate and ammonia. L-Asp has been introduced for the treatment of childhood acute lymphoblastic leukemia (ALL) since the 1960s because ALL cells lack AsnS expression and depend on extracellular asparagine uptake for survival. When plasma asparagine is depleted by systemic L-Asp administration, intracellular protein biosynthesis ceases and ALL cells die. The low expression of AsnS in ALL cells is due to hypermethylation of the AsnS gene. The CpG island methylation status of the AsnS gene promoter is associated with Asp sensitivity and its hypomethylation status correlates with Asp resistance and is an adverse prognosticator of patient survival (118). ENKTCL cells are even more sensitive to L-Asp than ALL cells (25). L-Asp was first used in combination treatment of ENKTCL by Murase et al. in 1986 (24). Around 2000, several case reports showed that L-Asp monotherapy induced durable CR in patients with R/R ENKTCL (119–121). Yong et al. reported a cohort of 18 (7 early-stage and 11 advanced-stage) Anth-resistant ENKTCL patients treated with L-Asp, vincristine, and dexamethasone followed by RT (if applicable). The CR rate after CT was 55.6%, and the 5-year OS rate of the whole cohort was 55.6% (122). Subsequent *in vivo* studies by Ando et al. showed that NK-cell leukemia/lymphoma cell lines were selectively sensitive to L-Asp among multiple tested anti-cancer agents. Further examination of tumor samples revealed that AsnS mRNA expression levels in lymphoma cells were inversely corelated with clinical responses to L-Asp treatment (25). These findings were subsequently confirmed by other studies (123, 124). Obviously, ENKTCL has the similar biological property to ALL (Figure 4). Likewise, the low expression

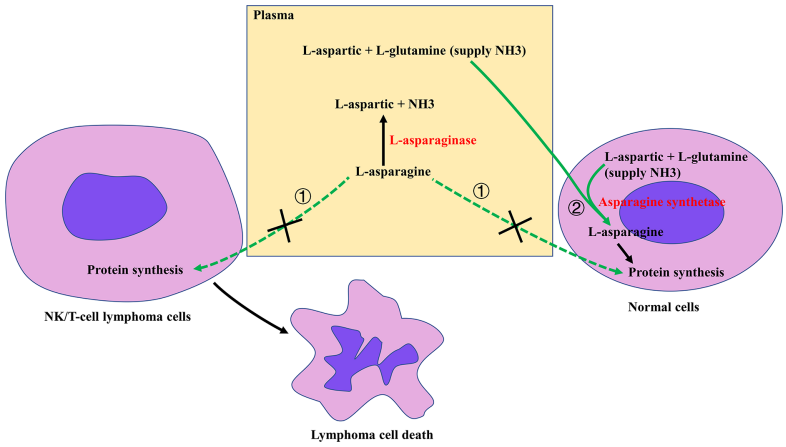


FIGURE 4
Overview of the mechanism of action of asparaginase (Asp) against NK/T-cell lymphoma (NKTCL). Due to the lack of asparagine synthetase (AsnS), NKTCL cells depend on the uptake of extracellular L-asparagine from the circulation (pathway ①) for protein synthesis. Administration of Asp hydrolyzes serum asparagine to aspartic acid and ammonia (NH3), thereby inhibiting tumor cell protein synthesis and ultimately leading to tumor cell death. In contrast, all normal cells in the body have two pathways to obtain L-asparagine for protein synthesis: taking extracellular L-asparagine from the circulation (pathway ①) and synthesizing their own L-asparagine from aspartic acid and NH3 *via* AsnS (pathway ②). When pathway ① is blocked, normal cells can still obtain adequate L-asparagine *via* pathway ② to meet their metabolic needs.

of AsnS gene in ENKTCL cells may be due to genome-wide DNA hypermethylation (125).

4.3 L-Asp and pegaspargase

The use of Asp in the treatment of ALL has been intensively studied. Its optimal therapeutic effect depends on complete and sustained depletion of serum asparagine (126). The serum half-life ($t_{1/2}$) of native *E. coli* L-Asp is 1.25 days (127). When using native Asp, daily administration is unnecessary. Instead, it can be administered at 2- to 3-day intervals. It is crucial, however, that the drug should be administered throughout the treatment period to achieve a complete and sustained depletion of serum asparagine (126). If L-Asp is administered for 4 or 7 days at 3-week intervals, starved cancer cells may be revived by regaining asparagine during the Asp-absent intervals. This may explain, at least in part, the unsatisfactory outcomes in some studies using L-Asp. Currently, L-Asp is largely replaced by polyethylene glycol-conjugated Asp (pegaspargase, PEG-Asp). The serum $t_{1/2}$ of PEG-Asp is 5.73 days, making it a 2-week dosing interval (127). The incidence of hypersensitivity to PEG-Asp is lower than that to native L-Asp (128).

Theoretically, both forms of Asp have similar anticancer activity, but in practice, L-Asp is inferior to PEG-Asp (Figure 5). Part of solid

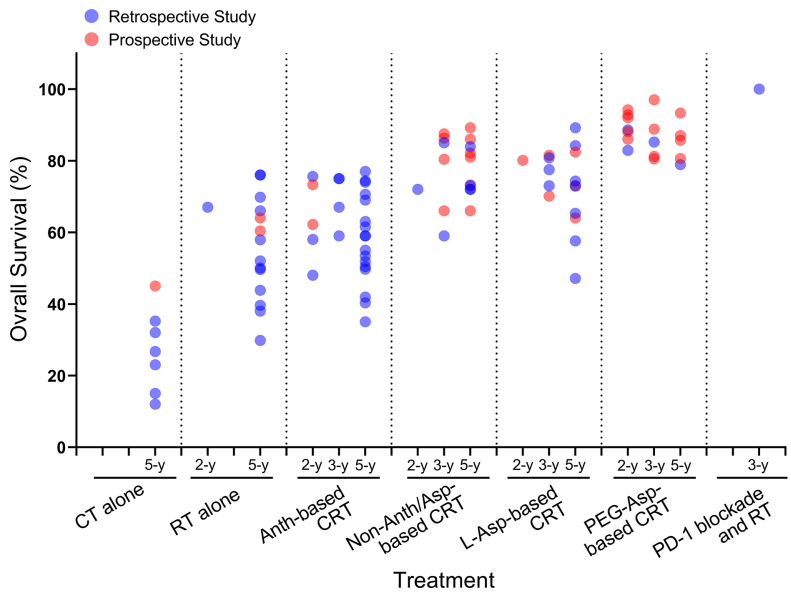


FIGURE 5
OS trends in early-stage ENKTCL patients treated with different modalities. CT, chemotherapy; RT, radiotherapy; Anth, anthracycline; CRT, chemoradiotherapy; Asp, asparaginase; PEG-Asp, pegaspargase; OS, overall survival. Data cited from (4, 27–32, 34–37, 39, 40, 42–46, 48–82, 84–97).

evidence comes from two prospective studies comparing L-Asp with PEG-Asp in patients with ENKTCL. One study by Kim et al. compared L-Asp *vs.* PEG-Asp in combination with the IMEP regimen in 41 newly diagnosed stage IV or Anth-resistant ENKTCL patients. L-Asp was delivered on days 1, 3, 5, 7, 9, and 11 of each cycle of CT, and PEG-Asp was given every 3 weeks. The results showed that the CR rate was higher in the PEG-Asp group (73.7% *vs.* 45.5%; P = 0.067) (129). In another recent randomized controlled study, 80 newly diagnosed ENKTCL patients were assigned to the DDGP (dexamethasone, cisplatin, gemcitabine, and PEG-Asp, repeated at 3-week intervals) arm or the SMILE (dexamethasone, methotrexate, ifosfamide, etoposide, and L-Asp, L-Asp given at 3-week intervals on days 3 to 9) arm. The results showed that the 3-year PFS (56.6% *vs.* 41.8%, P = 0.004) and 5-year OS (74.3% *vs.* 51.7%, P = 0.02) in the DDGP arm were significantly higher than those in the SMILE arm (130). L-Asp-based CT was inferior to PEG-Asp-based CT, at least in part due to the long L-Asp dosing interval between two courses of CT. Besides, higher toxicity-related mortality in the second study was also responsible for the poorer outcome in the SMILE arm (17.5% in the SMILE arm *vs.* 2.5% in the DDGP arm).

4.4 Individualized administration of Asp

The efficacy of Asp-based CT will be further enhanced if individualized treatment is given. The main disadvantages of Asp are hypersensitivity and silent inactivation, both of which are attributed to the production of neutralizing anti-Asp antibodies, occurring in 30-70% of patients during L-Asp treatment (131). Silent inactivation refers to the phenomenon of neutralizing antibodies being present in the absence of any clinical signs of allergy. Anti-Asp antibodies may result in faster Asp clearance, lower serum Asp concentrations, and higher risk of relapse (132, 133). PEG-Asp should not be given to patients who develop anti-*E. coli* Asp antibodies. Instead, Erwinia L-Asp which has different antigenic epitope to *E. coli* Asp is an alternative (134). For PEG-Asp, in addition to anti-Asp antibodies, there is another problem. Anti-PEG antibodies produced after PEG-Asp treatment can also lead to rapid Asp clearance and reduced efficacy (135). Moreover, Asp is essentially a protein that may have significantly different pharmacokinetics, pharmacodynamics, and immunogenicity in patients of different races and ages. For example, the $t_{1/2}$ of PEG-Asp is 7.1 days in South American adults and 5.73 days in Caucasian children (127, 136). Therefore, it is better to monitor the efficiency of asparagine depletion during treatment to achieve optimal efficacy and avoid ineffective medication.

Asp depletion efficiency can be evaluated by serum Asp concentration, presence of anti-Asp antibodies, and Asp activity. Relatively, Asp activity assay remains the best option in practice due to the lack of an anti-Asp antibody test that differentiates between inactivating or non-inactivating antibodies and the rapid ex vivo metabolism of asparagine in the presence of Asp (131). Currently, in the absence of detailed data on Asp metabolism in adult ENKTCL patients, the PEG-Asp activity monitoring algorithm proposed by Archie et al. can be adopted to optimize PEG-Asp dosing (137). Briefly, the algorithm consists of two steps: the first Asp activity monitoring is performed 4 - 7 days after PEG-Asp administration. Asp activity < 0.05 IU/mL indicates the presence of neutralizing antibodies, so treatment should be switched to Erwinia Asp. On the other hand, if Asp activity is ≥ 0.05 IU/mL, a second Asp activity monitoring should be performed 2 weeks after PEG-Asp administration. A second test result of < 0.025 IU/mL and a first test result of < 1.0 IU/mL indicate the presence of accelerated clearance, so the treatment should be switched to Erwinia Asp. If the second test result is < 0.025 IU/mL and the first test result is ≥ 1.0 IU/mL, or the second test level is between 0.025 and 0.1 IU/mL, there are three options: monitoring Asp activity after next dose, increasing PEG-Asp frequency, or switching to Erwinia Asp. If the second test level is ≥ 0.1 IU/mL, the scheduled PEG-Asp administration can be continued (Figure 6). For ENKTCL, if silent inactivation or hypersensitivity occurs and Erwinia L-Asp is not available, RT (for early-stage disease) or second-line treatment (for advance-stage disease) should be moved forward.

In addition, the dose of PEG-Asp used in current practice may not be optimal. As Asp is an enzyme, when the substrate (asparagine) is saturated, the pharmacological effects (both efficacy and toxicity) of Asp

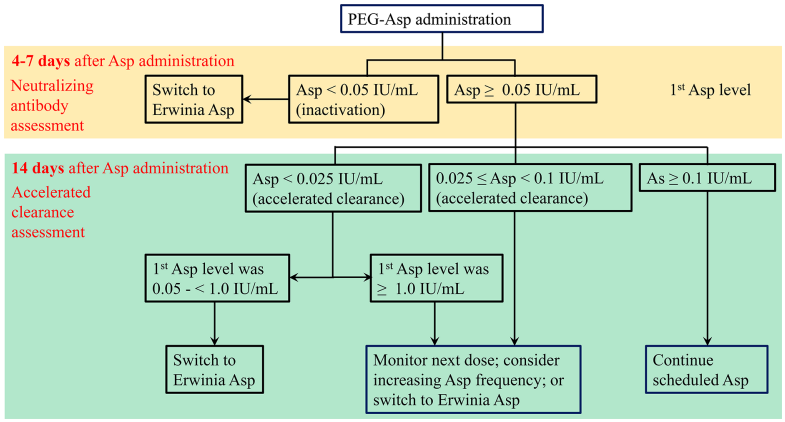


FIGURE 6
PEG-Asp activity monitoring algorithm for assessing possible silent inactivation by neutralizing antibodies and/or accelerated clearance (137).

do not change with increasing dose. This has been confirmed in practice. Kloons et al. conducted a trial to evaluate individualized dosing of PEG-Asp in pediatric ALL patients. They demonstrated that a median dose of 450 IU/m^2 PEG-Asp was enough to achieve adequate Asp activity levels and sufficient asparagine depletion, and that the reduced dose of PEG-Asp had similar toxicity to the standard dose of PEG-Asp (138). More importantly, the frequency of Asp treatment matters. As noted above, optimal therapeutic efficacy of Asp depends on complete and sustained depletion of serum asparagine. When used in combination with other cytotoxic agents, PEG-Asp is usually repeated every 3 weeks. However, approximately 20% of patients are unable to maintain adequate levels of Asp activity in the third week of each 3-week interval (136), so PEG-Asp should be repeated every two weeks if Asp activity levels are not monitored (139).

4.5 Best partner of Asp

It seems that it does not matter which drugs are combined with Asp in combination therapy. On the one hand, ENKTCL is intrinsically resistant to cytotoxic agents other than Asp. On the other hand, there is no evidence that one combination is more favorable than the other, regardless of toxicity. To date, two randomized controlled studies have comparatively evaluated PEG-Asp-based regimens for ENKTCL, and both obtained similar efficacy across treatment arms (Table 1). Huang et al. reported preliminary results of P-GemOx (PEG-Asp, gemcitabine, and oxaliplatin) + thalidomide *vs*. AspMetDex (PEG-Asp, methotrexate, and dexamethasone) at the 2019 ASH conference. They observed similar CR rates (60.0% *vs*. 55.0%), 3-year PFS and OS (detailed data not reported) between the two arms of 165 patients with newly diagnosed or R/R disease (143). Wei et al. compared SVILE (ifosfamide, PEG-Asp, vindesine, etoposide, and dexamethasone) with P-GemOx in 103 treatment-naïve patients. The CR rates after three cycles of CT (38.9% *vs*. 39.4% for early-stage disease, $P = 0.789$; 6.2% *vs*. 11.1% for advanced-stage disease, $P = 1.000$), 3-year PFS (88.3% *vs*. 93.9% for early-stage disease, $P = 0.469$; 46.2% *vs*. 65.7% for advanced-stage disease, $P = 0.703$), and 3-year OS (88.8% *vs*. 97.0% for early-stage disease, $P = 0.130$; 68.8% *vs*. 72.2% for advanced-stage disease, $P = 0.729$) were all similar between the two arms (69). In addition, Wang et al. treated 30 patients with PEG-Asp alone in a prospective phase 2 study. Two cycles of PEG-Asp were delivered concurrently with RT and 4 more cycles after RT. The results were excellent, with 2-year PFS of 90.9% and OS of 92.8% (67). Obviously, a more simplified regimen is more favorable when drug toxicity is considered. While this does not mean that those partners of the Asp scheme are of no values. A positive thought about Asp partners is that ENKTCL cells become sensitive to these partners when they are starved for asparagine deficiency following Asp administration. Based on the fact that aggressive chemotherapies result in higher toxicities rather than better efficacy, we can conclude that the highly toxic partners are unnecessary when combined with Asp. We suggest that more resource-consuming comparisons of Asp combination with different cytotoxic agents are unnecessary without the introduction of innovative concepts.

5 Staging methods for ENKTCL

Staging is very important for ENKTCL because of its solid cancer features: the majority of patients present with early-stage disease and RT is a curative treatment; the extent of local tumor invasiveness (LTI) is the strongest prognosticator in patients with early-stage disease (7, 31, 144). It is believed that RT alone is sufficient for patients with very early-stage disease. However, there is no consensus on how to define very early-stage disease. Future randomized controlled trials may answer this question, but an appropriate staging method is a prerequisite.

The Ann Arbor system is by far the conventional and most widely used staging method. This staging method was originally designed for Hodgkin lymphoma with predominantly lymph node involvement and does not take into account the extent of LTI. However, ENKTCL is exclusively an extranodal lymphoma. When used to assess localized ENKTCL, the Ann Arbor system fails to indicate the extent of LTI to guide treatment decisions. To compensate for the shortcomings of the Ann Arbor system, three ENKTCL-specified staging systems have been proposed.

Kim et al. proposed a Korea staging system in 2009 to classify ENKTCL into limited disease and extensive disease (141). However,

TABLE 1 Staging systems for ENKTCL.

Staging system	Staging rule	Advantage	Disadvantage
Ann Arbor (140)	Stage I, single extranodal lesion without nodal involvement; stage II, stage I or II nodal extent with limited contiguous extranodal involvement; stage IV, additional non-contiguous extranodal involvement	Easy to use	Stage I includes highly heterogenous disease due to varying extent of LTI
Korea (141)	Limited disease: Ann Arbor stage I/II UAT disease without LTI; extensive disease: Ann Arbor stage I/II UAT disease with LTI or stage III/IV UAT disease, and non-UAT disease.	Easy to use	Both limited and extensive diseases include highly heterogenous disease
TNM (7)	T stage is based on the anatomical structures involved; N stage is based on the extent of RLNM; all lesions beyond the UAT and regional lymph nodes are defined as M1.	Tumor burden and survival risk stratified well.	Only UAT disease is included; too complex and inconvenient for use
CA (142)	Stage I, confined to nasal cavity or nasopharynx without LTI and RLNM; stage II, non-UAT disease or UAT disease with LTI, without RLNM; stage III, disease with RLNM; stage IV, non-RLNM or disseminated disease	Easy to use; Stage I, III, and IV reflect tumor burden and survival risk well	Stage II includes heterogenous disease due to varying extent of LTI.

LTI, local tumor involvement; UAT, upper aerodigestive tract; RLNM, regional lymph node metastasis; CA, the Chinese Southwest Oncology Group and Asia Lymphoma Study Group.

for extensive disease, the prognosis and treatment strategies for Ann Arbor stage I/II disease with LTI and disseminated disease are obviously different. Further, for limited disease, the prognosis of Ann Arbor stage I disease is obviously different from that of Ann Arbor stage II disease. Given the solid cancer features of ENKTCL, we previously proposed a TNM (Tumor-Node-Metastasis) staging system (7). Obviously, locoregional disease is better stratified because this staging system is based solely on the extent of anatomical structures involved by the lymphoma. However, due to the complex anatomy of the UAT, this TNM staging system is too complex and inconvenient to use. Recently, the Chinese Southwest Oncology Group and the Asia Lymphoma Study Group (CA) proposed a staging method called the CA system. This method classifies Ann Arbor stage I disease into stage I or II based on the presence or absence of LTI, while stage III in CA system was identical to stage II in Ann Arbor system (142). A retrospective study comparing the CA system and the Ann Arbor system in 205 patients found that the CA system had better prognostic value than the Ann Arbor system (145). The CA system fully considers the prognostic value of both LTI and regional lymph node metastasis. Also, it is easy to use. However, CA stage II still includes a group of heterogeneous disease, as the extent of TLI varies greatly between patients, ranging from minimal to extensive infiltration around the UAT. Overall, among these staging methods (Table 2), the CA system is currently preferable, but the optimal staging method remains to be determined.

6 Treatment of early-stage ENKTCL

6.1 RT

The current National Comprehensive Cancer Network (NCCN) guidelines recommend combined chemoradiotherapy (CRT) for fit patients and RT alone for unfit patients with early-stage nasal ENKTCL. RT has an essential role in improved OS and PFS in patients with early-stage nasal ENKTCL (88, 146, 147). The 5-year OS rate in patients with early-stage disease treated with CT alone is only 12% to 45% (Figure 4) (4, 31, 32, 51, 59, 88, 91, 148). Emphatically, RT can't be omitted in patients who have achieved CR after induction CT. According to a multicenter study by the China Lymphoma Collaborative Group (CLCG), for Ann Arbor stage I/II ENKTCL patients who reached CR after Asp-based CT, the 5-year OS was 84.9% and 58.9% in patients with and without RT, respectively (149).

TABLE 2 Prospective randomized controlled studies in ENKTCL.

Author	Disease stage	Treatment modality	Arm	N	CR rate (%)	PFS (%)	OS (%)
Ma et al., 2009 (93)	I/II	CT-RT	CEOP	38	4CC: 21.1; ET: 94.4	2y: 65.8	2y: 73.3
			CEOP + semustine	37	4CC: 27.1; ET: 87.1	2y: 62.2	2y: 62.2
Wei et al., 2020 (69)	I/II	CT-RT-CT	SVILE	36	3CC: 38.9; ET: 83.4	3y: 88.3	3y: 88.8
			P-GemOx	33	3CC: 39.4; ET: 97.0	3y: 93.9	3y: 97.0
Zhang et al., 2021 (77)	I/II	RT alone	RT	35	ET: 48.6	5y: 56.5	5y: 60.4
		CT-RT	DDGP	30	ET: 73.3	5y: 82.9	5y: 85.7
Chai et al., 2022 (75)	I/II	RT-CT	GDP + chidamide	37	ET: 83.8	2y: 75.2; 5y: 67.5	2y: 89.2; 5y: 89.2
			GDP	37	ET: 78.4	2y: 70.2; 5y: 66.7	2y: 83.8; 5y: 81.0
Huang et al., 2019 (143)[a]	I-IV	CT-RT	P-GemOx + thalidomide	85	4CC: 60.0	3-y: 61.4[b]	3-y: 63.4[b]
			AspMetDex	80	4CC: 55.0		
Wei et al., 2020 (69)	III/IV	CT alone	SVILE	16	3CC: 6.2; ET: 68.8	3y: 46.2	3y: 68.8
			P-GemOx	18	3CC: 11.1; ET: 61.1	3y: 65.7	3y: 72.2
Wang et al., 2022 (130)	III/IV [c]	CT alone	DDGP	40	ET: 67.5	3y: 56.5	5y: 74.3
			SMILE	40	ET: 47.5	3y: 41.8	5y: 51.7

CR, complete response; PFS, progression-free survival; OS, overall survival; CT, chemotherapy; RT, radiotherapy; CEOP, cyclophosphamide, vincristine, etoposide, and prednisone; CC, cycles of chemotherapy; ET, end of treatment; SVILE, ifosfamide, PEG-Asp, vindesine, etoposide, and dexamethasone; P-GemOx, PEG-Asp, gemcitabine, and oxaliplatin; DDGP, PEG-Asp, gemcitabine, cisplatin and dexamethasone; GDP, gemcitabine, cisplatin, and dexamethasone; AspMetDex, PEG-Asp, methotrexate, and dexamethasone; SMILE, dexamethasone, methotrexate, ifosfamide, L-asparaginase, and etoposide.

[a]This was a multicenter randomized phase 2 trial. The analysis included 107 patents with newly diagnosed early-stage disease and 58 patients with advanced-stage or R/R disease. The CR rates were from patients with both early-stage and advanced-stage disease;

[b]The survival data were for the whole cohort. Separate data for each arm were not reported;

[c]This study adopted the CA staging system and included Ann Arbor stage II disease. PEG-Asp was used in the DDGP arm, while L-Asp in the SMILE arm.

During the early decades, patients receiving RT often had unsatisfactory outcomes due to the use of suboptimal radiation doses (34, 88). Patient outcomes did not improve significantly until the 1970s with the use of a higher dose of 50 Gy, which is recognized necessary to achieve long-term survival (88, 150). Modern RT for ENKTCL (including risk-adapted therapy, target volume, and dose guidelines) has been elaborately described by Qi et al. (151).

6.2 CT

In the Anth era, the 5-year OS was 47.3-83% in Ann Arbor stage I/II patients receiving RT alone (31–34, 37, 152–154) and 37.9-76% in those receiving combined CRT (29, 30, 32, 33, 37, 40, 46). There was no convincing evidence that adding CT to RT resulted in additional survival benefit (28, 30, 32, 33, 37, 40, 44, 152, 155, 156). However, this status has changed after the introduction of Asp. A randomized controlled study and a large cohort retrospective study both demonstrated the benefits of adding Asp-based CT. Zhang et al. randomized 65 patients with early-stage ENKTCL into RT alone group or DDGP (cisplatin, dexamethasone, PEG-Asp, and gemcitabine) followed by RT group. The 5-year PFS (56.5% *vs.* 82.9%, P = 0.023) and OS (60.4% *vs.* 85.7%, P = 0.040) were significant higher in the combined CRT group (Table 1) (77). Nevertheless, not all patients with early-stage disease can benefit from the addition of Asp-based CT. Zheng et al. evaluated the survival benefit of Asp-based *vs.* non-Asp-based CT plus RT in a retrospective cohort of 376 patients with early-stage ENKTCL. They stratified patients into low-, intermediate- and high-risk groups based on 5 clinical parameters (age > 60 years, stage II, elevated lactate dehydrogenase, poor performance status, and LTI), and found that Asp-based CT significantly improved 5-year OS in intermediate- and high-risk patients (84.4% *vs.* 74.5%, P = 0.014) (157). How to select patients who can benefit from the addition of Asp-based CT needs to be defined in randomized controlled studies. The survival trends in patient with early-stage ENKTCL treated with different types of CT are showed in Figure 5.

Another unanswered issue about CT is that how many CT courses are needed for early-stage ENKTCL. As shown in Table 3, most studies used 3 to 6 cycles of CT, and there is no evidence that short-course CT is inferior to long-course CT. A short-course of two cycles of modified SMILE CT and sequential RT in 18 cases with early-stage ENKTCL at the Memorial Sloan Kettering Cancer Center showed a post-CT CR rate of 67% and a 5-year OS of 83.3% (162). The outcomes were similar to studies with long-course CT. The optimal number of CT courses needs to be determined in randomized controlled studies.

6.3 Combined modality treatment of CT and RT

There are 3 combined modalities of CT and RT for early-stage ENKTCL: sequential method (CT followed by RT, or RT followed by CT), sandwich method (CT before and after RT), and concurrent method (CT during the period of RT). There is no available evidence showing which modality is more preferable at the moment. The sequential and sandwich methods are mainly used in China, while concurrent method is mainly used in Japan and Korea. The development of sequential and sandwich modalities in the early days was based on the understanding that this aggressive tumor requires aggressive CT, which would not be tolerated when administered concurrently with RT.

In the Anth era, early disease progression frequently occurred in patients treated with induction CT due to resistance, so the importance of upfront RT was emphasized (57, 80, 163). However, increased risk of systemic relapse was also observed in patients receiving upfront RT (59). In the current Asp era, early disease progression is not a big concern as most patients are sensitive to Asp-based treatment. Two multicenter retrospective studies of large cohorts evaluated how the sequence of CT and RT affects outcomes of patients treated primarily with Asp-based CT. Based on data from 1,360 patients, the China Lymphoma Collaborative Group Study found that patients treated with CT followed by RT had similar survival to those treated with RT followed by CT (164). Kwong et al. compared sequential CRT *vs.* concurrent CRT in 303 cases and observed similar survival as well (165). The optimal sequence of CT and RT needs to be defined in randomized controlled studies.

In today's view, aggressive CT is unnecessary for ENKTCL. Mild regimens, such as P-GemOx (GELOX) and DDGP, have equal or better efficacy and a more favorable safety profile than aggressive regimens (50, 69, 70, 130, 143). Given the trend towards more simplified CT, the feasibility of concurrent CRT should be reevaluated. Recent studies have showed that Asp alone or Asp combined with immunotherapy also yielded excellent efficacy in patients with early-stage ENKTCL when combined with RT (27, 67). These studies, although using small sample sizes, suggest that more simplified, more effective, and less toxic regimens are feasible.

6.4 Anti-PD-1/PD-L1 immunotherapy

Given the high activity in advanced-stage ENKTCL, anti-PD-1/PD-L1 immunotherapy is being tried in early-stage disease. Sun et al. recently reported the results of a retrospective study of early-stage ENKTCL treated with PEG-Asp combined with a PD-1 inhibitor, anlotinib (a multi-tyrosine kinase inhibitor approved in China for lung cancer), and sequential RT. Patient outcomes were excellent, with 100% 3-year PFS and OS, but a limitation of the study was that only 8 patients were included (27). The role of anlotinib in this combination was unknown, but the combination of the two most powerful ENKTCL drugs (PEG-Asp and PD-1 inhibitor) deserves further investigation in more patients. A phase 2 trial of this regimen is pending (NCT03936452), and a phase 3 randomized controlled trial of PEG-Asp-based CRT with or without PD-1 blockade therapy in early-stage ENKTCL is ongoing (NCT04365036). Several studies are currently underway to examine the efficacy of more simplified immunotherapy-based treatment approaches in patients with early-stage ENKTCL: PD-1 inhibitor and PEG-Asp combined with RT (NCT04676789), PD-1 inhibitor, PEG-Asp, and chidamide combined with RT (NCT04414969), PD-1 inhibitor monotherapy (NCT03728972), and PD-1 inhibitor concurrently with RT (NCT04417166, NCT05477264, and NCT05149170).

TABLE 3 Single arm prospective studies in NKTCL.

Author	Disease status	N	Asp	CT regimen used	Treatment modality	Courses of CT	CR rate (%)	PFS (%)	OS (%)
Lee et al., 2006 (35)	Stage I/II	16		IMEP	CT-RT	6	6CC: 69.0; ET: 81	–	3y: 80.4
Kim et al., 2009 (42)	Stage I/II	30		VIPD	CCRT-CT	Weekly DDP + 3	ET: 80	3y: 85.2	3y: 86.3
Yamaguchi et al., 2009 (95, 96)	Stage I/II	33		DeVIC	CCRT	3	ET: 75.0	2y: 67.0 5y: 67.0	2y: 78.0 5y: 73.0
Jiang et al., 2012 (45, 97)	Stage I/II	26	L-Asp	LVP	CT-RT-CT	2 + (2–4)	2CC: 42.3; ET: 80.8	2y: 80.6 5y: 64.0	2y: 88.5 5y: 64.0
Aviles et al., 2013 (51)	Stage I/II	202		CMED	RT-CT	6	ET: 91.0	–	5y: 86.0
Lin et al., 2013 (49)	Stage I/II	31	L-Asp	CHOP	CT-RT	6	4CC: 71.5; ET: 81.6	2y: 81.0	2y: 80.1
Wang et al., 2013 (50)	Stage I/II	27	L/P-Asp	GELOX	CT-RT	2 + 4	2CC: 55.6; ET: 74.1	2y: 86.0	2y: 86.0
Ke et al., 2014 (52)	Stage I/II	32		GDP	CCRT-CT	Weekly DDP + 3	ET: 84.4	3y: 84.4	3y: 87.5
Kim et al., 2014 (54)	Stage I/II	44		IMEP	CT-RT	6	6CC: 27.0; ET: 67.0	3y: 56.0	3y: 66.0
Kim et al., 2014 (53)	Stage I/II	30	L-Asp	IMEP	CCRT-CT	weekly DDP + 2	ET: 87.0	5y: 60.0	5y: 73.0
Tsai et al., 2015 (55)	Stage I/II	33		DVIP	CCRT-CT	2 DEP + 2	ET: 42.0	2y: 64.0 5y: 60.0	2y: 73.0 5y: 66.0
Yoon et al., 2016 (61)	Stage I/II	28	L-Asp	IMEP	CCRT-CT	Weekly DDP + 2	ET: 82.1	3y: 74.1	3y: 81.5
Jiang et al., 2017 (62)	Stage I/II	66	L-Asp	DEP	CT-CCRT-CT	2 + 2 DDP + 2	ET: 83.3	3y: 67.4	3y: 70.1
Xu et al., 2017 (63)	Stage I/II	40	P-Asp	MESA	CT-RT-CT	2 + 2	2CC: 71.1; ET: 89.5	2y: 89.1	2y: 92.0
Qi et al., 2018 (64)	Stage I/II	40		GDP	RT-CT	4	ET: 95.0	2y: 84.7 5y: 79.4	2y: 89.9 5y: 82.1
Zheng et al., 2018 (65)	Stage I/II	21	P-Asp	CHOP	RT-CT	6	ET: 90.5	–	3y: 80.5
Liu et al., 2020 (66)	Stage I/II	30	P-Asp	DICE	RT-CT	3	ET: 96.7	5y: 86.0	5y: 87.0
Wang et al., 2020 (67)	Stage I/II	30	P-Asp	P-Asp alone	CCRT-CT	2 + 4	ET: 100	2y: 90.9	2y: 92.8
Wei et al., 2020 (68)	Stage I/II	26	P-Asp	GDP -ML	CT-RT-CT	2 + 2	ET: 76.9	–	2y: 88.1
Zhu et al., 2020 (70)	Stage I/II	30	P-Asp	GDP	CCRT-CT	Weekly DDP + 3	ET: 93.3	5y: 89.4	5y: 93.3
Zhang et al., 2021 (71)	Stage I/II	81	L-Asp[!]	DICE	CT-RT	4	4CC: 11.1; ET: 84.0	5y: 63.4	5y: 82.4
Hu et al., 2022 (72)	Stage I/II	64	P-Asp	COEPL	CT-CCRT-CT	2 + 2 (VLP) + 2	ET: 82.0	3y: 78.1	3y: 81.2
Wang et al., 2022 (73)	Stage I/II	31	P-Asp	GAD-M	CT-RT-CT	(2–4) + (4–2)	2CC: 54.8; ET: 90.3	3y: 80.4 3y: 80.6	3y: 77.0 5y: 80.6
Zhu et al., 2022 (74)	Stage I/II	52	P-Asp	GELAD	CT-RT-CT	2 + 2	2CC: 46.2; ET: 92.3	2y: 90.4 4y: 90.4	2y: 94.2 4y: 94.2
Lee et al., 2006 (35)	Stage III/IV	8		IMEP	CT alone		13.0	–	mOS: 2.7m 3y: 30%
Kim et al., 2009 (99)	R/R	32		IMEP	CT alone		37.5	mTTF: 3.7m	mOS: 8.2m 5y: 24.8

(Continued)

TABLE 3 Continued

Author	Disease status	N	Asp	CT regimen used	Treatment modality	Courses of CT	CR rate (%)	PFS (%)	OS (%)
Jaccard et al., 2011 (100)	R/R	19	L-Asp	AspMetDex	CT-RT/HSCT		61.0	mPFS: 12.2m	mOS: 12.2m
Yamaguchi et al., 2011 (101)	Stage IV/R/R	38	L-Asp	SMILE	CT-HSCT (allo/auto)		45.0	1y: 53	1y: 55
Shi et al., 2015 (158)	R/R	16		Chidamide			6.0	–	–
Zheng et al., 2018 (65)	Stage III/IV	12	P-Asp	CHOP	CT alone		50.0	–	–
Wei et al., 2020 (68)	Stage III/IV	18	P-Asp	GDP-ML	CT-HSCT (auto)		33.3	2y: 33.2	2y: 35.6
Kim et al., 2020 (159)	R/R	21		Avelumab			24.0	mPFS: 2.7m	–
Song et al., 2021 (114)	Stage III/IV	27	L-Asp	VIDL	CT-HSCT (auto)		63.0	mPFS: 13.2m	mOS: 27.0m
Hu et al., 2022 (72)	Stage III/IV	16	P-Asp	COEP	CT-HSCT (auto)		55.6	3y: 45.7	3y: 48.1
Gao et al., 2020 (160)	Asp-R	37		Sintilimab + chidamide			44.4	1y: 66.0	1y: 79.1
Huang et al., 2021 (161)	Asp-R	32		Daratumumab			0	mPFS: 53.0d	mOS: 141.0d
Tao et al., 2021 (111)	Asp-R	28		Sintilimab			21.4	–	1y: 82.1 2y: 78.6
Huang et a. 2022 (98)	Asp-R	78		GEMSTONE-201			37.2		2y: 54.6

IMEP, ifosfamide, methotrexate, etoposide, and prednisone; DDP, cisplatin; VIPD, etoposide, ifosfamide, dexamethasone, and cisplatin; DeVIC, dexamethasone, etoposide, ifosfamide, and carboplatin; LVP, L-Asp, vincristine, and prednisone; GELOX, gemcitabine, L/P-Asp, and oxaliplatin; DICE, dexamethasone, ifosfamide, etoposide, and cisplatin; DEP, dexamethasone, etoposide, and cisplatin; DVIP, dexamethasone, etoposide, ifosfamide, and cisplatin; MESA, methotrexate, etoposide, dexamethasone, and PEG-Asp; CMED, cyclophosphamide, methotrexate, etoposide, and dexamethasone; SMILE, dexamethasone, methotrexate, ifosfamide, L-asparaginase, and etoposide; AspMetDex, L-asparaginase, methotrexate, and dexamethasone; HSCT, hematopoietic stem cell transplantation; DICE, dexamethasone, ifosfamide, cisplatin, and etoposide; GDP-ML, gemcitabine, dexamethasone, cisplatin, methotrexate, and PEG-Asp; COEPL, cyclophosphamide, vincristine, etoposide, prednisone, and P-Asp; VLP, vincristine, pegaspargase, and prednisone; GAD-M, gemcitabine, PEG-Asp, dexamethasone, and methotrexate; GELAD, gemcitabine, etoposide, PEG-Asp, dexamethasone; VIDL, etoposide, ifosfamide, dexamethasone, and L-Asp; Asp-R, asparaginase-resistant. ! L-ASP was delivered on d1-4.

7 Treatment of advanced-stage and R/R ENKTCL

7.1 CT

The survival of patients with advanced-stage ENKTCL is extremely poor. The current NCCN guidelines recommend Asp-based CT for advanced-staged disease. As shown in Figure 3, the CR rate of patients treated with Asp-absent CT (including Anth- and non-Anth-based CT) ranged from 13.0% to 37.5%, and the 5-year OS ranged from 16.7% to 30.0%. The efficacy of Asp-based CT is better than that of Asp-absent CT, but it is still unsatisfactory. In a prospective cohort study of the International T-cell Project, including 166 patients from 40 centers in 14 countries across four continents (Asia, Europe, North America, and South America), the median OS was only 10 months (4). As in early-stage disease, aggressive CT in advanced-stage disease may result in greater toxicity rather than greater efficacy (166). The median OS was several months as well in patients treated with SMILE or modified SMILE regimen and hematopoietic stem cell transplantation (HSCT) (162, 167). Patients with relapsed disease after front-line treatment had even worse survival. A multicenter retrospective study analyzing 179 patients with R/R ENKTCL from four countries found a median second OS of 6.4 months after relapse (168). Patients with extranasal ENKTCL had similar survival to those with advanced-stage nasal ENKTCL. The median OS was 2.83 to 9 months for gastrointestinal ENKTCL (169–172), 9.5 months for testicular disease (173), and 15.5 to 29 months for cutaneous ENKTCL (174, 175). These data indicate that extranasal ENKTCL should be managed like advanced-stage nasal ENKTCL.

7.2 HSCT

The role of HSCT in the treatment of ENKTCL is controversial. Auto-HSCT did not lead to better outcomes compared to Asp-based CT (176, 177). Several small cohort retrospective studies have evaluated the efficacy of allo-HSCT in patients with advanced-stage ENKTCL. A Japanese study of 28 patients (22 with NKTCL, 3 with blastic NK-cell lymphoma, and 3 with aggressive NK-cell leukemia) concluded that 2-year PFS and OS were 34% and 40%, respectively (178). In another study of 12 patients, 7 cases survived in remission with a median follow-up of 13 months (179). After investigating 18 patients with advanced-stage or R/R ENKTCL who underwent allo-HSCT, a multicenter study by the Asia Lymphoma Study Group observed 5-year PFS and OS of 51% and 57%, respectively (180). In a non-Asian cohort with 27 patients undergoing HSCT (14 with auto-HSCT and 13 with allo-HSCT), the 3-year OS was 64% for consolidative auto-HSCT in first-line treatment and 39% for allo-HSCT in salvage treatment (181). These data seem encouraging, but

there was patient selection bias in these studies, as patients who received HSCT generally had favorable performance status and good response to previous treatment. Besides, it may not be better than Asp-based CT (Figure 3). There is no doubt that HSCT will move to late-line treatment with the increasing number of novel drugs today.

7.3 RT

Given the sensitivity of ENKTCL to RT, RT is used in selected patients with advanced-stage disease. According to the International T-cell Project, patients with advanced-stage disease receiving combined CRT had significantly better survival than those receiving CT alone (3-year OS, 66% *vs*. 24%; 5-year OS, 58% *vs*. 24%; both Ps < 0.001) (4). However, there was clearly a selection bias. Patients who received RT inevitably had lower tumor burden and better response to induction CT than those who did not receive RT. Nevertheless, it is suggested that RT can be delivered to selected patients with oligometastases.

7.4 Anti-PD-1/PD-L1 immunotherapy

The positive rate of PD-L1 in ENKTCL cells is 39-100% (8). Overexpression of PD-L1 induced by EBV infection, on the one hand, is a potential mechanism by which ENKTCL avoids immune surveillance (182, 183), on the other hand, is a predictor of favorable response to PD-1 blockade treatment (159, 160). Kwong et al. first reported that PD-1 blockade was highly active in R/R ENKTCL in a series of 7 cases (26). Its outstanding efficacy was subsequently confirmed in clinical trials. In a phase 2 study, 28 patients with Asp-resistant ENKTCL were treated with the PD-1 inhibitor sintilimab. The CR rate and objective response rate (ORR) were 21.4% and 75%, respectively, and the 2-year OS was 78.6% (111). In another phase 2 trial of 78 cases with Asp-resistant ENKTCL treated with the anti-PD-L1 antibody sugemalimab, the CR was 37.2% and the 2-year OS was 54.6% (98). Clearly, the median second OS was > 2 years in both trials. The current NCCN guidelines recommend anti-PD-1 immunotherapy for Asp-resistant R/R ENKTCL. Promising results have also been observed in patients treated with immunotherapy combined with small molecule targeted drugs, such as histone deacetylase inhibitors (HDACi) (160, 184, 185). The combination of PD-1 inhibitor and HDACi chidamide was evaluated in a prospective phase Ib/II study in patients with Asp-resistant ENKTCL. The preliminary analysis of 37 cases showed that the CR rate, 1-year PFS, and OS was 44.4%, 66.0%, and 79.1%, respectively (160). The combined treatment showed activity even in patients with immunotherapy-resistant lymphoma, as HDACi also has immunomodulatory effects beyond anticancer effect (185, 186). Clinical trials investigating the efficacy of PD-1 blockade combined with a DNA demethylating inhibitor (DNMTi) (NCT04279379) or anti-CD38 antibody (NCT04763616) in R/R ENKTCL are ongoing.

Due to its high activity, immunotherapy has recently been used in the front-line treatment of advanced-stage disease. Cai et al. treated 9 newly diagnosed stage III/IV ENKTCL cases using a PD-1 inhibitor in combination with the P-GemOx regimen. The CR rate, 1-year PFS, and OS was 77.8%, 66.7%, and 100%, respectively (109). Although a small cohort retrospective study, it suggests that the combination of the two most powerful drugs (PEG-Asp and PD-1 blockade) may be a good option for front-line therapy of advanced-stage ENKTCL, and that aggressive CT may not be necessary in the modern era. Additional results of a prospective study (NCT04127227) of this combination treatment are pending. A more simplified regimen combing PD-1 blockade and PEG-Asp is currently being tested in prospective trials (NCT04096690 and NCT04004572) in patients with newly diagnosed advanced-stage ENKTCL.

7.5 Other immunotherapies

ENKTCL patients are universally EBV positive, making the viral protein latent membrane proteins (LMP) interesting treatment targets. LMP-targeted therapy has shown encouraging activity in several studies. In a phase 2 study, Kim et al. created autologous EBV-specific T cells in 47 patients with advanced-stage or R/R ENKTCL. The CR rate was 30% in 10 R/R patients receiving the cell therapy (187). Bollard et al. treated 29 patients with EBV-related lymphoma using LMP-specific cytotoxic T lymphocytes (CTL). The results showed that 11 of 21 patients with R/R disease achieved CR at the time of CTL infusion (188). Cho et al. treated 13 patients (11 early-stage patients and 2 advanced-stage patients) with EBV LMP-specific CTL cells when CR was achieved following CT, RT, and/or HSCT. The 4-year OS and PFS were 100% and 90%, respectively (189). Ando et al. developed an EBV-induced pluripotent stem cell (iPSC)-derived LMP-specific CTL that exhibited robust ENKTCL suppressive effects *in vitro* and *in vivo* (190). More clinical trials of EBV-targeted T cell therapy are underway (NCT03789617 and NCT03671850).

A subset of ENKTCL cells express CD30 and CD38, both of which have available targeted drugs. The anti-CD30 antibody conjugate brentuximab vedotin (BV) has been reported to be effective in individual cases (191, 192). In a BV phase 2 study of 33 patients with R/R CD30-positive non-Hodgkin lymphoma, 7 had ENKTCL. One ENKTCL patient achieved CR and another ENKTCL patient achieved partial response (PR) (193). The current NCCN guidelines recommend BV monotherapy for Asp-resistant R/R ENKTCL. The combination of BV with PD-1 inhibition (NCT05316246) and anti-CD30 CAR-T therapy (NCT04952584, NCT04008394, and NCT04526834) are currently under investigation in patients with CD30+ R/R lymphocyte malignancies. The anti-CD38 antibody daratumumab has been examined in a phase 2 study in patients with R/R ENKTCL with an ORR of 25% and a median PFS of 53 days (161) (Table 3). Zhang et al. screened a panel of biomarkers (B7-H3, CD70, TIM-3, VISTA, ICAM-1, and PD-1) in NKTCL cell lines and found that B7-H3 (CD276) was highly and homogeneously expressed in these cells. Therefore, they constructed a novel anti-B7-H3/CD3 bispecific T-cell engaging antibody and B7-H3-redirected CAR-T cells, both of which showed antitumor activity *in vitro* and *in vivo* (194). CD7 is positive in 84.8% of patients with ENKTCL. In a recently reported phase 1 stage study of 20 cases with CD7-positive R/R T-ALL or T-cell lymphoblastic lymphoma, 19 patients achieved bone marrow CR and 5 achieved extramedullary CR (195). A prospective trial of anti-CD7 CAR-T cell therapy in CD7-positive T-cell lymphoma (including ENKTCL) is ongoing (NCT04004637).

ENKTCL is an IL-2-dependent cancer (196). The binding of IL-2 to IL2α (CD25) exerts pro-inflammatory effects and promotes lymphomagenesis and drug resistance (197, 198). Therefore, blocking IL2-CD25 binding is a potential therapeutic strategy. Wang et al. have launched a prospective trial after reporting a R/R ENKTCL patient who responded well to anti-CD25 antibody therapy (NCT04337593).

Among these immunotherapies under investigation, anti-LMP CAR-T therapy or EBV-specific T cell therapy might be the most promising treatment.

7.6 Small molecule drugs

Epigenetic modifiers, including *MLL2*, *MLL3*, *BCOR*, *TET2*, *EP300*, and *ARID1A*, are mutated in about 24.8% of cases with ENKTCL (9). Accordingly, epigenetic regulation is an important treatment strategy for this disease. The HDACi chidamide has been approved in China for the treatment of R/R PTCL, including ENKTCL. In a phase 2 study of chidamide in patients with R/R PTCL, the CR rate was 6% in 16 patients with ENKTCL (158). When two additional real world studies were included, the pooled CR rate was 16% (ORR 38%), involving a total of 115 R/R ENKTCL patients (158, 199, 200). Romidepsin and belinostat are HDAC inhibitors used in western countries. The current NCCN guidelines recommend HDACi for Asp-resistant R/R ENKTCL. The DNMTi azacytidine and decitabine are being actively tested in combination treatment in patients with R/R ENKTCL (NCT04899414 and NCT04279379). Moreover, common genetic aberrations (18.2%) in ENKTCL involve genes related to the JAK-STAT pathway (*JAK3*, *JAK2*, *STAT3*, *STAT5B*, *SOCS1*, and *PTPRK*). *JAK* or *STAT* activating mutations lead to constitutive activation of the JAK-SATAT pathway, which plays a major role in ENKTCL cell growth and survival (9, 201). These findings make JAK an interesting target for the treatment of ENKTC. The efficacy of JAK inhibitor in R/R T- and NK-cell lymphoma is currently under investigation (NCT02974647). Mutations in genes associated with the RAS-MAPK pathway (*MAP3Ks*, *BRAF*, and *EPH1A*) occur in 14.4% of ENKTCL cases (9). Alisertib, which targets aurora kinase A, a downstream molecule of MAPK, has been used in 5 cases of R/R ENKTCL as part of two studies, but only one patient achieved PR (202, 203). XPO1 is a promising target for the treatment of both hematological and non-hematological cancers (204, 205). Preliminary results from a phase Ib study of the XPO1 inhibitor ATG-010 plus CT in heavily pretreated patients with R/R PTCL and ENKTCL have been reported at the 2021 ASH meeting. ORR and CR were observed in 3 and 2 of the 5 ENKTCL cases analyzed, respectively (206). The final results of this trial are pending (NCT04425070). PI3K inhibitors (PI3Ki) have demonstrated encouraging activity in R/R PTCL patients in multiple trials (207–209). Currently, several trials are assessing the efficacy and safety of PI3Ki combined with HDACi or other agents in patient with R/R PTCL, including ENKTCL (NCT05083208, NCT04774068, and NCT04639843). The above-mentioned targeted therapies are illustrated in Figure 7. In addition, deregulation of apoptosis through *TP53* mutations provides a further growth advantage for this disease (210). Targeting the TP53-MDM2 interaction is also a potential treatment approach. MDM2 inhibitors are currently being tested intensely in various cancers, including lymphomas (211). To date, small molecule drugs, including HDACi, JAK inhibitor, aurora kinase A inhibitor, only demonstrated mild efficacy in T/NK-cell lymphomas. PI3Ki showed higher response rates than these drugs, but only limited data exist and long-term

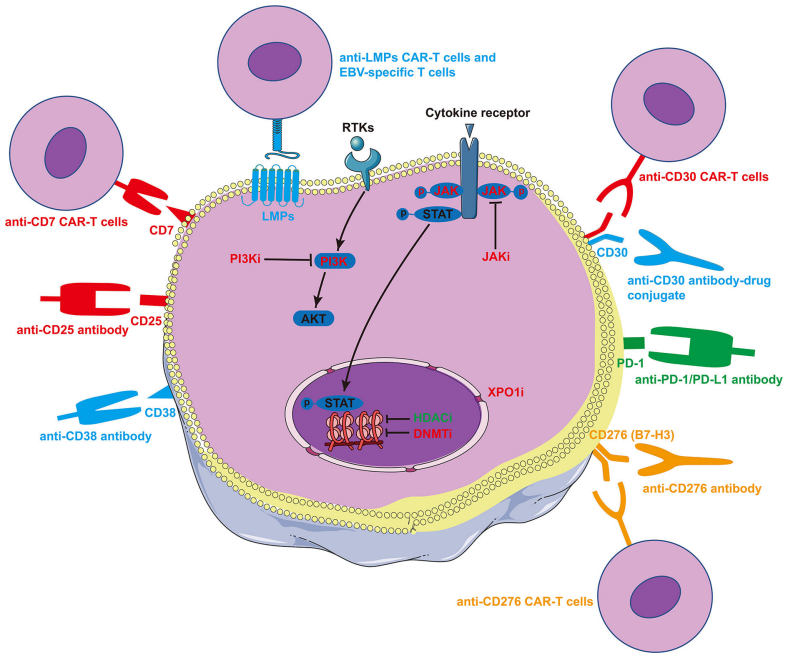


FIGURE 7
Schematic illustration of targeted therapies in ENKTCL. Green indicates that the targeted therapies have been widely used in practice; cyan indicates that the therapies are being investigated in early-stage clinical trials; orange indicates that the therapies have shown activity in animal models; and red indicates that the therapies are currently under investigation in clinical trials.

efficacy still need to be observed. At present and in the near future, these drugs might be choices in late line treatment or as partner drugs in combined treatment for ENKTCL.

8 Biomarkers for treatment decision making

8.1 Predictive markers

Biomarker-driven individualized and precision treatment is the way toward better efficacy, lower toxicity, and higher cost-performance. The genetic landscapes of ENKTCL have been described in several studies with relatively large sample sizes in recent years. *DDX3X*, *TP53*, *BCOR*, *STAT3*, and *MLL2* are the most commonly mutated genes that act as tumor suppressors or epigenetic modifiers or participate in signaling pathways (JAK-STAT, NF-κB, and RAS-MAPK) (8, 212–215). *TP53* mutation was identified as an adverse prognosticator in two studies (212, 214) and *DDX3X* in one study (212), but the predictive value of these genes was inconsistently reported in others (213, 215).

PD-L1 rearrangement is a marker of response to PD-1 blockade treatment. Lim et al. sequenced tumor samples from 19 R/R ENKTCL patients treated with the PD-1 inhibitor pembrolizumab. All 4 cases with complete and durable responses harbored *PD-L1* rearrangement, while all 10 non-responders were wild-type *PD-L1*. Clearly, *PD-L1* rearrangement is 100% specific in identifying responders to immunotherapy. In this study, PD-L1 expression levels were not associated with clinical response (216). However, higher PD-L1 expression levels did correlate with better immunotherapy response in two prospective studies (159, 160). The predictive value of *PD-L1* rearrangement on clinical response needs to be verified in more patients.

8.2. Molecular subtypes of ENKTCL

Molecular subtyping may help identify patients more likely to benefit from a specific treatment. The following three studies explored the molecular subtyping of ENKTCL and are summarized in Table 4. Xiong et al. proposed a molecular subtyping scheme based on an integrated analysis of the genomic and transcriptomic features of ENKTCL. Patients were classified into three subtypes: HEA subtype, enriched in T cell gene expression and mutations in epigenetic regulators (*EP300*, *HDAC9*, and *ARID1A*); TSIM subtype, characterized by aberrations in tumor suppressors (*TP53* mutation and del6q21) and immune modulators (JAK-STAT mutation/amplification and amp9p24.1/PD-L1/L2 locus); and MB subtype, enriched in *MYC*-associated aberrations, mainly *MGA* mutations, and loss of heterozygosity (LOH) at the *BRDT* locus. This subtyping scheme has prognostic value in patients with advanced-stage disease and may have value in individualized treatment decision-making (213). Dong et al. classified ENKTCL as C1 to C7 based on genome-wide mutation and genomic copy number alteration analysis.

TABLE 4 Molecular subtyping schemes of ENKTCL published in recent years.

Author	Subtype	Representative genomic alterations or immune characteristics	Prognosis	Potentially effective treatment
Xiong et al. (213)	HEA	Mutations in *HDAC9*, *EP300*, and *ARID1A*	Good	HDAC inhibitor
	TSIM	Mutations in JAK-STAT pathway and *TP53*, amp*JAK2* locus; amp17q21.2/*STAT3*/*5B*/*5A* locus, amp9p24.1/*PD-L1/2* locus, del6q21	Intermediate	PD-1 blockade
	MB	*MGA* mutation, 1p22.1/*BRDT* LOH	Poor	MYC inhibition
Dong et al. (214)	C1	Higher CN complexity including gains and losses of 17q21(*STAT3*), 8q24(*MYC*), and del19q	Intermediate	-
	C2	*KMT2D* mutation and chr2 gain	Intermediate	-
	C3	*NOTCH2* mutation and del17p	Intermediate	-
	C4	*DDX3X* mutation and del1p36	Intermediate	-
	C5	CN gain of chr19q/q13 and *JAK3* gain	Good	-
	C6	Aberrations in RAS/RAF/MAPK pathway, *JAK3*, *BCOR*, and *TP53*	Poor	-
	C7	*TET2* loss and *ARID1B* mutation	Good	-
Lim et al. (215)	GPM	Mutations in *BCOR*, *JAK3*, *KRAS*, *MYH11*, *DCC*, *ITK*, *NOTCH1*, *FAS*, *RET*, *BIRC3*, *MLLT1*, *LRP1B*, *NRG1*	Poor	-
Cho et al. (217)	Immune tolerance	High-Treg counts (> 500/HPF)	Good	Good response to PD-1 blockage
	Immune evasion-A	High cytotoxic T-cell counts, high PD-L1 expression, low Treg counts (PD-L1 > 10%)	Intermediate	Intermediate response to PD-1 blockage
	Immune evasion-B	Not otherwise specified	Intermediate	Intermediate response to PD-1 blockage
	Immune silenced	Immune response exhausted (Process-type CD68 > 90%)	Poor	Poor to PD-1 blockage

According to this classification, patients in C5 and C7 have a good prognosis, while patients in C6 have the worst prognosis (214). Lim et al. generated a genomic prognostic model (GPM) based on next-generation sequence of 260 ENKTCL tumors in which mutations in 13 genes (*BCOR*, *JAK3*, *KRAS*, *MYH11*, *DCC*, *ITK*, *NOTCH1*, *FAS*, *RET*, *BIRC3*, *MLLT1*, *LRP1B*, and *NRG1*) were associated with poorer survival. The representative genomic alterations and prognostic values of subtypes vary largely among these studies. This discrepancy is at least partially attributable to the inclusion of patients with heterogeneous disease status (mixed early-stage and advanced-stage disease) and treatments. Future subtyping studies should be conducted in patients receiving homogeneous treatment.

In addition, Cho et al. developed an immune subtyping model that classifies ENKTCL into four tumor immune microenvironment subgroups using three immunohistochemical markers, FOXP3, PD-L1, and CD68. The four subgroups were named immune tolerance, immune evasion-A, immune evasion-B, and immune silenced. The response rate to pembrolizumab was 100% (1/1) in the immune tolerance group, 60% (3/5) in the immune evasion group, and 0 (0/5) in the immune-silenced group (217). This subtyping method may guide immunotherapy but needs to be verified in more patients.

9 Conclusions

Survival of ENKTCL patients has improved significantly in the past two decades, mainly due to the great advances in RT technology and the introduction of Asp and anti-PD-/PD-L1 immunotherapy. RT is essential for early-stage disease. Asp-based CT benefits a proportion of patients with early-stage disease. Asp and PD-1/PD-L1 inhibitors are milestones in advanced-stage disease treatment. Their combination can further improve patient outcomes. The efficacy of Asp could be optimized by individualized administration. In the treatment of both early-stage and advanced-stage diseases, there is a trend toward more simplified regimens, less toxicity, and higher efficacy. Relevant clinical trials are currently underway. Small molecule inhibitors, monoclonal antibodies, and manufactured T cell therapies are under intensive investigation. EBV-targeted T cell therapies might be the most promising new treatment in the near future. In the future, there is no need to spend more resources comparing different combinations of Asp with cytotoxic agents. Instead, more efforts should be made to optimize the use of Asp and immunotherapy to maximize efficacy and minimize toxicity, explore ways to overcome resistance to Asp and immunotherapy, determine the optimal combination therapy of CT and RT, identify novel treatment targets, and define subpopulations who may benefit more from specific treatments.

Author contributions

ZY, ZHY and YL: conceptualization and methodology. ZY and SY: data curation and formal analysis. ZW and WZ: software and visualization. ZY: original draft. YL and ZHY: supervision, project administration, review and editing. All authors contributed to the article and approved the submitted version.

Conflict of interest

The authors declare that the research was conducted in the absence of any commercial or financial relationships that could be construed as a potential conflict of interest.

Publisher's note

All claims expressed in this article are solely those of the authors and do not necessarily represent those of their affiliated organizations, or those of the publisher, the editors and the reviewers. Any product that may be evaluated in this article, or claim that may be made by its manufacturer, is not guaranteed or endorsed by the publisher.

References

1. Yoon SE, Song Y, Kim SJ, Yoon DH, Chen TY, Koh Y, et al. Comprehensive analysis of peripheral T-cell and natural killer/T-cell lymphoma in Asian patients: A multinational, multicenter, prospective registry study in Asia. *Lancet Reg Health West Pac* (2021) 10:100126. doi: 10.1016/j.lanwpc.2021.100126

2. Aviles A. Nasal NK/T-cell lymphoma. a comparative analysis of a Mexican population with the other populations of Latin-America. *Mediterr J Hematol Infect Dis* (2015) 7(1):e2015052. doi: 10.4084/MJHID.2015.052

3. Hernandez-Ruiz E, Alvarado-Ibarra M, Juan Lien-Chang LE, Banda-Garcia L, Aquino-Salgado JL, Barragan-Ibanez G, et al. Epidemiology and clinical characteristics of non-Hodgkin lymphoma in Mexico. *World J Oncol* (2021) 12(1):28–33. doi: 10.14740/wjon1351

4. Fox CP, Civallero M, Ko YH, Manni M, Skrypets T, Pileri S, et al. Survival outcomes of patients with extranodal natural-killer T-cell lymphoma: a prospective cohort study from the international T-cell project. *Lancet Haematol* (2020) 7(4):e284–e94. doi: 10.1016/S2352-3026(19)30283-2

5. Yang Y, Wang Y, Liu X, He X, Zhang LL, Wu G, et al. Progression-free survival at 24 months and subsequent survival of patients with extranodal NK/T-cell lymphoma: a China lymphoma collaborative group (CLCG) study. *Leukemia* (2021) 35(6):1671–82. doi: 10.1038/s41375-020-01042-y

6. Kim TM, Lee SY, Jeon YK, Ryoo BY, Cho GJ, Hong YS, et al. Clinical heterogeneity of extranodal NK/T-cell lymphoma, nasal type: a national survey of the Korean cancer study group. *Ann Oncol* (2008) 19(8):1477–84. doi: 10.1093/annonc/mdn147

7. Yan Z, Huang HQ, Wang XX, Gao Y, Zhang YJ, Bai B, et al. A TNM staging system for nasal NK/T-cell lymphoma. *PloS One* (2015) 10(6):e0130984. doi: 10.1371/journal.pone.0130984

8. Sun KM, Wong YH, Cheung KC, Yuen CM, Chan YT, Lai WJ, et al. Update on molecular diagnosis in extranodal NK/T-cell lymphoma and its role in the era of personalized medicine. *Diagnostics (Basel)* (2022) 12(2). doi: 10.3390/diagnostics12020409

9. Kim H, Ko YH. The pathologic and genetic characteristics of extranodal NK/T-cell lymphoma. *Life (Basel)* (2022) 12(1). doi: 10.3390/life12010073

10. Montes-Mojarro IA, Fend F, Quintanilla-Martinez L. EBV and the pathogenesis of NK/T cell lymphoma. *Cancers (Basel)* (2021) 13(6). doi: 10.3390/cancers13061414

11. McBride P. Photographs of a case of rapid destruction of the nose and face. *1897. J Laryngol Otol* (1991) 105(12):1120. doi: 10.1017/s0022215100118407

12. Hargrove SW, Fodden JH, Rhodes AJ. Malignant granuloma of the nose. *Lancet* (1946) 2(6426):596–9. doi: 10.1016/s0140-6736(46)91056-2

13. Singh MM, Stokes JF, Drury RA, Walshe JM. The natural history of malignant granuloma of the nose. *Lancet* (1958) 1(7017):401–3. doi: 10.1016/s0140-6736(58)90717-7

14. Takahara M, Kumai T, Kishibe K, Nagato T, Harabuchi Y. Extranodal NK/T-cell lymphoma, nasal type: Genetic, biologic, and clinical aspects with a central focus on Epstein-Barr virus relation. *Microorganisms* (2021) 9(7). doi: 10.3390/microorganisms9071381

15. Ishii Y, Yamanaka N, Ogawa K, Yoshida Y, Takami T, Matsuura A, et al. Nasal T-cell lymphoma as a type of so-called "lethal midline granuloma". *Cancer* (1982) 50 (11):2336–44. doi: 10.1002/1097-0142(19821201)50:11<2336::AID-CNCR2820501120>3.0.CO;2-C

16. Vilde JL, Perronne C, Huchon A, Leport C, Gehanno P, Marche C, et al. Association of Epstein-Barr virus with lethal midline granuloma. *N Engl J Med* (1985) 313(18):1161. doi: 10.1056/NEJM198510313131816

17. Ng CS, Chan JK, Lo ST. Expression of natural killer cell markers in non-hodgkin's lymphomas. *Hum Pathol* (1987) 18(12):1257–62. doi: 10.1016/s0046-8177(87)80410-0

18. Harris NL, Jaffe ES, Stein H, Banks PM, Chan JK, Cleary ML, et al. A revised European-American classification of lymphoid neoplasms: A proposal from the international lymphoma study group. *Blood* (1994) 84(5):1361–92. doi: 10.1182/blood.V84.5.1361.1361

19. Jaffe ES, Chan JK, Su IJ, Frizzera G, Mori S, Feller AC, et al. Report of the workshop on nasal and related extranodal angiocentric T/Natural killer cell lymphomas. *Definitions differential diagnosis Epidemiol Am J Surg Pathol* (1996) 20(1):103–11. doi: 10.1097/00000478-199601000-00012

20. Jaffe ES, Harris NL, Stein H, Vardiman J. *WHO classification of tumours: Pathology and genetics of tumours of haematopoietic and lymphoid tissues. 3rd ed*. Lyon, France: IARC Press (2001).

21. McArthur GAD, Dew HR. Malignant granuloma of the nose. *J Laryngol Otol* (1925) 40:378–80. doi: 10.1017/S0022215100027481

22. Woods R. Observations ON MALIGNANT GRANULOMA OF THE NOSE. *Br Med J* (1921) 2(3159):65–6 1. doi: 10.1136/bmj.2.3159.65

23. Vonleden H, Schiff M. Antimetabolite therapy in midline lethal granuloma. *Arch Otolaryngol* (1964) 80:460–8. doi: 10.1001/archotol.1964.00750040472016

24. Murase T, Suzuki M, Toyama K. [Complete remission obtained by sequential chemotherapy of l-asparaginase and continuous infusion of bleomycin (ABLE protocol) in a case of refractory diffuse large cell lymphoma of a paranasal origin]. *Rinsho Ketsueki* (1986) 27(2):252–6.

25. Ando M, Sugimoto K, Kitoh T, Sasaki M, Mukai K, Ando J, et al. Selective apoptosis of natural killer-cell tumours by l-asparaginase. *Br J Haematol* (2005) 130 (6):860–8. doi: 10.1111/j.1365-2141.2005.05694.x

26. Kwong YL, Chan TSY, Tan D, Kim SJ, Poon LM, Mow B, et al. PD1 blockade with pembrolizumab is highly effective in relapsed or refractory NK/T-cell lymphoma failing l-asparaginase. *Blood* (2017) 129(17):2437–42. doi: 10.1182/blood-2016-12-756841

27. Sun P, Wang Y, Yang H, Chen C, Nie M, Sun XQ, et al. Combination of anti-PD-1 antibody, anlotinib and pegaspargase "Sandwich" with radiotherapy in localized natural Killer/T cell lymphoma. *Front Immunol* (2022) 13:766200. doi: 10.3389/fimmu.2022.766200

28. Kim GE, Lee SW, Chang SK, Park HC, Pyo HR, Kim JH, et al. Combined chemotherapy and radiation versus radiation alone in the management of localized angiocentric lymphoma of the head and neck. *Radiother Oncol* (2001) 61(3):261–9. doi: 10.1016/s0167-8140(01)00428-5

29. Kim WS, Song SY, Ahn YC, Ko YH, Baek CH, Kim DY, et al. CHOP followed by involved field radiation: is it optimal for localized nasal natural killer/T-cell lymphoma? *Ann Oncol* (2001) 12(3):349–52. doi: 10.1023/a:1011144911781

30. Cheung MM, Chan JK, Lau WH, Ngan RK, Foo WW. Early stage nasal NK/T-cell lymphoma: clinical outcome, prognostic factors, and the effect of treatment modality. *Int J Radiat Oncol Biol Phys* (2002) 54(1):182–90. doi: 10.1016/s0360-3016(02)02916-4

31. You JY, Chi KH, Yang MH, Chen CC, Ho CH, Chau WK, et al. Radiation therapy versus chemotherapy as initial treatment for localized nasal natural killer (NK)/T-cell lymphoma: a single institute survey in Taiwan. *Ann Oncol* (2004) 15(4):618–25. doi: 10.1093/annonc/mdh143

32. Li CC, Tien HF, Tang JL, Yao M, Chen YC, Su IJ, et al. Treatment outcome and pattern of failure in 77 patients with sinonasal natural killer/T-cell or T-cell lymphoma. *Cancer* (2004) 100(2):366–75. doi: 10.1002/cncr.11908

33. Kim K, Chie EK, Kim CW, Kim IH, Park CI. Treatment outcome of angiocentric T-cell and NK/T-cell lymphoma, nasal type: radiotherapy versus chemoradiotherapy. *Jpn J Clin Oncol* (2005) 35(1):1–5. doi: 10.1093/jjco/hyi006

34. Isobe K, Uno T, Tamaru J, Kawakami H, Ueno N, Wakita H, et al. Extranodal natural killer/T-cell lymphoma, nasal type: the significance of radiotherapeutic parameters. *Cancer* (2006) 106(3):609–15. doi: 10.1002/cncr.21656

35. Lee KW, Yun T, Kim DW, Im SA, Kim TY, Yoon SS, et al. First-line ifosfamide, methotrexate, etoposide and prednisolone chemotherapy +/- radiotherapy is active in stage I/II extranodal NK/T-cell lymphoma. *Leuk Lymphoma* (2006) 47(7):1274–82. doi: 10.1080/10428190600562823

36. Lee SH, Ahn YC, Kim WS, Ko YH, Kim K, Park K. The effect of pre-irradiation dose intense CHOP on anthracyline resistance in localized nasal NK/T-cell lymphoma. *Haematologica* (2006) 91(3):427–8.

37. Li YX, Yao B, Jin J, Wang WH, Liu YP, Song YW, et al. Radiotherapy as primary treatment for stage IE and IIE nasal natural killer/T-cell lymphoma. *J Clin Oncol* (2006) 24 (1):181–9. doi: 10.1200/JCO.2005.03.2573

38. Lee J, Suh C, Park YH, Ko YH, Bang SM, Lee JH, et al. Extranodal natural killer T-cell lymphoma, nasal-type: a prognostic model from a retrospective multicenter study. *J Clin Oncol* (2006) 24(4):612–8. doi: 10.1200/JCO.2005.04.1384

39. Wang B, Lu JJ, Ma X, Guo Y, Lu H, Hong X, et al. Combined chemotherapy and external beam radiation for stage IE and IIE natural killer T-cell lymphoma of nasal cavity. *Leuk Lymphoma* (2007) 48(2):396–402. doi: 10.1080/10428190601059795

40. Ma HH, Qian LT, Pan HF, Yang L, Zhang HY, Wang ZH, et al. Treatment outcome of radiotherapy alone versus radiochemotherapy in early stage nasal natural killer/T-cell lymphoma. *Med Oncol* (2010) 27(3):798–806. doi: 10.1007/s12032-009-9288-7

41. Yamaguchi M, Suzuki R, Kwong YL, Kim WS, Hasegawa Y, Izutsu K, et al. Phase I study of dexamethasone, methotrexate, ifosfamide, l-asparaginase, and etoposide (SMILE) chemotherapy for advanced-stage, relapsed or refractory extranodal natural killer (NK)/T-cell lymphoma and leukemia. *Cancer Sci* (2008) 99(5):1016–20. doi: 10.1111/j.1349-7006.2008.00768.x

42. Kim SJ, Kim K, Kim BS, Kim CY, Suh C, Huh J, et al. Phase II trial of concurrent radiation and weekly cisplatin followed by VIPD chemotherapy in newly diagnosed, stage IE to IIE, nasal, extranodal NK/T-cell lymphoma: Consortium for improving survival of lymphoma study. *J Clin Oncol* (2009) 27(35):6027–32. doi: 10.1200/JCO.2009.23.8592

43. Huang H, Lin Z, Lin X, Cai Q, Xia Z, Jiang W. Long-term outcomes of patients with newly diagnosed extranodal natural killer/T-cell lymphoma treated by etoposide, prednisone, vincristine, cyclophosphamide, and doxorubicin regimen: a single-institution experience. *Leuk Lymphoma* (2011) 52(6):1041–8. doi: 10.3109/10428194.2011.561388

44. Li YX, Liu QF, Wang WH, Jin J, Song YW, Wang SL, et al. Failure patterns and clinical implications in early stage nasal natural killer/T-cell lymphoma treated with primary radiotherapy. *Cancer* (2011) 117(22):5203–11. doi: 10.1002/cncr.26167

45. Jiang M, Zhang H, Jiang Y, Yang Q, Xie L, Liu W, et al. Phase 2 trial of "sandwich" l-asparaginase, vincristine, and prednisone chemotherapy with radiotherapy in newly diagnosed, stage IE to IIE, nasal type, extranodal natural killer/T-cell lymphoma. *Cancer* (2012) 118(13):3294–301. doi: 10.1002/cncr.26629

46. Wang L, Xia ZJ, Huang HQ, Lu Y, Zhang YJ. Cyclophosphamide, doxorubicin, vincristine, and prednisone (CHOP) in the treatment of stage IE/IIE extranodal natural killer/T cell lymphoma, nasal type: 13-year follow-up in 135 patients. *Int J Hematol* (2012) 96(5):617–23. doi: 10.1007/s12185-012-1174-y

47. Lee J, Cho SG, Chung SM, Ryu MR, Kim SH, Jang HS, et al. Retrospective analysis of treatment outcomes for extranodal NK/T-cell lymphoma (ENKL), nasal type, stage I-IIE: single institute experience of combined modality treatment for early localized nasal extranodal NK/T-cell lymphoma (ENKL). *Ann Hematol* (2013) 92(3):333–43. doi: 10.1007/s00277-012-1630-z

48. Lee J, Kim CY, Park YJ, Lee NK. Sequential chemotherapy followed by radiotherapy versus concurrent chemoradiotherapy in patients with stage I/II extranodal natural killer/T-cell lymphoma, nasal type. *Blood Res* (2013) 48(4):274–81. doi: 10.5045/br.2013.48.4.274

49. Lin N, Song Y, Zheng W, Tu M, Xie Y, Wang X, et al. A prospective phase II study of l-asparaginase- CHOP plus radiation in newly diagnosed extranodal NK/T-cell lymphoma, nasal type. *J Hematol Oncol* (2013) 6:44. doi: 10.1186/1756-8722-6-44

50. Wang L, Wang ZH, Chen XQ, Li YJ, Wang KF, Xia YF, et al. First-line combination of gemcitabine, oxaliplatin, and l-asparaginase (GELOX) followed by involved-field radiation therapy for patients with stage IE/IIE extranodal natural killer/T-cell lymphoma. *Cancer* (2013) 119(2):348–55. doi: 10.1002/cncr.27752

51. Aviles A, Neri N, Fernandez R, Huerta-Guzman J, Nambo MJ. Combined therapy in untreated patients improves outcome in nasal NK/T lymphoma: results of a clinical trial. *Med Oncol* (2013) 30(3):637. doi: 10.1007/s12032-013-0637-1

52. Ke QH, Zhou SQ, Du W, Liang G, Lei Y, Luo F, et al. Concurrent IMRT and weekly cisplatin followed by GDP chemotherapy in newly diagnosed, stage IE Nasal, extranodal NK/T-cell lymphoma. *Blood Cancer J* (2014) 4:e267. doi: 10.1038/bcj.2014.88

53. Kim SJ, Yang DH, Kim JS, Kwak JY, Eom HS, Hong DS, et al. Concurrent chemoradiotherapy followed by l-asparaginase-containing chemotherapy, VIDL, for localized nasal extranodal NK/T cell lymphoma: CISL08-01 phase II study. *Ann Hematol* (2014) 93(11):1895–901. doi: 10.1007/s00277-014-2137-6

54. Kim TM, Kim DW, Kang YK, Chung J, Song HS, Kim HJ, et al. A phase II study of ifosfamide, methotrexate, etoposide, and prednisolone for previously untreated stage I/II extranodal natural killer/T-cell lymphoma, nasal type: a multicenter trial of the Korean cancer study group. *Oncologist* (2014) 19(11):1129–30. doi: 10.1634/theoncologist.2014-0305

55. Tsai HJ, Lin SF, Chen CC, Chen TY, Su WC, Hwang WL, et al. Long-term results of a phase II trial with frontline concurrent chemoradiotherapy followed by consolidation chemotherapy for localized nasal natural killer/T-cell lymphoma. *Eur J Haematol* (2015) 94(2):130–7. doi: 10.1111/ejh.12405

56. Wang H, Wuxiao ZJ, Zhu J, Wang Z, Wang KF, Li S, et al. Comparison of gemcitabine, oxaliplatin and l-asparaginase and etoposide, vincristine, doxorubicin, cyclophosphamide and prednisone as first-line chemotherapy in patients with stage IE to IIE extranodal natural killer/T-cell lymphoma: a multicenter retrospective study. *Leuk Lymphoma* (2015) 56(4):971–7. doi: 10.3109/10428194.2014.939964

57. Zang J, Li C, Luo SQ, Wang JH, Xu M, Zhao LN, et al. Early radiotherapy has an essential role for improving survival in patients with stage I-II nasal-type of NK/T cell lymphoma treated with l-asparaginase-containing chemotherapy–a single institution experience. *Ann Hematol* (2015) 94(4):583–91. doi: 10.1007/s00277-014-2244-4

58. Michot JM, Mazeron R, Danu A, Lazarovici J, Ghez D, Antosikova A, et al. Concurrent etoposide, steroid, high-dose ara-c and platinum chemotherapy with radiation therapy in localised extranodal natural killer (NK)/T-cell lymphoma, nasal type. *Eur J Cancer* (2015) 51(16):2386–95. doi: 10.1016/j.ejca.2015.07.009

59. Moon JH, Lee BH, Kim JA, Lee YJ, Chae YS, Yhim HY, et al. Clinical impact of induction treatment modalities and optimal timing of radiotherapy for the treatment of limited-stage NK/T cell lymphoma. *Leuk Res* (2016) 49:80–7. doi: 10.1016/j.leukres.2016.08.015

60. Dong LH, Zhang LJ, Wang WJ, Lei W, Sun X, Du JW, et al. Sequential DICE combined with l-asparaginase chemotherapy followed by involved field radiation in newly diagnosed, stage IE to IIE, nasal and extranodal NK/T-cell lymphoma. *Leuk Lymphoma* (2016) 57(7):1600–6. doi: 10.3109/10428194.2015.1108415

61. Yoon DH, Kim SJ, Jeong SH, Shin DY, Bae SH, Hong J, et al. Phase II trial of concurrent chemoradiotherapy with l-asparaginase and MIDLE chemotherapy for newly diagnosed stage I/II extranodal NK/T-cell lymphoma, nasal type (CISL-1008). *Oncotarget* (2016) 7(51):85584–91. doi: 10.18632/oncotarget.11319

62. Jiang M, Zhang L, Xie L, Zhang H, Jiang Y, Liu WP, et al. A phase II prospective study of the "Sandwich" protocol, l-asparaginase, cisplatin, dexamethasone and etoposide chemotherapy combined with concurrent radiation and cisplatin, in newly diagnosed, I/II stage, nasal type, extranodal natural killer/T-cell lymphoma. *Oncotarget* (2017) 8 (30):50155–63. doi: 10.18632/oncotarget.16334

63. Xu PP, Xiong J, Cheng S, Zhao X, Wang CF, Cai G, et al. A phase II study of methotrexate, etoposide, dexamethasone and pegaspargase sandwiched with radiotherapy in the treatment of newly diagnosed, stage IE to IIE extranodal natural-Killer/T-Cell lymphoma, nasal-type. *EBioMedicine* (2017) 25:41–9. doi: 10.1016/j.ebiom.2017.10.011

64. Qi F, Wang WH, He XH, Chen B, Gui L, Fang H, et al. Phase 2 study of first-line intensity modulated radiation therapy followed by gemcitabine, dexamethasone, and cisplatin for high-risk, early stage extranodal nasal-type NK/T-cell lymphoma: The GREEN study. *Int J Radiat Oncol Biol Phys* (2018) 102(1):61–70. doi: 10.1016/j.ijrobp.2018.05.046

65. Zheng W, Gao Y, Ke X, Zhang W, Su L, Ren H, et al. PEG-L-CHOP treatment is safe and effective in adult extranodal NK/T-cell lymphoma with a low rate of clinical hypersensitivity. *BMC Cancer* (2018) 18(1):910. doi: 10.1186/s12885-018-4782-y

66. Liu Y, Xue K, Xia Z, Jin J, Wang J, Sun H, et al. Radiotherapy followed by DICEP regimen in treatment of newly diagnosed, stage IE/IIE, extranodal NK/T-cell lymphoma patients. *Cancer Med* (2020) 9(15):5400–5. doi: 10.1002/cam4.3207

67. Wang H, Wang L, Li C, Wuxiao Z, Chen G, Luo W, et al. Pegaspargase combined with concurrent radiotherapy for early-stage extranodal natural Killer/T-cell lymphoma, nasal type: A two-center phase II study. *Oncologist* (2020) 25(11):e1725–e31. doi: 10.1634/theoncologist.2020-0144

68. Wei C, Cao X, Zhang W, Zhang Y, Wang W, Zhang L, et al. Combined gemcitabine, cisplatin, dexamethasone, methotrexate, and pegaspargase (GDP-ML) for patients with newly diagnosed extranodal natural killer/T cell lymphoma, nasal type: a single arm, single center, prospective phase 2 study. *Ann Hematol* (2020) 99(12):2801–9. doi: 10.1007/s00277-020-04036-z

69. Wei L, Yang L, Ye J, Cong J, Li X, Yao N, et al. Outcomes of patients treated with SVILE vs. p-GemOx for extranodal natural killer/T-cell lymphoma, nasal type: a prospective, randomized controlled study. *Cancer Biol Med* (2020) 17(3):795–804. doi: 10.20892/j.issn.2095-3941.2020.0160

70. Zhu F, Liu T, Pan H, Xiao Y, Li Q, Liu X, et al. Long-term outcomes of upfront concurrent chemoradiotherapy followed by p-GDP regimen in newly diagnosed early stage extranodal nasal-type NK/T cell lymphoma: A prospective single-center phase II study. *Med (Baltimore)* (2020) 99(33):e21705. doi: 10.1097/MD.0000000000021705

71. Zhang Y, Liu Y, Xia Z, Jin J, Xue K, Wang J, et al. Phase II study of sequential chemoradiotherapy with l-asparaginase, dexamethasone, ifosfamide, cisplatin, and etoposide (DICE-l) in the early stage of extranodal natural killer (NK)/T-cell lymphoma. *Ann Transl Med* (2021) 9(14):1178. doi: 10.21037/atm-21-3525

72. Hu S, Lin N, Liu J, Sun Y, Liu W, Wang X, et al. A prospective phase II study of pegaspargase-COEP plus radiotherapy in patients with newly diagnosed extra-nodal NK/T-cell lymphoma. *Front Oncol* (2022) 12:839252. doi: 10.3389/fonc.2022.839252

73. Wang Y, Wang CQ, Sun P, Liu PP, Yang H, Wang HY, et al. Phase II study of gemcitabine, peg-asparaginase, dexamethasone and methotrexate regimen for newly diagnosed extranodal natural Killer/T-cell lymphoma, nasal type: Final analysis with long-term follow-up and rational research for the combination. *Front Oncol* (2022) 12:796738. doi: 10.3389/fonc.2022.796738

74. Zhu Y, Tian S, Xu L, Ma Y, Zhang W, Wang L, et al. GELAD chemotherapy with sandwiched radiotherapy for patients with newly diagnosed stage IE/IIE natural killer/T-cell lymphoma: a prospective multicentre study. *Br J Haematol* (2022) 196(4):939–46. doi: 10.1111/bjh.17960

75. Chai Y, Chen B, Qi F, Fang H, Qi SN, Guo RY, et al. First-line chemoradiation with or without chidamide (tucidinostat) in patients with early stage intermediate- and high-risk early-stage extranodal nasal-type natural killer/T-cell lymphoma: a randomized phase 2 study in China. *Int J Radiat Oncol Biol Phys* (2022) 113(4):833–44. doi: 10.1016/j.ijrobp.2022.04.001

76. Zhang Y, Ma S, Cai J, Yang Y, Jing H, Shuang Y, et al. Sequential p-GEMOX and radiotherapy for early-stage extranodal natural killer/T-cell lymphoma: A multicenter study. *Am J Hematol* (2021) 96(11):1481–90. doi: 10.1002/ajh.26335

77. Zhang L, Wang Y, Li X, Li L, Wang X, Sun Z, et al. Radiotherapy vs sequential pegaspargase, gemcitabine, cisplatin and dexamethasone and radiotherapy in newly diagnosed early natural killer/T-cell lymphoma: A randomized, controlled, open-label, multicenter study. *Int J Cancer* (2021) 148(6):1470–7. doi: 10.1002/ijc.33329

78. Hu Y, Chen M, Song Y, Liu X, Gou F, Zhang J, et al. Study of l-asparaginase, vincristine, and dexamethasone combined with intensity-modulated radiation therapy in early-stage nasal NK/T-cell lymphoma. *Am J Clin Oncol* (2020) 43(4):257–62. doi: 10.1097/COC.0000000000000647

79. Tian S, Li R, Wang T, Wang S, Tao R, Hu X, et al. Gemcitabine, dexamethasone, and cisplatin (GDP) chemotherapy with sandwiched radiotherapy in the treatment of newly diagnosed stage IE/IIE extranodal natural killer/T-cell lymphoma, nasal type. *Cancer Med* (2019) 8(7):3349–58. doi: 10.1002/cam4.2214

80. Qi F, Chen B, Wang J, Lin X, Qi S, Yang J, et al. Upfront radiation is essential for high-risk early-stage extranodal NK/T-cell lymphoma, nasal type: comparison of two sequential treatment modalities combining radiotherapy and GDP (gemcitabine, dexamethasone, and cisplatin) in the modern era. *Leuk Lymphoma* (2019) 60 (11):2679–88. doi: 10.1080/10428194.2019.1599111

81. Su C, Nguyen KA, Bai HX, Balaji D, Cao Y, Karakousis G, et al. Comparison of chemoradiotherapy with radiotherapy alone for early-stage extranodal natural killer/T-cell lymphoma, nasal type in elderly patients. *Leuk Lymphoma* (2018) 59(6):1406–12. doi: 10.1080/10428194.2017.1379078

82. Liu T, Zhu F, Xiao Y, Li Q, Liu X, Yang K, et al. Pegaspargase, gemcitabine, dexamethasone, and cisplatin (P-GDP) combined chemotherapy is effective for newly diagnosed extranodal NK/T-cell lymphoma: a retrospective study. *Cancer Manag Res* (2018) 10:5061–9. doi: 10.2147/CMAR.S179567

83. Bennani NN, Tun AM, Carson KR, Geiger JL, Maeda LS, Savage KJ, et al. Characteristics and outcome of extranodal NK/T-cell lymphoma in north America: A retrospective multi-institutional experience. *Clin Lymphoma Myeloma Leuk* (2021) 22(5): e300–9. doi: 10.1016/j.clml.2021.10.018

84. Li JW, Li YJ, Zhong MZ, Liu XL, Li J, Li KL, et al. Efficacy and tolerance of GELOXD/P-GEMOXD in newly diagnosed nasal-type extranodal NK/T-cell lymphoma: A multicenter retrospective study. *Eur J Haematol* (2018) 100(3):247–56. doi: 10.1111/ejh.13004

85. Li J, Li Y, Zhong M, Liu W, Liu X, Li J, et al. A multicenter retrospective comparison of sequential versus sandwich chemoradiotherapy for stage IE-IIE extranodal natural Killer/T-cell lymphoma, nasal type. *J Cancer* (2018) 9(9):1598–606. doi: 10.7150/jca.24310

86. Yamaguchi M, Suzuki R, Oguchi M, Asano N, Amaki J, Akiba T, et al. Treatments and outcomes of patients with extranodal natural Killer/T-cell lymphoma diagnosed between 2000 and 2013: A cooperative study in Japan. *J Clin Oncol* (2017) 35(1):32–9. doi: 10.1200/JCO.2016.68.1619

87. Wei W, Wu P, Li L, Zhang ZH. Effectiveness of pegaspargase, gemcitabine, and oxaliplatin (P-GEMOX) chemotherapy combined with radiotherapy in newly diagnosed, stage IE Nasal-type, extranodal natural killer/T-cell lymphoma. *Hematology* (2017) 22 (6):320–9. doi: 10.1080/10245332.2016.1264163

88. Vargo JA, Patel A, Glaser SM, Balasubramani GK, Farah RJ, Marks SM, et al. The impact of the omission or inadequate dosing of radiotherapy in extranodal natural killer T-cell lymphoma, nasal type, in the united states. *Cancer* (2017) 123(16):3176–85. doi: 10.1002/cncr.30697

89. Qian M, Tao H, Xu W, Ji H. A systematic comparison of treatment modalities for nasal extranodal natural killer/T-cell lymphoma in early stages between concurrent chemoradiotherapy and sequential chemotherapy. *Onco Targets Ther* (2017) 10:3617–23. doi: 10.2147/OTT.S136386

90. Huang Y, Yang J, Liu P, Zhou S, Gui L, He X, et al. Intensity-modulated radiation therapy followed by GDP chemotherapy for newly diagnosed stage I/II extranodal natural killer/T cell lymphoma, nasal type. *Ann Hematol* (2017) 96(9):1477–83. doi: 10.1007/s00277-017-3046-2

91. Cao J, Lan S, Shen L, Si H, Zhang N, Li H, et al. A comparison of treatment modalities for nasal extranodal natural killer/T-cell lymphoma in early stages: The efficacy of CHOP regimen based concurrent chemoradiotherapy. *Oncotarget* (2017) 8(12):20362–70. doi: 10.18632/oncotarget.13614

92. Kim TH, Kim JS, Suh YG, Cho J, Yang WI, Suh CO. The roles of radiotherapy and chemotherapy in the era of multimodal treatment for early-stage nasal-type extranodal natural Killer/T-cell lymphoma. *Yonsei Med J* (2016) 57(4):846–54. doi: 10.3349/ymj.2016.57.4.846

93. Ma X, Guo Y, Pang Z, Wang B, Lu H, Gu YJ, et al. A randomized phase II study of CEOP with or without semustine as induction chemotherapy in patients with stage IE/IIE extranodal NK/T-cell lymphoma, nasal type in the upper aerodigestive tract. *Radiother Oncol* (2009) 93(3):492–7. doi: 10.1016/j.radonc.2009.08.045

94. Wei L, Wang J, Ye J, Yang L, Cong J, Li X, et al. Long-term outcomes of patients treated with an EPOCHL regimen as first-line chemotherapy for newly diagnosed extranodal natural killer/T-cell lymphoma: a retrospective single-center study. *Leuk Lymphoma* (2020) 61(2):337–43. doi: 10.1080/10428194.2019.1663421

95. Yamaguchi M, Tobinai K, Oguchi M, Ishizuka N, Kobayashi Y, Isobe Y, et al. Concurrent chemoradiotherapy for localized nasal natural killer/T-cell lymphoma: An updated analysis of the Japan clinical oncology group study JCOG0211. *J Clin Oncol* (2012) 30(32):4044–6. doi: 10.1200/JCO.2012.45.6541

96. Yamaguchi M, Tobinai K, Oguchi M, Ishizuka N, Kobayashi Y, Isobe Y, et al. Phase I/II study of concurrent chemoradiotherapy for localized nasal natural killer/T-cell lymphoma: Japan clinical oncology group study JCOG0211. *J Clin Oncol* (2009) 27 (33):5594–600. doi: 10.1200/JCO.2009.23.8295

97. Zhang L, Jiang M, Xie L, Zhang H, Jiang Y, Yang QP, et al. Five-year analysis from phase 2 trial of "sandwich" chemoradiotherapy in newly diagnosed, stage IE to IIE, nasal type, extranodal natural killer/T-cell lymphoma. *Cancer Med* (2016) 5(1):33–40. doi: 10.1002/cam4.569

98. Huang H, Tao R, Yang Y, Cen H, Zhou H, Guo Y, et al. GEMSTONE-201: Preplanned primary analysis of a multicenter, single-arm, phase 2 study of sugemalimab (suge) in patients (pts) with relapsed or refractory extranodal natural killer/T cell lymphoma (R/R ENKTL). *J Clin Oncol* (2022) 40(16_suppl):7501. doi: 10.1200/JCO.2022.40.16_suppl.7501

99. Kim BS, Kim DW, Im SA, Kim CW, Kim TY, Yoon SS, et al. Effective second-line chemotherapy for extranodal NK/T-cell lymphoma consisting of etoposide, ifosfamide, methotrexate, and prednisolone. *Ann Oncol* (2009) 20(1):121–8. doi: 10.1093/annonc/mdn551

100. Jaccard A, Gachard N, Marin B, Rogez S, Audrain M, Suarez F, et al. Efficacy of l-asparaginase with methotrexate and dexamethasone (AspaMetDex regimen) in patients with refractory or relapsing extranodal NK/T-cell lymphoma, a phase 2 study. *Blood* (2011) 117(6):1834–9. doi: 10.1182/blood-2010-09-307454

101. Yamaguchi M, Kwong YL, Kim WS, Maeda Y, Hashimoto C, Suh C, et al. Phase II study of SMILE chemotherapy for newly diagnosed stage IV, relapsed, or refractory extranodal natural killer (NK)/T-cell lymphoma, nasal type: the NK-cell tumor study group study. *J Clin Oncol* (2011) 29(33):4410–6. doi: 10.1200/JCO.2011.35.6287

102. Ji J, Liu T, Xiang B, Liu W, He C, Chen X, et al. A study of gemcitabine, l-asparaginase, ifosfamide, dexamethasone and etoposide chemotherapy for newly diagnosed stage IV, relapsed or refractory extranodal natural killer/T-cell lymphoma, nasal type. *Leuk Lymphoma* (2014) 55(12):2955–7. doi: 10.3109/10428194.2014.907894

103. Wang YQ, Yang Y, Zhuo HY, Zou LQ, Jiang Y, Jiang M. Trial of LVDP regimen (L-asparaginase, etoposide, dexamethasone, and cisplatin, followed by radiotherapy) as first-line treatment for newly diagnosed, stage III/IV extranodal natural killer/T cell lymphoma. *Med Oncol* (2015) 32(2):435. doi: 10.1007/s12032-014-0435-4

104. Kim M, Kim TM, Kim KH, Keam B, Lee SH, Kim DW, et al. Ifosfamide, methotrexate, etoposide, and prednisolone (IMEP) plus l-asparaginase as a first-line therapy improves outcomes in stage III/IV NK/T cell-lymphoma, nasal type (NTCL). *Ann Hematol* (2015) 94(3):437–44. doi: 10.1007/s00277-014-2228-4

105. Ding H, Chang J, Liu LG, Hu D, Zhang WH, Yan Y, et al. High-dose methotrexate, etoposide, dexamethasone and pegaspargase (MEDA) combination chemotherapy is effective for advanced and relapsed/refractory extranodal natural killer/T cell lymphoma: a retrospective study. *Int J Hematol* (2015) 102(2):181–7. doi: 10.1007/s12185-015-1809-x

106. Zhou Z, Li X, Chen C, Li X, Zhang L, Li L, et al. Effectiveness of gemcitabine, pegaspargase, cisplatin, and dexamethasone (DDGP) combination chemotherapy in the treatment of relapsed/refractory extranodal NK/T cell lymphoma: a retrospective study of 17 patients. *Ann Hematol* (2014) 93(11):1889–94. doi: 10.1007/s00277-014-2136-7

107. Wang JH, Wang L, Liu CC, Xia ZJ, Huang HQ, Lin TY, et al. Efficacy of combined gemcitabine, oxaliplatin and pegaspargase (P-gemox regimen) in patients with newly diagnosed advanced-stage or relapsed/refractory extranodal NK/T-cell lymphoma. *Oncotarget* (2016) 7(20):29092–101. doi: 10.18632/oncotarget.8647

108. Liang JH, Wang L, Peter Gale R, Wu W, Xia Y, Fan L, et al. Efficacy of pegaspargase, etoposide, methotrexate and dexamethasone in newly diagnosed advanced-stage extra-nodal natural killer/T-cell lymphoma with the analysis of the prognosis of whole blood EBV-DNA. *Blood Cancer J* (2017) 7(9):e608. doi: 10.1038/bcj.2017.88

109. Cai J, Liu P, Huang H, Li Y, Ma S, Zhou H, et al. Combination of anti-PD-1 antibody with p-GEMOX as a potentially effective immunochemotherapy for advanced natural killer/T cell lymphoma. *Signal Transduct Target Ther* (2020) 5(1):289. doi: 10.1038/s41392-020-00331-3

110. Liu W, Yang Y, Qi S, Wang Y, He X, Zhang L, et al. Treatment, survival, and prognosis of advanced-stage natural Killer/T-cell lymphoma: An analysis from the China lymphoma collaborative group. *Front Oncol* (2020) 10:583050. doi: 10.3389/fonc.2020.583050

111. Tao R, Fan L, Song Y, Hu Y, Zhang W, Wang Y, et al. Sintilimab for relapsed/refractory extranodal NK/T cell lymphoma: a multicenter, single-arm, phase 2 trial (ORIENT-4). *Signal Transduct Target Ther* (2021) 6(1):365. doi: 10.1038/s41392-021-00768-0

112. Li J, Li J, Zhong M, Zhou H, Yu B. The clinical features and survival outcome of 107 newly diagnosed advanced stage extranodal NK/T-cell lymphoma cases: A triple-center study. *Cancer Manag Res* (2021) 13:1541–9. doi: 10.2147/CMAR.S292293

113. Wang X, Hu J, Dong M, Ding M, Zhu L, Wu J, et al. DDGP vs. SMILE in Relapsed/Refractory extranodal natural Killer/T-cell lymphoma, nasal type: A retrospective study of 54 patients. *Clin Transl Sci* (2021) 14(1):405–11. doi: 10.1111/cts.12893

114. Song GY, Yoon DH, Suh C, Moon JH, Baek DW, Kim JS, et al. Open-label, single arm, multicenter phase II study of VIDL induction chemotherapy followed by upfront autologous stem cell transplantation in patients with advanced stage extranodal NK/T-cell lymphoma. *Bone Marrow Transplant* (2021) 56(5):1205–8. doi: 10.1038/s41409-020-01160-2

115. Yamaguchi M, Kita K, Miwa H, Nishii K, Oka K, Ohno T, et al. Frequent expression of p-glycoprotein/MDR1 by nasal T-cell lymphoma cells. *Cancer* (1995) 76(11):2351–6. doi: 10.1002/1097-0142(19951201)76:11<2351::AID-CNCR2820761125>3.0.CO;2-1

116. Ahn HK, Kim SJ, Hwang DW, Ko YH, Tang T, Lim ST, et al. Gemcitabine alone and/or containing chemotherapy is efficient in refractory or relapsed NK/T-cell lymphoma. *Invest New Drugs* (2013) 31(2):469–72. doi: 10.1007/s10637-012-9889-4

117. Pokrovsky VS, Vinnikov D. L-asparaginase for newly diagnosed extra-nodal NK/T-cell lymphoma: systematic review and meta-analysis. *Expert Rev Anticancer Ther* (2017) 17(8):759–68. doi: 10.1080/14737140.2017.1344100

118. Akahane K, Kimura S, Miyake K, Watanabe A, Kagami K, Yoshimura K, et al. Association of allele-specific methylation of the ASNS gene with asparaginase sensitivity and prognosis in T-ALL. *Blood Adv* (2022) 6(1):212–24. doi: 10.1182/bloodadvances.2021004271

119. Obama K, Tara M, Niina K. L-asparaginase induced complete remission in Epstein-Barr virus positive, multidrug resistant, cutaneous T-cell lymphoma. *Int J Hematol* (1999) 69(4):260–2.

120. Nagafuji K, Fujisaki T, Arima F, Ohshima K. L-asparaginase induced durable remission of relapsed nasal NK/T-cell lymphoma after autologous peripheral blood stem cell transplantation. *Int J Hematol* (2001) 74(4):447–50. doi: 10.1007/BF02982090

121. Obama K, Tara M, Niina K. L-asparaginase-Based induction therapy for advanced extranodal NK/T-cell lymphoma. *Int J Hematol* (2003) 78(3):248–50. doi: 10.1007/BF02983802

122. Yong W, Zheng W, Zhang Y, Zhu J, Wei Y, Zhu D, et al. L-asparaginase-based regimen in the treatment of refractory midline nasal/nasal-type T/NK-cell lymphoma. *Int J Hematol* (2003) 78(2):163–7. doi: 10.1007/bf02983387

123. Liu WJ, Wang H, Peng XW, Wang WD, Liu NW, Wang Y, et al Asparagine synthetase expression is associated with the sensitivity to asparaginase in extranodal natural killer/T-cell lymphoma *in vivo* and *in vitro*. *Onco Targets Ther* (2018) 11:6605–15. doi: 10.2147/OTT.S155930

124. Li Y, Zhang X, Hu T, Han L, Li R, Wen J, et al. Asparagine synthetase expression and its potential prognostic value in patients with NK/T cell lymphoma. *Oncol Rep* (2014) 32(2):853–9. doi: 10.3892/or.2014.3237

125. Mundy-Bosse BL, Weigel C, Wu YZ, Abdelbaky S, Youssef Y, Casas SB, et al. Identification and targeting of the developmental blockade in extranodal natural Killer/T-cell lymphoma. *Blood Cancer Discovery* (2022) 3(2):154–69. doi: 10.1158/2643-3230.BCD-21-0098

126. Asselin B, Rizzari C. Asparaginase pharmacokinetics and implications of therapeutic drug monitoring. *Leuk Lymphoma* (2015) 56(8):2273–80. doi: 10.3109/10428194.2014.1003056

127. Asselin BL, Whitin JC, Coppola DJ, Rupp IP, Sallan SE, Cohen HJ. Comparative pharmacokinetic studies of three asparaginase preparations. *J Clin Oncol* (1993) 11(9):1780–6. doi: 10.1200/JCO.1993.11.9.1780

128. Chen SH. Asparaginase therapy in pediatric acute lymphoblastic leukemia: A focus on the mode of drug resistance. *Pediatr Neonatol* (2015) 56(5):287–93. doi: 10.1016/j.pedneo.2014.10.006

129. Kim HJ, Ock CY, Kim TM, Lee SH, Lee JY, Jung SH, et al. Comparison of native escherichia coli l-asparaginase versus pegylated asparaginase, in combination with ifosfamide, methotrexate, etoposide, and prednisolone, in extranodal NK/T-cell lymphoma, nasal type. *Cancer Res Treat* (2018) 50(3):670–80. doi: 10.4143/crt.2017.051

130. Wang X, Zhang L, Liu X, Li X, Li L, Fu X, et al. Efficacy and safety of a pegasparaginase-based chemotherapy regimen vs an l-asparaginase–based chemotherapy regimen for newly diagnosed advanced extranodal natural Killer/T-cell lymphoma. *JAMA Oncol* (2022) 8(7):1035–41. doi: 10.1001/jamaoncol.2022.1968

131. Van Trimpont M, Peeters E, De Visser Y, Schalk AM, Mondelaers V, De Moerloose B, et al. Novel insights on the use of l-asparaginase as an efficient and safe anti-cancer therapy. *Cancers (Basel)* (2022) 14(4). doi: 10.3390/cancers14040902

132. Kawedia JD, Liu C, Pei D, Cheng C, Fernandez CA, Howard SC, et al. Dexamethasone exposure and asparaginase antibodies affect relapse risk in acute lymphoblastic leukemia. *Blood* (2012) 119(7):1658–64. doi: 10.1182/blood-2011-09-381731

133. Liu C, Kawedia JD, Cheng C, Pei D, Fernandez CA, Cai X, et al. Clinical utility and implications of asparaginase antibodies in acute lymphoblastic leukemia. *Leukemia* (2012) 26(11):2303–9. doi: 10.1038/leu.2012.102

134. Hak LJ, Relling MV, Cheng C, Pei D, Wang B, Sandlund JT, et al. Asparaginase pharmacodynamics differ by formulation among children with newly diagnosed acute lymphoblastic leukemia. *Leukemia* (2004) 18(6):1072–7. doi: 10.1038/sj.leu.2403351

135. Armstrong JK, Hempel G, Koling S, Chan LS, Fisher T, Meiselman HJ, et al. Antibody against poly(ethylene glycol) adversely affects PEG-asparaginase therapy in acute lymphoblastic leukemia patients. *Cancer* (2007) 110(1):103–11. doi: 10.1002/cncr.22739

136. Douer D, Yampolsky H, Cohen LJ, Watkins K, Levine AM, Periclou AP, et al. Pharmacodynamics and safety of intravenous pegaspargase during remission induction in adults aged 55 years or younger with newly diagnosed acute lymphoblastic leukemia. *Blood* (2007) 109(7):2744–50. doi: 10.1182/blood-2006-07-035006

137. Bleyer A, Asselin BL, Koontz SE, Hunger SP. Clinical application of asparaginase activity levels following treatment with pegaspargase. *Pediatr Blood Cancer* (2015) 62(6):1102–5. doi: 10.1002/pbc.25299

138. Kloos RQH, Pieters R, Jumelet FMV, Jumelet FMV, van den Bos C. Individualized asparaginase dosing in childhood acute lymphoblastic leukemia. *J Clin Ocol* (2020) 38(7):715–24. doi: 10.1200/jco.19.02292

139. Rizzari C, Citterio M, Zucchetti M, Conter V, Chiesa R, Colombini A, et al. A pharmacological study on pegylated asparaginase used in front-line treatment of children with acute lymphoblastic leukemia. *Haematologica* (2006) 91(1):24–31.

140. Cheson BD, Fisher RI, Barrington SF, Cavalli F, Schwartz LH, Zucca E, et al. Recommendations for initial evaluation, staging, and response assessment of Hodgkin and non-Hodgkin lymphoma: the lugano classification. *J Clin Oncol* (2014) 32(27):3059–68. doi: 10.1200/JCO.2013.54.8800

141. Kim TM, Heo DS. Extranodal NK / T-cell lymphoma, nasal type: new staging system and treatment strategies. *Cancer Sci* (2009) 100(12):2242–8. doi: 10.1111/j.1349-7006.2009.01319.x

142. Hong H, Li Y, Lim ST, Liang C, Huang H, Yi P, et al. A proposal for a new staging system for extranodal natural killer T-cell lymphoma: a multicenter study from China and Asia lymphoma study group. *Leukemia* (2020) 34(8):2243–8. doi: 10.1038/s41375-020-0740-1

143. Huang H-q, Yan G, Su H, Huang Y, Gao Y, Xiaoxiao W, et al. Clinical outcome of an multicentre, randomized, phase II clinical trial for patients with extranodal NK/T cell lymphoma treated by p-gemox or aspametdex. *Blood* (2019) 134(Supplement_1):1569. doi: 10.1182/blood-2019-123478

144. Kim TM, Park YH, Lee SY, Kim JH, Kim DW, Im SA, et al. Local tumor invasiveness is more predictive of survival than international prognostic index in stage I

(E)/II(E) extranodal NK/T-cell lymphoma, nasal type. *Blood* (2005) 106(12):3785–90. doi: 10.1182/blood-2005-05-2056

145. Wu W, Ren K, Li N, Luo Q, Xu C, Zou L. Evaluation of different staging systems and prognostic analysis of nasal-type extranodal NK/T-cell lymphoma based on consistent LVDP chemotherapy regimen. *Transl Oncol* (2022) 21:101437. doi: 10.1016/j.tranon.2022.101437

146. Li YY, Feng LL, Niu SQ, Wang HY, Zhang LL, Wang L, et al. Radiotherapy improves survival in early stage extranodal natural killer/T cell lymphoma patients receiving asparaginase-based chemotherapy. *Oncotarget* (2017) 8(7):11480–8. doi: 10.18632/oncotarget.14006

147. Yang Y, Zhu Y, Cao JZ, Zhang YJ, Xu LM, Yuan ZY, et al. Risk-adapted therapy for early-stage extranodal nasal-type NK/T-cell lymphoma: Analysis from a multicenter study. *Blood* (2015) 126(12):1424–32. doi: 10.1182/blood-2015-04-639336

148. Sakata K, Hareyama M, Ohuchi A, Sido M, Nagakura H, Morita K, et al. Treatment of lethal midline granuloma type nasal T-cell lymphoma. *Acta Oncol* (1997) 36(3):307–11. doi: 10.3109/02841869709001268

149. Deng XW, Wu JX, Wu T, Zhu SY, Shi M, Su H, et al. Radiotherapy is essential after complete response to asparaginase-containing chemotherapy in early-stage extranodal nasal-type NK/T-cell lymphoma: A multicenter study from the China lymphoma collaborative group (CLCG). *Radiother Oncol* (2018) 129(1):3–9. doi: 10.1016/j.radonc.2018.04.026

150. Fauci AS, Johnson RE, Wolff SM. Radiation therapy of midline granuloma. *Ann Intern Med* (1976) 84(2):140–7. doi: 10.7326/0003-4819-84-2-140

151. Qi SN, Li YX, Specht L, Oguchi M, Tsang R, Ng A, et al. Modern radiation therapy for extranodal nasal-type NK/T-cell lymphoma: Risk-adapted therapy, target volume, and dose guidelines from the international lymphoma radiation oncology group. *Int J Radiat Oncol Biol Phys* (2021) 110(4):1064–81. doi: 10.1016/j.ijrobp.2021.02.011

152. Chen HH, Fong L, Su IJ, Ting LL, Hong RL, Leung HW, et al. Experience of radiotherapy in lethal midline granuloma with special emphasis on centrofacial T-cell lymphoma: A retrospective analysis covering a 34-year period. *Radiother Oncol* (1996) 38(1):1–6. doi: 10.1016/0167-8140(95)01668-6

153. Smalley SR, Cupps RE, Anderson JA, Ilstrup DM, McDonald TJ, Weiland LH, et al. Polymorphic reticulosis limited to the upper aerodigestive tract–natural history and radiotherapeutic considerations. *Int J Radiat Oncol Biol Phys* (1988) 15(3):599–605. doi: 10.1016/0360-3016(88)90300-8

154. Liang R, Todd D, Chan TK, Chiu E, Choy D, Loke SL, et al. Nasal lymphoma. A retrospective analysis of 60 cases. *Cancer* (1990) 66(10):2205–9.

155. Kim BS, Kim TY, Kim CW, Kim JY, Heo DS, Bang YJ, et al. Therapeutic outcome of extranodal NK/T-cell lymphoma initially treated with chemotherapy–result of chemotherapy in NK/T-cell lymphoma. *Acta Oncol* (2003) 42(7):779–83. doi: 10.1080/02841860310010682

156. Barrionuevo C, Zaharia M, Martinez MT, Taxa L, Misad O, Moscol A, et al. Extranodal NK/T-cell lymphoma, nasal type: Study of clinicopathologic and prognosis factors in a series of 78 cases from Peru. *Appl Immunohistochem Mol Morphol* (2007) 15(1):38–44. doi: 10.1097/01.pai.0000205062.27174.56

157. Zheng X, He X, Yang Y, Liu X, Zhang LL, Qu BL, et al. Association of improved overall survival with decreased distant metastasis following asparaginase-based chemotherapy and radiotherapy for intermediate- and high-risk early-stage extranodal nasal-type NK/T-cell lymphoma: A CLCG study. *ESMO Open* (2021) 6(4):100206. doi: 10.1016/j.esmoop.2021.100206

158. Shi Y, Dong M, Hong X, Zhang W, Feng J, Zhu J, et al. Results from a multicenter, open-label, pivotal phase II study of chidamide in relapsed or refractory peripheral T-cell lymphoma. *Ann Oncol* (2015) 26(8):1766–71. doi: 10.1093/annonc/mdv237

159. Kim SJ, Lim JQ, Laurensia Y, Cho J, Yoon SE, Lee JY, et al. Avelumab for the treatment of relapsed or refractory extranodal NK/T-cell lymphoma: An open-label phase 2 study. *Blood* (2020) 136(24):2754–63. doi: 10.1182/blood.2020007247

160. Gao Y, Huang H, Wang X, Bai B, Zhang L, Xiao Y, et al. Anti-PD-1 antibody (Sintilimab) plus histone deacetylase inhibitor (Chidamide) for the treatment of refractory or relapsed extranodal natural Killer/T cell lymphoma, nasal type (r/r-ENKTL): Preliminary results from a prospective, multicenter, single-arm, phase Ib/II trial (SCENT). *Blood* (2020) 136(Supplement 1):39–40. doi: 10.1182/blood-2020-134665

161. Huang H, Zhu J, Yao M, Kim TM, Yoon DH, Cho SG, et al. Daratumumab monotherapy for patients with relapsed or refractory natural killer/T-cell lymphoma, nasal type: An open-label, single-arm, multicenter, phase 2 study. *J Hematol Oncol* (2021) 14(1):25. doi: 10.1186/s13045-020-01020-y

162. Ghione P, Qi S, Imber BS, Seshan V, Moskowitz A, Galasso N, et al. (mSMILE) and intensity-modulated radiotherapy (IMRT) for extranodal NK-T lymphoma nasal type in a single-center population. *Leuk Lymphoma* (2020) 61(14):3331–41. doi: 10.1080/10428194.2020.1811864

163. Cui Y, Yao Y, Chen M, Jiang Y, Ren Q. The optimal timing of radiotherapy in the combination treatment of limited-stage extranodal natural killer/T-cell lymphoma, nasal type: An updated meta-analysis. *Ann Hematol* (2021) 100(12):2889–900. doi: 10.1007/s00277-021-04700-y

164. Qi SN, Yang Y, Zhang YJ, Huang HQ, Wang Y, He X, et al. Risk-based, response-adapted therapy for early-stage extranodal nasal-type NK/T-cell lymphoma in the modern chemotherapy era: A China lymphoma collaborative group study. *Am J Hematol* (2020) 95(9):1047–56. doi: 10.1002/ajh.25878

165. Kwong YL, Kim SJ, Tse E, Oh SY, Kwak JY, Eom HS, et al. Sequential chemotherapy/radiotherapy was comparable with concurrent chemoradiotherapy for stage I/II NK/T-cell lymphoma. *Ann Oncol* (2018) 29(1):256–63. doi: 10.1093/annonc/mdx684

166. Pokrovsky VS, Vinnikov D. Defining the toxicity of current regimens for extranodal NK/T cell lymphoma: a systematic review and metaproportion. *Expert Rev Anticancer Ther* (2019) 19(1):93–104. doi: 10.1080/14737140.2019.1549992

167. Kim SJ, Park S, Kang ES, Choi JY, Lim DH, Ko YH, et al. Induction treatment with SMILE and consolidation with autologous stem cell transplantation for newly diagnosed stage IV extranodal natural killer/T-cell lymphoma patients. *Ann Hematol* (2015) 94(1):71–8. doi: 10.1007/s00277-014-2171-4

168. Lim SH, Hong JY, Lim ST, Hong H, Arnoud J, Zhao W, et al. Beyond first-line non-anthracycline-based chemotherapy for extranodal NK/T-cell lymphoma: Clinical outcome and current perspectives on salvage therapy for patients after first relapse and progression of disease. *Ann Oncol* (2017) 28(9):2199–205. doi: 10.1093/annonc/mdx316

169. Kim JH, Lee JH, Lee J, Oh SO, Chang DK, Rhee PL, et al. Primary NK-/T-cell lymphoma of the gastrointestinal tract: clinical characteristics and endoscopic findings. *Endoscopy* (2007) 39(2):156–60. doi: 10.1055/s-2006-945114

170. Zheng S, Ouyang Q, Li G, Xu H, Jiang M, Cui D, et al. Primary intestinal NK/T cell lymphoma: a clinicopathologic study of 25 Chinese cases. *Arch Iran Med* (2012) 15(1):36–42. doi: 012151/AIM.0011

171. Jiang M, Chen X, Yi Z, Zhang X, Zhang B, Luo F, et al. Prognostic characteristics of gastrointestinal tract NK/T-cell lymphoma: an analysis of 47 patients in China. *J Clin Gastroenterol* (2013) 47(8):e74–9. doi: 10.1097/MCG.0b013e31829e444f

172. Au WY, Weisenburger DD, Intragumtornchai T, Nakamura S, Kim WS, Sng I, et al. Clinical differences between nasal and extranasal natural killer/T-cell lymphoma: A study of 136 cases from the international peripheral T-cell lymphoma project. *Blood* (2009) 113(17):3931–7. doi: 10.1182/blood-2008-10-185256

173. Huang Y, Shi X, Zhong P, Wang Y, Xiao H, Zhou X, et al. *De novo* testicular extranodal NK/T-cell lymphoma: A clinicopathologic study of 21 cases with review of additional 18 cases in the literature. *Am J Surg Pathol* (2019) 43(4):549–58. doi: 10.1097/PAS.0000000000001210

174. Lee WJ, Jung JM, Won CH, Chang SE, Choi JH, Chan Moon K, et al. Cutaneous extranodal natural killer/T-cell lymphoma: a comparative clinicohistopathologic and survival outcome analysis of 45 cases according to the primary tumor site. *J Am Acad Dermatol* (2014) 70(6):1002–9. doi: 10.1016/j.jaad.2013.12.023

175. Jiang L, Li P, Quan Q, Chen P, Qiu H, Zhang B. Cutaneous extranodal natural killer (NK) / T - cell lymphoma: A comprehensive clinical features and outcomes analysis of 71 cases. *Leuk Res* (2020) 88:106284. doi: 10.1016/j.leukres.2019.106284

176. Kwong YL. High-dose chemotherapy and hematopoietic SCT in the management of natural killer-cell malignancies. *Bone Marrow Transplant* (2009) 44(11):709–14. doi: 10.1038/bmt.2009.239

177. Tse E, Zhao WL, Xiong J, Kwong YL. How we treat NK/T-cell lymphomas. *J Hematol Oncol* (2022) 15(1):74. doi: 10.1186/s13045-022-01293-5

178. Murashige N, Kami M, Kishi Y, Kim SW, Takeuchi M, Matsue K, et al. Allogeneic haematopoietic stem cell transplantation as a promising treatment for natural killer-cell neoplasms. *Br J Haematol* (2005) 130(4):561–7. doi: 10.1111/j.1365-2141.2005.05651.x

179. Ennishi D, Maeda Y, Fujii N, Kondo E, Shinagawa K, Ikeda K, et al. Allogeneic hematopoietic stem cell transplantation for advanced extranodal natural killer/T-cell lymphoma, nasal type. *Leuk Lymphoma* (2011) 52(7):1255–61. doi: 10.3109/10428194.2011.572322

180. Tse E, Chan TS, Koh LP, Chng WJ, Kim WS, Tang T, et al. Allogeneic haematopoietic SCT for natural killer/T-cell lymphoma: a multicentre analysis from the Asia lymphoma study group. *Bone Marrow Transplant* (2014) 49(7):902–6. doi: 10.1038/bmt.2014.65

181. Brammer JE, Chihara D, Poon LM, Caimi P, de Lima M, Ledesma C, et al. Management of advanced and Relapsed/Refractory extranodal natural killer T-cell lymphoma: An analysis of stem cell transplantation and chemotherapy outcomes. *Clin Lymphoma Myeloma Leuk* (2018) 18(1):e41–50. doi: 10.1016/j.clml.2017.10.001

182. Bi XW, Wang H, Zhang WW, Wang JH, Liu WJ, Xia ZJ, et al. PD-L1 is upregulated by EBV-driven LMP1 through NF-kappaB pathway and correlates with poor prognosis in natural killer/T-cell lymphoma. *J Hematol Oncol* (2016) 9(1):109. doi: 10.1186/s13045-016-0341-7

183. Chen BJ, Chapuy B, Ouyang J, Sun HH, Roemer MG, Xu ML, et al. PD-L1 expression is characteristic of a subset of aggressive b-cell lymphomas and virus-associated malignancies. *Clin Cancer Res* (2013) 19(13):3462–73. doi: 10.1158/1078-0432.CCR-13-0855

184. Wang J, Gao YS, Xu K, Li XD. Combination of atezolizumab and chidamide to maintain long-term remission in refractory metastatic extranodal natural killer/T-cell lymphoma: A case report. *World J Clin cases* (2022) 10(5):1609–16. doi: 10.12998/wjcc.v10.i5.1609

185. Yan Z, Yao S, Liu Y, Zhang J, Li P, Wang H, et al. Durable response to sintilimab and chidamide in a patient with pegaspargase- and immunotherapy-resistant NK/T-cell lymphoma: Case report and literature review. *Front Oncol* (2020) 10:608304. doi: 10.3389/fonc.2020.608304

186. Wang C, Liu Y, Dong L, Li X, Yang Q, Brock MV, et al. Efficacy of decitabine plus anti-PD-1 camrelizumab in patients with Hodgkin lymphoma who progressed or relapsed after PD-1 blockade monotherapy. *Clin Cancer Res* (2021) 27(10):2782–91. doi: 10.1158/1078-0432.CCR-21-0133

187. Kim WS, Oki Y, Kim SJ, Yoon SE, Ardeshna KM, Lin Y, et al. Autologous EBV-specific T cell treatment results in sustained responses in patients with advanced extranodal NK/T lymphoma: results of a multicenter study. *Ann Hematol* (2021) 100(10):2529–39. doi: 10.1007/s00277-021-04558-0

188. Bollard CM, Gottschalk S, Torrano V, Diouf O, Ku S, Hazrat Y, et al. Sustained complete responses in patients with lymphoma receiving autologous cytotoxic T lymphocytes targeting Epstein-Barr virus latent membrane proteins. *J Clin Oncol* (2014) 32(8):798–808. doi: 10.1200/JCO.2013.51.5304

189. Cho SG, Kim N, Sohn HJ, Lee SK, Oh ST, Lee HJ, et al. Long-term outcome of extranodal NK/T cell lymphoma patients treated with postremission therapy using EBV LMP1 and LMP2a-specific CTLs. *Mol Ther* (2015) 23(8):1401–9. doi: 10.1038/mt.2015.91

190. Ando M, Ando J, Yamazaki S, Ishii M, Sakiyama Y, Harada S, et al. Long-term eradication of extranodal natural killer/T-cell lymphoma, nasal type, by induced pluripotent stem cell-derived Epstein-Barr virus-specific rejuvenated T cells *in vivo*. *Haematologica* (2020) 105(3):796–807. doi: 10.3324/haematol.2019.223511

191. Poon LM, Kwong YL. Complete remission of refractory disseminated NK/T cell lymphoma with brentuximab vedotin and bendamustine. *Ann Hematol* (2016) 95(5):847–9. doi: 10.1007/s00277-016-2627-9

192. Kim HK, Moon SM, Moon JH, Park JE, Byeon S, Kim WS. Complete remission in CD30-positive refractory extranodal NK/T-cell lymphoma with brentuximab vedotin. *Blood Res* (2015) 50(4):254–6. doi: 10.5045/br.2015.50.4.254

193. Kim SJ, Yoon DH, Kim JS, Kang HJ, Lee HW, Eom HS, et al. Efficacy of brentuximab vedotin in relapsed or refractory high-CD30-Expressing non-Hodgkin lymphomas: Results of a multicenter, open-labeled phase II trial. *Cancer Res Treat* (2020) 52(2):374–87. doi: 10.4143/crt.2019.198

194. Zheng M, Yu L, Hu J, Zhang Z, Wang H, Lu D, et al. Efficacy of B7-H3-Redirected BiTE and CAR-T immunotherapies against extranodal nasal natural Killer/T cell lymphoma. *Transl Oncol* (2020) 13(5):100770. doi: 10.1016/j.tranon.2020.100770

195. Lu P, Liu Y, Yang J, Zhang X, Yang X, Wang H, et al. Naturally selected CD7 CAR-T therapy without genetic manipulations for T-ALL/LBL: first-in-human phase 1 clinical trial. *Blood* (2022) 140(4):321–34. doi: 10.1182/blood.2021014498

196. Kagami Y, Nakamura S, Suzuki R, Iida S, Yatabe Y, Okada Y, et al. Establishment of an IL-2-dependent cell line derived from 'nasal-type' NK/T-cell lymphoma of CD2+, sCD3-, CD3epsilon+, CD56+ phenotype and associated with the Epstein-Barr virus. *Br J Haematol* (1998) 103(3):669–77. doi: 10.1046/j.1365-2141.1998.01029.x

197. Wang L, Li LR, Zhang L, Wang JW. The landscape of new drugs in extranodal NK/T-cell lymphoma. *Cancer Treat Rev* (2020) 89:102065. doi: 10.1016/j.ctrv.2020.102065

198. Wang L, Bi XW, Zhu YJ, He YZ, Lai QY, Xia ZJ, et al. IL-2Ralpha up-regulation is mediated by latent membrane protein 1 and promotes lymphomagenesis and chemotherapy resistance in natural killer/T-cell lymphoma. *Cancer Commun (Lond)* (2018) 38(1):62. doi: 10.1186/s40880-018-0334-8

199. Liu W, Zhao D, Liu T, Niu T, Song Y, Xu W, et al. A multi-center, real-world study of chidamide for patients with relapsed or refractory peripheral T-cell lymphomas in China. *Front Oncol* (2021) 11:750323. doi: 10.3389/fonc.2021.750323

200. Shi Y, Jia B, Xu W, Li W, Liu T, Liu P, et al. Chidamide in relapsed or refractory peripheral T cell lymphoma: A multicenter real-world study in China. *J Hematol Oncol* (2017) 10(1):69. doi: 10.1186/s13045-017-0439-6

201. Picod A, Martino S, Cervera P, Manuceau G, Arca M, Wittner M, et al. Deregulated JAK3 mediates growth advantage and hemophagocytosis in extranodal nasal-type natural killer/T-cell lymphoma. *Haematologica* (2022) 107(9):2218–25. doi: 10.3324/haematol.2021.280349

202. Venkatakrishnan K, Kim TM, Lin CC, Thye LS, Chng WJ, Ma B, et al. Phase 1 study of the investigational aurora a kinase inhibitor alisertib (MLN8237) in East Asian cancer patients: pharmacokinetics and recommended phase 2 dose. *Invest New Drugs* (2015) 33(4):942–53. doi: 10.1007/s10637-015-0258-y

203. Barr PM, Li H, Spier C, Mahadevan D, LeBlanc M, Ul Haq M, et al. Phase II intergroup trial of alisertib in relapsed and refractory peripheral T-cell lymphoma and transformed mycosis fungoides: SWOG 1108. *J Clin Oncol* (2015) 33(21):2399–404. doi: 10.1200/JCO.2014.60.6327

204. Landes JR, Moore SA, Bartley BR, Doan HQ, Rady PL, Tyring SK. The efficacy of selinexor (KPT-330), an XPO1 inhibitor, on non-hematologic cancers: A comprehensive review. *J Cancer Res Clin Oncol* (2022). doi: 10.1007/s00432-022-04247-z

205. Azmi AS, Uddin MH, Mohammad RM. The nuclear export protein XPO1 - from biology to targeted therapy. *Nat Rev Clin Oncol* (2021) 18(3):152–69. doi: 10.1038/s41571-020-00442-4

206. Huang H, Gao Y, Zhang H, Zhou K, Wu J, Cai Z, et al. XPO1 inhibitor (ATG-010) plus chemotherapy per investigator's choice for heavily pretreated patients with relapsed or refractory (R/R) peripheral T-cell lymphoma (PTCL) and extranodal NK/T-cell lymphoma (ENKTL):Preliminary results from a multicenter, single-arm, phase ib study (TOUCH trial). *Blood* (2021) 138(Supplement 1):2452. doi: 10.1182/blood-2021-147100

207. Jin J, Cen H, Zhou K, Xu X, Li F, Wu T, et al. A phase ib study of a PI3Kδ inhibitor linperlisib in patients with relapsed or refractory peripheral T-cell lymphoma. *Hematological Oncology* (2021) 39(S2 supplement abstract):300–1. doi: 10.1002/hon.128_2880

208. Horwitz SM, Koch R, Porcu P, Oki Y, Moskowitz A, Perez M, et al. Activity of the PI3K-delta,gamma inhibitor duvelisib in a phase 1 trial and preclinical models of T-cell lymphoma. *Blood* (2018) 131(8):888–98. doi: 10.1182/blood-2017-08-802470

209. Huen A, Haverkos BM, Zain J, Radhakrishnan R, Lechowicz MJ, Devata S, et al. Phase I/Ib study of tenalisib (RP6530), a dual PI3K delta/gamma inhibitor in patients with Relapsed/Refractory T-cell lymphoma. *Cancers (Basel)* (2020) 12(8). doi: 10.3390/cancers12082293

210. de Mel S, Hue SS, Jeyasekharan AD, Chng WJ, Ng SB. Molecular pathogenic pathways in extranodal NK/T cell lymphoma. *J Hematol Oncol* (2019) 12(1):33. doi: 10.1186/s13045-019-0716-7

211. Zhu H, Gao H, Ji Y, Zhou Q, Du Z, Tian L, et al. Targeting p53-MDM2 interaction by small-molecule inhibitors: Learning from MDM2 inhibitors in clinical trials. *J Hematol Oncol* (2022) 15(1):91. doi: 10.1186/s13045-022-01314-3

212. Jiang L, Gu ZH, Yan ZX, Zhao X, Xie YY, Zhang ZG, et al. Exome sequencing identifies somatic mutations of DDX3X in natural killer/T-cell lymphoma. *Nat Genet* (2015) 47(9):1061–6. doi: 10.1038/ng.3358

213. Xiong J, Cui BW, Wang N, Dai YT, Zhang H, Wang CF, et al. Genomic and transcriptomic characterization of natural killer T cell lymphoma. *Cancer Cell* (2020) 37(3):403–19 e6. doi: 10.1016/j.ccell.2020.02.005

214. Dong G, Liu X, Wang L, Yin W, Bouska A, Gong Q, et al. Genomic profiling identifies distinct genetic subtypes in extra-nodal natural killer/T-cell lymphoma. *Leukemia* (2022) 36(8):2064–75. doi: 10.1038/s41375-022-01623-z

215. Lim JQ, Huang D, Chan JY, Laurensia Y, Wong EKY, Cheah DMZ, et al. A genomic-augmented multivariate prognostic model for the survival of natural-killer/T-cell lymphoma patients from an international cohort. *Am J Hematol* (2022) 97(9):1159–69. doi: 10.1002/ajh.26636

216. Lim JQ, Huang D, Tang T, Tan D, Laurensia Y, Peng RJ, et al. Whole-genome sequencing identifies responders to pembrolizumab in relapse/refractory natural-killer/T cell lymphoma. *Leukemia* (2020) 34(12):3413–9. doi: 10.1038/s41375-020-1000-0

217. Cho J, Kim SJ, Park WY, Kim J, Woo J, Kim G, et al. Immune subtyping of extranodal NK/T-cell lymphoma: a new biomarker and an immune shift during disease progression. *Mod Pathol* (2020) 33(4):603–15. doi: 10.1038/s41379-019-0392-8

frontiers | Frontiers in Oncology

TYPE Original Research
PUBLISHED 10 February 2023
DOI 10.3389/fonc.2023.1119886

Check for updates

OPEN ACCESS

EDITED BY
Shariq Qayyum,
Brigham and Women's Hospital and Harvard Medical School, United States

REVIEWED BY
Masa Zdralevic,
University of Montenegro, Montenegro
Patricia Altea-Manzano,
KU Leuven, Belgium
Syed Mohammad Faisal,
Jazan University, Saudi Arabia

*CORRESPONDENCE
Zhiqian Zhang
zlzqzhang@bjmu.edu.cn

†These authors share first authorship

SPECIALTY SECTION
This article was submitted to Cancer Immunity and Immunotherapy, a section of the journal Frontiers in Oncology

RECEIVED 09 December 2022
ACCEPTED 06 January 2023
PUBLISHED 10 February 2023

CITATION
Song Q, Zhang K, Sun T, Xu C, Zhao W and Zhang Z (2023) Knockout of ENO1 leads to metabolism reprogramming and tumor retardation in pancreatic cancer. *Front. Oncol.* 13:1119886. doi: 10.3389/fonc.2023.1119886

COPYRIGHT
© 2023 Song, Zhang, Sun, Xu, Zhao and Zhang. This is an open-access article distributed under the terms of the Creative Commons Attribution License (CC BY). The use, distribution or reproduction in other forums is permitted, provided the original author(s) and the copyright owner(s) are credited and that the original publication in this journal is cited, in accordance with accepted academic practice. No use, distribution or reproduction is permitted which does not comply with these terms.

Knockout of ENO1 leads to metabolism reprogramming and tumor retardation in pancreatic cancer

Qingru Song†, Kai Zhang†, Tianjiao Sun, Congcong Xu, Wei Zhao and Zhiqian Zhang*

Key Laboratory of Carcinogenesis and Translational Research (Ministry of Education), Department of Cell Biology, Peking University Cancer Hospital & Institute, Beijing, China

The shift in glucose utilization from oxidative phosphorylation to glycolysis is the hallmark of tumor cells. The overexpression of ENO1, one of the key enzymes in the glycolysis process, has been identified in several cancers, however, its role in pancreatic cancer (PC) is yet unclear. This study identifies ENO1 as an indispensable factor in the progression of PC. Interestingly, ENO1-knockout could inhibit cell invasion and migration and prevent cell proliferation in pancreatic ductal adenocarcinoma (PDAC) cells (PANC-1 and MIA PaCa-2); meanwhile, tumor cell glucose uptake and lactate excretion also decreased significantly. Furthermore, ENO1-knockout reduced colony formation and tumorigenesis in both *in vitro* and *in vivo* tests. In total, after ENO1 knockout, 727 differentially expressed genes (DEGs) were identified in PDAC cells by RNA-seq. Gene Ontology enrichment analysis revealed that these DEGs are mainly associated with components such as the 'extracellular matrix' and 'endoplasmic reticulum lumen', and participate in the regulation of signal receptor activity. Kyoto Encyclopedia of Genes and Genomes pathway analysis revealed that the identified DEGs are associated with pathways, such as 'fructose and mannose metabolism', 'pentose phosphate pathway, and 'sugar metabolism for amino and nucleotide. Gene Set Enrichment Analysis showed that ENO1 knockout promoted the upregulation of oxidative phosphorylation and lipid metabolism pathways-related genes. Altogether, these results indicated that ENO1-knockout inhibited tumorigenesis by reducing cell glycolysis and activating other metabolic pathways by altering the expression of *G6PD, ALDOC, UAP1*, as well as other related metabolic genes. Concisely, ENO1, which plays a vital role in the abnormal glucose metabolism in PC, can be exploited as a target to control carcinogenesis by reducing aerobic glycolysis.

KEYWORDS

ENO1 DEGs, ENO1-knockout, pancreatic cancer (PC), tumor metabolism, tumorigenicity

1 Introduction

Pancreatic cancer (PC) is a malignant tumor of the digestive system and has a high mortality rate (1). It progresses rapidly and in the lack of specific symptoms and biomarkers, its early diagnosis is challenging (2). Therefore, it is crucial to find new targets for early diagnosis and treatment of PC. The special hypoxic microenvironment involves metabolic reprogramming in pancreatic ductal adenocarcinoma (PDAC) (3). Aerobic glycolysis instead of mitochondrial oxidative phosphorylation (OXPHOS) is used for energy production, known as the "Warburg effect" (4). Glycolysis supports the vigorous growth of cancer cells by producing various substrates (5). Therefore, metabolic regulation by downregulating key glycolytic enzymes can be a novel therapy for PC.

Enolase, one of the key enzymes in glycolysis, converts 2-phosphoglycerate to phosphoenolpyruvate (6). It has 4 isoforms: ENO1 (α-enolase) is expressed in most tissues, while ENO3 (β-Enolase) is mainly expressed in muscles. Meanwhile, ENO2 (γ-Enolase) and ENO4 are mainly found in neural tissue and mouse spermatozoa, respectively (7, 8). In addition to glycolytic functions, ENO1 plays various roles in the pathophysiological environment, including cell growth, cell invasion, ischemia and hypoxia, immune tolerance, allergic reaction, metastasis, tumorigenesis and inflammatory responses, etc (9–11).

The multifunctional glycolytic enzyme ENO1 has been shown to be commonly over-expressed in various human cancers including PC (12, 13). High expression of ENO1 is positively correlated with clinical stage, lymph node metastasis, and poor prognosis in PC. ENO1 promotes pancreatic cancer cells migration and metastasis through combining with integrins and uPAR (14). *In vivo*, the monoclonal antibody that block the binding of ENO1 with plasminogen inhibits metastasis formation of PDAC cells (15). In genetically engineered mice with pancreatic cancer, ENO1 DNA vaccine elicits antitumor immune responses by decreasing numbers of myeloid-derived suppressor cells and T-regulatory cells and increasing T-helper 1 and 17 responses to prolong survival (16). ENO1 may function as a promising and clinically-relevant molecular target for immunotherapeutic strategy, particularly in pancreatic cancer (15–17).

Herein, we knocked out ENO1 in pancreatic cancer cell lines and evaluated its impact on maintaining the Warburg effect and tumor growth through biochemical and functional approaches. We show that ENO1 knockout decreased PDAC cell growth, and suppressed tumorigenesis by altering the expression of metabolic pathway-related genes to trigger the metabolic patterns shift from glycolysis to OXPHOS and other metabolic pathways.

2 Materials and methods

2.1 Cell culture

Two kinds of human PDAC cell lines, PANC-1 and MIA PaCa-2, were obtained from the American Type Culture Collection (ATCC). The cells were cultured in DMEM (Dulbecco's Modified Eagle Medium) added with 10% fetal bovine serum (FBS), penicillin (Thermo Fisher Scientific, USA), and 100 μg/mL of streptomycin (Thermo Fisher Scientific, USA) at 37°C and 5% CO_2.

2.2 Vector construction and ENO1-knockout stable cell line

The single guide RNA (sgRNA) sequences were obtained based on the *ENO1* gene sequence and cloned into the LentiCRISPR v2 plasmid using the BsmBI site and primers 5'-TCGCGGGAATCCCACTGTTG-3'(forward) and 5'-CAACAGTGGGATTCCCGCGA-3' (reverse). For ENO1 knockout cells, we generated the recombinant lentiviruses using ViraPower Packaging Mix (Invitrogen, CA). The two knockout cell lines were obtained by infecting with lentiviruses for 48 h, followed by 2mg/L puromycin (Thermo Fisher Scientific, USA) selection for 14 days. The selected cells were subcultured to obtain the monoclonal cells. Eventually, ENO1 knockouts were confirmed by detecting ENO1 protein deficiency in corresponding cells using Western blotting.

2.3 Western blotting

Total cell proteins were extracted after cell lysis in RIPA lysis buffer (Solarbio, R0010). The protein-transferred PVDF membrane (Millipore, PVH00010) was incubated in 5% non-fat milk at 25°C for 1 h, followed by washing in 1×TBST. Next, the membrane was incubated with ENO1 antibodies (Sigma-Aldrich, WH0002023M1) for 1 h. After washing in TBST, the membrane was incubated with HRP-conjugated goat anti-mouse antibodies (ZSGB-BIO, ZB-2305, 1:100000) for 1 hr at room temperature. Immobilon™ Western Chemiluminescent HRP substrate (Millipore, WBKLS0500) was used to illuminate the protein bands.

2.4 Cell Counting Kit-8 (CCK-8) proliferation assay

Cells (5×10^3 cells/well) were seeded in 96-well plates. The cell viability was detected every 24 h for 4 days using the CCK-8 Kit (Dojindo, CK04) according to the manufacturer's instructions. Briefly, 10% CCK-8 solution was added to each well for 2 h, and then sample optical density (OD) was recorded at 485 nm using a microplate reader (BMG LABTECH) to determine the cell proliferation rate.

2.5 Colony formation assay

Cancer cells (1000 cells/well) were seeded into 6-well plates. After 2 to 3 weeks, colonies were immobilized with 4% paraformaldehyde (PFA) for 15 min. Then, the cells were stained with 0.1% crystal violet (CV) for 15 min. The stained cells were photographed with a Canon digital camera EOS M50 and counted by ImageJ software after washing. Colony formation rate is determined by counting the colonies numbers formed per 100 cells.

2.6 Transwell assay

Cells resuspended in DMEM without FBS were seeded into the upper chamber of the transwell chamber (Corning, CLS3422) at a cell density of 4×10^4 cells/well. Then, 800 µL DMEM supplemented with 20% FBS was added to the well under the chamber. The cells adhering to the upper layer of the chamber were swabbed after 24 h and then immobilized in 4% PFA for 15 min. Cells were stained with CV and then photographed and counted in four randomly selected fields under a stereomicroscope (Olympus, Japan). For the invasion assay, Matrigel (Corning, 356237) was coated on the 8 µm pores polycarbonate membrane of the transwell chamber. 4×10^4 cells were planted into each well and cultured for 48 h and the cell migration was estimated. The migration and invasion capacity was assessed by the number of cells that migrated and stained by crystal violet in a photograph. Each experiment was repeated thrice.

2.7 Glucose consumption and lactate production

Cells were seeded into 6-well plates and the DMEM medium was changed every 12 h. 500 µl of the medium was collected at 0 and 8 h of incubation to measure the initial and final concentrations of glucose and lactate, respectively, using a Silman M900 bioprocess biochemistry analyzer. Finally, the cells were digested with 0.25% trypsin solution (Thermo Fisher Scientific, USA) and counted through the countess 3 automated cell counter (Thermo Fisher Scientific, USA). The lactate and glucose levels were normalized based on cell count.

2.8 Soft agar assay

600 µl of 0.6% agar (Sigma, A1296) was added to each well of a 24-well plate. After the 0.6% agar solidified, the digested cells mixed with 0.3% agar were inoculated into the same at 600 µl/well; each well contained 1000 cells. The colonies that were >50 µm in diameter were photographed and counted under a stereomicroscope (Olympus, Japan) after three weeks.

2.9 Tumorigenicity assay in NOG mice

8-week-old male NOD-SCID IL-2 receptor gamma null (NOG) mice were used to access the tumorigenesis role of ENO1. The mice were divided into two groups (control and test groups) with 6 mice each. 2×10^6 cells were subcutaneously transplanted into the two sides of the NOG mice. The corresponding tumor sizes in mice were recorded every 5 days. The tumor volume was calculated using the formula $V = L*W^{2}*0.5$, where L and W represent the largest and the smallest diameters, respectively. After 5-6 weeks, the mice were sacrificed for tumor collection. All animal protocols were approved by the Peking University Cancer Hospital Animal Care and Use Committee, China.

2.10 RNA-sequencing

The cells were lysed with TRIzol reagent (Invitrogen,15596018); the library construction and RNA-sequencing were conducted by Novogene Co., Ltd (Tianjin, China). The raw sequencing data have been deposited in the Genome Sequence Archive (GSA) database under accession number HRA001089. All of the data are also available as the sequence read archive (SRA) format in the National Center for Biotechnology Information (NCBI) with the accession number of SRP414959. The gene expression differences were analyzed using the DEseq2 software (1.20.0). Data with p-value <0.05 after adjustment were considered significantly different. The Gene Ontology (GO) and KEGG (Kyoto Encyclopedia of Genes and Genomes) pathway enrichment analyses of differentially expressed genes (DEGs) were accomplished by clusterProfiler (3.4.4); GO terms with a p-value <0.05 were considered significantly enriched. Gene set enrichment analysis (GSEA) results were visualized by Omicshare Online tools.

2.11 Quantitative real-time PCR (q-RT-PCR)

Total cell RNA was extracted using the RNeasy® Mini Kit (QIAGEN,74104) as previously described (18). 2 µg of total RNA, Oligo-$(dT)_{15}$, dNTPs, and MMLV reverse transcriptase (Invitrogen, 28025-021) were mixed for cDNAs synthesis. qRT-PCR was performed using the Biosystems 7500 real-time PCR system. The gene expressions were estimated by the $2^{-\Delta\Delta Ct}$ method. The used primers are listed as follows:

GPX7:5′-CGACTTCAAGGCGGTCAACATC-3′ (forward), 5′-TCGGTAGTGCTGGTCTGTGAAG-3′ (reverse); RGN:5′-GGAGGAAGTGTCCAACTCTCTG-3′ (forward), 5′-CAATGGTGGCAACATAGCCTCC-3′ (reverse); GMPPA:5′-GGACAGTGAGAGCCTCTTCAAG-3′ (forward), 5′-TCGAGTTCAGGATGAGCACCTC-3′ (reverse); G6PD:5′-CTGTTCCGTGAGGACCAGATCT-3′ (forward), 5′-TGAAGGTGAGGATAACGCAGGC-3′(reverse); GFPT2:5′-GCTCATCGTGATTGGCTGTGGA-3′ (forward), 5′-CAACCATCACAGGAAGCTCAGTC-3′ (reverse); MGST1:5′-GCCAATCCAGAAGACTGTGTAGC-3′ (forward), 5′-AGGAGGCCAATTCCAAGAAATGG-3′ (reverse); GSTM4:5′-TGGAGAACCAGGCTATGGACGT-3′ (forward),5′-CCAGGAACTGTGAGAAGTGCTG-3′ (reverse); GAPDH:5′-GACCCCTTCATTGACCTCAAC-3′ (forward), 5′-CTTCTCCATGGTGGTGAAGA-3′ (reverse).

2.12 TIMER and GEPIA based gene expression and prognostic value analysis of ENO1 in human cancers

The TIMER (https://cistrome.shinyapps.io/timer/) and GEPIA databases (http://gepia2.cancer-pku.cn/#analysis) were used to analyze the difference in ENO1 expression levels between the human cancers and paired normal tissue. ENO1 expression levels (Log_2TPM) are displayed using box plots, with statistical significance of differential expression evaluated using the Wilcoxon test in the

TIMER 2.0 version. We use log2 (TPM + 1) for log-scale and match TCGA normal and GTEx data in GEPIA databases analysis. Furthermore, The Kaplan-Meier Plotter database (http://kmplot.com/analysis/) was used to find the prognostic value of ENO1 expression level in human cancers. We choose mRNA (RNA-seq) to start KM Plotter for pan-cancer. Patients are splited by selecting best cutoff value automatically.

2.13 Statistical analysis

Data were analyzed by GraphPad Prism 8. The data differences were assessed by t-test and those with p-value <0.05 were considered statistically significant.

3 Results

3.1 ENO1 is significantly upregulated in human pancreatic cancer and other cancer tissues

The results from the TIMER database showed that ENO1 expression was significantly higher in most human cancers tissue compared to adjacent normal tissue, such as in BLCA (bladder urothelial carcinoma), BRCA (breast invasive carcinoma), CHOL (cholangiocarcinoma), COAD (colon adenocarcinoma), ESCA (esophageal carcinoma), HNSC (head and neck cancer), KIRC (kidney renal papillary cell carcinoma), KIRP (kidney renal papillary carcinoma), LIHC (liver hepatocellular carcinoma), LUAD (lung adenocarcinoma), LUSC (lung squamous cell carcinoma), PRAD (prostate adenocarcinoma), READ (rectum adenocarcinoma), STAD (stomach adenocarcinoma), THCA (thyroid carcinoma) and UCEC (uterine corpus endometrial carcinoma). Notably, ENO1 expression was significantly lower only in KICH (kidney chromophobe) (Figure 1A). Similarly, GEPIA data also showed that ENO1 expression was high in most cancer types, which was consistent with TIMER analysis. The expression of ENO1 is significantly greater in PAAD (pancreatic adenocarcinoma) tumor tissues (T) than in normal tissues (N) with the highest Log_2FC value (Figure 1B and Supplementary Figure 1A). Altogether, these results suggested that ENO1 may promote the occurrence of various cancers including pancreatic cancer.

3.2 ENO1 is a prognostic biomarker in various cancers including pancreatic cancer

The prognostic value of ENO1 expression level in human cancers was analyzed using the Kaplan-Meier plotter database. We found that ENO1 upregulation was associated with poor overall survival (OS) in BLCA (n = 404, HR = 1.6, P = 0.0016; Figure 2A), BRCA (n = 1089,

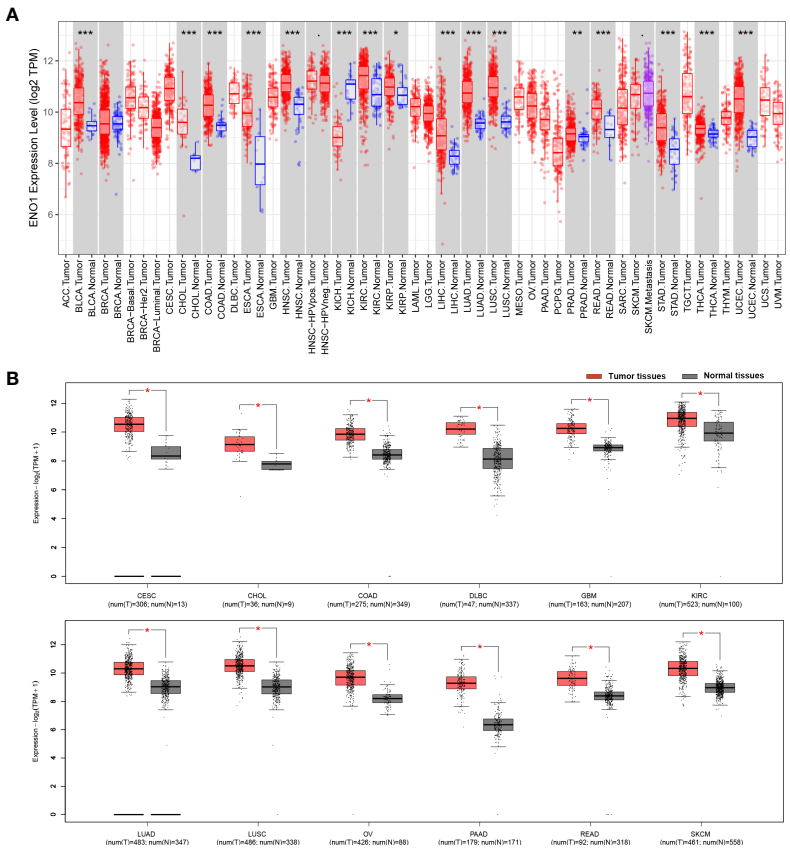


FIGURE 1
ENO1 expression is mostly upregulated different cancer types. ENO1 expression levels in different cancers and paired normal tissue were screened from the TCGA database using **(A)** TIMER (*P < 0.05, **P < 0.01, ***P < 0.001) and **(B)** GEPIA. T, tumor tissues; N, normal tissues.

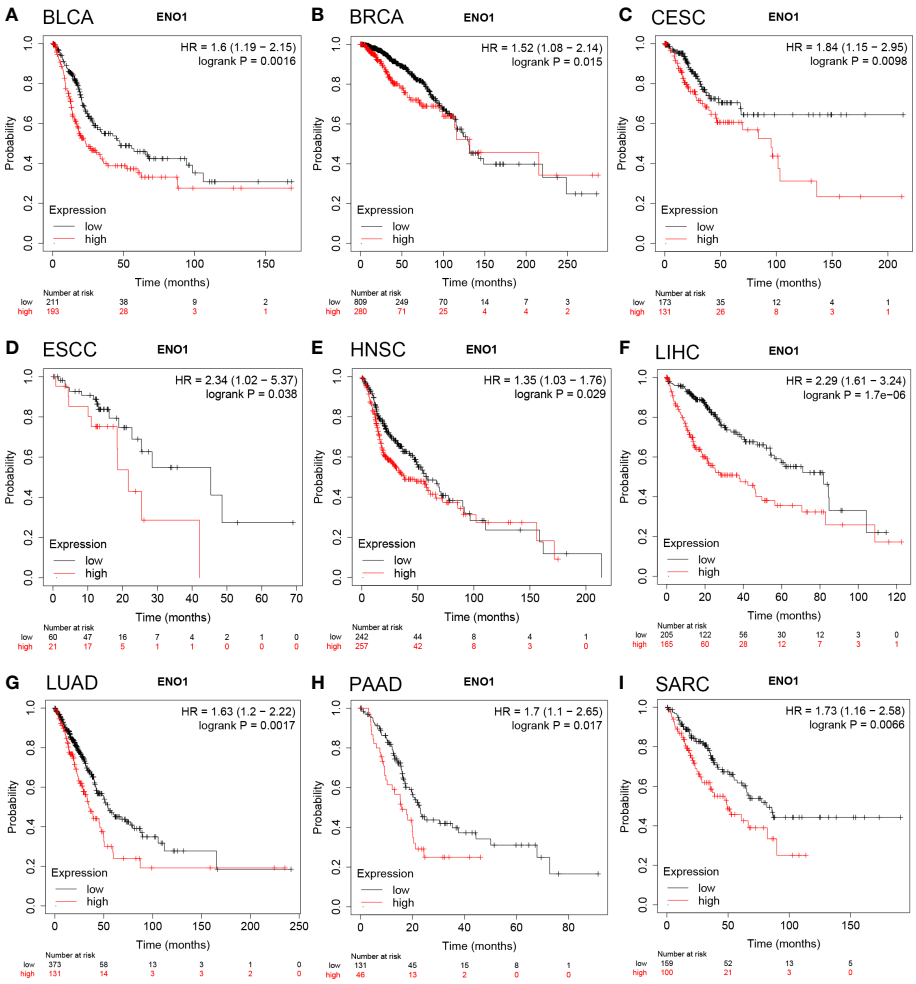


FIGURE 2
Overall survival of cancer patients was associated with high expression levels of ENO1 as analyzed by the Kaplan-Meier plotter database. **(A–I)** High ENO1 expression levels were related to worse overall survival in BLCA (n = 404), BRCA (n = 1089), CESC (n = 304), ESCC (n = 81), HNSC (n = 499), LIHC (n = 370), LUAD (n = 504), PAAD (n = 177) and SARC (n = 259).

HR = 1.52, P = 0.015; Figure 2B), CESC (cervical squamous cell carcinoma) (n = 304, HR = 1.84, P = 0.0098; Figure 2C), ESCC (esophageal squamous cell carcinoma) (n = 81, HR = 2.34, P = 0.038; Figure 2D), HNSC (n = 499, HR = 1.35, P = 0.029; Figure 2E), LIHC (n = 370, HR = 2.29, P = 1.7e-06; Figure 2F), LUAD (n = 504, HR = 1.63, P = 0.0017; Figure 2G), PAAD (n = 177, HR = 1.7, P = 0.017; Figure 2H) and SARC (sarcoma) (n = 259, HR = 1.73, P = 0.0066; Figure 2I). In addition, patients with higher ENO1 expression level had poor relapse-free survival (RFS) in BRCA, LIHC, PAAD, SARC, and TGCT (testicular germ cell tumors). More details of ENO1-RFS relationships were analyzed by the Kaplan-Meier plotter database (Supplementary Figure 1B–F). Concisely, overexpression of ENO1 was found associated with poor prognosis in multiple tumor types.

3.3 ENO1 knockout significantly reduced the growth and colony formation rate of PDAC cells

To examine the biological function(s) of ENO1 in PC, we knocked out ENO1 in PANC-1 and MIA PaCa-2 cells (Figure 3A). Both the ENO1-knockout and corresponding control cells were cultured and tested for cell viability using the CCK-8 assay. The cell growth curves (reflected by OD values) revealed that ENO1 knockout markedly inhibited the cell proliferation in both the PDAC cells (Figure 3B). The cells were cultured for 10-15 days, the colonies were immobilized and stained, and then photographed and counted. We found that the colony numbers of the ENO1 knockout cells were sharply decreased compared to the corresponding control cells. ENO1 knockout decreased the proliferation abilities of PANC-1 and MIA PaCa-2 cells significantly compared with the control cells (Figures 3C, D). Thus, knockout of ENO1 could inhibit the proliferation of PDAC cells.

3.4 ENO1 knockout decreased the cell migration, invasion, and glycolysis in PDAC cells

The effect of ENO1 knockout on cell migration and invasion in PDAC cells was evaluated by transwell assay. We found that fewer cells migrated through the polycarbonate membrane in the ENO1

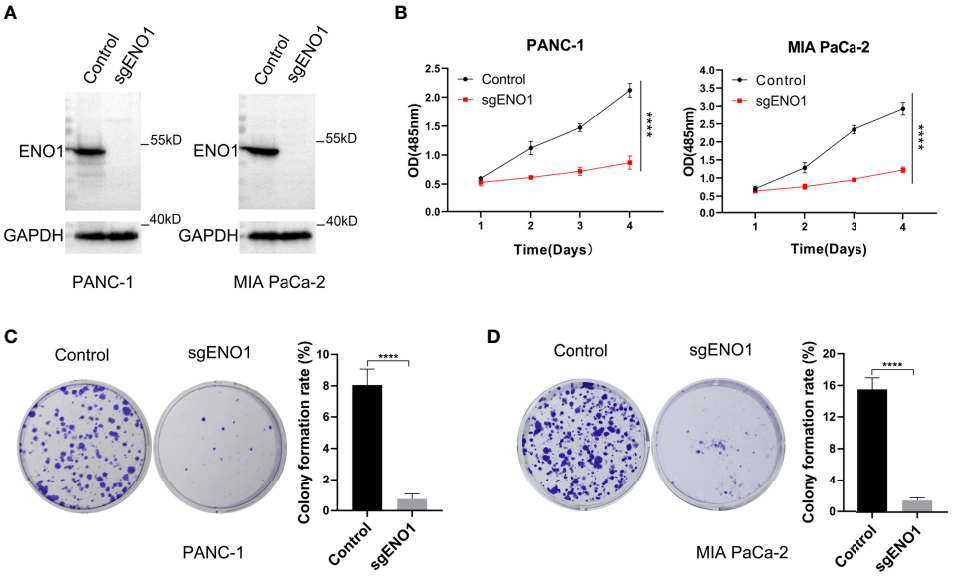


FIGURE 3
ENO1 knockout reduced the proliferation and colony formation ability of pancreatic cancer cells. **(A)** ENO1 knockout was validated by Western Blotting in PANC-1 and MIA PaCa-2 cells. **(B)** The cell proliferation (CCK-8 assay) and **(C, D)** colony formation rates were estimated in PANC-1 and MIA PaCa-2 cells after ENO1 knockout. 500 cells/well were seeded into the 6-well plates; ****P <0.0001.

knockout groups than in the control groups (Figures 4A, B). Consistently, when the polycarbonate membrane of the chamber was coated with Matrigel, the number of cells invading through the polycarbonate membrane was lower in the ENO1 knockout groups than in the control groups (Figures 4C, D). These results revealed that ENO1 knockout significantly decreased the migration and invasion of PDAC cells. To examine the effect of ENO1 knockout on glycolysis, we detected the possible change in glucose and lactate concentrations in the two PDAC cells. The corresponding cell culture media were collected at 0 and 8 h to estimate the amounts of glucose and lactate, reflecting any possible change in glucose uptake and lactate secretion after ENO1 knockout. We found that the glucose consumption and lactate production in both the ENO1 knockout PDAC cells were significantly lower compared to that in corresponding control cells (Figures 4E, F). This indicated that ENO1 knockout reduces glucose metabolism levels in PDAC cells.

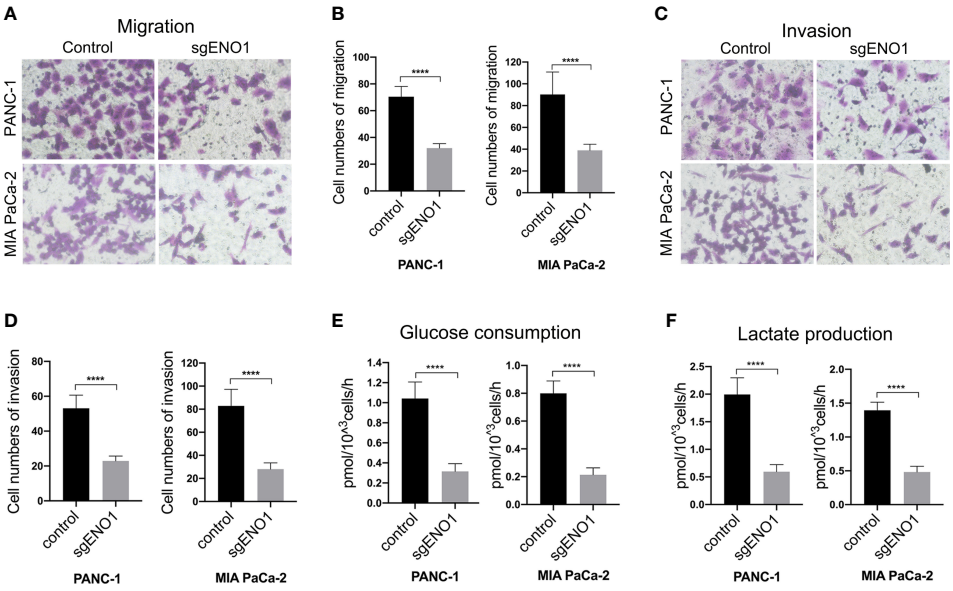


FIGURE 4
ENO1 knockout reduced cell migration, invasion, and glycolysis in PDAC cells. **(A, B)** The cell migration and **(C, D)** invasion decreased significantly after ENO1 knockout in PANC-1 and MIA PaCa-2 cells (transwell assay, ×200, n=3, error bars indicate S.D). **(E)** Glucose consumption and **(F)** lactate production significantly reduced after ENO1 knockout in PANC-1 and MIA PaCa-2 cells; ****P<0.0001.

3.5 ENO1 knockout inhibited the tumorigenicity of PDAC cells

Cells were seeded into 24-well plates and cultured in 0.3% agar for 2-3 weeks. We found that the colony numbers were significantly lower in the ENO1 knockout groups than in the control groups (Figures 5A, B). This indicated that ENO1 knockout markedly reduced the tumorigenicity of PDAC cells *in vitro*. For *in vivo* assay, 2×10^6 control or ENO1 knockout cells were subcutaneously inoculated into NOG mice. The tumor size was recorded every 5 days to obtain the growth curves. The results showed that tumor sizes were significantly smaller in ENO1 knockout mice than in control mice, indicating that ENO1 knockout reduced the tumorigenicity of PDAC cells (Figures 5C, D).

3.6 ENO1 knockout induced compensatory upregulation of other metabolic pathways in PC

After examining the biological function of ENO1 in PC, we tried to understand its underlying molecular mechanism in abnormal cell metabolism in PC. Accordingly, RNA-seq was conducted to find the DEGs after ENO1 knockout in PANC-1 cells (Supplementary Table 1). The heatmap from the transcriptome sequencing data revealed 727 DEGs (p-value <0.05), including 370 upregulated and 357 downregulated genes (Figure 6A). These DEGs were also analyzed by a volcano map, which showed the overall changes in gene expression after ENO1 knockout. The red and green dots represent the upregulated and downregulated DEGs, respectively (Figure 6B).

Furthermore, the identified DEGs were subjected to GO and KEGG pathway enrichment analysis. GO terms are defined as biological processes (BP), molecular functions (MF), and cellular components (CC). Based on the GO enrichment analysis, the top 20 GO terms of upregulated and downregulated genes were selected based on the -$\log_{10}$ (P-value) (Supplementary Figures 2A–F). The top 10 GO terms indicated that the main BP terms enriching the DEGs were heart development and the regulation of signaling receptor activity; the enriched CC terms were extracellular matrix and dendrites; the enriched MF terms were receptor ligand and regulator activity (Figure 6C). KEGG pathway analysis was used to annotate the DEGs related physiological and biochemical reaction pathways; the top 20 pathways were selected based on -$\log_{10}$ level (P-value). Many pathways showed substantial changes between the knockout and control cells (Figure 6D). These pathways include the cancer pathways, Rap1 signaling pathway, Wnt signaling pathway, and many metabolic pathways. The number and percentages of the DEGs belonging to these pathways are listed in Figure 6D.

To understand how ENO1 participates in the abnormal metabolism of PDAC cells, we mainly focused on the identified cell metabolism-associated pathways, including the pentose phosphate pathway and metabolism of fructose, mannose, glutathione, amino, and nucleotide sugar. The DEGs involved in these four metabolic pathways and their relative expression levels (sgENO1 vs control) are listed in Supplementary Table 2. These DEGs may be the regulatory targets of ENO1. We randomly selected 7 DEGs to validate the RNA-seq data by qRT-PCR, including 5 upregulated and 2 downregulated genes. We found that RNA-seq data were consistent with qRT-PCR (Figure 6E).

In addition, we performed GSEA to explore the potential downstream pathways of ENO1. GSEA highlighted that ENO1

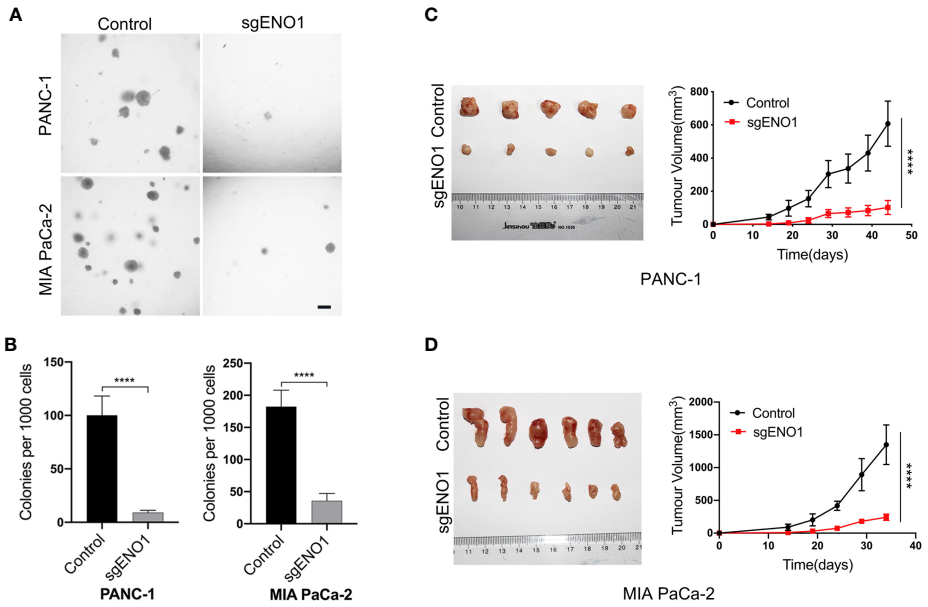


FIGURE 5
ENO1 knockout reduced tumorigenicity of PDAC cells. **(A, B)** The colony formation ability of PANC-1 and MIA PaCa-2 cells reduced after ENO1 knockout; scale bars, 100 μm. **(C, D)** The mice tumor growth curves originated from subcutaneous injection of ENO1 knockout and control cells are shown. (each group had 6 mice, one mouse died in the PANC-1 cell group); ****P<0.0001.

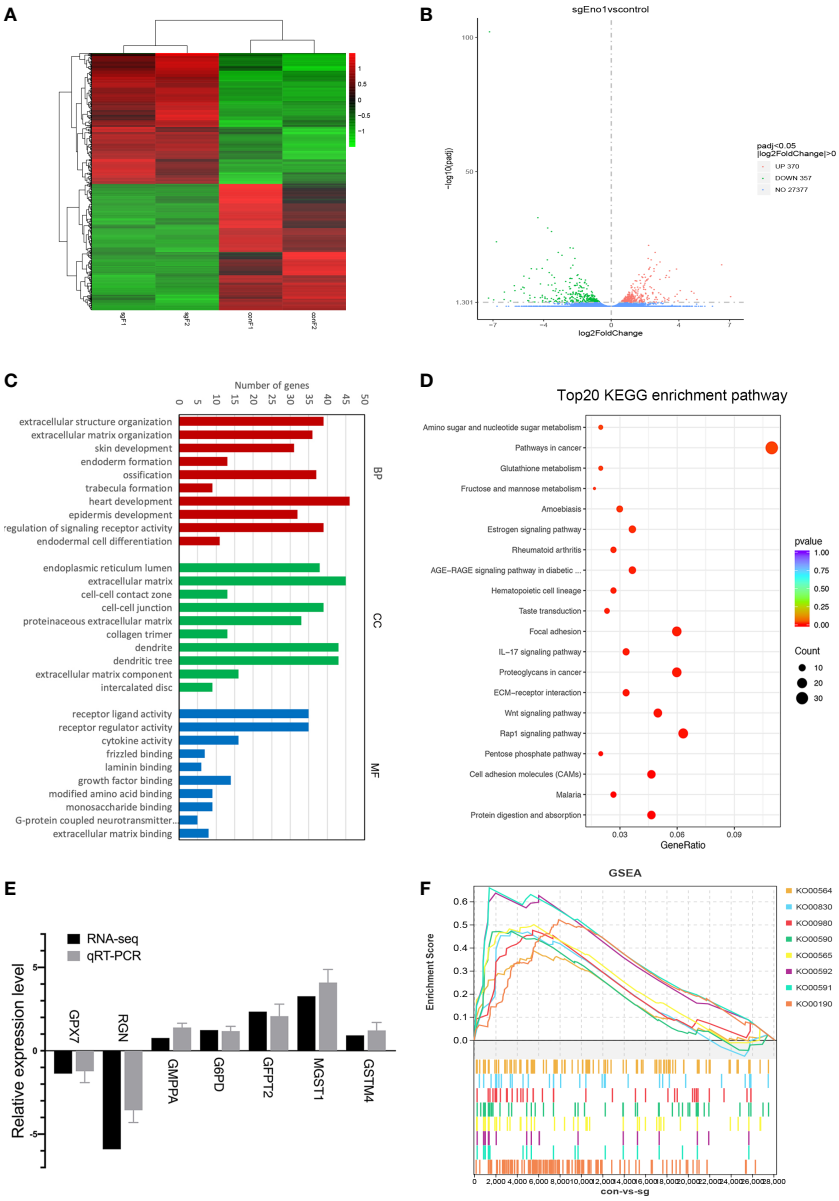


FIGURE 6
RNA-seq analysis of DEGs in control and ENO1 knockout groups. **(A)** A heatmap and **(B)** Volcano Plot of DEGs between ENO1 knockout and control cells: X-axis: the log2 (fold change); Y-axis: -log10 (Padj). Red and green dots represent the significantly upregulated and downregulated DEGs, respectively. **(C)** GO enrichment analysis of DEGs: X-axis, GO terms enriched in the BP, CC, and MF categories; Y-axis, the numbers of DEGs. **(D)** A scatterplot shows the DEGs enriched KEGG pathways: X-axis, the ratios of the DEGs involved in the pathways; Y-axis, the top 20 KEGG pathways based on -$\log_{10}$ (P-value). The bubble size and color respectively denote the number of DEGs and p-value of the corresponding KEGG pathways. **(E)**. qRT-PCR was used to validate the RNA-seq data; the X-axis shows the 7 randomly selected DEGs and Y-axis shows their relative expression levels. Grey and black columns represent the qRT-PCR and RNA-seq expression data, respectively. **(F)** GSEA plots illustrate the significant enrichment of metabolism-related upregulated genes in ENO1 knockout cells.

knockout in PANC-1 cells positively associated with various genes related to oxidative phosphorylation (KO00190), ether lipid metabolism (KO00565), arachidonic acid metabolism (KO00590), linoleic acid metabolism (KO00591), alpha-linolenic acid metabolism (KO00592), retinol metabolism (KO00830), glycerophospholipid metabolism (KO00564), and metabolism of xenobiotics by cytochrome P450 (KO00980) (Figure 6F). The GSEA plots, nominal p-value, FDR q-value, enrichment score (ES) and normalized ES nominated specifical metabolism pathways upregulated after ENO1 knockout are shown in Supplementary Figures 3A–H. The pathways were mainly associated with the activation of mitochondrial oxidative phosphorylation and lipid metabolism.

4 Discussion

Identifying the key regulators of PC is an important research challenge for the timely diagnosis and treatment of PC (19). In PC, tumor cells undergo reprogrammed metabolism to meet energy requirements and support malignant behaviors. Notably, dysregulation of ENO1 has been associated with several cancers (14, 20, 21).

Multivariate analyses have shown that overexpression of ENO1 can be a predictor of tumor progression (11, 13). These studies suggest ENO1 is a promising therapeutic and diagnostic target in human tumors.

Here, we show that ENO1 is widely expressed in normal human tissues and is significantly upregulated in most TCGA (The Cancer Genome Atlas) cancer patients. Furthermore, OS analysis found that high expression of ENO1 was significantly associated with poor prognosis of BLCA, BRCA, CESC, ESCC, HNSC, LIHC, LUAD, PAAD, and SARC cancers. Concerning the RFS, high expression of ENO1 was significantly related to poor prognosis of BRCA, LIHC, SARC, PAAD, and TGCT cancers. These findings are consistent with prior studies showing a correlation of high ENO1 expression and poorer survival in cancer patients (22, 23). These data highlighted ENO1 as an oncogene in various cancers.

Recent study have shown that ENO1 overexpression promoted proliferation, invasion and migration of SKCM cells; and increased pyruvate and lactate production (24). Subsequently, we explored the hypothesis that ENO1 is one of the leading regulators of the Warburg effect and thus plays a major role in carcinogenesis and tumor maintenance. We found that ENO1 knockout markedly reduced the cell proliferation, migration, and invasion of PDAC cells; meanwhile, glycolysis levels and tumorigenicity were also reduced. RNA-seq analysis identified key 727 DEGs after ENO1 knockout, which are mainly distributed in the extracellular matrix and endoplasmic reticulum, and participate in the regulation of signal receptor activity. KEGG pathway enrichment analysis revealed that the DEGs were related to key cellular metabolism pathways, including the pentose phosphate pathway, and the metabolism of fructose, mannose, glutathione, and others. In addition, RAS oncogene family members RAP1B, RHOH and Wnt family member WNT9A expression level were significantly down-regulated in ENO1 knockout group. Interestingly, we found that the expression levels of stem cell marker CD24 and CD34 were significantly decreased after knockout of ENO1. This is consistent with the report that ENO1 regulates stem cell-like properties in cancer cells (25).

In this study, we found that ENO1 knockout in PDAC cells affected the expression of abundant metabolism-related genes, confirming that the inhibition of ENO1 decreases proliferation and also suppresses tumor growth *in vivo* and *in vitro*. G6PD in the pentose phosphate pathway was upregulated after ENO1 knockout, suggesting a shift of glucose metabolism to the pentose phosphate pathway in PDAC cells. It seems that ENO1 silencing can redistribute excessive glucose to the pentose phosphate pathway, decreasing lactate levels. Metabolic pattern changes can promote autophagy and fatty acid oxidation, reducing the growth of cancer cells (26). ENO1 knockout downregulated ALDOC levels in fructose and mannose metabolic pathways. The aberrant expression of aldolase family members has been demonstrated to promote tumor progression; ALDOC is upregulated in various cancers and acts as a regulator of Wnt signaling (27). The knockdown of ALDOC reduces cell growth, glucose uptake, and glycolysis in cancer cells (28). Silencing of UAP1 inhibited the growth and colony formation of cancer cells (29). Our RNA-seq data showed that UAP1 levels decreased affecting the amino and nucleotide sugar metabolism pathway. These genes may be indispensable to ENO1-mediated regulation of cell metabolism in PC, however, the biological functions of other DEGs in PC must be examined in the future. Meanwhile, GSEA revealed that genes encoding for mitochondrial functions and lipid metabolism were significantly upregulated in ENO1 knockout cells, indicating a shift in metabolism patterns in cancer cells.

In summary, our findings show the metabolic analysis following ENO1 knockout. ENO1 is a potential oncogene and its knockout may suppress the tumorigenicity of PDAC cells by triggering the metabolic pattern change from glycolysis to other metabolic pathways such as pentose phosphate pathway, mitochondrial OXPHOS and lipid metabolism. ENO1 can be exploited as a therapeutical target for reducing aerobic glycolysis in PC. Inhibition of ENO1 alone or in combination with other pathways activated by ENO1 knockout, opens novel avenues for future cancer therapeutic approaches. Nonetheless, this study had certain limitations. We mainly validated the biological functions of ENO1 in PDAC cells by examining "loss-of-function", while "gain-of-function" studies can further uncover the mechanism of ENO1 activating intracellular and extracellular signals in cancer cells.

Data availability statement

The datasets presented in this study can be found in online repositories. The names of the repository/repositories and accession number(s) can be found below: The raw sequencing data have been deposited in the Genome Sequence Archive (GSA) database under accession number HRA001089. All of the data are also available as the sequence read archive (SRA) format in the National Center for Biotechnology Information (NCBI) with the accession number of SRP414959.

Ethics statement

The animal study was reviewed and approved by Peking University Cancer Hospital Animal Care and Use Committee.

Author contributions

ZZ, QS, and KZ designed the study. QS and KZ did experiments. QS, KZ, TS, and CX finished computational analysis. WZ provided expert consultation. ZZ, QS, and KZ wrote the manuscript. ZZ supervised the study. All authors contributed to the article and approved the submitted version.

Funding

This work was funded by the National Natural Science Foundation of China (Grant No. 81730075 and 82030080), and the National Key Research and Development Program of China (Grant No. 2016YFC1303400 and 2021YFA1300604).

Acknowledgments

The authors would acknowledge all the people contributed to this research.

Conflict of interest

The authors declare that the research was conducted in the absence of any commercial or financial relationships that could be construed as a potential conflict of interest.

Publisher's note

All claims expressed in this article are solely those of the authors and do not necessarily represent those of their affiliated organizations, or those of the publisher, the editors and the reviewers. Any product that may be evaluated in this article, or claim that may be made by its manufacturer, is not guaranteed or endorsed by the publisher.

Supplementary material

The Supplementary Material for this article can be found online at: https://www.frontiersin.org/articles/10.3389/fonc.2023.1119886/full#supplementary-material

References

1. Siegel RL, Miller KD, Jemal A. Cancer statistics, 2020. *CA Cancer J Clin* (2020) 70:7–30. doi: 10.3322/caac.21590

2. Singhi AD, Koay EJ, Chari ST, Maitra A. Early detection of pancreatic cancer: Opportunities and challenges. *Gastroenterology* (2019) 156:2024–40. doi: 10.1053/j.gastro.2019.01.259

3. Shukla SK, Mulder SE, Singh PK. Hypoxia-mediated *In vivo* tumor glucose uptake measurement and analysis. *Methods Mol Biol* (2018) 1742:107–13. doi: 10.1007/978-1-4939-7665-2_10

4. Vander Heiden MG, Cantley LC, Thompson CB. Understanding the warburg effect: The metabolic requirements of cell proliferation. *Science* (2009) 324:1029–33. doi: 10.1126/science.1160809

5. Yang J, Ren B, Yang G, Wang H, Chen G, You L, et al. The enhancement of glycolysis regulates pancreatic cancer metastasis. *Cell Mol Life Sci* (2020) 77:305–21. doi: 10.1007/s00018-019-03278-z

6. Wold F, Ballou CE. Studies on the enzyme enolase. *J Biol Chem* (1957) 227:301–12. doi: 10.1016/S0021-9258(18)70816-8

7. Pancholi V. Multifunctional alpha-enolase: Its role in diseases. *Cell Mol Life Sci* (2001) 58:902–20. doi: 10.1007/PL00000910

8. Nakamura N, Dai Q, Williams J, Goulding EH, Willis WD, Brown PR, et al. Disruption of a spermatogenic cell-specific mouse enolase 4 (eno4) gene causes sperm structural defects and male infertility. *Biol Reprod* (2013) 88:90. doi: 10.1095/biolreprod.112.107128

9. Fan SS, Zong M, Zhang H, Lu Y, Lu TB, Fan LY. Decreased expression of alpha-enolase inhibits the proliferation of hypoxia-induced rheumatoid arthritis fibroblasts-like synoviocytes. *Mod Rheumatol* (2015) 25:701–7. doi: 10.3109/14397595.2015.1014141

10. Razorenova OV, Ivanov AV, Budanov AV, Chumakov PM. Virus-based reporter systems for monitoring transcriptional activity of hypoxia-inducible factor 1. *Gene* (2005) 350:89–98. doi: 10.1016/j.gene.2005.02.006

11. Capello M, Ferri-Borgogno S, Cappello P, Novelli F. α-enolase: A promising therapeutic and diagnostic tumor target. *FEBS J* (2011) 278:1064–74. doi: 10.1111/j.1742-4658.2011.08025.x

12. Hsiao KC, Shih NY, Fang HL, Huang TS, Kuo CC, Chu PY, et al. Surface α-enolase promotes extracellular matrix degradation and tumor metastasis and represents a new therapeutic target. *PloS One* (2013) 8:e69354. doi: 10.1371/journal.pone.0069354

13. Song Y, Luo Q, Long H, Hu Z, Que T, Zhang X, et al. Alpha-enolase as a potential cancer prognostic marker promotes cell growth, migration, and invasion in glioma. *Mol Cancer* (2014) 13:65. doi: 10.1186/1476-4598-13-65

14. Principe M, Borgoni S, Cascione M, Chattaragada MS, Ferri-Borgogno S, Capello M, et al. Alpha-enolase (ENO1) controls alpha v/beta 3 integrin expression and regulates pancreatic cancer adhesion, invasion, and metastasis. *J Hematol Oncol* (2017) 10:16. doi: 10.1186/s13045-016-0385-8

15. Principe M, Ceruti P, Shih NY, Chattaragada MS, Rolla S, Conti L, et al. Targeting of surface alpha-enolase inhibits the invasiveness of pancreatic cancer cells. *Oncotarget* (2015) 6:11098–113. doi: 10.18632/oncotarget.3572

16. Cappello P, Rolla S, Chiarle R, Principe M, Cavallo F, Perconti G, et al. Vaccination with ENO1 DNA prolongs survival of genetically engineered mice with pancreatic cancer. *Gastroenterology* (2013) 144:1098–106. doi: 10.1053/j.gastro.2013.01.020

17. Cappello P, Tomaino B, Chiarle R, Ceruti P, Novarino A, Castagnoli C, et al. An integrated humoral and cellular response is elicited in pancreatic cancer by alpha-enolase, a novel pancreatic ductal adenocarcinoma-associated antigen. *Int J Cancer* (2009) 125:639–48. doi: 10.1002/ijc.24355

18. Zhao W, Wang L, Han H, Jin K, Lin N, Guo T, et al. 1B50-1, a mAb raised against recurrent tumor cells, targets liver tumor-initiating cells by binding to the calcium channel alpha2delta1 subunit. *Cancer Cell* (2013) 23:541–56. doi: 10.1016/j.ccr.2013.02.025

19. Ryan DP, Hong TS, Bardeesy N. Pancreatic adenocarcinoma. *N Engl J Med* (2014) 371:1039–49. doi: 10.1056/NEJMra1404198

20. Qian X, Xu W, Xu J, Shi Q, Li J, Weng Y, et al. Enolase 1 stimulates glycolysis to promote chemoresistance in gastric cancer. *Oncotarget* (2017) 8:47691–708. doi: 10.18632/oncotarget.17868

21. Zhu X, Yu H, Li B, Quan J, Zeng Z, Li G, et al. Targetting an LncRNA P5848-ENO1 axis inhibits tumor growth in hepatocellular carcinoma. *Biosci Rep* (2019) 39:11. doi: 10.1042/BSR20180896

22. Muller FL, Colla S, Aquilanti E, Manzo VE, Genovese G, Lee J, et al. Passenger deletions generate therapeutic vulnerabilities in cancer. *Nature* (2012) 488:337–42. doi: 10.1038/nature11331

23. Cappello P, Principe M, Bulfamante S, Novelli F. Alpha-enolase (ENO1), a potential target in novel immunotherapies. *Front Biosci (Landmark Ed)* (2017) 22:944–59. doi: 10.2741/4526

24. Zhang K, Tian R, Zhang W, Li Y, Zeng N, Liang Y, et al. α-enolase inhibits apoptosis and promotes cell invasion and proliferation of skin cutaneous melanoma. *Mol Biol Rep* (2022) 49:8241–50. doi: 10.1007/s11033-022-07540-9

25. Yang T, Shu X, Zhang HW, Sun LX, Yu L, Liu J, et al. Enolase 1 regulates stem cell-like properties in gastric cancer cells by stimulating glycolysis. *Cell Death Dis* (2020) 11:870. doi: 10.1038/s41419-020-03087-4

26. Capello M, Ferri-Borgogno S, Riganti C, Chattaragada MS, Principe M, Roux C, et al. Targeting the warburg effect in cancer cells through ENO1 knockdown rescues oxidative phosphorylation and induces growth arrest. *Oncotarget* (2016) 7:5598–612. doi: 10.18632/oncotarget.6798

27. Caspi M, Perry G, Skalka N, Meisel S, Firsow A, Amit M, et al. Aldolase positively regulates of the canonical wnt signaling pathway. *Mol Cancer* (2014) 13:164. doi: 10.1186/1476-4598-13-164

28. Fan K, Wang J, Sun W, Shen S, Ni X, Gong Z, et al. MUC16 c-terminal binding with ALDOC disrupts the ability of ALDOC to sense glucose and promotes gallbladder carcinoma growth. *Exp Cell Res* (2020) 394:112118. doi: 10.1016/j.yexcr.2020.112118

29. Ntellas P, Dadouli K, Perivoliotis K, Sogka E, Pentheroudakis G, Ioannou M, et al. Microvessel density and impact of angiogenesis on survival of resected pancreatic cancer patients: A systematic review and meta-analysis. *Pancreas* (2019) 48:233–41. doi: 10.1097/MPA.0000000000001237

frontiers | Frontiers in Immunology

TYPE Original Research
PUBLISHED 23 February 2023
DOI 10.3389/fimmu.2023.1111319

Check for updates

OPEN ACCESS

EDITED BY
Shariq Qayyum,
Brigham and Women's Hospital and Harvard Medical School, United States

REVIEWED BY
Syed Mohammad Faisal,
Jazan University, Saudi Arabia
Aditya Yashwant Sarode,
Columbia University, United States
Aftab Alam,
University at Buffalo, United States

*CORRESPONDENCE
Yuyan Zhu
yyzhu@cmu.edu.cn
Du Shi
dushi@cmu.edu.cn

†These authors have contributed equally to this work

SPECIALTY SECTION
This article was submitted to Cancer Immunity and Immunotherapy, a section of the journal Frontiers in Immunology

RECEIVED 29 November 2022
ACCEPTED 14 February 2023
PUBLISHED 23 February 2023

CITATION
Xu Y, Xia Z, Sun X, Wei B, Fu Y, Shi D and Zhu Y (2023) Identification of a glutamine metabolism reprogramming signature for predicting prognosis, immunotherapy efficacy, and drug candidates in bladder cancer. *Front. Immunol.* 14:1111319. doi: 10.3389/fimmu.2023.1111319

COPYRIGHT
© 2023 Xu, Xia, Sun, Wei, Fu, Shi and Zhu. This is an open-access article distributed under the terms of the Creative Commons Attribution License (CC BY). The use, distribution or reproduction in other forums is permitted, provided the original author(s) and the copyright owner(s) are credited and that the original publication in this journal is cited, in accordance with accepted academic practice. No use, distribution or reproduction is permitted which does not comply with these terms.

Identification of a glutamine metabolism reprogramming signature for predicting prognosis, immunotherapy efficacy, and drug candidates in bladder cancer

Yan Xu[1†], Zhixiu Xia[2†], Xiaoyu Sun[3], Baojun Wei[1], Yang Fu[1], Du Shi[1*] and Yuyan Zhu[1*]

[1]Department of Urology, The First Hospital of China Medical University, Shenyang, China, [2]Colorectal Tumor Surgery Ward, Department of General Surgery, Shengjing Hospital of China Medical University, Shenyang, China, [3]Department of Pharmacology, School of Pharmacy, China Medical University, Shenyang, China

Background: Bladder cancer is the most common malignancy of the urinary system. However, patient prognosis and treatment outcomes in bladder cancer are difficult to predict owing to high tumor heterogeneity. Given that abnormal glutamine metabolism has been identified as a key factor driving the progression of bladder cancer, it is necessary to assess the prognosis and therapeutic efficacy of bladder cancer treatments based on an analysis of glutamine metabolism-related genes.

Methods: We used bladder cancer sample data downloaded from The Cancer Genome Atlas to identify glutamine metabolism-related genes as prognostic markers, and established a novel Glutamine Metabolism Immunity Index (GMII) based on univariate and multivariate COX regression analyses. On the basis of GMII values, bladder cancer patients were divided into high- and low-risk groups, and systematic analysis was conducted for clinical features, somatic mutations, immune cell infiltration, chemotherapeutic response, and immunotherapeutic efficacy. Candidate small-molecule drugs targeting the GMII core target proteins were identified based on molecular docking analysis.

Results: The GMII consisting of eight independent prognostic genes was established to be an excellent tool for predicting the survival in patients with bladder cancer and was validated using multiple datasets. Compared with patients in the high-risk group, those in the low-risk group had significantly better responses to gemcitabine and immune checkpoint blockade. In addition, we predicted 12 potential small-molecule drugs that could bind to three of the GMII core target proteins.

Conclusions: The GMII can be used to accurately predict the prognosis and immunotherapeutic response of bladder cancer patients, as well as candidate small-molecule drugs. Furthermore, the novel "Glutamine Metabolism-related Gene"-guided strategy for predicting survival and chemo-immunotherapeutic efficacy may also be applicable for cancers other than bladder cancer.

KEYWORDS

bladder cancer, glutamine metabolism, immunotherapy efficacy, prognosis, molecular docking

Background

Bladder cancer is the most common malignancy affecting the urinary system, for which there is high recurrence and mortality rates worldwide (1, 2). Despite advances in surgical treatment, cisplatin-based chemotherapy, and immunotherapy for bladder cancer patients, the 5-year overall survival rate remains low, ranging from 23% to 48% (3). With continued bladder cancer progression, tumor cells require larger amounts of nutrients to sustain their growth, resulting in abnormal metabolism within the tumor microenvironment (4). In this regard. aberrant metabolic pathways have previously been identified as potentially effective biomarkers and therapeutic targets in cancer (5), and prognostic and therapeutic predictions based on such pathways can contribute to enhancing comprehensive individualized treatment outcomes.

Glutamine, which is considered the most abundant and versatile free amino acid (6). is bound by amino acid transporters, following which, it is enzymatically converted to glutamate by glutaminase. Glutamate is subsequently metabolized to α-ketoglutarate *via* glutamate dehydrogenase or transaminase, which then enters the tricarboxylic acid cycle (TCA) to replenish circulating metabolites (7). In many types of cancer, including bladder cancer, glutamine metabolism is dysregulated, which is integral to the rapid proliferation of most tumor cells (8). Given that the efficiency of glutamine import and metabolism is essential for cancer cell viability (9), glutamine is viewed as an attractive target for cancer antimetabolite therapy. Several proteins and enzymes are used as biomarkers to guide tumor diagnosis and treatment, and in this regard, the findings of recent studies have indicated that whereas the primary energy source for most cells is glucose, some immune cells metabolize glutamine at a higher rate under conditions of catabolic stress (10, 11). Glutamine serves as an important source of reduced nitrogen to fuel the synthesis of biomacromolecules, such as nucleotides, that are important for tumor cell proliferation, invasion, and immune escape. However, glutamine is also an essential metabolite for immune cell activation and antitumor effects in the tumor microenvironment (12). Consequently, it is also necessary to take into consideration glutamine metabolism from the perspective of tumor immunotherapy (13, 14). Although glucose metabolism in the context of bladder cancer has been widely studied, the role played by glutamine metabolism in this cancer type is still unclear. Consequently, it is necessary to assess the prognostic importance of glutamine metabolism in bladder cancer based on glutamine metabolism-related genes, and to predict which bladder cancer patient subtypes would respond better to immunotherapy and chemotherapy.

In this study, we molecularly subtyped bladder cancer patients based on glutamine metabolism-related genes and combined a range of statistical algorithms to construct a Glutamine Metabolism Immunity Index (GMII) comprising eight genes involved in glutamine metabolism. We used this GMII to predict tumor immune cell infiltration, chemotherapeutic response, and immunotherapeutic effect, and conducted comprehensive validations. In addition, on the basis of molecular docking analysis, we identified potential small-molecule drugs that bind effectively to glutamine metabolism core target proteins.

Materials and methods

Data sources and preprocessing

We from the cancer genome atlas (TCGA) database (https://portal.gdc.cancer.gov/) to download the bladder cancer patients (including 414 samples of bladder cancer and 19 adjacent non tumor samples) expression of the spectral data, clinical information, somatic mutation. From Gene Expression Omnibus (GEO) database (https://cancergenome.nih.gov/) download GSE13507 (n = 165) and GSE32894 (n = 224) as an independent verification of the queue. The list of genes involved in glutamine metabolism was obtained from the GenesCards database.

Analysis of differentially expressed glutamine genes

The R package "limma" was used to perform the difference analysis with the cutoff value set to p value<0.05. Gene Ontology (GO) and Kyto Encyclopedia of Genes and Genomes (KEGGE) analyses were performed using R package clusterProfiler. The STRING database was used to analyze protein-protein interactions (PPI) (15), and Cytoscape was used to visualize PPI networks (16). We identified key modules by using the 'MCODE'

plug-in in Cytoscape, and used seven algorithms commonly used in 'cytohubba' plug-in (Closeness, Degree, EPC, Radiality, Stress, MCC, MNC) to identify Hub genes. TRRUST databasewas used to predict the transcription factor (TF) of Hub gene (17).

Identification of glutamine metabolism-associated clusters

Bladder cancer samples were clustered by R package "ConsensusClusterPlus" to identify molecular subtypes related to glutamine metabolism. The R package "Survival" was used to perform Kaplan-Meier (KM) survival curves to compare outcomes between the two clusters.

Construction and validation of prognostic features from glutamine metabolism-related genes and their derived GMII

Univariate Cox regression analysis was used to screen out the genes associated with overall survival (OS) of bladder cancer, and multivariate Cox regression analysis was used to establish GMII. The Glutamine Metabolism Immunity Index (GMII) was calculated for each patient according to the following formula: Glutamine Metabolism Immunity Index (GMII) = Coef(Gene1) × Expr (Gene1) + Coef(Gene2) × Expr(Gene2) +…… Coef(Genen) × Expr(Genen). Expr(Genen) represents the expression level of a specific gene, and Coef(Genen) represents the coefficient in multivariate Cox analysis. The prognostic value of the features was verified by KM analysis and Receiver Operation Characteristic (ROC) curve, and the prognostic characteristics were verified by GSE13507. Univariate and multivariate Cox analyses were performed to determine whether the characteristics were independent risk factors. According to the clinical characteristic parameters, the correlation and stratification analysis between GMII and clinical characteristics were performed, and the nomogram was constructed to compare the consistency between predicted and actual survival rates by 1-year, 3-year and 5-year calibration maps.

Pan-cancer analysis

The GSCALite platform was used to analyze the eight genes of GMII (18). Fourteen pairs of normal and tumor tissue samples were selected for differential expression analysis. The prognosis of eight GMII genes was analyzed in 33 pan-cancer cancers. Gene set variation analysis (GSVA) was used to score the expression of these eight genes in each pan-cancer sample, and the GSVA score was obtained. The GSVA score was used to analyze the expression, prognosis and immune cell infiltration of these genes in pan-cancer. We also performed mutational analyses of the eight genes, including single nucleotide variation, copy number variation and methylation. Through CTRP database, we analyzed the expression levels and drug sensitivity of eight genes of GMII.

Immunohistochemical analysis

Build GMII gene immunohistochemical from Human Protein Atlas (HPA) database (https://www.proteinatlas.org/) (19).

Gene set enrichment analysis

We performed GSEA analysis by R package "clusterProfiler" to evaluate the main enrichment pathways in high-GMII groups to explore the underlying biological mechanisms. Filter for | NES |> 1, nominal p value < 0.05. Sample replacement was tested 1000 times, and clustering analysis of enriched gene sets was performed using the R package "enrichplot". Reference genomes include Hallmark, c5go, and c2kegg.

Gene mutation analysis

We calculated the tumor mutation burden (TMB) for each patient from somatic mutation data and compared TMB between high-GMII and low-GMII groups. The waterfall map is depicted through the R package "Maftools", showing the mutation landscape of the high-GMII and low-GMII groups. We also performed mutually exclusive and collaborative analyses of genes with the highest frequency of mutations in the high-GMII and low-GMII groups. Finally, somatic mutations of GMII genes were identified by cBioPortal database.

Immunogenomic landscape analysis

CIBERSORT method used to quantify infiltrating immune cell ratio (https://cibersort.stanford.edu/) (20). The proportion of 22 immune cells (B-naive cells, B-cell memory, plasma cells, T-cell CD8, T-cell CD4 naive, T-cell follicular helper cells, T-cell CD4 memory resting, T-cell CD4 memory activation, regulatory T cells (Tregs), γδ cells, monocytes, activation) was calculated by CIBERSORT method NK cells, resting NK cells, macrophage M0, macrophage M1, macrophage M2, resting dendritic cells, activated dendritic cells, resting mast cells, activated mast cells, eosinophils, and neutrophils). Samples with P<0.05 indicated that the proportion of immune cells calculated by CIBERSORT was correct. The tumor purity, stromal score, immune score and ESTIMATE scorewere calculated for each tumor sample by R package "ESTIMATE" (21). A single sample Gene set enrichment analysis (ssGSEA) algorithm was used to assess the immune infiltration between the two groups based on 28 immune cell types. XCELL, QUANTISEQ, MCPCOUNTER, EPIC and CIBERSORT-ABS software were also used to quantify the relative proportion of immune cell infiltration.

Analysis of chemotherapeutic drug sensitivity between different GMII groups

From tumor susceptibility multiple omics (GDSC) database (https://www.cancerrxgene.org/) (22), download the cancer gene expression data of different drugs, through the calculation of R packages "pRRophetic" IC50 to assess patient response to common chemotherapy drugs.

Prediction of immunotherapy response

Tumor Immune Dysfunction and Exclusion (TIDE) algorithm was used to infer the clinical response of patients to immunotherapy (23). High TIDE scores were associated with poorer immunotherapy. In addition, we extracted the IMvigor210 dataset, a group of clinical information on the treatment of urothelial carcinoma by anti-PD-L1 monoclonal antibody (atezolizumab) (24). The relationship between bladder cancer anti-PD-1 and anti-CTLA4 by Immunophenoscores (IPS) scores and GMII. The IPS score is a predictive score for a patient's response to anti-PD-1 and anti-ctLA-4 treatments (25). was downloaded from TCIA database (https://tcia.at/home). These results were used to evaluate the predictive value of GMII for immune checkpoint therapy.

Molecular docking simulation

We used MOE software to screen FDA-approved drugs that bind to target proteins and perform molecular docking simulations. Protein structures of core targets were collected from the PDB database and FDA-approved drugs were collected from the zinc15 database and converted to 3D structures in MOE by energy minimization. We optimized the protonation state of the protein and the direction of hydrogen at the PH of LigX 7 and the temperature of 300K. Finally, we studied the binding mode of PPARG, SLC7A9 and GALK1 with small molecule drugs by rigid docking simulation.

Statistical analysis

Survival curves were drawn using the Kaplan-Meier method. Wilcoxon test and Kruskal-Wallis test were used for comparison between two groups and more than two groups, respectively. Correlation was assessed by Spearman correlation analysis. A P value of 0.05 or less was considered statistically significant. All statistical analyses were performed by R (version 4.1.1).

Results

Identification of genes related to glutamine metabolism and their biological functions

The flow chart of this study is shown in Figure S1. We obtained 501 genes related to glutamine metabolism from the GeneCards database, and the screening criteria were that the correlation score was greater than 8 and they were protein-coding genes. Differential analysis of BC and normal bladder tissues yielded 301 genes. GO and KEGG analysis were performed to investigate the functions of these genes related to glutamine metabolism. The GO results showed that the genes related to glutamine metabolism were mainly enriched in the biological functions related to energy and metabolism. KEGG results showed that genes related to glutamine metabolism were enriched in signaling pathways such as carbon metabolism, AMPK signaling pathway and amino acid production (Figures 1A, B). PPI networks were analyzed by STRING database and visualized by Cytoscape to obtain three main network diagrams (Figures 1C–E). The common Hub genes were obtained by seven algorithms in Cytoscape software and the transcription factors of Hub genes were predicted in TRRUST database (Figures 1F, G).

Identification of clusters related to glutamine metabolism and correlation analysis between clusters and immune microenvironment

Clustering analysis of bladder cancer patients with glutamine metabolism-related genes obtained after differential analysis showed that BC patients were best divided into two clusters, with good internal consistency and stability of each Cluster (Figure 2A). The general characteristics of Cluster 1 and Cluster 2 are shown in Table S1. The survival curve showed that Cluster2 had a poor prognosis ($p < 0.05$) (Figure 2B). There were significant differences in clinical parameters such as age, gender, subtype, grade, clinical stage, M and race of bladder cancer between the two clusters. Compared with patients with C1 bladder cancer, the proportions of patients older than 60, male, non-papillary invasive subtype, high grade, high stage, M1, white and Asian in patients with C2 bladder cancer were significantly higher than those in patients with C1 bladder cancer ($p < 0.05$) (Figure 2C).

We analyzed the immune microenvironment between the two clusters. Through ESITIMATE algorithm, according to the Cluster 2 has higher ESITIMATE score, immune score, score matrix and lower purity of tumor (Figure 2D). The CIBERSORT algorithm showed that Cluster 2 had higher immune cell infiltration (Figure 2E). Patients' response to immune checkpoint inhibitors was negatively correlated with TIDE score. We found that TIDE score of Cluster 2 patients was significantly higher than that of Cluster 1 patients ($p < 0.05$), indicating that Cluster 2 patients had poor effect on immune checkpoint inhibitors (Figure 2F).

Construction and validation of the GMII

To construct a risk model associated with glutamine metabolism and its derived GMII, eight genes with independent prognostic value were identified by univariate and multivariate Cox analyses to construct GMII (Figure 3A). Coefficients for each gene in GMII (Figure 3B). Correlation analysis between GMII and survival status showed that higher GMII was associated with

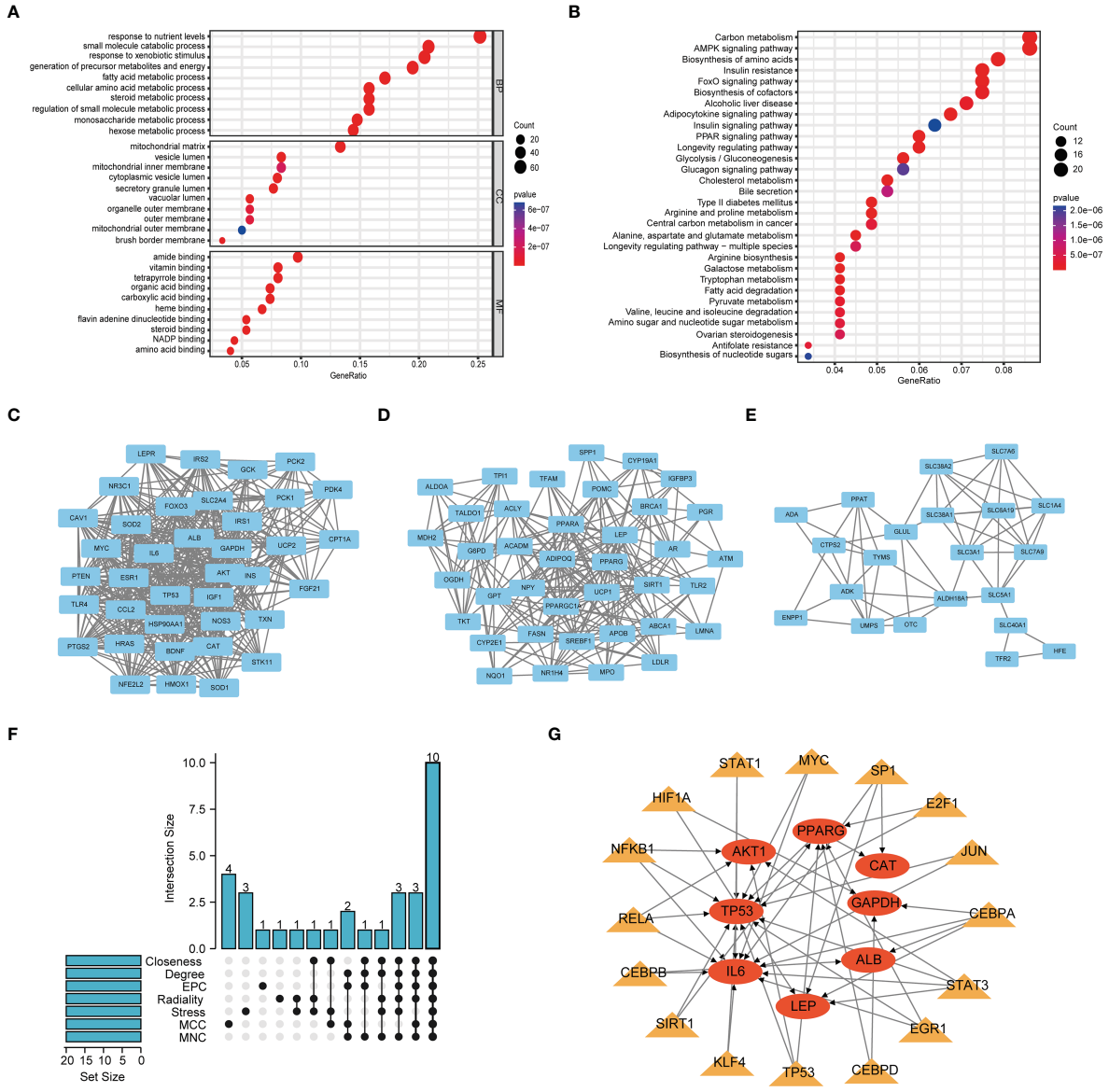


FIGURE 1
Function and subnetwork analysis of genes related to glutamine metabolism. **(A)** The top 10 rich terms for Biological Progress(BP), Cellular Component(CC) and Molecular Function(MF) in GO analysis. **(B)** The top 30 rich terms in KEGG's analysis. **(C–E)** MCODE plug-in gets three main network modules. **(F)** UpSet of cytohubba plug-in seven algorithms. **(G)** Transcription factors predicted by TRRUST for Hub genes. Circles represent genes and triangles represent transcription factors.

higher mortality (Figure 3C). Patients in the high-GMII group had a worse prognosis than those in the low-GMII group ($p < 0.05$) (Figure 3D). To verify the predictive value of this GMII, GSE13507 and GSE32894 were used to verify that the mortality rate in the high-GMII group was significantly higher than that in the low-GMII group ($p < 0.05$) (Figures 3E, F). The area under the 1-year, 3-year and 5-year ROC curves were 0.747, 0.714 and 0.743, respectively (Figure 3G), suggesting that GMII could better predict the short-term and long-term survival status of bladder cancer patients. The general characteristics of TCGA, GSE13507 and GSE32894 patients are shown in Table S2. Univariate and multivariate regression analyses showed that GMII was an independent risk factor (Figures 3H, I). Based on the results of multivariate analysis, a nomogram was constructed based on GMII, age, clinical stage, and T stage, with GMII accounting for the majority of the total score (Figure 3J). Calibration curves showed that the predicted and actual 1 -, 3 -, and 5-year survival rates were consistent with the reference lines (Figure 3K).

The expression of five of the eight GMII genes (TALDO1, AHCY, FASN, GALK1 and SLC7A9) in bladder cancer tissues was higher than that in normal tissues, while ENPP1, CYP19A1 and HSPG2 were down-regulated in tumor tissues ($p < 0.05$) (Figure S2A). Immunohistochemical data of HPA showed that FASN showed moderate staining in the cytoplasm and nucleus of urothelial cancer cells, but no staining was detected in normal bladder tissues. HSPG2 showed high staining in the cytoplasm and

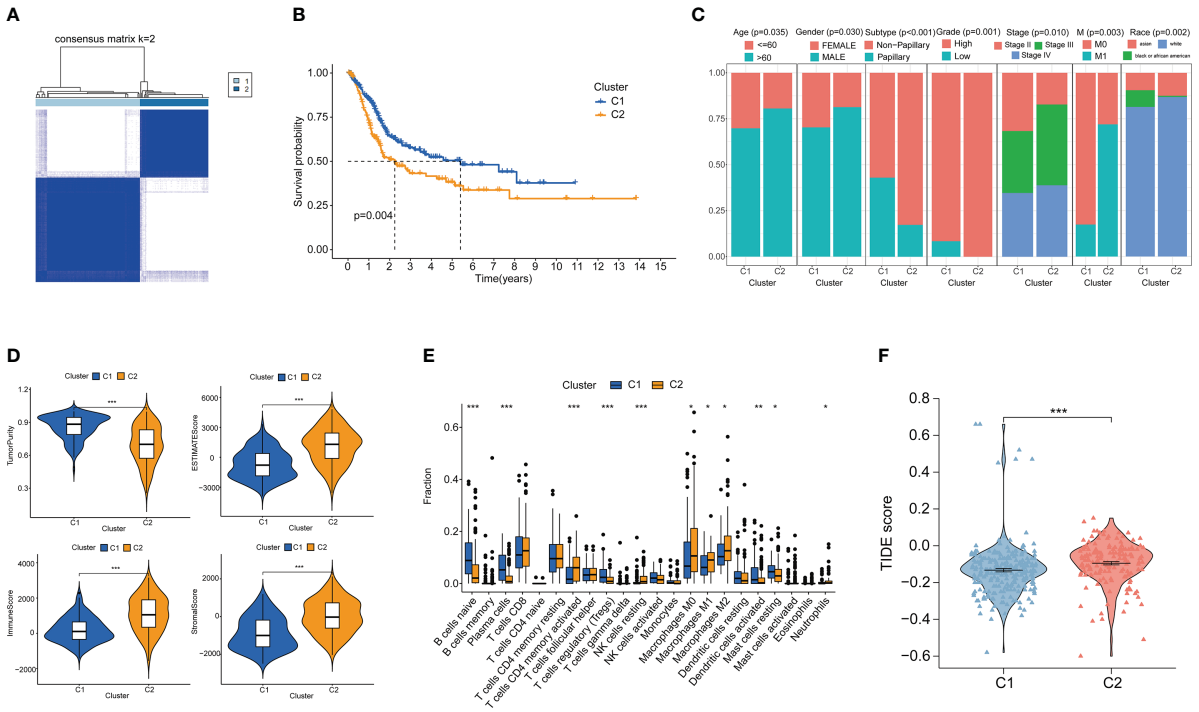


FIGURE 2
Cluster analysis and the association between different clusters with tumor microenvironments and immunotherapy. **(A)** Consensus clustering heat map when k=2. **(B)** Survival curves of two clusters. **(C)** Age, Gender, Subtype, Grade, Stage, M stage and Race between the two clusters. **(D)** Differences in tumor purity, ESITIMATE score, stroma and immune cells between the two clusters. **(E)** CIBERSORT score of immune cell infiltration between the two clusters. **(F)** TIDE score was used to compare the immunotherapy effect between Cluster 1 and Cluster 2. $*p < 0.05$ 、 $**p < 0.01$, $***p < 0.001$.

nucleus of normal bladder cells, but no staining was detected in urothelial carcinoma cells (Figure S2B). Glutamine Related Genes (GRGs) is highly expressed in most tumor tissues and is a high risk factor (Figures S3A, B). Gene set variation analysis (GSVA) was performed on 8 GRGs, and GSVA score was positively correlated with the expression of representative gene sets. Most tumor tissues had significantly higher GSVA scores than normal tissues (Figure S3C). GSVA score was significantly correlated with the prognosis of bladder cancer ($p < 0.05$), including overall survival (OS), progression-free survival (PFS) and disease-free survival (DSS) (Figure S3D). We further evaluated the correlation between GSVA score and immune cell infiltration and showed that GSVA score was significantly correlated with immune cell infiltration in bladder cancer ($p < 0.05$) (Figure S3E). We also collected the features of published prognostic models for bladder cancer and compared the GMII features with their prognostic prediction accuracy. The results showed that GMII values were superior to other models in terms of prognostic prediction (Figure S4).

Clinical correlations analysis of GMII

To further verify the clinical significance of GMII, we analyzed the differences in GMII between different clinical characteristics groups. The results showed that patients with Cluster 2, Non-papillary infiltration, lymphovascular invasion, High Grade, stage III-IV, M1 and N1-3 had higher GMII, suggesting that the higher the GMII, the more advanced the tumor (Figure 4A). Stratified analysis showed that GMII could significantly differentiate the prognosis of almost all clinical subgroups, with patients in the high-GMII group having a worse prognosis (Figure S5). To investigate the pathways that regulate tumorigenesis in the high-GMII group, we performed GSEA analysis, and the results showed that, The high GMII group was significantly enriched in high glutamine metabolism, glutamine synthesis and decomposition ($p < 0.05$) (Figure 4B). In addition, the high-GMII group was significantly enriched in carcinogenesis, angiogenesis, and epithelial-mesenchymal transition (EMT) pathways ($p < 0.05$) (Figure 4C). Glycolysis and myosynthesis were the features with the highest NES in the high-GMII group (Figures 4D, E).

Relationship between GMII and immune microenvironment

Previous studies have shown that glutamine metabolism and tumor microenvironment play an important role in tumor development (7, 26). The ESTIMATE algorithm found that the high GMII group had lower tumor purity (Figure 5A) and higher ESTIMATE score (Figure 5B), immune score (Figure 5C) and

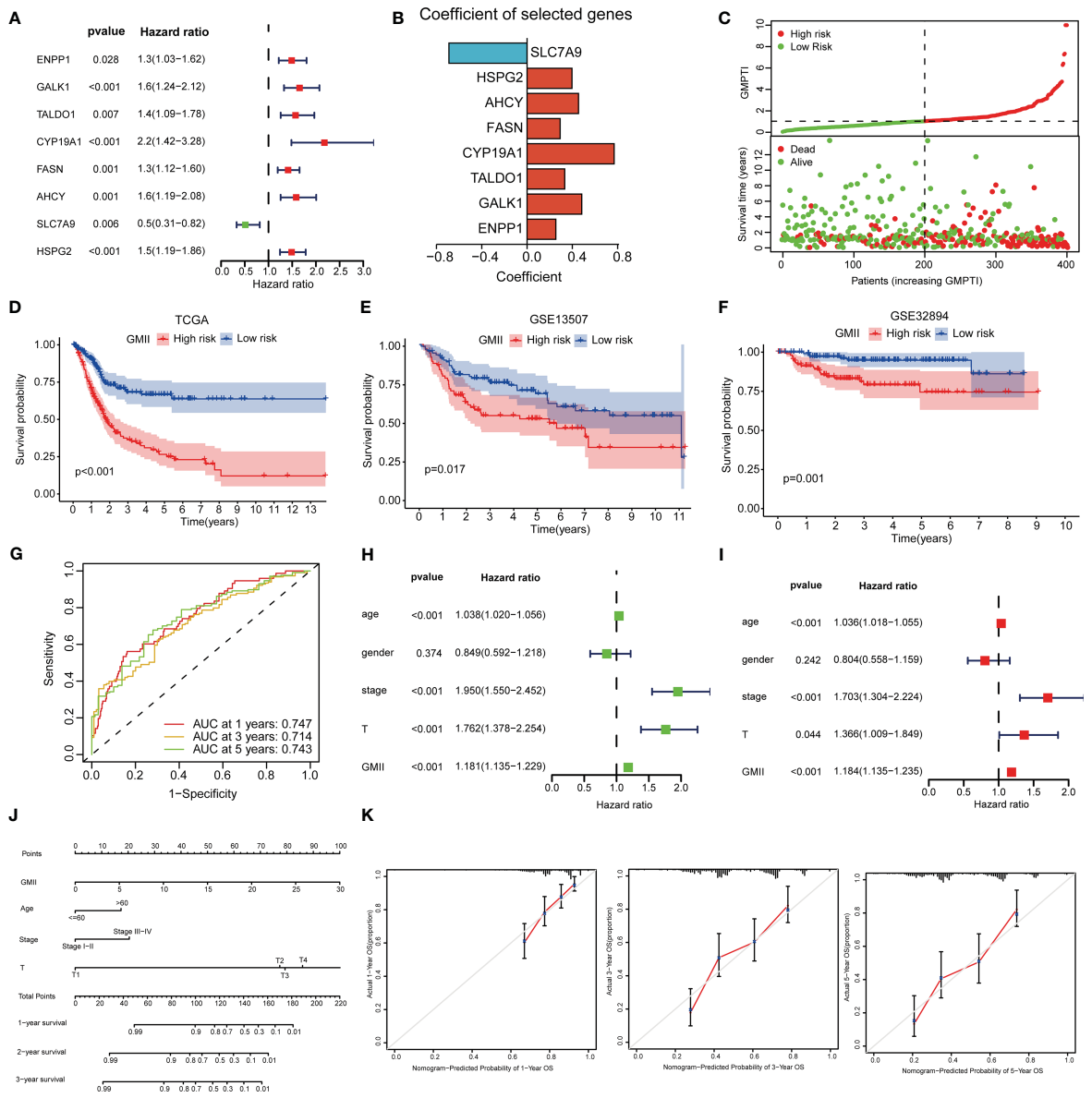


FIGURE 3
Construction of prognostic treatment index related to glutamine metabolism and validation of external data sets. **(A)** Forest maps of eight GRGs obtained by multivariate Cox analysis. **(B)** Construct eight GRGs coefficients of GMII. **(C)** Survival state of TCGA queue. **(D)** Kaplan-Meier survival curve of the TCGA cohort. **(E)** Kaplan-Meier survival curve of the GSE13507 cohort. **(F)** Kaplan-Meier survival curve of the GSE32894 cohort. **(G)** ROC curve of TCGA queue. **(H, I)** univariate and multivariate regression analysis. **(J)** Histogram based on GMII, age, clinical stage, and T-stage. **(K)** Calibration curves show the consistency of 1-year, 3-year, and 5-year survival rates predicted from bias-adjusted prognostic columns with actual survival rates.

stromal score (Figure 5D). CIBERSORT algorithm showed that the level of CD8 T cells in the high-GMII group was significantly lower than that in the low-GMII group ($p < 0.05$), and the level of immunosuppressive M2-type macrophages was increased in the high-GMII group, suggesting that the high-GMII group had higher immunosuppressive activity and promoted tumor progression (Figure 5E). We found correlations between GMII and a variety of immune cells using different software (Figure 5F). The ssGSEA algorithm results showed that the high-GMII group had higher immune cell infiltration and immune-related functions and pathways than the low-GMII group (Figure 5G).

Relationship between GMII and somatic cell mutation

TMB is an important predictor of immunotherapy and chemotherapy. To further investigate the association of GMII with somatic mutations in cancer cells, we used single nucleotide variation data to investigate differences in genomic mutations between high-GMII and low-GMII groups. TP53, TTN, KMT2D, MUC16 and ARID1A were the top five genes with the highest mutation frequency in high-GMII and low-GMII populations, but the mutation frequency of each gene was different between the two

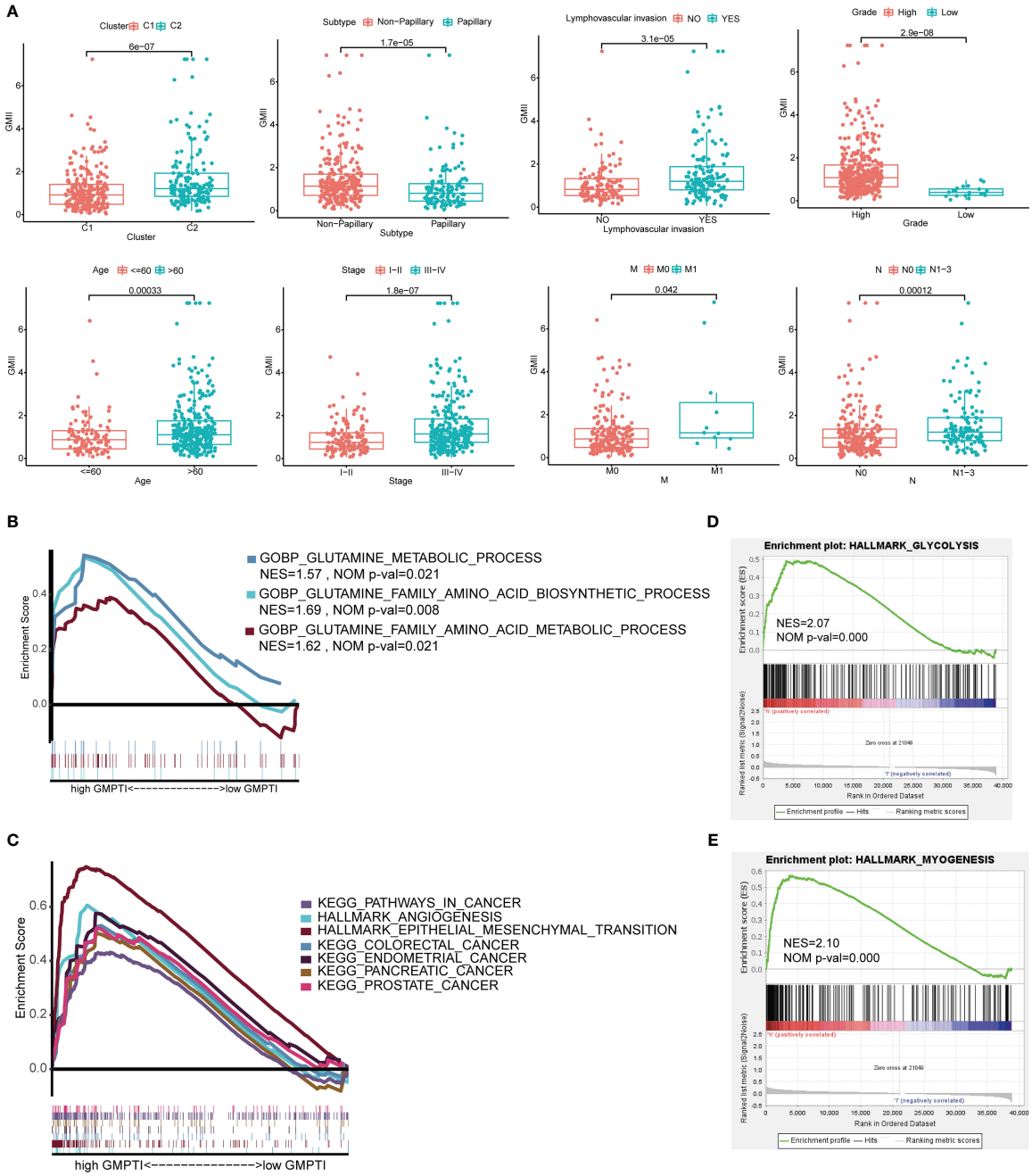


FIGURE 4
Correlation between GMII and clinical traits and gene set enrichment analysis in high-GMII group. **(A)** Differences in GMII between different clinical feature groups. **(B)** Pathways related to glutamine metabolism are abundant in the high-GMII group. **(C)** Glycolysis was significantly enriched in the high-GMII group. **(D)** Pathways associated with tumor development and progression are abundant in the high-GMII group. **(E)** Muscle synthesis was significantly enriched in the high-GMII group.

groups (Figures 6A, B). Through mutual exclusion and cooperation analysis among mutated genes, it was found that there was gene mutation synergy between most genes, and significant mutational mutual exclusion of TP53-ARID1A and EP300-ZFHX4 was found in the high-GMII group (Figure 6C). Significant mutational mutual exclusion of TP53-FGFR3 and KMT2D-FGFR3 was also found in the low-GMII group (Figure 6D). There were no differences in TMB between the two groups or in survival curves between the high and low TMB groups (Figure S6A, B). After TMB combined with GMII, the prognosis of the high TMB+ low GMII group was significantly better than that of the low TMB+ high GMII group (Figure S6C). In addition, the mutation rate of eight genes in GMII was detected in the cBioPortal database, and it was found that the mutation rate was low (Figure 6E).

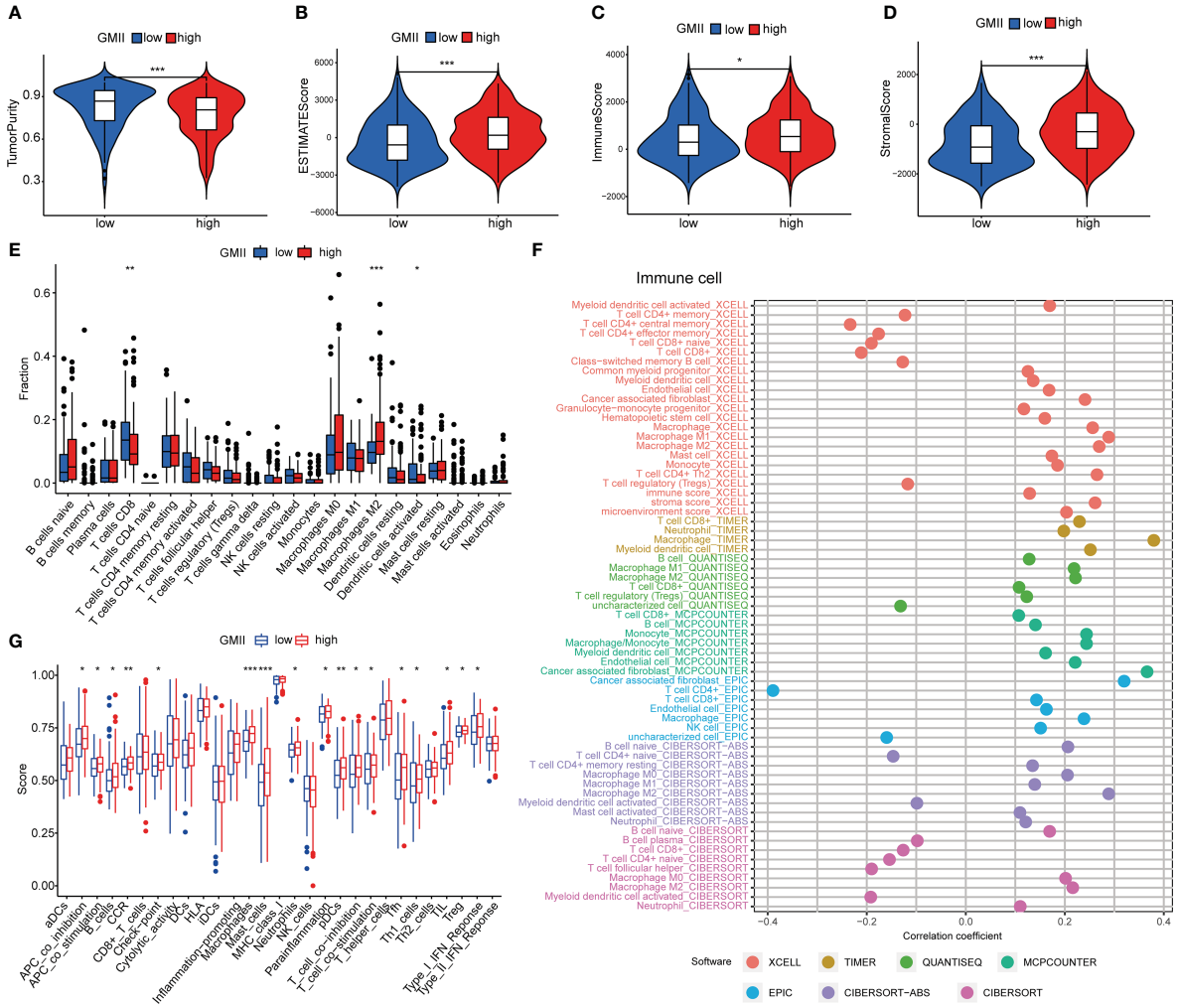


FIGURE 5
Immune cell infiltration in high-GMII and low-GMII groups. Tumor purity **(A)**, ESTIMATE score **(B)**, immune score **(C)**, and stromal score **(D)** between high – and low-GMII populations. **(E)** CIBERSORT algorithm was used to analyze the contents of immune cell infiltration in high-GMII and low-GMII groups. **(F)** Different software evaluated the correlation between immune scores and immune cells. **(G)** ssGSEA algorithm showed immune cell infiltration of immune-related functions and pathways in high-GMII and low-GMII groups. *$p < 0.05$ 、 **$p < 0.01$, ***$p < 0.001$.

Prediction of chemotherapy effects by the GMII

To investigate the potential of GMII for predicting the response to chemotherapytic therapy, We first downloaded data from the GDSC database on the response of high-GMII and low-GMII populations to common chemotherapy agents. The results showed that many common bladder cancer chemotherapy drugs had significant differences among high-GMII groups ($p<0.05$). Gemcitabine, as the most common chemotherapy drugs for bladder cancer, had significantly lower IC50 values in the low-GMII group than in the high-GMII group ($p<0.05$), suggesting that Gemcitabine may have better efficacy in the low-GMII group (Figure 7A). We also mapped the 3D structures of chemotherapeutic agents with differences between the two groups using the PubChem database (Figure S7). The relationship between GRGs and drug sensitivity was analyzed from cellMiner database, and the histograms of the top five drugs with the highest correlation between genes and drug sensitivity were drawn. Positive correlation indicates that stronger gene expression is more sensitive to drugs, while negative correlation indicates that stronger gene expression is more resistant to drugs. Among them, up-regulation of FASN expression may lead to enhanced sensitivity of patients to most drugs (Figure 7B). In addition, GDSC database was used to analyze the relationship between drug sensitivity and mRNA expression of the eight GRGs used to construct GMII. Contrary to cellMiner database, positive correlation represented that gene expression was related to drug resistance, while negative correlation represented that gene expression was related to drug sensitivity. The relationship between AHCY gene expression and chemotherapy-drug sensitivity is extensive, and HSPG2 has the highest correlation with most chemotherapy-drug sensitivity, among which HSPG2 is correlated with Dasatinib sensitivity in both databases (Figure 7C). These results suggest that the expression changes of genes constructing GMII may be effective indicators for predicting drug response and as potential therapeutic targets.

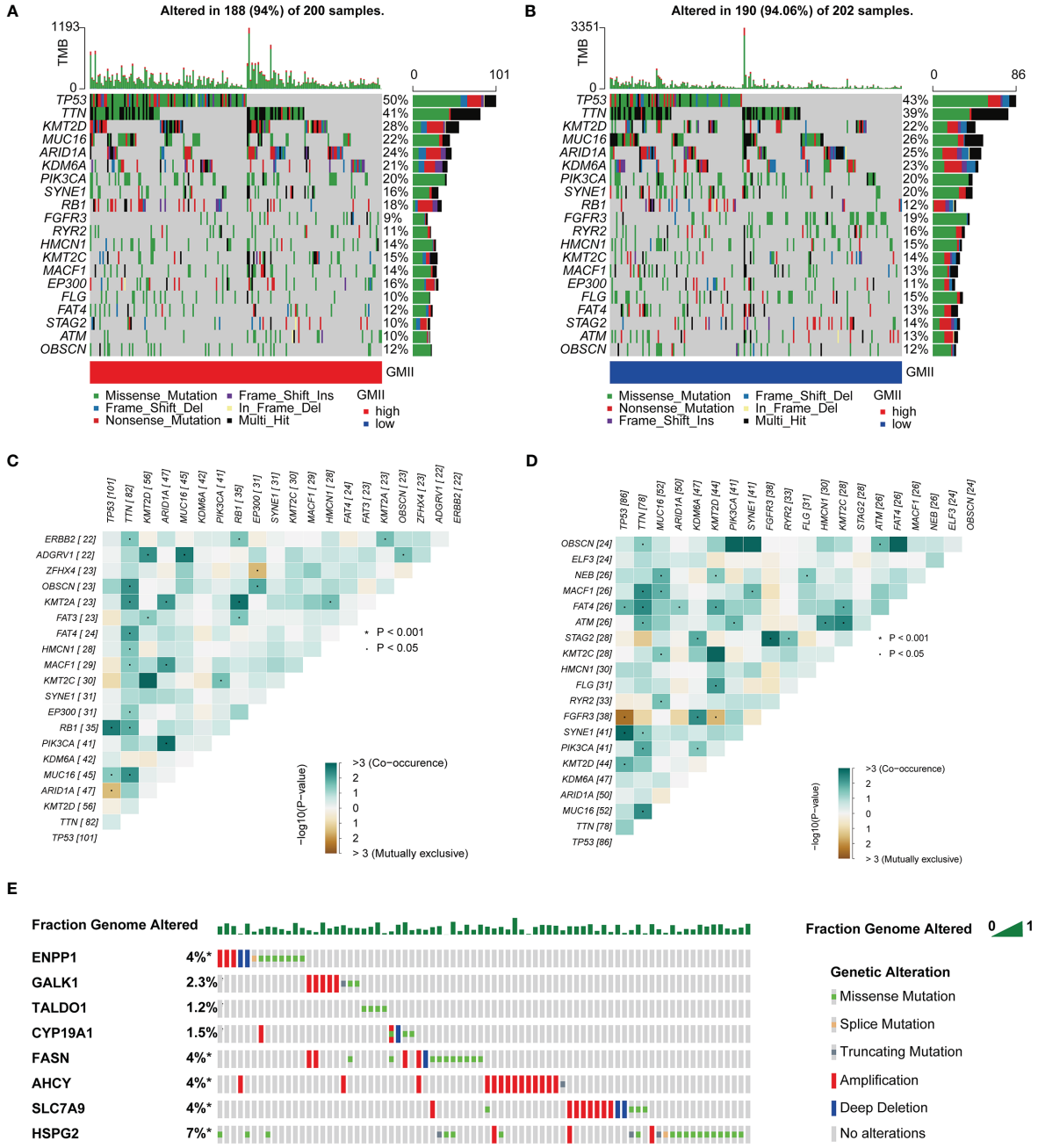


FIGURE 6
Association of GMII with genetic changes. Waterfall diagrams of somatic mutations in high-GMII **(A)** and low-GMII **(B)** groups. Mutual exclusion and synergistic heat maps of mutated genes in high-GMII **(C)** and low-GMII **(D)** groups. **(E)** Mutation rates of the eight GRGs that constructed GMII.

Prediction of immunotherapy efficacy by the GMII

Immune checkpoint inhibitors have provided clinical benefits in the treatment of a variety of tumors. By analyzing the correlation between genes in GMII and common immune checkpoints, we found that genes with the highest correlation with glutamine metabolism were significantly negatively correlated with PD-1/PD-L1 expression. For example, SLC7A9, a glutamine transporter, and FASN, a key enzyme in the metabolism of glutamine into fatty acids. These results indicated an inverse correlation between glutamine metabolism and PD-1/PD-L1 expression (Figure 8A). The expression of most immune checkpoints was different between the high-GMII group and the low-GMII group ($p < 0.05$) (Figure S8). Higher TIDE scores were associated with poorer immune checkpoint blockade therapy and shorter survival, and higher TIDE scores in the high-GMII group suggested poorer response to immune checkpoint blockade therapy (Figure 8B). The results of IMvigor210 dataset showed that there was a significant difference in GMII between the immunotherapy response group and the non-response group ($p<0.05$), and the GMII was lower in the response group (Figure 8C). The scores of IPS, IPS-PD1 blocker, IPS-CTLA4

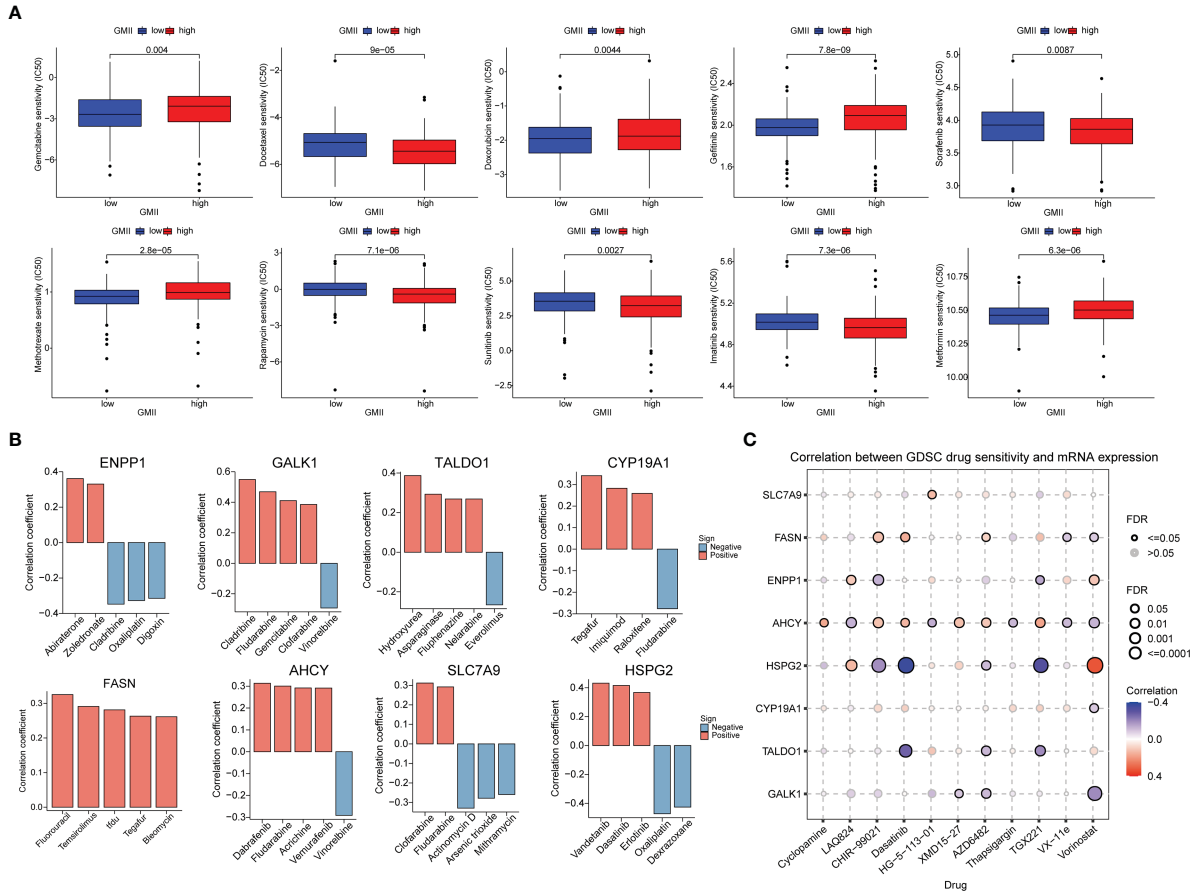


FIGURE 7
Effect of GMII on drug sensitivity. **(A)** Differences in response to commonly used chemotherapy drugs between high-GMII and low-GMII groups. **(B)** Construct the correlation between GMII gene and drug sensitivity. **(C)** Correlation between GDSC drug sensitivity and mRNA expression levels of eight genes that construct GMII.

blocker, and IPS-PD1-CTLA4 co-blocker were lower in the high-GMII group, indicating that the high-GMII group had a poor effect of anti-PD1, anti-CTLA4, and anti-PD1-CTLA4 co-treatment (Figure 8D). These results suggest that GMII may be associated with immunotherapy in bladder cancer patients.

Identification of core target proteins and prediction of drug candidates

In order to identify the core targets of genes related to glutamine metabolism, we constructed a PPI network through the STRING database (confidence score greater than 0.4), found the most closely related subnetwork to the GMII gene and found the core gene PPARG by "MCODE" in Cytoscape software (Figure S9). PPARG is located at the hub of the network and has the highest degree among all nodes. SLC7A9 is potentially used as a glutamine transporter and GAPK1 as a targeted receptor with small molecule inhibitors of kinases. We obtained X-ray structures of PPARG, SLC7A9 and GALK1 from the PDB database to screen 1379 FDA-approved drugs potentially targeting PPARG, SLC7A9 and GALK1. We used rigid docking in MOE to simulate the binding mode of small molecule drugs to PPARG, SLC7A9 and GALK1, where the interaction relationship between target proteins and candidate small molecules is shown in Table S3. We show the top four small-molecule drugs with the highest binding ability to PPARG (Bosulif, Candesartan, Centany, and Nefazodone) (Figures 9A–D) and the top four small-molecule drugs with the highest binding ability to SLC7A9 (Propantheline, Naloxeg) ol, Cobicistat and Fosinopril) (Figures 9E–H) and the top four small-molecule drugs with the highest GALK1 binding capacity (Propantheline, Ipratropium, Cangrelor and Lopinavir) (Figures 9I–L). For example, Bosulif (ZINC000022448983) forms hydrogen bonds with PPARG amino acid residues Met-348, Met-364 and His-449, among which Met-348 and Met-364 act as hydrogen bond acceptor and His-449 act as hydrogen bond donor. Naloxegol (ZINC000095564694) forms hydrogen bonds with SLC7A9 non-transmembrane amino acid residues Lys-53, Ser-57, Lys-145 and Thr-434, among which Ser-57 and Thr-434 act as hydrogen bond acceptor. Lys-53 and Lys-145 act as hydrogen bond donors. Cangrelor (ZINC000085537017) formed hydrogen bond and ion bond related interaction with GAPK1 amino acid residues Arg-228 and Arg-105, among which Arg-228 and Arg-105 were hydrogen bond donors. In addition, these small molecules form van der Waals

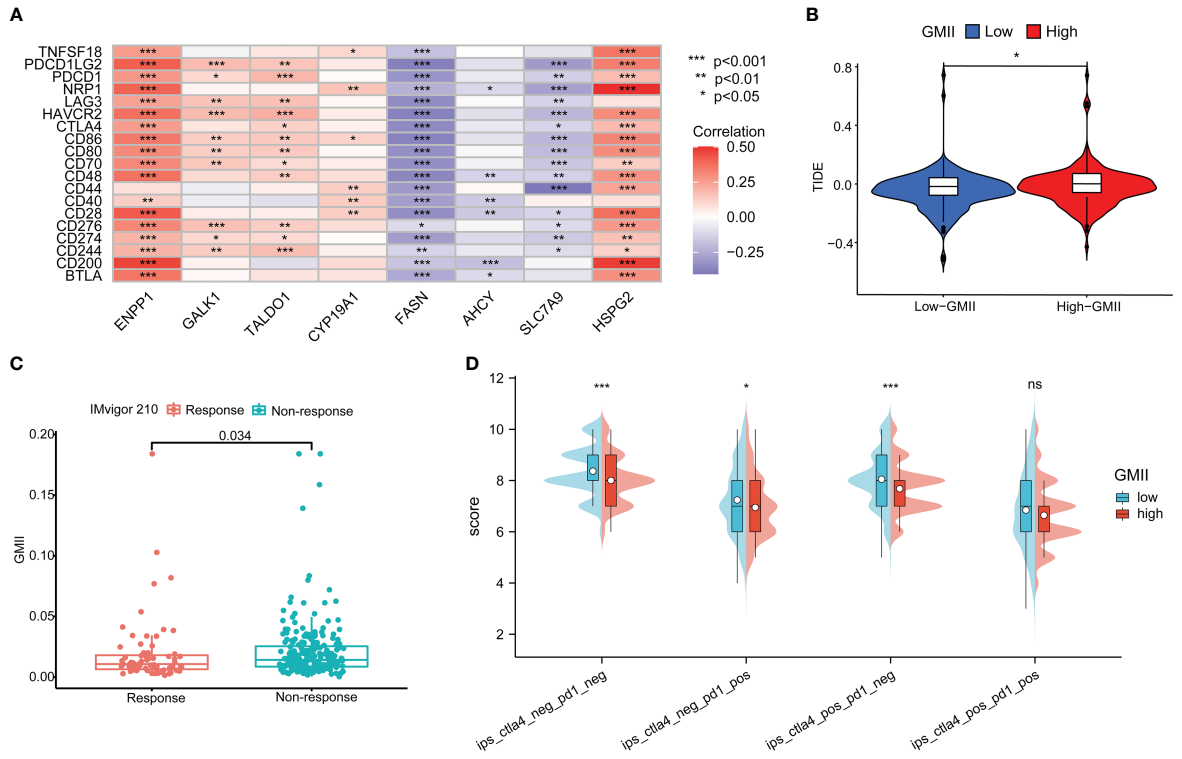


FIGURE 8
Application of GMII in immunotherapy prediction. **(A)** GMII gene expression was associated with common immune checkpoints. **(B)** TIDE scores were used to compare immunotherapy efficacy between high-GMII and low-GMII groups. **(C)** The IMvigor 210 database analyzed GMII in the responding and non-responding groups to immunotherapy. **(D)** The difference in response between high-GMII and low-GMII groups to PD1- or no-CTLA4 blockers, PD1 blockers, CTLA4 blockers, and PD1-CTLA4 co-blockers. *$p < 0.05$ 、 **$p < 0.01$, ***$p < 0.001$. ns, Non Significance.

(VDW) interactions with residues around the protein receptor, which contribute to the binding energy between small molecules and PPARG.

Discussion

Abnormal glutamine metabolism is considered a key factor driving the progression of solid tumors such as bladder cancer (8) (27); and consequently, there is an urgent need to identify more reliable and accurate glutamine metabolism-related markers that can be used to predict bladder cancer patient survival and immunotherapeutic response. In this study, we established the GMII consisting of eight glutamine metabolism-related genes (*ENPP1*, *GALK1*, *TALDO1*, *CYP19A1*, *FASN*, *AHCY*, *SLC7A9*, and *HSPG2*), a high value of which is associated with poor prognosis in bladder cancer patients. For comparative purposes, we evaluated the efficacy of other prognostic models for bladder cancer, which showed that the predictive performance of GMII was superior to that of all other assessed models. Furthermore, the GMII could be used to differentiate among patients with different levels of immune checkpoint expression, and predict their therapeutic response to ICI therapy. Moreover, on the basis of in silico molecular docking analysis, we identified potential drugs that can modulate the core target proteins of glutamine metabolism. Thus, aberrant glutamine metabolism signaling, as a reliable predictor of bladder cancer prognosis and immunotherapeutic response, may provide valuable insights for establishing effective therapeutic approaches for the treatment of bladder cancer.

In our previous study, we attempted to predict the prognosis of bladder cancer patients and their treatment response based on overall metabolic profiles (28). However, despite accumulating evidence that tumor-specific metabolic phenotypes are closely associated with prognosis and treatment response, there has to date been an insufficient assessment of gene signature indices focusing on key amino acid metabolic pathways, such as that involved in glutamine metabolism (13). In this study, we found that the GMII value is inversely associated with most immune checkpoint genes. We established that the TIDE score based on the high-GMII group (high GMII value) was significantly higher than that of the low-GMII group, indicating that ICI therapy is less effective for the treatment of patients with a high-GMII score. IPS has been established to be a better predictor of immunotherapy response in cancer patients undergoing anti-PD-1 and anti-CTLA-4 treatment (25). and we found that levels of IPS, IPS-PD1, IPS-CTLA4, and IPS-PD1-CTLA4 co-blockers were lower in the high-GMII group, thereby indicating that anti-PD-1 and anti-CTLA-4 treatments were less effective in the treatment of high-GMII group patients. Consistent with our observations, among patients in the IMvigor210 cohort with urothelial carcinoma, significant differences in GMII have been identified in the responders and non-responders to PD-L1 therapy. In the present study, we assessed

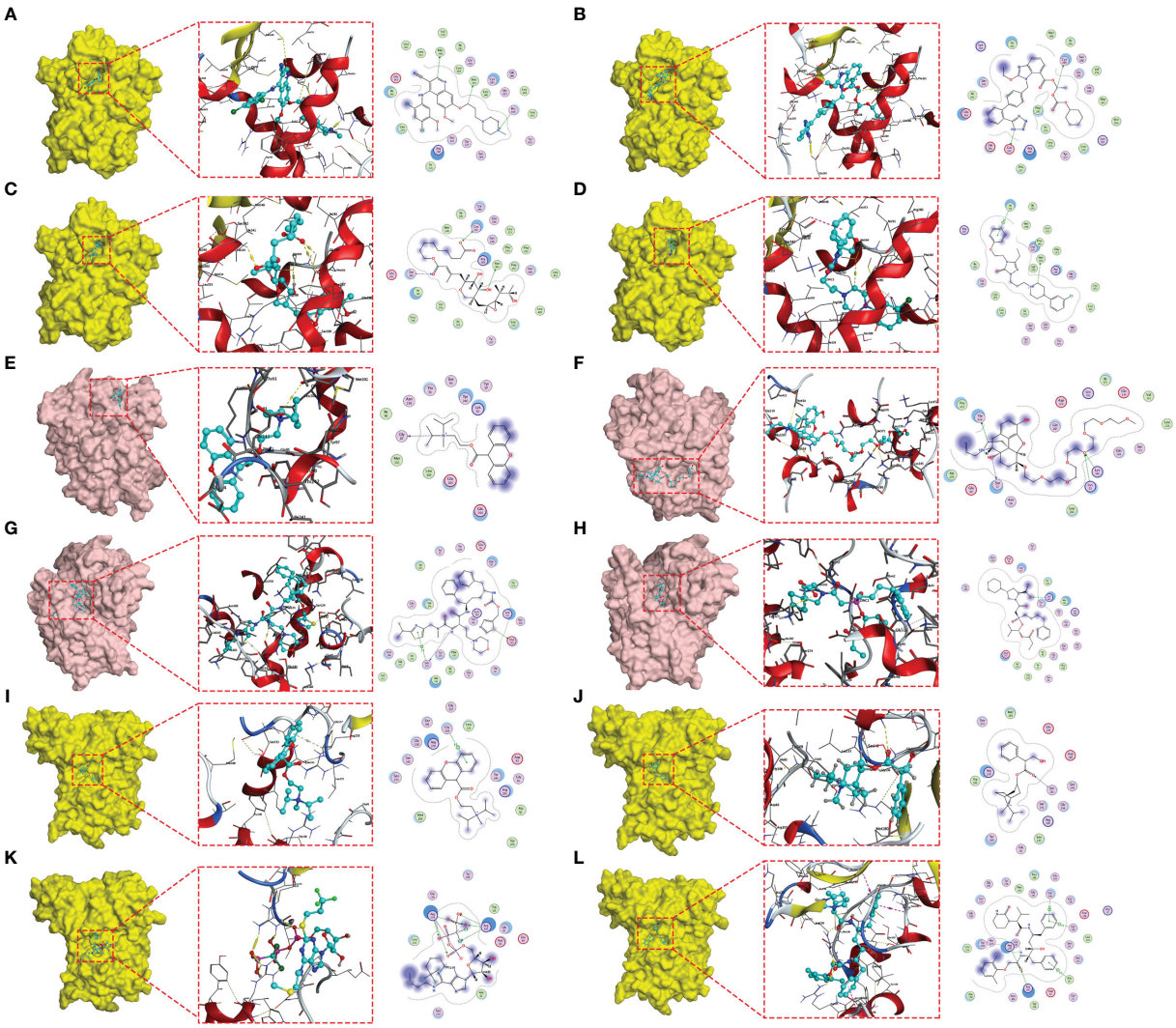


FIGURE 9
Molecular docking posture. Candidate drugs and target proteins screened using molecular docking. The Figure shows the docking position of the PPARG active pocket with Bosulif **(A)**, Candesartan **(B)**, Centany **(C)** and Nefazodone **(D)**. Docking position of the SLC7A9 active pocket with Propantheline **(E)**, Naloxegol **(F)**, Cobicistat **(G)** and Fosinopril **(H)**. Docking position of GALK1 active pocket with Propantheline **(I)**, Ipratropium **(J)**, Cangrelor **(K)** and Lopinavir **(L)**.

the responses of bladder cancer patients to common chemotherapeutic drugs based on their IC50 values and calculated the association between gene expression and drug sensitivity, which revealed significant differences in the responses to common chemotherapeutic drugs such as gemcitabine in the two GMII groups. These findings thus indicate that the risk model we constructed and the derived GMII can serve as effective indicators for assessing the response of bladder cancer patients to chemotherapy and immunotherapy, and may provide useful guidance for the future treatment of these patients.

The roles of the eight GMII genes in glutamine metabolism-related pathways can be characterized as follows. (1) Amino acid transport: Unlike SLC1A5, which is currently widely targeted in clinical studies, our analysis indicates that SLC7A9 is important for bladder cancer (29). Multiple studies have shown that SLC7A9 plays an essential role as a transporter of different amino acids for tumors, as these compete with immune cells for nutrients (30, 31). (2) Glutamate production: AHCY has a strong copper-binding capacity and is highly expressed, resulting in elevated glutamine levels (32, 33). GALK1 is a key enzyme in the catabolism of galactose, which can be further converted to glutamate by other enzymes (34). (3) Glutamate metabolism: FASN is a central regulator of *de novo* fatty acid synthesis that promotes the anabolic biosynthesis of fatty acids from citrate (7). *TALDO1* encodes a transaldolase (TA) that promotes nucleotide synthesis and the metabolic scavenging of ROS (35). and CYP19A1 is a cytochrome P450 (CYP) enzyme with immunomodulatory effects (36). (4) (4) Immune cell-related metabolism: ENPP1 promotes tumor cell metastasis and tumor immune escape (37). and HSPG2 is a cell-surface antigen that regulates NK cell activation (Figure 10). Given that the expression patterns of the aforementioned eight glutamine metabolic genes associated with tumorigenesis and regulation of the tumor immune microenvironment, the glutamine metabolism-related risk model and its derived GMII

can be considered to closely reflect the prognosis of bladder cancer and predict the effects of chemotherapy and immunotherapy.

Our systematic study of immunological and chemotherapeutic differences between low- and high-GMII groups has provided important insights into the mechanisms underlying aberrant glutamine metabolism in bladder cancer and the predictive utility of the GMII. In this regard, the findings of several previous studies have revealed the key roles of glutamine metabolism and the tumor immune microenvironment in tumor progression (12). Bladder cancer cells have been established to utilize immune checkpoint molecules such as PD-L1 to induce immune escape, thereby generating an immunosuppressive tumor microenvironment around bladder cancer cells (38),. In addition, bladder cancer cells have been shown to induce the activation of tumor-associated macrophages and regulatory T (Treg) cells, which in turn suppresses the antitumor activity of CD8+ cytotoxic T cells (39, 40). By constructing the GMII for glutamine metabolism-related genes to identify their response to immunotherapy, we found that patients in the low-GMII group (low glutamine metabolism) showed a more significant response to PD-L1 and PD-1 blockade treatment. Correspondingly, we found that although patients in the high-GMII group (high glutamine metabolism) were characterized by higher immune infiltration, they also harbored a larger number immunosuppressive cells, such as Treg cells and M2 subtype macrophages, which are known to suppress anti-tumor CD8+ T cells. Indeed, we detected a significant reduction in the proportion of CD8+ T cells among patients in the high-GMII group. Overall, this further highlights the fact that specific immune microenvironments promote the progression of bladder cancer and govern the responses to immunotherapy. Consistent with this scenario, the findings of a recent study have revealed that by activating the EGFR/ERK/c-Jun pathway, glutamine deprivation can promote the upregulation of PD-L1 in bladder cancer cells (8). Moreover, blocking glutamine can induce different metabolic processes to overcome the immune escape of tumors and enhance the efficacy of immunotherapy (41, 42). These observations thus provide evidence to indicate a complex dynamic regulatory relationship between glutamine metabolism and the tumor immune microenvironment (43). Accordingly, the characterization of glutamine metabolism may represent a novel approach for screening treatment-receptive patients and enhancing the efficacy of immunotherapy. Conversely, however, the findings of previous studies have indicated that glutamine metabolism can provide raw materials for the over-activated glycolysis and oxidative phosphorylation of tumor cells, and by promoting metabolic homeostasis, can also contribute to inducing tumor cell resistance to chemotherapeutic drugs (44–46). The perturbation of glutamine metabolism has also been shown to enhance sensitivity to gemcitabine in different types of solid tumors (47). On the basis of the aforementioned observations, we further analyzed differences between the different glutamine metabolism groups with respect to the efficacy of responses to common chemotherapeutic drugs, and found that patients in the low-GMII group were characterized by a more pronounced sensitivity to common chemotherapeutic drugs such as gemcitabine. These findings thus indicate that characterizing glutamine metabolism can also serve as a reasonable and effective method for screening receptive patients and enhancing the efficacy of chemotherapy. Consequently, targeting glutamine metabolism combined with PD-1/PD-L1 checkpoint blockade therapy and/or chemotherapy could represent a potentially effective therapeutic strategy for improving treatment outcomes among bladder cancer patients.

As a further application of GMII efficacy prediction, we demonstrated the feasibility of combining core target and structure-based approaches to identify drug candidates. On the basis of a PPI network constructed using genes associated with glutamine metabolism, we identified PPARG as the major hub gene, and by employing molecular docking software, we used PPARG, SLC7A9, and GALK1 as small-molecule drug targets to screen for potential drugs from among those in the FDA-approved drug library. We accordingly found that the first four small molecules with the highest PPARG binding ability (Bosulif, Cadesartan, Centany and Nefazodone) bind to the NR-LBD domain of PPARG protein and prevent it from binding to the nuclear ligand. The top four small molecules with the highest GALK1 binding fraction (Propantheline, Ipratropium, Cangrelor and

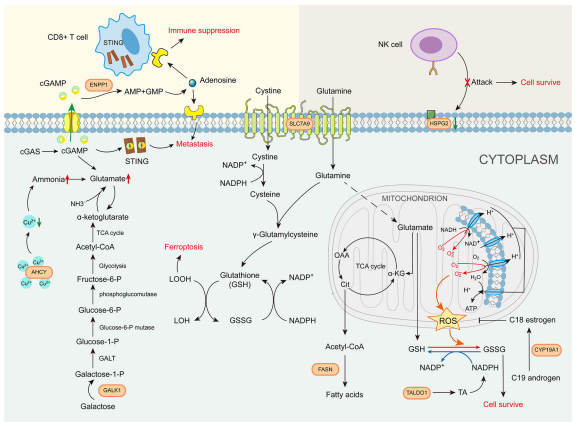


FIGURE 10
The role of glutamine metabolism immunity index gene in glutamine metabolism-related pathways.

Lopinavir) bind to the ATP-binding site of GALK1, blocking ATP occupation and thus affecting the protein kinase function of GALK1. PPARG acts as a nuclear receptor that regulates multiple biological functions, including adipogenesis, metabolism, and immunity (48). and PPARG signaling has been reported to have an important influence on immune rejection in patients with bladder cancer (49). Among the four small molecule drugs with the highest affinity for PPARG, bosulif has been reported in clinical trials for chronic myeloid leukemia (50). In addition, propantheline, which can be used to enhance the efficacy of antiretroviral drugs, can target SLC7A9, which in turn affects the amino acid nutrition of the tumor microenvironment and thus tumor cell survival. Cangrelor, which has been shown to be beneficial for intraoperative antiplatelet therapy, and lopinacir, which has been used in the treatment of severe COVID-19, were found to have high affinity for GALK1 (51, 52). Although the specific mechanisms of action of these small-molecule compounds remain to be further investigated, our findings indicate that they have potential utility for tumor immunotherapy, particularly among bladder cancer patients with abnormal glutamine metabolism.

Despite our important findings, this study does have certain limitations. Notably, our analysis, and hence conclusions, are based on data obtained from public databases, which may accordingly have led to inherent case selection bias. In addition, although our findings were validated based on assessments using multiple external datasets, the evaluation of a larger number of clinical cases is necessary to further verify the accuracy of our results. Finally, further *in vivo* and *in vitro* experiments are needed to examine the function of GRGs in bladder cancer.

Conclusion

In conclusion, based on the in-depth analysis of multiple aspects of bladder cancer based on the risk model and its derived GMII, we found that GMII can better predict the prognosis and immunotherapy response in BC patients. This study provides useful clues for the discovery of novel prognostic and therapeutic biomarkers and small-molecule drug targets from the perspective of oncogenic amino acid metabolic reprogramming. In an era when immunotherapy offers great promise for various cancer treatments, GMII provides guidance for the clinical diagnosis and individualized comprehensive treatment of bladder cancer.

Data availability statement

The original contributions presented in the study are included in the article/Supplementary Material. Further inquiries can be directed to the corresponding authors.

Author contributions

YX: formal analysis, data curation, conceptualization, writing original draft. ZX: formal analysis, visualization. XS: software, investigation. BW: investigation. YF: investigation. DS: software, supervision. YZ: conceptualization,writing—review and editing, supervision, project administration, funding acquisition. All authors contributed to the article and approved the submitted version.

Funding

This work was supported by the national natural science foundation of China (grants 81672523).

Conflict of interest

The authors declare that the research was conducted in the absence of any commercial or financial relationships that could be construed as a potential conflict of interest.

Publisher's note

All claims expressed in this article are solely those of the authors and do not necessarily represent those of their affiliated organizations, or those of the publisher, the editors and the reviewers. Any product that may be evaluated in this article, or claim that may be made by its manufacturer, is not guaranteed or endorsed by the publisher.

Supplementary material

The Supplementary Material for this article can be found online at: https://www.frontiersin.org/articles/10.3389/fimmu.2023.1111319/full#supplementary-material

SUPPLEMENTARY TABLE 1
Clinical statistical analysis of Cluster 1 and Cluster 2.

SUPPLEMENTARY TABLE 2
General characteristics of patients with TCGA, GSE13507 and GSE32894.

SUPPLEMENTARY TABLE 3
Interaction between target protein and candidate small molecules

SUPPLEMENTARY FIGURE 1
Flow chart of this study

SUPPLEMENTARY FIGURE 2
Immunohistochemistry analysis of FASN and HSPG2. **(A)** Differential expression of eight GMII-building GRGs between tumor tissue and normal tissue in the TCGA cohort. **(B)** Immunohistochemical results of FASN and HSPG2 in tumor and normal tissues. * $p < 0.05$, ** $p < 0.01$, *** $p < 0.001$.

SUPPLEMENTARY FIGURE 3
Pan-cancer analysis. **(A, B)** Differential expression levels and prognostic analysis of genes between tumor and normal tissues. **(C, D)** Difference level of GSVA scores and prognostic analysis between normal and tumor tissues. **(E)** The relationship between GRGs expression and immune cell infiltration. Red means positive correlation, blue means negative correlation. * $p < 0.05$, ** $p < 0.01$, *** $p < 0.001$, #FDR<0.05.

SUPPLEMENTARY FIGURE 4
Comparison of GMII index with other prognostic models of bladder cancer

SUPPLEMENTARY FIGURE 5
Prognosis curve among clinical subgroups

SUPPLEMENTARY FIGURE 6
Analysis of tumor mutation load. **(A)** TMB differences between high-GMII and low-GMII groups. **(B)** Survival curves of high-TMB and low-TMB groups. **(C)** Survival curve after combination of TMB and GMII.

SUPPLEMENTARY FIGURE 7
3D structures of chemotherapeutic drugs with differences between the two groups.

SUPPLEMENTARY FIGURE 8
Differences in the expression of common immune checkpoints between high-GMII and low-GMII groups.

SUPPLEMENTARY FIGURE 9
Subnetwork and core gene PPARG most closely related to GMII gene.

References

1. Sung H, Ferlay J, Siegel RL, Laversanne M, Soerjomataram I, Jemal A, et al. Global cancer statistics 2020: GLOBOCAN estimates of incidence and mortality worldwide for 36 cancers in 185 countries. *CA: Cancer J Clin* (2021) 71(3):209–49. doi: 10.3322/caac.21660

2. Seiler R, Ashab HAD, Erho N, van Rhijn BWG, Winters B, Douglas J, et al. Impact of molecular subtypes in muscle-invasive bladder cancer on predicting response and survival after neoadjuvant chemotherapy. *Eur urol* (2017) 72(4):544–54. doi: 10.1016/j.eururo.2017.03.030

3. Kuroki L, Guntupalli SR. Treatment of epithelial ovarian cancer. *BMJ (Clinical Res ed)* (2020) 371:m3773. doi: 10.1136/bmj.m3773

4. Sanli O, Dobruch J, Knowles MA, Burger M, Alemozaffar M, Nielsen ME, et al. Bladder cancer. *Nat Rev Dis primers.* (2017) 3:17022. doi: 10.1038/nrdp.2017.22

5. Beatty A, Fink LS, Singh T, Strigun A, Peter E, Ferrer CM, et al. Metabolite profiling reveals the glutathione biosynthetic pathway as a therapeutic target in triple-negative breast cancer. *Mol Cancer Ther* (2018) 17(1):264–75. doi: 10.1158/1535-7163.MCT-17-0407

6. Cruzat V, Macedo Rogero M, Noel Keane K, Curi R, Newsholme P. Glutamine: Metabolism and immune function, supplementation and clinical translation. *Nutrients* (2018) 10(11):1564. doi: 10.3390/nu10111564

7. Yang L, Venneti S, Nagrath D. Glutaminolysis: A hallmark of cancer metabolism. *Annu Rev Biomed engineering.* (2017) 19:163–94. doi: 10.1146/annurev-bioeng-071516-044546

8. Wang L, Xu T, Yang X, Liang Z, Zhang J, Li D, et al. Immunosuppression induced by glutamine deprivation occurs *via* activating PD-L1 transcription in bladder cancer. *Front Mol biosci* (2021) 8:687305. doi: 10.3389/fmolb.2021.687305

9. Xia L, Oyang L, Lin J, Tan S, Han Y, Wu N, et al. The cancer metabolic reprogramming and immune response. *Mol cancer.* (2021) 20(1):28. doi: 10.1186/s12943-021-01316-8

10. Newsholme P. Why is l-glutamine metabolism important to cells of the immune system in health, postinjury, surgery or infection? *J Nutr* (2001) 131(9 Suppl):2515S–22S. doi: 10.1093/jn/131.9.2515S

11. Cruzat VF, Krause M, Newsholme P. Amino acid supplementation and impact on immune function in the context of exercise. *J Int Soc Sports Nutr* (2014) 11(1):61. doi: 10.1186/s12970-014-0061-8

12. Faiena I, Ueno D, Shuch B. Glutamine and the tumor immune microenvironment. *Eur Urol.* (2019) 75(5):764–5. doi: 10.1016/j.eururo.2019.01.015

13. DeBerardinis RJ. Tumor microenvironment, metabolism, and immunotherapy. *N Engl J Med* (2020) 382(9):869–71. doi: 10.1056/NEJMcibr1914890

14. Oh MH, Sun IH, Zhao L, Leone RD, Sun IM, Xu W, et al. Targeting glutamine metabolism enhances tumor-specific immunity by modulating suppressive myeloid cells. *J Clin Invest* (2020) 130(7):3865–84. doi: 10.1172/JCI131859

15. Franceschini A, Szklarczyk D, Frankild S, Kuhn M, Simonovic M, Roth A, et al. STRING v9.1: protein-protein interaction networks, with increased coverage and integration. *Nucleic Acids Res* (2013) 41(Database issue):D808–15. doi: 10.1093/nar/gks1094

16. Smoot ME, Ono K, Ruscheinski J, Wang PL, Ideker T. Cytoscape 2.8: New features for data integration and network visualization. *Bioinf (Oxford England)* (2011) 27(3):431–2. doi: 10.1093/bioinformatics/btq675

17. Han H, Cho JW, Lee S, Yun A, Kim H, Bae D, et al. TRRUST v2: An expanded reference database of human and mouse transcriptional regulatory interactions. *Nucleic Acids Res* (2018) 46(D1):D380–d6. doi: 10.1093/nar/gkx1013

18. Liu CJ, Hu FF, Xia MX, Han L, Zhang Q, Guo AY. GSCALite: A web server for gene set cancer analysis. *Bioinf (Oxford England).* (2018) 34(21):3771–2. doi: 10.1093/bioinformatics/bty411

19. Uhlén M, Fagerberg L, Hallström BM, Lindskog C, Oksvold P, Mardinoglu A, et al. Proteomics. Tissue-based map of the human proteome. *Sci (New York NY).* (2015) 347(6220):1260419. doi: 10.1126/science.1260419

20. Chen B, Khodadoust MS, Liu CL, Newman AM, Alizadeh AA. Profiling tumor infiltrating immune cells with CIBERSORT. *Methods Mol Biol* (2018) 1711:243–59. doi: 10.1007/978-1-4939-7493-1_12

21. Yoshihara K, Shahmoradgoli M, Martínez E, Vegesna R, Kim H, Torres-Garcia W, et al. Inferring tumour purity and stromal and immune cell admixture from expression data. *Nat Commun* (2013) 4:2612. doi: 10.1038/ncomms3612

22. Yang W, Soares J, Greninger P, Edelman EJ, Lightfoot H, Forbes S, et al. Genomics of drug sensitivity in cancer (GDSC): A resource for therapeutic biomarker discovery in cancer cells. *Nucleic Acids Res* (2013) 41(Database issue):D955–61. doi: 10.1093/nar/gks1111

23. Jiang P, Gu S, Pan D, Fu J, Sahu A, Hu X, et al. Signatures of T cell dysfunction and exclusion predict cancer immunotherapy response. *Nat Med* (2018) 24(10):1550–8. doi: 10.1038/s41591-018-0136-1

24. Rosenberg JE, Hoffman-Censits J, Powles T, van der Heijden MS, Balar AV, Necchi A, et al. Atezolizumab in patients with locally advanced and metastatic urothelial carcinoma who have progressed following treatment with platinum-based chemotherapy: A single-arm, multicentre, phase 2 trial. *Lancet* (2016) 387 (10031):1909–20. doi: 10.1016/S0140-6736(16)00561-4

25. Charoentong P, Finotello F, Angelova M, Mayer C, Efremova M, Rieder D, et al. Pan-cancer immunogenomic analyses reveal genotype-immunophenotype relationships and predictors of response to checkpoint blockade. *Cell Rep* (2017) 18 (1):248–62. doi: 10.1016/j.celrep.2016.12.019

26. Hanahan D, Weinberg RA. Hallmarks of cancer: the next generation. *Cell* (2011) 144(5):646–74. doi: 10.1016/j.cell.2011.02.013

27. Sun N, Liang Y, Chen Y, Wang L, Li D, Liang Z, et al. Glutamine affects T24 bladder cancer cell proliferation by activating STAT3 through ROS and glutaminolysis. *Int J Mol Med* (2019) 44(6):2189–200. doi: 10.3892/ijmm.2019.4385

28. Tang C, Yu M, Ma J, Zhu Y. Metabolic classification of bladder cancer based on multi-omics integrated analysis to predict patient prognosis and treatment response. *J Trans Med* (2021) 19(1):205. doi: 10.1186/s12967-021-02865-8

29. Fotiadis D, Kanai Y, Palacín M. The SLC3 and SLC7 families of amino acid transporters. *Mol aspects Med* (2013) 34(2-3):139–58. doi: 10.1016/j.mam.2012.10.007

30. Baba H, Kanda M, Sawaki K, Nakamura S, Ueda S, Shimizu D, et al. SLC7A9 as a potential biomarker for lymph node metastasis of esophageal squamous cell carcinoma. *Ann Surg Oncol* (2022) 29(4):2699–709. doi: 10.1245/s10434-021-11001-1

31. Lin L, Yee SW, Kim RB, Giacomini KM. SLC transporters as therapeutic targets: Emerging opportunities. *Nat Rev Drug discovery.* (2015) 14(8):543–60. doi: 10.1038/nrd4626

32. Farms WB, Godfrey DA, Askari A. Effect of copper-deficient diet on metabolism in rat auditory structures. *Hearing Res* (1993) 67(1-2):45–50. doi: 10.1016/0378-5955(93)90230-X

33. Vizán P, Di Croce L, Aranda S. Functional and pathological roles of AHCY. *Front Cell Dev Biol* (2021) 9:654344. doi: 10.3389/fcell.2021.654344

34. Roser M, Josic D, Kontou M, Mosetter K, Maurer P, Reutter W. Metabolism of galactose in the brain and liver of rats and its conversion into glutamate and other amino acids. *J Neural Transm (Vienna Austria 1996).* (2009) 116(2):131–9. doi: 10.1007/s00702-008-0166-9

35. Ding Y, Gong C, Huang D, Chen R, Sui P, Lin KH, et al. Synthetic lethality between HER2 and transaldolase in intrinsically resistant HER2-positive breast cancers. *Nat Commun* (2018) 9(1):4274. doi: 10.1038/s41467-018-06651-x

36. Effner R, Hiller J, Eyerich S, Traidl-Hoffmann C, Brockow K, Triggiani M, et al. Cytochrome P450s in human immune cells regulate IL-22 and c-kit *via* an AHR feedback loop. *Sci Rep* (2017) 7:44005. doi: 10.1038/srep44005

37. Li J, Duran MA, Dhanota N, Chatila WK, Bettigole SE, Kwon J, et al. Metastasis and immune evasion from extracellular cGAMP hydrolysis. *Cancer discovery.* (2021) 11 (5):1212–27. doi: 10.1158/2159-8290.CD-20-0387

38. Tran L, Xiao JF, Agarwal N, Duex JE, Theodorescu D. Advances in bladder cancer biology and therapy. *Nat Rev Cancer.* (2021) 21(2):104–21. doi: 10.1038/s41568-020-00313-1

39. Schneider AK, Chevalier MF, Derré L. The multifaceted immune regulation of bladder cancer. *Nat Rev Urol* (2019) 16(10):613–30. doi: 10.1038/s41585-019-0226-y

40. Colombo MP, Piconese S. Regulatory-t-cell inhibition versus depletion: The right choice in cancer immunotherapy. *Nat Rev Cancer.* (2007) 7(11):880–7. doi: 10.1038/nrc2250

41. Altman BJ, Stine ZE, Dang CV. From Krebs to clinic: Glutamine metabolism to cancer therapy. *Nat Rev Cancer.* (2016) 16(10):619–34. doi: 10.1038/nrc.2016.71

42. Leone RD, Zhao L, Englert JM, Sun IM, Oh MH, Sun IH, et al. Glutamine blockade induces divergent metabolic programs to overcome tumor immune evasion. *Sci (New York NY).* (2019) 366(6468):1013–21. doi: 10.1126/science.aav2588

43. Ramapriyan R, Caetano MS, Barsoumian HB, Mafra ACP, Zambalde EP, Menon H, et al. Altered cancer metabolism in mechanisms of immunotherapy resistance. *Pharmacol Ther* (2019) 195:162–71. doi: 10.1016/j.pharmthera.2018.11.004

44. Wappler J, Arts M, Röth A, Heeren RMA, Peter Neumann U, Olde Damink SW, et al. Glutamine deprivation counteracts hypoxia-induced chemoresistance. *Neoplasia (New York NY).* (2020) 22(1):22–32. doi: 10.1016/j.neo.2019.10.004

45. Hensley CT, Wasti AT, DeBerardinis RJ. Glutamine and cancer: Cell biology, physiology, and clinical opportunities. *J Clin Invest* (2013) 123(9):3678–84. doi: 10.1172/JCI69600

46. Prasad P, Ghosh S, Roy SS. Glutamine deficiency promotes stemness and chemoresistance in tumor cells through DRP1-induced mitochondrial fragmentation. *Cell Mol Life Sci CMLS.* (2021) 78(10):4821–45. doi: 10.1007/s00018-021-03818-6

47. Chen R, Lai LA, Sullivan Y, Wong M, Wang L, Riddell J, et al. Disrupting glutamine metabolic pathways to sensitize gemcitabine-resistant pancreatic cancer. *Sci Rep* (2017) 7(1):7950. doi: 10.1038/s41598-017-08436-6

48. Lehrke M, Lazar MA. The many faces of PPARgamma. *Cell* (2005) 123(6):993–9. doi: 10.1016/j.cell.2005.11.026

49. Tate T, Xiang T, Wobker SE, Zhou M, Chen X, Kim H, et al. Pparg signaling controls bladder cancer subtype and immune exclusion. *Nat Commun* (2021) 12(1):6160. doi: 10.1038/s41467-021-26421-6

50. Hochhaus A, Gambacorti-Passerini C, Abboud C, Gjertsen BT, Brümmendorf TH, Smith BD, et al. Bosutinib for pretreated patients with chronic phase chronic myeloid leukemia: Primary results of the phase 4 BYOND study. *Leukemia* (2020) 34(8):2125–37. doi: 10.1038/s41375-020-0915-9

51. Cao B, Wang Y, Wen D, Liu W, Wang J, Fan G, et al. A trial of lopinavir-ritonavir in adults hospitalized with severe covid-19. *New Engl J Med* (2020) 382(19):1787–99. doi: 10.1056/NEJMoa2001282

52. Arabi YM, Gordon AC, Derde LPG, Nichol AD, Murthy S, Beidh FA, et al. Lopinavir-ritonavir and hydroxychloroquine for critically ill patients with COVID-19: REMAP-CAP randomized controlled trial. *Intensive Care Med* (2021) 47(8):867–86. doi: 10.1007/s00134-021-06448-5

10.3389/fimmu.2023.1111319

Glossary

TCGA	The Cancer Genome Atlas
GEO	Gene Expression Omnibus
BC	Bladder Cancer
GRGs	Glutamine related Genes
GMII	Glutamine Metabolism Immunity Index
ENPP1	Ectonucleotide pyrophosphatase/phosphodiesterase 1
GALK1	Galactokinase 1
TALDO1	Transaldolase 1
CYP19A1	Cytochrome P450 Family 19 Subfamily A Member 1
FASN	Fatty Acid Synthase
AHCY	Adenosylhomocysteinase
SLC7A9	Solute Carrier Family 7 Member 9
HSPG2	Heparan Sulfate Proteoglycan 2
PD-1	Programmed cell death 1
PD-L1	Programmed cell death 1 ligand 1
CTLA4	Cytotoxic T-lymphocyte-associated protein 4
ICB	Immune checkpoint blockade
OS	Overall survival
ROC	Receiver Operation Characteristic
NES	Normalized enrichment score
TMB	Tumor mutation burden
IC50	half maximal inhibitory concentration
GDSC	Genomics of Drug Sensitivity in Cancer
PPI	protein–protein interaction
KM	Kaplan–Meier
ssGSEA	single-sample gene set enrichment analysis
TIDE	tumor immune dysfunction and exclusion
GSEA	gene set enrichment analysis
GO	Gene Ontology
KEGG	Kyoto Encyclopedia of Genes and Genomes
LAG3	Lymphocyte Activating 3
IDO1	Indoleamine 2, 3-Dioxygenase 1
PFS	Progression-free survival
DSS	Disease-free survival
TP53	Tumor Protein P53
TTN	Titin
KMT2D	Lysine Methyltransferase 2D
MUC16	Mucin 16
ARID1A	AT-Rich Interaction Domain 1A
EP300	E1A Binding Protein P300
ZFHX4	Zinc Finger Homeobox 4
FGFR3	Fibroblast Growth Factor Receptor 3
ADCC	Antibody-dependent cytotoxicity
ROS	Reactive oxygen species
GPX4	glutathione peroxidase 4
GSH	reduced glutathione
TCA	tricarboxylic acid

(Continued)

Continued

frontiers | Frontiers in Immunology

TYPE Review
PUBLISHED 06 March 2023
DOI 10.3389/fimmu.2023.1120684

Check for updates

OPEN ACCESS

EDITED BY
Mohd Wajid Ali Khan,
University of Hail, Saudi Arabia

REVIEWED BY
Subuhi Sherwani,
University of Hail, Saudi Arabia
Syed M. Faisal,
University of Michigan Medical School,
United States

*CORRESPONDENCE
Haibo Lu
luhaibo@hrbmu.edu.cn
Shengjun Ji
drshengjunji@163.com
Yutian Zhao
drzhaoyutian@163.com

†These authors have contributed equally to this work

SPECIALTY SECTION
This article was submitted to Cancer Immunity and Immunotherapy, a section of the journal Frontiers in Immunology

RECEIVED 10 December 2022
ACCEPTED 20 February 2023
PUBLISHED 06 March 2023

CITATION
Zhu J, Lian J, Xu B, Pang X, Ji S, Zhao Y and Lu H (2023) Neoadjuvant immunotherapy for colorectal cancer: Right regimens, right patients, right directions? *Front. Immunol.* 14:1120684. doi: 10.3389/fimmu.2023.1120684

COPYRIGHT
© 2023 Zhu, Lian, Xu, Pang, Ji, Zhao and Lu. This is an open-access article distributed under the terms of the Creative Commons Attribution License (CC BY). The use, distribution or reproduction in other forums is permitted, provided the original author(s) and the copyright owner(s) are credited and that the original publication in this journal is cited, in accordance with accepted academic practice. No use, distribution or reproduction is permitted which does not comply with these terms.

Neoadjuvant immunotherapy for colorectal cancer: Right regimens, right patients, right directions?

Jiahao Zhu[1†], Jie Lian[1†], Benjie Xu[1], Xiangyi Pang[1], Shengjun Ji[2*], Yutian Zhao[3*] and Haibo Lu[1*]

[1]Department of Outpatient Chemotherapy, Harbin Medical University Cancer Hospital, Harbin, Heilongjiang, China, [2]Department of Radiotherapy and Oncology, The Affiliated Suzhou Hospital of Nanjing Medical University, Gusu School, Nanjing Medical University, Suzhou, Jiangsu, China, [3]Department of Radiotherapy and Oncology, The Affiliated Hospital of Jiangnan University, Wuxi, Jiangsu, China

Neoadjuvant chemoradiotherapy (NACRT) or chemotherapy (NACT) followed by radical resection and then adjuvant therapy is considered the optimal treatment model for locally advanced colorectal cancer (LACRC). A recent total neoadjuvant therapy (TNT) strategy further improved the tumour regression rate preoperatively and reduced local-regional recurrence in locally advanced rectal cancer (LARC). However, distant metastasis was still high, and little overall survival benefit was obtained from these preoperative treatment models. According to mismatch repair protein expression, MSI-H/dMMR and non-MSI-H/pMMR statuses were defined in colorectal cancer (CRC) patients. Due to the special features of biologics in MSI-H/dMMR CRC patients, this subgroup of patients achieved little treatment efficacy from chemoradiotherapy but benefited from immune checkpoint inhibitors (ICIs). The KEYNOTE-177 trial observed favourable survival outcomes in metastatic CRC patients treated with one-line pembrolizumab with tolerable toxicity. Given the better systemic immune function, increased antigenic exposure, and improved long-term memory induction before surgery, neoadjuvant ICI (NAICI) treatment was proposed. The NICHE trial pioneered the use of NAICI treatment in LACRC, and recent reports from several phase II studies demonstrated satisfactory tumour downsizing in CRC. Preclinical rationales and preliminary early-phase human trials reveal the feasibility of NAICI therapy and the therapeutic efficacy provided by this treatment model. Better tumour regression before surgery also increases the possibility of organ preservation for low LARC. However, the optimal treatment strategy and effective biomarker identification for beneficiary selection remain unknown, and potential pitfalls exist, including tumour progression during neoadjuvant treatment due to drug resistance and surgery delay. Given these foundations and questions, further phase II or III trials with large samples need to be conducted to explore the right regimens for the right patients.

KEYWORDS

colorectal cancer, immune checkpoint blockade, immunotherapy, microsatellite instability, neoadjuvant treatment

Introduction

Colorectal cancer (CRC) remains the second leading cause of cancer-related mortality worldwide, with an estimated 93 5000 deaths in 2020 (including 576,858 deaths from colon cancer and 339,022 deaths from rectal cancer), accounting for 10% of all cancer types (1). Locally advanced CRC (LACRC) invading adjacent tissues and/or regional lymph nodes occur in 36% of initially diagnosed patients, and distant metastatic diseases occur in 22%. According to the statistics reported by the National Cancer Institute (USA), the 5-year overall survival (OS) rates for colon and rectal cancers are 64% and 67%, respectively (2).

Surgery combined with chemotherapy and radiotherapy remains the standard component of curative multimodal treatment approaches for LACRC. OS and disease-free survival (DFS) benefits from postoperative adjuvant chemotherapy were observed for LACRC patients in previous clinical trials (3–8). However, approximately 30% of CRC patients delayed or even refused adjuvant chemotherapy after curative resection because of postoperative complications and poor physical condition, and less than half of the eligible patients received a full course of chemotherapy, which reduced the therapeutic efficacy (9–11). To improve the possibility of completing chemotherapy prior to surgery, increase the drug concentration surrounding the tumour, eradicate potential micrometastases, reduce the risk of recurrence and distant metastasis, reduce the tumour bulk to achieve more complete resection, and assess the chemosensitivity of disease to predict the subsequent outcome, neoadjuvant chemotherapy (NACT) was proposed and applied to the treatment of CRC. The results of the FOxTROT trial and another randomized trial conducted in Germany raised the possibility of cure for CRC patients treated with neoadjuvant therapy, especially for those who achieved pathological complete response (pCR) (12, 13). However, an improved response may not translate into a survival benefit in locally advanced CRC (14–16). Then potential NACT regimen was explored. Oxaliplatin was added as the second cytotoxic agent during standard neoadjuvant chemoradiotherapy for locally advanced rectal cancer (LARC) patients in the PETACC-6 trial, but tumour response and survival benefits were not observed (17). Another phase II clinical study (PRODIGE 22) was terminated early due to the high grade of toxicities and unsatisfactory tumour regression (18).

The impressive tumour response of microsatellite instability high (MSI-H) or deficient mismatch repair (dMMR) metastatic CRC (mCRC) opened the era of immunotherapies for CRC in 2015 (19). The KEYNOTE-177 study suggested that immune checkpoint inhibitors (ICIs) have absolute advantages compared with traditional chemotherapy combined with targeted therapy in dMMR mCRC, which shows promising future opportunities for the use of ICIs for resectable CRC in the neoadjuvant setting (20). The NICHE trial reported favourable outcomes in which the pCR rate reached 60% for dMMR colon cancer patients who received a neoadjuvant immunotherapy regimen combining nivolumab (an anti-PD-1 inhibitor) with ipilimumab (an anti-CTLA-4 inhibitor) (21). In the VOLTAGE trial, 60% of dMMR LARC patients and 30% of proficient mismatch repair (pMMR) LARC patients who received NACRT followed by nivolumab achieved pCR (22). ICIs have a distinct toxicity profile and potential patterns of response compared with traditional cytotoxic chemotherapies (23, 24). Theoretically, more antigen surrounding the tumour could prime effective systemic immunity to eradicate potential metastatic disease in the neoadjuvant setting as opposed to the adjuvant use of this treatment postoperatively (25). In this review, we summarize the recent clinical developments of neoadjuvant ICI (NAICI) treatment in CRC and discuss the pitfalls and future directions of this approach.

Management of locally advanced CRC

The primary aims of neoadjuvant treatment in LACRC are to achieve radical (R0) resection, decrease local recurrence and distant metastasis by pathological downstaging and eradicate occult micrometastatic disease with tolerable toxicity. Achieving a high rate of sphincter savings is also pursued in LARC. Breakthroughs of pCR or clinical complete response (cCR) achievement and organ preservation seem to have been made due to the application of radiotherapy and diverse neoadjuvant polychemotherapy patterns in LARC. Given the poor compliance of LARC patients, in which one-third of these patients refused to receive postoperative adjuvant chemotherapy and only 43% received 95% of the planned 5-fluorouracil (5-FU) dose in the standard neoadjuvant treatment model (EORTC 22921 study), adjuvant chemotherapy was proposed to be delivered before surgery, namely, total neoadjuvant therapy (TNT) treatment model (11). A significant downsize of the tumour before resection was observed in TNT models (26, 27), and the CAO/ARO/AIO-12 and OPRA trials further compared the therapeutic efficacy between the consolidation and induction treatment patterns in LARC (28, 29). Results of the two studies demonstrated that consolidation chemotherapy TNT model seems to have a better pCR rate, sphincter-saving rate and compliance than the induction model. Due to the higher rates of local-regional recurrence and relative fixed spatial position compared with colon cancer, radiotherapy is commonly applied in rectal cancer, especially for those mid-low rectal cancer. In terms of neoadjuvant radiotherapy in the TNT model, two radiotherapy methods are mainly applied in these trials: a short-course radiation scheme (5×5 Gy) and a long-course radiation scheme (25×2 Gy or 28×2 Gy). No difference in DFS was observed between the two radiotherapy model groups in the POLISH II and STELLAR trials (30, 31). The AVACROSS study reported an increase in the pCR rate to 36% at the cost of more serious surgery-associated complications when bevacizumab was added to induction chemotherapy (32). Poly ADP-ribose polymerase inhibitors (e.g., veliparib) and DNA protein kinase inhibitors (e.g., peposertib) are being evaluated in combination with NACRT or chemotherapy before surgery during TNT (22, 33–35). However, these studies are at an exploratory stage, and relative sequence studies deserve consideration. Overall, the TNT treatment model could improve the pCR rate for LARC compared with the traditional chemoradiotherapy model, which is consistent with the results obtained from three recent meta-analyses, while the survival benefits from TNT vary and deserve further investigation (36–38).

Limited literature has reported on neoadjuvant treatment in locally advanced colon cancer. Neoadjuvant chemotherapy with the OxMdG (fluorouracil and oxaliplatin) regimen achieved significant downstaging with acceptable gastrointestinal toxicity compared with standard postoperative chemotherapy in LACC, albeit with a low rate of pCR (2%) (12). The PRODIGE 22 study was stopped early due to a lack of efficacy in the FOLFOX (Folinic acid, fluorouracil, and oxaliplatin) combined with cetuximab arm (18). Another phase II trial analysed the therapeutic effects of panitumumab added to chemotherapy before surgery for LACC without KRAS, BRAF or PIK3CA mutations (39). The outcomes of this study showed that local recurrence was decreased to 26% and DFS was increased to 31% in patients with tumour downstaging, despite the high incidence of grade 3 skin rash. To date, there are no standard preoperative chemotherapy options for LACC, and an individual therapy model guided by multiplex gene testing or more accurate tumour and lymph node staging based on imaging before resection may provide new ideas for the treatment of this disease.

Tumour regression grading (TRG) systems are commonly used in gastrointestinal malignancies treated with neoadjuvant therapy, typically chemotherapy or radiochemotherapy. These categorizing methods assess the degree of tumour regressive changes by identifying fibrosis in relation to the residual tumour or evaluating the volume of the residual tumour in relation to the primary tumour lesions. TRGs could provide valuable prognostic information, and complete tumour regression has been confirmed to be closely associated with better survival and a lower recurrence rate in LARC (40). However, TRG cannot serve as a clinical research end-point due to the high numbers of versions of grading criteria and unclear conclusions on whether this classification system has advantages over the UICC/AJCC TNM staging systems. pCR is still used as a surrogate endpoint in neoadjuvant trials. NAICI trials have also adopted major pathological response (MPR) as the main endpoint, indicating that less than 10% of viable tumour tissues exist at primary sites after surgery in CRC and other cancers (41). Whether MPR could predict the survival of CRC patients who receive NAICI and serve as a surrogate for survival warrants further clarification and investigation.

Rationale for NAICI in LACRC

Advantages of NAICI in LACRC

T-cell activation mainly depends on T-cell receptor (TCR) signalling participating in recognizing tumour antigens. Then, the immune response is activated, which is characterized by a large number of different T-cell clones (42). Tumour-infiltrating T cells, especially CD8+ T cells, have long been considered to have a close association with improving survival and reducing locoregional recurrence and distant metastasis by recognizing and killing specific tumour cells (43, 44). However, several immune checkpoint molecules, mainly cytotoxic T-lymphocyte-associated antigen-4 (CTLA-4), programmed death-1 (PD-1), and programmed death-ligand 1 (PD-L1), suppress T-cell-mediated antitumour immune responses in the tumour microenvironment (TME) (45–47). Meanwhile, high PD-L1 expression levels in tumour cells also contribute to the exhaustion and apoptosis of T cells (48) (Figure 1A). The clinical application of ICIs targeting CTLA-4 or PD-1/PD-L1 to reactivate the immune response against cancer have achieved favourable outcomes in advanced CRC, especially for patients with MSI-H/dMMR (20, 49). However, the benefits of survival are still not satisfactory from ICIs as adjuvant therapy, probably due to the significant decrease in tumour antigens and local-regional blood vessel and draining lymph node damage after surgery, which limit immune-mediated tumour cell killing and long-term tumour-specific immunological memory (Figure 1B). ICIs administered as neoadjuvant therapy instead of in an adjuvant setting may be considered to improve clinical outcomes. A greater expansion of T-cell clones in the peripheral blood because of a wider range of tumour antigen exposure and better survival were observed in preclinical mouse models when an ICIs were given preoperatively rather than postoperatively (25).

Potential synergistic mechanism between NAICI and NACRT in LACRC

Cytotoxic agents commonly used in the NACT of CRC mainly include oxaliplatin and 5-FU or its derivatives. Oxaliplatin could induce immunogenic cell death (ICD), a kind of regulated cell death, due to the ability to stimulate the pre-apoptotic release of calreticulin and to promote the release of high-mobility group box 1 protein (HMGB1) (50). ICD increases the intracellular antigen concentration and improves the availability of antigen-presenting cells (APCs), thus contributing to antigen presentation to cytotoxic T-lymphocytes and their priming. Oxaliplatin is also reported to enhance the antigen presentation capacity of tumour cells by increasing the surface expression of MHC class I, contributing to the more effective activation of T cells and ICI-based immunotherapy *in vivo* (51). Moreover, the combined use of oxaliplatin and 5-FU was observed to promote APC maturation in a colon cancer mouse model (52). In addition to regulating antigen presentation, the addition of oxaliplatin upregulated PD-L1 expression on tumour cells in a murine model of CRC and improved tumour control (53, 54). High expression of PD-L1 in tumour nests was found to have a close association with favourable outcomes after neoadjuvant chemotherapy and chemoradiotherapy (55, 56). Oxaliplatin was shown to increase the relative proportion of CD8+ T cells and promote the recruitment of cytotoxic T cells into the TME but selectively deplete B cells in BALB/c mice (57). Another study further demonstrated that chemotherapy with the FOLFOX regimen could regulate the tumour-infiltrating CD8+ T-cell exhaustion stage into effector functional status in CRC (58). 5-FU was found to activate cytotoxic T cells by contributing to the exhaustion of myeloid-derived suppressor cells *via* programmed cell death (59). The mechanisms of chemoimmunotherapy discovered in CRC provide promising prospects for use of NAICI

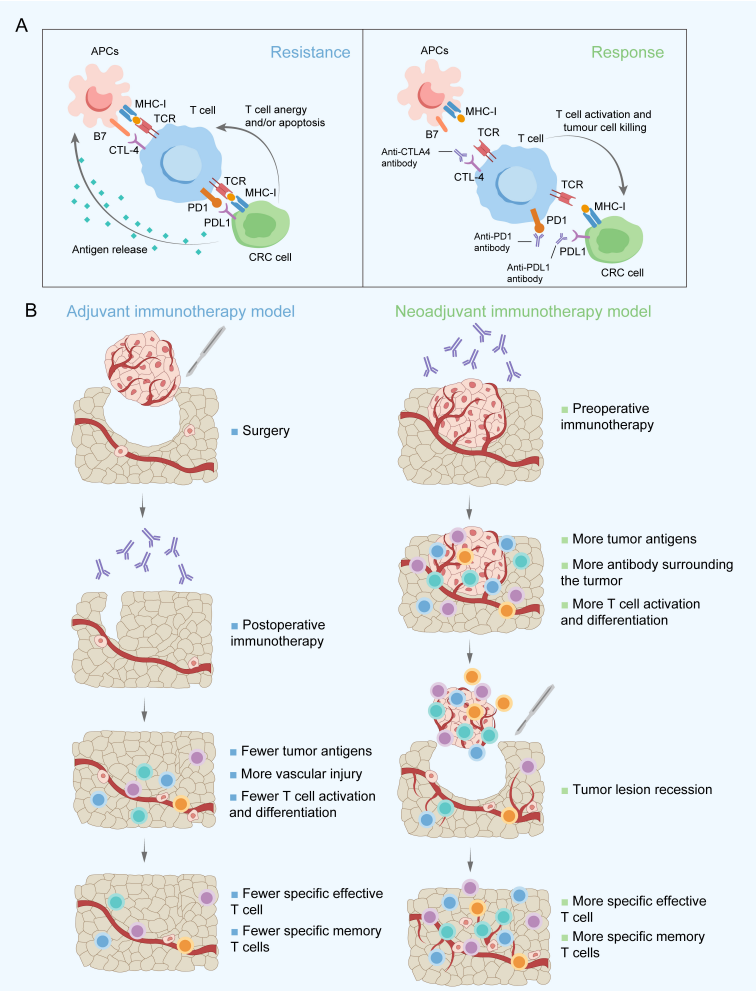


FIGURE 1
Main targets of immune checkpoint inhibitors applied in the clinic **(A)** and proposed rationale for immunotherapy administered postoperatively and preoperatively **(B)**. APCs, Antigen-presenting cells; CRC, Colorectal cancer; CTLA-4, Cytotoxic T-lymphocyte-associated antigen-4; MHC-I, Major histocompatibility complex class I; PD-1, Programmed death-1; PD-L1, Programmed death-ligand 1; TCR, T-cell receptor.

together with oxaliplatin-based chemotherapy, warranting further exploration of the optimal therapeutic strategies to achieve a higher tumour response rate (Figure 2A).

Radiation mainly utilized in the neoadjuvant treatment of LARC reduces tumour size and improves local-regional disease control. Meanwhile, the immunostimulatory effects induced by radiotherapy and the potential possibility of improving antitumour immunity cannot be ignored. Tumour cell damage caused by irradiation releases a large amount of damage-associated molecular patterns, activating Toll-like receptors and other receptors on APCs, ultimately leading to phagocytosis *via* natural killer (NK) cells or macrophages and immunological signal priming. Type I interferons (IFNs) secreted by activated APCs contribute to APC maturation in the lymph node, antigen presentation function improvement through autocrine signalling, and CD8+ T-cell activation, proliferation, and migration into the TME *via* the paracrine pathway (60). Then, tumour-specific T cells secrete type II IFN to recruit T cells into tumour tissues and upregulate the expression of MHC-I on tumour cells with a feedback mechanism under radiation intervention (61) (Figure 2B). APCs also induce the generation of durable and transferrable memory responses mainly dependent on CD4+ helper T cells by presenting the tumour neoantigens to T cells (62). Overall, chemoradiotherapy was found to contribute to recruiting immune cells into the tumour site and upregulating immune checkpoint expression to promote to the synergistic enhancement of ICI therapy efficacy, which suggests a new and favourable approach to neoadjuvant therapeutic modalities for LACRC.

Differences in the immune landscape between dMMR and pMMR in CRC

CRCs with MSI-H status account for approximately 15% of all cases of this disease. This special subtype of CRC marked with dMMR always has a high overall tumour mutation burden (TMB), which was reported to have a significant association with better ICIs

treatment effects (63). High TMB means more neoantigen generation and thus recruits a large number of tumour-infiltrating immune cells, such as cytotoxic T cells, into the TME. The proportions of CD8+ T cells and CD4+ functional subsets were dramatically increased (64). To balance the immune response and protect normal host tissues, T-cell inhibitory ligands, such as CD80 and CD86 of the B7 family and PD-L1 as well as regulatory T cells (Tregs), are correspondingly upregulated in tumour cells to bind coinhibitory receptors, including PD-L1 and CTLA4 (19, 65) (Figure 3A). A consensus has been reached that early stage (not including stage IV) CRC and oesophageal adenocarcinoma with MSI-H status indeed have a higher rate of PD-L1 positive expression and high TMB at the same time compared with other tumours (66).

Interestingly, a recent study further divided MSI-H CRC into two major categories: MSI-H1 and MSI-H2 (67). Better OS was observed in the MSI-H2 group than in the MSI-H1 group (P = 0.042). Immune microenvironment differences between the two groups of CRC mainly involved the distribution of M2 macrophages and the expression of PD-L2. The anti-inflammatory and immune suppression functions of enriched M2 macrophages and T-cell inhibition functions of PD-L2 leading to immune regulatory disorder may contribute to the poor survival in the MSI-H1 subset. This finding is consistent with the fact that approximately 40%-60% of MSI-positive tumour patients cannot benefit from ICIs treatment (68). High immune heterogeneity also exists in pMMR or microsatellite stability (MSS) CRC. Dienstmann et al. proposed four consensus molecular subgroups (CMSs), including CMS1 (MSI immune), CMS2 (canonical), CMS3 (metabolic) and CMS4 (mesenchymal) based on the gene expression of CRC (69). CMS2, characterized by WNT and MYC activation, has better survival than the other CMSs, while CMS1, with the biological features of strong activation of immune evasion pathways, has worse survival after recurrence. CMS1 and CMS3 decreased while CMS2 increased as the tumour location moved distally, and CMS2 accounted for most rectal cancers (Figure 3B). Another study further investigated the relationship between the CMSs and the immune subtypes (C1-C6) established by Thorsson et al. (68, 70). This study discovered that the *IFN-γ–dominant* subtype (C2) has enhanced activation of immune system pathways and dominates in CMS1 (53%), while

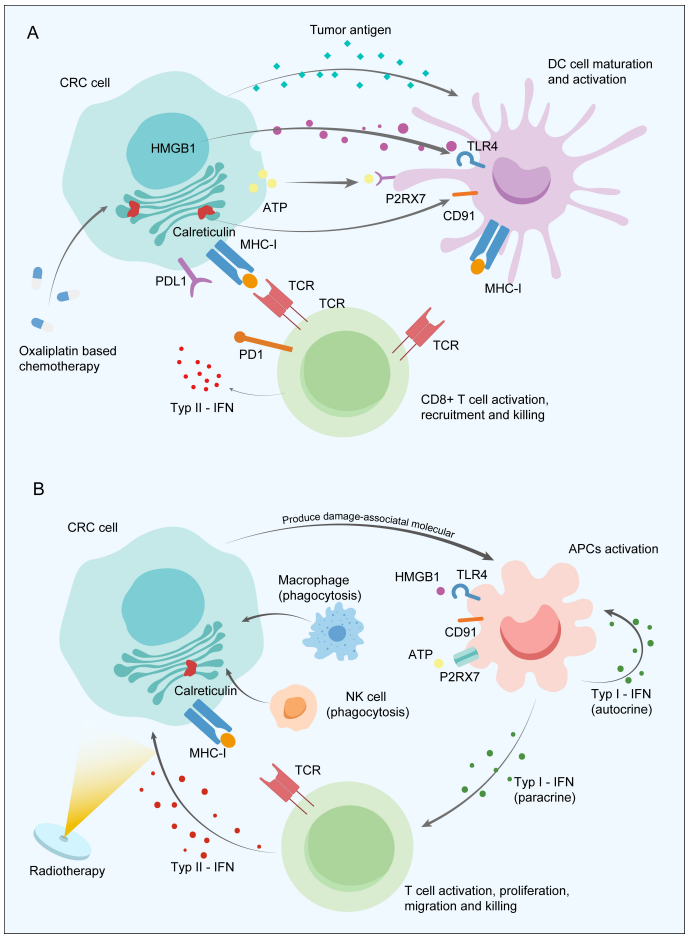


FIGURE 2
Potential synergistic mechanism between neoadjuvant immune checkpoint inhibitor and neoadjuvant chemotherapy **(A)** and radiotherapy **(B)** in colorectal cancer. APCs, Antigen-presenting cells; ATP, Adenosine triphosphate; CRC, Colorectal cancer; HMGB1, High-mobility group box 1 protein; IFNs, Type I interferons; MHC-I, Major histocompatibility complex class I; NK cells, Natural killer cells; P2RX7, Purinergic Receptor P2X 7 PD-1; Programmed death-1; PD-L1, Programmed death-ligand 1; TCR, T-cell receptor; TLR4, Toll Like Receptor 4.

the *wound healing* subgroup (C1), mainly depending on metabolic pathways, occupies most of CMS2 (91%), CMS3 (77%) and CMS4 (77%). CMS2 and the *IFN-γ–dominant subtype* share a similar immune status, including strong immune activation (higher proportions of activated CD8+ T cells, activated CD4+ T cells, Tregs, dendritic cells, and M1/M2 polarization) as well as the upregulation of immune checkpoints (CTLA-4 and PD-1/PD-L1), which means that these subgroups of CRC patients may benefit more from ICIs treatment. Galon et al. observed that approximately 45% of MSS CRCs and 65% of MSI-H CRCs had a higher Immunoscore, an effective indicator for CRC relapse prediction based on the expression of CD3+ and CD8+ T cells surrounding the tumour, which could achieve a favourable antitumour response, while the rest with a low Immunoscore may be unable to benefit from ICIs treatment (71). Therefore, differences in the immune landscape between MSI-H and non-MSI-H CRC were observed, but high immune heterogeneity also existed in their respective subgroups (Figure 3C).

Right regimens? NAICI strategies in CRC

Several large clinical studies have demonstrated survival advantages of MSI-H/dMMR mCRC treated with ICIs compared with traditional chemotherapy combined with or without ICIs therapy (19, 20, 49). The detection of MSI/MMR status for patients with an initial diagnosis of CRC recommended by the 2021 National Comprehensive Cancer Network (NCCN) guidelines makes the application of ICIs in early CRC possible (72, 73). In addition, the 2022 version of the NCCN guidelines also first recommend single PD-1 blockade (pembrolizumab) or a combination of anti-PD1 (nivolumab) and anti-CTL-4 (ipilimumab) as an alternative treatment for potentially resectable MSI-H/dMMR mCRC during the preoperative stage and MSI-H/dMMR cT4b colon cancer (74, 75). In terms of MSI-H/dMMR LACRC, several finished or ongoing clinical trials have explored the treatment efficacy of NAICI, and favourable outcomes have been achieved in some of these studies. MSS/pMMR CRC, accounting for approximately 85% of all CRC, benefit little from ICIs, which is a challenge for clinicians. Fortunately, the combination of ICIs and chemoradiotherapy has been widely applied in the neoadjuvant setting in recent clinical trials and has significantly improved tumour regression. Here, we summarize the clinical trials on the application of ICIs in the neoadjuvant treatment of CRC patients (Table 1).

Due to the special clinicopathological and molecular biological features of MSI-H/dMMR CRC, the early-stage patients of these subgroups could not benefit from adjuvant chemotherapy. The phase II clinical trial NICHE (NCT03026140) adopted the combination of nivolumab and ipilimumab as the neoadjuvant

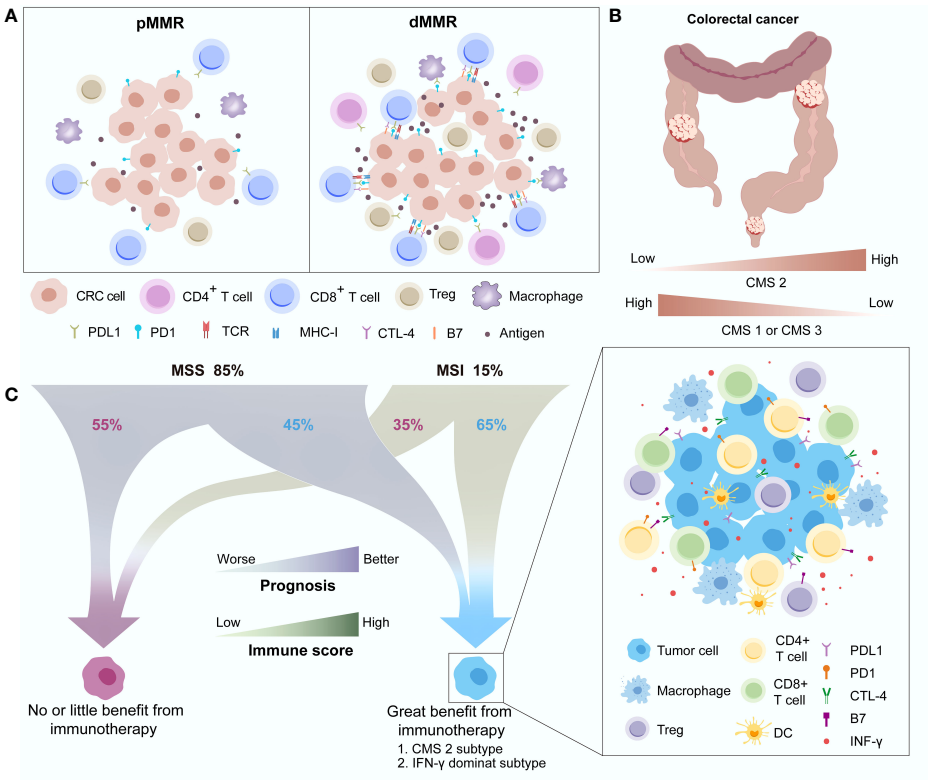


FIGURE 3
Differences in the immune landscape between pMMR and dMMR in CRC **(A)** and the distribution **(B)** and characteristics **(C)** of different immune subgroups. CMS, Consensus molecular subgroup; CRC, Colorectal cancer; CTLA-4, Cytotoxic T-lymphocyte-associated antigen-4; DC, Dendritic cell; dMMR, Deficient mismatch repair; IFN-γ, Interferon gamma; MSI, Microsatellite instability; MSS, Microsatellite stability; PD-1, Programmed death-1; PD-L1, Programmed death-ligand 1; pMMR, Proficient mismatch repair; TCR, T-cell receptor.

regimen to explore the NAICI treatment efficacy (21). The short-term outcomes showed that all of the dMMR status patients achieved a pathological response with tolerable adverse effects. This study preliminarily proves that nonmetastatic colon cancer patients could benefit from NAICI and indicates that NAICI has become more acceptable and has a potentially wide application in CRC, especially for those with dMMR status. A recent updated oral report of this study showed that the pCR rate increased to 69%, and the NICHE-2 study with a single arm also showed a similar pCR rate (67%) (80, 81). The NICOLE study (NCT04123925) investigated the treatment efficacy of single ICIs before surgery in early-stage colon cancer without detecting MMR status (82). The results showed that all patients underwent radical resection without delay. The outcomes of the two studies suggest that NAICI treatment with a combination of anti-PD-1 and anti-CTL-4 agents seems to achieve better tumour regression than the application of a single anti-PD-1 agent. In terms of survival, only the NICHE study reported that no recurrence occurred in dMMR colon cancer patients with a median follow-up of 32 months, while 6% patients with pMMR status suffered from relapse with a median follow-up of 28 months. The long-term survival results of these clinical trials are expected.

In LARC, several studies have investigated whether adding ICIs before surgery to the standard neoadjuvant treatment model could further improve the tumour regression rate. In the VOLTAGE-A study (NCT02948348), nivolumab consolidation treatment were added between the period of standard NACRT and radical surgery in LARC patients with MSS or MSI-H status (22). Thirty percent (11/37) and 60% (3/5) of LARC patients with MSS status and MSI-H status, respectively, achieved pCR. Immune-related adverse effects were tolerable, and no treatment-related deaths occurred. This study pioneered the use of NAICIs in the traditional standard neoadjuvant treatment of LARC. The PANDORA study (NCT04083365) added durvalumab NAICI consolidation immunotherapy in the traditional neoadjuvant treatment strategy of LARC, and the pCR rate reached 32.7% (18/55) (85). However, the improved pCR rate of this clinical trial does not seem to exceed that of the TIMING trial, where the pCR rate increased to 38% in the MSS status subgroup (26). Then, NSABP FR-2 (NCT03102047) study added a NAICI treatment regimen with durvalumab between NACRT and surgery, and the outcomes of this clinical trial obtained a pCR of 22.2% and a cCR of 31.1% in MSS rectal cancer patients (84). BFH-NCRTPD (NCT04911517) reached a similar CR rate of 58.3% with a small sample. Tislelizumab were added during NACRT and before operation in this study (78). The TNT treatment model significantly improves the tumour regression rate with tolerable advances in LARC. Therefore, this kind of treatment model also serves as a good platform for NAICI treatment research in CRC. Similar to the different timings of chemotherapy intervention in TNT, various NAICI application models also exist in different clinical trials. In the PKUCH 04 study (NCT04340401),.7 (33.3%) achieved pCR among 21 patients who underwent surgery, and 4 obtained cCR or near cCR among those who chose the "watch and wait" strategy (86). No severe adverse events were observed. A study by Li et al. retrospectively analysed the pCR rate in pMMR/MSS LARC patients treated with a combination of TNT and ICIs (89). The results showed that 6 patients achieved pCR (30%) among the 20 patients who underwent surgery, and 3 patients achieved cCR among the 4 patients who refused to undergo surgery. Nine patients with pCR or cCR suffered from mild chemoradiotherapy and immune-related adverse effects, and no severe adverse effects were observed in any of these patients. Another retrospective study with a similar TNT treatment model without adding ICIs in the same patient group also reported a pCR rate of 29%, which suggests that this kind of ICIs intervention model seems to provide an additional therapeutic benefits (90). Two phase II studies, AVANA (NCT03854799) and NRG-GI002 (NCT02921256), investigated tumour regression when single ICIs were added concurrently with NACRT in LARC (76, 83). The TNT treatment model was applied in both clinical trials. In the AVANA study, a total of 23% (22/96) of patients achieved pCR, and 61.5% (59/96) of patients obtained an MPR. Another randomized controlled study, NRG-GI002, adopted a similar concurrent NAICI application model for stage II-III rectal cancer patients with high risk in the experimental group. However, no significant difference in the pCR rate was observed between the experimental group (31.9%) and the control group (29.4%) without pembrolizumab treatment.

All of the clinical trials in LARC above suggest that the pCR rate was not significantly improved when an NAICI was added to the TNT model. A potential reason is that long-term neoadjuvant radiotherapy damages the local immune system, limiting the immune response and reducing the additional efficacy of immunotherapy besides the prolonged surgical interval. Short-term neoadjuvant radiotherapy reduces impaired immune function and has noninferior treatment efficacy compared with long-term regimens in LARC according to the STELLAR and RAPIDO trials (16, 31). A study by Zhang et al. (NCT04231552) explored the treatment model of short-term neoadjuvant radiotherapy (5×5 Gy) followed by chemotherapy and ICI treatment in LARC patients (88). pCR rate was significantly increased to 46%. The interval between neoadjuvant treatment and surgery was greatly decreased, and no severe immune-related adverse events were observed. The AVERECTAL study also applied short-term neoadjuvant radiotherapy and increased the cycles of mFOLFOX6 and ICI before surgery in LARC patients (77). The pCR rate in this study significantly improved to 37.5% compared with 16% in the previous control group. A recent oral report of TORCH (NCT04518280), in which short-course neoadjuvant radiotherapy was administered, also showed an amazingly high CR rate (CR rate: 81.8%, 9/11; pCR rate: 77.8%, 7/9) in MSS LARC (87). The short-term neoadjuvant radiotherapy model seems to have a higher probability of achieving pCR in LARC when combined with an NAICI. The ongoing PRIME-PR (NCT04621370) study is directly comparing the tumour regression difference between short-term and long-term neoadjuvant radiotherapy in the TNT treatment model with NAICI in LARC (91). The TORCH (NCT04518280) study is

10.3389/fimmu.2023.1120684

TABLE 1 Reported studies involving neoadjuvant immunotherapy trials in CRC.

Identifier	Trial name	Enrollment	Location	Trial design	CR rate n (%)	MPR rate n (%)	Grade 3-4 AEs n (%)	Reference
NCT03854799	AVANA	101 (MSI-H:1, MSS:38, Rest unknown)	Rectal cancer	Single-arm, Stage II-III, Phase II, nCRT (50.4Gy+Cape) + Ave 10 mg/kg q2w×6 cycles → TME (8-10w after the end of nCRT)	pCR: 22 (23)	59 (61.5)	8% (non-immune related) and 4% (immune-related)	(76)
NCT03503630	Averectal	44	Rectal Cancer	Single-arm, Stage II-III, Phase II, SCRT(5x5Gy) → FOLFOX+ Ave 10 mg/kg q2w×6 cycles → TME (3-4w after last treatment)	pCR:15 (37.5)	27 (67.5)	Grade 3: 25 (58.1%) and Grade 4: 5 (11.6%)	(77)
NCT04911517	BFH-NCRTPD	pMMR: 20	Rectal Cancer	Single-arm, Stage II-III, Phase II, nCRT (50Gy+Cape) + Tisl 200mg q3w×3 cycles → Surgery → Adjuvant chemotherapy with CapeOx	pCR: 7 (58.3)	NR	3 (25) (enteritis, oral ulcer and hyperthyroidism)	(78)
NCT04165772		dMMR: 16	Rectal Cancer	Single-arm, Stage II-III, Phase II, Dost 500mg q3w×3 cycles → nCRT (50.4Gy+Cape) → TME	cCR: 12 (100)	NR	0	(79)
NCT03026140	NICHE	dMMR: 32 pMMR: 33	Colon cancer	Randomized, Stage I-III, Phase II, Ipi 1mg/kg×1 cycle + Nivo 3mg/kg q2w×2 cycle → Surgery (pMMR patients were randomly assigned to receive celecoxib from D1 until the day before surgery)	pCR: dMMR: 22 (68.8) pMMR: 4(13.3)	dMMR:31 (96.9) pMMR: 7 (23.3)	7 (10.7)	(80)
NCT03026140	NICHE-2	dMMR: 112	Colon cancer	Single-arm, Stage I-III, Phase II, Ipi 1mg/kg×1 cycle + Nivo 3mg/kg q2w×2 cycle → Surgery	pCR: 72 (67)	102 (95)	5 (4) (immune-related) and 15 (13) (surgery-related)	(81)
NCT04123925	NICOLE	dMMR: 3 pMMR:19	Colon cancer	Single-arm, Stage II-III, Phase II, Nivo 240 mg q2w×2 cycles → Surgery	NR	dMMR: 0 pMMR: 3 (15.8)	1 (4.5) (diarrhea)	(82)
NCT02921256	NRG-GI002	Pemb arm: 90 Control arm: 95	Rectal Cancer	Randomized, Stage II-III, Phase II, Pemb arm: FOLFOX×4m + nCRT(50.4Gy+Cape)+Pemb 200mg q3w×6 cycles → Surgery (8-12w after radiotherapy), Control arm: FOLFOX×4m + nCRT(50.4Gy+Cape) → Surgery (8-12w after radiotherapy)	pCR: Pemb arm: NR (31.9) Control arm: NR (29.4) cCR: Pemb arm: NR (13.9) Control arm: NR (13.6)	NR	Pemb arm: 48.2% (during nCRT) and 37.3% (after nCRT) Control arm: NR	(83)
NCT03102047	NSABP FR-2	MSS: 45	Rectal Cancer	Single-arm, Stage II-III, Phase II, nCRT → Durv 750mg q2w×4 cycles → Surgery (8-12w after radiotherapy)	pCR: 10 (22.2) cCR: 14 (31.1)	NR	NR	(84)

(Continued)

TABLE 1 Continued

Identifier	Trial name	Enrollment	Location	Trial design	CR rate n (%)	MPR rate n (%)	Grade 3-4 AEs n (%)	Reference
NCT04083365	PANDORA	60	Rectal Cancer	Single-arm, Stage II-III, Phase II, nCRT (50.4Gy+Cape) + Durv 1500mg q4w×3 cycles → Surgery (after 10-12w from neoadjuvant therapy)	pCR: 18 (32.7)	NR	4 (7.3) (diarrhea, skin toxicity, transaminase increase, lipase increase and pancolitis)	(85)
NCT04340401	PKUCH 04	dMMR: 27	Rectal Cancer	Single-arm, Stage II-III, Phase II, CapeOX + Cam 200mg q3w×3 cycles → Radiotherapy (45Gy) → CapeOX q3w×2 cycles → Surgery	pCR: 7 (33.3)	7 (33.3)	lymphopenia (24%), diarrhea (8%), and thrombocytopenia (4%)	(86)
NCT04518280	TORCH	Arm A: 35 Arm B: 32	Rectal Cancer	Randomized, Stage II-III, Phase II, Arm A: SCRT(5x5Gy) → CapeOX + Tori 240mg q3w×6 cycles → TME, Arm B: CapeOX + Tori 240mg q3w×2 cycles → SCRT(5x5Gy) → CapeOX + Tori 240mg q3w×4 cycles → TME	MSS: CR: 9 (81.8) pCR: 7 (77.8)	NR	Grade 3: 4 (36.4%) and Grade 4: 0	(87)
NCT02948348	VOLTAGE-A	MSS: 37 MSI-H: 5	Rectal cancer	Single-arm, Stage II-III, Phase Ib/II, nCRT (50.4Gy+Cape) + Nivo 240mg q2w×5 cycles → Surgery → Adjuvant chemotherapy with FOLFOX or XELOX	pCR: MSS: 11 (30) MSI-H: 3(60)	MSS: 14 (38) MSI-H: NR	2 (myasthenia and interstitial nephritis	(22)
NCT04231552		dMMR: 1 pMMR: 28 Unknown: 1	Rectal Cancer	Single-arm, Stage II-III, Phase II, SCRT(5x5Gy) → CapeOX + Cam 200mg q3w×2 cycles → Surgery (1w after last immunotherapy)	pCR: dMMR: 1 (100) pMMR: 12 (46.2)	NR	8 (26.7) (leukopenia, anemia and neutropenia)	(88)

Clinical trial details can be accessed at ClinicalTrials.gov database. AEs, Adverse effects; Ave, avelumab; Cam, Camrelizumab; CapeOX, capecitabine and oxaliplatin; Cap, capecitabine; cCR, Clinical complete response; CR, Complete response; D, day; dMMR, Deficient mismatch repair; Dost, Dostarlimab; Durv, Durvalumab; FOLFOX, folinic acid, fluorouracil and oxaliplatin; Ipi, Ipilimumab; MPR, Major pathologic response; MSI-H, Microsatellite instability-high; MSS, Microsatellite stability; m, Months; NCT, National Clinical Trial; Nivo, Nivolumab; nCRT, Neoadjuvant chemoradiotherapy; NR, Not report; Pemb, Pembrolizumab; pMMR, Proficient mismatch repair; pCR, Pathological complete response; SCRT, Short-course radiotherapy; Tisl, Tislelizumab; TME, Total mesorectal excision; W, Week; XELOX, Xeloda and oxaliplatin.

further investigating the optimal intervention timing of NAICI and neoadjuvant chemotherapy administration for short-term neoadjuvant radiotherapy in the same population (92). Additionally, the REGINA study (NCT04503694) explored the therapeutic effect of the combination of nivolumab and regorafenib when administered before and after standard preoperative short-course radiation therapy in LARC (79). A recent study (NCT04165772) demonstrated that NAICI therapy with single dostarlimab, a PD-1 inhibitor, followed by radiotherapy without chemotherapy also achieved favourable tumour regression in dMMR stage II-III LARC (93). A total of 12 patients were enrolled, and all these patients achieved cCR. These completed or ongoing studies are currently in clinical phase II with limited examples, and the results of these studies are worthy of reflection and expectation. More large-size clinical trials with optimized treatment strategies are warranted. These currently recruiting studies are summarized in Table 2.

Right patients? Potential biomarkers in NAICI

Currently, MSI/MMR status detection has been widely used for selecting potential patients who could benefit from immunotherapy in CRC and other solid tumours. A higher percentage of MSI-H/dMMR status subgroup patients benefited in terms of better tumour regression with NAICI treatment in the NICHE study and longer survival with first-line ICI treatment in the KEYNOTE-177 study (20, 21). MSI/MMR status seems to be an effective biomarker for predicting the response to immunotherapy, but only approximately 10% of localized CRCs and approximately 5% of mCRCs have MSI-H/dMMR status, and a few of MSS/pMMR CRC patients were also reported to benefit from ICI treatment (98, 99). Therefore, more precise and reliable predictors need to be identified. TMB, a biomarker measuring the somatic mutations per coding area of a tumour genome, may serve as a supplementary immunotherapy

predictor in MSS/pMMR CRC (100). Similar to MSI-H/dMMR CRC, which have a 20 times higher mutation burden than non-MSI-H/pMMR CRC, a higher TMB is associated with a greater number of neoantigens produced and presented, enhancing immunogenicity and improving immunotherapeutic efficacy (101, 102). KEYNOTE-158 showed that the higher TMB subgroup shares a similar objective response rate regardless of MSI status in solid tumours (103). Then, two clinical trials preliminarily confirmed the treatment efficacy predictive value of TMB in CRC patients with MSS status who received immunotherapy (104, 105). TMB was detected in tumour tissue in the REGONIVO study, and a higher objective response rate (50% vs. 35.3%) and better median progression-free survival (12.5 vs. 7.9 months) were observed in the higher TMB group. Another CCTG CO.26 study also showed a better OS in CRC patients with TMB ≥ 28, in which plasma TMB was analysed with cfDNA in blood samples. Another tumor neoantigents related biomarker was POLE/POLD 1. Mutations in the POLE exonuclease domain disturbs the function of proofreading exonuclease activity required to replicate DNA with high fidelity and cause a high mutation burden in somatic cells (106). Most POLE-mutated CRCs have MSS or MSI-L statuses, while increased CD8+ T-cell infiltration, higher expression of T

TABLE 2 Ongoing perspective studies involving neoadjuvant immunotherapy trials in resectable CRC.

Identifier	Trial name	Country	Estimated enrollment cases	Location	Trial design	Primary endpoint (s)	Estimated study Completion (year)	Reference
NCT04643041	BASKET	China	dMMR:47	Rectal cancer	Single-arm, NR, NR, Anti-PD-1 Antibody 200mg q3w×4 cycles → W&W	1-year DFS	2026	
NCT04621370	PRIME-RT	United Kingdom	48	Rectal cancer	Randomized, Stage II-III, Phase II, Arm A: Durv 1500mg×1 cycles → SCRT(5x5Gy) → FOLFOX×6 cycles+Durv 1500mg q4w → W&W or Surgery, Arm B: Durv 1500mg×1 cycles → Radiotherapy(50Gy+Cape) +Durv 1500mg q4w×1 cycles → FOLFOX×4 cycles+Durv 1500mg q4w → W&W or Surgery	CR	2025	(91)
NCT04503694	REGINA	Belgium	6	Rectal cancer	Single-arm, Stage II-III, Phase II, Nivo 240mg q2w×2 cycles +regorafenib 80mg d1-14 → SCRT(5x5Gy) → Nivo 240mg q2w×2 cycles+regorafenib 80mg d1-14 → TME → Adjuvant chemotherapy	pCR	2028	(79)
NCT03127007	R-IMMUNE	Belgium	54	Rectal cancer	Randomized, Stage II-III, Phase I/II, Arm A: nCRT (45-50Gy+5-FU) +Atez 1200mg q3w×4 cycle → Surgery, Arm B: nCRT (45-50Gy+5-FU) → Surgery	AEs, pCR	2023	
NCT04124601	CHINOREC	Austria	80	Rectal cancer	Randomized, Stage II-III, Phase II, Arm A: nCRT (50Gy+Cape) → Surgery Arm B: nCRT (50Gy+Cape) → Ipi 1mg/kg×1 cycle → Nivo 3mg/kg q2w×3 cycle → Surgery	AEs	2023	(94)
NCT04293419	DUREC	Spain	58	Rectal cancer	Single-arm, Stage II-III, Phase II, FOLFOX×4 cycles+Durv 1500mg q4w×3 cycles → nCRT (50.4Gy+Cape)+Durv 1500mg	pCR	2025	

(Continued)

TABLE 2 Continued

Identifier	Trial name	Country	Estimated enrollment cases	Location	Trial design	Primary endpoint (s)	Estimated study Completion (year)	Reference
					q4w×2 cycles → Durv 1500mg q4w×1 cycles → Surgery			
NCT04017455	TARZAN	Netherlands	38	Rectal cancer	Single-arm, Resectable disease, Phase II, Radiotherapy → Beva 5mg/kg×1 cycle → Beva 5mg/kg +Atez 840mg×2 cycle → Atez 840mg×1 cycle → Surgery	cCR	2024	
NCT04906044	STARS-RC03	China	30	Rectal cancer	Single-arm, Stage II-III, Phase I, SCRT+chemotherapy+Tile → Surgery	AEs	2028	
NCT04130854	INNATE	American	58	Rectal cancer	Randomized, Stage II-III, Phase I/II, Arm A: SCRT(5x5Gy) +APX005M (an Anti-CD40 Agonist) 0.3mg/kg×1 cycle → APX005M 0.3mg/kg +FOLFOX×5 cycle → FOLFOX×1 cycle → TME, Arm B: SCRT(5x5Gy)→ FOLFOX×6 cycle → TME	pCR	2023	
NCT03299660		Australia	37	Rectal cancer	Single-arm, Stage II-III, Phase II, nCRT (50.4Gy+Cape or 5-FU) → Ave 10 mg/kg q2w×4 cycles → Surgery	pCR	2023	(95)
NCT04304209		China	195	Rectal cancer	Randomized, Stage II-III, Phase II/III, dMMR group: Sint 200mg q3w×4 cycles → Surgery or W&W → Adjuvant Sint ± CapeOX, pMMR group-1: nCRT (50Gy +CapeOX) + Sint 200mg q3w×4 cycles → Surgery or W&W → Adjuvant CapeOX×4 cycles, pMMR group-2: nCRT (50Gy +CapeOx) → Surgery or W&W → Adjuvant CapeOX×4 cycles	pCR	2026	(96)
NCT04109755	PEMREC	Switzerland	MSS: 25	Rectal cancer	Single-arm, Stage II-III, Phase II, SCRT(5x5Gy) + Pemb 200 mg q3w×4 cycle → Surgery	TRG	2028	(97)
NCT04411524		China	MSI-H: 50	Rectal cancer	Single-arm, Stage II-III, Phase II, Anti-PD-1 Antibody×2 cycles → nCRT (50Gy+Cape +Irinotecan) → Anti-PD-1 Antibody×3 cycles → TME → Adjuvant XELOX×6 cycles	pCR	2022	
NCT04411537		China	MSS: 50	Rectal cancer	Single-arm, Stage II-III, Phase II, Anti-PD-1 Antibody×2 cycles → nCRT (50Gy+Cape +Irinotecan) → Anti-PD-1 Antibody×3 cycles → TME → Adjuvant XELOX×6 cycles	pCR	2022	

(Continued)

TABLE 2 Continued

Identifier	Trial name	Country	Estimated enrollment cases	Location	Trial design	Primary endpoint (s)	Estimated study Completion (year)	Reference
NCT04443543		China	222	Rectal cancer	Non-Randomized, Stage II-III, Phase II, MSS group: XELIRI or FOLFIRINOX (cycles of chemotherapy depend on patient tumor responses) → Surgery or W&W MSI-H group: nCRT (50Gy +XELIRI or FOLFIRINOX) → Tisl 200mg×3 cycles → Surgery or W&W	cCR	2026	
NCT04357587		American	dMMR:10	Rectal cancer	Single-arm, Stage II-III, Phase I, nCRT (50Gy+Cape) + Pemb 200mg q3w×3 cycles → TME	AEs, Tolerability, Feasibility	2022	
NCT03921684		Israel	29	Rectal cancer	Single-arm, Stage II-III, Phase II, nCRT (50.4Gy+Cape) → FOLFOX+Nivo 240mg q2w×3 cycle → Surgery	pCR, AEs	2025	
NCT04558684		China	30	Rectal cancer	Single-arm, Stage II-III, Phase I/II, SCRT(5x5Gy) → CapeOX + Cam 200mg q3w×6 cycles → W&W or Surgery	cCR	2023	
NCT04663763		China	MSS: 32 MSI-H: 8	Rectal cancer	Single-arm, Stage II-III, Phase II, SCRT(5x5Gy) → CapeOX + Sint 200mg q3w×4 cycles → TME → Adjuvant CapeOX×4 cycles	pCR	2025	
NCT04636008		China	dMMR:20	Rectal cancer	Single-arm, Stage II-III, Phase Ib/II, SCRT(5x5Gy) → Sint 200mg q2w×3 cycles → Surgery	AEs	2022	
NCT03985891	JSFOL	China	40	Colon cancer	Randomized, Stage II-III, Phase I/II, Arm A: FOLFOX+JS001 (an Anti-PD-1 Antibody) 3mg/kg q2w×6 cycles → Surgery, Arm B: FOLFOX×6 cycles → Surgery	pCR, rCR, ORR	2026	
NCT05202314	NACSOC-02	China	20	Colon cancer	Single-arm, Resectable disease, Phase NR, Cam 200mg q3w×2 cycles +FOLFOX×3 cycles or CapeOx×2 cycles → Surgery	pCR	2026	
NCT04625803		China	64	Colon cancer	Single-arm, Stage II-III, Phase II, FOLFOX+Cam 200 mg q2w×5 cycles+Apatinib×2 m → Surgery → FOLFOX+Cam 200 mg q2w×7 cycles	TRG	2025	
NCT05231850		China	dMMR:70	Colon cancer	Single-arm, Stage II-III, Phase II, Tisl 200mg q3w until disease progression, unacceptable or withdrawal of consent	DFS	2027	

(Continued)

TABLE 2 Continued

Identifier	Trial name	Country	Estimated enrollment cases	Location	Trial design	Primary endpoint (s)	Estimated study Completion (year)	Reference
NCT03926338	PICC	China	dMMR: 100	Colorectal cancer	Randomized, Stage II-III, Phase I/II, Arm A: Tori 3mg/m^2 q2w +Celecoxib×3m or 6m → Surgery Arm B: Tori 3mg/m^2 q2w×3m or 6m → Surgery	pCR	2024	

Clinical trial details can be accessed at ClinicalTrials.gov database. 5-FU, 5-fluorouracil; AEs, Adverse effects; Atez, Atezolizumab; Ave, avelumab; Beva, bevacizumab; Cam, Camrelizumab; CapeOX, capecitabine and oxaliplatin; cCR, Cap, capecitabine; cCR, Clinical complete response; CR, Complete response; D, day; DFS, Disease free survival; dMMR, Deficient mismatch repair; Durv, Durvalumab; FOLFOX, folinic acid, fluorouracil and oxaliplatin; Ipi, Ipilimumab; m, Month; MSI-H, Microsatellite instability-high; MSS, Microsatellite stability; NCT, National Clinical Trial; Nivo, Nivolumab; nCRT, Neoadjuvant chemoradiotherapy; NR, Not report; ORR, Overall response rate; Pemb, Pembrolizumab; pMMR, Proficient mismatch repair; pCR, Pathological complete response; PD-1, programmed death-1; rCR, Radiographic complete response; SCRT, Short-course radiotherapy; Sint, Sintilimab; TME, Total mesorectal excision; Tori, Toripalimab; TRG, Tumor regression grade; W, Week; W&W, Watch & wait; XELIRI, Xeloda and irinotecan; XELOX, Xeloda and oxaliplatin; FOLFIRINOX, folinic acid, fluorouracil, irinotecan and oxaliplatin.

lymphocyte markers and effector cytokines, and upregulation of PD-1, PD-L1, and CTLA-4 could also be observed in these POLE-mutated CRCs (107, 108). Given that POLE-mutated CRCs have similar immune features to their MSI-H status counterparts, the application of immunotherapy deserves exploration, and therapeutic efficacy warrants investigation in POLE-mutated CRC.

Recently, B2M mutations were also found to be associated with clinical response in CRC patients treated with anti-PD-1 therapy. These mutations disturbed MHC class I antigen presentation, reduced T-cell activation, and contributed to immune escape. Different forms of B2M mutations showed the opposite prediction value in CRC. Primary B2M mutations were more frequently observed in MMR-deficient CRC, and complete B2M loss has a significant association with less recurrence and metastasis in CRC (109). However, acquired B2M mutations were reported to result in resistance to ICIs (65). Theoretically, PD-L1 expression could serve as a good clinical response predictor for tumours treated with anti-PD-1 therapy. The predictive value of PD-L1 expression has been confirmed in non-small cell lung cancer and gastric cancer, and PD-L1 detection with immunohistochemical staining has been widely used to guide the application of ICIs treatment in these tumours (110, 111). However, PD-L1 expression did not seem to be associated with prognosis in CRC patients (19, 49). Both of the two genes participate in the stimulation of immune effector cells, and the unusual prognostic role of the two genes in CRC treated with anti-PD1 therapy warrants further elucidation of the potential mechanism.

A previous study demonstrated that a higher density of tumour-infiltrating lymphocytes (TILs), especially CD8-positive T cells, surrounding CRC tumours was significantly associated with a better ICIs treatment response (112). In the NICHE study, CD8-positive T-cell infiltration (TCI) and CD8-positive PD-1-positive TCI were found to be higher in dMMR status colon cancer than that in its pMMR counterpart. Further molecular and immunophenotypic analyses revealed that CD8-positive PD-1-positive TCI could predict the ICIs treatment response in pMMR colon cancer and was considered an effective predictor for ICIs therapy (21). In addition to CD8-positive TCI, the density of CD3-positive T cells was also found to be a more favourable prognostic biomarker in CRC than common histopathological prognostic factors (43). The Immunoscore was proposed as a standardized method to assess the density of both intra- and extratumoral CD3-positive T cells and CD8-positive T cells in colon cancer (44). Its favourable prognostic predictive value has been validated in 3539 patients with stage I-III colon cancer from 14 expert centres in 13 countries. Further validation of the Immunoscore in CRC is ongoing in a multicentre clinical trial (NCT01688232). Another phase II study (NCT04262687) evaluated the treatment efficacy of a chemotherapy regimen of XELOX (xeloda and oxaliplatin) and bevacizumab combined with pembrolizumab in unresectable mCRC patients with an MSS status and a higher level of immune infiltration. More precise and reliable predictive biomarkers need to be identified to select potential patients who could benefit from ICIs treatment.

Right directions? Pitfalls and promise of NAICI in CRC

The current outcomes reported from completed or ongoing clinical trials have revealed that tumour regression benefits from the application of NAICI in locally advanced CRC, but the optimal timing and strategies of immunotherapy remain unknown, and beneficiary identification needs further exploration. Additionally, several concerns regarding ICIs treatment should not be ignored. One concern is that early progression of disease during the period of neoadjuvant treatment due to drug resistance may result in CRC patients losing their best surgical chances. As shown in the results of the PANDORA study, local and/or metastatic tumour progression occurred in 3 patients before surgery (85). The potential mechanisms of ICIs treatment resistance are complicated. Grasso et al. investigated the potential immune escape mechanisms in MSI-H/dMMR CRC patients (113). They found that genetic alterations influenced the multiple steps of immune activation. Changes in the WNT signalling pathway impaired immune recognition. Genetic alterations, including a biallelic loss of β2 microglobulin (β2M), an

MHC class I component, and single-copy loss events in HLA molecules lead to antigen presentation defects. Alterations in immune response–related genes involved in T-cell reactions, B-cell differentiation and NK cell activity contributed to weakened immune function. These potential immune pathway changes may cause immune tolerance and intrinsic resistance to ICIs treatment. Among these various mechanisms, *IFN-γ* signalling was found to play a key role in immunotherapy resistance. *IFN-γ* signalling initiated by T cells could induce PD-L1 expression through JAK-STAT signalling and interfere with the combination of CTLA-4 and the costimulatory molecule B7. Melanoma patients with JAK-STAT signalling-related gene mutations experienced tumour recurrence after responding to anti-PD-1 therapy (114). *IFN-γ* signalling-related gene mutations caused a nonresponse to anti-CTLA-4 treatment (115).

Another concern is the immune-related adverse events (irAEs) that occur during NAICI treatment in CRC. Severe irAEs prolong the interval between neoadjuvant treatment and surgery, increase the possibility of potential distant metastasis, and even cause mortality. Theoretically, patients who receive NAICI treatment may be more vulnerable to severe irAEs due to the more functional immune system compared with late cancer. Colitis is the most common irAE in patients treated with ipilimumab monotherapy, while hypothyroidism, rash, and diarrhoea are more commonly observed in patients treated with nivolumab and pembrolizumab (116). A retrospective study by Han et al. reported that 58.3% of dMMR CRC patients were treated with anti-PD1 neoadjuvant monotherapy, including pembrolizumab or nivolumab, and 16.7% of these patients experienced grade 3-4 irAEs (117). A combination of anti-PD1 and anti-CTL-4 immune drugs was applied in the NICHE study; 13% of patients suffered from grade 3-4 immune treatment-related toxicity, and none of the patients delayed radical resection (21). In a study by Zhang et al., camrelizumab (anti-PD-1) and chemotherapy were applied after short-course radiotherapy, and no grade 3-4 irAEs were observed (77). Outcomes of these small sample clinical trials showed that severe irAEs, mainly colitis, that occurred during NAICI treatment in CRC were uncommon and manageable and did not affect the timing of surgery. However, the number of patients enrolled in these studies was limited, and potential irAEs still warrant full and serious consideration in daily practice.

Except for these pitfalls, the application of NAICI therapy further improves the possibility of organ preservation (OP) in LARC patients. For patients who achieve cCR after neoadjuvant treatment, whether rectal resection should be performed is controversial. Harba-Gamal et al. first proposed the watch and wait (W&W) strategy in 2004 (13). They advised carrying out close follow-up rather than performing total mesorectal excision for these cCR LARC patients. This strategy preserves functional issues and avoids the complications of surgery, including anal dysfunction and sexual dysfunction, which improves the quality of life of these patients. A secondary analysis of the OPRA clinical trial analysed the differences in survival and OP rates among LARC patients who achieved cCR, near complete response (nCR), or incomplete clinical response (iCR) after TNT treatment (118). cCR and nCR patients were assigned to the W&W strategy, while iCR patients were recommended to undergo total mesorectal excision. The outcome of this analysis demonstrated that the 3-year OP rates in cCR and nCR patients were 79% and 52%, respectively, and the 3-year DFS in the iCR group was lower than that in the other two groups. However, no significant difference in the 3-year OS was observed among these three subgroups. They recommended the W&W strategy as a feasible treatment model for LARC patients who achieved cCR or nCR after neoadjuvant therapy. Long-lasting benefits have been observed in several cancers if favourable immunotherapy efficacy was obtained from initial immune treatment (80, 119, 120). Maintenance immunotherapy may further improve the long-term OP and DFS rates in LARC patients who achieved cCR or nCR after NAICI therapy, especially for those in the MSI-H/dMMR subgroup. Further large sample size preclinical validation studies are warranted.

Future prospects

The optimal intervention timing of immunotherapy, ideal duration of ICIs, appropriate dose of immune drugs, and combination strategy of ICIs and cytotoxic agents before surgery are unknown now. A large number of early exploratory clinical trials are ongoing. The treatment model of short-course radiotherapy followed by 4-5 cycles of anti-PD1 therapy combined with fluorouracil- or its derivative-based chemotherapy before surgery in CRC seems to be more ideal according to reports to date. Screening of beneficiaries of immunotherapy remains based on the MSI/MMR status, while some MSI-H/dMMR CRC patients could not benefit from ICIs treatment, and some MSS/pMMR patients could achieve a good clinical response from immunotherapy. Therefore, response-associated genetic signatures covering neoantigen load, immune system response to tumour or antigen load and any defects in reaction initiation should be established (42). Pathological alterations, TME changes and potential mechanisms of ICIs resistance could be deeply investigated with residual viable tumour tissues obtained after NAICI therapy by surgical resection. Single-cell analysis of these tumour specimens could reveal immune evasion mechanisms from multiple dimensions. Findings from such studies may convert immunologically “cold” tumours to “hot” tumours and lead to the development of new treatment combinations to improve ICIs treatment efficacy. Robust biomarker identification will also reduce the risk of patients suffering from severe irAEs. Additionally, a higher level of tumour antigen-specific circulating T cells induced by NAICI could develop a long-lasting effector-memory T-cell pool (25, 121, 122). This finding may provide a potential survival benefit for patients treated with NAICI who achieved cCR or nCR if maintenance immunotherapy was administered without surgery.

Conclusion

The application of neoadjuvant therapy in CRC downsizes the tumours preoperatively and improves local and systemic control of

the disease, but no significant OS benefit was observed in previous clinical trials (36–38). Favourable outcomes were obtained in dMMR mCRC patients from treatment with pembrolizumab monotherapy as first-line therapy. The administration of ICIs was pioneered in LACRC in the neoadjuvant setting, which yielded impressive results especially in MSI-H/dMMR patients (20). Possible reason is due to the enhanced T-cell activation when a more functional immune system encountered more antigenic exposure before operation. However, optimum NAICI treatment regimen establishment and effective biomarker identification for beneficiary screening need further exploration. In summary, greater cooperation between clinicians and tumour immunologists contributes to a deeper understanding of the mechanisms of action of ICIs and to the development of robust theoretical foundations for the improvement of ICIs treatment efficacy in cancers.

Author contributions

JZ, SJ, YZ and HL conceived and designed this study. JL, BX, and XP drew figures and tables. JL, BX, and XP collected and updated clinical trial data. JZ wrote the manuscript and HL revised the manuscript. All authors contributed to the article and approved the submitted version.

Funding

This work was supported by the National Natural Science Foundation of China (grant nos. U20A20376), Beijing Award Foundation (grant nos. YXJL-2020-0818-0478), Wu Jieping Medical Foundation (grant no. 320.6750.2020-19-20), Heilongjiang Province Postdoctoral Science Foundation (grant no. LBHZ21189), Harbin Medical University Innovative Science Research Funded Project (grant no. 31041220028), China Postdoctoral Science Foundation (grant no. 2022MD713747), Gusu Health Talent Program (GSWS2020067), Harbin Medical University Innovative Science Research Funded Project (grant no. 2022-KYYWF-0289).

Conflict of interest

The authors declare that the research was conducted in the absence of any commercial or financial relationships that could be construed as a potential conflict of interest.

Publisher's note

All claims expressed in this article are solely those of the authors and do not necessarily represent those of their affiliated organizations, or those of the publisher, the editors and the reviewers. Any product that may be evaluated in this article, or claim that may be made by its manufacturer, is not guaranteed or endorsed by the publisher.

References

1. Sung H, Ferlay J, Siegel RL, Laversanne M, Soerjomataram I, Jemal A, et al. Global cancer statistics 2020: GLOBOCAN estimates of incidence and mortality worldwide for 36 cancers in 185 countries. *CA Cancer J Clin* (2021) 71(3):209–49. doi: 10.3322/caac.21660

2. *Colorectal cancer: Statistics* (2022). Available at: https://www.cancer.net/cancer-types/colorectal-cancer/statistics.

3. Sargent D, Sobrero A, Grothey A, O'Connell MJ, Buyse M, Andre T, et al. Evidence for cure by adjuvant therapy in colon cancer: observations based on individual patient data from 20,898 patients on 18 randomized trials. *J Clin Oncol* (2009) 27(6):872–7. doi: 10.1200/JCO.2008.19.5362

4. André T, Boni C, Navarro M, Tabernero J, Hickish T, Topham C, et al. Improved overall survival with oxaliplatin, fluorouracil, and leucovorin as adjuvant treatment in stage II or III colon cancer in the MOSAIC trial. *J Clin Oncol* (2009) 27(19):3109–16. doi: 10.1200/JCO.2008.20.6771

5. Yothers G, O'Connell MJ, Allegra CJ, Kuebler JP, Colangelo LH, Petrelli NJ, et al. Oxaliplatin as adjuvant therapy for colon cancer: updated results of NSABP c-07 trial, including survival and subset analyses. *J Clin Oncol* (2011) 29(28):3768–74. doi: 10.1200/JCO.2011.36.4539

6. Haller DG, Tabernero J, Maroun J, de Braud F, Price T, Van Cutsem E, et al. Capecitabine plus oxaliplatin compared with fluorouracil and folinic acid as adjuvant therapy for stage III colon cancer. *J Clin Oncol* (2011) 29(11):1465–71. doi: 10.1200/JCO.2010.33.6297

7. The National Comprehensive Cancer Network. *NCCN clinical practice guidelines in oncology, colon cancer. version 1.2012* (2012). Available at: https://www.nccn.org.

8. Ahiko Y, Shida D, Kudose Y, Nakamura Y, Moritani K, Yamauchi S, et al. Recurrence hazard of rectal cancer compared with colon cancer by adjuvant chemotherapy status: a nationwide study in Japan. *J Gastroenterol* (2021) 56(4):371–81. doi: 10.1007/s00535-021-01771-6

9. Bosset JF, Calais G, Mineur L, Maingon P, Stojanovic-Rundic S, Bensadoun RJ, et al. Fluorouracil-based adjuvant chemotherapy after preoperative chemoradiotherapy in rectal cancer: long-term results of the EORTC 22921 randomised study. *Lancet Oncol* (2014) 15(2):184–90. doi: 10.1016/S1470-2045(13)70599-0

10. Sainato A, Cernusco Luna Nunzia V, Valentini V, De Paoli A, Maurizi ER, Lupattelli M, et al. No benefit of adjuvant fluorouracil leucovorin chemotherapy after neoadjuvant chemoradiotherapy in locally advanced cancer of the rectum (LARC): long term results of a randomized trial (I-CNR-RT). *Radiother Oncol* (2014) 113 (2):223–9. doi: 10.1016/j.radonc.2014.10.006

11. Bosset JF, Collette L, Calais G, Mineur L, Maingon P, Radosevic-Jelic L, et al. Chemotherapy with preoperative radiotherapy in rectal cancer. *N Engl J Med* (2006) 355(11):1114–23. doi: 10.1056/NEJMoa060829

12. Foxtrot Collaborative Group. Feasibility of preoperative chemotherapy for locally advanced, operable colon cancer: the pilot phase of a randomised controlled trial. *Lancet Oncol* (2012) 13(11):1152–60. doi: 10.1016/S1470-2045(12)70348-0

13. Habr-Gama A, Perez RO, Nadalin W, Sabbaga J, Ribeiro U Jr, Silva e Sousa AH Jr, et al. Operative versus nonoperative treatment for stage 0 distal rectal cancer following chemoradiation therapy: long-term results. *Ann Surg* (2004) 240(4):711–7; discussion 717-8. doi: 10.1097/01.sla.0000141194.27992.32

14. Cercek A, Goodman KA, Hajj C, Weisberger E, Segal NH, Reidy-Lagunes DL, et al. Neoadjuvant chemotherapy first, followed by chemoradiation and then surgery, in the management of locally advanced rectal cancer. *J Natl Compr Canc Netw* (2014) 12 (4):513–9. doi: 10.6004/jnccn.2014.0056

15. Seymour MT, Morton DInternational FOxTROT Trial Investigators. FOxTROT: an international randomised controlled trial in 1052 patients (pts) evaluating neoadjuvant chemotherapy (NAC) for colon cancer. *J Clin Oncol* (2019) 37:15_suppl:3504–4. doi: 10.1200/JCO.2019.37.15_suppl.3504

16. Bahadoer RR, Dijkstra EA, van Etten B, Marijnen CAM, Putter H, Kranenbarg EM, et al. Short-course radiotherapy followed by chemotherapy before total mesorectal excision (TME) versus preoperative chemoradiotherapy, TME, and optional adjuvant chemotherapy in locally advanced rectal cancer (RAPIDO): a randomised, open-label, phase 3 trial. *Lancet Oncol* (2021) 22(1):29–42. doi: 10.1016/S1470-2045(20)30555-6

17. Schmoll HJ, Stein A, Van Cutsem E, Price T, Hofheinz RD, Nordlinger B, et al. Pre- and postoperative capecitabine without or with oxaliplatin in locally advanced rectal cancer: PETACC 6 trial by EORTC GITCG and ROG, AIO, AGITG, BGDO, and FFCD. *J Clin Oncol* (2021) 39(1):17–29. doi: 10.1200/JCO.20.01740

18. Karoui M, Rullier A, Piessen G, Legoux JL, Barbier E, De Chaisemartin C, et al. Perioperative FOLFOX 4 versus FOLFOX 4 plus cetuximab versus immediate surgery for high-risk stage II and III colon cancers: A phase II multicenter randomized controlled trial (PRODIGE 22). *Ann Surg* (2020) 271(4):637–45. doi: 10.1097/SLA.0000000000003454

19. Le DT, Uram JN, Wang H, Bartlett BR, Kemberling H, Eyring AD, et al. PD-1 blockade in tumors with mismatch-repair deficiency. *N Engl J Med* (2015) 372 (26):2509–20. doi: 10.1056/NEJMoa1500596

20. Andre T, Amonkar M, Norquist JM, Shiu KK, Kim TW, Jensen BV, et al. Health-related quality of life in patients with microsatellite instability-high or mismatch repair deficient metastatic colorectal cancer treated with first-line pembrolizumab versus chemotherapy (KEYNOTE-177): an open-label, randomised, phase 3 trial. *Lancet Oncol* (2021) 22(5):665–77. doi: 10.1016/S1470-2045(21)00064-4

21. Chalabi M, Fanchi LF, Dijkstra KK, Van den Berg JG, Aalbers AG, Sikorska K, et al. Neoadjuvant immunotherapy leads to pathological responses in MMR-proficient and MMR-deficient early-stage colon cancers. *Nat Med* (2020) 26(4):566–76. doi: 10.1038/s41591-020-0805-8

22. Yuki S, Bando H, Tsukada Y, Inamori K, Komatsu Y, Homma S, et al. Short-term results of VOLTAGE-a: Nivolumab monotherapy and subsequent radical surgery following preoperative chemoradiotherapy in patients with microsatellite stable and microsatellite instability-high locally advanced rectal cancer. *J Clin Oncol* (2020) 38:15_suppl:4100–0. doi: 10.1200/JCO.2020.38.15_suppl.4100

23. Chiou VL, Burotto M. Pseudoprogression and immune-related response in solid tumors. *J Clin Oncol* (2015) 33:3541–3. doi: 10.1200/JCO.2015.61.6870

24. Brahmer JR, Lacchetti C, Schneider BJ, Atkins MB, Brassil KJ, Caterino JM, et al. Management of immune-related adverse events in patients treated with immune checkpoint inhibitor therapy: American society of clinical oncology clinical practice guideline. *J Clin Oncol* (2018) 36:1714–68. doi: 10.1200/JCO.2017.77.6385

25. Liu J, Blake SJ, Yong MC, Harjunpää H, Ngiow SF, Takeda K, et al. Improved efficacy of neoadjuvant compared to adjuvant immunotherapy to eradicate metastatic disease. *Cancer Discovery* (2016) 6(12):1382–99. doi: 10.1158/2159-8290.CD-16-0577

26. Garcia-Aguilar J, Chow OS, Smith DD, Marcet JE, Cataldo PA, Varma MG, et al. Effect of adding mFOLFOX6 after neoadjuvant chemoradiation in locally advanced rectal cancer: A multicentre, phase 2 trial. *Lancet Oncol* (2015) 16(8):957–66. doi: 10.1016/S1470-2045(15)00004-2

27. Cercek A, Roxburgh CSD, Strombom P, Smith JJ, Temple LKF, Nash GM, et al. Adoption of total neoadjuvant therapy for locally advanced rectal cancer. *JAMA Oncol* (2018) 4(6):e180071. doi: 10.1001/jamaoncol.2018.0071

28. Fokas E, Schlenska-Lange A, Polat B, Klautke G, Grabenbauer GG, Fietkau R, et al. Chemoradiotherapy plus induction or consolidation chemotherapy as total neoadjuvant therapy for patients with locally advanced rectal cancer: Long-term results of the CAO/ARO/AIO-12 randomized clinical trial. *JAMA Oncol* (2022) 8(1): e215445. doi: 10.1001/jamaoncol.2021.5445

29. Vaccaro CA, Yazyi FJ, Ojra Quintana G, Santino JP, Sardi ME, Beder D, et al. Locally advanced rectal cancer: Preliminary results of rectal preservation after neoadjuvant chemoradiotherapy. *Cir Esp* (2016) 94(5):274–9. doi: 10.1016/j.ciresp.2015.12.007

30. Ciseł B, Pietrzak L, Michalski W, Wyrwicz L, Rutkowski A, Kosakowska E, et al. Long-course preoperative chemoradiation versus 5 × 5 gy and consolidation chemotherapy for clinical T4 and fixed clinical T3 rectal cancer: long-term results of the randomized polish II study. *Ann Oncol* (2019) 30(8):1298–303. doi: 10.1093/annonc/mdz186

31. Jin J, Tang Y, Hu C, Jiang LM, Jiang J, Li N, et al. Multicenter, randomized, phase III trial of short-term radiotherapy plus chemotherapy versus long-term chemoradiotherapy in locally advanced rectal cancer (STELLAR). *J Clin Oncol* (2022) 40(15):1681–92. doi: 10.1200/JCO.21.01667

32. Nogué M, Salud A, Vicente P, Arrivi A, Roca JM, Losa F, et al. Addition of bevacizumab to XELOX induction therapy plus concomitant capecitabine-based chemoradiotherapy in magnetic resonance imaging-defined poor-prognosis locally advanced rectal cancer: the AVACROSS study. *Oncologist* (2011) 16(5):614–20. doi: 10.1634/theoncologist.2010-0285

33. Czito BG, Deming DA, Jameson GS, Mulcahy MF, Vaghefi H, Dudley MW, et al. Safety and tolerability of veliparib combined with capecitabine plus radiotherapy in patients with locally advanced rectal cancer: A phase 1b study. *Lancet Gastroenterol Hepatol* (2017) 2(6):418–26. doi: 10.1016/S2468-1253(17)30012-2

34. Capdevila J, Macias Declara I, Carmen Riesco Martinez M, Maurel J, Hernando J, Alonso V, et al. Phase II study of durvalumab plus total neoadjuvant therapy (TNT) in locally advanced rectal cancer: the GEMCAD-1703 DUREC trial. *J Clin Oncol* (2020) 38(15_suppl):TPS4122. doi: 10.1200/JCO.2020.38.15_suppl.TPS4122

35. Romesser PB, Holliday EB, Phillip T, Garcia-Carbonero R, Capdevila J, Tuli R, et al. A multicenter phase Ib/II study of DNA-PK inhibitor peposertib (M3814) in combination with capecitabine and radiotherapy in patients with locally advanced rectal cancer. *J Clin Oncol* (2021) 39:3_suppl:TPS144. doi: 10.1200/JCO.2021.39.3_suppl.TPS144

36. Petrelli F, Trevisan F, Cabiddu M, Sgroi G, Bruschieri L, Rausa E, et al. Total neoadjuvant therapy in rectal cancer: A systematic review and meta-analysis of treatment outcomes. *Ann Surg* (2020) 271(3):440–8. doi: 10.1097/SLA.0000000000003471

37. Kasi A, Abbasi S, Handa S, Al-Rajabi R, Saeed A, Baranda J, et al. Total neoadjuvant therapy vs standard therapy in locally advanced rectal cancer: A systematic review and meta-analysis. *JAMA Netw Open* (2020) 3(12):e2030097. doi: 10.1001/jamanetworkopen.2020.30097

38. Liu S, Jiang T, Xiao L, Yang S, Liu Q, Gao Y, et al. Total neoadjuvant therapy (TNT) versus standard neoadjuvant chemoradiotherapy for locally advanced rectal cancer: A systematic review and meta-analysis. *Oncologist* (2021) 26(9):e1555–66. doi: 10.1002/onco.13824

39. Jakobsen A, Andersen F, Fischer A, Jensen LH, Jørgensen JC, Larsen O, et al. Neoadjuvant chemotherapy in locally advanced colon cancer. a phase II trial. *Acta Oncol* (2015) 54(10):1747–53. doi: 10.3109/0284186X.2015.1037007

40. Mace AG, Pai RK, Stocchi L, Kalady MF. American Joint committee on cancer and college of American pathologists regression grade: a new prognostic factor in rectal cancer. *Dis Colon Rectum* (2015) 58(1):32–44. doi: 10.1097/DCR.0000000000000266

41. Topalian SL, Taube JM, Pardoll DM. Neoadjuvant checkpoint blockade for cancer immunotherapy. *Science* (2020) 367(6477):eaax0182. doi: 10.1126/science.aax0182

42. Versluis JM, Long GV, Blank CU. Learning from clinical trials of neoadjuvant checkpoint blockade. *Nat Med* (2020) 26(4):475–84. doi: 10.1038/s41591-020-0829-0

43. Galon J, Costes A, Sanchez-Cabo F, Kirilovsky A, Mlecnik B, Lagorce-Pagès C, et al. Type, density, and location of immune cells within human colorectal tumors predict clinical outcome. *Science* (2006) 313(5795):1960–4. doi: 10.1126/science.1129139

44. Pagès F, Mlecnik B, Marliot F, Bindea G, Ou FS, Bifulco C, et al. International validation of the consensus immunoscore for the classification of colon cancer: a prognostic and accuracy study. *Lancet* (2018) 391(10135):2128–39. doi: 10.1016/S0140-6736(18)30789-X

45. Pardoll D. Cancer and the immune system: Basic concepts and targets for intervention. *Semin Oncol* (2015) 42(4):523–38. doi: 10.1053/j.seminoncol.2015.05.003

46. Mocellin S, Nitti D. CTLA-4 blockade and the renaissance of cancer immunotherapy. *Biochim Biophys Acta* (2013) 1836(2):187–96. doi: 10.1016/j.bbcan.2013.05.003

47. Salmaninejad A, Valilou SF, Shabgah AG, Aslani S, Alimardani M, Pasdar A, et al. PD-1/PD-L1 pathway: Basic biology and role in cancer immunotherapy. *J Cell Physiol* (2019) 234(10):16824–37. doi: 10.1002/jcp.28358

48. Dong H, Strome SE, Salomao DR, Tamura H, Hirano F, Flies DB, et al. Tumor-associated B7-H1 promotes T-cell apoptosis: a potential mechanism of immune evasion. *Nat Med* (2002) 8(8):793–800. doi: 10.1038/nm730

49. Lenz HJ, Van Cutsem E, Luisa Limon M, Luisa Limon M, Wong KYM, Hendlisz A, et al. First-line nivolumab plus low-dose ipilimumab for microsatellite instability-High/Mismatch repair-deficient metastatic colorectal cancer: The phase II CheckMate 142 study. *J Clin Oncol* (2022) 40(2):161–70. doi: 10.1200/JCO.21.01015

50. Tesniere A, Schlemmer F, Boige V, Kepp O, Martins I, Ghiringhelli F, et al. Immunogenic death of colon cancer cells treated with oxaliplatin. *Oncogene* (2010) 29 (4):482–91. doi: 10.1038/onc.2009.356

51. Park SJ, Ye W, Xiao R, Silvin C, Padget M, Hodge JW, et al. Cisplatin and oxaliplatin induce similar immunogenic changes in preclinical models of head and neck cancer. *Oral Oncol* (2019) 95:127–35. doi: 10.1016/j.oraloncology.2019.06.016

52. Hong X, Dong T, Yi T, Hu J, Zhang Z, Lin S, et al. Impact of 5-fu/oxaliplatin on mouse dendritic cells and synergetic effect with a colon cancer vaccine. *Chin J Cancer Res* (2018) 30(2):197–208. doi: 10.21147/j.issn.1000-9604.2018.02.03

53. Wang W, Wu L, Zhang J, Wu H, Han E, Guo Q. Chemoimmunotherapy by combining oxaliplatin with immune checkpoint blockades reduced tumor burden in colorectal cancer animal model. *Biochem Biophys Res Commun* (2017) 487(1):1–7. doi: 10.1016/j.bbrc.2016.12.180

54. Ledys F, Klopfenstein Q, Truntzer C, Arnould L, Vincent J, Bengrine L, et al. RAS status and neoadjuvant chemotherapy impact CD8+ cells and tumor HLA class I expression in liver metastatic colorectal cancer. *J Immunother Cancer* (2018) 6(1):123. doi: 10.1186/s40425-018-0438-3

55. Zhang S, Bai W, Tong X, Bu P, Xu J, Xi Y. Correlation between tumor microenvironment-associated factors and the efficacy and prognosis of neoadjuvant therapy for rectal cancer. *Oncol Lett* (2019) 17(1):1062–70. doi: 10.3892/ol.2018.9682

56. Chen TW, Huang KC, Chiang SF, Chen WT, Ke TW, Chao KSC. Prognostic relevance of programmed cell death-ligand 1 expression and CD8+ TILs in rectal cancer patients before and after neoadjuvant chemoradiotherapy. *J Cancer Res Clin Oncol* (2019) 145(4):1043–53. doi: 10.1007/s00432-019-02874-7

57. Stojanovska V, Prakash M, McQuade R, Fraser S, Apostolopoulos V, Sakkal S, et al. Oxaliplatin treatment alters systemic immune responses. *BioMed Res Int* (2019) 2019:4650695. doi: 10.1155/2019/4650695

58. Guan Y, Kraus SG, Quaney MJ, Daniels MA, Mitchem JB, Teixeiro E. FOLFOX chemotherapy ameliorates CD8 T lymphocyte exhaustion and enhances checkpoint blockade efficacy in colorectal cancer. *Front Oncol* (2020) 10:586. doi: 10.3389/fonc.2020.00586

59. Kanterman J, Sade-Feldman M, Biton M, Ish-Shalom E, Lasry A, Goldshtein A, et al. Adverse immunoregulatory effects of 5FU and CPT11 chemotherapy on myeloid-derived suppressor cells and colorectal cancer outcomes. *Cancer Res* (2014) 74 (21):6022–35. doi: 10.1158/0008-5472.CAN-14-0657

60. Musella M, Manic G, De Maria R, Vitale I, Sistigu A. Type-i-interferons in infection and cancer: Unanticipated dynamics with therapeutic implications. *Oncoimmunology* (2017) 6(5):e1314424. doi: 10.1080/2162402X.2017.1314424

61. Burnette BC, Liang H, Lee Y, Chlewicki L, Khodarev NN, Weichselbaum RR, et al. The efficacy of radiotherapy relies upon induction of type i interferon-dependent innate and adaptive immunity. *Cancer Res* (2011) 71(7):2488–96. doi: 10.1158/0008-5472.CAN-10-2820

62. Bishnupuri KS, Alvarado DM, Khouri AN, Shabsovich M, Chen B, Dieckgraefe BK, et al. IDO1 and kynurenine pathway metabolites activate PI3K-akt signaling in the

neoplastic colon epithelium to promote cancer cell proliferation and inhibit apoptosis. *Cancer Res* (2019) 79(6):1138–50. doi: 10.1158/0008-5472.CAN-18-0668

63. Lemery S, Keegan P, Pazdur R. First FDA approval agnostic of cancer site - when a biomarker defines the indication. *N Engl J Med* (2017) 377(15):1409–12. doi: 10.1056/NEJMp1709968

64. Zhang P, Liu M, Cui Y, Zheng P, Liu Y. Microsatellite instability status differentially associates with intratumoral immune microenvironment in human cancers. *Brief Bioinform* (2021) 22(3):bbaa180. doi: 10.1093/bib/bbaa180

65. Le DT, Durham JN, Smith KN, Wang H, Bartlett BR, Aulakh LK, et al. Mismatch repair deficiency predicts response of solid tumors to PD-1 blockade. *Science* (2017) 357(6349):409–13. doi: 10.1126/science.aan6733

66. Luchini C, Bibeau F, Ligtenberg MJL, Singh N, Nottegar A, Bosse T, et al. ESMO recommendations on microsatellite instability testing for immunotherapy in cancer, and its relationship with PD-1/PD-L1 expression and tumour mutational burden: a systematic review-based approach. *Ann Oncol* (2019) 30(8):1232–43. doi: 10.1093/annonc/mdz116

67. Hu W, Yang Y, Qi L, Chen J, Ge W, Zheng S. Subtyping of microsatellite instability-high colorectal cancer. *Cell Commun Signal* (2019) 17(1):79. doi: 10.1186/s12964-019-0397-4

68. Soldevilla B, Carretero-Puche C, Gomez-Lopez G, Al-Shahrour F, Riesco MC, Gil-Calderon B, et al. The correlation between immune subtypes and consensus molecular subtypes in colorectal cancer identifies novel tumour microenvironment profiles, with prognostic and therapeutic implications. *Eur J Cancer* (2019) 123:118–29. doi: 10.1016/j.ejca.2019.09.008

69. Dienstmann R, Vermeulen L, Guinney J, Kopetz S, Tejpar S, Tabernero J. Consensus molecular subtypes and the evolution of precision medicine in colorectal cancer. *Nat Rev Cancer* (2017) 17(2):79–92. doi: 10.1038/nrc.2016.126

70. Thorsson V, Gibbs DL, Brown SD, Wolf D, Bortone DS, Ou Yang TH, et al. The immune landscape of cancer. *Immunity* (2018) 48(4):812–30.e14. doi: 10.1016/j.immuni.2018.03.023

71. Mlecnik B, Bindea G, Angell HK, Maby P, Angelova M, Tougeron D, et al. Integrative analyses of colorectal cancer show immunoscore is a stronger predictor of patient survival than microsatellite instability. *Immunity* (2016) 44(3):698–711. doi: 10.1016/j.immuni.2016.02.025

72. The National Comprehensive Cancer Network. *NCCN clinical practice guidelines in oncology, colon cancer. version 1.2021* (2021). Available at: https://www.nccn.org.

73. The National Comprehensive Cancer Network. *NCCN clinical practice guidelines in oncology, rectal cancer. version 1.2021* (2021). Available at: https://www.nccn.org.

74. The National Comprehensive Cancer Network. *NCCN clinical practice guidelines in oncology, colon cancer. version 1.2022* (2022). Available at: https://www.nccn.org.

75. The National Comprehensive Cancer Network. *NCCN clinical practice guidelines in oncology, rectal cancer. version 1.2022* (2022). Available at: https://www.nccn.org.

76. Salvatore L, Bensi M, Corallo S, Bergamo F, Pellegrini I, Rasola C, et al. Phase II study of preoperative (PREOP) chemoradiotherapy (CTRT) plus avelumab (AVE) in patients (PTS) with locally advanced rectal cancer(LARC): the AVANA study. *J Clin Oncol* (2021) 39:15_suppl:abstr3511. doi: 10.1200/JCO

77. Shamseddine A, Zeidan Y, Bouferraa Y, Turfa R, Kattan J, Mukherji D, et al. SO-30 efficacy and safety of neoadjuvant short-course radiation followed by mFOLFOX-6 plus avelumab for locally-advanced rectal adenocarcinoma: Averectal study. *Ann Oncol* (2021) 32:3_suppl:S215. doi: 10.1016/j.annonc.2021.05.054

78. Yao HW, Yang ZY, Gao JL, Zhang X, Wu G, Wei D, et al. Safety and efficacy evaluation of long course neoadjuvant chemoradiotherapy plus tislelizumab followed by total mesorectal excision for locally advanced rectal cancer: Short-term results of a multicenter, phase II study. *J Clin Oncol* (2022) 40:16_suppl:e15599–9. doi: 10.1200/JCO.2022.40.16_suppl.e15599

79. Bregni G, Senti C, Reina AE, Gkolfakis P, Moretti L, Veron A, et al. 505TiP REGINA: A phase II trial of neoadjuvant regorafenib (rego) in combination with nivolumab (nivo) and short-course radiotherapy (SCRT) in intermediate-risk, stage II-III rectal cancer (RC). *Ann Oncol* (2021) 32:5_suppl:579. doi: 10.1016/j.annonc.2021.08.1024

80. Verschoor YL, Berg JV, Beets G, Sikorska K, Aalbers A, Van Lent A, et al. Neoadjuvant nivolumab, ipilimumab, and celecoxib in MMR-proficient and MMR-deficient colon cancers: Final clinical analysis of the NICHE study. *J Clin Oncol* (2022) 40:16_suppl:3511–1. doi: 10.1200/JCO.2022.40.16_suppl.3511

81. Chalabi M, Verschoor YL, Berg JV, Sikorska K, Beets G, Lent AV, et al. Neoadjuvant immune checkpoint inhibition in locally advanced MMR-deficient colon cancer: The NICHE-2 study. *Ann Oncol* (2022) 33:suppl_7:S808–69. doi: 10.1016/annonc/annonc1089

82. Avallone A, Stefano AD, Pace U, Catteau A, Di Gennaro E, Tatangelo F, et al. Neoadjuvant nivolumab in early stage colorectal cancer. *Ann Oncol* (2020) 31:suppl_4:S449. doi: 10.1016/j.annonc.2020.08.602

83. Rahma OE, Yothers G, Hong TS, Russell MM, You YN, Parker W, et al. Use of total neoadjuvant therapy for locally advanced rectal cancer: Initial results from the pembrolizumab arm of a phase 2 randomized clinical trial. *JAMA Oncol* (2021) 7(8):1225–30. doi: 10.1001/jamaoncol.2021.1683

84. George TJ, Yothers G, Jacobs SA, Finley GG, Wade JL, Rocha Lima CM, et al. Phase II study of durvalumab following neoadjuvant chemoRT in operable rectal cancer: NSABP FR-2. *J Clin Oncol* (2022) 40:4_suppl:99. doi: 10.1200/JCO.2022.40.4_suppl.099

85. Tamberi S, Grassi E, Zingaretti C, Papiani G, Pini S, Corbelli J, et al. A phase II study of capecitabine plus concomitant radiation therapy followed by durvalumab (MEDI4736) as preoperative treatment in rectal cancer: PANDORA study final results. *J Clin Oncol* (2022) 40:17_suppl:LBA3513. doi: 10.1200/JCO.2022.40.17_suppl.LBA3513

86. Wu A, Li Y, Ji D, Zhang L, Zhang X, Cai Y, et al. PKUCH 04 trial: Total neoadjuvant chemoradiation combined with neoadjuvant PD-1 blockade for pMMR/MSS locally advanced middle to low rectal cancer. *J Clin Oncol* (2022) 40:16_suppl:3609. doi: 10.1200/JCO.2022.40.16_suppl.3609

87. Wang Y, Shen L, Wan J, Zhang H, Wu R, Wang J, et al. Short-course radiotherapy combined with CAPOX and toripalimab for the total neoadjuvant therapy of locally advanced rectal cancer: a randomized, prospective, multicentre, double-arm, phase II trial (TORCH). *J Clin Oncol* (2022) 40:16_suppl:e15602–2. doi: 10.1200/JCO.2022.40.16_suppl.e15602

88. Lin ZY, Cai M, Zhang P, et al. Short-course radiotherapy and subsequent CAPOX plus camrelizumab followed by delayed surgery for locally advanced rectal cancer:Short-term results of a phase II trial. *J Clin Oncol* (2021) 39:3_suppl:63–3. doi: 10.1200/JCO.2021.39.3_suppl.63

89. Li YJ, Zhang L, Dong QS, Cai Y, Zhang YZ, Wang L, et al. Short-term outcome of programmed cell death protein1 (PD-1) antibody combined with total neoadjuvant chemoradiotherapy in the treatment of locally advanced middle-low rectal cancer with high risk factors. *Chin J Gastrointest Surg* (2021) 24(11):998–1007. doi: 10.3760/cma.j.cn441530-20210927-00386

90. Zhao Y, Zhu J, Yang B, Gao Q, Xu Y, Wei X, et al. Retrospective study of total neoadjuvant therapy for locally advanced rectal cancer. *Future Oncol* (2022) 18(6):691–700. doi: 10.2217/fon-2021-0644

91. Hanna CR, O'Cathail SM, Graham JS, et al. Durvalumab (MEDI 4736) in combination with extended neoadjuvant regimens in rectal cancer: a study protocol of a randomised phase II trial (PRIME-RT). *Radiat Oncol* (2021) 16(1):163. doi: 10.1186/s13014-021-01888-1

92. Wang Y, Shen L, Wan J, Saunders M, Samuel L, Harrison M, et al. Short-course radiotherapy combined with CAPOX and toripalimab for the total neoadjuvant therapy of locally advanced rectal cancer: a randomized, prospective, multicentre, double-arm, phase II trial (TORCH). *BMC Cancer* (2022) 22(1):274. doi: 10.1186/s12885-022-09348-z

93. Cercek A, Lumish M, Sinopoli J, Weiss J, Shia J, Lamendola-Essel M, et al. PD-1 blockade in mismatch repair-deficient, locally advanced rectal cancer. *N Engl J Med* (2022) 386(25):2363–76. doi: 10.1056/NEJMoa2201445

94. Laengle J, Kuehrer I, Pils D, Stift A, Teleky B, Herbst F, et al. Interim analysis of neoadjuvant chemoradiotherapy with sequential ipilimumab and nivolumab in rectal cancer (CHINOREC): A prospective randomized, open-label, multicenter, phase II clinical trial. *J Clin Oncol* (2022) 40:16_suppl:e15604–4. doi: 10.1200/JCO.2022.40.16_suppl.e15604

95. Michael M, Wong R, Gill SS, Goldstein D, Ngan S, Heriot AG, et al. Phase II trial PD-L1/PD-1 blockade avelumab with chemoradiotherapy for locally advanced resectable T3B-4/N1-2 rectal cancer: The ave-rec trial. *J Clin Oncol* (2019) 37:15_suppl:TPS3622–TPS3622. doi: 10.1200/JCO.2019.37.15_suppl.TPS3622

96. Chen G, Wang F, Xiao WW, Jin Y, Zhang RX, Cai P, et al. Pd1 antibody sintilimab for dMMR/MSI-h locally advanced rectal cancer: An open-label, phase 2, single-arm study (cohort a). *J Clin Oncol* (2021) 39:15_suppl:e15602–2. doi: 10.1200/JCO.2021.39.15_suppl.e15602

97. Kossler T, Nicolas B, Dutoit V, Puppa G, Tsantoulis P, Frossard JL, et al. A phase II study to evaluate safety and efficacy of neoadjuvant pembrolizumab and radiotherapy in localized MSS rectal cancer. *J Clin Oncol* (2020) 38:4_suppl:TPS272–2. doi: 10.1200/JCO.2020.38.4_suppl.TPS272

98. Fabrizio DA, George TJJr, Dunne RF, Frampton G, Sun J, Gowen K, et al. Beyond microsatellite testing: assessment of tumor mutational burden identifies subsets of colorectal cancer who may respond to immune checkpoint inhibition. *J Gastrointest Oncol* (2018) 9(4):610–7. doi: 10.21037/jgo.2018.05.06

99. Chen EX, Jonker DJ, Kennecke HF, Berry SR, Couture F, Ahmad CE, et al. CCTG CO.26 trial: A phase II randomized study of durvalumab (D) plus tremelimumab (T) and best supportive care (BSC) versus BSC alone in patients (pts) with advanced refractory colorectal carcinoma (rCRC). *J Clin Oncol* (2019) 37:4_suppl:481–1. doi: 10.1200/JCO.2019.37.4_suppl.481

100. Fan A, Wang B, Wang X, Nie Y, Fan D, Zhao X, et al. Immunotherapy in colorectal cancer: current achievements and future perspective. *Int J Biol Sci* (2021) 17(14):3837–49. doi: 10.7150/ijbs.64077

101. Tumeh PC, Harview CL, Yearley JH, Shintaku IP, Taylor EJ, Robert L, et al. PD-1 blockade induces responses by inhibiting adaptive immune resistance. *Nature* (2014) 515(7528):568–71. doi: 10.1038/nature13954

102. Rooney MS, Shukla SA, Wu CJ, Getz G, Hacohen N. Molecular and genetic properties of tumors associated with local immune cytolytic activity. *Cell* (2015) 160(1-2):48–61. doi: 10.1016/j.cell.2014.12.033

103. Marabelle A, Fakih M, Lopez J, Shah M, Shapira-Frommer R, Nakagawa K, et al. Association of tumour mutational burden with outcomes in patients with advanced solid tumours treated with pembrolizumab: prospective biomarker analysis of the multicohort, open-label, phase 2 KEYNOTE-158 study. *Lancet Oncol* (2020) 21(10):1353–65. doi: 10.1016/S1470-2045(20)30445-9

104. Shitara K, Hara H, Takahashi N, Kojima T, Kawazoe A, Asayama M, et al. Updated results from a phase ib trial of regorafenib plus nivolumab in patients with advanced colorectal or gastric cancer (REGONIVO, EPOC1603). *J Clin Oncol* (2020) 38:4_suppl:135–5. doi: 10.1200/JCO.2020.38.4_suppl.135

105. Chen EX, Jonker DJ, Loree JM, Kennecke HF, Berry SR, Couture F, et al. CCTG CO.26: Updated analysis and impact of plasma-detected microsatellite stability (MSS) and tumor mutation burden (TMB) in a phase II trial of durvalumab (D) plus tremelimumab (T) and best supportive care (BSC) versus BSC alone in patients (pts) with refractory metastatic colorectal carcinoma (rmCRC). *J Clin Oncol* (2019) 37:15_suppl:3512–2. doi: 10.1200/JCO.2019.37.15_suppl.3512

106. Hino H, Shiomi A, Kusuhara M, Kagawa H, Yamakawa Y, Hatakeyama K, et al. Clinicopathological and mutational analyses of colorectal cancer with mutations in the POLE gene. *Cancer Med* (2019) 8(10):4587–97. doi: 10.1002/cam4.2344

107. Wang F, Zhao Q, Wang YN, Jin Y, He MM, Liu ZX, et al. Evaluation of POLE and POLD1 mutations as biomarkers for immunotherapy outcomes across multiple cancer types. *JAMA Oncol* (2019) 5(10):1504–6. doi: 10.1001/jamaoncol.2019.2963

108. Domingo E, Freeman-Mills L, Rayner E, Glaire M, Briggs S, Vermeulen L, et al. Somatic POLE proofreading domain mutation, immune response, and prognosis in colorectal cancer: a retrospective, pooled biomarker study. *Lancet Gastroenterol Hepatol* (2016) 1(3):207–16. doi: 10.1016/S2468-1253(16)30014-0

109. Koelzer VH, Baker K, Kassahn D, Baumhoer D, Zlobec I. Prognostic impact of β-2-microglobulin expression in colorectal cancers stratified by mismatch repair status. *J Clin Pathol* (2012) 65(11):996–1002. doi: 10.1136/jclinpath-2012-200742

110. Garon EB, Rizvi NA, Hui R, Leighl N, Balmanoukian AS, Eder JP, et al. Pembrolizumab for the treatment of non-small-cell lung cancer. *N Engl J Med* (2015) 372(21):2018–28. doi: 10.1056/NEJMoa1501824

111. Hersom M, Jørgensen JT. Companion and complementary diagnostics-focus on PD-L1 expression assays for PD-1/PD-L1 checkpoint inhibitors in non-small cell lung cancer. *Ther Drug Monit* (2018) 40(1):9–16. doi: 10.1097/FTD.0000000000000460

112. Huh JW, Lee JH, Kim HR. Prognostic significance of tumor-infiltrating lymphocytes for patients with colorectal cancer. *Arch Surg* (2012) 147(4):366–72. doi: 10.1001/archsurg.2012.35

113. Grasso CS, Giannakis M, Wells DK, Hamada T, Mu XJ, Quist M, et al. Genetic mechanisms of immune evasion in colorectal cancer. *Cancer Discov* (2018) 8(6):730–49. doi: 10.1158/2159-8290.CD-17-1327

114. Kalbasi A, Ribas A. Tumour-intrinsic resistance to immune checkpoint blockade. *Nat Rev Immunol* (2020) 20(1):25–39. doi: 10.1038/s41577-019-0218-4

115. Barrueto L, Caminero F, Cash L, Makris C, Lamichhane P, Deshmukh RR. Resistance to checkpoint inhibition in cancer immunotherapy. *Transl Oncol* (2020) 13 (3):100738. doi: 10.1016/j.tranon.2019.12.010

116. Kanani A, Veen T, Søreide K. Neoadjuvant immunotherapy in primary and metastatic colorectal cancer. *Br J Surg* (2021) 108(12):1417–25. doi: 10.1093/bjs/znab342

117. Han K, Tang JH, Liao LE, Jiang W, Sui QQ, Xiao BY, et al. Neoadjuvant immune checkpoint inhibition improves organ preservation in T4bm0 colorectal cancer with mismatch repair deficiency: A retrospective observational study. *Dis Colon Rectum* (2022). doi: 10.1097/DCR.0000000000002466

118. Thompson H, Kim JK, Yuval JB, Verheij F, Patil S, Gollub MJ, et al. Survival and organ preservation according to clinical response after total neoadjuvant therapy in locally advanced rectal cancer patients: A secondary analysis from the organ preservation in rectal adenocarcinoma (OPRA) trial. *J Clin Oncol* (2021) 39:15_suppl:3509–9. doi: 10.1200/JCO.2021.39.15_suppl.3509

119. Aggarwal C, Thompson JC, Black TA, Katz SI, Fan R, Yee SS, et al. Clinical implications of plasma-based genotyping with the delivery of personalized therapy in metastatic non-small cell lung cancer. *JAMA Oncol* (2019) 5(2):173–80. doi: 10.1001/jamaoncol.2018.4305

120. Han J, Zhao Y, Shirai K, Molodtsov A, Kolling FW, Fisher JL, et al. Resident and circulating memory T cells persist for years in melanoma patients with durable responses to immunotherapy. *Nat Cancer* (2021) 2(3):300–11. doi: 10.1038/s43018-021-00180-1

121. Liu J, Rozeman EA, O'Donnell JS, Allen S, Fanchi L, Smyth MJ, et al. Batf3+ DCs and type I IFN are critical for the efficacy of neoadjuvant cancer immunotherapy. *Oncoimmunology* (2018) 8(2):e1546068. doi: 10.1080/2162402X.2018.1546068

122. Smith KN, Llosa NJ, Cottrell TR, Siegel N, Fan H, Suri P, et al. Persistent mutant oncogene specific T cells in two patients benefitting from anti-PD-1. *J Immunother Cancer* (2019) 7(1):40. doi: 10.1186/s40425-018-0492-x

Glossary

5-FU	5-fluorouracil
AJCC	American Joint Committee on Cancer
APCs	Antigen-presenting cells
B2M	Beta-2-Microglobulin
BRAF	V-raf murine sarcoma viral oncogene homolog B1
CapeOX	Capecitabine and oxaliplatin
cCR	Clinical complete response
CCR5	C-C chemokine receptor type 5
CD3+	Cluster of differentiation 3 positive
CD4+	Cluster of differentiation 4 positive
CD8+	Cluster of differentiation 8 positive
cfDNA	Circluting-tumor DNA
CMSs	Consensus molecular subgroups
CRC	Colorectal cancer
CTLA-4	Cytotoxic T-lymphocyte-associated antigen-4
CXCR3	Cxc chemokine receptor 3
DFS	Disease free survival
dMMR	Deficient mismatch repair
FOLFIRINOX	Fluorouracil
irinotecan	and oxaliplatin
FOLFOX	Folinic acid, fluorouracil, and oxaliplatin
HMGB1	High-mobility group box 1 protein
ICD	Induce immunogenic cell death
ICIs	Immune checkpoint inhibitors
iCR	Incomplete clinical response
IFNs	Type I interferons
IFN-γ	Interferon gamma
irAEs	Immune-related adverse events
JAK-STAT	Janus kinase-Signal transducer and activator of transcription
KRAS	Kirsten rats arcomaviral oncogene homolog
LACRC	Locally advanced colorectal cancer
LARC	Locally advanced rectal cancer
mCRC	metastatic colorectal cancer
MHC-I	Major histocompatibility complex class I
MPR	Major pathological response
MSI	Microsatellite instability
MSI-H	Microsatellite instability high
MSI-L	Microsatellite instability low
MSS	Microsatellite stability
NACT	Neoadjuvant chemotherapy
NACRT	neoadjuvant chemoradiotherapy
NAICI	Neoadjuvant Immune checkpoint inhibitor
NCCN	National Comprehensive Cancer Network
nCR	Near complete response
NK cells	Natural killer cells
OP	Organ preservation
OS	Overall survival
OxMdG	Fluorouracil and oxaliplatin
pCR	Pathological complete response
PD-1	Programmed death-1
PD-L1	Programmed death-ligand 1
PI3KCA	Phosphatidylinositol-4,5-bisphosphate 3-kinase, catalytic subunit alpha
pMMR	Proficient mismatch repair
POLD 1	polymerase delta 1
POLE	Polymerase epsilon
TCI	T-cell infiltration
TCR	T-cell receptor
TILs	Tumour-infiltrating lymphocytes
TMB	Tumour mutation burden
TME	Tumour microenvironment
TNM	Tumor, node, metastasis
TNT	Total neoadjuvant therapy
Tregs	regulatory T cells
TRG	Tumour regression grading
UICC	Union for International Cancer Control
W&W	watch and wait
XELOX	Xeloda and oxaliplatin
β2M	β2 microglobulin

(Continued)

Continued

frontiers | Frontiers in Immunology

TYPE Original Research
PUBLISHED 15 March 2023
DOI 10.3389/fimmu.2023.1141712

Check for updates

OPEN ACCESS

EDITED BY
Mohd Wajid Ali Khan,
University of Hail, Saudi Arabia

REVIEWED BY
Andrea Canellada,
University of Buenos Aires, Argentina
Subuhi Sherwani,
University of Hail, Saudi Arabia

*CORRESPONDENCE
Ashish Ranjan
ashish.ranjan@okstate.edu

SPECIALTY SECTION
This article was submitted to Cancer Immunity and Immunotherapy, a section of the journal Frontiers in Immunology

RECEIVED 10 January 2023
ACCEPTED 27 February 2023
PUBLISHED 15 March 2023

CITATION
Singh A and Ranjan A (2023) Adrenergic receptor signaling regulates the CD40-receptor mediated anti-tumor immunity. *Front. Immunol.* 14:1141712. doi: 10.3389/fimmu.2023.1141712

COPYRIGHT
© 2023 Singh and Ranjan. This is an open-access article distributed under the terms of the Creative Commons Attribution License (CC BY). The use, distribution or reproduction in other forums is permitted, provided the original author(s) and the copyright owner(s) are credited and that the original publication in this journal is cited, in accordance with accepted academic practice. No use, distribution or reproduction is permitted which does not comply with these terms.

Adrenergic receptor signaling regulates the CD40-receptor mediated anti-tumor immunity

Akansha Singh and Ashish Ranjan*

Department of Physiological Sciences, College of Veterinary Medicine, Oklahoma State University, Stillwater, OK, United States

Introduction: Anti-CD40 agonistic antibody (αCD40), an activator of dendritic cells (DC) can enhance antigen presentation and activate cytotoxic T-cells against poorly immunogenic tumors. However, cancer immunotherapy trials also suggest that αCD40 is only moderately effective in patients, falling short of achieving clinical success. Identifying factors that decrease αCD40 immune-stimulating effects can aid the translation of this agent to clinical reality.

Method/Results: Here, we reveal that β-adrenergic signaling on DCs directly interferes with αCD40 efficacy in immunologically cold head and neck tumor model. We discovered that β-2 adrenergic receptor (β2AR) activation rewires CD40 signaling in DCs by directly inhibiting the phosphorylation of IκBα and indirectly by upregulating levels of phosphorylated-cAMP response element-binding protein (pCREB). Importantly, the addition of propranolol, a pan β-Blocker reprograms the CD40 pathways, inducing superior tumor regressions, increased infiltration of cytotoxic T-cells, and a reduced burden of regulatory T-cells in tumors compared to monotherapy.

Conclusion: Our study highlights an important mechanistic link between stress-induced β2AR signaling and reduced αCD40 efficacy in cold tumors, providing a new combinatorial approach to improve clinical outcomes in patients.

KEYWORDS

immunotherapy, Anti-CD40 agonist antibody, propranalol, adrenergic signaling, anti-tumor immunity

1 Introduction

The unique ability of dendritic cells (DCs) to cross-present antigens to CD8+ T-cells makes them the most potent antigen-presenting cells (APCs) in anti-tumor immunity cascade. This is highly promising, but DCs with dysregulated CD receptor signaling fail to respond significantly to tumor antigens, resulting in poor antigen presentation and T-cell mediated tumor clearance. To overcome this challenge, the use of anti-CD40 agonistic antibody (αCD40), an activator of APCs has grown with the goal of enhancing the

proportions of functional/activated DCs and subsequent activation of cytotoxic T-cells (1, 2). However, immunologically cold tumors can generate redundant immune evasive mechanisms to inhibit αCD40 immune activation by released tumor antigens, and clinical trials have shown that this approach is moderately effective as a monotherapy (3). Also, αCD40's short circulatory half-life and toxicity can further limit its clinical utility (4–6). Thus, therapeutic approaches that increase sensitivity to αCD40 immunotherapy and thereby reduce the required treatment doses are needed to improve outcomes in patients with cold tumors. Herein, we aimed to dissect the role of β2-adrenergic signaling in αCD40 treatment, thereby providing a mechanistic and pharmacological basis to improve outcomes in clinical settings.

Adrenergic signaling mediated stress and anti-tumor immunity are intricately linked and demonstrate an inverse relationship. The sympathetic nervous system is closely associated with the body's immune system since both primary and secondary lymphoid organs are permeated by post-ganglionic sympathetic neurons (7). The neurotransmitters (norepinephrine or NE) released from adrenergic neurons during stress can bind to the β2-adrenergic receptor (β2AR) present on tumor cell membranes. This binding activates anti-apoptotic pathways *via* adenylyl cyclase to induce rapid tumor growth rates, metastasis, chemo- and radio-resistance (8–11). The released NE also engages with macrophages, DCs, or T-cells to enhance macrophage polarization from M1 to M2 type, increases the production of anti-inflammatory cytokines, and reduces the proliferative capacities of cytotoxic T-cells (8, 12). Several studies have already demonstrated that β-ARs expressed on DCs decline pro-inflammatory cytokine secretion (13–16), antigen uptake (17), antigen presentation (18, 19), and migration capabilities (15, 20). What is not known is how the complementary activation mechanisms of αCD40 and β2AR influence DC effector functions, and whether targeting these signaling pathways concurrently would translate into superior tumor control relative to monotherapies.

Among the β2AR inhibitors, Propranolol, an FDA approved Pan-Beta blocker has been shown to improve outcomes of radiation (21), Immune checkpoint inhibitors (ICI) (22–24) & chemotherapies (25) in pre-clinical tumor models. Mechanistically, propranolol remodels tumor microenvironment by increasing the infiltration of effector CD8+ T-cells and declining suppressor cell populations. Propranolol hydrochloride is also being investigated in clinical trials as supportive therapy for prostate cancer (26) and stage IIIC-IV melanoma, and as part of combinatorial regimens of recurrent or metastatic urothelial cancer with anti-PD1 ICI (27), and radiation therapy for esophageal cancer (28). Based on these promising features, the aims of this study were two-fold. First, we assessed the implications of β-adrenergic signaling on DCs activation and maturation mediated by αCD40. Next, we evaluated the ability of propranolol to improve local αCD40 *in-situ* immunotherapy of poorly immunogenic head and neck tumors (MOC2). *In-situ* therapies utilize direct injection of immunostimulatory reagents into tumors to disrupt local immunosuppression, thereby reducing the dosage and associated toxicities. Our data shows that blocking β2AR can enhance the *in-situ* αCD40 efficacy against the MOC2 tumor model at suboptimal doses, thereby providing a translation basis of this approach for clinical use.

2 Materials

RPMI media (11875093), DMEM (11965092), Fetal bovine serum, FBS (10082147), Penicillin-Streptomycin, PenStrep (15140122), PBS (10010023), Collagenase IV (17104019), Pierce BCA Protein Assay (23228) were procured from ThermoFisher/Gibco, Waltham, MA, USA. Murine GM-CSF (315–03) was purchased from PeproTech, Cranbury, NJ, USA. Isoproterenol-HCL (16504), BSA (A7030) was purchased from MiliporeSigma, St. Louis, MO, USA. αCD40 (FGk45) from BioXcell West lebanon, NH. APC-Cy7 anti-CD45 (557659), Pe-Cy7 anti-CD45 (552848), BB515 anti-MHC-II (565254), BV421 anti-CD40 (562846) were purchased from BD Biosciences, San Jose, CA, USA. PerCP anti-CD3 (100326), BV785 anti-CD4 (100453), PE-Cy7 anti-CD8 (100722), APC-Cy7 anti-CD11c (117324), FITC anti-MHC-II (107605), PE anti-CD86 (105008), and ELISA MAX™ Deluxe Set Mouse IL-6 (431304), IL1b (432604) and IL-12 (433604) was procured from BioLegend, San Diego, CA, USA. TRIzol Reagent (15596026), PE anti-GranzymeB (12–8898–82), AF488 anti-FOXP3 (53–5773–82), unconjugated GAPDH (AM4300) antibody and MTT (3-(4,5-Dimethylthiazol-2-yl)-2,5-Diphenyltetrazolium Bromide) (M6494) were purchased from Invitrogen, Waltham, MA, USA. Unconjugated Phospho-IkBα (2859S), Phospho-CREB (9198S), IkBα (4814T) and CREB (9197T) antibodies were purchased from Cell Signaling Technology, Inc. Danvers, MA, USA. iScript™ gDNA Clear cDNA Synthesis Kit (1725034), iTaq Universal SYBR Green Supermix (1725124) was purchased from Bio-Rad, Hercules, CA, USA. IL-6, IL-1b, IL-10, and GAPDH primers were ordered from IDT, Coralville, IA, USA. The Quantikine™ Mouse IL-10 (M1000B) immunoassay was procured from R&D Systems, Inc., Minneapolis, MN, USA. Mouse OSCC (MOC2) cell line (EWL002-FP) was purchased from Kerafast, Boston, MA, USA.

3 Methods

3.1 Generation of tumor cell lysate, and bone marrow-derived Dendritic cells (BMDCs) for cytotoxicity and signaling studies

The lysate was generated by sonicating 10,000 MOC2 cells using Branson Sonifier 450 and centrifuging the lysate to harvest whole or partially lysed cells. The protein content of the whole lysate was determined using a BCA assay kit.

Female mice aged 8-12 weeks were utilized to generate bone marrow-derived DCs (BMDCs) through culturing of the harvested marrow cells with RPMI media that was enriched with FBS, Penicillin-Streptomycin, and GM-CSF. On the 5th day, the BMDCs were harvested, and their CD11c expression was confirmed using flow cytometry (≥80% CD11c+) and these cells

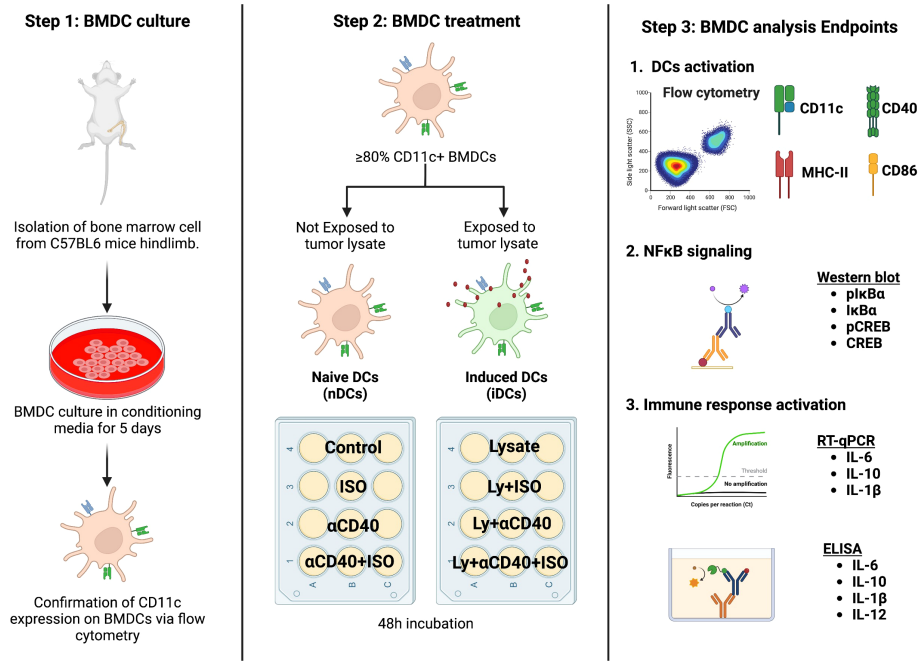


FIGURE 1
A schematic representation of the *in-vitro* BMDC isolation and treatment plan is shown. Bone marrow cells derived from C57BL/6 female mice were cultured in DC conditioning media and the expression of CD11c was confirmed after 5 days of culture. BMDCs with ≥80% CD11c expression were categorized as naïve (nDCs) or induced DCs (iDCs) based on exposure to MOC2 tumor cell lysate. The cells were then treated with 1 μM ISO (a β2AR agonist) and 10 μg/ml αCD40 (a CD40 agonist) for 48 hours before analysis. Schematic created with BioRender.com.

were used for subsequent experiments as described in Figure 1. Briefly, the BMDCs were divided into two groups: naïve BMDCs (nDCs, untreated with tumor cell lysate) and induced DCs (iDCs, treated with tumor cell lysate). 25,000 BMDCs were treated with 1μM Isoproterenol (non-selective β2AR agonist, ISO), 10μg/ml αCD40 or 100 μg/ml tumor cells lysate and incubated for 48h in RPMI with 100ng/ml GM-CSF to assess cytotoxicity using the MTT assay (following manufacturer's protocol), and for other mechanistic assays as described in following sections. For co-treatments, BMDCs were pretreated with 1μM ISO for 1h before being subjected to αCD40 or tumor cell lysate and incubated for 48h.

3.2 *In-vitro* and *in-vivo* immune cell analysis using flow cytometry

Briefly, iDCs and nDCs were washed with cold FACS buffer (PBS + 2% FBS) and stained for 30mins on ice in dark for CD11c, MHC-II, CD86 & CD40. Cells were washed twice with cold FACS buffer before acquisition on BD™ LSRII instrument. For *in-vivo* studies, MOC2 tumor samples from mice were cut into ~1cm pieces and digested with 200 U/ml Collagenase IV solution. Digested tumors were passed through 70 μm cell strainers and incubated in RBC lysis buffer (Invitrogen) for 10min. Single-cell suspensions were washed with cold FACS buffers and stained for 30mins on ice in dark. Data was analyzed using Flowjo software v.10.8.1 (Treestar Inc., Ashland, OR, USA) and cells were gated as follows- CD45+ CD3+ (Total T-cells), CD45+ CD3+ CD4+ CD8- (T_H, CD4+ T helper cells), CD45+ CD3+ CD8- CD4+ FOXP3+ (Treg, Regulatory T-cells), CD45+ CD3+ CD4- CD8+ (T_C, CD8+ T-cells), CD45+ CD3+ CD4- CD8+ GZMB+ (Effector cytotoxic T-cells), CD45+ CD11c+ (DC, Dendritic cells), CD45+ CD11c+ MHC-II+ CD86+ (Activated DCs), CD45+ CD11c+ MHC-II+ CD40+ (Matured DCs). Channel gating (Figure S1) and compensations were done using unstained cells, single-stained cells, and appropriate FMOs.

3.3 RT-qPCR analysis for cytokine gene expression in nDC and iDCs

RNA was extracted from treated and untreated nDCs and iDCs using TRIzol reagent followed by DNase treatment. cDNA was prepared from 1μg of total RNA using cDNA synthesis kit following manufacturer protocol. SYBR green based real-time analysis was done to detect the expression of IL-1β, IL-6 & IL-10 genes using GAPDH as a housekeeping gene. PCR mixture contained 1μl cDNA, 10μl SYBR green master mix (2X), and 100nM of each reverse and forward primer in a total volume of 20μl. PCR was run using settings of 95°C for 15s and 60°C for 60s for 35 cycles, on 7500 Fast Real-Time PCR system, Applied Biosystem. ΔC_T for the gene target was calculated by subtracting GAPDH C_T values for each replicate and represented as $2^{\wedge}\Delta C_T$ in the bar graph. Primer sequences are given in Table 1.

TABLE 1 Mouse primer sequences used for RT-PCR.

Gene	5′ Primer sequence Forward	5′ Primer sequence Reverse
IL-1b	TGGACCTTCCAGGAT GAGGACA	GTTCATCTCGGAGCC TGTAGTG
IL-6	ACAACCACGGCCTTC CCTACTT	CACGATTTCCCAGAGA ACATGTG
IL-10	CGGGAAGACAATAAC TGCACCC	CGGTTAGCAGTATGT TGTCCAGC
GAPDH	CATCACTGCCACCCA GAAGACTG	ATGCCAGTGAGCTTCC CGTTCAG

3.4 Western blot analysis of NFκB pathway targets and quantification of released cytokine

nDC and iDC were lysed and the total protein amount was estimated using BCA assay. An equal amount of cell lysate (30μg) was loaded on SDS-PAGE (BioRad, MiniPROTEAN Tetra System), and transferred to NC membrane (BioRad Trans-Blot Turbo) for 30min run at a constant voltage of 25V. Blots were blocked using 3% BSA solution for 1h at RT and stained with anti-pIkBα, anti-IkBα, anti-pCREB, and anti-CREB antibodies overnight at 4°C. Blots were washed in TBST buffer before incubating with appropriate secondary antibodies for 1h at RT, and imaged using BioRad, ChemiDoc™ MP Imaging System. Blots were stripped using mild stripping buffer (Glycine, pH2) and re-stained with anti-GAPDH antibody for 1h at RT following the above-mentioned procedure. To create intensity graphs, the intensities of pIkBα, IkBα, pCREB1, CREB, and GAPDH bands were measured using ImageJ software. The background intensities were subtracted from each blot. The intensities of pIkBα, IkBα, pCREB, or CREB were then normalized by dividing them with the GAPDH band intensities and represented as ratios of the phosphorylated to unphosphorylated IkBα or CREB on a bar graph. Data were analyzed using 2 independent BMDC experiments. ELISA was also performed to quantify the released cytokines, IL-6, IL-1β, IL-10 & IL-12, in 50μl of iDC culture supernatants following the manufacturer's protocol.

3.5 MOC2 *in-vivo* study design

All animal associated procedures were approved by Oklahoma State University Animal Care and Use Committee. For tumor inoculation, MOC2 cells (purchased from Kerafast, Boston, MA, USA) cultured in DMEM media supplemented with 10% v/v FBS & 100U/ml PenStrep, harvested at 70-80% confluency were washed with sterile cold PBS before inoculations. 8-weeks old C57BL/6 female mice were injected subcutaneously with 1.5 X 10^5 MOC2 cells in the flank region. Propranolol-HCl (10 mg/kg B.W.) resuspended in sterile PBS was injected subcutaneously from day 5 onwards daily until mice euthanasia. Tumor volumes were measured daily using a caliper (3-in Digital caliper, UltraTECH) and calculated using the formula (L*W*W)/2. Once tumors reached an average volume of ~50 mm^3, 30 μg of αCD40 antibody was injected intratumorally. Two doses were given 8 days apart, and mice were euthanized 4-wk post-inoculation. Tumors were harvested for immune cell analysis using flow cytometry.

3.6 Statistical analysis

All analyses were performed using Prism v.9.4.0 software (GraphPad Software Inc. La Jolla, CA, USA). Treatment groups were compared using Two-tailed Unpaired T-tests. For group analysis with multiple variables, One-way ANOVA with either Tukey or Bonferroni multiple comparison test, and Two-way ANOVA were used as applicable. P values less than 0.05 was considered significant and represented as * P <0.05, ** P <0.005, *** P <0.0005, **** P <0.0001.

4 Results

4.1 β2AR signaling reduced the surface expression of co-stimulatory molecules on nDCs and iDCs.

β2AR agonist treated nDCs showed significantly reduced CD11c+ expression and viability (~40%) relative to untreated control, but these effects were not observed upon exposure to MOC2 tumor lysates in iDCs (Figures 2A–C). Also, the MHC-II, CD86 & CD40 expressions significantly decreased in both nDCs and iDCs with ISO (Figures 2B, C, E & Figure S2), but the average fold decrease was more pronounced in iDCs compared to nDCs (~MHC-II [83% vs 74%], CD86 [70% vs 53%] & CD40 [80% vs 24.1%]; Figure 2D).

4.2 β2AR signaling reduced αCD40 priming abilities of nDCs and iDCs.

Unlike iDCs, nDCs that were co-treated with αCD40 and ISO showed significantly reduced cell viability compared to αCD40 alone (Figure 3A). Additionally, although the MHC-II and CD86 expression on CD11c+ cells and percentage of CD40+ cell modified similarly for nDCs and iDCs (Figure 3B, C & Figure S2), however, the MFI of CD40 expression on iDC was significantly reduced relative to nDC (Figure S2), indicating an overall decline in the αCD40 mediated priming of iDCs following β2AR activation (Figures 3D, E).

4.3 β2AR signaling reengineered CD40 signaling by inhibiting phosphorylation of IκBα subunit of the Ikk complex to alter cytokine production.

The activator of NFkB1 & NFkB2 complexes, i.e. IKK complex, was analyzed by targeting phosphorylated IkBα (pIkBα, Ser32) using western blot and represented as the ratio of phosphorylated and unphosphorylated IkBα band intensities. In both nDCs and iDCs, a significant increase in intracellular levels of pIkBα vs IkBα was

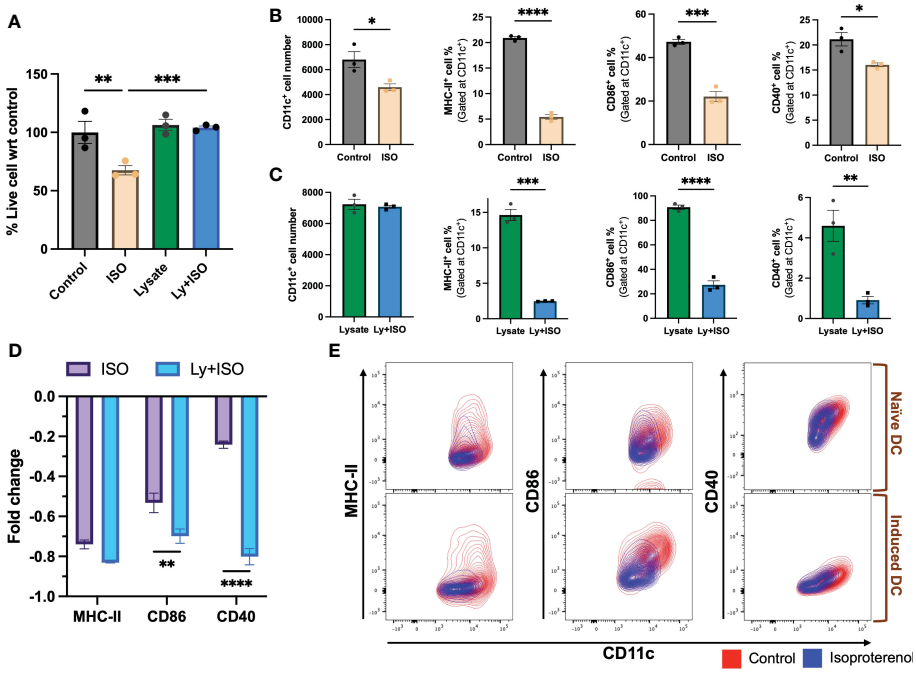


FIGURE 2
The impact of ISO (1μM) treatment on the viability and surface expression of co-stimulatory molecules on CD11c+ expressing naïve DC (nDCs) and tumor lysate induced DCs (iDCs) was evaluated after 48 hours. **(A)** ISO reduced nDCs viability, while having no effect on iDCs. **(B, C)** Both nDCs and iDCs treated with ISO showed significant decreases in surface expression of co-stimulatory molecules, MHC-II+, CD86+ and CD40+. **(D)** iDCs exposed to ISO showed a higher decrease in MHC-II, CD86 and CD40 surface expression compared to nDCs. The fold change was calculated by comparing the ISO treated population to the respective control (untreated nDCs or lysate-only treated iDCs) using the formula [(ISO treated population/Control population)-1]. **(E)** The results are demonstrated by representative contour plots of MHC-II+, CD86+ and CD40+ cell populations, showing the intensity of ISO treated nDCs and iDCs overlaid with their respective controls. Statistical analysis was carried out using unpaired t-test, One-way ANOVA & Two-way ANOVA tests where applicable. *P* values less than 0.05 were considered significant. * *P* <0.05, ** *P* <0.005, *** *P* <0.0005, **** *P* <0.0001.

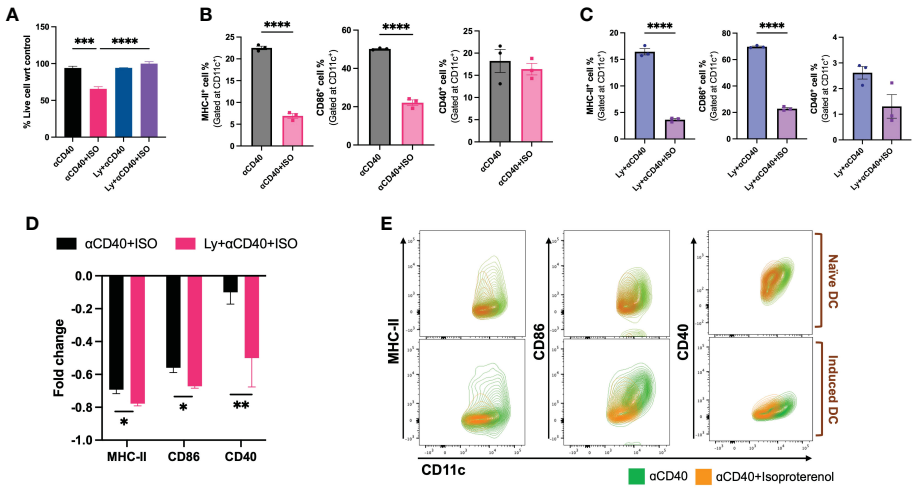


FIGURE 3
Viability & frequencies of MHC-II+, CD86+ & CD40+ nDCs and iDCs exposed to 10 μg/ml αCD40 and 1μM ISO for 48h. **(A)** A significant decrease in the viability of αCD40 treated nDCs with ISO treatment was observed in absence of tumor lysate stimulation. **(B, C).** The population of MHC-II+ and CD86+ nDC and iDC was reduced with ISO and αCD40 co-treatment, however, CD40+ population remain unchanged in nDCs but reduced in iDCs. **(D)** Decrease in the surface expression of co-stimulatory molecules was significantly higher in αCD40-treated iDCs compared to nDCs. Fold change in a cell population with ISO treatment was calculated using αCD40 only treated nDCs and iDCs as control and using the formula: [(ISO treated population/Control population)-1]. **(E)** The results are demonstrated by representative contour plots of MHC-II+, CD86+ and CD40+ cell populations, showing the intensity of ISO treated nDCs and iDCs overlaid with their respective αCD40 treatment controls. Statistical analysis was carried out using unpaired T-test, One-way ANOVA & Two-way ANOVA tests where applicable. *P* values less than 0.05 were considered significant. *** *P* <0.0005, **** *P* <0.0001.

observed with αCD40 treatment, but pIkBα levels declined significantly with αCD40+ISO cotreatment (~1.5-fold in nDCs and ~4-fold in iDCs). Also, the levels of phosphorylated CREB (pCREB, Ser133) relative to unphosphorylated CREB (CREB) decreased slightly in nDCs with αCD40 treatment, but this phenomenon was more evident in iDCs. The addition of ISO (± αCD40) significantly increased the levels of pCREB in both nDCs and iDCs (Figure 4A). To understand the association of IKK complex activation with cytokines production, the gene expression of IL-1b, IL-6 & IL-10 in iDCs was quantified. Expression of IL-10 decreased, and IL-1b & IL-6 increased in presence of αCD40 in iDCs. In contrast, ISO significantly decreased the expression of IL-1b and IL-6 and increased the expression of IL-10 in αCD40 treated iDCs. (Figure 4B). These were similarly observed in culture supernatant with significant decreases in pro-inflammatory cytokine levels of IL-1β, IL-6, and IL-12 and an increase in anti-inflammatory IL-10 levels in αCD40+ISO treated iDCs relative to αCD40 treated cells (Figure 4C).

4.4 αCD40 and propranolol combination achieved superior MOC2 tumor suppression and induction of anti-tumor immunity

Propranolol mediated efficacy of αCD40 *in-situ* vaccination (ISV) in the MOC2 model was evaluated by comparing tumor growth up to 4 weeks post-inoculation (see Figure 5A schematic). αCD40 and propranolol induced partial to moderate reduction of tumor growth compared to the untreated control, but the combined treatment achieved a significant suppression of tumor growth rates compared to the control ($p<0.05$; Figure 5B). We also evaluated the percentage of T-cells and their functional counterparts in the tumor. Data showed a significant increase in the frequency of tumor-infiltrating CD45+ CD3+ T-cells in the combination regimen compared to control which was not observed with monotherapies (Figure 5C). Notably, a significantly higher infiltration of CD8+ T-cells in Prop+αCD40 treated tumors (~24%) relative to untreated tumors (9%) and αCD40 (~15%) was noted. A significantly higher numbers of CD8+ T cells vs CD4+ T cells was observed with combination treatment compared to control and Prop alone treated tumors. A non-statistically significant decrease in regulatory T-cells (CD4+ Foxp3+) populations and an increase in cytotoxic T-cells (CD8+ GZMB+) was observed with all therapies compared to control but their ratio demonstrated a significantly higher number of cytotoxic T-cells vs Tregs in αCD40 and Prop+αCD40 groups compared to the untreated control. Further, the addition of Prop enhanced CD45+ CD11c+ cells by 2.5-fold in treated tumors compared to untreated and αCD40 treated tumors (Figure 5D). Additionally, the mean population of MHC-II & CD86 double-positive cells increased from ~11% in untreated tumors to ~13% in αCD40, and ~16% in Prop+αCD40 & Prop alone treatments. Importantly, the MHC-II+ CD40+ double-positive DCs in Prop +αCD40 treated tumors showed the highest enhancement (~3-fold, $p<0.05$) vs untreated tumors, and Prop and αCD40 monotherapies

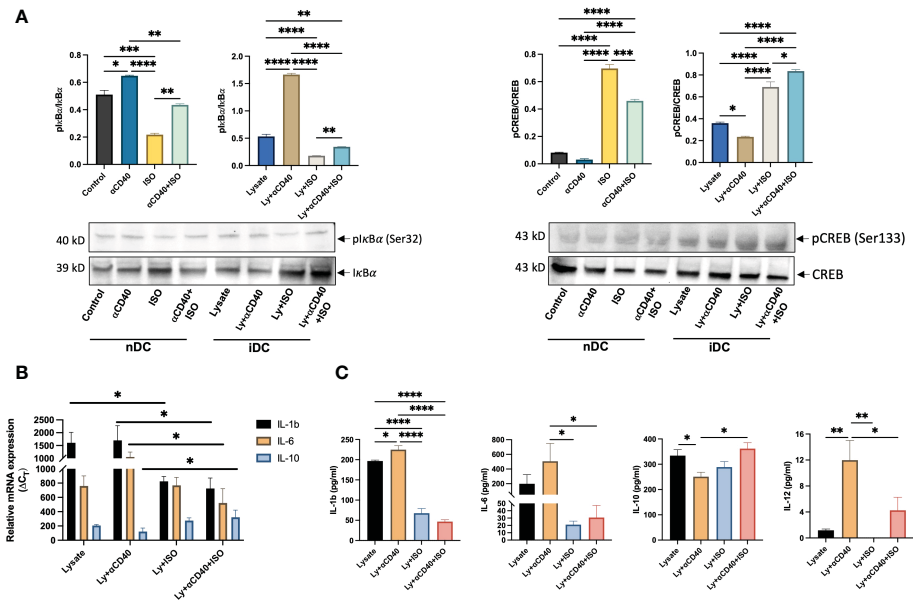


FIGURE 4
Analysis of Phosphorylated IkBα and CREB levels in nDCs and iDCs treated with ISO (1μM) and αCD40 (10 μg/ml) for 48h. **(A)** Western blots showed reduced pIkBα levels compared to unphosphorylated IkBα in the presence of ISO in both αCD40 treated nDCs and iDCs. ISO treatment increased pCREB levels in both nDCs and iDCs, with or without αCD40 treatment. The ratio of phosphorylated to unphosphorylated forms is shown as the intensity graphs. Respective GAPDH blots used to normalize the band intensities are shown in Figures S4A, B and the normalized band intensities are summarized in Figure S5C. **(B)** Gene expression analysis revealed that αCD40+ISO treatment significantly decreased IL-1β & IL-6 levels in iDCs compared to αCD40 treatment alone, and increased IL-10 expression in these cells. The results are expressed as 2^ΔCT with respect to GAPDH levels. **(C)** The release of IL-1β, IL-6 & IL-10 in the culture supernatant of co-treated iDCs showed a similar trend, with αCD40-mediated increase in released IL-12 significantly declining with ISO treatment. Statistical analysis was carried out using One-way ANOVA. *P* values less than 0.05 were considered significant. * *P* <0.05, ** *P* <0.005, *** *P* <0.0005, **** *P* <0.0001.

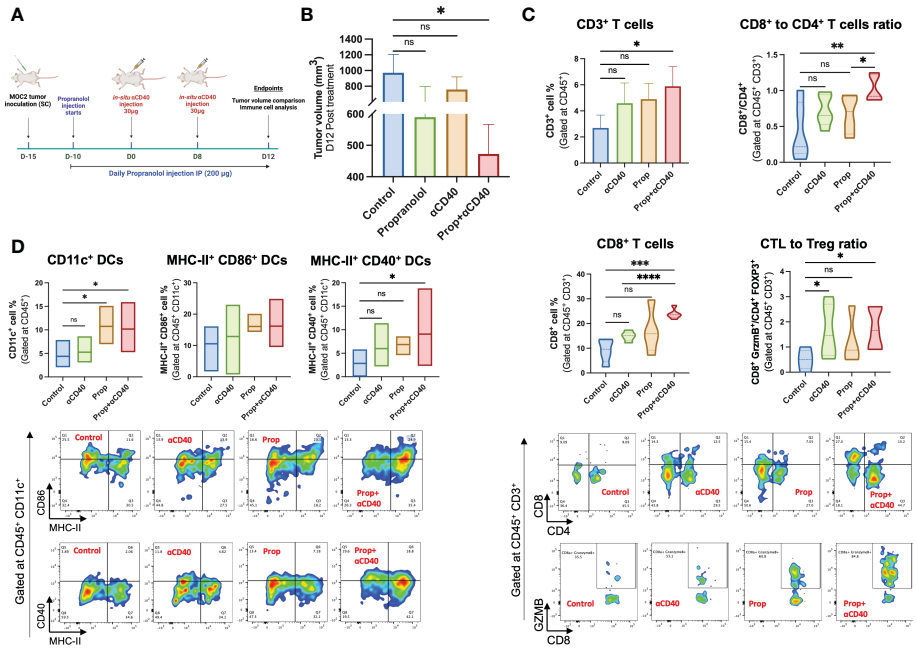


FIGURE 5
Treatment design of the murine efficacy and immune-evaluation study. **(A)** Propranolol (10mg/kg of BW) was administered subcutaneously daily 5 days post-inoculation. Two 30 μg αCD40 intratumoral injections were administered at 8 days intervals in the tumor (~50 mm^3 volume). Mean tumor volume and anti-tumor immune cells were compared on day 28 post-inoculation (Timeline created with BioRender.com). **(B)** The combination of Prop+αCD40 demonstrated a significant reduction in tumor volume compared to the control on day 28 post-inoculation, while monotherapies did not show any significant differences. These results suggest that the combination therapy of Prop+αCD40 is more effective in reducing tumor growth compared to either Prop or αCD40 alone. Immune cells infiltrating MOC2 tumors (n=5 mice/group) analyzed by flow cytometry showed superior immunomodulation with Prop+αCD40. **(C)** Frequencies of CD3+ T-cells, especially CD8+ T-cells infiltrating tumors were enhanced at the highest level by combination treatment vs untreated control and monotherapies. The ratio of cytotoxic T-cells (CD8+ GZMB+) to T regulatory cells (CD4+ Foxp3+) was increased significantly in αCD40 treated groups relative to the control. **(D)** CD11c+, MHC-II+ CD86+ double positive (gated at CD45+ CD11c+) & MHC-II+ CD40+ double positive (gated at CD45+ CD11c+) dendritic cell frequencies showed significant enhancements in the presence of Prop and αCD40. Statistical analysis was carried out using One-way ANOVA & Two-way ANOVA multiple comparison tests. *P* values less than 0.05 were considered significant. * P <0.05, ** P <0.005, *** P <0.0005, **** P <0.0001. ns, nonsignificant.

(~2-fold). (All immune cell population data are presented in Supplementary Table 1.)

5 Discussion

Prior research has shown that NE-mediated adrenergic receptor activation inhibits the activation, differentiation, and effector functions of T-cells (29–32) and modulates the cytokines and chemokines production from macrophages, monocytes, and DCs (7, 33, 34). β2AR signaling can also polarize macrophages from M1 to M2 type, thereby enhancing anti-inflammatory cytokines like IL-10, IL-4 & IL-13, and decreasing pro-inflammatory cytokines like INFγ, TNFα, IL1β, CCL2, CCL3 and CCL4 to cause tumor progression (35–39). Considering that CD40 pathways mainly impact APCs, the reported roles of β2AR signaling on macrophages and DCs piqued our interest in understanding their ability to modulate their functions and impact therapeutic outcomes. We found that β2AR signaling limits DCs function in the presence of tumor antigens by decreasing the expression of MHC-II, CD86, and CD40.

Our data disagrees with a previous study (40) that showed no effects on MHC-II & CD86 expression in NE and LPS stimulated DCs. We believe that unlike LPS that works *via* TLR4, DAMPs & PAMPs present in tumor cell lysate can induce DC activations through multiple signaling mechanisms (TLR3, TLR4, RAGE, etc.) on DCs (41, 42), thereby generating dramatic different immunoactivities with β2AR activation vs LPS alone. To demonstrate this, we compared the stimulation of BMDCs with two types of cancer cell lysates (B16F10 melanoma and MOC2 oral squamous carcinoma) to that of LPS treatments. Our results showed that LPS-treated BMDCs did not exhibit any changes in MHC-2 and CD86 surface expression, while BMDC stimulation with B16F10 and MOC2 tumor cell lysates resulted in differential MHC-2 expression in response to ISO treatment (as shown in Figure S3). While we did not investigate the specific mechanisms behind the differences in MHC-2 and CD86 expression on DCs with the various types of cell lysates, our data still provides strong evidence that the expression of immunomodulatory markers on DCs is dependent on the composition of the ligand/antigen pool.

The use of Pan Beta-blocker like propranolol enhances the efficacy of immunotherapy by blocking β2AR signaling on progenitor and functional immune cells to result in better therapeutic outcomes (22, 27, 31). We looked at the effects of β2AR activation on DCs in presence of αCD40 in BMDCs. β2AR signaling can regulate NFκB pathways by inhibiting phosphorylation of IkBα through enhanced β-Arrestin2 protein production (43, 44). We found that activation of β2AR on αCD40

treated DCs significantly decreased the levels of pIkBα and enhanced the accumulation of unphosphorylated IkBα in cells, thereby suggesting the suppression of DC maturation and CD40-mediated NFκB activation. β2AR signaling has also been shown to activate cAMP/PKA pathways and subsequent CREB phosphorylation. We observed higher levels of pCREB in ISO treated nDCs and iDCs (Figure 4A). Phosphorylated (p) CREB can compete with activated NFκB for the DNA binding sites. Thus, we propose that pCREB may indirectly interfere with αCD40 mediated DC priming (see Figure 6 schematic), to decrease the production of pro-inflammatory cytokines and co-stimulatory molecules (e.g. decreased IL-6 and IL-1B expression and enhanced IL-10 production in iDCs) (45, 46). We noticed similar trends in the cytokines produced in the culture supernatants. The ability of DCs to activate T cells is often evaluated by measuring IL-12 production and co-stimulatory molecules (47, 48), so we examined the IL-12 released from these cells and found that ISO treatment had a significant impact on the release of IL-12 from αCD40-treated induced DCs (iDCs). Thus, we propose that activation of β2AR signaling in αCD40-treated naïve and induced DCs transforms the DC population into an immune-tolerant type, both by blocking NFκB activation and indirectly promoting CREB activation.

Propranolol has been shown to improve the functions of naïve and activated immune cells (22, 27, 31). Since β2AR activation subverted αCD40 signaling in BMDCs, we also investigated the effects of pharmacological β2AR blocking on therapeutic outcomes of αCD40 in immunologically cold MOC2 tumors (49). Despite the improvements made in the potency of CD40 monoclonal antibodies (mAbs) through approaches such as engineering the Fc region, the use of αCD40 immunotherapy in clinics is still faced with challenges due to its associated toxicities. These toxicities include liver damage, low platelet count, cytokine release syndrome (CRS), and hyper-immune activation (2, 50, 51). Also, the widespread expression of the CD40 receptor on both immune and non-immune cells in tumors and other organs leads to broad activation of CD40-expressing cells, limiting the treatment dose of αCD40 mAbs and causing non-specific toxicity. Therefore, we employed a lower dose of αCD40 antibody (30μg; 2X) with Propranolol *via* intratumoral route to overcome the dose-limiting toxicities associated with higher quantities of αCD40 (4). β-blocker with αCD40 treatment significantly suppressed tumor growth at suboptimal doses compared to untreated control, and the outcomes were comparable to a prior report administering higher αCD40 dosage (50μg) and greater frequency (3X) of treatment in the melanoma model (52). MOC2 tumors show a high presence of Tregs and minimal populations of CD8 T-cells (53, 54). Blocking β2AR in mice tumor models can increase lymphocyte infiltration, and lower M1 to M2 polarization of macrophage and Treg population (22, 30, 55, 56). Our findings demonstrate that the combination of Prop+αCD40 effectively modulates the tumor microenvironment, leading to a pronounced increase in CD8+ T cell and cytotoxic T cell infiltration, and a reduction in Tregs compared to tumors treated with monotherapies or untreated control. Surface expression of MHC and co-stimulatory molecules on DCs are known to correlate with enhanced T cell activation and its effector functions (57–61). Blocking β2AR signaling with Prop significantly increased intratumoral CD11c+ populations, and when combined with αCD40 treatment, the number of double-positive MHC-II+ CD40+ DCs significantly increased. This suggests that the combination treatment facilitated robust anti-tumor immune cell priming and maturation. The

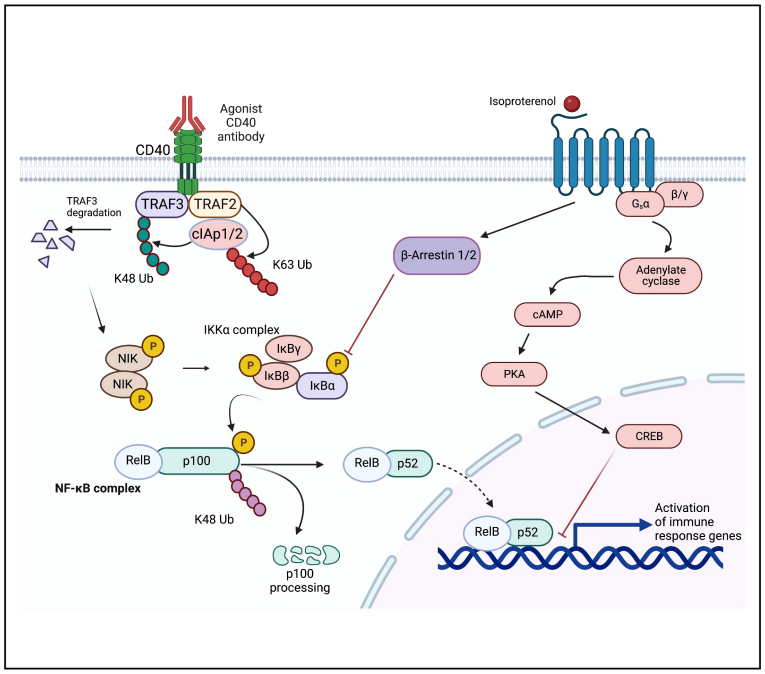


FIGURE 6
Proposed mechanism of β2AR signaling mediated re-engineering of CD40-CD40L signaling in DCs. An increase in intracellular pIkBα (pIkBα) level with αCD40 treatment is reversed by β2AR signaling, thereby resulting in an altered cytokine production and immuno-retardation of anti-tumor response. Adapted from "NF-KB Signaling Pathway", by BioRender.com (2022). Retrieved from https://app.biorender.com/biorender-templates.

increased presence of dendritic cells in the tumor microenvironment, facilitated by Prop treatment, provided a stronger foundation for αCD40 immune therapy. As a result, the combination treatment showed a significant improvement in adaptive anti-tumor immunity compared to control, unlike monotherapies. For *in-vivo* studies, our goal was to include a true untreated control to simulate clinical conditions and evaluate the immunological synergism between αCD40 & Propranolol. PBS is not a standard treatment for head and neck tumors and other types of tumors. Therefore, previous pre-clinical studies, including ours, have used untreated controls relative to PBS to assess the effectiveness of *in-situ* vaccination or parenteral treatment (52, 62–64). Additionally, studies by Hu et al., Singh et al., and others have shown that PBS or non-relevant/isotype control antibody treatments do not enhance tumor control compared to propranolol or αCD40 alone (64–68). Future studies may include PBS (or an isotype control antibody) to further confirm the feasibility of the proposed combination therapy in the MOC2 murine model.

Thus, our investigation provides the foundational basis for improving αCD40 immunotherapy by the use of β-blockers. This combination can be particularly relevant for cold TMEs and can reverse β2AR signaling mediated tumor cell survival seen previously (69, 70). We found that the combination of Prop+αCD40 enhanced therapeutic and anti-tumor immune responses compared to control, however, some changes were not statistically different from monotherapies. Further studies are needed to optimize treatment dosages and timelines to achieve a pronounced tumor remission. Gender-specific differences in β-blocker response and immune cell characteristics should also be explored to gain a deeper understanding of the therapeutic outcomes (71).

Data availability statement

The original contributions presented in the study are included in the article/Supplementary Material. Further inquiries can be directed to the corresponding author.

Ethics statement

The animal study was reviewed and approved by Oklahoma State University Animal Care and Use Committee.

Author contributions

AR and AS conceived the project and designed the study goals. AS performed the experiments and analyzed the data. AR and AS wrote the manuscript. All authors contributed to the article and approved the submitted version.

Funding

We acknowledge the National Cancer Institute of the National Institutes of Health under award number R01CA260974, and the Kerr Endowed Chair at Oklahoma State University for supporting this research.

Conflict of interest

The authors declare that the research was conducted in the absence of any commercial or financial relationships that could be construed as a potential conflict of interest.

Publisher's note

All claims expressed in this article are solely those of the authors and do not necessarily represent those of their affiliated organizations, or those of the publisher, the editors and the reviewers. Any product that may be evaluated in this article, or claim that may be made by its manufacturer, is not guaranteed or endorsed by the publisher.

Supplementary material

The Supplementary Material for this article can be found online at: https://www.frontiersin.org/articles/10.3389/fimmu.2023.1141712/full#supplementary-material

SUPPLEMENTARY FIGURE 1
Gating strategy used for the analysis of BMDCs.

SUPPLEMENTARY FIGURE 2
Mean fluorescence intensities of different surface markers, MHC-II **(A)**, CD86 **(B)**, and CD40 **(C)** analyzed on CD11c gated BMDCs. Population percentage is shown in Figure 2 and Figure 3. Statistical analysis was carried out using One-way ANOVA. *P* values less than 0.05 were considered significant. * *P* <0.05, *** *P* <0.0005, **** *P* <0.0001.

SUPPLEMENTARY FIGURE 3
MHC-II and CD86 expression on CD11c+ BMDCs under different stimulation. **(A)** 10,000 BMDC (>80% CD11c+) were stimulated with 1 μg/ml LPS and in combination with 10 μg/ml αCD40 for 48h showed a significant increase in MHC-II and CD86 expression. Upon ISO treatment, LPS alone stimulated BMDCs demonstrated no change in MHC-II and CD86 expression whereas it decreased in LPS+αCD40 treated BMDCs. **(B)** BMDCs treated with 100 μg/ml B16F10 tumor cell lysate showed a significant decrease in MHC-II expression which increased with the addition of αCD40. With ISO treatment, MHC-II expression further increased in these cells whereas CD86 expression decreased. **(C)** BMDCs treated with 100 μg/ml MOC2 tumor cell lysate alone and with αCD40 showed a similar pattern of MHC-II expression as B16F10 lysate stimulated cells but MHC-II and CD86 expression decreased upon ISO treatment. Statistical analysis was carried out using One-way ANOVA. *P* values less than 0.05 were considered significant. * *P* <0.05, ** *P* <0.005, *** *P* <0.0005, **** *P* <0.0001.

SUPPLEMENTARY FIGURE 4
Western blots of phosphorylated and unphosphorylated IkBα **(A)** & CREB **(B)**, presented in Figure 4A, are shown with their respective GAPDH blots used for normalization. **(C)** Table summarizing normalized band intensities of target proteins represented as a ratio of phosphorylated and unphosphorylated forms of IkBα & CREB in Figure 4A.

SUPPLEMENTARY TABLE 1
Frequencies of immune cells analyzed in murine MOC2 tumor model treated with β2AR antagonist (Prop) and CD40 agonist (αCD40).

References

1. Beatty GL, Li Y, Long KB. Cancer immunotherapy: Activating innate and adaptive immunity through CD40 agonists. *Expert Rev Anticancer Ther* (2017) 17 (2):175–86. doi: 10.1080/14737140.2017.1270208

2. Vonderheide RH, Flaherty KT, Khalil M, Stumacher MS, Bajor DL, Hutnick NA, et al. Clinical activity and immune modulation in cancer patients treated with CP-870,893, a novel CD40 agonist monoclonal antibody. *J Clin Oncol* (2007) 25(7):876–83. doi: 10.1200/JCO.2006.08.3311

3. Rüter J, Antonia SJ, Burris HA, Huhn RD, Vonderheide RH. Immune modulation with weekly dosing of an agonist CD40 antibody in a phase I study of patients with advanced solid tumors. *Cancer Biol Ther* (2010) 10(10):983–93. doi: 10.4161/cbt.10.10.13251

4. Li DK, Wang W. Characteristics and clinical trial results of agonistic anti-CD40 antibodies in the treatment of malignancies. *Oncol Lett* (2020) 20(5):176. doi: 10.3892/ol.2020.12037

5. Vonderheide RH, Glennie MJ. Agonistic CD40 antibodies and cancer therapy. *Clin Cancer Res* (2013) 19(5):1035–43. doi: 10.1158/1078-0432.CCR-12-2064

6. Bajor DL, Mick R, Riese MJ, Huang AC, Sullivan B, Richman LP, et al. Long-term outcomes of a phase I study of agonist CD40 antibody and CTLA-4 blockade in patients with metastatic melanoma. *Oncoimmunol* (2018) 7(10):e1468956. doi: 10.1080/2162402X.2018.1468956

7. Bucsek MJ, Giridharan T, MacDonald CR, Hylander BL, Repasky EA. An overview of the role of sympathetic regulation of immune responses in infectious disease and autoimmunity. *Int J Hyperthermia* (2018) 34(2):135–43. doi: 10.1080/02656736.2017.1411621

8. Wang W, Cao X. Beta-adrenergic signaling in tumor immunology and immunotherapy. *Crit Rev Immunol* (2019) 39(2):93–103. doi: 10.1615/CritRevImmunol.2019031188

9. Eng JW, Reed CB, Kokolus KM, Pitoniak R, Utley A, Bucsek MJ, et al. Housing temperature-induced stress drives therapeutic resistance in murine tumour models through β2-adrenergic receptor activation. *Nat Commun* (2015) 6:6426. doi: 10.1038/ncomms7426

10. He J-J, Zhang W-H, Liu S-L, Chen Y-F, Liao C-X, Shen Q-Q, et al. Activation of β-adrenergic receptor promotes cellular proliferation in human glioblastoma. *Oncol Lett* (2017) 14(3):3846–52. doi: 10.3892/ol.2017.6653

11. Cole SW, Sood AK. Molecular pathways: Beta-adrenergic signaling in cancer. *Clin Cancer research: an Off J Am Assoc Cancer Res* (2012) 18(5):1201–6. doi: 10.1158/1078-0432.CCR-11-0641

12. Bucsek MJ, Qiao G, MacDonald CR, Giridharan T, Evans L, Niedzwecki B, et al. β-adrenergic signaling in mice housed at standard temperatures suppresses an effector phenotype in CD8(+) T cells and undermines checkpoint inhibitor therapy. *Cancer Res* (2017) 77(20):5639–51. doi: 10.1158/0008-5472.CAN-17-0546

13. Goyarts E, Matsui M, Mammone T, Bender AM, Wagner JA, Maes D, et al. Norepinephrine modulates human dendritic cell activation by altering cytokine release. *Exp Dermatol* (2008) 17(3):188–96. doi: 10.1111/j.1600-0625.2007.00677.x

14. Maestroni GJ. Short exposure of maturing, bone marrow-derived dendritic cells to norepinephrine: impact on kinetics of cytokine production and Th development. *J Neuroimmunol* (2002) 129(1-2):106–14. doi: 10.1016/S0165-5728(02)00188-1

15. Maestroni GJ, Mazzola P. Langerhans cells beta 2-adrenoceptors: role in migration, cytokine production, Th priming and contact hypersensitivity. *J Neuroimmunol* (2003) 144(1-2):91–9. doi: 10.1016/j.jneuroim.2003.08.039

16. Nijhuis LE, Olivier BJ, Dhawan S, Hilbers FW, Boon L, Wolkers MC, et al. Adrenergic β2 receptor activation stimulates anti-inflammatory properties of dendritic cells in vitro. *PloS One* (2014) 9(1):e85086. doi: 10.1371/journal.pone.0085086

17. Yanagawa Y, Matsumoto M, Togashi H. Enhanced dendritic cell antigen uptake *via* alpha2 adrenoceptor-mediated PI3K activation following brief exposure to noradrenaline. *J Immunol* (2010) 185(10):5762–8. doi: 10.4049/jimmunol.1001899

18. Seiffert K, Hosoi J, Torii H, Ozawa H, Ding W, Campton K, et al. Catecholamines inhibit the antigen-presenting capability of epidermal langerhans cells. *J Immunol* (2002) 168(12):6128–35. doi: 10.4049/jimmunol.168.12.6128

19. Hervé J, Dubreil L, Tardif V, Terme M, Pogu S, Anegon I, et al. β2-adrenoreceptor agonist inhibits antigen cross-presentation by dendritic cells. *J Immunol* (2013) 190(7):3163–71. doi: 10.4049/jimmunol.1201391

20. Maestroni GJ. Dendritic cell migration controlled by alpha 1b-adrenergic receptors. *J Immunol* (2000) 165(12):6743–7. doi: 10.4049/jimmunol.165.12.6743

21. Chen M, Qiao G, Hylander BL, Mohammadpour H, Wang XY, Subjeck JR, et al. Adrenergic stress constrains the development of anti-tumor immunity and abscopal responses following local radiation. *Nat Commun* (2020) 11(1):1821. doi: 10.1038/s41467-019-13757-3

22. Fjæstad KY, Rømer AMA, Goitea V, Johansen AZ, Thorseth ML, Carretta M, et al. Blockade of beta-adrenergic receptors reduces cancer growth and enhances the response to anti-CTLA4 therapy by modulating the tumor microenvironment. *Oncogene* (2022) 41(9):1364–75. doi: 10.1038/s41388-021-02170-0

23. Kokolus KM, Zhang Y, Sivik JM, Schmeck C, Zhu J, Repasky EA, et al. Beta blocker use correlates with better overall survival in metastatic melanoma patients and improves the efficacy of immunotherapies in mice. *Oncoimmunol* (2018) 7(3):e1405205. doi: 10.1080/2162402X.2017.1405205

24. Bucsek MJ, Qiao G, MacDonald CR, Giridharan T, Evans L, Niedzwecki B, et al. β-adrenergic signaling in mice housed at standard temperatures suppresses an effector phenotype in CD8. *Cancer Res* (2017) 77(20):5639–51. doi: 10.1158/0008-5472.CAN-17-0546

25. Pasquier E, Street J, Pouchy C, Carre M, Gifford AJ, Murray J, et al. β-blockers increase response to chemotherapy *via* direct antitumour and anti-angiogenic mechanisms in neuroblastoma. *Br J Cancer* (2013) 108(12):2485–94. doi: 10.1038/bjc.2013.205

26. Chang PY, Huang WY, Lin CL, Huang TC, Wu YY, Chen JH, et al. Propranolol reduces cancer risk: A population-based cohort study. *Medicine* (2015) 94(27):e1097. doi: 10.1097/MD.0000000000001097

27. Gandhi S, Pandey MR, Attwood K, Ji W, Witkiewicz AK, Knudsen ES, et al. Phase I clinical trial of combination propranolol and pembrolizumab in locally advanced and metastatic melanoma: Safety, tolerability, and preliminary evidence of antitumor activity. *Clin Cancer Res* (2021) 27(1):87–95. doi: 10.1158/1078-0432.CCR-20-2381

28. Liao X, Chaudhary P, Qiu G, Che X, Fan L. The role of propranolol as a radiosensitizer in gastric cancer treatment. *Drug Des Devel Ther* (2018) 12:639–45. doi: 10.2147/DDDT.S160865

29. Zalli A, Bosch JA, Goodyear O, Riddell N, McGettrick HM, Moss P, et al. Targeting ß2 adrenergic receptors regulate human T cell function directly and indirectly. *Brain Behav Immun* (2015) 45:211–8. doi: 10.1016/j.bbi.2014.12.001

30. Qiao G, Chen M, Mohammadpour H, MacDonald CR, Bucsek MJ, Hylander BL, et al. Chronic adrenergic stress contributes to metabolic dysfunction and an exhausted phenotype in T cells in the tumor microenvironment. *Cancer Immunol Res* (2021) 9 (6):651–64. doi: 10.1158/2326-6066.CIR-20-0445

31. Qiao G, Bucsek MJ, Winder NM, Chen M, Giridharan T, Olejniczak SH, et al. β-adrenergic signaling blocks murine CD8. *Cancer Immunol Immunother* (2019) 68 (1):11–22. doi: 10.1007/s00262-018-2243-8

32. Estrada LD, Agac D, Farrar JD. Sympathetic neural signaling *via* the beta2-adrenergic receptor suppresses T-cell receptor-mediated human and mouse CD8(+) T-cell effector function. *Eur J Immunol* (2016) 46(8):1948–58. doi: 10.1002/eji.201646395

33. Halder N, Lal G. Cholinergic system and its therapeutic importance in inflammation and autoimmunity. *Front Immunol* (2021) 12:660342. doi: 10.3389/fimmu.2021.660342

34. Scanzano A, Cosentino M. Adrenergic regulation of innate immunity: a review. *Front Pharmacol* (2015) 6:171. doi: 10.3389/fphar.2015.00171

35. Gill SK, Marriott HM, Suvarna SK, Peachell PT. Evaluation of the anti-inflammatory effects of β-adrenoceptor agonists on human lung macrophages. *Eur J Pharmacol* (2016) 793:49–55. doi: 10.1016/j.ejphar.2016.11.005

36. Grailer JJ, Haggadone MD, Sarma JV, Zetoune FS, Ward PA. Induction of M2 regulatory macrophages through the β2-adrenergic receptor with protection during endotoxemia and acute lung injury. *J Innate Immun* (2014) 6(5):607–18. doi: 10.1159/000358524

37. Roewe J, Higer M, Riehl DR, Gericke A, Radsak MP, Bosmann M. Neuroendocrine modulation of IL-27 in macrophages. *J Immunol* (2017) 199 (7):2503–14. doi: 10.4049/jimmunol.1700687

38. Victoni T, Salvator H, Abrial C, Brollo M, Porto LCS, Lagente V, et al. Human lung and monocyte-derived macrophages differ with regard to the effects of β. *Respir Res* (2017) 18(1):126. doi: 10.1186/s12931-017-0613-y

39. Sharma M, Patterson L, Chapman E, Flood PM. Salmeterol, a long-acting β2-adrenergic receptor agonist, inhibits macrophage activation by lipopolysaccharide from porphyromonas gingivalis. *J Periodontol* (2017) 88(7):681–92. doi: 10.1902/jop.2017.160464

40. Takenaka MC, Araujo LP, Maricato JT, Nascimento VM, Guereschi MG, Rezende RM, et al. Norepinephrine controls effector T cell differentiation through β2-adrenergic receptor-mediated inhibition of NF-κB and AP-1 in dendritic cells. *J Immunol* (2016) 196(2):637–44. doi: 10.4049/jimmunol.1501206

41. González FE, Gleisner A, Falcón-Beas F, Osorio F, López MN, Salazar-Onfray F. Tumor cell lysates as immunogenic sources for cancer vaccine design. *Hum Vaccin Immunother* (2014) 10(11):3261–9. doi: 10.4161/21645515.2014.982996

42. Chiang CL, Kandalaft LE, Tanyi J, Hagemann AR, Motz GT, Svoronos N, et al. A dendritic cell vaccine pulsed with autologous hypochlorous acid-oxidized ovarian cancer lysate primes effective broad antitumor immunity: from bench to bedside. *Clin Cancer Res* (2013) 19(17):4801–15. doi: 10.1158/1078-0432.CCR-13-1185

43. Gao H, Sun Y, Wu Y, Luan B, Wang Y, Qu B, et al. Identification of beta-arrestin2 as a G protein-coupled receptor-stimulated regulator of NF-kappaB pathways. *Mol Cell* (2004) 14(3):303–17. doi: 10.1016/S1097-2765(04)00216-3

44. Kizaki T, Shirato K, Sakurai T, Ogasawara JE, Oh-ishi S, Matsuoka T, et al. Beta2-adrenergic receptor regulate toll-like receptor 4-induced late-phase NF-kappaB activation. *Mol Immunol* (2009) 46(6):1195–203. doi: 10.1016/j.molimm.2008.11.005

45. O'Sullivan BJ, Thomas R. CD40 ligation conditions dendritic cell antigen-presenting function through sustained activation of NF-kappaB. *J Immunol* (2002) 168(11):5491–8. doi: 10.4049/jimmunol.168.11.5491

46. Hostager BS, Bishop GA. CD40-mediated activation of the NF-κB2 pathway. *Front Immunol* (2013) 4:376. doi: 10.3389/fimmu.2013.00376

47. Tugues S, Burkhard SH, Ohs I, Vrohlings M, Nussbaum K, Vom Berg J, et al. New insights into IL-12-mediated tumor suppression. *Cell Death Differ* (2015) 22 (2):237–46. doi: 10.1038/cdd.2014.134

48. Kaka AS, Foster AE, Weiss HL, Rooney CM, Leen AM. Using dendritic cell maturation and IL-12 producing capacity as markers of function: A cautionary tale. *J Immunother* (2008) 31(4):359–69. doi: 10.1097/CJI.0b013e318165f5d2

49. Wakiyama H, Furusawa A, Okada R, Inagaki F, Kato T, Maruoka Y, et al. Increased immunogenicity of a minimally immunogenic tumor after cancer-targeting near infrared photoimmunotherapy. *Cancers* (2020) 12(12). doi: 10.3390/cancers12123747

50. Johnson P, Challis R, Chowdhury F, Gao Y, Harvey M, Geldart T, et al. Clinical and biological effects of an agonist anti-CD40 antibody: A cancer research UK phase I study. *Clin Cancer Res* (2015) 21(6):1321–8. doi: 10.1158/1078-0432.CCR-14-2355

51. Berner V, Liu H, Zhou Q, Alderson KL, Sun K, Weiss JM, et al. IFN-gamma mediates CD4+ T-cell loss and impairs secondary antitumor responses after successful initial immunotherapy. *Nat Med* (2007) 13(3):354–60. doi: 10.1038/nm1554

52. Singh MP, Sethuraman SN, Ritchey J, Fiering S, Guha C, Malayer J, et al. In-situ vaccination using focused ultrasound heating and anti-CD-40 agonistic antibody enhances T-cell mediated local and abscopal effects in murine melanoma. *Int J Hyperthermia* (2019) 36(sup1):64–73. doi: 10.1080/02656736.2019.1663280

53. Judd NP, Allen CT, Winkler AE, Uppaluri R. Comparative analysis of tumor-infiltrating lymphocytes in a syngeneic mouse model of oral cancer. *Otolaryngol Head Neck Surg* (2012) 147(3):493–500. doi: 10.1177/0194599812442037

54. Moore EC, Cash HA, Caruso AM, Uppaluri R, Hodge JW, Van Waes C, et al. Enhanced tumor control with combination mTOR and PD-L1 inhibition in syngeneic oral cavity cancers. *Cancer Immunol Res* (2016) 4(7):611–20. doi: 10.1158/2326-6066.CIR-15-0252

55. Daher C, Vimeux L, Stoeva R, Peranzoni E, Bismuth G, Wieduwild E, et al. Blockade of beta-adrenergic receptors improves CD8(+) T-cell priming and cancer vaccine efficacy. *Cancer Immunol Res* (2019) 7(11):1849–63. doi: 10.1158/2326-6066.CIR-18-0833

56. Mohammadpour H, MacDonald CR, McCarthy PL, Abrams SI, Repasky EA. beta2-adrenergic receptor signaling regulates metabolic pathways critical to myeloid-derived suppressor cell function within the TME. *Cell Rep* (2021) 37(4):109883. doi: 10.1016/j.celrep.2021.109883

57. Wu H, Chen J, Song S, Yuan P, Liu L, Zhang Y, et al. β2-adrenoceptor signaling reduction in dendritic cells is involved in the inflammatory response in adjuvant-induced arthritic rats. *Sci Rep* (2016) 6:24548. doi: 10.1038/srep24548

58. Tas SW, Vervoordeldonk MJ, Hajji N, Schuitemaker JH, van der Sluijs KF, May MJ, et al. Noncanonical NF-kappaB signaling in dendritic cells is required for indoleamine 2,3-dioxygenase (IDO) induction and immune regulation. *Blood* (2007) 110(5):1540–9. doi: 10.1182/blood-2006-11-056010

59. Tang M, Diao J, Gu H, Khatri I, Zhao J, Cattral MS. Toll-like receptor 2 activation promotes tumor dendritic cell dysfunction by regulating IL-6 and IL-10 receptor signaling. *Cell Rep* (2015) 13(12):2851–64. doi: 10.1016/j.celrep.2015.11.053

60. Ferris ST, Durai V, Wu R, Theisen DJ, Ward JP, Bern MD, et al. cDC1 prime and are licensed by CD4. *Nature* (2020) 584(7822):624–9. doi: 10.1038/s41586-020-2611-3

61. Liang B, Workman C, Lee J, Chew C, Dale BM, Colonna L, et al. Regulatory T cells inhibit dendritic cells by lymphocyte activation gene-3 engagement of MHC class II. *J Immunol* (2008) 180(9):5916–26. doi: 10.4049/jimmunol.180.9.5916

62. Singh MP, Sethuraman SN, Miller C, Malayer J, Ranjan A. Boiling histotripsy and in-situ CD40 stimulation improve the checkpoint blockade therapy of poorly immunogenic tumors. *Theranostics* (2021) 11(2):540–54. doi: 10.7150/thno.49517

63. Wakabayashi R, Kono H, Kozaka S, Tahara Y, Kamiya N, Goto M. Transcutaneous codelivery of tumor antigen and resiquimod in solid-in-Oil nanodispersions promotes antitumor immunity. *ACS Biomater Sci Eng* (2019) 5 (5):2297–306. doi: 10.1021/acsbiomaterials.9b00260

64. Knorr DA, Dahan R, Ravetch JV. Toxicity of an fc-engineered anti-CD40 antibody is abrogated by intratumoral injection and results in durable antitumor immunity. *Proc Natl Acad Sci U S A* (2018) 115(43):11048–53. doi: 10.1073/pnas.1810566115

65. Hu Q, Liao P, Li W, Hu J, Chen C, Zhang Y, et al. Clinical use of propranolol reduces biomarkers of proliferation in gastric cancer. *Front Oncol* (2021) 11:628613. doi: 10.3389/fonc.2021.628613

66. Singh M, Vianden C, Cantwell MJ, Dai Z, Xiao Z, Sharma M, et al. Intratumoral CD40 activation and checkpoint blockade induces T cell-mediated eradication of melanoma in the brain. *Nat Commun* (2017) 8(1):1447. doi: 10.1038/s41467-017-01572-7

67. Pasquier E, Ciccolini J, Carre M, Giacometti S, Fanciullino R, Pouchy C, et al. Propranolol potentiates the anti-angiogenic effects and anti-tumor efficacy of chemotherapy agents: implication in breast cancer treatment. *Oncotarget* (2011) 2 (10):797–809. doi: 10.18632/oncotarget.343

68. MacDonald CR, Bucsek MJ, Qiao G, Chen M, Evans L, Greenberg DJ, et al. Adrenergic receptor signaling regulates the response of tumors to ionizing radiation. *Radiat Res* (2019) 191(6):585–9. doi: 10.1667/RR15193.1

69. Gysler SM, Drapkin R. Tumor innervation: peripheral nerves take control of the tumor microenvironment. *J Clin Invest* (2021) 131(11). doi: 10.1172/JCI147276

70. Brunskole Hummel I, Reinartz MT, Kälble S, Burhenne H, Schwede F, Buschauer A, et al. Dissociations in the effects of β2-adrenergic receptor agonists on cAMP formation and superoxide production in human neutrophils: support for the concept of functional selectivity. *PloS One* (2013) 8(5):e64556.

71. Wang S, Cowley LA, Liu XS. Sex differences in cancer immunotherapy efficacy, biomarkers, and therapeutic strategy. *Molecules* (2019) 24(18). doi: 10.1371/journal.pone.0064556

frontiers | Frontiers in Immunology

TYPE Original Research
PUBLISHED 29 March 2023
DOI 10.3389/fimmu.2023.1162213

Check for updates

OPEN ACCESS

EDITED BY
Michael Evangelopoulos,
Northwestern University, United States

REVIEWED BY
Ritika Tewari,
Benaroya Research Institute, United States
Nemat Ali,
King Saud University, Saudi Arabia
Bishal Singh,
MRC Laboratory of Molecular Biology (LMB), University of Cambridge, United Kingdom

*CORRESPONDENCE
Saif Khan
sf.khan@uoh.edu.sa;
saifkhan.bio@gmail.com
Mohd Wajid Ali Khan
mw.khan@uoh.edu.sa;
wajidkhan11@gmail.com

SPECIALTY SECTION
This article was submitted to Cancer Immunity and Immunotherapy, a section of the journal Frontiers in Immunology

RECEIVED 09 February 2023
ACCEPTED 13 March 2023
PUBLISHED 29 March 2023

CITATION
Khan S, Khan MWA, Sherwani S, Alouffi S, Alam MJ, Al-Motair K and Khan S (2023) Directional preference for glioblastoma cancer cell membrane encapsulated nanoparticle population: A probabilistic approach for cancer therapeutics. *Front. Immunol.* 14:1162213. doi: 10.3389/fimmu.2023.1162213

COPYRIGHT
© 2023 Khan, Khan, Sherwani, Alouffi, Alam, Al-Motair and Khan. This is an open-access article distributed under the terms of the Creative Commons Attribution License (CC BY). The use, distribution or reproduction in other forums is permitted, provided the original author(s) and the copyright owner(s) are credited and that the original publication in this journal is cited, in accordance with accepted academic practice. No use, distribution or reproduction is permitted which does not comply with these terms.

Directional preference for glioblastoma cancer cell membrane encapsulated nanoparticle population: A probabilistic approach for cancer therapeutics

Saif Khan[1,2]*, Mohd Wajid Ali Khan[2,3]*, Subuhi Sherwani[4], Sultan Alouffi[2,5], Mohammad Jahoor Alam[2,4], Khalid Al-Motair[2] and Shahper Khan[6]

[1]Department of Basic Dental and Medical Sciences, College of Dentistry, University of Ha'il, Ha'il, Saudi Arabia, [2]Medical and Diagnostic Research Centre, University of Ha'il, Ha'il, Saudi Arabia, [3]Department of Chemistry, College of Sciences, University of Ha'il, Ha'il, Saudi Arabia, [4]Department of Biology, College of Sciences, University of Ha'il, Ha'il, Saudi Arabia, [5]Department of Clinical Laboratory Sciences, College of Applied Medical Sciences, University of Ha'il, Ha'il, Saudi Arabia, [6]Interdisciplinary Nanotechnology Centre, Aligarh Muslim University, Aligarh, India

Background: Selective cancer cell recognition is the most challenging objective in the targeted delivery of anti-cancer agents. Extruded specific cancer cell membrane coated nanoparticles, exploiting the potential of homotypic binding along with certain protein-receptor interactions, have recently proven to be the method of choice for targeted delivery of anti-cancer drugs. Prediction of the selective targeting efficiency of the cancer cell membrane encapsulated nanoparticles (CCMEN) is the most critical aspect in selecting this strategy as a method of delivery.

Materials and methods: A probabilistic model based on binding scores and differential expression levels of Glioblastoma cancer cells (GCC) membrane proteins (factors and receptors) was implemented on python 3.9.1. Conditional binding efficiency (CBE) was derived for each combination of protein involved in the interactions. Selective propensities and Odds ratios in favour of cancer cells interactions were determined for all the possible combination of surface proteins for 'k' degree of interaction. The model was experimentally validated by two types of Test cultures.

Results: Several Glioblastoma cell surface antigens were identified from literature and databases. Those were screened based on the relevance, availability of expression levels and crystal structure in public databases. High priority eleven surface antigens were selected for probabilistic modelling. A new term, Break-even point (BEP) was defined as a characteristic of the typical cancer cell membrane encapsulated delivery agents. The model predictions lie within ±7% of the experimentally observed values for both experimental test culture types.

Conclusion: The implemented probabilistic model efficiently predicted the directional preference of the exposed nanoparticle coated with cancer cell membrane (in this case GCC membrane). This model, however, is developed and validated for glioblastoma, can be easily tailored for any type of cancer involving CCMEN as delivery agents for potential cancer immunotherapy. This probabilistic model would help in the development of future cancer immunotherapeutic with greater specificity.

KEYWORDS

glioblastoma, encapsulated nanoparticle, cancer cell membrane, probabilistic model, homotypic binding, human serum albumin nanoparticles

Introduction

Cancer cell targeting is the most critical step towards its successful therapy. Researchers have employed a myriad of techniques to achieve this selective targeting thereby alleviating undesirable consequences (1–4). Recently, biodegradable nanoparticles coated with extruded target cancer cell membranes, were employed to selectively identify target cancer cells. This specificity originates from homotypic binding of differentially expressed extracellular regions of transmembrane proteins (5–7). Glioma cells are well known for differential expression of several membrane associated surface antigens/proteins (8, 9). This characterizes GBM (Glioblastoma multiforme) cell as suitable candidate/s for selective identification built on homotypic interaction of cell surface proteins/antigens (10–13). Nanoparticles coated with extruded cell membranes from glioma cells, harboring similar levels of differentially expressed surface antigens/proteins, was employed by several researchers to selectively target GBM cells (14–17). Glioma cell surface harbors several receptor-factor complexes. These surface receptor-factor couples possess high affinity for each other. These heterotypic surface interactions are critical for progression and/or inhibition of glioma cell proliferation (9). Hetero-complexes of surface-receptor couples are well defined and explored by several studies (8, 10–16). These hetero complexes (involving receptor- factor couple) may offer significant hinderance to the homotypic selective force exploited by the Cancer cell membrane encapsulated nanoparticles (CCMEN) employed for selectively differentiating healthy cells from GBM cells. The magnitude and direction (favour or opposition) of heterotypic interaction play decisive role in determining the selective potential of the CCMEN. The magnitude (or the strength) and direction of the heterotypic interactions depends upon the differential expression pattern of the receptor-factor couples in glioma cells w.r.t healthy cells. Several studies report expression levels of such receptor-factor couples (18–20). Expression levels may also be extracted from databases such as Gene Expression Omnibus (GEO, 21), Human Protein Atlas (HPA, 22) and The Cancer Genome Atlas (TCGA, 23).

Probabilistic models have been developed for patient-specific combination cancer treatments based on sequencing data and functional assay of the drug (24). Other approachesinvolve the application of probabilistic models for the prediction of the metastatic spread of the tumor (25). In the present study we have encoded a probabilistic model in python 3.9.1 based on the binding potential and expression levels of the surface receptors/proteins (SP) on Glioblastoma cancer cells (GCC), Normal healthy cells (NHC) and their corresponding protein Factors (F). The objective of this model is not only to determine the directional preference of the exposed CCMEN population, but also to characterize the CCMEN for a range of degree of interaction of SP. This model, however, is developed and validated for Glioblastoma, can be easily tailored for any type of cancer involving CCMEN as delivery agents.

Material and methods

Expression levels

Normalized surface gene (receptors) and secreted factors (gene) expression levels for healthy normal brain cells were determined from the Human Protein Atlas (HPA) and GEO (Gene Expression Omnibus) datasets. Secreted levels of the IL-13 (Interleukin-13) for normal healthy brain cells was considered as a baseline (since it has the minimum expression level) and all other gene expression levels (factors and receptors) were represented w.r.t to IL-13. Over/repressed levels of genes (receptors and factors) were determined from the GEO series GSE147352. This series includes 85 adult (age range from 22-81 years) grade Glioblastoma tissues, 18 lower grade glioma tissues and 15 normal brain tissues characterized by rRNA-depleted total RNAseq. Only 85 adult grade glioblastoma and 15 normal brain tissues were included in this study. Altered glioblastoma levels of gene expression was represented as folds (Table 1) for each gene considered in this study.

Determination of binding efficiency (Intrinsic affinities)

RCSB Protein data bank (PDB) database was used to retrieve three-dimensional structure of surface protein as well as their respective ligand/s. Discovery studio suit was used to optimize the

TABLE 1 Expression Levels and Glioblastoma fold change.

Receptors				
Receptor Gene	Description	NEX	rNX	FC
PDGFRA	Platelet derived growth factor receptor	7.24	72.43	11.1
TGFB2R	Transforming Growth Factor beta Type II Receptor	5.21	52.14	3.58
EGFR	Epidermal growth factor receptor	4	40	17.19
Met R.	Hepatocyte growth receptor	2.7	27	1.95
IL4R	Interleukin-4 receptor	4.2	42	2.28
IL-13R	Interleukin-13 receptor	7.34	73.43	4.48
Tfr2	Transferrin receptor	0.45	4.5	0.41
Kdr	Vascular endothelial growth factor receptor	1.96	19.57	2.55
FGFR1	Fibroblast growth factor receptor	12.4	124	1.67
PLAUR	Urokinase plasminogen activator surface receptor	2.63	26.29	10.24
ITGA2B	Integrin	1.69	16.86	0.71
Factors Gene	***Factors***	***NEX***	***rNX***	***FC***
PDGF	Platelet derived growth factor	12.77	127.71	1.95
TGF	Transforming Growth Factor	8.79	87.86	2.51
EGF	Epidermal growth factor	0.27	2.71	1.36
HGF	Hepatocyte growth factor	1.31	13.14	1.41
IL-4	Interleukin-4	0.2	2	1.1
IL-13	Interleukin-13	0.1	1	1.9
Tf	Transferrin	7.86	78.57	1.17
VEGF	Vascular endothelial growth factor	6.09	60.86	10.21
FGF2	Fibroblast growth factor	10.16	101.57	1.33
PLAU	Urokinase plasminogen activator	0.87	8.71	32.64
TNC	Tenascin-C	1.79	17.86	78.92

NEX, Original Normal brain cell expression levels; rNX, Normal brain cell expression levels w.r.t Interlukin-13; FC, Glioblastoma expr levels vs normal brain cell (fold change: The fold change is derived as the ratio of relative rNX (Normal brain cell expression levels w.r.t Interlukin-13 shown in the table) to relative glioblastoma expression levels w.r.t Interlukin-13 not shown in the table but represented as Fold change FC). Relative glioblastoma expression levels w.r.t Interlukin-13 can be obtained simply by dividing FC by rNX.

three-dimensional structures. We removed unwanted redundant molecules. All the protein-protein interactions involving native receptor-factor complex are redocking results since these are available in either protein databank or other predicted databases, all receptor-receptor and non-native cross receptor-factor interactions were determined by performing protein-protein docking. Haddock 2.4 online server (https://wenmr.science.uu.nl/haddock2.4/) was used to do docking and to predict the strength of interaction between ligand-protein as well as protein-protein. The best dock was selected that was based on two parameters i.e Haddock score and Z-score. Prodigy webserver (https://wenmr.science.uu.nl/prodigy/) was used to find out binding affinity between ligand-protein as well as protein-protein. The intrinsic binding scores (BS) are reported in database repository RDO_datasets (link provided in Database availability statement)

Probabilistic model

A probabilistic model was developed to determine the interaction probabilities (and eventually odds ratios) for the receptor (R) surface proteins (SP) and their combinations present on the glioma CCMEN. The interaction probabilities (P) of individual and combinations of SP receptors on CCMEN were determined towards GCC, NHC and F. The model has the following assumptions:

1. A specific SP or their combination undergoes interaction with the SP on any of the following: GCC only, GCC + F, NHC only, NHC + F or F only.
2. A SP or their combination cannot interact with the SP on both GCC and NHC simultaneously.

3. Atleast one SP interacts with any one instance of the SP of the following: GCC only or NHC only or F only or GCC + F or NHC + F.
4. Interaction of the SP or their combination with the secreted "F only" represents no interaction with either GCC or NHC.
5. No Factor-Factor interactions are considered in this study
6. All other interactions were assumed to result in zero net preference to the specific cell or Factor type.

Probabilities were derived from the conditional binding efficiency (CBE) of surface proteins on CCMEN towards the SP on cell type (GCC or NHC) and/or F. CBE were derived from the BS. Since CBE depends upon the protein type and its conditional expression level (Glioblastoma positive: GCC/F or Negative: NHC; Table 1). Final CBE values were derived from the following Eq.1

$$CBE = \text{BS} * \text{MIN}\left(\frac{\text{SP}_{NEX} \text{ on CCMEN, } \text{SP}_{NEX} \text{ on } \frac{\text{GCC}}{\text{NHC}}}{\text{F}}\right)^{*} \quad \text{Eq.1}$$

$$\text{MIN}\left(\frac{SP_{FC} \text{ on CCMEN, } \text{SP}_{FC} \text{ on } \frac{\text{GCC}}{\text{NHC}}}{\text{F}}\right)$$

Where,

MIN = select the lower value among the choices.

SP_{NEX} = Surface Protein normal/native expression level

SP_{FC} = Surface Protein Fold change (Glioblastoma positive: GCC/F or Negative: NHC)

The model assumes that any number of surface protein types on CCMEN may undergo interaction with the SP of GCC/NHC or F. The degree of interaction (k) is defined as the number of SP on CCMEN undergoing interaction simultaneously. Probabilities were calculated for degree of interactions ranging from one to n (n =11) proteins considered in this study (Table 1). Except for single protein interaction, several combinations of proteins may be derived depending upon the degree of interaction. The number of possible combinations (PC) for a given degree of interaction (k) is given by the following equation (Eq.2)

$$PC = \frac{n!}{(n-k)! \times k!} \quad \text{Eq.2}$$

Where,

$n!$ = factorial of total number of protein types considered in the study (11 in this case).

$k!$ = factorial of degree of interaction (range from 1 to 11)

Probabilities (P) were calculated for each combination assuming null to full factor interactions. The degree of factor interaction (k_F) is defined as the number of factors interacting with a certain combination of degree k ($0 \geq k_F \geq k$). Binding strengths (BST) and probabilities were calculated for each type of combination. BST_{GCC} and P_{GCC} of interaction towards GCC, BST_{NHC} and P_{NHC} of interaction towards NHC and BST_F and P_F of interaction towards F. Each combination is further subdivided based on number of factors interacting for a given combination (k_F). The subclasses range from zero F interaction (Full cell type Interaction: GCC/NHC) to full F Interaction (zero cell type Interaction: F). BST and P of interaction was determined for each class and its subdivision. The hierarchy of probabilistic model classes and subclasses is represented in the flowchart (Figure 1).

(P_{GCC}: probability of Interaction with GCC, P_{NHC}: probability of Interaction with NHC, P_F: probability of Interaction with F, n=11)

The model was implemented in python (3.9.1).

Conditional expected value calculation

Expected value ($E(x)$) of a random variable x is defined as the sum of the probability-weighted average of all the possible realization of the discreet variable. The Expected value is the arithmetic mean of several independently selected outcomes. In this case the expected values of binding strength were determined (from the probabilistic model discussed above) for each class (k) and subclass (k_F) based on their respective conditional probabilities (Conditional probability is defined as the likelihood of an event or outcome occurring, based on the occurrence of a previous event or outcome, in this case depending class: k and corresponding subclass: k_F)

$$E(x)_{k,k_F} = \sum_{i=1}^{i=\frac{n!}{(n-k)! \times k!}} P_{k,k_F}^{BST_i^{k,k_F}} \times BST_i^{k,k_F}$$

Here:$E(x)_{k,kF}$ is the expected value of the k^{th} class and k_F subclass; n=11.

$P_{k,k_F}^{BST_i^{k,k_F}}$ is the conditional probability value of the i^{th} combination for the k^{th} class and subclass k_F.

BST_i^{k,k_F} is the binding strength of the individual or specific combination of SP for the k^{th} class and subclass k_F.

Determination of selective propensities

Selective propensity (S_p) is defined as the affinity of the SP on CCMEN or their combination for a particular degree of protein interaction (k and subclass k_F) towards SP on GCC, NHC or F. S_p for a typical SP combination (for a specific k and k_F) were derived by representing the BSTs (for GCC, NHC and F) as vectors on the x, y and z axis in a three-dimensional space (Figure 2). $S_{p,\ GCC/NHC/F}$:

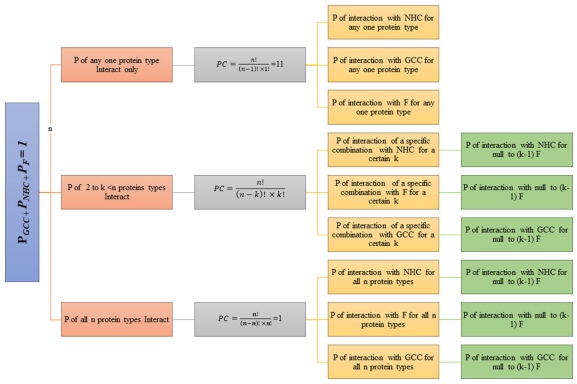


FIGURE 1
Probabilistic Model.

selective propensity towards GCC/NHC/F is given by Eq.3-5

$$S_{p,\ GCC} = 90° - R°_{x,\ GCC} \quad \text{Eq.3}$$

Here : $R°_x$ = *Angle of the resultant vector with x – axis*, *x-axis* represents GCC

$$S_{p,\ NHC} = 90° - R°_{x,\ NHC} \quad \text{Eq.4}$$

Here : $R°_x$ = *Angle of the resultant vector with x – axis*, *x-axis* represents NHC

$$S_{p,\ F} = 90° - R°_{x,\ F} \quad \text{Eq.5}$$

Here : $R°_x$ = *Angle of the resultant vector with x – axis*, *x-axis* represents F

$R°_{x,\ GCC/NHC/F}$ was determined as the ratio of the resultant vector R_x, (calculated by Eq.6-11) with the BST for GCC/NHC/F on the *x-axis* (*x-axis* was cycled through BSTs for GCC, NHC and F sequentially)

$$R_{x,\ GCC} = \sqrt[2]{BST^2_{x,GCC} + BST^2_{y,NHC} + BST^2_{z,F}} \quad \text{Eq.6}$$

$$R_{x,\ NHC} = \sqrt[2]{BST^2_{x,NHC} + BST^2_{y,GCC} + BST^2_{z,F}} \quad \text{Eq.7}$$

$$R_{x,\ F} = \sqrt[2]{BST^2_{x,F} + BST^2_{y,GCC} + BST^2_{z,NHC}} \quad \text{Eq.8}$$

$$R°_{x,\ GCC} = Degrees\left(\frac{BST_{x,GCC}}{R_{x,\ GCC}}\right) \quad \text{Eq.9}$$

$$R°_{x,\ NHC} = Degrees\left(\frac{BST_{x,NHC}}{R_{x,\ NCC}}\right) \quad \text{Eq.10}$$

$$R°_{x,\ F} = Degrees\left(\frac{BST_{x,F}}{R_{x,\ F}}\right) \quad \text{Eq.11}$$

S_p is directly proportional to the pull of the SP or their combination towards the axis of interest (*x-axis*). Selective propensities (S_p) of each protein type or their combination for a particular degree of interaction (*k* and for their subclasses k_F) were derived from Eq.3-5.

Experimental validation of model predictions

An *In vitro* validation experiment was designed to determine the accuracy of the probabilistic model prediction for GCC binding efficiency of the exposed CCMEN population. The initial (exposed) and final concentration of the CCMEN was determined in terms of Na^+/K^+ ATPase α-1 cell surface receptor concentration (μg/mL). This receptor is present on the glioblastoma cell membrane encapsulating the HSA-Nanoparticle (described in the database repository RDO_datasets). The concentration was determined by direct binding ELISA for Na^+/K^+ ATPase α-1 cell surface receptor.

Standard plot for Na+/K+ ATPase α-1 is given in database repository RDO_datasets: Standard Plot. The *ln* fitting equation (Eq.12) with $R^2 = 0.9158$ is given as

$$Absorbance\ (nm) = 0.2657ln(\text{Na} + /\text{K} + \text{ATPase}\ \alpha - 1\ \mu g/mL) + 1.072 \quad \text{Eq.12}$$

Overnight culture of Glioblastoma cancer cells (GCC cells) 10,000 (U87MG) or both: GCC cells and peripheral blood mononuclear cells (PBMCs) in a ratio of 1:1 (5000:5000) were prepared separately in a total volume of 200 μl of complete RPMI medium. CCMEN (5 μg/ml) was added to the Test cultures: Test culture I: GCC + F (released from GCC cells) and Test culture II: GCC + NHC + F (released from GCC and NHC cells) and incubated for 30 mins (duration standardized previously data not provided here). The contents of the test culture were centrifuged after incubation to separate the supernatant for Test culture I and Test culture II. The supernatant was subjected to direct binding ELISA for Na+/K+ ATPase α-1 cell surface receptor (refer to database repository RDO_datasets for details). The fraction of CCMEN population binding the GCC was determined from Eq. 13.

$$\%\ of\ CCMEN\ bound\ to\ GCC = \frac{conc.\ of\ CCMEN_{exposed}\ (^{\mu g}/_{mL}) - conc.\ of\ CCMEN_{supernatant\ I\ or\ II}\ (^{\mu g}/_{mL})}{conc.\ of\ CCMEN_{exposed}\ (^{\mu g}/_{mL})} \text{x}\ 100 \quad \text{Eq.13}$$

Note:- All the experiments were performed in triplicate and average value were reported.

Preparation of CCMEN (CCM-c/m-HSA-Cis NPs)

Synthesize of CCMEN was carried out using a previously reported extrusion approach with slight modifications (6, 26). First, cell membrane was isolated from a glioblastoma cancer cell line U87MG. Second, a dual delivery mode HSA NPs was synthesised using cationic HSA (c-HSA) and manno-pyranoside HSA (m-HSA). Both c-HSA (5 mg; 10%) and m-HSA (10 mg; 20%) were mixed together using distilled water. Five gram of cisplatin (free base form) was added to 50 ml of distilled water, and then this was added to the above mixture of albumin in a ratio of 1% w/v in total 10 ml. The mixture will be emulsified using centrifugation at 10,000 rpm for 2 minutes. The pellet was collected and homogenized using a glass homogenizer resulting primary emulsion. Furthermore, a high-pressure homogenizer was used and primary emulsion was passed through (7-9 times) at a pressure of 20,000 psi to get c/m-HSA-Cis NPs. c/m-HSA-Cis NPs were passed through a 200 nm filter. Filtered c/m-HSA-Cis NPs were stored at −80°C for future experiments. Finally, isolated cancer cell membrane (CCM) was 10-15 times extruded physically using a 400 nm polycarbonate membrane and the resulting vesicles were mixed with c/m-HSA-Cis NPs. The mixture was further

extruded through a 200 nm polycarbonate membrane to get the final product CCM-c/m-HSA-Cis NPs.

Results

A probabilistic model was implemented in python to predict the fraction of CCMEN directed towards specific cell type (GCC/NHC) or protein F. Both tabular and graphical results were generated from this tool. The tabular results were presented as.csv files. Several types of.csv files were generated. BST_k_GCC/NHC/F.csv files represent the calculated binding strength for all the possible combinations of the SP of CCMEN towards SP of GCC/NHC/F for k degree of interaction ($1 \le k \le 11$). Column headers: Prot_comb represents the receptor numeric code for the specific protein combination (refer to Table 1 for numeric receptor code: R_code), BST@kf = N is the binding strength for N factor interaction ($0 \le N \le k$). BST@k_interactions.csv file tabulates the overall binding strengths (summation of BST for all combinations) of SP on CCMEN for k interaction ($1 \le k \le 11$) towards GCC (first row), NHC (second row) and Factors (third row). P_k_GCC/NHC/F.csv tabulate the absolute probability of interaction derived from the probabilistic model for all the possible combinations of the SP of CCMEN towards SP of GCC/NHC/F for k degree of interaction ($1 \le k \le 11$). Column header: P@kf = N is the probability of binding of the specific protein combination (refer to Table 1 for numeric receptor code: R_code) for N factor interaction ($0 \le N \le k$). P@K_interactions.csv file tabulates the overall absolute probabilities of binding (summation of probabilities for all combinations) of SP on CCMEN for k interaction ($1 \le k \le 11$) towards GCC (first row), NHC (second row) and Factors (third row). The distribution of overall binding probabilities as a function of $1 \le k \le 11$ is given in Figure 2. SP_k_GCC/NHC/F.csv tabulate the selective propensity (as discussed in methods section) of all the possible combinations of the SP of CCMEN towards SP of GCC/NHC/F for k degree of interaction ($1 \le k \le 11$). Column headers: Sp_,prot_comb represents the average selective propensity of the specific SP combination towards GCC/NHC/F, Sp@kf = N is the selective propensity of the specific SP combination for N factor interactions. SP@K_interactions.csv file tabulates the overall selective propensity of binding (summation of selective propensities for all combinations from BST@k_interactions.csv) for SP on CCMEN@k interaction ($1 \ge k \le 11$) towards GCC (first row), NHC (second row) and Factors (third row).

EBST_k_GCC/NHC/F.csv files reports the probabilistic Expected Value $E(x)_{k,kF}$ for $BST^{k,kF}$ (binding strength for k interaction and k_F factor interactions) towards GCC/NHC/F. Column headers: EBST_Overall is the overall probabilistic $E(x)_k$of binding strength for k degree of interaction towards GCC/NHC/F, EBST@kf=N is the probabilistic $E(x)_{k,kF}$ of binding strength for k degree of interaction and N Factor interactions towards GCC/NHC/F. EBST_k_interactions.csv summarizes the $E(x)_k$ of BST for GCC, NHC and F for $1 \le k \le n$. ESP_k_GCC/NHC/F.csv files tabulates the probabilistic $E(x)_{k,kF}$ of selective propensity towards GCC/NHC/F. Column headers: EBST_Overall is the overall probabilistic $E(x)_k$ of S_p for k degree of interaction towards GCC/NHC/F, EBST@kf=N is the probabilistic $E(x)_{k,kF}$ of S_p for k degree of interaction and N Factor interactions towards GCC/NHC/F. ESP_k_interactions.csv summarizes the $E(x)_k$ of S_p for GCC, NHC and F for $1 \le k \le n$. $E(x)_k$ results for BST and S_p are reported in database repository RDO_datasets (link provided in Database availability statement).

S_p for individual surface receptor protein (Table 1) on CCMEN were determined as function of their average respective CBEs towards GCC, NHC and F (Eq. 3-11), Figures 3A–C presents the unscaled S_p, $_{GCC}$, $S_{p,NHC}$ and $S_{p,F}$ of individual surface receptor protein as vectors in a 3D interstitial space. The 2D red plane represents threshold boundary below which the arrows parallel to x-axis represents the individual protein directed towards cell type/proteins on the x-axis. The labels on the three axis *(x, y and z)* represents arbitrary positional coordinates within the interstitial space. $E(x)_k$ $S^k_{p,NHC}$ and $S^k_{p,F}$ were determined for all possible k interactions ($1 \le k \le n = 11$; Figures 3D–F, File: SP@K_interactions.csv). $S^{k,k_F}_{p,GCC}$ and $S^{k,k_F}_{p,F}$ were determined for all possible k interactions ($1 \le k \le n = 11$) and factor interactions k_F ($0 \le k_F \le 11$). Figure 4 presents the distribution for the $S^{k,k_F}_{p,GCC}$ in contrast to $S^{k,k_F}_{p,F}$ up till three factor interactions (rest are provided in database repository RDO_datasets). 3D quiver plots were also determined for $S^{k,k_F}_{p,NHC}$ and reported in in database repository RDO_datasets.

Fraction of population having $S^{k,k_F}_{p,GCC}$ and $S^{k,k_F}_{p,F} > 45°$ and the respective odds ratios in favour of GCC (Figure 5A) and F (Figure 5B) of the fractional population were determined for all classes of interaction level ($1 \le k \ge 11$) and their corresponding subclass (leaves of network) of factor interaction ($0 \le k_F \le 11$). This was reported as Kamada-kawai network plots (Figures 5A, B). The size of nodes corresponds to the fractional population of CCMEN encapsulated nanoparticle (directed towards GCC: Figure 5A and towards F: Figure 5B) for the specific class 'k' (Intermediary nodes; refer to color codes in the figure for specific degree of interaction) and/or subclass 'k_F' (leaf nodes; refer to color codes in the figure for specific degree of factor interaction). Each node label (Figure 5A) = odds ratio of the fractional population in favour GCC interaction for the specific class 'k' and subclass 'k_F'/ fraction of population directed towards GCC for the specific class 'k' and subclass 'k_F'. Each node label (Figure 5B) = odds ratio of the fractional population in favour of F interaction for the specific class 'k' and subclass 'k_F'/fraction of population directed towards F for

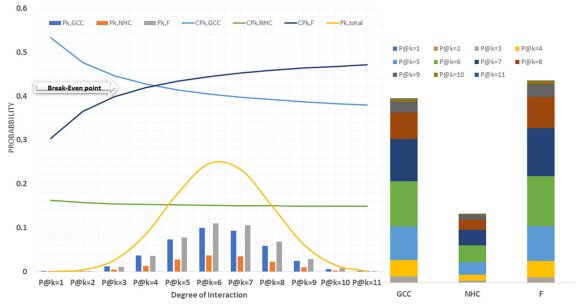


FIGURE 2
Probability distribution @k interactions; P:Probability, CP: conditional probability.

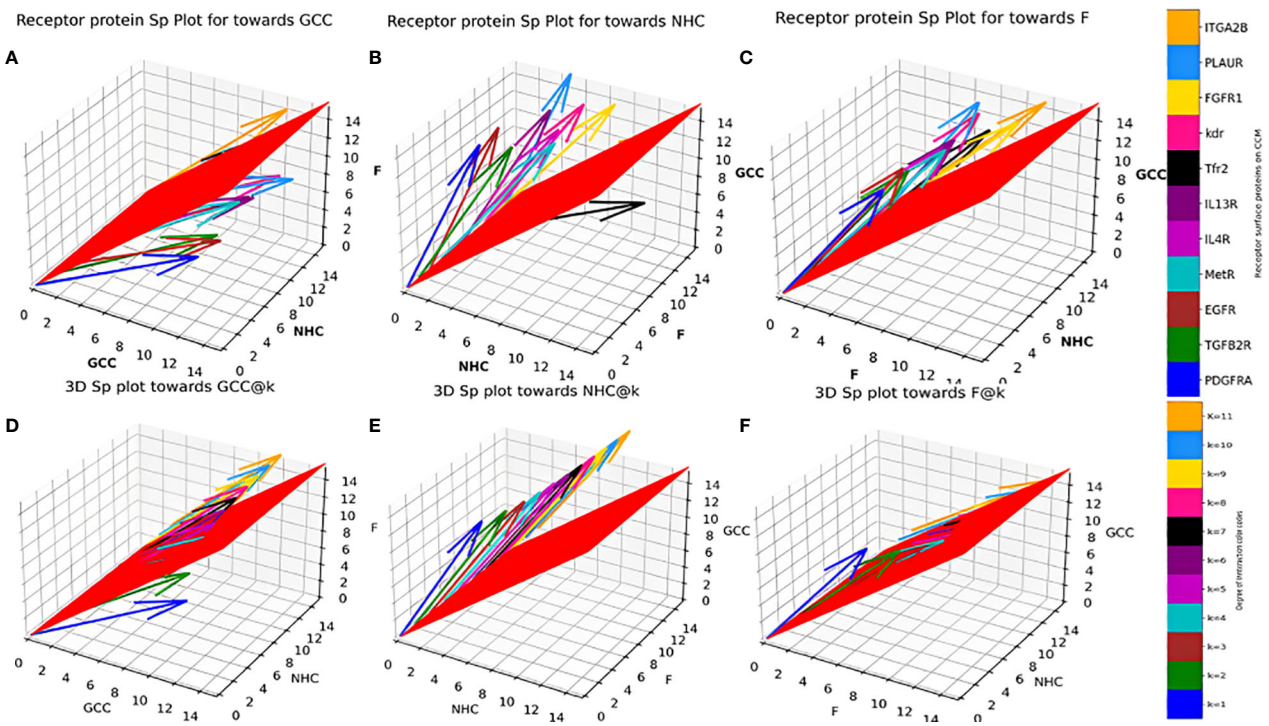


FIGURE 3
Individual Protein vs Degree of interaction quiver plots; 3D S_p plot for Individual surface proteins towards **(A)** GCC, **(B)** NHC and **(C)** F; 3D S_p plot @k interactions towards **(D)** GCC, **(E)** NHC and **(F)** F.

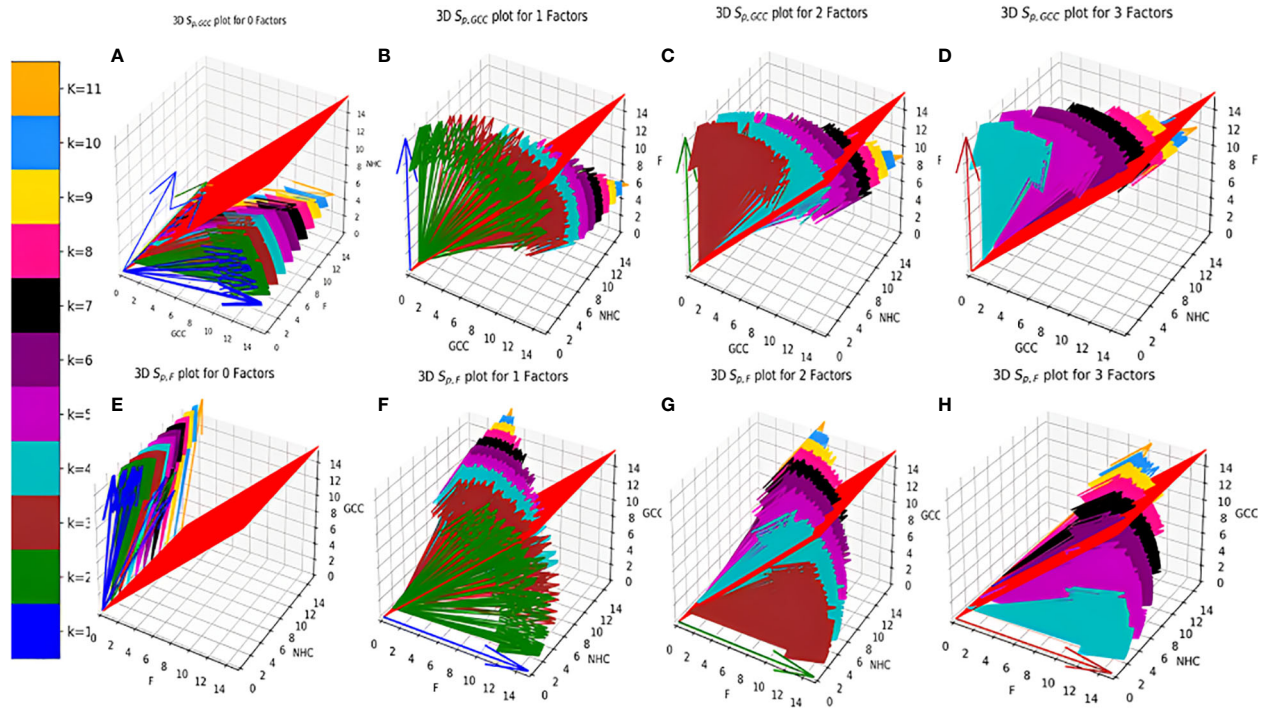


FIGURE 4
Distribution of $S_{p,GCC}^{k,k_F}$ Vs $S_{p,F}^{k,k_F}$ **(A–D)**. $S_{p,GCC}^{k,k_F}$ **(E–H)**. $S_{p,F}^{k,k_F}$. **(A)** zero Factors; **(B)** 1 Factor; **(C)** 2 Factors; **(D)** 3 Factors; **(E)** zero Factors; **(F)** 1 Factor; **(G)** 2 Factors; **(H)** 3 Factors.

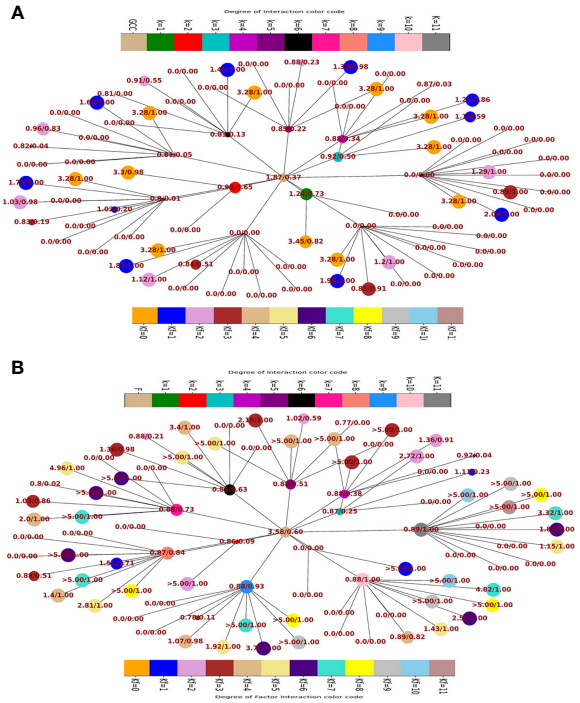


FIGURE 5
(A) Network plot of class wise fractional distribution of $S_{p,GCC}^{k,k_F}$ and corresponding odds ratio: node label = odds ratio of the fractional population in favour GCC interaction for the specific class '*k*' and subclass 'k_F'/fraction of population directed towards GCC for the specific class '*k*' and subclass 'k_F'. **(B)** Network plot of class wise fractional distribution of $S_{p,GCC}^{k,k_F}$ and corresponding odds ratio: node label = odds ratio of the fractional population in favour of F interaction for the specific class '*k*' and subclass 'k_F'/fraction of population directed towards F for the specific class '*k*' and subclass 'k_F'.

the specific class '*k*' and subclass 'k_F'. Kamada-kawai network plots for $S_{p,NHC}^{k,k_F} > 45°$ and the respective odds ratios in favour of NHC of the fractional population of CCMEN encapsulated nanoparticle directed towards NHC are provided as in database repository RDO_datasets. $E(x)_k$,s_p and $E(x)_k$,s_p for a particular *k* degree of interactions are given in Figure 6. The horizontal bar for $E(x)_k$,s_p represents the threshold ($E(x)_k$,$s_p \geq s_p$=45°) required propensity to be directed towards *x*-axis (cycled through GCC, NHC and F).

The distribution of resultant $E(x)_k$of $S_{p,k}$ towards GCC is portrayed in Figure 6C. resultant $E(x)_k$profile of $S_{p,k}$ towards NHC and F are provided in in database repository RDO_datasets. Ultimate directional preference (GCC, NHC, F and NNDP) of the CCMEN (Figure 5A, B). NNDP corresponds to the fraction of nanoparticles having no net directional preference (NNDP) and hence their fate is unpredictable. The GCC, NHC and F fraction of nanoparticle have a net directional preference towards the GCC, NHC and F respectively.

Discussion

This study and associated python tool were designed to determine the fraction of CCMEN directed towards the cancer cell (in this case GCC, NHC and extracellular Factors F). This was derived by implementing a probabilistic model (discussed in the methods section) based on the CBE of the of surface receptor proteins on CCMEN for GCC, NHC and F. Eq. 1 explains the derivation of CBE from BS. BS is multiplied with the expression fold change of the contributing (R-R or R-F) proteins having the lower fold change of the two interacting proteins. This magnify/reduce the BS as a function of expression level simultaneously keeping it within the bounds defined by the lower expression fold change. Three types of CBEs were derived: CBE for interaction of SP on CCMEN and GCC (input file: cmcc.csv), CBE for interaction of SP on CCMEN and NHC (input file: cmnc.csv) and CBE for interaction of SP on CCMEN and F (input file: cmf.csv). The probabilistic model reveals the BST and corresponding probabilities of all the possible ways (combinations) the CCMEN may interact with the GCC, NHC and/or F (model assumptions discussed before). Figure 2 highlight the probability distribution profile of CCMEN interaction with GCC, NHC and F. The distribution is mildly left skewed normal with peak at k=6. More than 80% of the exposed CCMEN population have protein interactions ranging from 5 to 8 surface receptors. It is interesting to note that the conditional probability (CP_k) for interaction of SP on CCMEN with GCC follows an inverse relationship with *k* (Figure 2). CP_k corresponds to the fractional population of CCMEN for a specific *k*. For $k \geq 5$ the fractional population directed towards Factors dominates over the fractional population targeting GCC. This point of intersection defined here as the Break-even point (BEP) corresponds to the first instance of $CP_{k,GCC}$ falling below either of the other two ($CP_{k,\ NHC}$ or $CP_{k,\ F}$). Higher is the value of BEP more is the fraction of CCMEN directed towards the cancer cells (in this case GCC). BEP ranges from 0 to *n*. Hence, BEP is hereby suggested as a critical scale for measurement of cancer cell targeting efficiency of CCMEN for given surface antigens (receptors).

Individual S_p for all the surface receptor proteins (except Tfr2 and ITGA2B, Table 1) on CCMEN are directed towards GCC. (Tfr2: towards NHC, and ITGA2B: no net directional preference, Figure 3A-C). However, a sharp contrast is observed in the directional preference of the CCMEN population obtained as a consequence of the real probabilistic picture (based on all possible combinations) from the probabilistic model. The dominant GCC directional preference of CCMEN fades away gradually when the $k \geq 5$ (Figures 3D–F). This may be accounted to the proportionally growing population of CCMEN interacting with the factors, with increasing "*k*". A detailed picture of the distribution of $S_{p,GCC}^{k,k_F}$ (Figures 4A–D) and $S_{p,F}^{k,k_F}$ (Figures 4E–H) reveals the effect of increasing factor interaction for all degrees of *k* ($1 \geq k \leq 11$, $k_F \leq 3$, distribution for $k_F \geq 4$ available in database repository RDO_datasets. It is obvious, that higher factor interactions are only possible at higher *k* values. It is important to note that the increase in the fractional population of CCMEN directed towards F (with increasing k_F) does not exactly correspond to the fractional loss of CCMEN population directed towards GCC. This fractional loss is distributed into three types of CCMEN population having different directional preferences. Type1: Directed towards F; Type2: Directed towards NHC (negligible in this case) and Type3: No Net directional preference (NNDP). CCMEN classified under NNDP

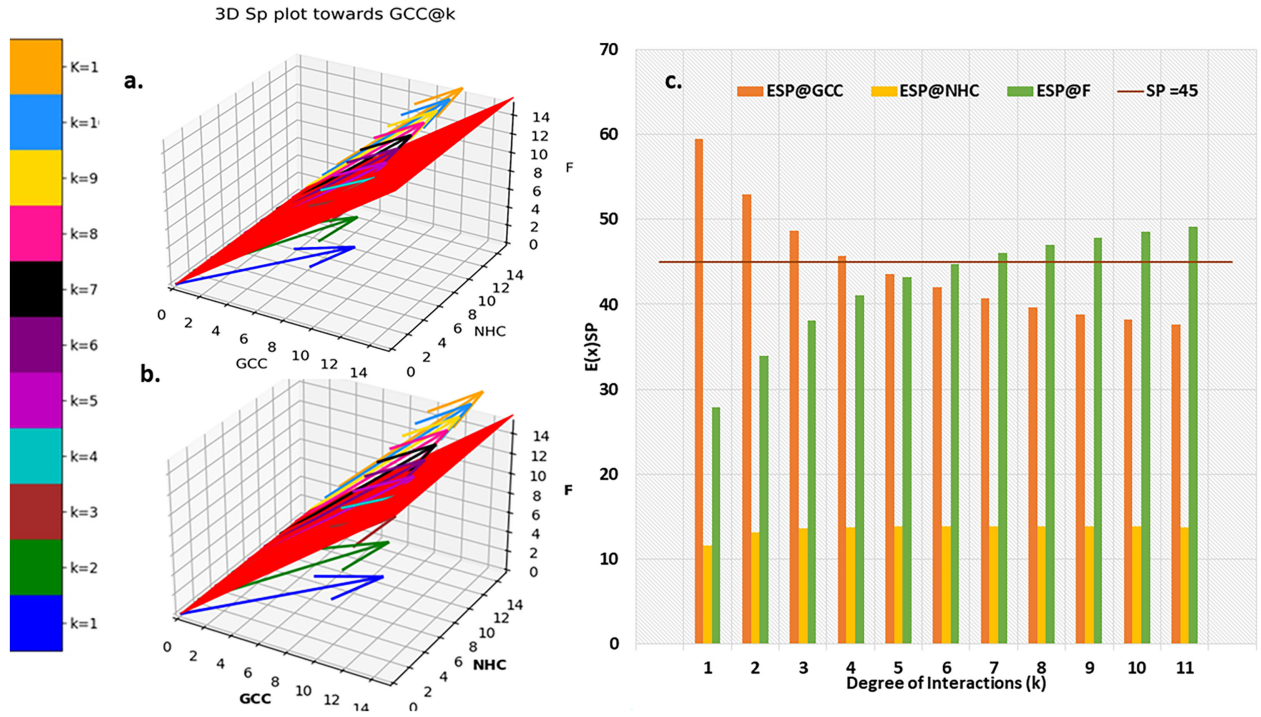


FIGURE 6
Probabilistic Expected Directional preference. **(A)** 3D S_p plot @k interactions towards **(B)** Resultant $E(x)_k$of $S_{p,k}$ **(C)** comparison of $E(x)_k$of $S_{p,k}$ for GCC, NHC and F.

category have almost equal propensities towards the three: GCC, NHC and F. $S^{k,k_F}_{p,GCC}$, $S^{k,k_F}_{p,F}$ and $S^{k,k_F}_{p,NHC}$ for CCMENs under NNDP are always < than the threshold 45° (red 2D plane) for all k and k_F values. As per the assumption no. 3 (refer to methods section: probabilistic model assumptions) NNDP population may be equally distributed among the three fates: GCC, NHC and F. In this case, NNDP population corresponds to 3% of the exposed CCMEN. GCC, NHC and F each will get an equal share of ~ 1%. This will be added up to the respective fractional population directed towards GCC, NHC and F derived from the model.

Kamada-kawai network plots (Figures 5A,B) reveal the fractional selective preference of each class (k: Intermediary nodes) and its corresponding subclass (k_F: Leaf Nodes). No direct proportionality is observed between odds ratio in favour of GCC and F interaction (nodes label: numerator; Figures 5A, B respectively) and fraction of population directed towards GCC and F (node labels: denominator; Figures 5A, B respectively). The fraction of CCMEN population directed towards GCC falls sharply as the degree of interaction increases. The odds ratio falls below 1 for $k_F \geq 3$ (for all k). The resultant conditional expected directional preference ($E(x)_k$of $S_{p,k}$ (refer to Methods section) for GCC (Figure 6B) exactly resemble the gross directional preference (Figure 6A). $E(x)_k$of $S_{p,k}$ for F increases gradually (as 'k' tends to 11) and jumps over the threshold (s_p=45°) for k≥6 (Figure 6C). Since the $E(x)_5$of $S_{p,5}$ for GCC, NHC and F falls short of the threshold this class (k =5) may be designated as the class with the highest NNDP population (Figure 6C). The overall odds ratio in favour of GCC interaction is almost double (1.87) for a CCMEN fractional population of 37% (directed towards GCC). This odds ratio prescribes a good fidelity of the selective preference of this fraction of population towards GCC. This population primarily corresponds to subclass $0 \geq k_F < 4$ (Figure 5A). 60% of the total exposed population of CCMEN is directed towards F with significantly high odds in favour of F interaction (3.58). This fraction of population primarily corresponds to subclass $5 \geq k_F < 11$ (Figure 5B). NHC appears to attract a negligible fraction of population (provided in database repository RDO_datasets). The present model has the following shortcomings, this model considers only three type of interactions **i.e** to GCC, NHC and Factors however in realistic scenarios there will be more interactions such as with certain immuno/inflammatory markers. The upcoming upgraded model will be more comprehensive and will include case specific interactions in addition to the present three dimensional. The upcoming model will be able to handle customised N-dimensional interactions. This model does not include Factor-Factor interactions. The upgraded model will be able to handle this type of interactions as well. As and when the model becomes more comprehensive in upcoming upgraded version it will be able to determine the net directional preference of more and more particle fraction thereby reducing the particles within NNDP fraction. The final prediction of the exposed CCMEN population (for Test culture type II, Figure 5A): GCC = 38% (37_{P_model} + 1_{NNDP})@Odds ratio in favour of GCC=1.87, NHC = 1% (0_{P_model} + 1_{NNDP}))@Odds ratio in favour of NHC=1.5 and F = 61% (60_{P_model} + 1_{NNDP}))@Odds ratio in favour of F=3.58. The model prediction for percentage/fraction of CCMEN (exposed) population directed towards GCC (for Test culture type I): GCC = 39% (39_{P_model} + 0_{NNDP}))@Odds ratio in favour of GCC=4.63, NHC = Absent in Test culture type I and F =

61% (61_{P_model} + 0_{NNDP})@Odds ratio in favour of F >5. Model predictions for test culture I were derived by supplying a zero matrix for NHC input file of CBE values (cmnc.csv). The fraction of CCMEN population directed towards GCC, F and NHC were determined experimentally as discussed in methods section (Experimental validation of model predictions: Eq 13). The model predictions lie within ±7% of the experimentally observed values for both (Test culture I and II). The probabilistic model efficiently predicts the directional preference of the nanoparticle population.

Conclusion

A probabilistic model based on binding scores and expression levels was implemented on python 3.9.1. The implemented probabilistic model efficiently predicted the directional preference (39%) of the exposed CCMEN towards Glioblastoma cancer cells. It is recommended to selectively include those surface antigen on the membrane encapsulated nanoparticles which enhance the value of BEP. Higher the value of BEP more is the fraction of CCMEN directed towards the Cancer cells. Present model may be applied to determine the directional preference of an entity (e.g Nanoparticle coated with cancer cell membrane) under the influence of three directional forces in three dimensions. However, upcoming versions will be able to deal with 'N' number of forces representing different attractive entities for Cancer cell membrane coated Nanoparticles in hyperspace.

Data availability statement

The original contributions presented in the study are included in the article/Supplementary Material. Further inquiries can be directed to the corresponding authors.

Author contributions

SaK developed the probabilistic model, and its assumptions, SaK and MK implemented the model in python, SS and SA performed necessary validation studies, MA and KA-M determined binding scores. ShK developed tailor designed nanoparticles for validation studies. All authors contributed to the article and approved the submitted version.

Funding

Deputy for Research & Innovation, Ministry of Education in Saudi Arabia (project number RDO-2002).

Acknowledgments

The authors extend their appreciation to the Deputy for Research & Innovation, Ministry of Education in Saudi Arabia for funding this research work through project number RDO-2002.

Conflict of interest

The authors declare that the research was conducted in the absence of any commercial or financial relationships that could be construed as a potential conflict of interest.

Publisher's note

All claims expressed in this article are solely those of the authors and do not necessarily represent those of their affiliated organizations, or those of the publisher, the editors and the reviewers. Any product that may be evaluated in this article, or claim that may be made by its manufacturer, is not guaranteed or endorsed by the publisher.

Supplementary material

The Supplementary Material for this article can be found online at: https://www.frontiersin.org/articles/10.3389/fimmu.2023.1162213/full#supplementary-material

References

1. Rosenblum D, Joshi N, Tao W, Karp JM, Peer D. Progress and challenges towards targeted delivery of cancer therapeutics. *Nat Commun* (2018) 9:1410. doi: 10.1038/s41467-018-03705-y

2. Kydd J, Jadia R, Velpurisiva P, Gad A, Paliwal S, Rai P. Targeting strategies for the combination treatment of cancer using drug delivery systems. *Pharmaceutics* (2017) 9 (4):46. doi: 10.3390/pharmaceutics9040046

3. Morales-Cruz M, Delgado Y, Castillo B, Figueroa CM, Molina AM, Torres A, et al. Smart targeting to improve cancer therapeutics. *Drug Des Devel Ther* (2019) 13:3753–72. doi: 10.2147/DDDT.S219489

4. Yoo J, Park C, Yi G, Lee D, Koo H. Active targeting strategies using biological ligands for nanoparticle drug delivery systems. *Cancers (Basel).* (2019) 11(5):640. doi: 10.3390/cancers11050640

5. Li R, He Y, Zhang S, Qin J, Wang J. Cell membrane-based nanoparticles: a new biomimetic platform for tumor diagnosis and treatment. *Acta Pharm Sin B* (2018) 8 (1):14–22. doi: 10.1016/j.apsb.2017.11.009

6. Harris JC, Scully MA, Day ES. Cancer cell membrane-coated nanoparticles for cancer management. *Cancers (Basel).* (2019) 11(12):1836. doi: 10.3390/cancers11121836

7. Jin J, Bhujwalla ZM. Biomimetic nanoparticles camouflaged in cancer cell membranes and their applications in cancer theranostics. *Front Oncol* (2020) 9:1560. doi: 10.3389/fonc.2019.01560

8. Rettig WJ, Chesa PG, Beresford HR, Feickert HJ, Jennings MT, Cohen J, et al. Differential expression of cell surface antigens and glial fibrillary acidic protein in human astrocytoma subsets. *Cancer Res* (1986) 46(12 Pt 1):6406–12.

9. Li YM, Hall WA. Cell surface receptors in malignant glioma. *Neurosurgery* (2011) 69(4):980–94. doi: 10.1227/NEU.0b013e318220a672

10. Kahlon KS, Brown C, Cooper LJ, Raubitschek A, Forman SJ, Jensen MC. Specific recognition and killing of glioblastoma multiforme by interleukin 13-zetakine redirected cytolytic T cells. *Cancer Res* (2004) 64:9160–6. doi: 10.1158/0008-5472.CAN-04-0454

11. Citri A, Yarden Y. EGF–ERBB signalling: towards the systems level. *Nat Rev Mol Cell Biol* (2006) 7(7):505–16. doi: 10.1038/nrm1962

12. Berezowska S, Schlegel J. Targeting ErbB receptors in high-grade glioma. *Curr Pharm design.* (2011) 17(23):2468–87. doi: 10.2174/138161211797249233

13. Boccaccio C, Comoglio PM. The MET oncogene in glioblastoma stem cells: implications as a diagnostic marker and a therapeutic target. *Cancer Res* (2013) 73 (11):3193–9. doi: 10.1158/0008-5472.CAN-12-4039

14. Wei X, Gao J, Zhan C, Xie C, Chai Z, Ran D, et al. Liposome-based glioma targeted drug delivery enabled by stable peptide ligands. *J Control. Release* (2015) 218:13–21. doi: 10.1016/j.jconrel.2015.09.059

15. Chai Z, Ran D, Lu L, Zhan C, Ruan H, Hu X, et al. Ligand-modified cell membrane enables the targeted delivery of drug nanocrystals to glioma. *ACS Nano.* (2019) 13(5):5591–601. doi: 10.1021/acsnano.9b00661

16. De Pasquale D, Marino A, Tapeinos C, Pucci C, Rocchiccioli S, Michelucci E, et al. Homotypic targeting and drug delivery in glioblastoma cells through cell membrane-coated boron nitride nanotubes. *Materials design.* (2020) 192:108742. doi: 10.1016/j.matdes.2020.108742

17. Khan M, Sherwani S, Khan S, Alouffi S, Alam M, Al-Motair K, et al. Insights into multifunctional nanoparticle-based drug delivery systems for glioblastoma treatment. *Molecules* (2021) 26(8):2262.

18. Markert JM, Fuller CM, Gillespie GY, Bubien JK, McLEAN LA, Hong RL, et al. Differential gene expression profiling in human brain tumors. *Physiol Genomics* (2001) 5(1):21–33. doi: 10.1152/physiolgenomics.2001.5.1.21

19. Freije WA, Castro-Vargas FE, Fang Z, Horvath S, Cloughesy T, Liau LM, et al. Gene expression profiling of gliomas strongly predicts survival. *Cancer Res* (2004) 64 (18):6503–10. doi: 10.1158/0008-5472.CAN-04-0452

20. Ghosh D, Funk CC, Caballero J, Shah N, Rouleau K, Earls JC, et al. A cell-surface membrane protein signature for glioblastoma. *Cell Syst* (2017) 4(5):516–29. doi: 10.1016/j.cels.2017.03.004

21. Edgar R, Domrachev M, Lash AE. Gene expression omnibus: NCBI gene expression and hybridization array data repository. *Nucleic Acids Res* (2002) 30 (1):207–10. doi: 10.1093/nar/30.1.207

22. Uhlén M, Fagerberg L, Hallström BM, Lindskog C, Oksvold P, Mardinoglu A, et al. Tissue-based map of the human proteome. *Science* (2015) 347(6220):1260419. doi: 10.1126/science.1260419

23. Weinstein JN, Collisson EA, Mills GB, Shaw KR, Ozenberger BA, Ellrott K, et al. The cancer genome atlas pan-cancer analysis project. *Nat Genet* (2013) 45(10):1113–20. doi: 10.1038/ng.2764

24. Berlow NE, Rikhi R, Geltzeiler M, Abraham J, Svalina MN, Davis LE, et al. Probabilistic modeling of personalized drug combinations from integrated chemical screen and molecular data in sarcoma. *BMC cancer.* (2019) 19:1–23. doi: 10.1186/s12885-019-5681-6

25. Altrock P, Liu L, Michor F. The mathematics of cancer: integrating quantitative models. *Nat Rev Cancer* (2015) 15:730–45. doi: 10.1038/nrc4029

26. Fang RH, Hu CM, Luk BT, Gao W, Copp JA, Tai Y, et al. Cancer cell membrane-coated nanoparticles for anticancer vaccination and drug delivery. *Nano letters.* (2014) 14(4):2181–8. doi: 10.1021/nl500618u

frontiers | Frontiers in Oncology

TYPE Original Research
PUBLISHED 30 March 2023
DOI 10.3389/fonc.2023.1097309

Check for updates

OPEN ACCESS

EDITED BY
Subhash Kumar Tripathi,
Seattle Children's Research Institute,
United States

REVIEWED BY
Desh Deepak Singh,
Amity University Rajasthan,
India
Deepak Parashar,
Medical College of Wisconsin,
United States
Himanshu Batra,
Harvard Medical School, United States

*CORRESPONDENCE
Bernardo L. Rapoport
brapoport@rosebankoncology.co.za

SPECIALTY SECTION
This article was submitted to
Breast Cancer,
a section of the journal
Frontiers in Oncology

RECEIVED 13 November 2022
ACCEPTED 09 March 2023
PUBLISHED 30 March 2023

CITATION
Rapoport BL, Steel HC, Benn CA, Nayler S, Smit T, Heyman L, Theron AJ, Hlatshwayo N, Kwofie LLI, Meyer PWA and Anderson R (2023) Dysregulation of systemic soluble immune checkpoints in early breast cancer is attenuated following administration of neoadjuvant chemotherapy and is associated with recovery of CD27, CD28, CD40, CD80, ICOS and GITR and substantially increased levels of PD-L1, LAG-3 and TIM-3.
Front. Oncol. 13:1097309.
doi: 10.3389/fonc.2023.1097309

COPYRIGHT
© 2023 Rapoport, Steel, Benn, Nayler, Smit, Heyman, Theron, Hlatshwayo, Kwofie, Meyer and Anderson. This is an open-access article distributed under the terms of the Creative Commons Attribution License (CC BY). The use, distribution or reproduction in other forums is permitted, provided the original author(s) and the copyright owner(s) are credited and that the original publication in this journal is cited, in accordance with accepted academic practice. No use, distribution or reproduction is permitted which does not comply with these terms.

Dysregulation of systemic soluble immune checkpoints in early breast cancer is attenuated following administration of neoadjuvant chemotherapy and is associated with recovery of CD27, CD28, CD40, CD80, ICOS and GITR and substantially increased levels of PD-L1, LAG-3 and TIM-3

Bernardo L. Rapoport [1,2,3*], Helen C. Steel [1], Carol A. Benn [3,4], Simon Nayler [3,5], Teresa Smit [2], Liezl Heyman [2], Annette J. Theron [1], Nomsa Hlatshwayo [1,6], Luyanda L.I. Kwofie [1,6], Pieter W.A. Meyer [1,6] and Ronald Anderson [1]

[1]Department of Immunology, Faculty of Health Sciences, University of Pretoria, Pretoria, South Africa, [2]Medical Oncology Centre of Rosebank, Johannesburg, South Africa, [3]Netcare Breast Care Centre, Johannesburg, South Africa, [4]Department of Surgery, Faculty of Health Sciences, University of the Witwatersrand, Johannesburg, South Africa, [5]Drs Gritzman & Thatcher Inc. Laboratories, University of the Witwatersrand Donald Gordon Medical Centre, Johannesburg, South Africa, [6]Department of Immunology, Tshwane Academic Division of the National Health Laboratory Service, Pretoria, South Africa

Neoadjuvant chemotherapy (NAC) may alter the immune landscape of patients with early breast cancer (BC), potentially setting the scene for more effective implementation of checkpoint-targeted immunotherapy. This issue has been investigated in the current study in which alterations in the plasma concentrations of 16 soluble co-stimulatory and co-inhibitory, immune checkpoints were measured sequentially in a cohort of newly diagnosed, early BC patients (n=72), pre-treatment, post-NAC and post-surgery using a Multiplex® bead array platform. Relative to a group of healthy control subjects (n=45), the median pre-treatment levels of five co-stimulatory (CD27, CD40, GITRL, ICOS, GITR) and three co-inhibitory (TIM-3, CTLA-4, PD-L1) soluble checkpoints were significantly lower in the BC patients vs. controls (p<0.021-p<0.0001; and p<0.008-p<0.00001, respectively). Following NAC, the plasma levels of six soluble co-stimulatory checkpoints (CD28, CD40, ICOS, CD27, CD80, GITR), all involved in activation of $CD8^+$ cytotoxic T cells, were significantly increased (p<0.04-p<0.00001), comparable with control values and remained at these levels post-surgery. Of the soluble co-inhibitory checkpoints, three (LAG-3, PD-L1, TIM-3) increased significantly post-NAC, reaching levels significantly greater

than those of the control group. PD-1 remained unchanged, while BTLA and CTLA-4 decreased significantly ($p<0.03$ and $p<0.00001$, respectively). Normalization of soluble co-stimulatory immune checkpoints is seemingly indicative of reversal of systemic immune dysregulation following administration of NAC in early BC, while recovery of immune homeostasis may explain the increased levels of several negative checkpoint proteins, albeit with the exceptions of CTLA-4 and PD-1. Although a pathological complete response (pCR) was documented in 61% of patients (mostly triple-negative BC), surprisingly, none of the soluble immune checkpoints correlated with the pCR, either pre-treatment or post-NAC. Nevertheless, in the case of the co-stimulatory ICMs, these novel findings are indicative of the immune-restorative potential of NAC in early BC, while in the case of the co-inhibitory ICMs, elevated levels of soluble PD-L1, LAG-3 and TIM-3 post-NAC underscore the augmentative immunotherapeutic promise of targeting these molecules, either individually or in combination, as a strategy, which may contribute to the improved management of early BC.

KEYWORDS

breast cancer, co-inhibitory checkpoints, co-stimulatory checkpoints, cytotoxic T cells, immunotherapy, immune dysregulation, neoadjuvant chemotherapy

Introduction

Notwithstanding the existence of profound immune dysregulation in advanced metastatic breast cancer (BC), it is now well recognized that early disease is also associated with both localized and systemic immune dysfunction (1–4). In the tumor microenvironment (TME), macrophages of the M2-like immunosuppressive phenotype appear to predominate (5–7), where they effectively exclude cytotoxic $CD8^+$ T cells from reaching their tumor targets (8). In the case of systemic immunosuppression in early BC, prominent mechanisms include decreased numbers and/or activation of conventional dendritic cells (1, 3, 4), as well as increased numbers of monocytes with an M2-like phenotype (6, 9).

Recently, soluble co-inhibitory immune checkpoint molecules (ICMs) have been implicated as being potential mediators of the systemic immune dysregulation, which is associated with certain types of malignancy (10, 11). Prominent among these soluble co-inhibitory ICMs are: i) cytotoxic T-lymphocyte-associated protein (CTLA-4); ii) programmed cell death protein 1 (PD-1) and its ligand, PD-L1; iii) lymphocyte activation gene 3 (LAG-3); and iv) T cell immunoglobulin and mucin-domain-containing protein 3 (TIM-3) (12). On the other hand, less is known about alterations in the systemic levels of co-stimulatory ICMs measured prior to and following treatment of various types of malignancy. Although the origins of soluble systemic ICMs remain unclear, leakage from the TME seems plausible. In this setting, soluble co-inhibitory ICMs may originate from tumor cells *per se*, as well as from structural cells such as cancer-associated fibroblasts and cells of the innate and adaptive immune systems recruited to the TME (13, 14). Soluble variant isoforms of the ICMs, which lack transmembrane domains, may arise from alternative RNA splicing, or, alternatively, by proteolytic detachment from cell membranes (10, 12). Importantly, soluble co-inhibitory ICMs appear to retain their biological activities (10, 12).

In the setting of early BC, neoadjuvant chemotherapy (NAC) preceding surgical excision of residual tumor tissue remains a cornerstone of the treatment of this malignancy and strategies to improve the clinical efficacy and safety of this pre-operative procedure are ongoing, including evaluation of the combination of co-inhibitory PD-L1-targeted immunotherapy with chemotherapy (15). Notably, however, the involvement of the various types of soluble ICMs as potential contributors to systemic immune dysregulation in early BC remains largely unexplored, as does the role of NAC and subsequent surgical resection in alleviating cancer-related immune dysfunction.

In accordance with our primary hypothesis, we have therefore compared the plasma concentrations of eight co-stimulatory, six co-inhibitory, and two dual-active ICMs in a cohort of early BC patients with those of a group of healthy control subjects, as well as the effects of NAC and surgery on the plasma levels of these immunoregulatory proteins. This is a follow-up to our previous study in which we reported that the plasma levels of a number of systemic soluble co-stimulatory and co-inhibitory ICMs were significantly decreased in a cohort of early BC patients relative to those of healthy controls, indicative of tumor-related immune dysregulation (16).

Patients and controls

Seventy-two female patients of the original cohort (n=98) (16) with early BC attending the Medical Oncology Centre of Rosebank, Johannesburg, South Africa, who had completed treatment (NAC) and surgery were deemed eligible for recruitment to the study. Eligibility criteria included: i) age ≥18 years; ii) Eastern Cooperative

Oncology Group (ECOG) performance status (PS) of 0, 1, or 2; iii) histologically confirmed BC (17) classified as clinical stage I, II or III according to the AJCC Breast Staging 8th Edition (18); iv) normal bone marrow, liver and renal function; v) NAC with anthracycline (A) and/or a taxane (T)-based chemotherapy regimen. Human epidermal growth factor receptor 2 (Her2) -positive patients received neoadjuvant trastuzumab-based treatment.

Exclusion criteria were as follows: i) prior systemic chemotherapy for BC within five years; ii) a history of any other malignancy during the preceding five years, with the exception of basal cell or squamous cell carcinoma of the skin treated with local resection only, as well as carcinoma *in situ* of the cervix; iii) patients with confirmed stage IV disease; iv) known seropositivity for human immunodeficiency virus (HIV) and/or hepatitis B or hepatitis C viruses; v) uncontrolled intercurrent illness including, but not limited to, active infection, symptomatic congestive heart failure, unstable angina pectoris, cardiac arrhythmia or psychiatric illness/social situations that would limit compliance with study requirements; vi) pregnancy or breast feeding; and vii) otherwise not deemed to be a good study candidate according to the sole discretion of the principal investigator (BLR).

The group of healthy female control participants (n=45, mean age = 49.9 years; range 24–70 years) was recruited almost exclusively from the female personnel of the Medical Oncology Centre of Rosebank and the Faculty of Health Sciences, University of Pretoria. Exclusion criteria included: i) those with uncontrolled medical conditions; and ii) any potential participant deemed unwell by the qualified nursing sister in attendance on the day of venepuncture. Immunohistochemical staining was performed for ER, PR, Her2, and Ki67. Fluorescence *in situ* hybridization (FISH) was used to confirm Her2 positivity. Clinical assessment of the primary tumor and lymph nodes was done using bi-dimensional caliper measurements of the primary tumor and axillary nodes. The lymph node positivity at presentation was assessed clinically, radiologically, or by sentinel lymph node biopsy. Sonographic assessments of the primary tumor and lymph nodes were performed regularly. The pathological complete response (pCR) was defined as the complete disappearance of invasive cancer in the breast and the absence of tumor cells in the axillary lymph nodes.

Ethics committee clearance

Permission to undertake this study and to draw blood from patients with early BC and from matched, healthy control subjects was granted by the Research Ethics Committee of the Faculty of Health Sciences, University of Pretoria, in full compliance with the World Medical Association Declaration of Helsinki 2013. Two submissions were approved: firstly, the BC study, and secondly, a submission in respect of the healthy control subjects (respective Approval Numbers 517/2017 and 762/2020). Prior, written informed consent was obtained from all participants.

Methods

Whole blood samples of 20 mL and 10 mL volumes were collected in ethylenediaminetetraacetic acid (EDTA)-containing vacutainers from the BC patients and control subjects, respectively, and the plasma promptly separated, aliquoted and stored at -80°C until the plasma concentrations of the various soluble co-inhibitory and co-stimulatory immune checkpoints were measured.

Soluble immune checkpoints

A Human Immuno-Oncology Checkpoint Protein Panel (Milliplex® MAP Kit, Merck, KGaA, Darmstadt, Germany; catalogue number HCKP1-11K-PX17) was used to simultaneously determine the plasma concentrations of 16 soluble immune checkpoint molecules namely, cluster of differentiation (CD)27, CD28, CD40, CD80, CD86, glucocorticoid-induced tumor necrosis factor receptor family-related protein (GITR) and its ligand GITRL, inducible T cell costimulator (ICOS), B and T lymphocyte attenuator (BTLA), herpes virus entry mediator (HVEM), Toll-like receptor (TLR)-2, CTLA-4, PD-1, PD-L1, LAG-3 and TIM-3. All reagents were provided by the manufacturer and the experimental protocol was followed as per the manufacturer's instructions. Briefly, plasma samples were thawed at room temperature and diluted at a ratio of 1:2 in assay buffer provided. Diluted plasma samples, standards and controls (25 µL) were added to the appropriately designated wells followed by the addition of the conjugated beads (25 µL). The plate was sealed with a foil cover and incubated for two hours at room temperature (25°C) with gentle agitation.

Following the incubation period, the plate was washed three times with 200 µL wash buffer using a Bio-Plex Pro Wash Station Magnetic Plate Washer (Bio-Rad Laboratories Inc., Hercules, CA, USA). Thereafter, 25 µL of detection antibodies were added to each well. The plate was sealed and incubated as described above for one hour at 25°C. This was followed by the addition of 25 µL streptavidin-phycoerythrin to each well. The plate was sealed again and incubated for a final 30 minutes as described above. The plate was then washed a further three times with 200 µL wash buffer. Sheath fluid (150 µL) was added to all wells and the beads were resuspended on a plate shaker for two minutes prior to being assayed on a Bio-Plex Suspension Array platform (Bio-Rad Laboratories Inc., Hercules, CA, USA). Bio-Plex Manager software 6.0 was used for bead acquisition and analysis of median fluorescence intensity. The results are reported as picograms (pg)/milliliter (mL) plasma.

Pathological complete response

As mentioned above, the pCR was defined as the complete disappearance of invasive cancer in the breast and the absence of tumor in the axillary lymph nodes.

Statistical analysis

The primary hypothesis was that significant differences exist in the plasma levels of soluble ICMs of newly diagnosed, early BC

patients measured pre-treatment, post-NAC and post-surgery. Data, presented as the median values with 95% confidence intervals, was prospectively obtained and levels of ICMs measured at the different stages of treatment were compared in the cohort of BC patients, as well as with those of healthy controls using the non-parametric Mann-Whitney U-test. Descriptive statistics were used to tabulate patient characteristics. A p value of < 0.05 was considered statistically significant. The area under the receiver-operating curve (AUC) was used as a measure of the discriminatory abilities of the soluble ICMs. The Youden index, a summary measure of the receiver -operating curve (ROC), was used as an agnostic method for choosing an optimal cut-off value on the biomarker value to illustrate potential clinical usefulness. NCSS software version 11 for Windows (USA) was used for statistical analyses.

Results

Patient demographics, breast cancer subtypes

The plasma levels of soluble ICMs were measured in 72 patients with early BC receiving NAC. Patient characteristics are summarized in Table 1. The patients had a median age of 54 years (range 29 – 85 years), of which 63.9% were post-menopausal, 34.7% pre-menopausal and 1.4% peri-menopausal. The predominant biological subtype was triple -negative BC (TNBC) (70.8%), with the remaining subtypes being Her2- positive (13.9%), luminal-A (1.4%) and luminal-B (12.5%). One patient had TNBC and luminal-B (1.4%). The tumor size was classified as follows: T1 patients (29.2%), T2 patients (58.3%), T3 patients 8.3% and T4 patients 4.2%. Half of the patients had nodal involvement (50%).

Soluble immune checkpoints

Comparisons between the plasma concentrations of the soluble co-stimulatory, co-inhibitory and dual ICMs for: i) the cohort of BC patients prior to initiation of NAC relative to those of the healthy control subjects; and ii) pre-treatment versus post-NAC are shown in Tables 2, 3, respectively, with the results expressed as the median values with 95% confidence limits. With respect to comparisons, the pre-treatment plasma concentrations of the soluble ICMs for the cohort of BC patients relative to those of the healthy control subjects, all of these were either significantly or numerically decreased, as reported previously (16). In the case of the eight soluble co-stimulatory ICMs, five of these, CD27, CD40, ICOS, GITR and GITRL, were significantly decreased (p<0.021-p<0.0001), while CD28, CD80 and CD86, were numerically decreased, but not significantly so (Table 2). Of the six co-inhibitory ICMs, three, namely CTLA-4, PD-L1 and TIM-3, were significantly decreased (p<0.008-p<0.00001) in the group of BC patients, while BTLA, LAG-3 and TIM-3 were numerically, but not significantly decreased. Of the two dual-active soluble ICMs, both HVEM and TLR-2 were lower in the group of BC patients, with only the former attaining statistical significance (p<0.0004).

TABLE 1 Demographic and clinical data of the cohort of newly diagnosed early breast cancer patients.

Patient Characteristics		
Age		
Median	54 years	
Range	29 - 85 years	
Menopausal Status		
Post-menopausal	46	63.89%
Pre-menopausal	25	34.72%
Peri-menopausal	1	1.39%
Grade		
1	1	1.39%
2	20	27.78%
3	49	68.06%
Unknown	2	2.78%
Tumor Size		
T1	21	29.17%
T2	42	58.33%
T3	6	8.33%
T4	3	4.17%
Nodal Status		
Positive	36	50.00%
Negative	36	50.00%
Stage		
1	12	16.67%
2A	32	44.44%
2B	20	27.78%
3	8	11.11%
Biological Type		
Her2 Positive	10	13.89%
Luminal A	1	1.39%
Luminal B	9	12.50%
TNBC	51	70.83%
TNBC & Luminal B	1	1.39%
Ki-67		
≤ 14%	3	4.17%
15 - 39%	23	31.94%
≥ 40%	45	62.50%
Unknown	1	1.39%

As shown in Table 3, following NAC, the plasma concentrations of six of the soluble co-stimulatory ICMs (CD27, CD28, CD40, CD 80, ICOS, and GITR increased significantly (p<0.04-p<0.00001) to

levels comparable with those of the control group, while GITRL was essentially unchanged and CD86 numerically lower. Of the soluble co-inhibitory ICMs, the plasma concentrations of three of these molecules (PD-L1, LAG-3, TIM-3) increased significantly (all $p<0.00001$) (Table 3). Levels of PD-1 remained similar to pre-treatment levels, while those of BTLA and CTLA-4 were significantly lower ($p<0.03$ and $p<0.00001$, respectively) (Table 3). Of the two dual-active soluble ICMs, the plasma concentrations of TLR-2 and HVEM increased significantly post-NAC ($p<0.02$ and $p<0.00001$, respectively) relative to pre-treatment values.

Notably, as shown in Table 4, the post-NAC plasma levels of PD-L1 and those of LAG-3 and TIM-3 in particular, were also significantly higher than those of the control group (percentage increases of 43.5, 209% and 97.6% for PD-L1, LAG-3 and TIM-3, respectively), with the levels of HVEM also being significantly higher (77%) than those of the control group (Table 4).

As shown in Table 5, on completion of NAC, no further statistically significant increases in the plasma concentrations of any of the 16 soluble ICMs were detected following surgical resection of residual tumor tissue. This observation seemingly indicates that NAC is the primary driver of alterations in the plasma levels of both co-stimulatory and co-inhibitory ICMs in our cohort of early BC patients.

Graphical representations depicting the progressive changes in the median plasma concentrations of each of the 16 ICMs throughout the course of NAC (pre-treatment, post-NAC and post-surgery) in relation to the corresponding median values of the control subjects are shown in Figure 1 (CD27, CD80, ICOS, GITR) and Figure 2 (LAG-3, PD-L1, TIM-3), and Supplementary Figure 1 (CD28, CD40, CD86, GITRL), Supplementary Figure 2 (BTLA, CTLA-4, PD-1) and Supplementary Figure 3 (TLR-2, HVEM).

Response to neoadjuvant chemotherapy

Patients received taxane and/or anthracycline/alkylating agent-based NAC. Patients who tested positive for Her2 also received trastuzumab. There were 44 pCRs (61%) in the entire cohort. The pCR rates for Her2-positive disease, luminal disease and TNBC were 80%, 30% and 65%, respectively. An example of a patient who attained a pCR is shown in Supplementary Figures 4–6. None of the soluble ICMs was predictive or prognostic for pCR in this patient cohort. Patients were recruited between 24 Jan 2018 to 18 Sep 2019. Follow-up continued, and the database was updated for this analysis until January 2020. Five patients relapsed, and one died at a median follow-up of 364 days (79 to 643). The progression-free survival (PFS) and overall survival (OS) data will be reported separately at maturity.

Discussion

In a forerunner to the current study, we recently reported that the plasma concentrations of a large group of soluble ICMs, comprising both co-stimulatory and co-inhibitory proteins, were significantly decreased in treatment-naïve, newly-diagnosed patients with early BC (n=98), relative to those of a cohort of healthy control subjects (n=45) (16). The current study is a follow-up to our earlier investigation and was designed to explore the immune-restorative potential of implementation of NAC and subsequent surgical resection of residual tumor tissue in the same, albeit somewhat smaller, cohort of early BC patients who completed both NAC and surgery (n=72). In terms of realization of our primary objectives, the following represent the most significant and novel findings: i) the plasma concentrations of five soluble co-stimulatory ICMs (CD27, CD40, GITRL, ICOS, GITR) were significantly lower than those of the control group pre-treatment, while those of CD28, CD80 and CD86 were numerically decreased, but not significantly so; ii) post-NAC, the plasma concentrations of six soluble co-stimulatory immune checkpoints (CD27, CD28, CD40, CD80, ICOS, GITR), all of which are involved in the activation of anti-tumor cytotoxic T cells (12), normalized; iii) recovery of the plasma levels of these six ICMs remained essentially unchanged following surgical resection; iv) the levels of three soluble co-inhibitory ICMs (PD-L1, LAG-3 and TIM-3) were also significantly lower in the cohort of early BC patients and increased significantly in magnitude relative to pre-treatment levels post-NAC, with no further augmentation post-surgery. Notably, and somewhat concerningly, the plasma levels of these three co-inhibitory ICMs were significantly higher, especially in the case of LAG-3 and TIM-3, than those of the control group.

Of the other soluble co-inhibitory ICMs, BTLA and CTLA-4 did not respond to NAC, remaining significantly decreased relative to their pre-treatment values, while the median level of soluble PD-1, which was comparable in both groups, remained unchanged. In the case of the persistently low levels of soluble CTLA-4, it is noteworthy that taxane has been reported to deplete the numbers of regulatory T cells (Tregs), a major cellular source of this ICM (19). However, further follow-up studies are necessary to establish if soluble CTLA-4 levels increase over time. Of the two dual-active soluble ICMs, the pre-treatment level of HVEM was significantly lower than that of the corresponding median control value, recovering post-NAC to values, which were considerably higher than those of the control group. In the case of soluble TLR-2, the median pre-treatment value for this dual-active ICM was comparable with that of the control group, increasing modestly, albeit significantly, post-NAC.

With respect to potential mechanisms that contribute to the increased systemic concentrations of the six soluble co-stimulatory ICMs following implementation of NAC in our cohort of early BC patients, it is noteworthy that the components of NAC, namely anthracycline, taxane, cyclophosphamide and platinum-based agents, are all effective inducers of immunogenic cell death, a process which restores anti-tumor immunity in the TME (20, 21). In this context, our findings are somewhat similar to a recently published study by Dong et al. (22). These authors reported that administration of the immunomodulatory agent, sorafenib, to patients with advanced hepatocellular carcinoma (n=53) resulted in significant increases in the median plasma concentrations of 11/16 of the soluble co-inhibitory and co-stimulatory ICMs tested, an effect which was evident after two weeks of therapy. Differences between our study and that of Dong et al., include the types of

TABLE 2 Comparison between newly diagnosed early breast cancer patients and control subjects with respect to the plasma concentrations of the soluble co-stimulatory, co-inhibitory and dual-activity immune checkpoints.

	ICM	Breast Cancer newly diagnosed (n=72)	Controls (n=45)	*p* value
		Median pg/mL (95%CI)	Median pg/mL (95%CI)	
Co-stimulatory	CD27	3342.45	4577.35	0.0243
		(2808.61 – 4107.68)	(3391.13 – 5784.85)	
	CD28	32914.45	46135.18	0.1248
		(29326.90 – 42636.04)	(27210.29 – 67544.10)	
	CD40	1523.32	1977.68	0.0210
		(1298.16 – 1777.45)	(1404.82 – 2569.56)	
	ICOS	15123.78	26506.65	0.0087
		(12471.47 – 19942.11)	(15897.52 – 31725.99)	
	GITR	1497.40	3797.68	0.0001
		(1053.33 – 1969.52)	(1993.96 – 5396.86)	
	GITRL	5886.13	7151.12	0.0199
		(4959.23 – 6681.22)	(5528.36 – 9878.41)	
	CD86	11585.17	14297.09	0.1734
		(9938.61 – 14646.29)	(9391.46 – 20525.14)	
	CD80	1678.33	2329.77	0.0735
		(1422.82 – 2039.65)	(1395.01 – 3042.87)	
Co-inhibitory	PD-1	12305.41	14917.48	0.5158
		(10260.08 – 15798.61)	(7874.92 – 21795.02)	
	PD-L1	1647.14	3342.62	0.0001
		(1269.54 – 2228.88)	(2628.64 – 4750.96)	
	CTLA-4	1566.38	2618.23	0.0079
		(1314.46 – 1890.81)	(1578.44 – 3110.47)	
	TIM-3	3897.66	5046.87	0.0005
		(3169.51 – 4330.5)	(4732.72 – 5958.87)	
	LAG-3	131275.90	150416.00	0.5868
		(106666.3 – 156881.5)	(94508.53 – 187997.2)	
	BTLA	13021.75	18147.26	0,2349
		(10277.82 – 18548.68)	(11461.86 – 25180.69)	
Dual	TLR-2	26831.35	30477.20	0,1806
		(21172.10 – 32396.97)	(20928.44 – 50302.64)	
	HVEM	1865.22	2290.19	0,0004
		(1671.15 – 2038.38)	(2079.46 – 2618.44)	

malignancy investigated, as well as types and duration of anticancer therapy; another notable difference between the two studies relates to the apparent absence of a group of healthy control subjects in the study reported by Dong et al. (22).

Given that the increases in the median plasma concentrations of the soluble co-stimulatory ICMs, together with associated clinical improvement in our BC patient cohort, may be linked to immunogenic cell death induced by NAC, the corresponding increases in the levels of the soluble co-inhibitory ICMs, PD-L1, LAG-3 and TIM-3, relative to those of the control group, do seem somewhat counterintuitive. Although this may relate to restoration of a balance in immune homeostasis, the unexpectedly high increases in the plasma levels of these co-inhibitory ICMs may, however, compromise the efficacy of therapeutic monoclonal

TABLE 3 Comparison of the concentrations of the soluble co-stimulatory, co-inhibitory and dual-activity immune checkpoints measured in the plasma of the cohort of early breast cancer patients before and after implementation of neoadjuvant chemotherapy (NAC).

	ICM	Breast Cancer newly diagnosed (n=72)	Post-NAC (n=72)	*p* value
		Median pg/ml (95%CI)	Median pg/ml (95%CI)	
Co-stimulatory	CD27	3342.45	5351.47	0.0001
		(2808.61 – 4107.68)	(4678.25 - 5894,.7)	
	CD28	32914.45	44277.76	0.0416
		(29326.90 – 42636.04)	(38319.44 – 51220.42)	
	CD40	1523.32	2030.72	0.0003
		(1298.16 – 1777.45)	(1792.5 – 2199.04)	
	ICOS	15123.78	26586.28	0.0002
		(12471.47 – 19942.11)	(20912.88 – 31335.04)	
	GITR	1497.40	4035.98	0.0001
		(1053.33 – 1969.52)	(3198.29 – 5204.35)	
	GITRL	5886.13	5339.99	0.8044
		(4959.23 – 6681.22)	(4728.24 – 6121.00)	
	CD86	11585.17	9922,61	0,2789
		(9938.61 – 14646.29)	(7890.94 – 11990.77)	
	CD80	1678.33	3048,74	0.0001
		(1422.82 – 2039.65)	(2522.82 – 3520.25)	
Co-inhibitory	PD-1	12305.41	13350.55	0.7859
		(10260.08 – 15798.61)	(10537.37 – 15491.33)	
	PD-L1	1647.14	4794.97	0.0001
		(1269.54 – 2228.88)	(4162.41 – 5731.71)	
	CTLA-4	1566.38	598,20	0.0001
		(1314.46 – 1890.81)	(472.91 – 768.78)	
	TIM-3	3897.66	9975.90	0.0001
		(3169.51 – 4330.5)	(8793.62 – 10515.70)	
	LAG-3	131275.90	464880.70	0.0001
		(106666.3 – 156881.5)	(309218.5 – 580137.6)	
	BTLA	13021.75	9987.98	0.0367
		(10277.82 – 18548.68)	(8255.35 – 12554.33)	
Dual	TLR-2	26831.35	33837.86	0.0258
		(21172.1 – 32396.97)	(28228.61 - 39571,02)	
	HVEM	1865.22	4047.29	0.0001
		(1671.15 – 2038.38)	(3610.92 – 4445.29)	

antibodies (mAbs). In this context, it is noteworthy that persistently elevated plasma levels of soluble LAG-3 and TIM-3, like PD-L1, are associated with decreased survival in patients with various types of advanced malignancies (23–26).

Current approaches in the treatment of early BC include NAC, which in the case of TNBC in particular, may also incorporate PD-1/PD-L1 blockading mAbs as mentioned above (15). Against this background, two recently published, randomized, placebo-controlled clinical trials in early TNBC are noteworthy, namely the IMpassion031(n=333 patients) and KEYNOTE-522 (n=1174 patients) trials, which evaluated the clinical efficacy of addition of co-inhibitory ICM-targeted immunotherapy with either atezolizumab (PD-L1-targeted mAb) or pembrolizumab (PD-1-targeted mAb) in combination with NAC, relative to that of

TABLE 4 Comparison of the plasma concentrations of the soluble co-inhibitory immune checkpoints, PD-L1, LAG-3 and TIM-3 and the soluble dual-activity checkpoint, HVEM, measured in the group of healthy control subjects and the cohort of early breast cancer patients post-neoadjuvant chemotherapy (NAC).

Checkpoint (pg/ml)	Controls (n=45)	Breast cancer patients post-NAC (n=72)	*p* value
PD-L1	3343 (2268.64-4750.96)*	4795 (4162.41-5731.71)	0.0010
LAG-3	150416 (94508.3-187997.2)	464881 (309218.5-580137.6)	0.00001
TIM-3	5047 (4732.72-5958.87)	9976 (8793.62-10515.70)	0.00001
HVEM	2290 (2079.46-2618.44)	4047 (3610.92-4445.29)	0.00001

*Results are expressed as the median values (95% CI).

placebo + NAC, respectively (27, 28). The authors reported significantly improved pCR responses and event-free survival rates, irrespective of tumor PD-L1 positivity, in the Impassion031 and KEYNOTE-522 clinical trials, respectively (27, 28). These observations have been confirmed in two recent systematic reviews and meta-analyses. The first of these, which encompassed six randomized controlled trials focused on early TNBC (n=2142 patients), reported that NAC in combination with PD-1/PD-L1 inhibitors also resulted in improved pCR rates and event-free survival (29). The second included eight randomized controlled trials, encompassing 4901 patients with both early and metastatic TNBC (four trials in each category) (30). The authors of this study

TABLE 5 Comparison of the plasma concentrations of the soluble co-stimulatory, co-inhibitory and dual-activity immune checkpoints measured in the plasma of the cohort of early breast cancer patients post-NAC and post-surgery.

	ICM	Post-NAC (n=72)	Post-Surgery (n=72)	*p* value
		Median pg/mL (95%CI)	Median pg/mL (95%CI)	
Co-stimulatory	CD27	5351.47	5427.68	0.8105
		(4678.25 – 5894.37)	(4411.67 – 6317.06)	
	CD28	44277.76	50058.18	0.5705
		(38319.44 – 51220.42)	(34830.52 – 64706.44)	
	CD40	2030.72	2054.12	0.6203
		(1792.50 – 2199.04)	(1820.74 – 2383.79)	
	ICOS	26586.28	29746.46	0.3751
		(20912.88 – 31335.04)	(24270.58 – 33438.89)	
	GITR	4035.98	4434,89	0.9777
		(3198.29 – 5204.35)	(3354.37 – 6046.58)	
	GITRL	5339.99	5927.89	0.5226
		(4728.24 – 6121.00)	(4860.76 – 7008.59)	
	CD86	9922.61	12439.80	0.2276
		(7890.94 – 11990.77)	(9566.36 – 14837.24)	
	CD80	3048.74	3611.23	0.6459
		(2522.82 – 3520.25)	(2754.67 – 4138.41)	
Co-inhibitory	PD-1	13350.55	15076.64	0.3102
		(10537.37 – 15491.33)	(12077.71 – 19383.37)	
	PD-L1	4794.97	5215.05	0.8667
		(4162.41 – 5731.71)	(4239.88 – 5969.17)	
	CTLA-4	598.20	687.76	0.8292
		(472.91 – 768.78)	(550.45 – 828.91)	
	TIM-3	9975.90	9615.77	1.0000

(Continued)

TABLE 5 Continued

	ICM	Post-NAC (n=72)	Post-Surgery (n=72)	*p* value
		Median pg/mL (95%CI)	Median pg/mL (95%CI)	
		(8793.62 – 10515.70)	(8440.15 – 10984.92)	
	LAG-3	464880.70	500133.40	0.5992
		(309218.5 – 580137.6)	(466624.6 – 500748.6)	
	BTLA	9987.98	12777.20	0.3217
		(8255.35 – 12554.33)	(9507.29 – 15003.63)	
Dual	TLR-2	33837.86	37042.86	0.7782
		(28228.61 - 39571.02)	(29069.20 – 45880.29)	
	HVEM	4047.29	3950.36	0.6259
		(3610.92 – 4445.29)	(3611.92 – 4381.72)	

reported improved OS and PFS in patients treated with immunotherapy together with chemotherapy relative to those treated with chemotherapy alone (30). Taken together, these various studies are consistent with a beneficial, immune-restorative interaction between NAC and co-inhibitory ICM-targeted immunotherapy.

Although these and other studies document significant advances that have been made in treating TNBC patients (27–37), the magnitude of this benefit, as well as long-term survival, do, however, remain relatively low. Moreover, most of the clinical research in the field of immunotherapy has been focused on targeting PD-L1. Limitations of our study include sample size, diversity of BC subtypes and data collected from a single institution. Moreover, different therapeutic PD-1/PD-L1 therapeutic monoclonal antibodies require different companion tests. Some assays involve determination of PD-L1 levels on the tumor cells, some on immune cells and some on both cell types. An additional caveat is that only PD-L1 is extensively used in clinical practice. Problematically, however, some tumor types respond to immunotherapy independently of PD-L1 expression. Clearly, additional research of the type described in the current study, investigating additional checkpoints and additional pathways is

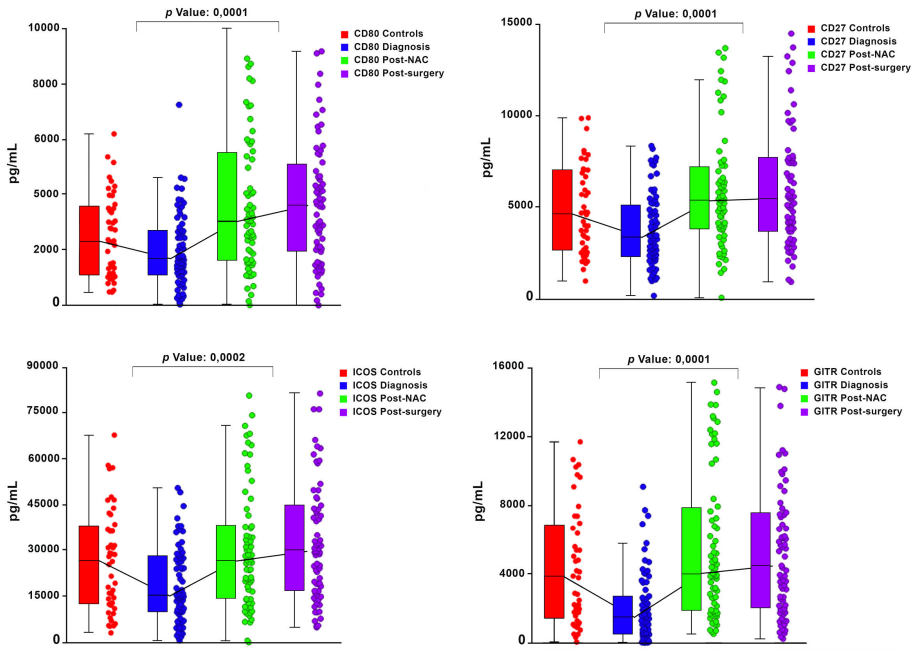


FIGURE 1
Box and whisker plots depicting the progressive changes in the median plasma concentrations (with 95% confidence limits) of four co-stimulatory immune checkpoints (CD27, CD80, ICOS and GITR) throughout the course of neoadjuvant chemotherapy (NAC) (pre-treatment/diagnosis, post-NAC and post-surgery) in relation to the corresponding median values of the control subjects. The *p* values represent the comparison between the pre-treatment/diagnosis and post-NAC values.

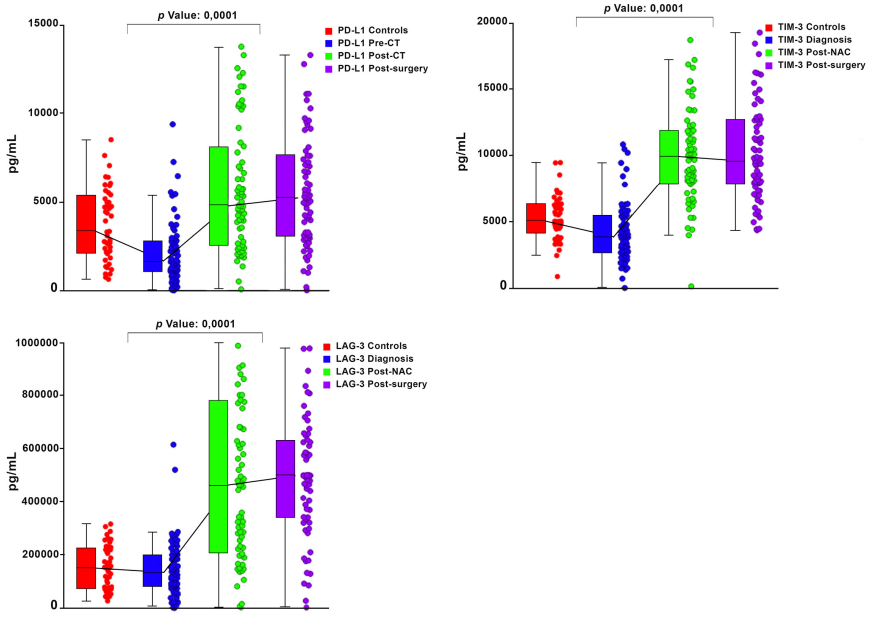


FIGURE 2
Box and whisker plots depicting the progressive changes in the median plasma concentrations (with 95% confidence limits) of three co-inhibitory immune checkpoints (PD-L1, TIM-3 and LAG-3) throughout the course of neoadjuvant chemotherapy (NAC) (pre-treatment/diagnosis, post-NAC and post-surgery) in relation to the corresponding median values of the control subjects. The *p* values represent the comparison between the pre-treatment/diagnosis and post-NAC values.

required to improve long-term outcomes. These include discerning insights into the mechanisms of resistance against immune checkpoint blockade and the cell types involved, as well as the identification of novel, reliable targets and biomarkers to predict responsiveness to treatment. Importantly, the results of the present study indicate, that co-inhibitory ICMs other than PD-L1, specifically LAG-3 and TIM-3, are also prominent in early BC patients following implementation of NAC and should therefore be considered as potential targets for future investigation in these patients as an adjunctive strategy to improve outcomes.

Conclusions

We previously described a state of systemic immune quiescence and immune dysregulation in patients with early BC, which was associated with decreased levels of soluble co-stimulatory and co-inhibitory ICMs. In the current follow-up study, we focused on the effect of NAC and surgery on the levels of these various ICMs. Novel findings originating from the current study include substantial increases in the levels of the majority of the soluble ICMs post-NAC, which did not change significantly post-surgery. Improvement in the levels of six of the co-stimulatory ICMs is indicative of immune- restoration, as all of these are involved in the activation of anti-tumor cytotoxic T cells. In the case of the co-inhibitory ICMs, we observed substantial increases in the levels of LAG-3, TIM-3 and PD-L1, identifying these ICMs as potential future targets in the management of TNBC. Although none of the 16 measured soluble plasma ICMs correlated with the pCR, an extended follow-up study involving a larger number of early BC patients is necessary to demonstrate possible associations of these soluble ICMs with OS and PFS.

Data availability statement

The raw data supporting the conclusions of this article will be made available by the authors, without undue reservation.

Ethics statement

Permission to undertake this study and to draw blood from patients with early BC and from matched, healthy control subjects was granted by the Research Ethics Committee of the Faculty of Health Sciences, University of Pretoria, in full compliance with the World Medical Association Declaration of Helsinki 2013. Two submissions were approved; firstly, the BC study, and secondly, a submission in respect of the healthy control subjects (respective Approval Numbers 517/2017 and 762/2020). Prior, written informed consent was obtained from all participants. The patients/participants provided their written informed consent to participate in this study.

Author contributions

BR, HS, SN, and RA conceptualized the study. BR, CB, and SN provided clinical oversight. HS, AT, NH, TS, LK, and LH were responsible for diligent processing and storage of blood/plasma

specimens and for performance of laboratory analyses of plasma specimens. BR, PM, and TS advised on aspects of statistical analysis of data. All authors contributed to the article and approved the submitted version.

Funding

This study was funded by a grant awarded to BR by the Cancer Association of South Africa (CANSA).

Conflict of interest

Author SN is a partner at Drs Gritzman & Thatcher Inc. Laboratories.

The remaining authors declare that the research was conducted in the absence of any commercial or financial relationships that could be construed as a potential conflict of interest.

Publisher's note

All claims expressed in this article are solely those of the authors and do not necessarily represent those of their affiliated organizations, or those of the publisher, the editors and the reviewers. Any product that may be evaluated in this article, or claim that may be made by its manufacturer, is not guaranteed or endorsed by the publisher.

Supplementary material

The Supplementary Material for this article can be found online at: https://www.frontiersin.org/articles/10.3389/fonc.2023.1097309/full#supplementary-material

SUPPLEMENTARY FIGURE 1
Box and whisker plots depicting the progressive changes in the median plasma concentrations (with 95% confidence limits) of three co-inhibitory immune checkpoints (BTLA, CTLA-4 and PD-1) throughout the course of neoadjuvant chemotherapy (NAC) (pre-treatment/diagnosis, post-NAC and post-surgery) in relation to the corresponding median values of the control subjects. The p values represent the comparison between pre-treatment/diagnosis and post-NAC values.

SUPPLEMENTARY FIGURE 2
Box and whisker plots depicting the progressive changes in the median plasma concentrations (with 95% confidence limits) of the remaining four co-stimulatory immune checkpoints (CD28, CD40, CD86 and GITRL) throughout the course of neoadjuvant chemotherapy (NAC) (pre-treatment/diagnosis, post-NAC and post-surgery) in relation to the corresponding median values of the control subjects. The p values represent the comparison between the pre-treatment/diagnosis and post-NAC values.

SUPPLEMENTARY FIGURE 3
Box and whisker plots depicting the progressive changes in the median plasma concentrations (with 95% confidence limits) of the two dual-activity immune checkpoints (TLR-2 and HVEM) throughout the course of neoadjuvant chemotherapy (NAC) (pre-treatment/diagnosis, post-NAC and post-surgery) in relation to the corresponding median values of the control subjects. The p values represent the comparison between the pre-treatment/diagnosis and post-NAC values.

SUPPLEMENTARY FIGURE 4
Histological photomicrographs of pre-treatment tissue of a patient who attained a pathological complete response. **(A)** x20 Magnification: Core biopsy hematoxylin and eosin (H&E) stained slide breast carcinoma no special type (NST), prior to therapy. **(B)** X10 Magnification: Positive E-Cadherin immunoperoxidase stain of tumor confirming ductal differentiation. **(C)** x20 Magnification: Estrogen receptor immunoperoxidase stain of tumor, showing no staining (ER negative).

SUPPLEMENTARY FIGURE 5
Histological photomicrographs of pre-treatment tissue of a patient who attained a pathological complete response. **(A)** x20 Magnification: Progesterone receptor immunoperoxidase stain of tumor (PR negative). **(B)** x20 Magnification: HER2 immunoperoxidase stain of tumor (HER2 negative). **(C)** x20 Magnification :Ki67 immunoperoxidase stain of tumor (90% of tumor cells staining positive).

SUPPLEMENTARY FIGURE 6
Histological photomicrographs of post-surgery tissue obtained during surgery of a patient who attained a pathological complete response. **(A)** X10 Magnification: Tumor bed post chemotherapy showing stromal fibrosis and dystrophic calcification with NO tumor cells H&E. **(B)** X10 Magnification: Tumor bed post chemotherapy showing loose fibrovascular response and elastosis with NO tumor cells H&E. **(C)** x20 Magnification: MNF116 (broad pancytokeratin) immunoperoxidase stain of tumor bed post chemotherapy showing NO residual staining tumor cells.

References

1. Allen BM, Hiam KJ, Burnett CE, Venida A, DeBarge R, Tenvooren I, et al. Systemic dysfunction and plasticity of the immune macroenvironment in cancer models. *Nat Med* (2020) 26:1125–34. doi: 10.1038/s41591-020-0892-6

2. Pinzon-Charry A, Ho CS, Maxwell T, McGuckin MA, Schmidt C, Furnival C, et al. Numerical and functional defects of blood dendritic cells in early- and late-stage breast cancer. *Br J Cancer* (2007) 97:1251–9. doi: 10.1038/sj.bjc.6604018

3. Meyer MA, Baer JM, Knolhoff BL, Nywening TM, Panni RZ, Su X, et al. Breast and pancreatic cancer interrupt IRF8-dependent dendritic cell development to overcome immune surveillance. *Nat Commun* (2018) 9:1250. doi: 10.1038/s41467-018-03600-6

4. Brand JS, Colzani E, Johansson ALV, Giesecke J, Clements M, Bergh J, et al. Infection-related hospitalizations in breast cancer patients: Risk and impact on prognosis. *J Infect* (2016) 72:650–8. doi: 10.1016/j.jinf.2016.04.003

5. Obeid E, Nanda R, Fu YX, Olopade OI. The role of tumor-associated macrophages in breast cancer progression (review). *Int J Oncol* (2013) 43:5–12. doi: 10.3892/ijo.2013.1938

6. Ramos RN, Rodriguez C, Hubert M, Ardin M, Treilleux I, Ries CH, et al. CD163+ tumor-associated macrophage accumulation in breast cancer patients reflects both local differentiation signals and systemic skewing of monocytes. *Clin Transl Immunol* (2020) 9:e1108. doi: 10.1002/cti2.1108

7. Mehta AK, Cheney EM, Hartl CA, Pantelidou C, Oliwa M, Castrillon JA, et al. Targeting immunosuppressive macrophages overcomes PARP inhibitor resistance in BRCA1-associated triple-negative breast cancer. *Nat Cancer* (2021) 2:66–82. doi: 10.1038/s43018-020-00148-7

8. Peranzoni E, Lemoine J, Vimeux L, Feuillet V, Barrin S, Kantari-Mimoun C, et al. Macrophages impede CD8 T cells from reaching tumor cells and limit the efficacy of anti-PD-1 treatment. *Proc Natl Acad Sci U.S.A.* (2018) 115:E4041–50. doi: 10.1073/pnas.1720948115

9. Zhang B, Cao M, He Y, Liu Y, Zhang G, Yang C, et al. Increased circulating M2-like monocytes in patients with breast cancer. *Tumour Biol* (2017) 39:1010428317711571. doi: 10.1177/1010428317711571

10. Li W, Syed F, Yu R, Yang J, Xia Y, Relich RF, et al. Soluble immune checkpoints are dysregulated in COVID-19 and heavy alcohol users with HIV infection. *Front Immunol* (2022) 13:833310. doi: 10.3389/fimmu.2022.833310

11. Malinga NZ, Siwele SC, Steel HC, Kwofie LLI, Meyer PWA, Smit T, et al. Systemic levels of the soluble co-inhibitory immune checkpoints, CTLA-4, LAG-3, PD-1/PD-L1 and TIM-3 are markedly increased in basal cell carcinoma. *Transl Oncol* (2022) 19:101384. doi: 10.1016/j.tranon.2022.101384

12. Gu D, Ao X, Yang Y, Chen Z, Xu X. Soluble immune checkpoints in cancer: Production, function and biological significance. *J Immunother Cancer* (2018) 6:132. doi: 10.1186/s40425-018-0449-0

13. Zhang H, Dutta P, Liu J, Sabri N, Song Y, Li WX, et al. Tumour cell-intrinsic CTLA4 regulates PD-L1 expression in non-small cell lung cancer. *J Cell Mol Med* (2019) 23:535–42. doi: 10.1111/jcmm.13956

14. Yoshikawa K, Ishida M, Yanai H, Tsuta K, Sekimoto M, Sugie T. Prognostic significance of PD-L1-positive cancer-associated fibroblasts in patients with triple-negative breast cancer. *BMC Cancer* (2021) 21:239. doi: 10.1186/s12885-021-07970-x

15. Brown LC, Loi S. Immune checkpoint inhibition in the treatment of early stage triple negative breast cancer: 2021 update. *Breast* (2022) 62 Suppl 1:S29–33. doi: 10.1016/j.breast.2021.12.018

16. Rapoport BL, Steel HC, Hlatshwayo N, Theron AJ, Meyer PWA, Nayler S, et al. Systemic immune dysregulation in early breast cancer is associated with decreased plasma levels of both soluble co-inhibitory and co-stimulatory immune checkpoint molecules. *Front Immunol* (2022) 13:823842. doi: 10.3389/fimmu.2022.823842

17. Dent R, Hanna WM, Trudeau M, Rawlinson E, Sun P, Narod SA. Pattern of metastatic spread in triple-negative breast cancer. *Breast Cancer Res Treat* (2009) 115:423–8. doi: 10.1007/s10549-008-0086-2

18. Amin MB, Greene FL, Edge SB, Compton CC, Gershenwald JE, Brookland RK, et al. The eighth edition AJCC cancer staging manual: Continuing to build a bridge from a population-based to a more "personalized" approach to cancer staging. *CA Cancer J Clin* (2017) 67:93–9. doi: 10.3322/caac.21388

19. Roselli M, Cereda V, di Bari MG, Formica V, Spila A, Jochems C, et al. Effects of conventional therapeutic interventions on the number and function of regulatory T cells. *Oncoimmunology* (2013) 2:e27025. doi: 10.4161/onci.27025

20. Fumet JD, Limagne E, Thibaudin M, Ghiringhelli F. Immunogenic cell death and elimination of immunosuppressive cells: A double-edged sword of chemotherapy. *Cancers* (2020) 12:2637. doi: 10.3390/cancers12092637

21. Hernández ÁP, Juanes-Velasco P, Landeira-Viñuela A, Bareke H, Montalvillo E, Góngora R, et al. Restoring the immunity in the tumor microenvironment: Insights into immunogenic cell death in onco-therapies. *Cancers* (2021) 13:2821. doi: 10.3390/cancers13112821

22. Dong MP, Enomoto M, Thuy LTT, Hai H, Hieu VN, Hoang DV, et al. Clinical significance of circulating soluble immune checkpoint proteins in sorafenib-treated patients with advanced hepatocellular carcinoma. *Sci Rep* (2020) 10:3392. doi: 10.1038/s41598-020-60440-5

23. Wang Q, Zhang J, Tu H, Liang D, Chang DW, Ye Y, et al. Soluble immune checkpoint-related proteins as predictors of tumor recurrence, survival, and T cell phenotypes in clear cell renal cell carcinoma patients. *J Immunother Cancer* (2019) 7:334. doi: 10.1186/s40425-019-0810-y

24. Maruhashi T, Sugiura D, Okazaki IM, Okazaki T. LAG-3: from molecular functions to clinical applications. *J Immunother Cancer* (2020) 8:e001014. doi: 10.1136/jitc-2020-001014

25. Orme JJ, Enninga EAL, Lucien-Matteoni F, Dale H, Burgstaler E, Harrington SM, et al. Therapeutic plasma exchange clears circulating soluble PD-L1 and PD-L1-positive extracellular vesicles. *J Immunother Cancer* (2020) 8:e001113. doi: 10.1136/jitc-2020-001113

26. Oh SY, Kim S, Keam B, Kim TM, Kim DW, Heo DS. Soluble PD-L1 is a predictive and prognostic biomarker in advanced cancer patients who receive immune checkpoint blockade treatment. *Sci Rep* (2021) 11:19712. doi: 10.1038/s41598-021-99311-y

27. Mittendorf EA, Zhang H, Barrios CH, Saji S, Jung KH, Hegg R, et al. Neoadjuvant atezolizumab in combination with sequential nab-paclitaxel and anthracycline-based chemotherapy versus placebo and chemotherapy in patients with early-stage triple-negative breast cancer (IMpassion031): A randomised, double-blind, phase 3 trial. *Lancet* (2020) 396:1090–100. doi: 10.1016/S0140-6736(20)31953-X

28. Schmid P, Cortes J, Dent R, Pusztai L, McArthur H, Kümmel S, et al. Event-free survival with pembrolizumab in early triple-negative breast cancer. *N Engl J Med* (2022) 386:556–67. doi: 10.1056/NEJMoa2112651

29. Xin Y, Shen G, Zheng Y, Guan Y, Huo X, Li J, et al. Immune checkpoint inhibitors plus neoadjuvant chemotherapy in early triple-negative breast cancer: A systematic review and meta-analysis. *BMC Cancer* (2021) 21:1261. doi: 10.1186/s12885-021-08997-w

30. Ji Q, Ding J, Hao M, Luo N, Huang J, Zhang W. Immune checkpoint inhibitors combined with chemotherapy compared with chemotherapy alone for triple-negative breast cancer: A systematic review and meta-analysis. *Front Oncol* (2021) 11:795650. doi: 10.3389/fonc.2021.795650

31. Solinas C, Gombos A, Latifyan S, Piccart-Gebhart M, Kok M, Buisseret L. Targeting immune checkpoints in breast cancer: An update of early results. *ESMO Open* (2017) 2:e000255. doi: 10.1136/esmoopen-2017-000255

32. Santa-Maria CA, Kato T, Park JH, Kiyotani K, Rademaker A, Shah AN, et al. A pilot study of durvalumab and tremelimumab and immunogenomic dynamics in metastatic breast cancer. *Oncotarget* (2018) 9:18985–96. doi: 10.18632/oncotarget.24867

33. Mina LA, Lim S, Bahadur SW, Firoz AT. Immunotherapy for the treatment of breast cancer: Emerging new data. *Breast Cancer* (2019) 11:321–8. doi: 10.2147/BCTT.S184710

34. Zou Y, Zou X, Zheng S, Tang H, Zhang L, Liu P, et al. Efficacy and predictive factors of immune checkpoint inhibitors in metastatic breast cancer: A systematic review and meta-analysis. *Ther Adv Med Oncol* (2020) 12:1758835920940928. doi: 10.1177/1758835920940928

35. Nanda R, Liu MC, Yau C, Shatsky R, Pusztai L, Wallace A, et al. Effect of pembrolizumab plus neoadjuvant chemotherapy on pathologic complete response in women with early-stage breast cancer: An analysis of the ongoing phase 2 adaptively randomized I-SPY2 trial. *JAMA Oncol* (2020) 6:676–84. doi: 10.1001/jamaoncol.2019.6650

36. Papadimitriou M, Liakouli Z, Papadimitriou CA. The role of immune checkpoint inhibitors in triple-negative breast cancer: Recent developments and future perspectives. *J Cancer Metastasis Treat* (2021) 7:63. doi: 10.20517/2394-4722.2021.138

37. Qureshi S, Chan N, George M, Ganesan S, Toppmeyer D, Omene C. Immune checkpoint inhibitors in triple negative breast cancer: The search for the optimal biomarker. *biomark Insights* (2022) 17:11772719221078774. doi: 10.1177/11772719221078774

frontiers | Frontiers in Immunology

TYPE Case Report
PUBLISHED 14 April 2023
DOI 10.3389/fimmu.2023.1178682

Check for updates

OPEN ACCESS

EDITED BY
Shariq Qayyum,
Brigham and Women's Hospital and
Harvard Medical School, United States

REVIEWED BY
Laura Deborah Locati,
University of Pavia, Italy
Todd Bartkowiak,
Vanderbilt University, United States

*CORRESPONDENCE
Shaoyan Liu
shaoyanliu.bj@263.net
Yi Cai
yicai108@gmail.com

†These authors contributed equally as co-first authors to this article.

SPECIALTY SECTION
This article was submitted to Cancer Immunity and Immunotherapy, a section of the journal Frontiers in Immunology

RECEIVED 03 March 2023
ACCEPTED 30 March 2023
PUBLISHED 14 April 2023

CITATION
Gui L, Zhu Y, Li X, He X, Ma T, Cai Y and Liu S (2023) Case report: Complete response of an anaplastic thyroid carcinoma patient with *NRAS* Q61R/*BRAF* D594N mutations to the triplet of dabrafenib, trametinib and PD-1 antibody. *Front. Immunol.* 14:1178682. doi: 10.3389/fimmu.2023.1178682

COPYRIGHT
© 2023 Gui, Zhu, Li, He, Ma, Cai and Liu. This is an open-access article distributed under the terms of the Creative Commons Attribution License (CC BY). The use, distribution or reproduction in other forums is permitted, provided the original author(s) and the copyright owner(s) are credited and that the original publication in this journal is cited, in accordance with accepted academic practice. No use, distribution or reproduction is permitted which does not comply with these terms.

Case report: Complete response of an anaplastic thyroid carcinoma patient with *NRAS* Q61R/*BRAF* D594N mutations to the triplet of dabrafenib, trametinib and PD-1 antibody

Lin Gui[1†], Yiming Zhu[2†], Xiaomo Li[3†], Xiaohui He[1†], Tonghui Ma[3], Yi Cai[4*] and Shaoyan Liu[2*]

[1]Department of Medical Oncology, National Cancer Center/National Clinical Research Center for Cancer/Cancer Hospital, Chinese Academy of Medical Sciences & Peking Union Medical College, Beijing Key Laboratory of Clinical Study on Anticancer Molecular Targeted Drugs, Beijing, China, [2]Department of Head and Neck Surgical Oncology, National Cancer Center/National Clinical Research Center for Cancer/Cancer Hospital, Chinese Academy of Medical Sciences & Peking Union Medical College, Beijing, China, [3]Genetron Health (Beijing) Technology, Co. Ltd, Beijing, China, [4]Independent Researcher, Ellicott City, Maryland, MD, United States

Anaplastic thyroid carcinoma, *BRAF* non-V600, *NRAS*, combination immunotherapy and targeted therapy, case report. Anaplastic thyroid carcinoma (ATC) is a rare type of thyroid cancer with a mortality rate near 100%. *BRAF* V600 and *NRAS* mutations are the most common drivers of ATC. While patients with *BRAF* V600-mutated ATC can be treated with BRAF-targeted therapy, there is no effective treatment for ATC driven by *NRAS* or non-V600 *BRAF* mutations. For patients with untargetable driver mutations, immunotherapy provides an alternative treatment option. Here, we present a metastatic ATC patient with PD-L1 positive (tumor proportion score of 60%) tumor and *NRAS* Q61R/*BRAF* D594N mutations, who progressed on PD-1 antibody sintilimab plus angiogenesis inhibitor anlotinib. The class 3 BRAF mutant D594N is sensitive to the inhibition of MEK inhibitor trametinib, and its oncogenic activity also depends on CRAF, which can be inhibited by BRAF inhibitor dabrafenib. For these reasons, the patient received a salvage treatment regime of dabrafenib, trametinib, and sintilimab, which resulted in a complete pathological response. To our best knowledge, this is the first report of successful treatment of ATC patients with concurrent *NRAS*/*BRAF* non-V600 mutations with the combination of immunotherapy and targeted therapy. Further investigation is required to decipher the mechanism by which the combination of dabrafenib/trametinib with PD-1 antibody overcomes initial immunotherapy resistance likely mediated by concurrent *BRAF* and *NRAS* mutations.

KEYWORDS

anaplastic thyroid carcinoma (ATC), BRAF non-V600E, NRAS, combination immunotherapy and targeted therapy, case report

Background

Anaplastic thyroid carcinoma (ATC) is one of the most aggressive solid tumors with a disease-specific mortality rate near 100% (1). Genomic profiling studies revealed that the major drivers of ATC are *TP53*, *TERT*, *BRAF*, and *NRAS* mutations (2). While ATC patients with *BRAF* V600 mutation are eligible for BRAF-targeted therapy, there is no effective treatment for *NRAS*-mutated ATC patients (1).

In the past decade, cancer immunotherapy has shifted the paradigm of cancer treatment. Based on the results of the KEYNOTE-158 trial, FDA approved PD-1 antibody pembrolizumab as a treatment option for patients with TMB-H (≥ 10 mut/Mb) solid tumors, which was also endorsed by the NCCN thyroid cancer guideline for ATC treatment (1). Of note, the KETNOTE-158 trial only included two patients with thyroid cancer. Recently, an investigational PD-1 antibody spartalizumab showed promising efficacy in a phase 2 trial of ATC, in which spartalizumab achieved an overall response rate (ORR) of 29% and 35% in the PD-L1 positive and high PD-L1 (≥ 50%) subgroups, respectively (3). Responses were seen in *BRAF* wild-type and *BRAF*-mutant patients. These results indicated that PD-1 antibody might be a treatment option for ATC patients with high PD-L1 expression, irrespective of their *BRAF* mutation status.

Both immune checkpoint blockade (ICB) and BRAF-targeted therapies have been approved for the treatment of *BRAF* V600-mutant melanoma (4). Of note, abnormal activation of the MAPK signaling can result in tumor-intrinsic resistance to ICB through the modulation of tumor microenvironment (TME) (5). The triplet combination of BRAF inhibitor (BRAFi), MEK inhibitor (MEKi), and PD-1/L1 antibodies have been tested in clinical trials of *BRAF* V600-mutant melanoma (6–8). Although the triplet regimes did not improve the response rate compared with the doublets, they improved the duration of response. Furthermore, two triplets improved progression-free survival (PFS) in the IMspire150 and KEYNOTE-022 trials (6, 7). Therefore, the NCCN guideline for cutaneous melanoma recommended two triplets regimes (vemurafenib/cobimetinib/atezolizumab and dabrafenib/trametinib/pembrolizumab) as first-line therapy options for unresectable or metastatic melanoma patients with *BRAF* V600 mutation (4).

According to the mechanisms of activation, BRAF mutants can be classified into three groups (9). Class 1 and 2 mutants function as RAS-independent monomers and dimers, respectively (9). Class 3 mutants have impaired kinase activity, and their oncogenic activity depends on RAS and CRAF (9). Because coexisting *BRAF* mutations synergize with *RAS* mutations in the amplification of downstream MAPK signaling, the treatment of solid tumors with coexisting *BRAF/RAS* mutations is more challenging than those with *BRAF* or *RAS* mutations alone. Here, we presented a PD-L1-positive metastatic ATC patient with coexisting *NRAS* and class 3 *BRAF* mutations. After progression on PD-1 antibody sintilimab plus an angiogenesis inhibitor anlotinib, she achieved a pathological complete response with the triplet regime of BRAFi dabrafenib, MEKi trametinib, and a domestic PD-1 antibody sintilimab (Figure 1A).

Case presentation

A 61-year-old female presented with a rapidly enlarging neck mass in November 2021. Contrast-enhanced computed tomography (CT) revealed a 1.9×1.8 cm nodule and a 3.2×2.6 cm nodule in the left and right thyroid lobes, respectively. She underwent surgical resection of partial thyroid right lobe and thyroid left lobe mass on Jan 25th, 2022. Postoperative histopathological examination confirmed multifocal anaplastic thyroid carcinoma with areas of necrosis and calcifications in the right lobe, and nodular goiter in the left. Immunohistochemical (IHC) staining was positive for Ki-67 (80%), Vimentin, TTF-1, P53, Cyclin D1, Pax-8, TG (weak, 1+), BRAF V600E (weak, 1+), and negative for AE1/AE3, CD56, Calcitonin, LCA, and HMB45 (Figure 1B). Two months later, a progressively enlarging mass appeared in her right neck, indicating disease progression (Figure 1A). PET-CT imaging revealed multiple hypoechoic nodules in cervical region VI, with the largest located in the center of 4.0×2.8 cm (Figures 1C, 2A). The patient was then referred to our hospital. She had a poor Eastern Cooperative Oncology Group (ECOG) performance status of 2, difficulty in breathing, and choking with deglutition.

Because radical surgery was not suitable, the patient was treated with anlotinib (10mg, QD, 2 weeks on/1 week off), a multi-targeted tyrosine kinase inhibitor targeting tumor angiogenesis and proliferation from May 13th. The lesion soon shrank by about 20%, and the patient's skin color returned to normal. Genetic testing of the resected tumor tissue with a multi-gene next-generation sequencing (NGS) panel (Onco Panscan^{TM}, Genetron Health) revealed a tumor mutational burden of 1.41 mutations per megabase (mut/Mb), microsatellite status stable (MSS), *TERT* promoter mutation, an *NRAS* Q61R mutation with a variant allele fraction (VAF) of 10.6%, and a *BRAF* D594N mutation with a VAF of 12.6% (Table 1). PD-L1 IHC assay (PD-L1 IHC 22C3 pharmDx assay, Agilent Technologies, Carpinteria, CA, USA) showed a TPS of 60% and a CPS of 80 (Figure 1B). We previously reported the successful treatment of a PD-L1-positive, *NRAS* Q61R-mutated metastatic ATC patient with sintilimab plus an angiogenesis inhibitor anlotinib (10). Given the similarity of these two ATC patients, sintilimab (200 mg, Q3W) was added on May 21st, 2022. Unfortunately, disease progression occurred, including neck mass enlargement to 4.4×3.0 cm, the reappearance of breathing difficulty, and choking with deglutition. And this doublet regime was left off after one cycle (Figures 1A, C).

MAPK signaling amplification driven by class 3 BRAF mutant D594N is sensitive to the inhibition of trametinib (9). Furthermore, the oncogenic activity of class 3 BRAF mutants depends on CRAF (11), which can be inhibited with dabrafenib (12). Of note, the efficacy of dabrafenib plus trametinib has not been established in *NRAS*-driven solid tumors. Given the coexistence of *NRAS* Q61R and *BRAF* D594N mutations, the patient was then treated with a salvage regime consisting of dabrafenib (75 mg, BID), trametinib (2 mg, QD), and sintilimab (200mg, Q3W) from Jun 10th, 2022. After nine days, regression of all metastases in the bilateral neck was noted, and breathing/swallowing returned to normal (Figures 1A, C).

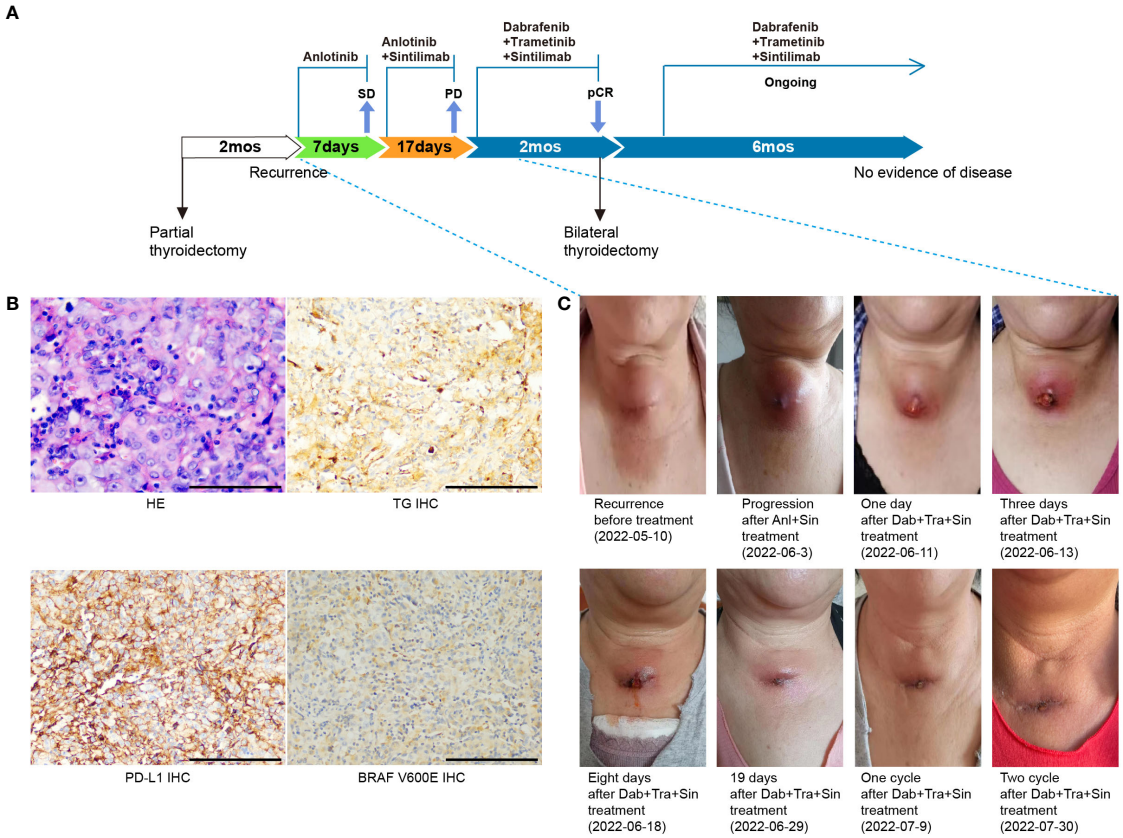


FIGURE 1
Case summary. **(A)** Summary of disease course and treatment procedure. pCR, pathological complete response; SD, stable disease; PD, progressive disease; mo, months. **(B)** H&E, TG, BRAF V600E and PD-L1 staining of the primary tumor. Scale bars: 50 μm. H&E: hematoxylin and eosin. **(C)** Representative images showing disease recurrence/progression on sintilimab plus anlotonib, and the patient's response to the triplet regime of sintilimab, dabrafenib, and trametinib.

After one cycle, the neck mass continued to shrink, and the ulcerated area was healed (Figures 1C, 2B). Fever (39.5°C) was the only adverse event observed during this triplet regime treatment. Her temperature returned to normal within 24 hours of taking off dabrafenib. The triplet regime was resumed after her temperature remained normal for 24 hours, and no subsequent fever occurred. After two cycles (six weeks) of treatment, radical surgery was evaluated as feasible (Figures 1C, 2C). The patient discontinued dabrafenib and trametinib on Aug 11th, 2022. And bilateral residual thyroidectomy plus neck lymph node dissection were performed the next day. Postoperative pathology indicated that she had a pathological complete response (pCR). Given the high risk of ATC patients with concomitant *BRAF*/*RAS* and *TERT* mutations (13), she continued on the triplet regime from Sep 20th and remained in remission with an excellent quality of life until the last follow-up in March 2023 (Figure 1A).

Discussion

The three major histological types of thyroid cancers are differentiated thyroid carcinoma (DTC), medullary thyroid carcinoma (MTC), and anaplastic thyroid carcinoma (ATC) (1). DTC represents more than 95% of thyroid cancer cases and has a very good prognosis. In contrast, ATC patients have a poor prognosis with a historical median overall survival (OS) of four months (14). ATC responds poorly to conventional thyroid cancer treatment options including surgery, radiation therapy, chemotherapy, and radioactive iodine (RAI) therapy (1). The NCCN guideline for thyroid carcinoma recommended that ATC patients with locally resectable disease can be treated with multimodal therapy, and those with actionable mutations (*BRAF*, *NTRK*, *ALK*, *RET*, MSI, dMMR, TMB-H) can be treated with targeted therapy or immunotherapy (1).

Recent genomic profiling studies revealed that activating *BRAF* and *RAS* mutations are major drivers of thyroid cancer. The TCGA study characterized the landscape of papillary thyroid carcinoma (PTC), the most common type of thyroid cancer (15). Among 496 PTC patients, 60% carried *BRAF* mutations, and 13% had *RAS* mutations. Compared to PTC, genomic studies of large ATC cohorts are rare. In one study of 126 ATC patients, 45% had *BRAF* alterations (all V600E except for 1 deletion), and 24% had *RAS* mutations (13). In another ATC cohort (n = 196), 41% had *BRAF* mutations and 27% had *RAS* mutations (2). Interestingly, the latter study also observed non-V600 *BRAF* mutations in PTC, one precursor of ATC. These rare *BRAF* alterations include *BRAF* fusions, K601E, G469A, V600_K601delinsE, V600_K601>D, V600_W604>R, and V600_S605>D. Of note, *BRAF* V600E

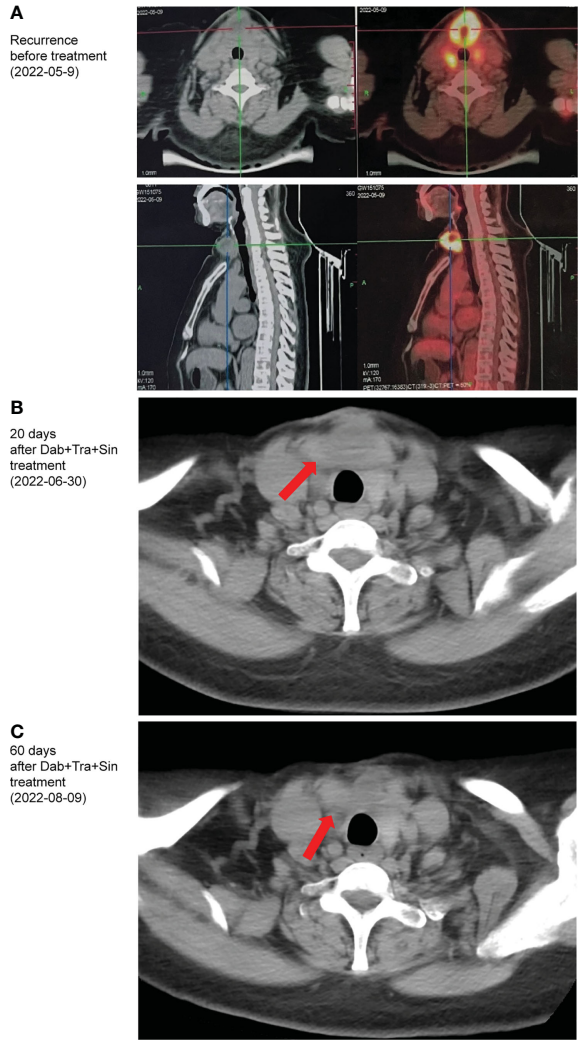


FIGURE 2
Computed tomography images showing the patient' recurrence **(A)**, as well as response to the triplet regime of sintilimab, dabrafenib, and trametinib after 20 **(B)**, 60 **(C)** days of treatment.

and *RAS*mutations are mutually exclusive in these thyroid cancer cohorts.

Abnormal activation of the RAF-RAS-MAPK signaling pathway is identified in more than 30% of human cancers (16). BRAF is an established therapeutic target in colorectal cancer (CRC), non-small cell lung cancer (NSCLC), melanoma, and ATC (17). Recently, FDA granted accelerated approval of dabrafenib in combination with trametinib for the treatment of almost all *BRAF* V600-mutated solid tumors. In contrast, there is no effective therapy for *NRAS*-mutated solid tumors. Furthermore, coexisting *NRAS* mutations can result in resistance to dabrafenib/trametinib (18, 19). Therefore, the treatment of solid tumors driven by *NRAS* mutation alone or in combination with *BRAF* mutations represents a clinical challenge.

Recent pieces of evidence indicated that immunotherapy could be an effective treatment option for ATC. In a single-center study, PD-1 antibody pembrolizumab or nivolumab achieved an overall response rate (ORR) of 16% in 13 advanced or metastatic ATC patients, including seven patients with *BRAF* V600E mutations (20). And responses were ongoing in four individuals. Similarly, in a phase 2 trial of advanced/metastatic ATC (n = 42), an investigational PD-1 antibody spartalizumab achieved an overall ORR of 19%, including three complete responses (CRs) and five partial responses (PRs) (3).

Given the poor prognosis and limited therapeutic options of ATC, several multitargeted tyrosine kinase inhibitors (TKIs) including sorafenib, sunitinib, imatinib, and pazopanib have been evaluated in clinical trials with unsatisfactory results. Anlotinib is a novel multitarget TKI which has been approved in China for the treatment of medullary thyroid cancer (MTC), (NSCLC), small cell lung cancer (SCLC), soft tissue sarcoma (STS) and radioactive iodine-refractory differentiated thyroid cancer (RAIR-DTC) (21, 22). In a single-arm phase 2 trial, neoadjuvant anlotinib therapy achieved an ORR of 76.9% in patients with advanced thyroid cancer (23). As most patients treated with TKI will develop resistance, the combination of PD-1 antibodies with TKIs has been proposed as a strategy to overcome TKI resistance in cancer patients. In a retrospective study at the MD Anderson Cancer Center, the addition of pembrolizumab to TKIs resulted in a best overall response (BOR) of 42% in ATC patients who progressed on TKIs (24). Sintilimab is a PD-1 antibody approved in China for the treatment of NSCLC, Hodgin's lymphoma, hepatocellular carcinoma, and esophageal squamous cell carcinoma (ESCC) (25). Recently, the combination of sintilimab and anlotinib has shown promising antitumor activity and tolerable safety profiles in cervical cancer, endometrial cancer, hepatocellular carcinoma, and biliary tract cancer (26–29).

Previously, we reported that sintilimab plus anlotinib achieved a remarkable response in a metastatic *NRAS*-mutated ATC patient

TABLE 1 Summary of NGS analysis.

Mutation Type	Gene	Nucleotide change	Amino acid change	Mutation effect	VAF (%)
Somatic	*BRAF*	c.1782T>G	p.Asp594Glu	Missense	12.6
	NRAS	c.182A>G	p.Gln61Arg	Missense	10.6
	CDK8	c.524G>C	p.G175A	Missense	10.8
	TERT	c.-124C>T	–	Promoter	33.6
MSS					
TMB low (1.41mutations/MB)					

VAF, variant allele frequency; MSI, microsatellite instability; MSS, microsatellite stable; TMB, tumor mutational burden.

with high PD-L1 expression (10). In this study, our patient briefly responded to anlotinib but quickly developed resistance to sintilimab plus anlotinib. We suspected that the distinct responses to sintilimab plus anlotinib in these two PD-L1-positive, *NRAS*-mutated ATC patients could be mediated by the class 3 *BRAF* mutation D594N, which synergizes with *RAS* mutations in the amplification of downstream MAPK signaling (9). The oncogenic activity of class 3 BRAF mutants depends on the kinase activity of CRAF (9), which can be inhibited by BRAFi dabrafenib. Furthermore, class 3 BRAF mutants are sensitive to the inhibition of MEKi trametinib (9). Although the antitumor activity of MAPK-targeted therapy has not been established in *NRAS*-mutated solid tumors, this approach could counteract the synergistic effect of coexisting *NRAS*/*BRAF* mutations and render the tumor sensitive to immunotherapy.

Activation of the MAPK pathway plays a key role in tumor-intrinsic resistance to immune checkpoint blockade (30). In patients with triple-negative breast cancer, activation of the RAS-MAPK pathway was associated with reduced tumor-infiltrating lymphocytes (TILs) (31). However, trametinib treatment upregulated the expression of PD-L1 and MHC-I/II in mouse mammary tumor-derived cell lines *in vitro* and *in vivo*. Similarly, in *BRAF* V600-mutant melanoma, hyperactivated MAPK signaling inhibits T cell infiltration through the production of VEGF, which was reversed by the administration of a BRAFi (32). Other studies showed that the addition of dabrafenib/trametinib to immune checkpoint blockade (ICB) resulted in higher antitumor activity than ICB alone (33, 34). These preclinical and clinical studies led to the hypothesis that the combination of immunotherapy and MAPK-targeted therapy might provide better clinical benefits than each alone. The efficacy of BRAFi/MEKi plus PD-1/PD-L1 antibody triplets in *BRAF*-mutated solid tumors has been tested in three pivotal trials of melanoma (IMspire150, KEYNOTE-022, COMBI-i). Based on the results of the IMspire150 trial, FDA approved the combination of BRAFi vemurafenib, MEKi cobimetinib, and PD-L1 antibody atezolizumab for the treatment of *BRAF* V600-mutated melanoma. Because class 3 BRAF mutants were resistant to vemurafenib but sensitive to trametinib, we selected the dabrafenib/trametinib doublet to combine with sintilimab as the salvage therapy for our patient, which achieved a complete pathological response.

In addition to triplet therapy, optimal sequencing of immunotherapy and targeted therapy represents another strategy to improve outcomes for patients with *BRAF*-mutated solid tumors. In murine models of *BRAF*/*NRAS*-driven melanoma, anti-PD-1/L1 antibody lead-in before MAPK inhibitor combination optimized antitumor activity by promoting T cell clonal expansion and macrophage polarization (35). Consistently, results of two trials (DREAMseq and SECOMBIT) showed that nivolumab/ipilimumab followed by BRAFi/MEKi doublets led to superior overall survival in patients with advanced *BRAF*-mutant melanoma when compared with the opposite treatment sequence (36, 37). Similarly, data from the phase 3 NEMO trial revealed that previous immunotherapy led to better clinical benefits of MEKi binimetinib in patients with *NRAS*-mutant melanoma (38). While these results were obtained in patients with *BRAF*/*NRAS*-mutant melanoma, we can not rule out the possibility that a brief preceding immunotherapy of our patient may also contribute to her response to the BRAFi/MEKi/PD-1 antibody triplet regime.

Given this patient's remarkable response, further investigation is required to explore the potential of the BRAFi/MEKi/PD-1 antibody triplet in patients with *NRAS*- or *BRAF*-mutated solid tumors refractory to immunotherapy and *BRAF*-targeted therapy. Furthermore, clinical trials of sequential immunotherapy and targeted therapy in ATC should be pursued.

Data availability statement

The original contributions presented in the study are included in the article/Supplementary Material. Further inquiries can be directed to the corresponding authors.

Ethics statement

Written informed consent was obtained from the individual(s) for the publication of any potentially identifiable images or data included in this article.

Author contributions

Concept and design: LG, SL, YZ, XH. Acquisition, analysis, and interpretation of data: LG, XL, YC. Drafting of the manuscript: YC, XL. Critical revision of the manuscript for important intellectual content: TM, XH, SL. Technical and material support: LG, XH, YZ. Study supervision: SL. All authors contributed to the article and approved the submitted version.

Acknowledgments

The authors are grateful to the patient for her kind cooperation.

Conflict of interest

XL and TM are employees of Genetron Health Beijing Technology, Co. Ltd.

The remaining authors declare that the research was conducted in the absence of any commercial or financial relationships that could be constructed as a potential conflict of interest.

Publisher's note

All claims expressed in this article are solely those of the authors and do not necessarily represent those of their affiliated organizations, or those of the publisher, the editors and the reviewers. Any product that may be evaluated in this article, or claim that may be made by its manufacturer, is not guaranteed or endorsed by the publisher.

References

1. Haddad RI, Bischoff L, Ball D, Bernet V, Blomain E, Busaidy NL, et al. Thyroid carcinoma, version 2.2022, NCCN clinical practice guidelines in oncology. *J Natl Compr Cancer Netw* (2022) 20:925–51. doi: 10.6004/jnccn.2022.0040

2. Pozdeyev N, Gay LM, Sokol ES, Hartmaier R, Deaver KE, Davis S, et al. Genetic analysis of 779 advanced differentiated and anaplastic thyroid cancers. *Clin Cancer Res* (2018) 24:3059–68. doi: 10.1158/1078-0432.CCR-18-0373

3. Capdevila J, Wirth LJ, Ernst T, Ponce Aix S, Lin CC, Ramlau R, et al. PD-1 blockade in anaplastic thyroid carcinoma. *J Clin Oncol* (2020) 38:2620–7. doi: 10.1200/JCO.19.02727

4. Swetter SM, Thompson JA, Albertini MR, Barker CA, Baumgartner J, Boland G, et al. NCCN guidelines® insights: Melanoma: Cutaneous, version 2.2021. *J Natl Compr Cancer Network* (2021) 19:364–76. doi: 10.6004/jnccn.2021.0018

5. Fares CM, Van Allen EM, Drake CG, Allison JP, Hu-Lieskovan S. Mechanisms of resistance to immune checkpoint blockade: Why does checkpoint inhibitor immunotherapy not work for all patients? *Am Soc Clin Oncol Educ book. Am Soc Clin Oncol Annu Meeting* (2019) 39:147–64. doi: 10.1200/EDBK_240837

6. Gutzmer R, Stroyakovskiy D, Gogas H, Robert C, Lewis K, Protsenko S, et al. Atezolizumab, vemurafenib, and cobimetinib as first-line treatment for unresectable advanced BRAF(V600) mutation-positive melanoma (IMspire150): primary analysis of the randomised, double-blind, placebo-controlled, phase 3 trial. *Lancet (London England)* (2020) 395:1835–44. doi: 10.1016/S0140-6736(20)30934-X

7. Ferrucci PF, Di Giacomo AM, Del Vecchio M, Atkinson V, Schmidt H, Schachter J, et al. KEYNOTE-022 part 3: a randomized, double-blind, phase 2 study of pembrolizumab, dabrafenib, and trametinib in BRAF-mutant melanoma. *J Immunother Cancer* (2020) 8(2):e001806. doi: 10.1136/jitc-2020-001806

8. Dummer R, Long GV, Robert C, Tawbi HA, Flaherty KT, Ascierto PA, et al. Randomized phase III trial evaluating spartalizumab plus dabrafenib and trametinib for BRAF V600-mutant unresectable or metastatic melanoma. *J Clin Oncol* (2022) 40:1428–38. doi: 10.1200/JCO.21.01601

9. Yao Z, Yaeger R, Rodrik-Outmezguine VS, Tao A, Torres NM, Chang MT, et al. Tumours with class 3 BRAF mutants are sensitive to the inhibition of activated RAS. *Nature* (2017) 548:234–8. doi: 10.1038/nature23291

10. Gui L, Liu S, Zhang Y, Shi Y. A remarkable and durable response to sintilimab and anlotinib in the first-line treatment of an anaplastic thyroid carcinoma without targetable genomic alterations: A case report. *OncoTargets Ther* (2021) 14:2741–6. doi: 10.2147/OTT.S305196

11. Trojaniello C, Vitale MG, Ascierto PA. Triplet combination of BRAF, MEK and PD-1/PD-L1 blockade in melanoma: the more the better? *Curr Opin Oncol* (2021) 33:133–8. doi: 10.1097/CCO.0000000000000709

12. King AJ, Arnone MR, Bleam MR, Moss KG, Yang J, Fedorowicz KE, et al. Dabrafenib; preclinical characterization, increased efficacy when combined with trametinib, while BRAF/MEK tool combination reduced skin lesions. *PloS One* (2013) 8:e67583. doi: 10.1371/journal.pone.0067583

13. Xu B, Fuchs T, Dogan S, Landa I, Katabi N, Fagin JA, et al. Dissecting anaplastic thyroid carcinoma: A comprehensive clinical, histologic, immunophenotypic, and molecular study of 360 cases. *Thyroid* (2020) 30:1505–17. doi: 10.1089/thy.2020.0086

14. Lin B, Ma H, Ma M, Zhang Z, Sun Z, Hsieh IY, et al. The incidence and survival analysis for anaplastic thyroid cancer: a SEER database analysis. *Am J Trans Res* (2019) 11:5888–96.

15. Cancer Genome Atlas Research Network. Integrated genomic characterization of papillary thyroid carcinoma. *Cell* (2014) 159:676–90. doi: 10.1016/j.cell.2014.09.050

16. Samatar AA, Poulikakos PI. Targeting RAS-ERK signalling in cancer: promises and challenges. *Nat Rev Drug Discovery* (2014) 13:928–42. doi: 10.1038/nrd4281

17. Bailey MH, Tokheim C, Porta-Pardo E, Sengupta S, Bertrand D, Weerasinghe A, et al. Comprehensive characterization of cancer driver genes and mutations. *Cell* (2018) 173:371–385.e18. doi: 10.1016/j.cell.2018.02.060

18. Chapman PB. Mechanisms of resistance to RAF inhibition in melanomas harboring a BRAF mutation. *Am Soc Clin Oncol Educ book. Am Soc Clin Oncol Annu Meeting* (2013) 33:e80–e82. doi: 10.1200/EdBook_AM.2013.33.80

19. Cabanillas ME, Dadu R, Iyer P, Wanland KB, Busaidy NL, Ying A, et al. Acquired secondary RAS mutation in BRAF(V600E)-mutated thyroid cancer patients treated with BRAF inhibitors. *Thyroid* (2020) 30:1288–96. doi: 10.1089/thy.2019.0514

20. Hatashima A, Archambeau B, Armbruster H, Xu M, Shah M, Konda B, et al. An evaluation of clinical efficacy of immune checkpoint inhibitors for patients with anaplastic thyroid carcinoma. *Thyroid* (2022) 32:926–36. doi: 10.1089/thy.2022.0073

21. Li S. Anlotinib: A novel targeted drug for bone and soft tissue sarcoma. *Front Oncol* (2021) 11:664853. doi: 10.3389/fonc.2021.664853

22. Lin Y, Qin S, Li Z, Yang H, Fu W, Li S, et al. Apatinib vs placebo in patients with locally advanced or metastatic, radioactive iodine-refractory differentiated thyroid cancer: The REALITY randomized clinical trial. *JAMA Oncol* (2022) 8:242–50. doi: 10.1001/jamaoncol.2021.6268

23. Huang NS, Wei WJ, Xiang J, Chen JY, Guan Q, Lu ZW, et al. The efficacy and safety of anlotinib in neoadjuvant treatment of locally advanced thyroid cancer: A single-arm phase II clinical trial. *Thyroid* (2021) 31:1808–13. doi: 10.1089/thy.2021.0307

24. Iyer PC, Dadu R, Gule-Monroe M, Busaidy NL, Ferrarotto R, Habra MA, et al. Salvage pembrolizumab added to kinase inhibitor therapy for the treatment of anaplastic thyroid carcinoma. *J immunotherapy Cancer* (2018) 6:68. doi: 10.1186/s40425-018-0378-y

25. Lu Z, Wang J, Shu Y, Liu L, Kong L, Yang L, et al. Sintilimab versus placebo in combination with chemotherapy as first line treatment for locally advanced or metastatic oesophageal squamous cell carcinoma (ORIENT-15): multicentre, randomised, double blind, phase 3 trial. *BMJ (Clinical Res ed.)* (2022) 377:e068714. doi: 10.1136/bmj-2021-068714

26. Xu Q, Wang J, Sun Y, Lin Y, Liu J, Zhuo Y, et al. Efficacy and safety of sintilimab plus anlotinib for PD-L1-Positive recurrent or metastatic cervical cancer: A multicenter, single-arm, prospective phase II trial. *J Clin Oncol* (2022) 40:1795–805. doi: 10.1200/JCO.21.02091

27. Wei W, Ban X, Yang F, Li J, Cheng X, Zhang R, et al. Phase II trial of efficacy, safety and biomarker analysis of sintilimab plus anlotinib for patients with recurrent or advanced endometrial cancer. *J Immunother Cancer* (2022) 10(5):e004338. doi: 10.1136/jitc-2021-004338

28. Chen X, Li W, Wu X, Zhao F, Wang D, Wu H, et al. Safety and efficacy of sintilimab and anlotinib as first line treatment for advanced hepatocellular carcinoma (KEEP-G04): A single-arm phase 2 study. *Front Oncol* (2022) 12:909035. doi: 10.3389/fonc.2022.909035

29. Jin S, Zhao R, Zhou C, Zhong Q, Shi J, Su C, et al. Feasibility and tolerability of sintilimab plus anlotinib as the second-line therapy for patients with advanced biliary tract cancers: An open-label, single-arm, phase II clinical trial. *Int J Cancer* (2022) 152 (8):1648–58. doi: 10.1002/ijc.34372

30. Kalbasi A, Ribas A. Tumour-intrinsic resistance to immune checkpoint blockade. *Nat Rev Immunol* (2020) 20:25–39. doi: 10.1038/s41577-019-0218-4

31. Loi S, Dushyanthen S, Beavis PA, Salgado R, Denkert C, Savas P, et al. RAS/MAPK activation is associated with reduced tumor-infiltrating lymphocytes in triple-negative breast cancer: Therapeutic cooperation between MEK and PD-1/PD-L1 immune checkpoint inhibitors. *Clin Cancer Res* (2016) 22:1499–509. doi: 10.1158/1078-0432.CCR-15-1125

32. Liu C, Peng W, Xu C, Lou Y, Zhang M, Wargo JA, et al. BRAF inhibition increases tumor infiltration by T cells and enhances the antitumor activity of adoptive immunotherapy in mice. *Clin Cancer Res* (2013) 19:393–403. doi: 10.1158/1078-0432.CCR-12-1626

33. Liu L, Mayes PA, Eastman S, Shi H, Yadavilli S, Zhang T, et al. The BRAF and MEK inhibitors dabrafenib and trametinib: Effects on immune function and in combination with immunomodulatory antibodies targeting PD-1, PD-L1, and CTLA-4. *Clin Cancer Res* (2015) 21:1639–51. doi: 10.1158/1078-0432.CCR-14-2339

34. Hu-Lieskovan S, Mok S, Homet Moreno B, Tsoi J, Robert L, Goedert L, et al. Improved antitumor activity of immunotherapy with BRAF and MEK inhibitors in BRAF(V600E) melanoma. *Sci Trans Med* (2015) 7:279ra41. doi: 10.1126/scitranslmed.aaa4691

35. Wang Y, Liu S, Yang Z, Algazi AP, Lomeli SH, Wang Y, et al. Anti-PD-1/L1 lead-in before MAPK inhibitor combination maximizes antitumor immunity and efficacy. *Cancer Cell* (2021) 39:1375–1387.e6. doi: 10.1016/j.ccell.2021.07.023

36. Atkins MB, Lee SJ, Chmielowski B, Tarhini AA, Cohen GI, Truong TG, et al. Combination dabrafenib and trametinib versus combination nivolumab and ipilimumab for patients with advanced BRAF-mutant melanoma: The DREAMseq trial-ECOG-ACRIN EA6134. *J Clin Oncol* (2023) 41:186–97. doi: 10.1200/JCO.22.01763

37. Ascierto PA, Mandalà M, Ferrucci PF, Guidoboni M, Rutkowski P, Ferraresi V, et al. Sequencing of ipilimumab plus nivolumab and encorafenib plus binimetinib for untreated BRAF-mutated metastatic melanoma (SECOMBIT): A randomized, three-arm, open-label phase II trial. *J Clin Oncol* (2023) 41:212–21. doi: 10.1200/JCO.21.02961

38. Dummer R, Schadendorf D, Ascierto PA, Arance A, Dutriaux C, Di Giacomo AM, et al. Binimetinib versus dacarbazine in patients with advanced NRAS-mutant melanoma (NEMO): a multicentre, open-label, randomised, phase 3 trial. *Lancet Oncol* (2017) 18:435–45. doi: 10.1016/S1470-2045(17)30180-8

frontiers | Frontiers in Immunology

TYPE Original Research
PUBLISHED 17 April 2023
DOI 10.3389/fimmu.2023.1179827

Check for updates

OPEN ACCESS

EDITED BY
Subhash Kumar Tripathi,
Seattle Children's Research Institute,
United States

REVIEWED BY
Swathi Merugu,
Memorial Sloan Kettering Cancer Center,
United States
Bishal Singh,
University of Cambridge, United Kingdom

*CORRESPONDENCE
Jonathan L. Bramson
bramsonj@mcmaster.ca

SPECIALTY SECTION
This article was submitted to Cancer Immunity and Immunotherapy, a section of the journal Frontiers in Immunology

RECEIVED 04 March 2023
ACCEPTED 27 March 2023
PUBLISHED 17 April 2023

CITATION
Afsahi A, Silvestri CM, Moore AE, Graham CF, Bacchiochi K, St-Jean M, Baker CL, Korneluk RG, Beug ST, LaCasse EC and Bramson JL (2023) LCL161 enhances expansion and survival of engineered anti-tumor T cells but is restricted by death signaling. *Front. Immunol.* 14:1179827. doi: 10.3389/fimmu.2023.1179827

COPYRIGHT
© 2023 Afsahi, Silvestri, Moore, Graham, Bacchiochi, St-Jean, Baker, Korneluk, Beug, LaCasse and Bramson. This is an open-access article distributed under the terms of the Creative Commons Attribution License (CC BY). The use, distribution or reproduction in other forums is permitted, provided the original author(s) and the copyright owner(s) are credited and that the original publication in this journal is cited, in accordance with accepted academic practice. No use, distribution or reproduction is permitted which does not comply with these terms.

LCL161 enhances expansion and survival of engineered anti-tumor T cells but is restricted by death signaling

Arya Afsahi[1,2,3], Christopher M. Silvestri[1,2,3], Allyson E. Moore[1,2,3], Carly F. Graham[1,2,3], Kaylyn Bacchiochi[2,3], Martine St-Jean[4], Christopher L. Baker[1,2,3], Robert G. Korneluk[4], Shawn T. Beug[4,5,6], Eric C. LaCasse[4] and Jonathan L. Bramson[1,2,3]*

[1]Centre for Discovery in Cancer Research, McMaster University, Hamilton, ON, Canada, [2]McMaster Immunology Research Center, McMaster University, Hamilton, ON, Canada, [3]Department of Medicine, McMaster University, Hamilton, ON, Canada, [4]Apoptosis Research Centre, Children's Hospital of Eastern Ontario Research Institute, Ottawa, ON, Canada, [5]Department of Biochemistry, Microbiology and Immunology, University of Ottawa, Ottawa, ON, Canada, [6]Centre for Infection, Immunity and Inflammation, University of Ottawa, Ottawa, ON, Canada

Background: The genesis of SMAC mimetic drugs is founded on the observation that many cancers amplify IAP proteins to facilitate their survival, and therefore removal of these pathways would re-sensitize the cells towards apoptosis. It has become increasingly clear that SMAC mimetics also interface with the immune system in a modulatory manner. Suppression of IAP function by SMAC mimetics activates the non-canonical NF-κB pathway which can augment T cell function, opening the possibility of using SMAC mimetics to enhance immunotherapeutics.

Methods: We have investigated the SMAC mimetic LCL161, which promotes degradation of cIAP-1 and cIAP-2, as an agent for delivering transient costimulation to engineered BMCA-specific human TAC T cells. In doing so we also sought to understand the cellular and molecular effects of LCL161 on T cell biology.

Results: LCL161 activated the non-canonical NF-κB pathway and enhanced antigen-driven TAC T cell proliferation and survival. Transcriptional profiling from TAC T cells treated with LCL161 revealed differential expression of costimulatory and apoptosis-related proteins, namely CD30 and FAIM3. We hypothesized that regulation of these genes by LCL161 may influence the drug's effects on T cells. We reversed the differential expression through genetic engineering and observed impaired costimulation by LCL161, particularly when CD30 was deleted. While LCL161 can provide a costimulatory signal to TAC T cells following exposure to isolated antigen, we did not observe a similar pattern when TAC T cells were stimulated with myeloma cells expressing the target antigen. We questioned whether FasL expression by myeloma cells may antagonize the costimulatory effects of LCL161. Fas-KO TAC T cells displayed superior expansion following antigen stimulation in the presence of LCL161,

suggesting a role for Fas-related T cell death in limiting the magnitude of the T cell response to antigen in the presence of LCL161.

Conclusions: Our results demonstrate that LCL161 provides costimulation to TAC T cells exposed to antigen alone, however LCL161 did not enhance TAC T cell anti-tumor function when challenged with myeloma cells and may be limited due to sensitization of T cells towards Fas-mediated apoptosis.

KEYWORDS

SMAC mimetics, engineered T cells, LCL161, multiple myeloma, cancer immunotherapy, adoptive T cell therapies

Introduction

T lymphocytes have robust anti-tumor capabilities, which has established them as a leading cellular candidate for adoptive cell therapy of cancer. However, naturally occurring anti-tumor T cells are rare due to immunological tolerance mechanisms that prevent self-reactivity. Synthetic biology has overcome this issue through the development of synthetic antigen receptors that can be engineered into T cells to redirect them towards a chosen antigen. We have developed a TCR-based synthetic receptor designed to co-opt TCR signaling, known as the T cell antigen coupler (TAC), which yields potent anti-tumor T cells with reduced off-tumor toxicity (1). The activation signal transduced through the TAC receptor results in robust cytotoxicity against tumor cells, cytokine expression, and cellular proliferation.

T cell activation can be enhanced with costimulatory signaling (2). Many synthetic antigen receptors, like chimeric antigen receptors (CARs), have incorporated costimulation into the receptor for greater benefit (3, 4). However, it remains unknown whether non-canonical signaling delivered through CARs, where the TCR signaling domain is physically linked to costimulatory signaling components, contributes to the serious toxicities associated with CAR-engineered T cell therapy (5). The TAC receptor was purpose-built to deliver a canonical T cell activation signal and, hence, does not incorporate costimulatory elements into the receptor design. We recognize that provision of costimulation may enhance TAC T cell function, and thus, are pursuing chemical biology strategies to do so *via* small molecule drugs that would enable temporal and titratable costimulation without compromising the basal T cell state.

Second mitochondria-derived activator of caspases (SMAC) mimetics are relatively novel drugs under investigation as anti-cancer agents, and several have proven tolerability in clinical trials. These compounds regulate both intrinsic and extrinsic apoptosis pathways, which are dysregulated in many cancers (6, 7). SMAC mimetics have been shown to impact NF-κB signaling pathways, resulting in T cell costimulation through non-canonical NF-κB (ncNF-κB) activation (8), and subsequent increased T cell survival (9). Current data indicates that combination of SMAC mimetics with anti-tumor T cells can result in combinatorial tumor cell killing through sensitization of tumor cells to TNFα (10, 11). However, little research has been conducted on the impact of SMAC mimetics on the engineered T cell product themselves.

Here we have investigated the use of the monovalent SMAC mimetic LCL161 as an agent for delivering transient costimulation to anti-myeloma TAC T cells and to understand what subsequent changes are occurring within the T cells. We confirmed the costimulatory effects of LCL161 under conditions where TAC T cells are stimulated with antigen alone and observed enhanced survival and proliferation of T cells. However, these effects were not tied directly to the magnitude of ncNF-κB activation and we further characterized the contributions of apoptosis-related proteins, CD30, FAIM3, and Fas, to the costimulatory outcomes. Under conditions where the T cells were co-cultured with myeloma cells, we failed to see an anti-tumor benefit of LCL161 except at doses that potentiate T cell death. Deletion of Fas enhanced the survival of T cells in the presence of LCL161 and lead to enhanced expansion. Thus, although LCL161 can provide costimulation to TAC T cells, these costimulatory properties did not enhance the anti-myeloma effect of non-edited TAC T cells.

Abbreviations: SMAC, second mitochondria-derived activator of caspases; IAP, inhibitor of apoptosis; NF-κB, nuclear factor kappa-light-chain-enhancer of activated B cells; cIAP1/2, cellular IAP 1 or 2; TAC, T cell antigen coupler; FAIM3, Fas apoptotic inhibitory molecule 3; TCR, T cell receptor; CAR, Chimeric antigen receptor; TNFRSF8, TNF receptor superfamily member 8; FCMR, Fc Mu receptor; XIAP, X-linked IAP

Results

LCL161-mediated costimulation of TAC T cells

T cell costimulation is multi-faceted and results in several downstream functional changes. Proliferative capacity and survival are two key parameters augmented by costimulation that are positively associated with clinical success of adoptive T cell therapy (12, 13), and thus were used as our primary functional readouts. To characterize the costimulatory properties of LCL161, a

dye-dilution proliferation assay using CellTrace Violet was used. To determine the dose of LCL161 that provided optimal costimulation, we stimulated non-engineered T cells and engineered BCMA-specific TAC T cells (14) through the TCR or TAC receptor alone using plate-bound agonistic anti-CD3 or 6-7 μm diameter polystyrene microbeads coated with BCMA, respectively. Both non-engineered and TAC-engineered T cells demonstrated increased entry into division and increased cell yield and viability after stimulation in the presence of increasing concentrations of LCL161, which plateaued between 0.5-1 μM (Supplemental Figure 1). Therefore, we selected a concentration of 0.625 μM LCL161 for further experiments.

We noted donor variation in the degree of costimulation engendered by LCL161. Therefore, we generated TAC T cells from a series of healthy and myeloma donors to garner broad insights regarding the influence of donor on the biological outcomes (Supplemental Figure 2, Supplemental Table 1).

Treatment of T cells with LCL161 should initiate ncNF-κB signaling by conversion of NF-κB2 p100 precursor to the active p52 subunit (8). TAC T cells were stimulated with plate-bound BCMA in the presence of 0.625 μM LCL161 or vehicle for 24 – 72 hours, after which the p52/p100 ratio were determined by western blot. The amount of immobilized BCMA was determined by serial dilution in a dye-dilution proliferation assay and a concentration of 0.05 μg/mL was chosen as it provided relatively weak stimulation to readily visualize LCL161 costimulation (data not shown). Stimulation with antigen and vehicle resulted in a limited increase in the p52/p100 ratio, whereas antigenic stimulation alongside LCL161 resulted in significantly greater conversion of p100 to p52 amongst all donors (Figure 1B) indicating activation of the signaling pathway. The relative conversion of p100 to p52 varied among the T cell products tested, indicating donor variability (Figure 1C).

Given the variability in ncNF-κB signaling when TAC T cells from different donors were stimulated with target in the presence of LCL161, we assessed the proliferation and survival of TAC T cells from the donors shown in Figure 1. TAC T cells stimulated with BCMA-coated beads and 0.625 μM LCL161 displayed significantly greater viability, total live cell yield, and overall percentage of cells entering division than those stimulated with beads and vehicle alone (Figures 2A, B). While all donors displayed some enhancement in these parameters in the presence of LCL161, the effect again varied among the donors (Supplemental Figure 3). We examined the relationship between p100 to p52 conversion and the proliferation metrics by creating a simple proliferation composite score (p_c) that averages the three metrics we have examined ($pc = \frac{viability + divided\,\% + cell\ \ yield}{3}$). We then compared this composite score to the area-under-the-curve of the p52:p100 ratio plots and found that there was no relationship between the absolute magnitude of NF-κB2 activation and the level of proliferation and survival enhancement delivered by LCL161 (Figure 2C, Supplemental Figure 4).

CD30 and FAIM3 are implicated in the costimulatory role of LCL161

To gain insight into the mechanism(s) by which LCL161 influences T cell biology we performed transcriptional profiling on TAC T cells from three donors (HN18, MM16, and L10) stimulated with BCMA-coated microbeads alongside LCL161 or vehicle for 24 or 72 hrs. After stimulation, RNA was collected and analyzed using the Clariom-S Pico human genechip, which covers >20,500 genes. We primarily observed differential expression of genes related to immune function and activation (Supplemental Figure 5; data available at GEO, GSE227986). Of particular interest to us were two genes highly affected by LCL161, *FCMR* (encoding FAIM3) and *TNFRSF8* (encoding CD30) (Figure 3A). FAIM3 (15, 16) and CD30 (17–19) are both involved in regulation of costimulation and apoptosis pathways in T cells and contribute to a balance of survival and death signaling. We confirmed the transcript data by measuring the surface expression of CD30 and FAIM3 on TAC T cells following stimulation with antigen and increasing concentration of LCL161. Indeed, we observed that antigen-mediated stimulation of TAC T cells in the presence LCL161 resulted in up- and down-regulation of CD30 and FAIM3, respectively, in $CD8^+$ TAC T cells (Figure 3B). A similar observation was seen with $CD4^+$ TAC T cells (data not shown).

We sought to investigate the roles of these proteins in LCL161-mediated costimulation. We speculated that reversing the LCL161-mediated repression and induction of FAIM3 and CD30, respectively, would alter the costimulatory effects of the drug. To investigate how these receptors influence the proliferative capacity and survival of T cells during extended stimulation, we genetically engineered our BCMA TAC T cells. To force constitutive expression of *FCMR* (FAIM3 OE), we inserted a copy of the cDNA upstream of the TAC receptor in the lentiviral vector used to engineer the T cells (Figure 3C). To remove *TNFRSF8* expression (CD30 KO), we deleted the gene using CRISPR/Cas9 with a triple gRNA approach (Figure 3D). As a control, we exposed BCMA TAC T cells to a non-targeting gRNA/Cas9 RNP to account for any effect of gRNA/Cas9 or electroporation on the T cells. We used genotyping to determine CD30 gene-disruption (Figure 3E) and phenotypic analysis to determine CD30 absence and FAIM3 forced surface expression (Figure 3F, G). To do so, we stimulated TAC T cells with anti-CD3 and high dose LCL161 to maximally induce CD30 and repress FAIM3. Under the effects of LCL161 we noted a marked reduction in CD30 expression on the cell surface of the gene-edited TAC T cells compared to controls (Figure 3F), although we were unable to achieve complete knock down of CD30 despite extensive optimization of the knock-out protocol. Similarly, forced expression of FAIM3 was successful and surface expression was maintained in the presence of LCL161 during stimulation (Figure 3G). Next, we evaluated the effects of CD3O knockout and/or constitutive FAIM3 on TAC T cell proliferation and survival following stimulation with antigen-coated microbeads in the presence of LCL161. Disruption of

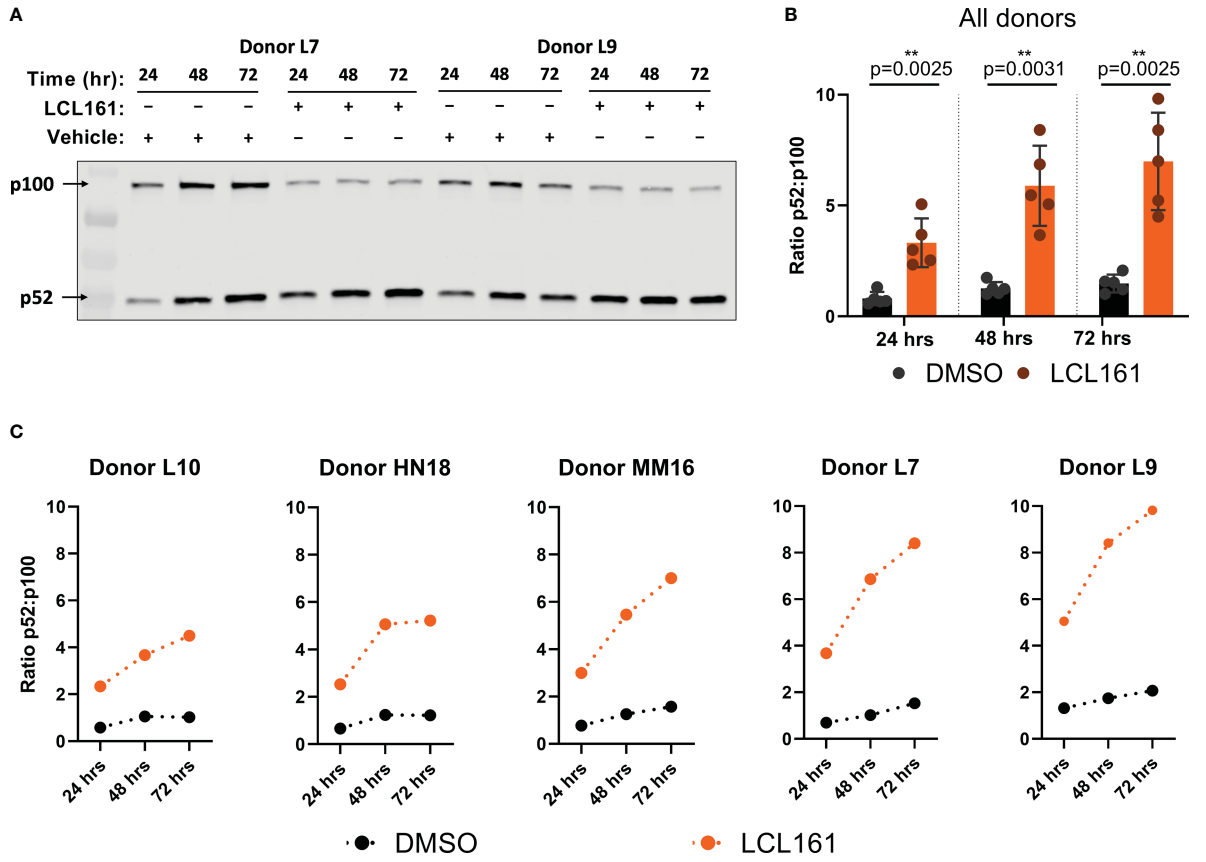


FIGURE 1
LCL161 activates the ncNF-κB signaling pathway in TAC T cells. 0.5x10^6 TAC T cells were stimulated on plates coated with 0.05 ng/mL BCMA-Fc and either DMSO or 0.625 μM LCL161. Cells were collected and lysates were processed, ran on 4-20% polyacrylamide gels, and immunoblotted for NF-κB2 p100/p52. **(A)** Representative western blot indicating levels of NF-κB2 p100 and p52. **(B-C)** Signal quantification and normalization using Li-Cor Empiria software. NF-κB2 p100 and p52 signal was quantified and normalized to total protein loaded per lane and a ratio was calculated. **(B)** n=5. **p<0.01 as calculated by two-tailed paired t test. **(C)** data from individual donors in **(B)** These data represent 2 independent experiments.

CD30 had a profound negative impact on the proliferative capacity of TAC T cells in multiple donors, even though we did not achieve complete disruption of the CD30 gene (Figure 3H). The effect of FAIM3 was variable; constitutive expression of FAIM3 impaired cell expansion of TAC T cells generated from donors L10 and L3 but had no impact on TAC T cells derived from donor L6. The combination of CD30-disruption and forced expression of FAIM3 also yielded variable outcomes as the combination further impaired the cell yield from Donor L10 TAC T cells, revealed no combinatorial effect with TAC T cells from Donor L3 and, in the case of TAC T cells from Donor L6, overexpression of FAIM3 counteracted the effects of CD30 deletion. These results demonstrate that the costimulatory effects of LCL161 on TAC T cells are CD30-dependent, while the role of FAIM3 in LCL161-mediated costimulation is variable and donor-dependent.

LCL161-mediated costimulation impairs TAC T cell expansion in co-culture with myeloma cells

To assess whether LCL161 could provide costimulatory benefit when TAC T cells were co-cultured with myeloma cells, we stimulated T cells with BCMA$^+$ MM.1S myeloma tumor cells in the presence or absence of 0.625 μM LCL161. The absolute proliferative response of the TAC T cells to the myeloma cell line was much more robust than the antigen-coated beads (Figure 4A; data from Figure 2 is included as a point of reference). Although MM.1S stimulation gave an overall stronger proliferative signal, the combination of LCL161 and MM.1S stimulation resulted in reduced expansion of the TAC T cells, which manifest as a decrease in TAC T cell numbers at the end of the co-culture, and there was no augmentation of survival or cells entering division as previously observed with bead stimulation (Figure 4B). These data reveal that while LCL161 costimulation was important when TAC T cells were stimulated with antigen alone, there may be opposing signals delivered by the tumor cells which mitigate the beneficial impacts of the LCL161.

T cell expansion can be limited by Fas-mediated death (20), and the reduced apoptosis threshold as a result of LCL161 targeting of IAPs may underpin the negative effects of LCL161 in the context of the T cell:myeloma cell cultures. Indeed, we confirmed that the tumor lines used in this study uniformly expressed FasL (Figure 4C). To address the possibility that Fas signaling mitigates the beneficial effects of LCL161, we removed Fas from the TAC T

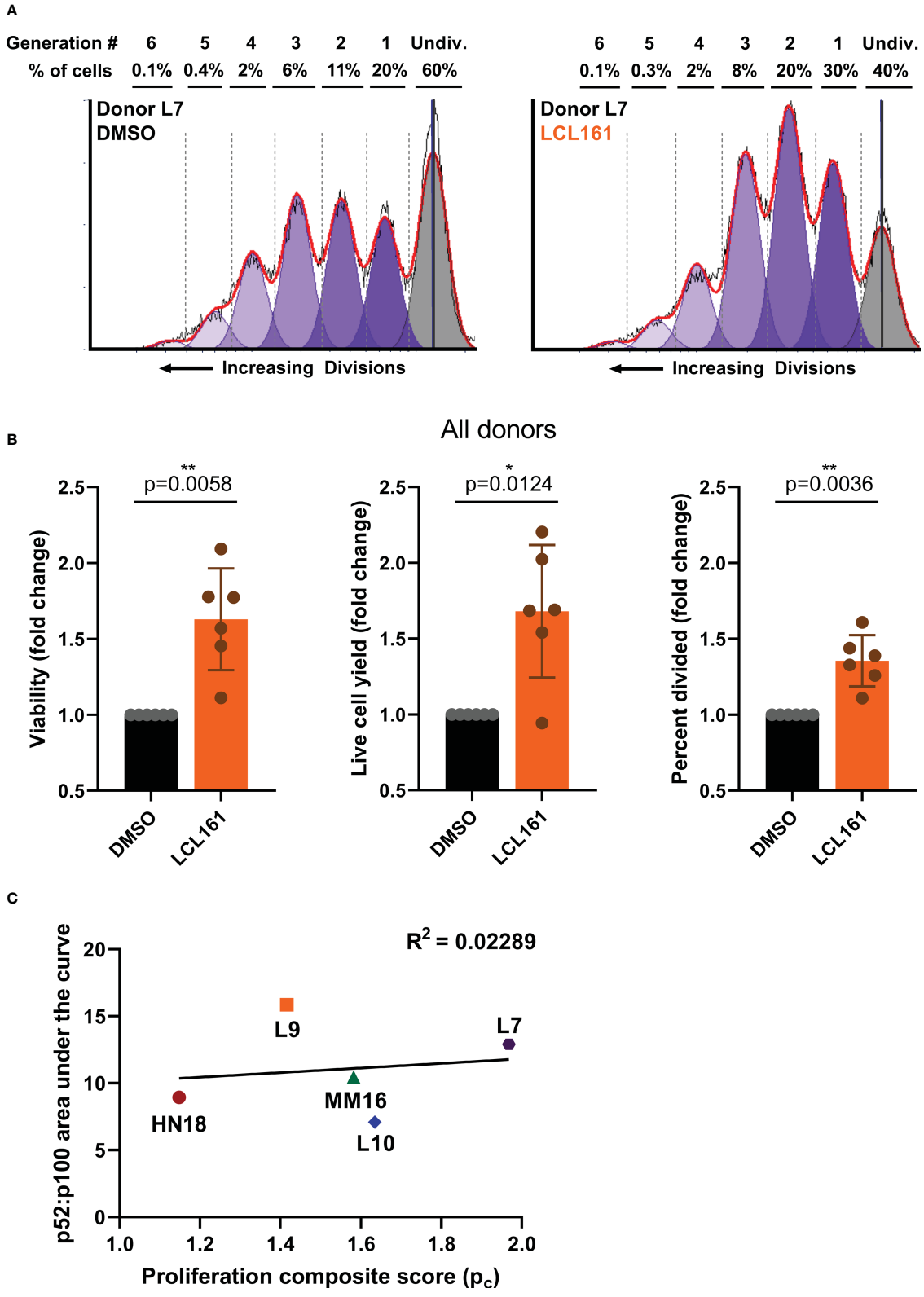


FIGURE 2
LCL161 treatment amplifies proliferation and enhances survival of antigen-stimulated TAC T cells. CTV-labelled TAC T cells were stimulated with Protein G polystyrene beads loaded with 50 ng BCMA-Fc/million beads at an E:T of 1:1 for 96 hours in the presence of 0.625 μM LCL161 or DMSO. T cells were harvested and stained for flow cytometric analysis. **(A)** representative flow plots with proliferation modeling, and **(B)** analyzed proliferation data from 5 donors, n=6; *p<0.05, **p<0.01 as calculated by two-tailed paired t test. These data represent 3 independent experiments. **(C)** Composite proliferation score was calculated as the average of the three proliferation parameters and compared to the area under the curve of the p52:p100 ratio curves in Figure 1C. A simple regression was calculated to determine linear fit.

10.3389/fimmu.2023.1179827

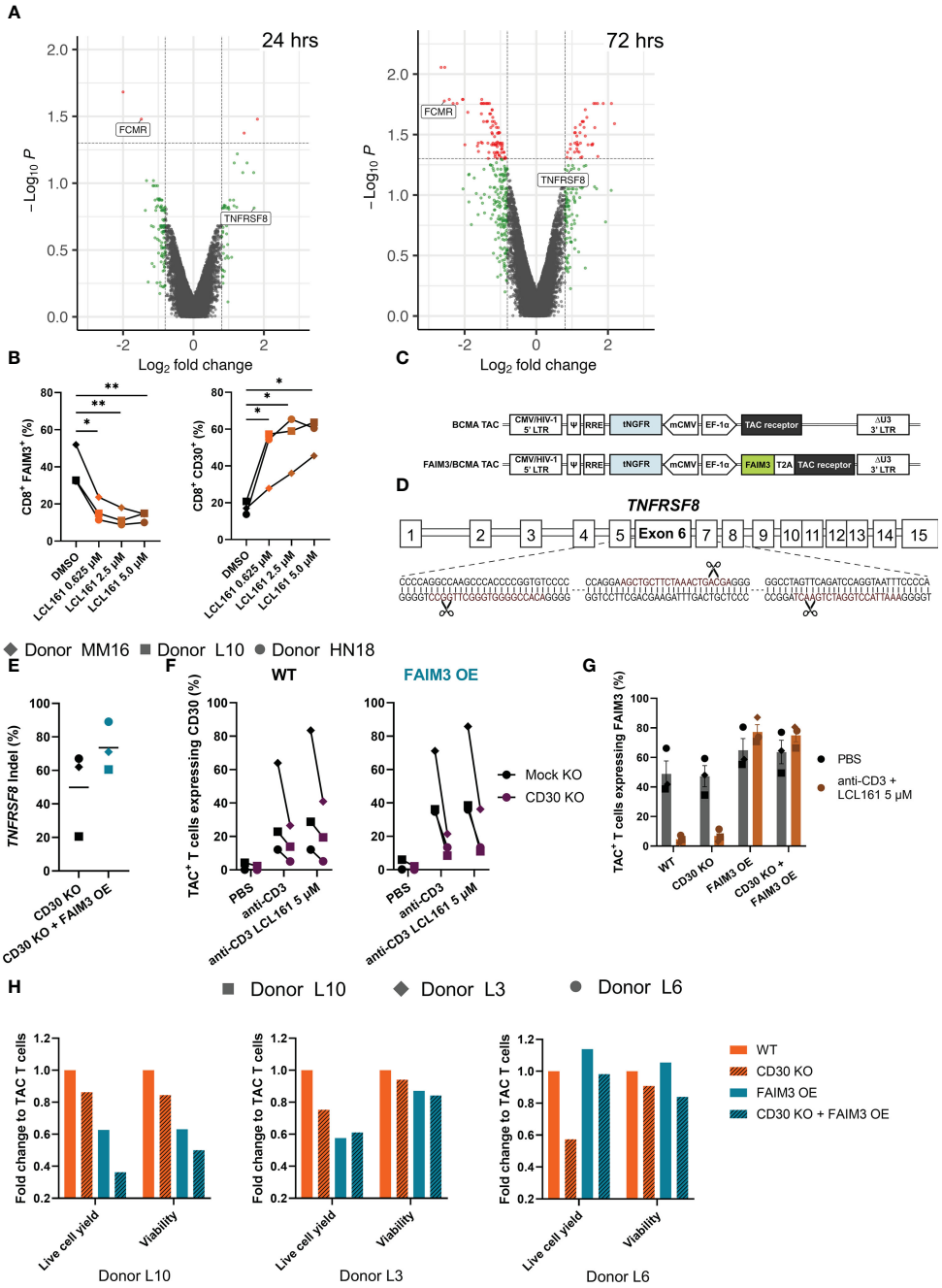


FIGURE 3
FAIM3 and CD30 mediate, in part, the costimulatory mechanisms of LCL161 in enhancing TAC T cell proliferation. **(A)** Cryopreserved TAC T cells were thawed into complete media, rested for 24 hrs, then 5x10^5 T cells were stimulated by 0.05 µg/mL plate-bound BCMA antigen for 24 or 72 hrs in the presence of DMSO or LCL161. After stimulation, cells were collected, homogenized, and RNA was collected. Transcripts were assessed using a Clariom-S Pico human genechip. n=3, 1 per donor (HN18, L10, MM16). Volcano plots of the 24 and 72 hour Clariom data were generated using a p-value threshold of 0.05 (red dots) and fold change of 1.75 (red or green dots). **(B)** Thawed and rested cryopreserved TAC T cells were stimulated for 72 hrs with BCMA-coated microbeads and LCL161 or vehicle. Cells were collected, stained, and analyzed by flow cytometry for FAIM3 and CD30 expression. **(C)** Schematic diagram of FAIM3 cDNA separated by a T2A sequence upstream of the TAC receptor within the lentiviral vector. **(D)** *TNFRSF8* was deleted by triple gRNA editing with CRISPR/Cas9, schematic indicates the sequence of gRNA (in red) and cut sites on the targeted exon. **(E-H)** BCMA TAC T cells ± FAIM3 overexpression (OE) were cultured as normal and edited on day 3 with CD30 multi-guide or negative control gRNA/Cas9 RNP by Neon electroporation. T cells were then cultured until day 14-15 and utilized fresh in assays. **(E)** TAC T cell genomic DNA was collected on day 13-14 of culture by extraction with Lucigen DNA extraction solution. The *TNFRSF8* exon 6 locus was amplified by PCR, sequenced by sanger sequencing, and indel frequency was computed using Synthego ICE. **(F-G)** BCMA TAC T cells ± FAIM3 OE were stimulated using 1 µg/mL plate-bound agonistic anti-CD3 antibody ± 5 µM LCL161 for 24 hrs (donor L10) or 72 hrs (donors L3 and L6). After stimulation T cells were collected and stained for **(F)** CD30 and **(G)** FAIM3 expression and analyzed by flow cytometry. **(H)** CTV-labelled TAC T cells were stimulated with 0.625 µM LCL161 and BCMA-coated microbeads at an E:T 1:1 for 96 hrs then analyzed by flow cytometry. Data was modeled using FCS Express 7 and values were normalized to wildtype TAC T cells. n=3. The data in panel B represent 1 independent experiment. The data in panels E – H represent 3 independent experiments.

cells by CRISPR-mediated gene-editing. Here, we reproducibly achieved a high efficiency KO at >80% in all cases (Figure 4D). The removal of Fas in the TAC T cells enhanced total cell yield, viability, and cells entering division of TAC T cells in the presence of 0.625 μM LCL161 when T cells were stimulated with antigen alone ("Beads"; Figure 4E). This effect was greater in cells treated with LCL161 rather than DMSO. Furthermore, we observed that the incidence of apoptotic T cells was reduced following stimulation with antigen alone in the presence of LCL161 when Fas was disrupted, supporting a role for Fas in limiting the costimulatory effects of LCL161, presumably through fratricide ("Beads"; Figure 4F). Removal of Fas from the TAC T cells did improve cell yield following stimulation with MM.1S, but did not impact viability, cell division or incidence of apoptosis in LCL161 treated T cells compared to DMSO ("MM.1S"; Figures 4E–F).

LCL161 enhancement of TAC T cell anti-tumor cytotoxicity is accompanied by T cell toxicity

Although we did not observe enhanced proliferation or survival on TAC T cells stimulated with myeloma tumor cell lines *in vitro*, we wondered if LCL161 would augment T cell-mediated cytotoxicity against myeloma cells. To this end, TAC T cells were co-cultured with myeloma cells in the presence of LCL161 and tumor viability was assessed. Enhanced killing of the tumor cells was only observed with high concentrations of LCL161 tested (5 μM; Figure 5A). In fact, a small change in concentration to 2.5 μM failed to provide enhanced killing (Figure 5B). Inhibition of the IAPs in tumor cells is predicted to result in increased sensitivity to TNF-mediated cell death by switching TNFα signaling from activation of the classical NF-κB pathway towards caspase-8 mediated apoptosis (21, 22), and we have observed that TAC T cell produce large amounts of TNFα upon stimulation by myeloma cell lines (Figure 5C). To address whether LCL161 augments TAC T cell killing through sensitization of the multiple myeloma tumor cells to TNFα, we cultured MM.1S or RPMI 8226 cell lines with 5 μM LCL161 +/- recombinant human TNF. MM.1S cells displayed a modest increase to cell death when treated with both LCL161 and TNF, whereas RPMI 8226 cells remained largely unaffected (Figure 5D). This was not entirely unexpected as there is considerable heterogeneity in susceptibility of MM cell lines to LCL161 (23), which may be in part be due to deletions of cIAP1/2 or other NF-κB-associated factors that occur in some multiple myelomas (24, 25). Investigating these two cell lines further showed a complete basal absence of cIAP2 and p100 in the RPMI 8226 cells (Supplemental Figure 6), which may explain the lack of sensitization to TNFα. Thus, the increased killing of the myeloma cell lines in the presence of higher concentration of LCL161 (5 μM) is likely due to something other than sensitization of TNFα-mediated killing.

The results in Figure 2 indicated that maximal costimulation of the T cells is achieved with an LCL161 concentration below 1 μM, however the results in Figure 5 indicated that concentrations of 5 μM were required to observe enhanced killing of myeloma tumor cells. We, therefore, explored the effect of 5 μM LCL161 on TAC T cells. While we observed that this high concentration of LCL161 could significantly enhance the percent of T cells that entered division (Figure 6A), we also noted a concomitant increase in activation induced cell death (AICD). We excluded strictly dead/necrotic cells and measured the portion of live TAC T cells that were sensitized by 5 μM LCL161 towards apoptosis by measuring active caspase-3 expression and the presence of phosphatidylserine on the outer membrane leaflet of TAC T cells stimulated with antigen-loaded beads for 48 hrs. We observed a trend towards increased proportion of stimulated TAC T cells entering apoptosis and decreased viability (Figure 6B). We questioned whether this observation might be explained by a second IAP target of LCL161, X-linked IAP (XIAP). As XIAP is a regulator of caspase-3, -7, and -9 related apoptotic pathways (26), depression of caspase-inhibition by XIAP at high concentrations of LCL161 may further potentiate T cells towards death (27). We stimulated T cells from two healthy donors (M12 and L15) with plate-bound BCMA-Fc and 5 μM LCL161 for 72 hours and examined the levels of XIAP within these cells, but we did not observe any difference in XIAP levels (Supplemental Figure 7). We questioned if the impact of Fas is more pronounced with high dose LCL161 due to sensitization of TAC T cells towards death at the 5 μM dose. Fas KO-TAC T cells were stimulated with antigen-coated beads or MM.1S myeloma cells and we assessed proliferative capacity, viability, and susceptibility to apoptosis in the presence of 5 μM LCL161 (Figures 6C–D). The deletion of Fas again manifested greater enhancement to proliferation and viability, and reduction to apoptosis in bead-stimulated T cells than MM.1S stimulated T cells. The mean absolute change in proliferation metrics and viability of Fas-deleted TAC T cells stimulated with bead-based antigen in the presence of 5 μM LCL161 was greater than previously measured at the lower 0.625 μM dose, suggesting that Fas limits T cell expansion under these conditions. Similar to the observation with 0.625 μM LCL161, TAC T cells stimulated with myeloma cells in the presence of 5 μM displayed enhanced accumulation of TAC T cell at the end of the culture period but no significant improvement to viability, which points to a mechanism unrelated to Fas.

Discussion

Unlike chimeric antigen receptors which require the inclusion of costimulation domains for optimal function (3), TAC receptors provide robust anti-tumor immunity without the need for engineered costimulation. Indeed, other synthetic receptor strategies that utilize TCR-centric designs also show potent function in the absence of costimulation (28, 29). These properties notwithstanding, costimulation promotes survival, greater proliferative capacity (30), and memory formation/persistence (31) – important traits for anti-tumor engineered T cell products (32). Herein we investigated a strategy for controlled and transient druggable delivery of costimulation using the clinical candidate, LCL161. We observed an enhancement to TAC T cell survival and proliferative capacity that was restricted at higher doses of LCL161, partially through a Fas-mediated mechanism (Figure 7).

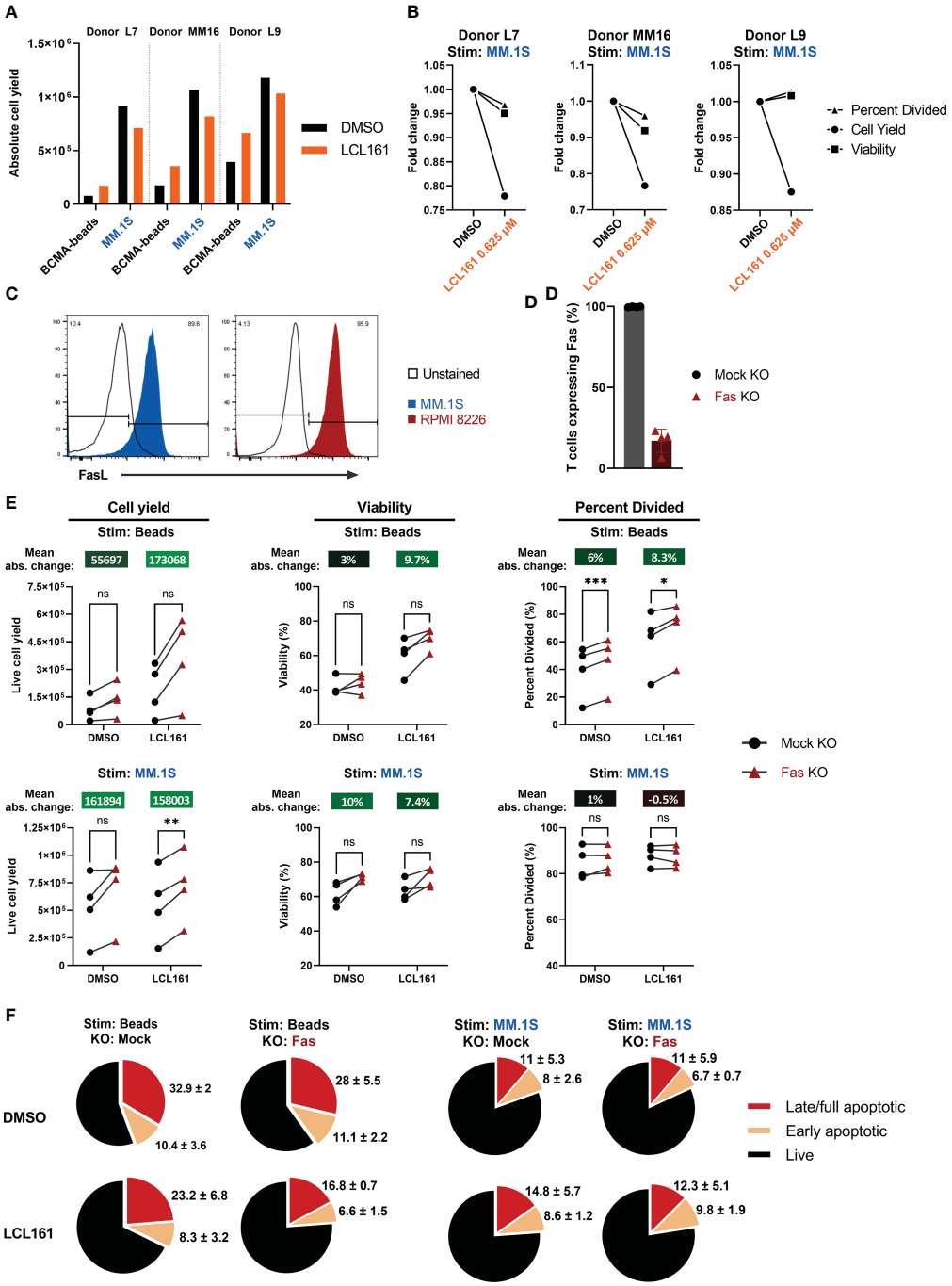


FIGURE 4
LCL161 does not enhance TAC T cell survival and proliferation when co-cultured with myeloma cells *in vitro* and is independent of Fas. **(A-B)** Thawed and rested cryopreserved BCMA TAC T cells were stimulated 1:1 with MM.1S tumor cells or BCMA-coated microbeads in the presence of 0.625 µM LCL161 for 96 hrs. Absolute cell count was enumerated using counting beads during flow cytometric analysis. The bead proliferation data displayed in **(A)** is shared in Figure 2B. **(B)** Proliferation metrics from TAC T cells stimulated with MM.1S cells were normalized to the vehicle control. **(C)** Cultured MM.1S and RPMI 8226 myeloma cells were stained for FasL expression and analyzed by flow cytometry. **(D–F)** BCMA TAC T cells were cultured as normal and edited on day 3 with Fas multi-guide or negative control gRNA/Cas9 RNP by Neon electroporation. T cells were then cultured until day 14-15 and utilized fresh in assays. n=4. **(D)** BCMA TAC T cells edited with mock or Fas RNP were stained for Fas expression on day 13-14 and analyzed by flow cytometry. **(E)** Mock or Fas-edited TAC T cells were stimulated 1:1 with MM.1S tumor cells or BCMA-coated microbeads and in the presence of 0.625 µM LCL161 or vehicle for 96 hrs. After stimulation, samples were stained, mixed with counting beads, and analyzed by flow cytometry. Proliferation metrics were modeled using FCS Express 7 software. Mean absolute change between mock and Fas KO is reported above each condition. **(F)** Mock or Fas-edited TAC T cells were stimulated 1:1 with MM.1S tumor cells or BCMA-coated microbeads and in the presence of 0.625 µM LCL161 or vehicle for 72 hrs. After stimulation, cells were stained for live/dead, fixed, and finally stained for phosphatidylserine (PS) on the outer membrane. Cells were analyzed by flow cytometry. Early apoptotic cells were defined as live/dead$^-$, PS$^+$, late/full apoptotic cells were defined as live/dead$^+$, PS$^+$. Pie charts represent mean values, with mean + standard deviation written outside the pie slice. n=3. These data represent 3 independent experiments. ns: not significant, *p<0.05, **p<0.01, and ***p<0.001 as calculated by paired t test with Holm-Šídák method.

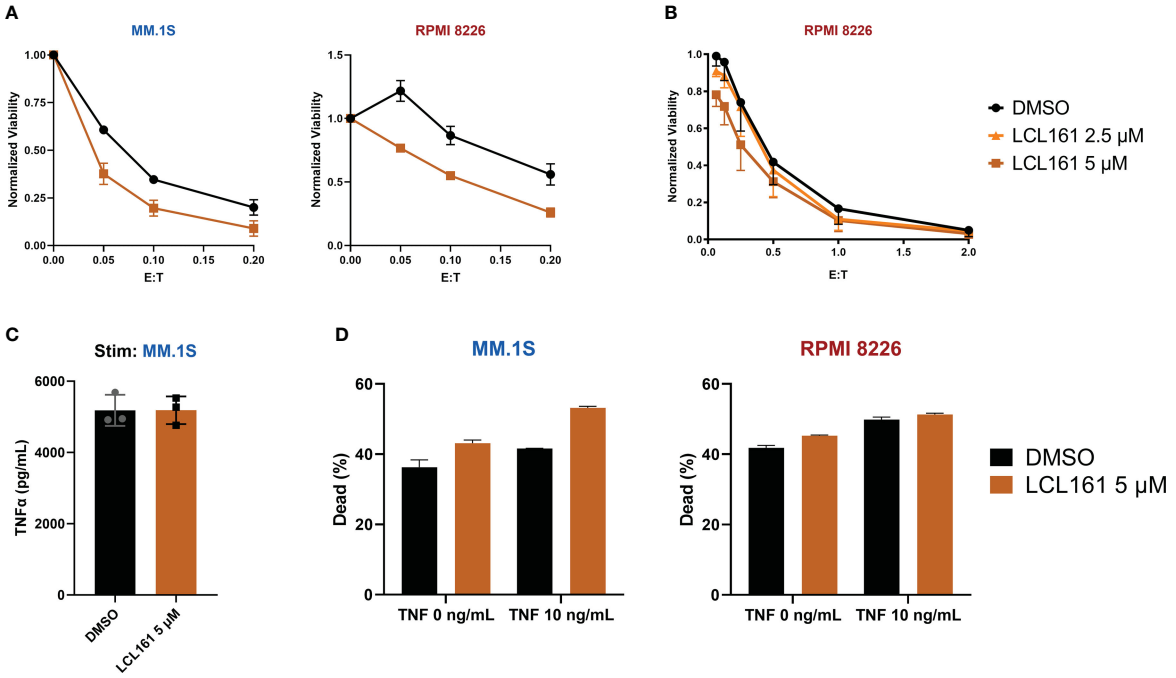


FIGURE 5
LCL161 sensitizes multiple myeloma cells to T cell cytotoxicity at higher doses. **(A)** 5x10^5 tumor cells were co-cultured with TAC T cells and 5 μM LCL161 or vehicle, in biological triplicate at various E:T for 24 hrs. After co-culture, cytotoxicity was measured through flow analysis and normalized to tumor-only controls; data shown as mean and SD. Data were generated with T cells from 3 different donors (L5, L6, L9) run independently in 1 experiment **(B)**. Luciferase-based cytotoxicity assay of TAC T cells co-cultured with effLuc+ myeloma cell lines for 48 hours in the presence of vehicle or LCL161. Samples were run in triplicate and normalized to tumor-only cell controls; data shown as mean and SEM. Data were generated with T cells from 3 different donors (L6, L7, L9) run independently in 1 experiment. **(C)** TAC T cells were stimulated with MM.1S cells at an E:T ratio of 1:1 in the presence of either DMSO or LCL161 for 24 hours and TNFα levels were measured in the supernatant. The data reflects technical triplicates **(D)** Multiple myeloma cell lines were incubated with DMSO or LCL161, in the presence of TNFα for 48 hrs. Cells were harvested, stained for viability, and analyzed by flow cytometry. The data reflects technical triplicates.

Our study employed engineered TAC T cells from both healthy donors and multiple myeloma patient donors to broaden the applicability and relevance of our findings. A reductionist antigen-on-bead system allowed us to fine tune signaling events and stringently study the effects of LCL161 on our engineered TAC T cells. Costimulation from IAP antagonism is mediated through the ncNF-κB pathway (8), an observation we corroborated. Low dose LCL161 potentiated processing of NF-κB2 p100 to p52 that increased for at least 72 hrs following TAC-mediated stimulation. Functionally, low dose LCL161 provided functional improvements to T cells measured by enhanced survival and expansion. We noted that the extent to which the LCL161 enhanced survival and expansion did not appear to correlate with the ratio of p100 to p52 conversion; for example, donor HN18 displayed little enhancement of proliferation with LCL161 yet strongly activated the ncNF-κB pathway. While the exact mechanism underpinning this donor-to-donor variability remains unclear, genechip transcriptional profiling identified numerous targets which led us to investigate in more detail the roles of CD30 and FAIM3 in LCL161-mediated enhancement of TAC T cell proliferation. How these receptors function is not fully elucidated within the field of T cell biology; research is mixed with some studies showing a pro-apoptotic capacity (17, 18), and others showing a costimulatory or survival property (15, 16, 19). CD30 is a well-known TNFRSF member that plays a pivotal role in T cell activation as well as providing survival signals for lymphomas that is cIAP-dependent (33). Indeed, SMAC mimetic treatment has been shown to provide similar cellular signals as CD30, intersecting on canonical and ncNF-κB signaling (34, 35). Our data with CD30 KO clearly demonstrated its requirement in enhancing proliferation and survival in the context of LCL161 treatment. The impact of FAIM3 overexpression was less clear due to donor variation, but the data indicated a trend towards restricting proliferation when it is constitutively expressed in TAC T cells. A recent report suggested that costimulation *via* FAIM3 was dependent on the availability of its ligand, IgM (16). We reasoned that bovine IgM present in our culture medium may not provide an appropriate ligand, so we added exogenous human IgM to our culture medium but found no additive effects with the FAIM3 overexpressing cells (data not shown).

Although we observed a slight enhancement to TAC T cell-mediated killing of multiple myeloma cells *in vitro* at high doses of LCL161 (5 μM), this effect did not persist with a 2-fold reduction in concentration. Indeed, we expanded our investigation to *in vivo*

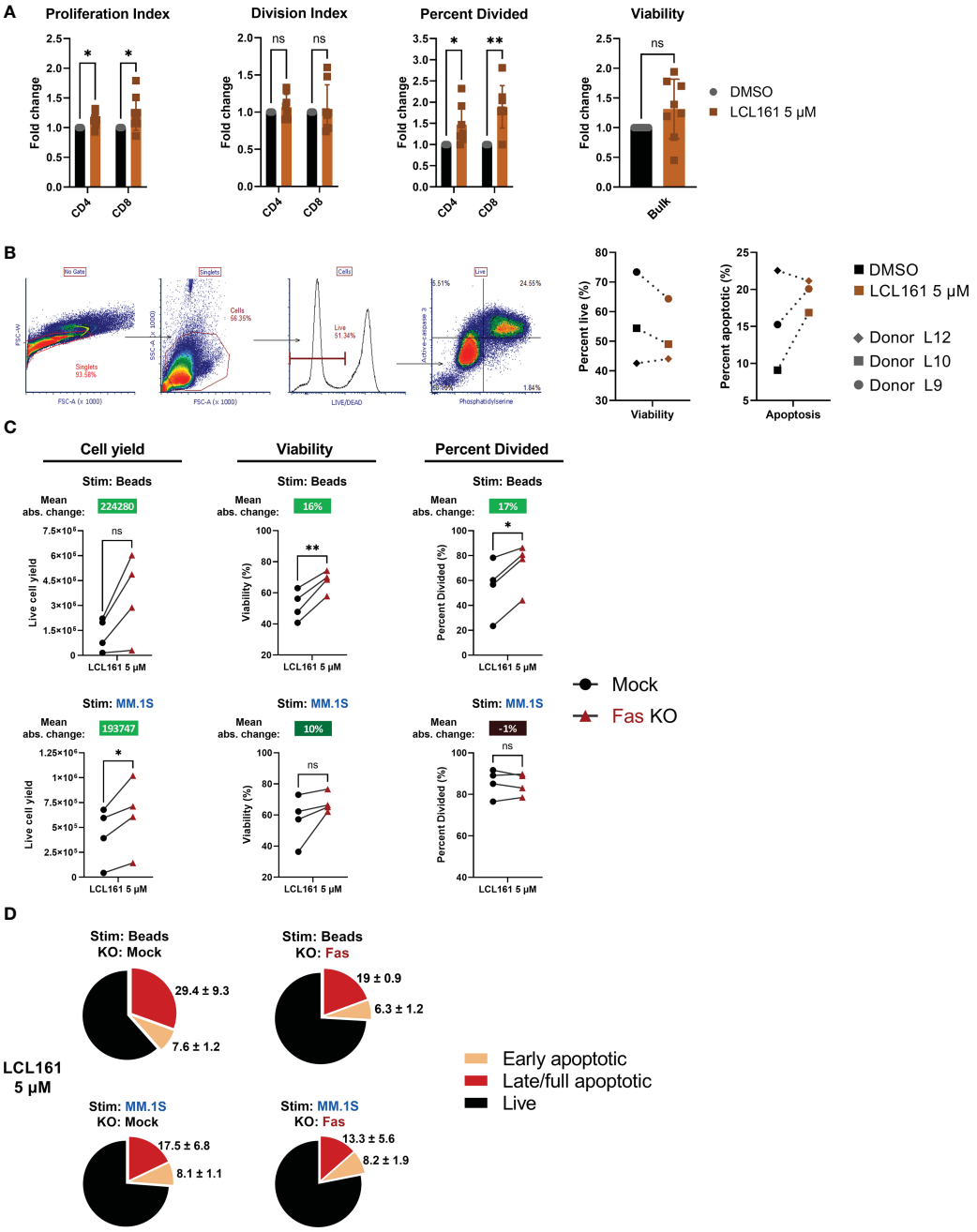


FIGURE 6
High dose LCL161 initiates activation induced cell death in stimulated TAC T cells that is responsive to Fas KO only in the case of antigen-alone stimulation. **(A)** TAC T cells labeled with CellTrace Violet were cultured with loaded beads at an E:T of 1:1 for 96 hrs. T cells were harvested and stained for flow cytometric analysis. Proliferation metrics were modeled with FCS Express 7. Proliferation and division indices are a measure of the average number of cells any or a dividing cell generates, respectively. Paired and unpaired parametric t tests with Holm-Šídák correction was used to calculate statistical significance; ns, P>0.05, *P<=0.05, **P<= 0.01. n=8, comprising 5 different donors generated in 7 independent experiments **(B)** TAC T cells were stimulated with protein G polystyrene beads coated with antigen-loaded microbeads for 48 hrs. Viability and proportion of apoptotic cells as defined by live/dead, phosphatidylserine and active-caspase 3 staining. Viable cells are defined as live/dead negative, and apoptotic cells defined as active caspase3$^+$ and PS$^+$. Data represent T cell products from 3 donors produced in 3 independent experiments. **(C)** CTV-labeled mock or Fas-edited TAC T cells stimulated 1:1 with MM.1S tumor cells or BCMA-coated microbeads and in the presence of 5 µM LCL161 or vehicle for 96 hrs. After stimulation, samples were stained, mixed with counting beads, and analyzed by flow cytometry. Proliferation metrics were modeled using FCS Express 7 software. Mean absolute change between mock and Fas KO is reported above each condition. Data were generated with T cells from 4 donors (L15, M12, M28, M46) produced in 3 independent experiments. **(D)** Mock or Fas-edited TAC T cells were stimulated 1:1 with MM.1S tumor cells or BCMA-coated microbeads and in the presence of 5 µM LCL161 or vehicle for 72 hrs. After stimulation, cells were stained for live/dead, fixed, and finally stained for phosphatidylserine. Cells were analyzed by flow cytometry. Early apoptotic cells were defined as live/dead$^-$, PS$^+$, late/full apoptotic cells were defined as live/dead$^+$, PS$^+$. Pie charts represent mean values, with mean + SD written outside the pie slice. Data were generated with T cells from 3 donors (M12, M28, M46) produced in 2 independent experiments.

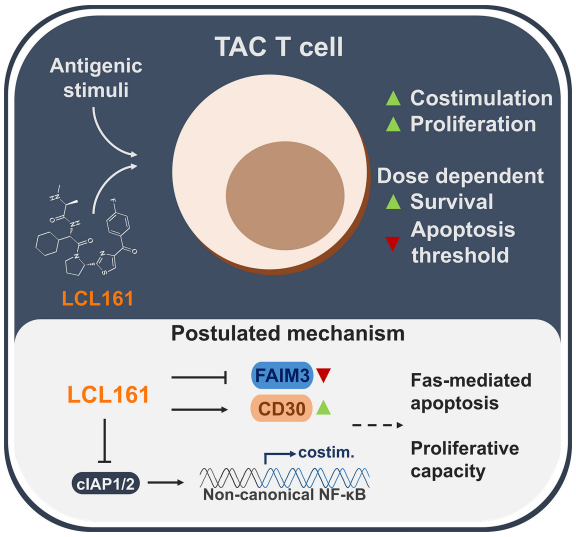


FIGURE 7
A summarized overview of the observations and postulated mechanisms of LCL161-effects on TAC T cell biology.

studies and similarly observed no benefit in anti-tumor activity of TAC T cells against system MM.1S xenografts (described in our recent publication (14)) when mice were concomitantly treated with either 25 or 75 mg/kg LCL161 (data not shown). Our data indicate that the negative effects of the drug on the T cell population need to be carefully considered. A balance between the costimulatory effects of LCL161 and unwanted induction of AICD in the T cells became evident as we titrated the dose of drug on activated T cells, an observation previously seen with non-engineered T cells at high doses of LCL161 (36). We suspected that knockdown of both cIAP1/2 and XIAP at higher doses of LCL161 could render the T cells more susceptible to full caspase-3 activation and subsequent cell death (27). This may be exacerbated by TNFα produced by the TAC T cells, which can further potentiate death signaling in the absence of cIAP1/2 (22, 37). We did not observe increased knockdown of XIAP at increasing LCL161 doses 72 hrs after antigenic stimulation. However, it is possible that XIAP is competitively inhibited rather than degraded, and thus is not suppressing caspase-activation or death signaling. Indeed, the apoptotic sensitization in the T cells may be transduced through death-receptor pathways as XIAP is known to restrict Fas-mediated apoptosis (38). As activated T cells express Fas and FasL for regulation and immune homeostasis (39), we speculated that expression of FasL on the tumor cells contributed to the restricted ability of LCL161 to enhance TAC T cell survival and proliferation in the context of myeloma cell stimulation. In addition to this, T cell fratricide through Fas-FasL interactions with neighbouring T cells would compound this effect. To address this, we knocked out expression of Fas on our TAC T cells and showed a reduction to T cell toxicity at the low and high doses of LCL161 with bead stimulation, supporting our hypothesis that LCL161 does reduce the threshold to apoptosis in activated T cells through Fas-driven fratricide. However, this effect did not translate as clearly to MM.1S cell-based stimulation which indicates that other factors or mediators are likely involved in the restriction of LCL161-mediated proliferative enhancement with myeloma cell lines. Fas-deletion recovers the loss of TAC T cell yield observed following MM.1S stimulation in the presence of 5 μM LCL161, which supports the hypothesis that the decline in T cell yield following stimulation with MM.1S is mediated, at least in part, through Fas signaling. Nevertheless, even in the absence of Fas, we do not observe an increase in TAC T cell viability or proliferation in the presence of LCL161, which suggests that LCL161-mediated costimulation is inconsequential in the presence of the full complement of adhesion molecules and costimulatory ligands (such as LFA-3 [40])] found on the myeloma cells. Indeed, we have detected CD137L and CD86 on RPMI 8226 and MM.1S cells by flow cytometry (data not shown).

Given that the myeloma lines RPMI 8226 and MM1S were resistant to LCL161 (23) and TNFα, we were able to tune our investigations to draw conclusions under the lens of a TAC T cell-centric observation and understand the impact on T cell biology. Our study highlights several pathways and mechanisms by which LCL161 integrates into T cell proliferation and survival, expanding our understanding of SMAC mimetics as enhancers of anti-cancer immunity (41). Additional refinement to SMAC mimetic small molecule drugs through medicinal chemistry, or development of direct cIAP1/2 antagonists, could increase the therapeutic threshold between costimulatory effects and unwanted sensitization to AICD. Beyond their use as drugs to activate costimulation in the context of cell therapy, the evidence that LCL161 can enhance T cell proliferation *ex vivo* in response to a reductionist stimulation suggests that small-molecule IAP antagonists may be of use during the manufacturing of engineered T cells through enhancement of proliferation.

Methods

Cell lines

Human myeloma cell lines RPMI-8226 (CCL-115; purchased from ATCC (Manassas, VA) and MM.1S (kindly provided by Dr. Kelvin Lee, Roswell Park Cancer Institute, NY) were cultured in RPMI 1640 (Gibco (Thermo Fisher Scientific), Waltham, MA), supplemented with 10% FBS (Gibco), 2 mM L-glutamine (BioShop Canada Inc., Burlington, ON, Canada), 10 mM HEPES (Roche Diagnostics, Laval, QC, Canada), 1 mM sodium pyruvate (Sigma-Aldrich Canada Co. (Millipore Sigma), Oakville, ON, Canada), 1 mM nonessential amino acids (Gibco), 100 U/mL penicillin (Gibco), and 100 μg/mL streptomycin (Gibco). To generate luciferase-expressing cell lines, parental RPMI 8226 or MM.1S cell lines were transduced with lentivirus encoding enhanced firefly luciferase (effLuc) (42) as well as puromycin N-acetyltransferase at an MOI 10 and selected in culture media supplemented with 8 μg/mL puromycin (InvivoGen, San Diego, CA). HEK293T cells (kindly provided by Dr. Megan Levings, University of British Columbia, Canada) were cultured in DMEM (Gibco), supplemented with 10%

FBS (Gibco), 2 mM L-glutamine (BioShop), 10 mM HEPES (Roche Diagnostics), 100 U/mL penicillin (Gibco), and 100 µg/mL streptomycin (Gibco), or 0.1 mg/mL normocin (InvivoGen). All cells were cultured at 37°C, 95% ambient air, 5% CO2, and routinely tested for mycoplasma contamination using the PlasmoTest detection kit (InvivoGen, San Diego, CA, USA).

Lentivirus production

Lentivirus encoding the BCMA-specific TAC receptor and truncated NGFR transduction marker (14) with or without FAIM3 was produced as previously described (43) using a third generation packaging system (44). Briefly, 12 x 10^6 HEK293T cells plated on a 15-cm dish (NUNC (Thermo Fisher Scientific)) were transfected with plasmids pRSV-REV (6.25 µg), pMD2.G (9 µg), pMDLg-pRRE (12.5 µg), and pCCL BCMA TAC (32 µg) encapsulated with Lipofectamine 2000 (Thermo Fisher Scientific) in Opti-MEM media (Gibco). 12-16 hours post-transfection, media was exchanged with HEK293 media supplemented with 1 mM sodium butyrate (Sigma-Aldrich). 24-36 hours later, supernatant was harvested, filtered through a 0.45 µm asymmetric polyethersulfone filter (Thermo Fisher Scientific) to remove cellular debris. Viral particles were then concentrated using an Amicon Ultra 15 100 kDa centrifugal filter (Millipore Sigma) and stored at -80°C. Viral titre (TU/mL) was determined post-thaw by serial dilution and transduction of HEK293T cells, and enumeration of percent $NGFR^+$ cells by flow cytometry.

Generation of engineered human T cells

Peripheral blood mononuclear cells (PBMCs) were obtained from healthy or myeloma patient donors who provided informed written consent in accordance with the Hamilton Integrated Research Ethics Board, or were collected from commercial leukapheresis products (HemaCare, Northridge, CA and STEMCELL Technologies, Vancouver, BC, Canada). In the case of leukapheresis products, samples were transported at room temperature and processed within 24 hrs of collection. Whole blood was collected from donors using BD CPT sodium heparin collection tubes (BD Biosciences). PBMCs were isolated from blood or leukapheresis by Ficoll-Paque Plus gradient centrifugation (Cytiva, Vancouver, BC, Canada) and cryopreserved in inactivated human AB serum (Corning, Corning, NY) containing 10% DMSO (Sigma-Aldrich), or in CryoStor10 (STEMCELL Technologies) for healthy donors, and RPMI (Gibco) containing 12.5% human serum albumin (Sigma-Aldrich) and 10% DMSO (Sigma-Aldrich) for myeloma patient donors. Samples were cryopreserved in an isopropanol controlled-rate freezer (Thermo Fisher Scientific) at -80°C for 24-72 hrs prior to long term storage in liquid nitrogen. Post-thaw, PBMCs were activated with 25 µL ImmunoCult soluble anti-CD3/28/2 tetrameric complexes (STEMCELL Technologies) per mL PBMC, and cultured in RPMI 1640 (Gibco) containing 10% FBS (Gibco), 2 mM L-glutamine (BioShop), 10 mM HEPES (Roche), 1 mM sodium pyruvate (Sigma-Aldrich), 1 mM non-essential amino acids (Gibco), 55 µM β-mercaptoethanol (Gibco), 100 U/mL penicillin (Gibco), 100 µg/mL streptomycin (Gibco), 1.5 ng/mL rhL-2 and 10 ng/mL rhIL-7 (PeproTech, Cranbury, NJ). 16-24 hours later, activated T cells were transduced with lentivirus at an MOI of 1-2. T cells edited by CRISPR/Cas9 were washed with 1x PBS on day 3 to remove soluble activator, otherwise T cells were washed on day 4. Transduced cells were enriched with the EasySep Human CD271 Positive Selection Kit II (STEMCELL Technologies) on day 7-10 of culture. Culture yields were enumerated every 2-3d and supplemented with cytokine-containing media to dilute cultures to ~ 1.0×10^6 cells/mL. Engineered T cell products were expanded for a total culture period of 14-15 days prior to use. In some cases, TAC T cell products were cryopreserved prior to use. In short, after culture cells were cryopreserved in CryoStor10 according to manufacturer's directions at 20×10^6 cells/mL (for downstream *in vitro* assays). Prior to use of cryopreserved TAC T cell products in any *in vitro* assay, cells were thawed according to manufacturer's directions and rested for 24 hrs in cytokine-containing media (as above). Mean viability and recovery were 85.5% (± 7.2% std. dev.; 95% CI [83.2, 87.7]) and 57.2% (± 16.4% std. dev.; 95% CI [52.1, 62.3]), n=42.

All assays were performed in T cell medium without cytokines; FBS lots were assessed compared to previous lots to ensure similar T cell manufacturing (expansion, viability, cryopreservation) and functionality (proliferation, cytotoxicity, and cytokine production).

CRISPR/Cas9 editing of T cells

T cell gene-editing was accomplished by electroporation of complexed gRNA/Cas9 ribonucleoprotein (RNP). To generate RNP, a triple sgRNA pool (Synthego, Redwood City, CA, USA) or negative control gRNA (IDT, Newark, NJ, USA) was complexed with 20 pmol Alt-R HiFi Cas9 V3 (IDT) at a 3:1 sgRNA , Cas9 molar ratio for 10-15 min at room temperature. Prior to electroporation activated T cells were pooled and washed with 1x PBS. $5x10^5$ T cells per electroporation were resuspended in buffer T (Thermo Fisher Scientific) and mixed with complexed RNP (20 pmol on a Cas9 basis) and shocked using a NEON electroporation system (Thermo Fisher Scientific) set to 1600 V, 10 ms pulse width, and 3 pulses. Immediately after electroporation, T cells were dispensed into antibiotic-free T cell medium containing rhIL-2 and rhIL-7. To edit the *TNFRSF8* gene, exon 6 was targeted with sgRNAs with sequences (5' – 3'), AAATTACCTGGATCTGAACT, AGCTGCTTCTAAACTGACGA, and ACACCGGGGTGGGCTTGGCC. To edit the *FAS* gene, exon 2 was targeted with sgRNAs with sequence (5' – 3'), CACU UGGGCAUUAACACUUU, UACAGUUGAGACUCAGAACU, and GUGUAACAUACCUGGAGGAC. Genomic DNA was collected from T cells on d14/15 with QuickExtract DNA extraction solution 1.0 (Lucigen, Hoddesdon, UK) following manufacturers instructions, and targeted exons were amplified by PCR and sequenced by sanger sequencing. Indel analysis was performed by Synthego ICE (45) with PCR/sequencing primers (5' – 3') for *TNFRSF8* exon 6, CTC CCCCTCATCTCAAGAGCTATC and TGAGCCTCAAAC

CAAAGCAAGA; *FAS* exon 2 TGAAGAACCTGAGATCCA AACTGCT and TGGTAGATCCTAATCAGTTTTGACATGA.

Flow cytometry

Flow cytometry data were collected with BD LSR II (V/B/R or V/B/YG/R laser configuration), BD LSR Fortessa (V/B/R laser configuration) or Beckman Coulter CytoFLEX LX (NUV/V/YG/B/R laser configuration) and analyzed using FCS Express v7 Software (DeNovo Software, Pasadena, CA).

Phenotypic characterization of T cell products

Surface expression of BCMA TAC constructs was determined by staining with recombinant human BCMA-Fc protein (R&D Systems, Minneapolis, MN), followed by goat anti-human IgG (to detect BCMA-Fc) and antibodies against markers CD4, CD8α, CD30, FAIM3, Fas, and/or NGFR. Antibody-fluorochrome combinations, cat #, and RRID# are indicated in the table following the materials section. Unless otherwise stated, all stains were done at room temperature for 30 minutes in PBS + 2% BSA + 2.5 mM EDTA. Staining was assessed by flow cytometry.

Transduction efficiency of TAC T cells was evaluated by co-expression of the TAC receptor and truncated NGFR in bulk, CD4, and/or CD8 populations (refer to Supplemental Figure 8 for gating strategy). Knockout of Fas was similarly detected (refer to Supplemental Figure 9).

To assess expression of FAIM3 and CD30 of unedited TAC T cells in response to LCL161, 72-hour cell stimulation with BCMA-coated microbeads and LCL161 (5 µM) or vehicle was used. FAIM3 expression was abrogated in response to stimulation, whereas CD30 expression required stimulation (refer to Supplemental Figure 10 for gating strategy). To assess expression of FAIM3 and CD30 on CD30-edited and/or FAIM3 overexpressing TAC T cells 72-hour stimulation with 1 µg/mL plate-bound agonistic anti-CD3 (clone, OKT3) and LCL161 (5 µM) or vehicle was utilized (refer to Supplemental Figure 11 for gating strategy).

In vitro cytotoxicity assay

For luciferase-based cytotoxicity assays TAC T cells were co-cultured in triplicate with $2.5x10^4$ luciferase-expressing RPMI 8226 or MM.1S cells in the presence of DMSO or LCL161 at indicated effector:target ratios for 48 hours at 37°C in opaque-white flat-bottom 96-well microplates. Following co-culture, 0.15 mg/mL D-Luciferin (Perkin Elmer, Waltham, MA) was added, and luminescence was measured with an open filter using a SpectraMax i3 (Molecular Devices, San Jose, CA) plate reader. Tumor cell viability was calculated as $\frac{(Emission-background)}{(Tumor\ alone-background)} \times 100$ %. For flow-based cytotoxicity assays, engineered T cells were co-cultured with $2.5x10^4$ RPMI 8226 or MM.1S cells with DMSO or LCL161 at indicated effector:target ratios for 24 hrs at 37°C. Following co-culture, samples were stained for NGFR, CD138, and viability and $CD138^+NGFR^-$ cell viability was utilized as a measure of tumor cell survival.

Microbead antigen loading

Protein G-conjugated ~6-7 µm polystyrene beads (Spherotech, Lake Forest, IL, USA) were coated with 50 ng BCMA-Fc chimera protein (R&D Systems, Minneapolis, MN, USA) per 10^6 beads in PBS + 0.1% BSA at a concentration of $5x10^6$ beads/mL and incubated rotating overnight at 4°C. Immediately prior to use, beads were resuspended in T cell medium without cytokines to achieve the desired effector:target ratio.

Proliferation assay

Engineered T cells were labelled with CellTrace Violet dye (Thermo Fisher Scientific) and stimulated with MM.1S tumor targets or antigen-coated microbeads at a 1:1 effector:target ratio (non-stimulated control wells were also plated to determine undivided peak for proliferation modeling). After 4 days at 37°C, co-cultures were stained with Live/Dead Fixable stain and antibodies against markers CD8α, CD4, NGFR, CD3, and/or CD138, and mixed with absolute counting beads (Thermo Fisher Scientific). Flow cytometry data were acquired as indicated above, refer to Supplemental Figure 12 for gating strategy. Results were analysed using Proliferation Plots in FCS Express 7. In short, non-stimulated control T cells were used to identify and fix a Starting Generation within Proliferation Fit Options. Proliferation Fit Statistics were used to calculate the percent of original cells that divided (percent divided). Absolute cell yield was calculated as,

$$cell\ \ count = \frac{\#\ CD3+\ live\ \ events}{\#\ \ bead\ \ events} \times \#\ \ beads\ \ loaded\ \ into\ \ sample.$$

Clariom-S RNA transcriptome analysis

$5x10^5$ TAC T cells were stimulated with 0.05 µg/mL plate-bound BCMA-Fc antigen in a 24-well plate in the presence of 0.625 µM LCL161 or DMSO for 24 or 72 hrs. After stimulation, T cells were collected, washed with 1x PBS to remove media, then processed to collect total RNA. For the 24 hour stimulation, dead cells were removed using the Miltenyi Dead Cell removal kit. Briefly, T cells were homogenized by centrifugation through QIAshredder columns (QIAGEN, Hilden, Germany), and RNA was purified from the resultant lysates by RNeasy Mini Plus (QIAGEN) RNA purification kit as per manufacturer's instructions. Purified RNA was assessed for quality above RIN>7 by NanoDrop OneC spectrophotometry (Thermo Fisher Scientific) and 2100 Bioanalyzer (Agilent, Santa Clara, CA, USA). Total RNA was hybridized using a Clariom-S Pico genechip (refer to GEO accession #GSE227986 for further details), and resultant data was analyzed using the Transcriptome Analysis Console (Thermo Fisher Scientific) to determine differential gene analysis (DGA) between DMSO and LCL161 group with donor as a

repeated measure. Raw and normalized data is available through the NCBI Gene Expression Omnibus repository under accession #GSE227986. To generate volcano plots, the differentially expressed gene were input using the EnhancedVolcano() package in R (46). Genes were identified as significant with a p-value below 0.05 and a fold change >1.75/<-1.75. Gene ontology (GO) over-representation analysis was conducted using the clusterProfiler() package in R (47–49). Specifically, the biological processes (BP) ontology was used to identify enriched pathways. A Benjamin & Hochberg (50) (BH) correction was applied *post-hoc* and gene sets were identified as significant with an adjusted p-value below 0.05. All analyses were performed using R Statistical Software [v4.2.1 (49)].

Western blotting

T cell NF-κB2 p100/p52 and XIAP analysis was accomplished by first stimulating 5x10^5 TAC T cells on 0.05 µg/mL plate-bound BCMA-Fc antigen in a 24-well plate in the presence of 0.625 µM LCL161 or DMSO for 24, 48, or 72 hrs. After stimulation, T cells were collected, washed twice in 1x PBS, then frozen as cell pellets at -20°C. Protein lysates were generated from cell pellets by lysis with RIPA lysis buffer (Thermo Fisher Scientific) containing protease inhibitors (Roche, Basel, Switzerland) for 15 min on ice, followed by 15 min centrifugation at 15000 RCF 4°C. Lysates were quantified by BCA assay (Thermo Fisher Scientific), and 8.5 (NKFB2) or 10 (XIAP) µg protein was loaded onto a 4-20% gradient gel (Bio-Rad). Proteins were then transferred to a nitrocellulose membrane, stained for total protein by REVERT 700 total protein stian (Li-COR Biosciences, Lincoln, NE, USA), and then blotted for NF-κB2 (Cell Signaling Technologies) or XIAP (Cell Signaling Technologies). All imaging was accomplished using an Odyssey Lx Imaging System (Li-COR Biosciences) set to auto mode. Blots were analyzed using Empiria Software (Li-COR Biosciences) where NF-κB2 p100/p52, or XIAP, signals were normalized to total protein signal of their respective wells (refer to Supplemental Figure 7 for an example). For analysis of tumor cells, MM.1S and RPMI 8226 cells were pelleted and lysed in an SDS-RIPA buffer (10 mM Tris-HCl, 150 mM NaCl, 10 mM KCl, 1 mM EDTA, 0.5% deoxycholic acid, 0.5% Tween 20, 0.5% NP-40, 0.1% SDS) with protease and phosphate inhibitor cocktail (MiliporeSigma) for 20 minutes on ice. Cells were then sonicated for 10 seconds at 20% amplitude before centrifugation and protein quantification by DC protein assay (Bio-Rad). Equal amount of protein (25 µg) was loaded onto 10% SDS-PAGE gels. Immunoblotting was performed overnight at 4°C with the primary antibodies, p100/p52 (Cell Signaling Technologies), NIK (Abcam, Cambridge, UK), β-Tubulin (DSHB, Iowa city, IA, USA), cIAP1/2 (MBL International, Woburn, MA, USA), and XIAP (MBL International). The next day, bound primary antibodies were probed with secondary antibodies conjugated to either Alexa Fluor680 (Thermo Fisher Scientific) or IRDye 800CW (Li-COR Biosciences) at room temperature for 1 hour, then blots were scanned on the Odyssey Infrared Imaging System (Li-COR Biosciences).

T cell apoptosis and AICD assay

T cell apoptosis was investigated by stimulating 5x10^5 engineered T cells 1:1 with antigen-loaded microbeads or MM.1S tumor cells for 24, 48, or 72 hrs in the presence of DMSO or LCL161 at indicated concentrations. Afterwards, cells were immediately stained with live/dead fixable viability dye at room temperature for 20 minutes, fixed with BD Cytofix, and stained for phosphatidylserine and CD3 surface expression on ice for 60 min. Cells were analyzed by flow cytometry and populations were defined as live (PS$^-$ live/dead$^-$), early apoptotic (PS$^+$ live/dead$^-$), and late apoptotic (PS$^+$ live/dead$^+$), refer to Supplemental Figure 13 for gating strategy.

To investigate AICD in TAC T cells, cells were stimulated as above with antigen-loaded microbeads for 48 hrs in the presence of DMSO or LCL161. Cells were stained with live/dead fixable viability dye at RT, fixed with BD Cytofix, stained for phosphatidylserine on ice for 60 min, permeabilized with BD Phosflow perm/wash I as per manufacturers guidelines, then stained intracellularly for active caspase 3. Percent apoptotic in live cells was defined as live/dead$^-$ PS$^+$ active-caspse3$^+$, refer to Figure 6B for gating strategy.

Tumor cell TNF-sensitivity assay

2x10^5 MM.1S or RPMI 8226 cells were incubated with 5 µM LCL161 or DMSO and in the presence of rhTNFα (BD Biosciences) at indicated concentrations for 48 hrs. After incubation, cells were collected and stained using a fixable live/dead dye. Samples were analyzed by flow cytometry to determine viability.

Statistics

All statistical analyses were performed in GraphPad Prism version 9.4 for Windows (San Diego, CA). Paired two tailed t tests, or multiple paired t tests using the Holm-Šídák method, were utilized to compare between two samples. An ordinary one-way ANOVA using the Dunnett multiple comparison test was used to compare the means of three or more unmatched groups. * = p > 0.05, ** = p > 0.01, *** = p > 0.001, and N.S. = not significant.TABLE

Reagents

Reagent	Source	Identifier
Goat anti-human IgG (H +L)-PE	Jackson ImmunoResearch	Cat# 109-115-098, RRID , AB_2337675
Anti-human CD4-Pacific Blue	BD Biosciences	Cat# 558116, RRID , AB_397037
Anti-human CD4-APC-H7	BD Biosciences	Cat# 560158, RRID , AB_1645478

(Continued)

Continued

Anti-human CD4-AlexaFluor 700	Thermo Fisher Scientific	Cat# 56-0048-82, RRID , AB_657741
Anti-human CD8α-AlexaFluor 700	Thermo Fisher Scientific	Cat# 56-0086-82, RRID , AB_657756
Anti-human CD8α-PerCP-Cyanine5.5	Thermo Fisher Scientific	Cat# 45-0088-42, RRID , AB_1582255
Anti-human CD30-PE	Miltenyi Biotec	Cat# 130-120-783, RRID , AB_2784118
Anti-human FAIM3-APC	BioLegend	Cat# 398103, RRID , AB_2876722
Anti-human NGFR-VioBright FITC	Miltenyi Biotec	Cat# 130-104-893, RRID , AB_2661084 Cat# 130-113-985, RRID , AB_2734063
Anti-human NGFR-Brilliant Violet 421	BD Biosciences	Cat# 562562, RRID , AB_2737657
Anti-human CD138-APC	BioLegend	Cat# 356505, RRID , AB_2561879
Anti-human CD3-Brilliant Violet 605	BioLegend	Cat# 300460, RRID , AB_2564380
Anti-human FasR-APC	BioLegend	Cat# 305612, RRID , AB_314550
Functional grade anti-human CD3	Thermo Fisher Scientific	Cat# 16-0037-85, RRID , AB_468855
Anti-NF-κB2 P100/p52	Cell Signaling Technologies	Cat# 4882, RRID , AB_10695537
Anti-human NIK	Abcam	Cat# ab7204, RRID , AB_2139765
Anti-cIAP1/2	MBL International	Cat# CY-P1041, RRID , AB_10950764
Anti-XIAP	MBL International	Cat# M044-3, RRID , AB_592998
Anti-XIAP	Cell Signaling Technologies	Cat# 2045, RRID , AB_2214866
Anti-β-Tubulin	Developmental Studies Hybridoma Bank	Cat# E7, RRID , AB_528499
IRDye 800CW goat anti-rabbit	Li-COR Biosciences	Cat# 926-32211, RRID , AB_621843
Anti-human FasL-PE	BD Biosciences	Cat# 564261, RRID , AB_2738713
Anti-phosphatidylserine-AlexaFluor 488	MilliporeSigma	Cat# 16-256, RRID , AB_492616
Anti-human active caspase 3-Alexa Fluor 647	BD Bioscience	Cat# 560626, RRID , AB_1727414
LIVE/DEAD fixable Near-IR dead cell stain	Thermo Fisher Scientific	Cat# L10119
Cytofix buffer	BD Biosciences	Cat# 554655
Phosflow perm/wash I	BD Bioscience	Cat# 557885
123count eBeads	Thermo Fisher Scientific	Cat# 01-1234-42

(Continued)

Continued

Protein G-conjugated ~6 µm polystyrene beads	Spherotech	Cat# PGP-60-5
Alt-R S.p. HiFi Cas9 Nuclease V3	Integrated DNA Technologies	Cat# 1081061
Pierce RIPA Lysis buffer	Thermo Fisher Scientific	Cat# 89901
cOmplete, Mini, EDTA-free protease inhibitor tablets	Roche	Cat# 04 693 159 001
Protease and Phosphatase Inhibitor Cocktail	MilliporeSigma	Cat# PPC1010
DC Protein Assay Kit	Bio-Rad	Cat# 5000111
Pierce BCA assay	Thermo Fisher Scientific	Cat# 23227
4-20% TGX pre-cast gel, 15 lanes	Bio-Rad	Cat# 4561096
0.2 µm nitrocellulose membrane	Bio-Rad	Cat# 1620112
REVERT 700 Total protein stain kit	Li-COR Biosciences	Cat# 926-11010
Intercept blocking buffer (TBS)	Li-COR Biosciences	Cat# 927-60001
Intercept Antibody Diluent (T20 TBS)	Li-COR Biosciences	Cat# 927-65001
CellTrace Violet	Thermo Fisher Scientific	Cat# C34557
D-Luciferin	Perkin Elmer	Cat# 122799
rhBCMA-Fc chimera	R&D Systems	Cat# 193-BC
rhTNFα	BD Biosciences	Cat# 554618
LCL161	Novartis	N/A

Data availability statement

The data presented in the study are deposited in the NCBI Gene Expression Omnibus repository, accession number GSE227986, released: https://www.ncbi.nlm.nih.gov/geo/query/acc.cgi?acc=GSE227986.

Ethics statement

The studies involving human participants were reviewed and approved by Hamilton Integrated Research Ethics Board. The patients/participants provided their written informed consent to participate in this study. The animal study was reviewed and approved by McMaster Animal Research Ethics Board.

Author contributions

AA, SB, EL, and JB conceptualized these studies. AA and JB designed experiments and interpreted results. AA, CS, AM, CG, CB, MS-J, and KB generated these data and performed analyses. AA and

JB wrote this manuscript. SB, EL, and CG edited the manuscript. All authors contributed to the article and approved the submitted version.

Funding

This research was funded by the Samuel Family Foundation, Inc. AA received support from the Ontario Graduate Scholarship and the Samuel Scholars Program. JB is supported by a Canadian Research Chair in Translational Cancer Immunology and the John Bienenstock Chair in Molecular Medicine. Additional funding support was through a CIHR Foundation grant to RK.

Acknowledgments

We would like to thank the healthy and myeloma patient PBMC donors for their generous donation of peripheral blood for these studies. This work has been presented in part at the BioCanRx Summit4CI conference and the Translational Research Cancer Centers Consortium annual meeting.

Conflict of interest

JB is a co-founder and shareholder of Triumvira Immunologics and is a paid consultant for Triumvira Immunologics. JB is a co-inventor on patents related to the BCMA TAC described in this manuscript and licensed to Triumvira Immunologics. CB is paid through a sponsored research agreement with Triumvira Immunologics. EL is a co-founder, shareholder, and chief scientific officer of Protaxis Therapeutics.

The remaining authors declare that the research was conducted in the absence of any commercial or financial relationships that could be construed as a potential conflict of interest.

Publisher's note

All claims expressed in this article are solely those of the authors and do not necessarily represent those of their affiliated organizations, or those of the publisher, the editors and the reviewers. Any product that may be evaluated in this article, or claim that may be made by its manufacturer, is not guaranteed or endorsed by the publisher.

Supplementary material

The Supplementary Material for this article can be found online at: https://www.frontiersin.org/articles/10.3389/fimmu.2023.1179827/full#supplementary-material

References

1. Helsen CW, Hammill JA, Lau VWC, Mwawasi KA, Afsahi A, Bezverbnaya K, et al. The chimeric tac receptor Co-opts the T cell receptor yielding robust anti-tumor activity without toxicity. *Nat Commun* (2018) 9(1):3049. doi: 10/gd27qr

2. Chen L, Flies DB. Molecular mechanisms of T cell Co-stimulation and Co-inhibition. *Nat Rev Immunol* (2013) 13(4):227–42. doi: 10.1038/nri3405

3. Savoldo B, Ramos CA, Liu E, Mims MP, Keating MJ, Carrum G, et al. Cd28 costimulation improves expansion and persistence of chimeric antigen receptor-modified T cells in lymphoma patients. *J Clin Invest* (2011) 121(5):1822–6. doi: 10.1172/JCI46110

4. Cappell KM, Kochenderfer JN. A comparison of chimeric antigen receptors containing Cd28 versus 4-1bb costimulatory domains. *Nat Rev Clin Oncol* (2021) 18 (11):715–27. doi: 10.1038/s41571-021-00530-z

5. Schmidts A, Wehrli M, Maus MV. Toward better understanding and management of car-T cell-associated toxicity. *Annu Rev Med* (2021) 72(1):365–82. doi: 10.1146/annurev-med-061119-015600

6. Dubrez L, Berthelet J, Glorian V. Iap proteins as targets for drug development in oncology. *Onco Targets Ther* (2013) 6:1285–304. doi: 10/gf5pjd

7. Boddu P, Carter BZ, Verstovsek S, Pemmaraju N. Smac mimetics as potential cancer therapeutics in myeloid malignancies. *Br J Haematol* (2019) 185(2):219–31. doi: 10.1111/bjh.15829

8. Dougan M, Dougan S, Slisz J, Firestone B, Vanneman M, Draganov D, et al. Iap inhibitors enhance Co-stimulation to promote tumor immunity. *J Exp Med* (2010) 207 (10):2195–206. doi: 10.1084/jem.20101123

9. Philipson BI, O'Connor RS, May MJ, June CH, Albelda SM, Milone MC. 4-1bb costimulation promotes car T cell survival through noncanonical nf-κb signaling. *Sci Signaling* (2020) 13(625). doi: 10/gg8fhh

10. Michie J, Beavis PA, Freeman AJ, Vervoort SJ, Ramsbottom KM, Narasimhan V, et al. Antagonism of iaps enhances car T-cell efficacy. *Cancer Immunol Res* (2019) 7 (2):183–92. doi: 10.1158/2326-6066.CIR-18-0428

11. Song EZ, Wang X, Philipson BI, Zhang Q, Thokala R, Zhang L, et al. The iap antagonist birinapant enhances chimeric antigen receptor T cell therapy for glioblastoma by overcoming antigen heterogeneity. *Mol Ther Oncolytics* (2022) 27:288–304. doi: 10.1016/j.omto.2022.11.004

12. Gardner RA, Finney O, Annesley C, Brakke H, Summers C, Leger K, et al. Intent-to-Treat leukemia remission by Cd19 car T cells of defined formulation and dose in children and young adults. *Blood* (2017) 129(25):3322–31. doi: 10.1182/blood-2017-02-769208

13. Finney OC, Brakke HM, Rawlings-Rhea S, Hicks R, Doolittle D, Lopez M, et al. Cd19 car T cell product and disease attributes predict leukemia remission durability. *J Clin Invest* (2019) 129(5):2123–32. doi: 10.1172/JCI125423

14. Bezverbnaya K, Moogk D, Cummings D, Baker CL, Aarts C, Denisova G, et al. Development of a b-cell maturation antigen-specific T-cell antigen coupler receptor for multiple myeloma. *Cytotherapy* (2021) 23(9):820–32. doi: 10.1016/j.jcyt.2021.05.007

15. Hitoshi Y, Lorens J, Kitada SI, Fisher J, LaBarge M, Ring HZ, et al. Toso, a cell surface, specific regulator of fas-induced apoptosis in T cells. *Immunity* (1998) 8 (4):461–71. doi: 10.1016/s1074-7613(00)80551-8

16. Meryk A, Pangrazzi L, Hagen M, Hatzmann F, Jenewein B, Jakic B, et al. Fcμ receptor as a costimulatory molecule for T cells. *Cell Rep* (2019) 26(10):2681–91.e5. doi: 10.1016/j.celrep.2019.02.024

17. Telford WG, Nam SY, Podack ER, Miller RA. Cd30-regulated apoptosis in murine Cd8 T cells after cessation of tcr signals. *Cell Immunol* (1997) 182(2):125–36. doi: 10.1006/cimm.1997.1228

18. Hombach AA, Rappl G, Abken H. Blocking Cd30 on T cells by a dual specific car for Cd30 and colon cancer antigens improves the car T cell response against Cd30 (-) tumors. *Mol Ther* (2019) 27(10):1825–35. doi: 10.1016/j.ymthe.2019.06.007

19. Gilfillan MC, Noel PJ, Podack ER, Reiner SL, Thompson CB. Expression of the costimulatory receptor Cd30 is regulated by both Cd28 and cytokines. *J Immunol* (1998) 160(5):2180. doi: 10.4049/jimmunol.160.5.2180

20. Yamamoto TN, Lee PH, Vodnala SK, Gurusamy D, Kishton RJ, Yu Z, et al. T Cells genetically engineered to overcome death signaling enhance adoptive cancer immunotherapy. *J Clin Invest* (2019) 129(4):1551–65. doi: 10.1172/JCI121491

21. Petersen SL, Wang L, Yalcin-Chin A, Li L, Peyton M, Minna J, et al. Autocrine tnfalpha signaling renders human cancer cells susceptible to smac-Mimetic-Induced apoptosis. *Cancer Cell* (2007) 12(5):445–56. doi: 10.1016/j.ccr.2007.08.029

22. Vince JE, Wong WW, Khan N, Feltham R, Chau D, Ahmed AU, et al. Iap antagonists target Ciap1 to induce tnfalpha-dependent apoptosis. *Cell* (2007) 131 (4):682–93. doi: 10.1016/j.cell.2007.10.037

23. Ramakrishnan V, Painuly U, Kimlinger T, Haug J, Rajkumar SV, Kumar S. Inhibitor of apoptosis proteins as therapeutic targets in multiple myeloma. *Leukemia* (2014) 28(7):1519–28. doi: 10/f6cbcm

24. Chesi M, Mirza NN, Garbitt VM, Sharik ME, Dueck AC, Asmann YW, et al. Iap antagonists induce anti-tumor immunity in multiple myeloma. *Nat Med* (2016) 22 (12):1411–20. doi: 10.1038/nm.4229

25. Demchenko YN, Glebov OK, Zingone A, Keats JJ, Bergsagel PL, Kuehl WM. Classical and/or alternative nf-kappab pathway activation in multiple myeloma. *Blood* (2010) 115(17):3541–52. doi: 10.1182/blood-2009-09-243535

26. Obexer P, Ausserlechner MJ. X-Linked inhibitor of apoptosis protein - a critical death resistance regulator and therapeutic target for personalized cancer therapy. *Front Oncol* (2014) 4:197. doi: 10.3389/fonc.2014.00197

27. Jost PJ, Grabow S, Gray D, McKenzie MD, Nachbur U, Huang DC, et al. Xiap discriminates between type I and type ii fas-induced apoptosis. *Nature* (2009) 460 (7258):1035–9. doi: 10.1038/nature08229

28. Baeuerle PA, Ding J, Patel E, Thorausch N, Horton H, Gierut J, et al. Synthetic truc receptors engaging the complete T cell receptor for potent anti-tumor response. *Nat Commun* (2019) 10(1):2087. doi: 10.1038/s41467-019-10097-0

29. Xu Y, Yang Z, Horan LH, Zhang P, Liu L, Zimdahl B, et al. A novel antibody-tcr (Abtcr) platform combines fab-based antigen recognition with Gamma/Delta-tcr signaling to facilitate T-cell cytotoxicity with low cytokine release. *Cell Discovery* (2018) 4(1):62. doi: 10.1038/s41421-018-0066-6

30. Appleman LJ, Berezovskaya A, Grass I, Boussiotis VA. Cd28 costimulation mediates T cell expansion *Via* il-2-Independent and il-2-Dependent regulation of cell cycle progression. *J Immunol* (2000) 164(1):144–51. doi: 10.4049/jimmunol.164.1.144

31. Boesteanu AC, Katsikis PD. Memory T cells need Cd28 costimulation to remember. *Semin Immunol* (2009) 21(2):69–77. doi: 10.1016/j.smim.2009.02.005

32. Chen GM, Chen C, Das RK, Gao P, Chen CH, Bandyopadhyay S, et al. Integrative bulk and single-cell profiling of premanufacture T-cell populations reveals factors mediating long-term persistence of car T-cell therapy. *Cancer Discovery* (2021) 11(9):2186–99. doi: 10.1158/2159-8290.CD-20-1677

33. Pierce JM, Mehta A. Diagnostic, prognostic and therapeutic role of Cd30 in lymphoma. *Expert Rev Hematol* (2017) 10(1):29–37. doi: 10.1080/17474086.2017.1270202

34. Csomos RA, Wright CW, Galban S, Oetjen KA, Duckett CS. Two distinct signalling cascades target the nf-kappab regulatory factor c-Iap1 for degradation. *Biochem J* (2009) 420(1):83–91. doi: 10.1042/BJ20082140

35. Kocab AJ, Veloso A, Paulsen MT, Ljungman M, Duckett CS. Effects of physiological and synthetic iap antagonism on c-Iap-Dependent signaling. *Oncogene* (2015) 34(43):5472–81. doi: 10.1038/onc.2015.3

36. Knights AJ, Fucikova J, Pasam A, Koernig S, Cebon J. Inhibitor of apoptosis protein (Iap) antagonists demonstrate divergent immunomodulatory properties in human immune subsets with implications for combination therapy. *Cancer Immunol Immunother* (2013) 62(2):321–35. doi: 10.1007/s00262-012-1342-1

37. Wu H, Tschopp J, Lin SC. Smac mimetics and tnfalpha: A dangerous liaison? *Cell* (2007) 131(4):655–8. doi: 10.1016/j.cell.2007.10.042

38. Bratton SB, Lewis J, Butterworth M, Duckett CS, Cohen GM. Xiap inhibition of caspase-3 preserves its association with the apaf-1 apoptosome and prevents Cd95- and bax-induced apoptosis. *Cell Death Differ* (2002) 9(9):881–92. doi: 10.1038/sj.cdd.4401069

39. Brunner T, Wasem C, Torgler R, Cima I, Jakob S, Corazza N. Fas (Cd95/Apo-1) ligand regulation in T cell homeostasis, cell-mediated cytotoxicity and immune pathology. *Semin Immunol* (2003) 15(3):167–76. doi: 10.1016/s1044-5323(03)00035-6

40. Bou Zerdan M, Nasr L, Kassab J, Saba L, Ghossein M, Yaghi M, et al. Adhesion molecules in multiple myeloma oncogenesis and targeted therapy. *Int J Hematol Oncol* (2022) 11(2). doi: 10.2217/ijh-2021-0017

41. Mo X, Tang C, Niu Q, Ma T, Du Y, Fu H. Htip: High-throughput immunomodulator phenotypic screening platform to reveal iap antagonists as anti-cancer immune enhancers. *Cell Chem Biol* (2019) 26(3):331–9.e3. doi: 10/gghgfm

42. Rabinovich BA, Ye Y, Etto T, Chen JQ, Levitsky HI, Overwijk WW, et al. Visualizing fewer than 10 mouse T cells with an enhanced firefly luciferase in immunocompetent mouse models of cancer. *Proc Natl Acad Sci U.S.A.* (2008) 105 (38):14342–6. doi: 10.1073/pnas.0804105105

43. Hammill JA, VanSeggelen H, Helsen CW, Denisova GF, Evelegh C, Tantalo DG, et al. Designed ankyrin repeat proteins are effective targeting elements for chimeric antigen receptors. *J Immunother Cancer* (2015) 3(1):55. doi: 10.1186/s40425-015-0099-4

44. Dull T, Zufferey R, Kelly M, Mandel RJ, Nguyen M, Trono D, et al. A third-generation lentivirus vector with a conditional packaging system. *J Virol* (1998) 72 (11):8463–71. doi: 10.1128/JVI.72.11.8463-8471.1998

45. Conant D, Hsiau T, Rossi N, Oki J, Maures T, Waite K, et al. Inference of crispr edits from Sanger trace data. *CRISPR J* (2022) 5(1):123–30. doi: 10.1089/crispr.2021.0113

46. Blighe K, Rana S, Lewis M. *Enhancedvolcano: Publication-ready volcano plots with enhanced colouring and labeling* (2018). Available at: https://github.com/kevinblighe/EnhancedVolcano.

47. Yu G, Wang LG, Han Y, He QY. Clusterprofiler: An r package for comparing biological themes among gene clusters. *OMICS* (2012) 16(5):284–7. doi: 10.1089/omi.2011.0118

48. Wu T, Hu E, Xu S, Chen M, Guo P, Dai Z, et al. Clusterprofiler 4.0: A universal enrichment tool for interpreting omics data. *Innovation (Camb)* (2021) 2(3):100141. doi: 10.1016/j.xinn.2021.100141

49. Team RC. *R: A language and environment for statistical computing*. Vienna, Austria: R Foundation for Statistical Computing (2022).

50. Benjamini Y, Hochberg Y. Controlling the false discovery rate: A practical and powerful approach to multiple testing. *J R Stat Society: Ser B (Methodological)* (1995) 57 (1):289–300. doi: 10.1111/j.2517-6161.1995.tb02031.x

frontiers | Frontiers in Oncology

TYPE Review
PUBLISHED 19 April 2023
DOI 10.3389/fonc.2023.1179947

Check for updates

OPEN ACCESS

EDITED BY
Subhash Kumar Tripathi,
Seattle Children's Research Institute,
United States

REVIEWED BY
Bishal Singh,
University of Cambridge, United Kingdom
Ritika Tewari,
Benaroya Research Institute, United States

*CORRESPONDENCE
Yanzhang Tian
tyz2030@163.com

SPECIALTY SECTION
This article was submitted to Cancer Immunity and Immunotherapy, a section of the journal Frontiers in Oncology

RECEIVED 05 March 2023
ACCEPTED 03 April 2023
PUBLISHED 19 April 2023

CITATION
Han P, Mo S, Wang Z, Xu J, Fu X and Tian Y (2023) UXT at the crossroads of cell death, immunity and neurodegenerative diseases. *Front. Oncol.* 13:1179947. doi: 10.3389/fonc.2023.1179947

COPYRIGHT
© 2023 Han, Mo, Wang, Xu, Fu and Tian. This is an open-access article distributed under the terms of the Creative Commons Attribution License (CC BY). The use, distribution or reproduction in other forums is permitted, provided the original author(s) and the copyright owner(s) are credited and that the original publication in this journal is cited, in accordance with accepted academic practice. No use, distribution or reproduction is permitted which does not comply with these terms.

UXT at the crossroads of cell death, immunity and neurodegenerative diseases

Pengzhe Han[1], Shaojian Mo[1,2], Zhengwang Wang[1], Jiale Xu[1], Xifeng Fu[1,2] and Yanzhang Tian[1,2]*

[1]Third Hospital of Shanxi Medical University, Shanxi Bethune Hospital, Shanxi Academy of Medical Sciences Tongji Shanxi Hospital, Taiyuan, China, [2]Department of Biliary and Pancreatic Surgery, Shanxi Bethune Hospital, Shanxi Academy of Medical Sciences, Tongji Shanxi Hospital, Taiyuan, China

The ubiquitous expressed transcript (UXT), a member of the prefoldin-like protein family, modulates regulated cell death (RCD) such as apoptosis and autophagy-mediated cell death through nuclear factor-κB (NF-κB), tumor necrosis factor-α (TNF-α), P53, P62, and methylation, and is involved in the regulation of cell metabolism, thereby affecting tumor progression. UXT also maintains immune homeostasis and reduces proteotoxicity in neurodegenerative diseases through selective autophagy and molecular chaperones. Herein, we review and further elucidate the mechanisms by which UXT affects the regulation of cell death, maintenance of immune homeostasis, and neurodegenerative diseases and discuss the possible UXT involvement in the regulation of ferroptosis and immunogenic cell death, and targeting it to improve cancer treatment outcomes by regulating cell death and immune surveillance.

KEYWORDS

UXT, apoptosis, immunity, neurodegenerative disease, autophagy

1 Introduction

The ubiquitous expressed transcript (UXT) gene is located at the Xp11.23–p11.22 locus, a region of strong biological significance that is affected by X gene inactivation. When retrieved from the National Center for Biotechnology Information (NCBI, https://www.ncbi.nlm.nih.gov/gene) UXT is also known as *STAP1* and *ART-27*. Recent studies have revealed that *UXT* plays an important role in cellular transformation and gene transcription by regulating the androgen receptor (AR), GATA4, nuclear factor-κB (NF-κB), and EVI1activities as cofactors (1–5). UXT is upregulated in various tumor tissues, including colorectal cancer (6), sarcoma (5), breast cancer (7, 8), and dedifferentiated skull-base chordomas (9). Therefore, UXT is considered a proto-oncogene in human cancers. UXT is downregulated in prostate cancer tissues, and its overexpression has been reported to inhibit prostate cancer cell growth (10–12). UXT may promote or suppress tumorigenesis depending on the tumor type and microenvironment (13).

Previous research has confirmed that: UXT contains two mRNA splicing variants that produce two UXT isoforms, UXT-V1 and UXT-V2, respectively. These two isoforms differ in their subcellular localization and actions, with the UXT-V2 protein mainly distributed in the nucleus and the UXT-V1 protein mainly distributed in the cytoplasm (14). At the same time, the expression of UXT-V1 is lower than that of UXT-V2. Some of the studies did not specifically state the isoforms; for those studies, "UXT" is used in this review.

Cell death is an important mechanism for maintaining the functional homeostasis of cells or organs (15). In the treatment of tumors, targeting or inducing tumor cell death is also the pathway of choice for most non-surgical treatment modalities for tumors, and therefore the study of the mechanisms regulating cell death is crucial (16). However, tumor cells are resistant to cell death. This involves activation of anti-apoptotic proteins, cellular autophagy, and epigenetic mechanisms. Chemotherapy resistance caused by them is a difficult problem in most cancer treatments (17). As the research of tumor treatment has advanced, the clinical treatment of tumor has entered the era of precision medicine. Targeted therapy and immunotherapy are gradually gaining attention (18). Cell death releases substances such as damage associated molecular patterns, ATP, DNA and inflammatory factors, which activate anti-tumor immune response. Thus, cell death induces different levels of immune response (19). Amyotrophic lateral sclerosis (ALS) is one of the neurodegenerative diseases. ALS is associated with neuroinflammation, immune response, and dysfunction due to neuronal death (20, 21).

There are some contradictory views among studies on the role of UXT. First, UXT-V2 can inhibit TNF-α-induced apoptosis by upregulating the expression of anti-apoptotic genes in the NF-κB signaling pathway (2). In addition, UXT can also inhibit P53 activity through murine double minute X (MDMX) or epigenetic mechanisms, thereby suppressing apoptosis (5, 22). However, UXT-V2 can also interact with sterile α and HEAT armadillo motif-containing protein (SARM) in mitochondria to promote apoptosis (23). Second, UXT can promote P62-mediated selective autophagy (24, 25). However, when UXT is downregulated, it can promote autophagy by decreasing mTOR activity or promoting autophagy lysosome formation (26, 27). Third, UXT-V1 knockdown inhibits type I IFN expression (28), and UXT-V2 is phosphorylated to impair the activation of NF-κB signaling pathway and attenuate host cell antiviral immune responses (29). However, UXT can inhibit the expression of type I IFN through the cGAMP-STING signaling pathway (25). Therefore, there is an urgent need to evaluate the role of UXT in different diseases. To this end, we present a comprehensive review on the different ways in which UXT regulates cell death and the progress of UXT research in immune regulation and neurodegenerative diseases based on the perspectives of cell death and immunity. We also discuss the possibility of UXT involvement in ferroptosis, immunogenic cell death, the improvement of the tumor immune microenvironment and immune response, and the regulation of neuro-degenerative disease progression. We reveal possible research trends and indicate some suggestions for future research.

2 The origin and degradation of UXT

The *UXT* gene encodes a protein of approximately 18 kDa and is widely expressed in human and mouse tissues (30). UXT is a member of the alpha-like prefoldin protein family that exhibits alpha-helical properties and has two isoforms, both of which are derived from the same chromosome. UXT is distributed in the nucleus, cytoplasm, and mitochondria. UXT-V2 is the shorter isoform, consisting of 157 amino acids, while UXT-V1 has 12 more amino acids (169 amino acids) at its N-terminal end compared with UXT-V2. These are called MVFPLPTPQEPI motif (31), which can bind to TRAF2 to mediate the TNFR1 apoptosis pathway, which is unique to UXT-V1. The UXT-V1 plasmid also generates the UXT-V2 isoform through translation at the second methionine of codon 13 (ATG2) (14). The subcellular localization of UXT correlates with the cell cycle. UXT binds to γ-microtubule proteins, suggesting that UXT is a centrosome component, and that its overexpression disrupts centrosome structure (11). UXT is also involved in mitosis and germ cell meiosis (32), and is essential for cell viability, with insufficient expression in cells leading to cell death (33).

Both UXT-V1 and UXT-V2 can be ubiquitinated. Both tumor suppressor protein LOX-PP and E3 ubiquitin ligase SCF (Fbxo7) can induce UXT-V2 ubiquitination and proteasome degradation (7, 14). UXT-V2 is highly expressed in breast cancer tissue, where it can inhibit ER activity. Endocrine therapy for ER-negative breast cancer is known to be less effective, and endocrine therapy for ER-positive patients also faces the dilemma of drug resistance and reduced sensitivity. This provides a new perspective on improving the poor response to endocrine therapy and resistance in breast cancer patients. E3 ubiquitin ligase SCF (Fbxo7) mediated ubiquitination of UXT-V1, but the cell abundance of UXT-V1 did not change significantly (14). The MVFPLPTPEPI motif at the N-terminal of UXT-V1 probably does not mediate ubiquitin binding of UXT-V1 to SCF (Fbxo7), at least not primarily. Although UXT-V1 is a short half-life protein, the regulation of its degradation remains unclear.

3 Apoptosis: one of the cell death pathways

Cell death is the end of cellular life. With the accumulation of experimental data in recent decades, multiple forms of cell death have been identified that are interconnected and complementary *via* mechanisms that regulate cellular homeostasis in living organisms. The Nomenclature Committee on Cell Death (NCCD) classifies cell death into regulatory cell death (RCD) and accidental cell death (ACD) based on environmental and environmental factors (34). RCD includes apoptosis (both endogenous and exogenous), necrosis, pyroptosis, ferroptosis, and autophagy-dependent cell death.

Targeting apoptotic pathways in tumor cells is a promising anticancer strategy (35, 36). Indeed, apoptosis, which is classified

into either endogenous or exogenous based on the activating pathways, can be activated by cellular stress, DNA damage, and immune surveillance pathways. The key step in the endogenous apoptosis pathway is an altered mitochondrial outer membrane permeability (MOMP) with the release of Cyto-chrome c from the mitochondria into the cell matrix; this is accompanied by the dysregulation of the B-cell lymphoma 2 (BCL-2) family such as BH3-only protein, which activates caspase-9-mediated apoptosis (34). Conversely, exogenous apoptosis is mediated by Fas, TNF receptor 1 (TNFR1), death receptor (DR) 4, and DR5 membrane protein receptors, which correspond to Fas ligand (FasL), TNF, or TNF-related apoptosis-inducing ligand (TRAIL) proteins, respectively, and subsequently cause apoptosis through the recruitment of Fas-associated death domain (FADD) and caspase-8, which further activates the cascade of cysteine activation and BID cleavage (34). BID serves as the "link" between endogenous and exogenous apoptosis, and is positively regulated by p53 at the transcriptional level (37), which can transmit the signal to the mitochondria and trigger a stronger apoptotic signal.

3.1 UXT and mitochondria

Mitochondria provide energy for cells through diverse metabolic functions and play a central role in apoptosis. Recent studies have shown that mitochondria also play a novel role as pro-inflammatory signaling hubs in some types of cell death, such as necrosis, ferroptosis, and pyroptosis (38). The distribution of mitochondria is regulated by the cytoskeleton, and mitochondrial aggregation in the perinuclear region is considered a feature of cell death.

UXT interacts with leucine-rich pentatricopeptide repeat containing protein (LRPPRC) through the SEC1 structural domain and participates in the LRPPRC complex by acting as a bridge between the LRPPRC actin-based cytoarchitecture and potential transcriptional complexes. The LRPPRC complex participates in the integration of cytoskeletal actin and microtubule networks, including vesicular transport, nucleocytoplasmic shuttling, nuclear chromosome remodeling, and transcriptional control (39). Subsequently, it was shown that UXT, as one of the subunits of the LRPPRC complex, acts through the microtubule (MT) cytoskeleton, where normal cells need adenosine triphosphate the most and thus influence mitochondrial distribution, and localizes mitochondria at the key functional sites of chromosome remodeling where errors trigger mitochondria-mediated cell death (40). Elevated levels of UXT may promote progressive mitochondrial aggregation and cell death through the association of UXT with LRPPRC (41). In recent years, several studies have investigated the influence of UXT on the cytoskeleton and its involvement in mitochondrial distribution. Previously, UXT was thought to affect mitochondrial distribution through LRPPRC. There is a lack of strong evidence on whether UXT affects mitochondrial repositioning through the cytoskeleton and the causal mechanistic studies of this in relation to cell death. Both UXT-V1 and UXT-V2 have been shown to interact with SARM in monocyte mitochondria, as observed under lipopolysaccharide (LPS) and polyinosinic:polycytidylic acid (poly I:C) simulated infection conditions (23). The interaction of UXT-V2 with SARM in the mitochondria increases SARM-induced exogenous apoptosis by increasing caspase-8 activity and mitochondrial membrane potential depolarization. In contrast, the interaction between UXT-V1 and SARM decreased caspase-8 activity and inhibited apoptosis.

The shift in mitochondrial membrane potential can regulate the release of apoptotic factors and mitochondrial membrane permeability (42); therefore, mitochondrial membrane potential plays an important role in apoptosis (43). Future studies should investigate how UXT acts through the mitochondria to affect apoptosis or other death pathways.

3.2 UXT and the NF-κB signaling pathway

The NF-κB family is composed of B cell-specific transcription factors that include c-REL, RelA (p65), RelB, NF-κB2 (p100/p52), NF-κB1 (p105/p50), and five DNA-binding proteins that bind to form homo- or heterodimers, which regulate gene transcription. When NF-κB is not activated in the cytoplasm, it binds to its specific repressor protein, IκB. When infection and stress damage occur in the body, TNF and interleukin-1 (IL-1) activate the IκB kinase (IKK) complex, trigger NF-κB translocation, activate the NF-κB signaling pathway, and regulate the transcription of target genes. NF-κB regulates innate and adaptive immune responses and modulates cell proliferation and apoptosis. NF-κB signaling pathways are involved in the development of cancer, diabetes, immune disorders, acquired immunodeficiency syndrome, COVID-19, and other diseases through their regulatory roles in inflammation, tumors, and immunity (44, 45). TNF is a pleiotropic cytokine belonging to the TNF superfamily. By binding to its cognate receptor, TNF-R1, it induces a signaling cascade that can lead to the upregulation of pro-inflammatory genes or cell death. TNF signaling is determined by the activity of two distinct spatiotemporal complexes: the TNF-R1 binding complex (complex-I), which drives NF-κB activation and the inflammatory response, and the secondary complex (complex-II), which can trigger cell death (46).

In prostate cancer cells, UXT-V2 acts as a transcriptional cofactor that interacts with P65 through the intact Rel homology structural domain (RHD) in response to TNF-α stimulation. UXT-V2 is passively recruited to NF-κB enhancers and functions as a nuclear chaperone to tightly regulate NF-κB target gene expression in the nucleus. Reduction in endogenous UXT-V2 significantly increases the propensity for TNF-α-induced apoptosis (2). The authors also found that in UXT-V1 knockdown cells, TNF-α synergistically activated caspase-8 and poly-ADP ribose polymerase (PARP), significantly promoting apoptosis, and the cells were highly sensitive to TNF-α induced apoptosis. To be specific, UXT-V1 in the cytoplasm blocked the recruitment of FADD by TRAF2 and inhibited the formation of complex - II (FADD-RIP-TRADD) through the N-terminal 12-amino acid motif-targeting complex -I (TRAF2-RIP-TRADD). Therefore, UXT-V1 inhibits TNF-α induced apoptosis by blocking the recruitment of the death receptor TNFR1 adaptor protein (31). The UXT is not controlled by the NF-κB signal path. The regulation

of complex- II by UXT-V1 and the regulation of nuclear events in NF-κB signaling pathway by UXT-V2 clarified the differences between the two isoforms of UXT, enriched the mechanism of action of UXT, provided direct evidence of UXT and cell death, and also hinted at the possibility of UXT participating in the regulation of tumor, inflammation and immunity through the NF-κB signaling pathway. Interestingly, there appears to be some contradiction between this and Sethurathinam's (23) findings. They proposed that UXT-V2 interacts with SARM in the mitochondria of monocytes to promote apoptosis, which UXT-V1 inhibits. UXT-V2 is mainly found in the nucleus, cytoplasm, and mitochondria. But most of it is in the nucleus. In addition to the differences between the cells themselves, different subcellular localization may involve different mechanisms, which does not rule out the possibility that they occur simultaneously.

The mechanism underlying the selective activation of the NF-κB signaling pathway by UXT is not fully understood. In COS-7 cells, LRP16 interacts with ART-27 and AR in an androgen-independent manner and participates in AR transactivation (47). Furthermore, LRP16, as an interacting factor of UXT, could be integrated into the NF-κB transcriptional enhancer in the nucleus to participate in the regulation of NF-κB. Meanwhile, increased TNF-α + cycloheximide (CHX)-induced apoptosis was observed in cells with downregulated LRP16 expression. Downregulation of LRP16 also increased cell sensitivity to TNF-α-induced apoptosis; the anti-apoptotic proteins X-linked inhibitor of apoptosis protein (XIAP) and FLICE-inhibitory protein (FLIP) were blocked (48). The mechanism of the interaction between UXT and LRP16 in cell death, such as apoptosis, has not been further investigated. In addition, UXT interacts specifically with the EZH1-SUZ12 complex to regulate the activation of NF-κB targets. EZH1and UXT knockdown significantly increased the percentage of apoptotic cells and the sensitivity of cells to apoptosis. The mechanism may be that EZH1 and UXT can regulate TNF and two induced anti-apoptosis genes, *BIRC2* (coding cIAP1) and *BIRC3* (coding cIAP2) (49). Therefore, UXT-V2 may co-regulate the nuclear events of NF-κB with LRP-16 and EZH1 (Figure 1).

3.3 UXT and the P53 signaling pathway

P53, also known as *TP53*, has tumor-suppressive effects. In normal cells, P53 binds to its inhibitors, mouse double minute 2 homolog (MDM2) and MDMX, and maintains low levels of activity. When activated in the presence of hypoxia, DNA damage, and stress, P53 induces apoptosis, cellular senescence, and cell cycle arrest. *P53* regulates energy metabolism, inflammation, and epithelial-mesenchymal transition and plays a central role in DNA damage repair. Importantly, *P53* can be mutated in various tumors (50, 51). The P53 pathway plays various roles in cell death, including apoptosis (52), autophagy (53), pyroptosis (54), necrosis (55), and ferroptosis (56). This may involve complex crosstalk with the NF-κB pathway (57).

Kyoto Encyclopedia of Genes and Genomes (KEGG) and gene ontology (GO) analyses revealed that genes differentially expressed before and after *UXT* knockdown in HCT116 cells were associated with the P53 pathway (49), which suggests a relationship between UXT and the P53 signaling pathway in tumors. The authors also confirmed in human osteosarcoma cells that UXT-V2 inhibits P53 activity by binding to MDMX, which further leads to a selective increase in NF-κB activity. This up-regulates the expression of hypoxia-inducible factor-1α (HIF-1α), which in turn significantly increases the expression of glycolytic genes, such as *glucose transporter (GLUT)-1/3, hexokinase (HK)-2/3, lactate dehydrogenase A (LDHA)*, and *enolase (ENO)*, promoting glycolysis (5). This shift confers a proliferation and survival advantage to tumor cells. The authors also demonstrated that UXT-V2 affects NF-κB activity by increasing the nuclear localization of P65.

In solid tumors, hypoxia is a pervasive growth environment in tumor tissue and is progressively exacerbated by reduced vascularity

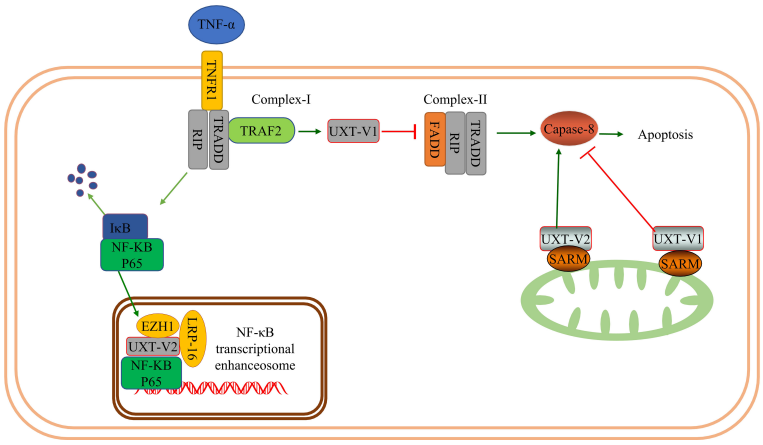


FIGURE 1
UXT and NF-κB signaling pathway: When TNF-α binds to TNFR1 and UXT-V1 binds to TRAF2, apoptosis is inhibited by inhibiting the formation of complex- II by inhibiting FADD recruitment. UXT-V1 binds to the SARM on the mitochondrial membrane and inhibits the activity of casepase8, thereby inhibiting cell apoptosis. UXT-V2 binds to SARM up-regulating the activity of casepase8 and promoting apoptosis. UXT-V2 acts as an NF-κB enhancer to regulate the transcription of downstream genes in the NF-κB signaling pathway. EZH1 and LRP-16 participate in the composition of the NF-κB enhanceosome.

in the tissue. The Warburg effect is a metabolic signature in which tumor cells rapidly break down glucose and glutamine through glycolysis while activating the expression of key enzymes to provide energy (58). This imparts a variety of properties, such as cellular resistance to death. Researchers have found that breast cancer cells exhibit increased anti-apoptotic properties when aerobic glycolysis is enhanced, while inhibition of HIF-1α inhibits aerobic glycolysis, reduces resistance to apoptosis, and promotes apoptosis (59). UXT-V2 is up-regulated in breast cancer tissues and cell lines, and down-regulates maternal expression 3 (MEG3) by binding to DNMT3B, thereby inhibiting the P53 signaling pathway (22).UXT-V2 also inhibits apoptosis and promotes the proliferation, migration, and invasion of breast cancer cells through its negative regulation of the P53 signaling pathway (22). This provides direct evidence that UXT modulates apoptosis *via* the P53 signaling pathway (Figure 2).

3.4 UXT and DNA methylation

DNA methylation is an epigenetic process. Cancer often shows overall DNA hypomethylation compared with healthy tissues. Methylation of CpG islands in promoter regions generally suppresses transcription; DNA methylation at CpG sites is the most common epigenetic inhibition of tumor suppressor genes in malignant tumors (60, 61). Regulation of genes involved in apoptosis, mediated by DNA methylation, may be an important mechanism for tumor cells to escape apoptosis, and changes in these related genes can occur in the form of hypomethylation to reactivate anti-apoptotic genes or in the form of hypermethylation to inhibit pro-apoptotic genes (62, 63).

DNA methylation can be catalyzed by the DNMT family of enzymes. In breast cancer cells, UXT-V2 interacts with DNMT3B to downregulate *MEG3* through methylation, and negatively regulates the *MEG3/P53* axis, thereby inhibiting apoptosis and promoting proliferation (22). Enhancer of zeste homologue 2 (EZH2) is a catalytic subunit of histone methyl-transferase and polycomb repressive complex 2 (PRC2), which can alter the expression of downstream target genes through H3K27me3 (64, 65). Subsequent studies have found that UXT promotes the formation of the PRC2 complex through interaction between UXT and EZH2 in the nucleus, thus promoting histone methyltransferase (HMTase) activity of EZH2. UXT inhibits transcription of tumor suppressor gene *homeobox A9 (HOXA9)* and *disabled homolog 2 (DAB2)*-interacting protein (DAB2IP), promoting proliferation, colony formation and migration of renal clear cell carcinoma (13). Meanwhile, UXT is highly expressed in breast cancer and that UXT suppresses RND3 epigenetically by recruiting EZH2 in breast cancer. After UXT knockdown, cell proliferation and metastasis are inhibited (66). This evidence suggests that UXT interacts with EZH2 in tumor cells.

Knockdown of EZH2 or DZNep(EZH2 inhibitor) can induce apoptosis of RKO and HCT116 cells, promote autophagy, inhibit G1/S transition, and increase the number of G1 phase cells (67). Meanwhile EZH2 modulates E2F1-dependent apoptosis through epigenetic regulation of Bcl-2 interacting mediator of cell death (BIM) expression (68). Therefore, EZH2 can regulate cell apoptosis, cell cycle and disease progression, playing a crucial role in the occurrence and development of tumors (64, 69). We speculate that UXT may regulate tumor cell apoptosis or other processes by recruiting EZH2 or stabilizing EZH2 as a chaperone (Figure 3).

In conclusion, UXT-V1/V2 may regulate apoptosis *via* multiple mechanisms . In the treatment of tumors, the deletion of pro-apoptotic genes or overexpression of anti-apoptotic genes causes the tumor to inhibit apoptosis. This inhibition leads to resistance to chemotherapy drugs and the development of multidrug resistance. UXT may be a potential diagnostic or therapeutic biomarker.

4 UXT and autophagy

Autophagy is a conserved mechanism in various cells, is divided into either non-selective or selective. Non-selective autophagy can be used to break down cellular proteins, lipids, and nucleic acids to maintain intracellular homeostasis when cell nutrition is deficient. In selective autophagy, misfolded and abnormally accumulated proteins can be broken down when the body is exposed to conditions such as hypoxia, oxidative stress, pathogen infection, and radiation (70, 71). Autophagy is involved in cell death and survival in cancers, neurodegenerative diseases, and metabolic disorders (72, 73). The NCCD classifies autophagy-dependent RCD as autophagy-dependent cell death (34). During cell death, autophagy can also activate apoptosis, ferroptosis, necrotic

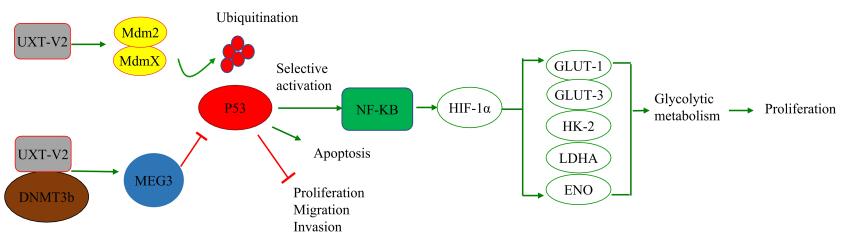


FIGURE 2
UXT and the P53 signaling pathway: UXT-V2 inhibits P53 by promoting ubiquitin degradation of P53 through MDMX. Down-regulation of P53 activity leads to selective activation of NF-κB signaling pathway, up-regulation of HIF-1α expression, promotion of glycolysis gene *GLUT-1/3, HK-2, LDHA, and ENO* expression, and promotion of glycolysis. These changes promote cell proliferation. By binding to DNMT3B, UXT-V2 downregulates MEG3 by methylation and thus inhibits the P53 signaling pathway. When P53 is suppressed, apoptosis is inhibited and cell proliferation, migration and invasion are promoted.

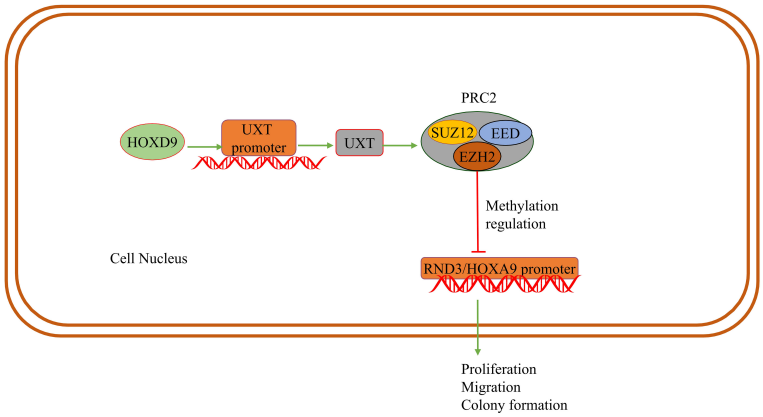


FIGURE 3
UXT and methylation: HOXD9 acts on the UXT promoter to up-regulate UXT expression. UXT promotes methyltransferase activity with EZH2 in PRC2 and methylates the promoter of the tumor suppressor gene *RND3/HOXA9*. The expression of RND3/HOXA9 is down-regulated and promotes tumor cell proliferation, migration and colony formation.

apoptosis, and other RCD modes through molecular pathways such as TRAIL and ferritin (70, 74–76). Notably, autophagy-dependent cell death should not be confused with other modes of RCD caused by autophagy (34, 73, 77). Mutations in genes associated with autophagy are associated with many human diseases, and the search for new therapeutic targets in the autophagy pathway has great potential (78).

UXT plays a role in late endosome/autophagosome–lysosome fusion events. Downregulation of UXT leads to an increase in the binding of tumor susceptibility gene 101(TSG101) vesicles to lysosomes, increases autophagy flux, and promotes the degradation of centrosomal protein of 55 kDa (CEP55) when TSG101 is overexpressed (26). In addition, UXT interacts with the mTOR protein, an essential negative regulator of autophagy. In mammals, the mTOR protein participates in the formation of mTOR complex 1 (mTORC1) and mTOR complex 2 (mTORC2) (79). mTORC1 limits the autophagic decomposition of cell components, inhibits the formation of autophagosomes, and plays a role in both the early and late stages of autophagy (80). Conversely, mTORC2 participates in the regulation of apoptosis and glucose homeostasis by interacting with protein kinase B (AKT). In the mouse photosensitive cell line 661W, after the conditional knockout of UXT, the decrease in mTOR activity promoted a significant increase in autophagy-related genes and the inhibition of autophagy-negative regulation genes, accompanied by a decrease in sequestosome 1 (SQSTM1) levels and an increase in microtubule-associated protein light chain (LC3)-II levels. Significant activation of autophagy increases the expression of pro-apoptotic genes and decreases that of anti-apoptotic genes (27). Eventually, photoreceptor apoptosis and the downregulation of retinal pigmentation-related genes lead to severe retinal degeneration and retinal dysfunction. Therefore, UXT plays a key role in promoting mTOR activity to prevent retinal degeneration.

In selective autophagy, P62 acts as a ubiquitin-dependent autophagy-selective receptor that binds to misfolded proteins and mediates protein autophagy degradation (71). P62 may also interact with TRAF6 and activate the NF-κB signaling pathway *via* the P62-TRAF6-NF-κB axis. Additionally, P62 is associated with exogenous apoptosis and autophagy, which can control cell death or survival (81). This hypothesis was partially supported by a subsequent study. UXT-V2 interacts with the autophagy receptor P62 through the LIM protein-binding (LB) domain and acts as an autophagy adapter for P62, regulating P62-mediated selective autophagy (24). Notably, UXT-V2 may act in the form of oligomers. In addition, UXT-V2 specifically interacts with STING1 and selectively autophagy degrades STING1 by promoting the interaction of P62 with STING1 (25). Therefore, UXT-V2 is involved in the selective autophagy degradation of proteins *via* P62 (Figure 4).

Excessive activation of autophagy can lead to ferroptosis (82). This unique cell death pattern is driven by iron-dependent phospholipid peroxidation and is regulated by iron therapy, redox homeostasis, mitochondrial activity, and lipid and glucose metabolism in the cell, with many signaling pathways (83). Ferroptosis is a mode of cell death involved in the progression of tumors and degenerative diseases. After the activation of autophagy, ferritin in fibroblasts and cancer cells can be degraded to promote ferroptosis (75).

Nuclear factor erythroid 2-related factor 2 (NRF2) and its main negative regulator Kelch-like ECH-associated protein 1 (KEAP1) are essential for maintaining redox, metabolism, and protein homeostasis and regulating inflammation (84). The P62-NRF2 pathway is strongly associated with ferroptosis. In hepatocellular carcinoma, the degradation of KEAP1 mediated by P62 assists the activation of NAD(P)H quinone dehydrogenase 1 (NQO1), heme oxygenase 1 (HO1), and ferritin heavy chain 1 (FTH1) downstream of NRF2. These downstream genes confer resistance to ferroptosis by altering iron metabolism and lipid peroxidation. Inhibition of NRF2 activation makes HCC cells more susceptible to ferroptosis both *in vitro* and *in vivo*. Thus, NRF2 activation inhibited ferroptosis in liver cancer cells (85). When autophagy is inhibited, the P62-KEAP1-NRF2 pathway protects HepG2 cells from alcohol-induced ferroptosis (86). The P62-KEAP1-NRF2 pathway also protects neuroblastoma cells from 6-OHDA-induced ferroptosis by activating HO1. Targeting the P62-

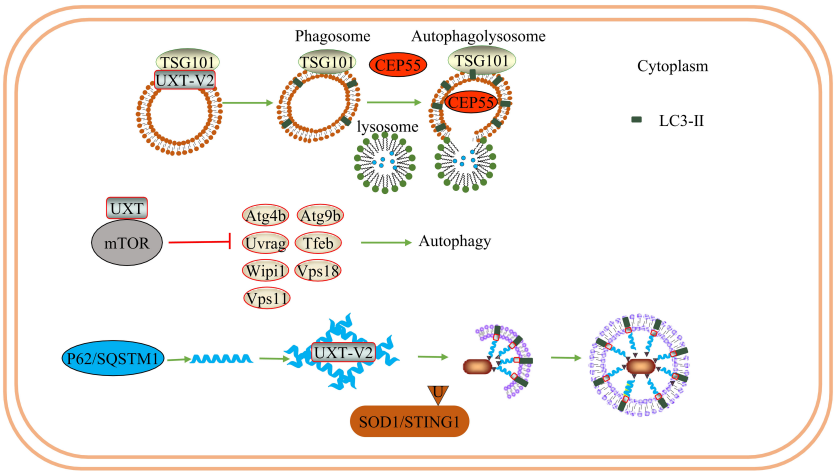


FIGURE 4
UXT and autophagy: UXT-V2 can be combined with TSG101. When UXT-V2 is down-regulated, it promotes the binding of TSG101-containing vesicles to lysosomes and promotes the degradation of CEP55. At the same time, the expression of LC3-II was up-regulated. UXT interact with mTOR, When UXT-V2 is down-regulated, autophagy promotes genetic *Atg4b/Uvrag/Wipi1/Vps11/Atg9b/Tfeb/Vps18* expression are suppressed. And then inhibit autophagy. P62 can form a strip α-helical structure. UXT-V2 promotes the interweaving of P62 into a network, increases the binding sites of P62 and LC3, and promotes the autophagy degradation of SOD1 aggregates and STING1.

KEAP1-NRF2 signaling pathway provides new insights into the treatment of Parkinson's disease (87). Similar studies have been performed on lung epithelial cells and neurons in spinal cord injury (88, 89). Thus, we speculate that UXT may regulate ferroptosis in cancer and neurodegenerative diseases through the P62-KEAP1-NRF2 signaling pathway.

Autophagy is a continuous and complex dynamic process, and the effects of UXT regulation on autophagy are not fully understood. Based on the results of previous studies, we believe that UXT may have a dual effect on autophagy regulation. When the expression of UXT is reduced, autophagy can be promoted by reducing the activity of mTOR or promoting the formation of autophagic lysosomes. In contrast, UXT can promote P62-mediated selective autophagy. Based on this, we discussed the possibility that UXT is involved in the regulation of ferroptosis *via* P62. UXT belongs to one of the subunits of pre-folded protein analogs and can act in the form of oligomers. Therefore, studies investigating the mechanism of UXT should consider that in addition to UXT alone, UXT may assist autophagy-related proteins in maintaining the correct protein conformation and function as chaperones, which then regulate autophagy.

5 UXT and immunity

The immune system is a complex and effective defense system of the human body. When bacteria, viruses, damaged cells, or tumor cells are used as antigens to stimulate immune cells, they can trigger innate or adaptive immune responses that maintain immune balance in the body. The immune system can also respond to the body's own components, and the destruction of cells or tissues can lead to autoimmune diseases. In the treatment of tumors, the weak immunogenicity of the tumor itself, inhibition of tumor cell apoptosis, tumor immunosuppressive cells in the tumor microenvironment (TME), and other factors can lead to tumor cells escaping immune surveillance. Cancer immunotherapy is to reactivate tumor immunity by improving immune cell function, immune checkpoint inhibitors, adoptive cell therapy and other methods (90). Thus, immunotherapy for tumors is considered promising.

MAVS is an antiviral protein complex in the mitochondria. Viral infection can activate the MAVS-TNFR3 signaling axis in the mitochondria. As a component of the MAVS signaling body in the mitochondria, UXT-V1 binds to TRAF3 *via* the N-terminal TRAF binding motif, mediates innate antiviral responses. When UXT-V1 is knockdown, the translocation of TRAF3/TRADD to the mitochondria is significantly blocked, which inhibits retinoic acid-inducible gene-I (RIG-I)-mediated IFN-β, IL-8, and interferon-stimulated gene factor 54 (ISG54). Therefore, UXT-V1 is critical for the virus-induced activation of NF-κB and IRF3 and is a positive regulator (28). UXT-V2 is phosphorylated by BGLF4 at the Thr3 site, which blocks the interaction between UXT-V2 and P65; this inhibits the transactivation of NF-κB, effectively weakening the immune response of host cells in the antiviral response, and facilitating the replication process of the virus (29).Therefore, UXT-V2 and UXT-V1 can regulate the innate immune response during viral infection. However, the two mechanisms differ. Since UXT-V1 is primarily present in the cytoplasm, it functions through the mitochondrial MAVS complex. UXT-V2 mainly exists in the nucleus and can act as a component of the NF-κB signal enhanceosome (Figure 5).

UXT has been shown to be an important negative regulator of type I IFN signaling. UXT also modulates the suppressive phenotype of Treg. Thus UXT may promote immunosuppression. Systemic lupus erythematosus(SLE) is an autoimmune disease characterized by overexpression of type I IFNs and ISGs. After DNA mimics or cGAMP stimulation, UXT specifically binds to STING1 and promotes the binding of STING1 to P62. UXT reduces

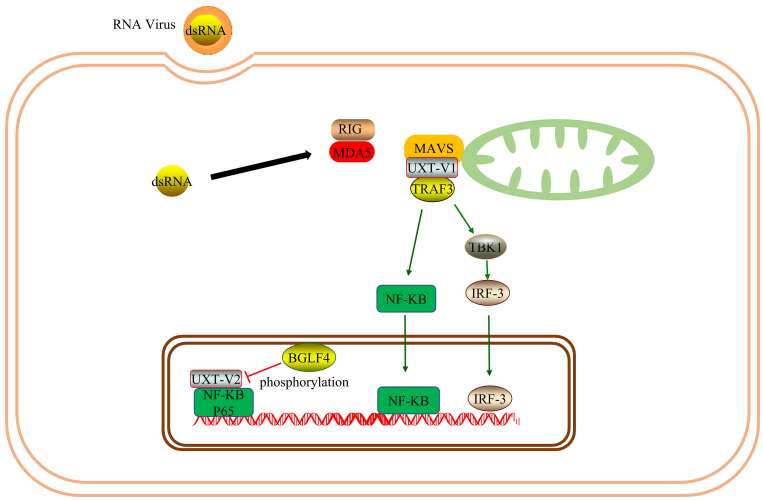


FIGURE 5
UXT promotes immune response: As one of the components of the MAVS signalosome, UXT-V1 promotes the nuclear translocation of IRF3 and NF-κB by binding to TRAF3, thus promoting innate immune response. UXT-V2 can be phosphorylated by BGLF4, disrupting its NF-κB enhanceosome function.

the production of type I IFN by selectively degrading STING1 (25). UXT can negatively regulate the cGAS-STING1 pathway. Notably, the authors performed a large-scale gene expression profiling using leukocytes and peripheral blood mononuclear cells from 1211 SLE patients and 139 healthy donors and confirmed that UXT expression was significantly impaired in SLE patients (25). This provides evidence for the involvement of UXT in the SLE process. In the TME, Tregs participate in the formation of the tumor inhibition microenvironment. Tregs are a subset of T cells and a T cell subtype with immunosuppressive effects primarily involved in adaptive immune responses and play an important role in maintaining immune self-tolerance and immune homeostasis (91). FOXP3, a member of the fox family, is a major regulator of Treg phenotype and immune-suppressive function (92). UXT-V2 is expressed in Tregs, traditional T (ConvT) cells, and B cells in blood samples from healthy volunteers. UXT-V2 directly regulates FOXP3 in Tregs and promotes its transcription by interacting with the proline-rich domain at the N-terminus of FOXP3 in the nucleus (93). Thus, UXT can regulate the inhibitory phenotype of Tregs by promoting the expression of FOXP3.

Based on these previous findings, we conclude that UXT may have a dual effect on innate immunity. UXT-V1/V2 modulates the NF-κB signaling pathway in different ways and modulates innate immunity. In contrast, UXT promotes selective autophagy and inhibits type I IFN production *via* cGAS-STING1 and adaptive immune responses by promoting Treg function. This could be related to the differences between cells and diseases, as well as the different mechanisms of UXT. As there are very few studies on UXT, we cannot rule out the possibility of their simultaneous occurrence. This requires interpretation from a more comprehensive perspective (Figure 6).

Immunogenic cell death (ICD) refers to the activation of the host adaptive immune response by substances released after cell death as endogenous (such as cell components) or exogenous (such as viruses) antigens after the stimulation of viral infection, chemotherapy drugs, and radiotherapy (34, 94). These changes cause cell death, and is different from traditional apoptosis. ICD stimulates the host immune system and enhances the immune response induced by immunotherapy (95, 96). Therefore, successful induction of ICD is important for improving current oncological treatment outcomes (97). Depending on the complexity of the immunosuppressive TME and the low immunogenicity of tumor cells, the sensitivity to tumor chemotherapy can be reduced, resulting in limited clinical efficacy. Therefore, a more efficient treatment strategy is urgently needed (98). The immune response is the basis of ICD. Manipulating the patient's immune system to activate the host immune response to the pathogenesis of cancer is a promising strategy. This may provide possible intervention measures to improve tumor metastasis and drug resistance (99).

Several studies have shown that STING1 is effectively activated by various factors that promote ICD in colon cancer and neuroblastoma cells (100, 101). Type I IFN, a cytokine released when tumor cells die, initiates adaptive immunity during ICD and promotes the maturation of antigen-presenting cells (94, 102). Type I IFN directly promotes DC maturation and links innate and adaptive immunities (103). As a subunit of the pre-folded protein family, UXT participates in tumor cell antigen exposure and antigen presentation, thereby affecting the number of tumor-infiltrating immune cells (TIICs) (104). In addition, Tregs recognize autologous and non-autologous antigens, including tumor antigens, and down-regulate dendritic cell function through CTLA-4, granulozyme/perforin, and IL-10, thereby disabling T cell activation responses and inducing immunosuppression and immune tolerance (105). Immune tolerance can hinder effective tumor immunity. Numerous Tregs infiltrate the human liver, lung, pancreas, and other tumors (106–108). Changes in tumor infiltration are critical to the outcome of antitumor drug therapy, and an increase in the proportion of Tregs indicates a poor treatment response (109). The removal of Tregs can reduce tumor immune tolerance, thereby improving the efficacy of tumor

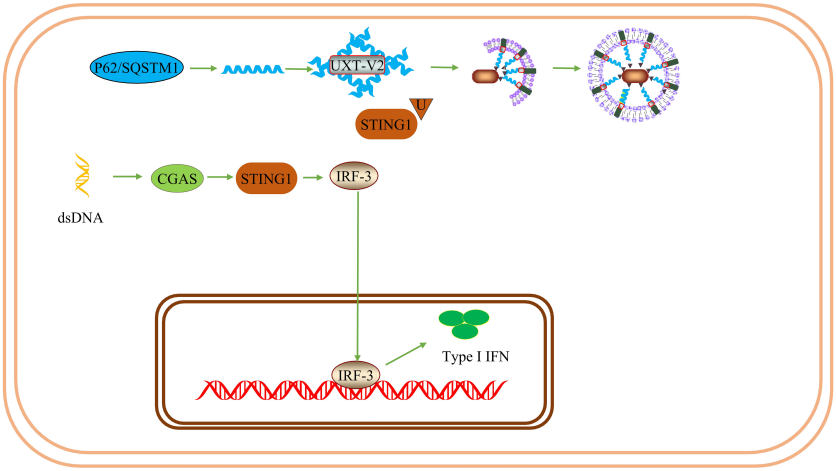


FIGURE 6
UXT inhibits the immune response: UXT-V2 negatively modulates the cGAS-STING1 signaling pathway by promoting the autophagy degradation of STING1 mediated by P62. These changes lead to a down-regulation of the type I IFN expression.

immunotherapy and increasing the risk of autoimmune diseases (110). Therefore, effective tumor immunity can also be obtained through systemic or local disruption of immune tolerance. EZH2 has been shown to maintain the immunosuppressive function of Tregs by modulating the transcription of Tregs cells (111). As described above, UXT interacts with EZH2 in the nucleus to promote the activity of the methyltransferase in which EZH2 is involved. Interestingly, blocking the function of EZH2 in Treg selectively breaks tolerance in the TME without inducing systemic autoimmune toxicity (112). Therefore, knocking down UXT to inhibit Tregs may create a favorable immune basis for the occurrence of ICD.

UXT may be involved in the regulation of ICD in two ways. On the one hand, UXT may enhance the immune response by modulating the expression of type I IFN and immunosuppressive cells, while on the other hand, UXT may also regulate antigen exposure and presentation and promote the maturation of antigen-presenting cells. UXT is down-regulated to reduce EZH2 recruitment, thereby improving the autoimmune toxicity caused by inhibition of Treg cells.

As previously indicated, UXT-V2 can up-regulate the expression of glycolysis-related genes and promote tumor glycolysis (5). Hypoxia is one of the characteristics of the TME in solid tumors. According to the Warburg effect, tumor cells prefer glycolysis for their energy supply even under aerobic conditions. A large amount of pyruvate is produced during glycolysis and that energy supply and is then converted into lactic acid by lactate dehydrogenase (LDH). Lactic acid is one of the main contributors to an acidic TME. In acidic TMEs, many tumor cells, including breast cancer cells, experience immuno-suppression (113). Lactic acid promotes the survival of melanoma cells in acidic TME (114). In addition, lactic acid plays an immunosuppressive role in the TME, increases tumor cell survival and promotes tumor immune escape (115).

Therefore, inhibition of glycolysis reduces the concentration of lactate to reshape the TME and enhance anti-tumor immunity (116). Several studies have shown that the inhibition of glycolysis promotes ICD induction in hepatocellular carcinoma (117). Thus, we speculate that targeting UXT to improve tumor metabolic reprogramming promotes ICD in tumor cells. Notably, lactic acid promotes the activity and recruitment of Tregs, which reduces the immune response of the cancer cells (118). Tregs express the lactate transporter monocarboxylate transporter 1 (MCT1) and transport lactate as a metabolic fuel (119) (Figure 7).

In summary, UXT can promote the function of Tregs, and, conversely, glycolysis in tumor tissues. These two factors may contribute to each other by exacerbating immunosuppression, immune escape, and promoting tumor progression. Therefore, targeted UXT may improve therapeutic effects by improving tumor cell metabolism in the TME. In addition, targeted UXT may promote ICD by improving tumor antigenicity, improving antigen presentation, and enhancing the immune response.

6 UXT and neurodegenerative diseases

ALS is a progressive neurodegenerative disease characterized by degeneration of motor neurons in the brain and spinal cord, accompanied by progressive muscle weakness. The ALS2 protein encoded by the *ALS2* gene is closely related to diseases of the nervous system, including ALS. The accumulation of abnormal proteins caused by mutations in ALS2 or other factors can cause many clinical symptoms or different diseases (120, 121). ALS results in paralysis and death within 2–5 years of onset.

ALS is a disease involving multiple systems and factors. Although the etiology and pathogenesis of ALS are not fully understood, research has shown that inflammatory responses in the peripheral and central nervous systems contribute to the injury of motor neurons and promote disease progression. The pathological processes of ALS2 involve endoplasmic reticulum stress, oxidative stress, neuroinflammation, and axonal transport

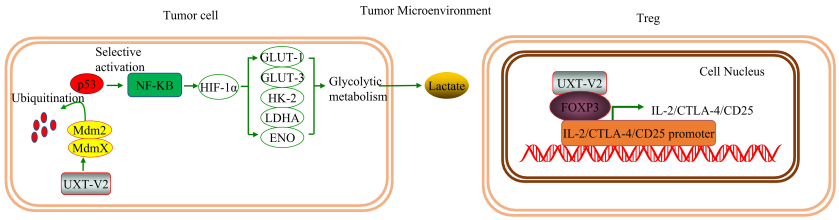


FIGURE 7
UXT regulates the tumor microenvironment: UXT-V2 promotes glycolysis by selectively activating the NF-κB signaling pathway by inhibiting the P53 signaling pathway. Glycolysis is promoted to increase lactate production and to acidify the TME. When UXT-V2 expression is up-regulated in Tregs, FOXP3 mRNA and protein levels are also up-regulated. UXT-V2 can also help maintain the inhibitory phenotype of Treg by binding to FoxP3 and stabilizing FOXP3 binding to *IL-2/CTLA-4/CD25* promoters.

dysfunction, and the study of the relationship between the structure and function of the ALS2 protein and the study of interacting proteins or chaperones will provide novel insights into the molecular pathogenesis of ALS (122) (Figure 8).

Several researchers have found that UXT interacts directly with ALS2 and is co-localized in the cytoplasm (123, 124). The UXT-V2 isoform protein specifically interacts with ALS2 *in vitro* and *in vivo* through its DH/PH region. In addition, UXT-V2 and ALS2 were colocalized in the cytoplasm of Neuro2a cells. Interestingly, their transcription appears to be synchronized throughout the cell cycle, with G0/G1 being the highest expression phase for both genes (125). Previous studies have found that overexpression of ALS2 triggers the Rac1/phosphatidylinositol 3-kinase/Akt3 anti-apoptotic pathway, thus inhibiting the toxicity of superoxide dismutase type 1 (SOD1) (126). The central nervous system is rich in SOD1, which accounts for approximately 1% of brain proteins. Mutated SOD1 exhibits definite neurotoxicity; SOD1 mutations are prone to form aggregates due to misfolding. SOD1 is associated with ALS. In addition, ALS2 has a protective effect on SOD1 and can bind to mutant SOD1 to inhibit its toxicity. As one of the subunits of a pre-folded protein analog, UXT may help to maintain the proper folding of mutant SOD1 close to the DH/PH region of ALS2 to some extent, thus assisting in its protective effect on SOD1.

Mutated P62 causes motor neuron degeneration in mice and zebrafish ALS models (127, 128). The interaction between UXT and the autophagy receptor P62 can prevent protein toxicity in neurons by facilitating autophagy degradation of protein polymers (24). Thus, UXT may play a protective role in ALS by acting as a chaperone protein, helping the protein maintain its normal conformation, or promoting selective autophagy to weaken endoplasmic reticulum stress caused by abnormal protein accumulation.

ALS-associated mutations enhance the accumulation of TAR DNA-binding protein 43 (TDP-43) in the cytoplasm and mitochondria (129). Accumulation of TDP-43 in the cytoplasm is a marker of ALS and has been linked to neuroinflammatory cytokines in patients with ALS. NF-κB and type I IFN can upregulate relevant inflammatory factors and promote disease progression in ALS. One study found that TDP-43 leads to the mitochondrial DNA (mtDNA) entering the cytoplasm after entering the mitochondria, activating IRF3, and upregulating NF-κB activity by activating the cGAS-STING signaling pathway. Remarkably, researchers have been able to delay neurodegeneration by downregulating the STING signal,

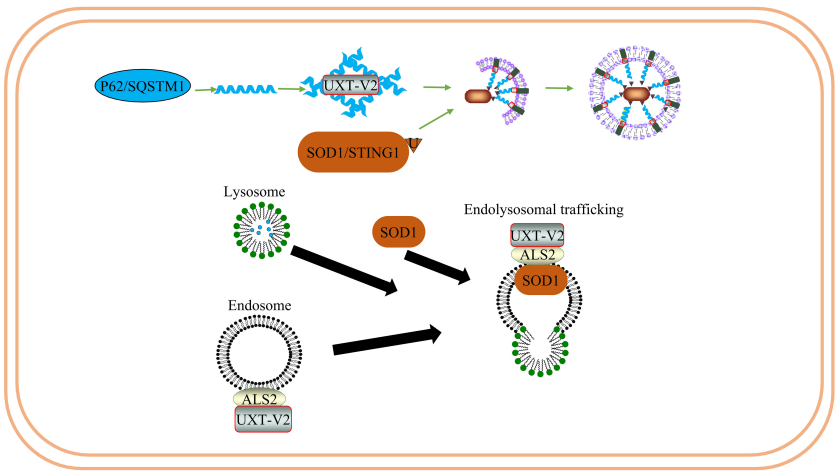


FIGURE 8
UXT regulates the degradation of SOD1 protein aggregates in ALS: UXT-V2 promotes autophagy degradation of P62 - mediated SOD1 protein aggregates. UXT-V2 promotes endolysosomal trafficking of SOD1 protein aggregates by binding to ALS2.

demonstrating the potential of targeting this pathway (130). In addition, STING can degrade the autolysosome pathway in the bone marrow cells. Blocking STING suppresses the overactive type I interferon response and inflammation in immune cells caused by a C9orf72 deficiency (131). Therefore, STING is an exciting potential target for ALS transformation therapy (132). UXT-V2 degrades STING through selective autophagy, negatively regulates the cGAS-STING1 signaling pathway, and reduces type I IFN production (25). We speculate that UXT may play a neuroprotective role in ALS by promoting autophagic degradation of STING and negatively regulating type I IFN.

Compared with the control group, one study found that the number of T cell subsets in patients with ALS significantly increased CD8 cytotoxic T cells and natural killer (NK) T cells, while Tregs significantly decreased. Tregs are also negatively correlated with disease progression. This indicates that patients with ALS exhibit systemic immune activation (133). A prospective multicenter human and animal experiment showed that Treg expansion was negatively correlated with disease progression rate and positively correlated with survival time. In addition, the expansion of Tregs was associated with a decrease in somatic cell size of motor neurons in SOD1 mutant mice, significant suppression of astrocyte and microglial immunoreactivity, and increased expression of neurotrophic factor genes in the spinal cord and peripheral nerves. Thus, Tregs have a protective effect on the nerves and may also inhibit toxic neuroinflammation in the central nervous system. The strategy of peripheral enhancement and neuroprotective activity of the Treg group may prove to be therapeutic in patients with ALS (134). Notably, it is generally safe and well-tolerated to inject Tregs into the body in combination with IL-2 subcutaneously after conducting a phase I uncontrolled clinical trial. This slows the progression of both the early and late stages of the disease (135). In subsequent randomized control trial and open-label extension, it was found that Treg/IL-2 treatment was safe, well-tolerated, and had a high Treg inhibition function (136) (Figure 9).

Therefore, the protective effect of Tregs on nerves in ALS has been preliminarily proven both theoretically and clinically. As mentioned earlier, UXT regulates Tregs through Foxp3. When UXT was overexpressed in Tregs, the binding of Foxp3 to *IL-2, CTLA-4, and CD25* increased. We speculate that UXT plays a neuroprotective role in ALS by negatively regulating the cGAS-STING1 signaling pathway and positively regulating the nuclear localization and stability of the Foxp3 protein, thereby inhibiting the progress of neuroinflammation in ALS.

The interaction between UXT and Down syndrome (DS) critical region gene 1 (DSCR1) on human chromosome 21 has been previously confirmed *in vitro* (137).

DSCR1 is also called calcineurin (RCAN) in subsequent studies and is believed to be involved in the pathogenesis of DS (138). RCAN homologues are upregulated in Alzheimer's disease, myocardial hypertrophy, diabetes, and degenerative neuropathy, as well as in external stressors (such as reactive oxygen species, Ca^{2+}, β-amyloid, and hormone changes) (139). Research on whether and how UXT may play a role in DS has not progressed.

7 Conclusions and future directions

Chemotherapy and radiotherapy play an irreplaceable role in tumor treatment. However, chemoresistance or multidrug resistance is a difficult problem that has plagued human beings for many years. UXT-V1 regulates TNF, induces the formation of the TNFR1 trimer, inhibits the recruitment of TNFR1 signal complex, and inhibits apoptosis. UXT-V2 inhibits cell apoptosis by promoting the expression of anti-apoptotic genes downstream of NF-κB and by epigenetic inhibition of the P53 signaling pathway. UXT-V2 interacts with the mitochondria and SARM to promote apoptosis. When the expression of UXT is reduced, it can promote autophagy by promoting the fusion of vesicles and lysosomes. It can also promote autophagy and cause photoreceptor apoptosis by interacting with mTOR. In addition, UXT interacts with P62 to

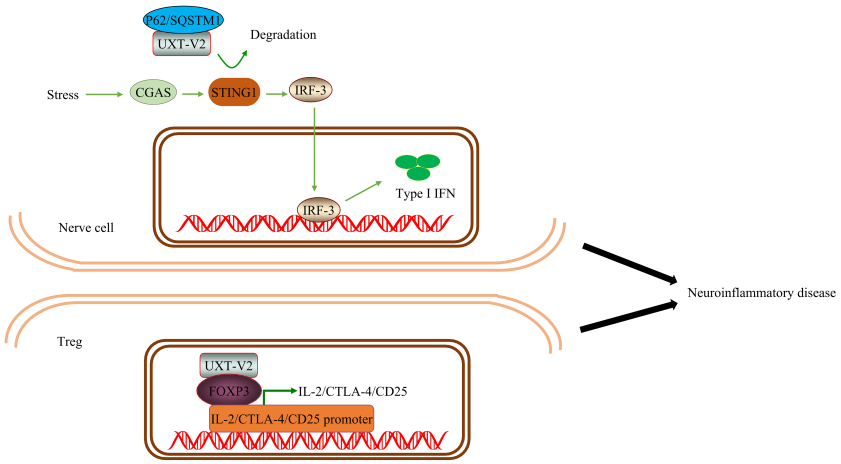


FIGURE 9
UXT regulates neuroinflammation in ALS: UXT-V2 down regulates the expression of type I IFN by autophagy degradation of STING1 mediated by P62. UXT-V2 promoted the inhibitory phenotype of Tregs by binding to FOXP3. Together, they improve neuroinflammation in neurodegenerative diseases.

promote selective autophagy mediated by P62. Thus, UXT can regulate apoptosis and autophagy in various ways and regulate the regulatory death of tumor cells. This suggests the possibility of UXT involvement in the diagnosis and treatment of tumors and in alleviating drug resistance to chemotherapy. The effect of the P62-KEAP1-NRF2 axis on ferroptosis in tumor cells has been previously reported; therefore, we discussed the possibility of UXT involvement in P62-mediated ferroptosis. We hope to further deepen the understanding of the effect of UXT on tumors from the perspective of regulatory cell death.

With the application of immune checkpoint inhibitors, CAR-T cells, adoptive immunotherapy, and other therapies, tumor immunotherapy is widely considered to be promising. In recent years, there has been a gradual increase in the study of UXT in the immunological community. UXT-V1 inhibits type I IFN expression through the cGAS-STING signaling pathway and participates in innate immune response. The cGAS-STING signaling pathway has a strong immune surveillance effect. Activation of the STING promotes a variety of anti-tumor effects, including T cell activation, DC maturation, and accelerated cancer cell death. STING also modulates inflammation and type I IFN induced disease progression in ALS and SLE. UXT interacts with the Foxp3 to regulate the inhibitory phenotype of Treg and participate in the adaptive immune response. Meanwhile UXT may also regulate gene transcription in Treg through EZH2.Treg is a type of $CD4^{+}$T cell that is immunosuppressive. This effect is seen in both tumors and ALS. UXT can promote autophagy degradation of STING and inhibitory phenotypes of Treg. This provides a clue to the immunosuppressive effects of UXT in diseases including tumors and neurodegenerative diseases. UXT can also up-regulate the expression of glycolytic genes through a crosstalk between the P53 and NF-κB pathways. This not only enhances tumor cell proliferation and anti-apoptotic advantage, but also promotes lactate production in TME. Lactate promotes the formation of the acid TME and acts as a fuel for Treg to maintain the immunosuppressive function of Treg. Therefore, UXT may have immunosuppressive function on the one hand and metabolic regulation on the other. Through the connection of these two aspects, it is possible not only to promote tumor cell survival, but also to cause more severe immunosuppression. Importantly, RIG-I-mediated expression of IFN, IL-8 and ISG54 can be suppressed by MAVS when UXT-V1 is down-regulated. Phosphorylation of UXT-V2 blocks the activation of NF-κB and attenuates the host's antiviral immune response.

The study of UXT in cell death and immunity is still in its infancy; therefore, the available data are limited, with some key questions requiring further explanation. First, in a specific disease or mechanism study, we must identify the isoforms and action forms of UXT. There are two isoforms of UXT with different cell distributions. Although UXT-V1 and UXT-V2 are distributed in the nucleus, cytoplasm and mitochondria, UXT-V1 is mostly found in the cytoplasm, while UXT-V2 in the nucleus. At the same time, except for the monomer form, the structure of UXT has the ability to form a hexamer. Second, there have been few studies of UXT interaction targets, mechanisms and related diseases. As a target discovered more than 20 years ago, UXT-related malignancies are more concentrated in breast and prostate cancers, where it is believed to regulate tumor progression and affect tumor prognosis. The mechanisms of UXT mainly involve NF-κB, P53, methylation, autophagy and androgen receptors. Therefore, research on other diseases and their mechanisms remains warranted.

Author contributions

PH, YT and XF contributed to conception and design of the study. PH and SM drafted and revised the manuscript. PH, SM, ZW and JX contributed to the production and modification of images. YT made critical revisions to important parts of the manuscript. All authors contributed to manuscript, and approved the submitted version.

Funding

This article was supported by Shanxi Provincial Department of Human Resources and Social Security, grant number 20210002; Shanxi Province 136 revitalization medical project (department of general surgery)

Conflict of interest

The authors declare that the research was conducted in the absence of any commercial or financial relationships that could be construed as a potential conflict of interest.

Publisher's note

All claims expressed in this article are solely those of the authors and do not necessarily represent those of their affiliated organizations, or those of the publisher, the editors and the reviewers. Any product that may be evaluated in this article, or claim that may be made by its manufacturer, is not guaranteed or endorsed by the publisher.

References

1. Markus SM, Taneja SS, Logan SK, Li W, Ha S, Hittelman AB, et al. Identification and characterization of ART-27, a novel coactivator for the androgen receptor n terminus. *Mol Biol Cell* (2002) 13(2):670–82. doi: 10.1091/mbc.01-10-0513

2. Sun S, Tang Y, Lou X, Zhu L, Yang K, Zhang B, et al. UXT is a novel and essential cofactor in the NF-kappaB transcriptional enhanceosome. *J Cell Biol* (2007) 178 (2):231–44. doi: 10.1083/jcb.200611081

3. Carter DR, Buckle AD, Tanaka K, Perdomo J, Chong BH. Art27 interacts with GATA4, FOG2 and NKX2.5 and is a novel co-repressor of cardiac genes. *PloS One* (2014) 9(4):e95253. doi: 10.1371/journal.pone.0095253

4. McGilvray R, Walker M, Bartholomew C. UXT interacts with the transcriptional repressor protein EVI1 and suppresses cell transformation. *FEBS J* (2007) 274 (15):3960–71. doi: 10.1111/j.1742-4658.2007.05928.x

5. Qi M, Ganapathy S, Zeng W, Zhang J, Little JB, Yuan ZM. UXT, a novel MDMX-binding protein, promotes glycolysis by mitigating p53-mediated restriction of NF-kappaB activity. *Oncotarget.* (2015) 6(19):17584–93. doi: 10.18632/oncotarget.3770

6. Yin J, Luo W, Zeng X, Zeng L, Li Z, Deng X, et al. UXT-AS1-induced alternative splicing of UXT is associated with tumor progression in colorectal cancer. *Am J Cancer Res* (2017) 7(3):462–72.

7. Sanchez-Morgan N, Kirsch KH, Trackman PC, Sonenshein GE. UXT is a LOX-PP interacting protein that modulates estrogen receptor alpha activity in breast cancer cells. *J Cell Biochem* (2017) 118(8):2347–56. doi: 10.1002/jcb.25893

8. Foschini MP, Morandi L, Sanchez AM, Santoro A, Mulè A, Zannoni GF, et al. Methylation profile of X-Chromosome–related genes in Male breast cancer. *Front Oncol* (2020) 10. doi: 10.3389/fonc.2020.00784

9. Asioli S, Zoli M, Guaraldi F, Sollini G, Bacci A, Gibertoni D, et al. Peculiar pathological, radiological and clinical features of skull-base de-differentiated chordomas. results from a referral centre case-series and literature review. *Histopathology.* (2020) 76(5):731–9. doi: 10.1111/his.14024

10. Taneja SS, Ha S, Swenson NK, Torra IP, Rome S, Walden PD, et al. ART-27, an androgen receptor coactivator regulated in prostate development and cancer. *J Biol Chem* (2004) 279(14):13944–52. doi: 10.1074/jbc.M306576200

11. Nwachukwu JC, Mita P, Ruoff R, Ha S, Wang Q, Huang SJ, et al. Genome-wide impact of androgen receptor trapped clone-27 loss on androgen-regulated transcription in prostate cancer cells. *Cancer Res* (2009) 69(7):3140–7. doi: 10.1158/0008-5472.CAN-08-3738

12. Nwachukwu JC, Li W, Pineda-Torra I, Huang HY, Ruoff R, Shapiro E, et al. Transcriptional regulation of the androgen receptor cofactor androgen receptor trapped clone-27. *Mol Endocrinology.* (2007) 21(12):2864–76. doi: 10.1210/me.2007-0094

13. Zeng J, Xiang W, Zhang Y, Huang C, Chen K, Chen Z. Ubiquitous expressed transcript promotes tumorigenesis by acting as a positive modulator of the polycomb repressive complex 2 in clear cell renal cell carcinoma. *BMC Cancer.* (2019) 19(1):874. doi: 10.1186/s12885-019-6069-3

14. Spagnol V, Oliveira CAB, Randle SJ, Passos PMS, Correia C, Simaroli NB, et al. The E3 ubiquitin ligase SCF(Fbxo7) mediates proteasomal degradation of UXT isoform 2 (UXT-V2) to inhibit the NF-kappaB signaling pathway. *Biochim Biophys Acta Gen Subj.* (2021) 1865(1):129754. doi: 10.1016/j.bbagen.2020.129754

15. He H, Huang J, Wu S, Jiang S, Liang L, Liu Y, et al. The roles of GTPase-activating proteins in regulated cell death and tumor immunity. *J Hematol Oncol* (2021) 14(1):171. doi: 10.1186/s13045-021-01184-1

16. Koren E, Fuchs Y. Modes of regulated cell death in cancer. *Cancer Discovery* (2021) 11(2):245–65. doi: 10.1158/2159-8290.CD-20-0789

17. Mohammad RM, Muqbil I, Lowe L, Yedjou C, Hsu HY, Lin LT, et al. Broad targeting of resistance to apoptosis in cancer. *Semin Cancer Biol* (2015) 35 Suppl(0): S78–S103. doi: 10.1016/j.semcancer.2015.03.001

18. Tsimberidou AM, Fountzilas E, Nikanjam M, Kurzrock R. Review of precision cancer medicine: evolution of the treatment paradigm. *Cancer Treat Rev* (2020) 86:102019. doi: 10.1016/j.ctrv.2020.102019

19. Rothlin CV, Hille TD, Ghosh S. Determining the effector response to cell death. *Nat Rev Immunol* (2021) 21(5):292–304. doi: 10.1038/s41577-020-00456-0

20. Liu Z, Li H, Hong C, Chen M, Yue T, Chen C, et al. ALS-associated E478G mutation in human OPTN (Optineurin) promotes inflammation and induces neuronal cell death. *Front Immunol* (2018) 9:2647. doi: 10.3389/fimmu.2018.02647

21. Puentes F, Malaspina A, van Noort JM, Amor S. Non-neuronal cells in ALS: role of glial, immune cells and blood-CNS barriers. *Brain Pathol* (2016) 26(2):248–57. doi: 10.1111/bpa.12352

22. Huang ZF, Tang YL, Shen ZL, Yang KY, Gao K. UXT, a novel DNMT3b-binding protein, promotes breast cancer progression *via* negatively modulating lncRNA MEG3/p53 axis. *Mol Ther Oncolytics.* (2022) 24:497–506. doi: 10.1016/j.omto.2021.12.008

23. Sethurathinam S, Singh LP, Panneerselvam P, Byrne B, Ding JL. UXT plays dual opposing roles on SARM-induced apoptosis. *FEBS Lett* (2013) 587(20):3296–302. doi: 10.1016/j.febslet.2013.08.033

24. Yoon MJ, Choi B, Kim EJ, Ohk J, Yang C, Choi YG, et al. UXT chaperone prevents proteotoxicity by acting as an autophagy adaptor for p62-dependent aggrephagy. *Nat Commun* (2021) 12(1):1955. doi: 10.1038/s41467-021-22252-7

25. Pan M, Yin Y, Hu T, Wang X, Jia T, Sun J, et al. UXT attenuates the CGAS-STING1 signaling by targeting STING1 for autophagic degradation. *Autophagy* (2022) 19(2):440–56. doi: 10.1080/15548627.2022.2076192

26. Lin YM, Chu PH, Ouyang P. Depletion of UXT, a novel TSG101 interaction protein, leads to enhanced CEP55 attenuation through lysosome degradation. *Biochem Biophys Res Commun* (2021) 542:59–64. doi: 10.1016/j.bbrc.2020.12.110

27. Pan M, Yin Y, Wang X, Wang Q, Zhang L, Hu H, et al. Mice deficient in UXT exhibit retinitis pigmentosa-like features *via* aberrant autophagy activation. *Autophagy.* (2021) 17(8):1873–88. doi: 10.1080/15548627.2020.1796015

28. Huang Y, Liu H, Ge R, Zhou Y, Lou X, Wang C. UXT-V1 facilitates the formation of MAVS antiviral signalosome on mitochondria. *J Immunol* (2012) 188 (1):358–66. doi: 10.4049/jimmunol.1102079

29. Chang LS, Wang JT, Doong SL, Lee CP, Chang CW, Tsai CH, et al. Epstein-Barr Virus BGLF4 kinase downregulates NF-kappaB transactivation through phosphorylation of coactivator UXT. *J Virol* (2012) 86(22):12176–86. doi: 10.1128/JVI.01918-12

30. Schroer A, Schneider S, Ropers H, Nothwang H. Cloning and characterization of UXT, a novel gene in human Xp11, which is widely and abundantly expressed in tumor tissue. *Genomics.* (1999) 56(3):340–3. doi: 10.1006/geno.1998.5712

31. Huang Y, Chen L, Zhou Y, Liu H, Yang J, Liu Z, et al. UXT-V1 protects cells against TNF-induced apoptosis through modulating complex II formation. *Mol Biol Cell* (2011) 22(8):1389–97. doi: 10.1091/mbc.e10-10-0827

32. Schafler ED, Thomas PA, Ha S, Wang Y, Bermudez-Hernandez K, Tang Z, et al. UXT is required for spermatogenesis in mice. *PloS One* (2018) 13(4):e0195747. doi: 10.1371/journal.pone.0195747

33. Zhao H, Wang Q, Zhang H, Liu Q, Du X, Richter M, et al. UXT is a novel centrosomal protein essential for cell viability. *Mol Biol Cell* (2005) 16(12):5857–65. doi: 10.1091/mbc.e05-08-0705

34. Galluzzi L, Vitale I, Aaronson SA, Abrams JM, Adam D, Agostinis P, et al. Molecular mechanisms of cell death: recommendations of the nomenclature committee on cell death 2018. *Cell Death Differ* (2018) 25(3):486–541. doi: 10.1038/s41418-017-0012-4

35. Carneiro BA, El-Deiry WS. Targeting apoptosis in cancer therapy. *Nat Rev Clin Oncol* (2020) 17(7):395–417. doi: 10.1038/s41571-020-0341-y

36. Singh P, Lim B. Targeting apoptosis in cancer. *Curr Oncol Rep* (2022) 24(3):273–84. doi: 10.1007/s11912-022-01199-y

37. Sax JK, Fei P, Murphy ME, Bernhard E, Korsmeyer SJ, El-Deiry WS. BID regulation by p53 contributes to chemosensitivity. *Nat Cell Biol* (2002) 4(11):842–9. doi: 10.1038/ncb866

38. Bock FJ, Tait SWG. Mitochondria as multifaceted regulators of cell death. *Nat Rev Mol Cell Biol* (2020) 21(2):85–100. doi: 10.1038/s41580-019-0173-8

39. Liu L, McKeehan WL. Sequence analysis of LRPPRC and its SEC1 domain interaction partners suggests roles in cytoskeletal organization, vesicular trafficking, nucleocytosolic shuttling, and chromosome activity. *Genomics.* (2002) 79(1):124–36. doi: 10.1006/geno.2001.6679

40. Liu L, Amy V, Liu G, McKeehan WL. Novel complex integrating mitochondria and the microtubular cytoskeleton with chromosome remodeling and tumor suppressor RASSF1 deduced by in silico homology analysis, interaction cloning in yeast, and colocalization in cultured cells. *In Vitro Cell Dev Biol Anim.* (2002) 38 (10):582–94. doi: 10.1290/1543-706X(2002)38<582:NCIMAT>2.0.CO;2

41. Moss TN, Vo A, McKeehan WL, Liu L. UXT (Ubiquitously expressed transcript) causes mitochondrial aggregation. *In Vitro Cell Dev Biol Anim* (2007) 43(3-4):139–46. doi: 10.1007/s11626-007-9016-6

42. Peng SY, Lin LC, Chen SR, Farooqi AA, Cheng YB, Tang JY, et al. Pomegranate extract (POMx) induces mitochondrial dysfunction and apoptosis of oral cancer cells. *Antioxidants (Basel)* (2021) 10(7):1117. doi: 10.3390/antiox10071117

43. Zaib S, Hayyat A, Ali N, Gul A, Naveed M, Khan I. Role of mitochondrial membrane potential and lactate dehydrogenase a in apoptosis. *Anticancer Agents Med Chem* (2022) 22(11):2048–62. doi: 10.2174/1871520621666211126090906

44. Taniguchi K, Karin M. NF-kappaB, inflammation, immunity and cancer: coming of age. *Nat Rev Immunol* (2018) 18(5):309–24. doi: 10.1038/nri.2017.142

45. Alharbi KS, Fuloria NK, Fuloria S, Rahman SB, Al-Malki WH, Javed Shaikh MA, et al. Nuclear factor-kappa b and its role in inflammatory lung disease. *Chem Biol Interact* (2021) 345:109568. doi: 10.1016/j.cbi.2021.109568

46. Annibaldi A, Meier P. Checkpoints in TNF-induced cell death: implications in inflammation and cancer. *Trends Mol Med* (2018) 24(1):49–65. doi: 10.1016/j.molmed.2017.11.002

47. Yang J, Zhao YL, Wu ZQ, Si YL, Meng YG, Fu XB, et al. The single-macro domain protein LRP16 is an essential cofactor of androgen receptor. *Endocr Relat Cancer.* (2009) 16(1):139–53. doi: 10.1677/ERC-08-0150

48. Wu Z, Li Y, Li X, Ti D, Zhao Y, Si Y, et al. LRP16 integrates into NF-kappaB transcriptional complex and is required for its functional activation. *PloS One* (2011) 6 (3):e18157. doi: 10.1371/journal.pone.0018157

49. Su S-K, Li C-Y, Lei P-J, Wang X, Zhao Q-Y, Cai Y, et al. EZH1/SUZ12 complex positively regulates the transcription of NF-κB target genes via interaction with UXT. *J Cell Sci* (2016) 129(12):2343–53. doi: 10.1242/jcs.185546

50. Vaddavalli PL, Schumacher B. The p53 network: cellular and systemic DNA damage responses in cancer and aging. *Trends Genet* (2022) 38(6):598–612. doi: 10.1016/j.tig.2022.02.010

51. Hassin O, Oren M. Drugging p53 in cancer: one protein, many targets. *Nat Rev Drug Discovery* (2022) 22(2):127–44. doi: 10.1038/s41573-022-00571-8

52. Doherty J, Baehrecke EH. Life, death and autophagy. *Nat Cell Biol* (2018) 20 (10):1110–7. doi: 10.1038/s41556-018-0201-5

53. White E. Autophagy and p53. *Cold Spring Harb Perspect Med* (2016) 6(4): a026120. doi: 10.1101/cshperspect.a026120

54. Hu Y, Wang B, Li S, Yang S. Pyroptosis, and its role in central nervous system disease. *J Mol Biol* (2022) 434(4):167379. doi: 10.1016/j.jmb.2021.167379

55. Weinlich R, Oberst A, Beere HM, Green DR. Necroptosis in development, inflammation and disease. *Nat Rev Mol Cell Biol* (2017) 18(2):127–36. doi: 10.1038/nrm.2016.149

56. Zhang L, Lu Y, Ma X, Xing Y, Sun J, Jia Y. The potential interplay between G-quadruplex and p53: their roles in regulation of ferroptosis in cancer. *Front Mol Biosci* (2022) 9:965924. doi: 10.3389/fmolb.2022.965924

57. Carrà G, Lingua MF, Maffeo B, Taulli R, Morotti A. P53 vs NF-κB: the role of nuclear factor-kappa b in the regulation of p53 activity and vice versa. *Cell Mol Life Sci* (2020) 77(22):4449–58. doi: 10.1007/s00018-020-03524-9

58. Cerella C, Dicato M, Diederich M. Modulatory roles of glycolytic enzymes in cell death. *Biochem Pharmacol* (2014) 92(1):22–30. doi: 10.1016/j.bcp.2014.07.005

59. Chen F, Chen J, Yang L, Liu J, Zhang X, Zhang Y, et al. Extracellular vesicle-packaged HIF-1alpha-stabilizing lncRNA from tumour-associated macrophages regulates aerobic glycolysis of breast cancer cells. *Nat Cell Biol* (2019) 21(4):498–510. doi: 10.1038/s41556-019-0299-0

60. Kinnaird A, Zhao S, Wellen KE, Michelakis ED. Metabolic control of epigenetics in cancer. *Nat Rev Cancer.* (2016) 16(11):694–707. doi: 10.1038/nrc.2016.82

61. Emran AA, Chatterjee A, Rodger EJ, Tiffen JC, Gallagher SJ, Eccles MR, et al. Targeting DNA methylation and EZH2 activity to overcome melanoma resistance to immunotherapy. *Trends Immunol* (2019) 40(4):328–44. doi: 10.1016/j.it.2019.02.004

62. Hervouet E, Vallette FM, Cartron PF. Impact of the DNA methyltransferases expression on the methylation status of apoptosis-associated genes in glioblastoma multiforme. *Cell Death Dis* (2010) 1:e8. doi: 10.1038/cddis.2009.7

63. Gopisetty G, Ramachandran K, Singal R. DNA Methylation and apoptosis. *Mol Immunol* (2006) 43(11):1729–40. doi: 10.1016/j.molimm.2005.11.010

64. Kim KH, Roberts CW. Targeting EZH2 in cancer. *Nat Med* (2016) 22(2):128–34. doi: 10.1038/nm.4036

65. Duan R, Du W, Guo W. EZH2: a novel target for cancer treatment. *J Hematol Oncol* (2020) 13(1):104. doi: 10.1186/s13045-020-00937-8

66. Hu XC, Chu J, Zhou Y, Li CC, Zhou GJ, Jiang GQ. HOXD9 transcriptionally induced UXT facilitate breast cancer progression *via* epigenetic modification of RND3. *Cell Signal* (2022) 90:110188. doi: 10.1016/j.cellsig.2021.110188

67. Yao Y, Hu H, Yang Y, Zhou G, Shang Z, Yang X, et al. Downregulation of enhancer of zeste homolog 2 (EZH2) is essential for the induction of autophagy and apoptosis in colorectal cancer cells. *Genes (Basel)* (2016) 7(10):83. doi: 10.3390/genes7100083

68. Wu ZL, Zheng SS, Li ZM, Qiao YY, Aau MY, Yu Q. Polycomb protein EZH2 regulates E2F1-dependent apoptosis through epigenetically modulating bim expression. *Cell Death Differ* (2010) 17(5):801–10. doi: 10.1038/cdd.2009.162

69. Comet I, Riising EM, Leblanc B, Helin K. Maintaining cell identity: PRC2-mediated regulation of transcription and cancer. *Nat Rev Cancer.* (2016) 16(12):803–10. doi: 10.1038/nrc.2016.83

70. Goodall ML, Fitzwalter BE, Zahedi S, Wu M, Rodriguez D, Mulcahy-Levy JM, et al. The autophagy machinery controls cell death switching between apoptosis and necroptosis. *Dev Cell* (2016) 37(4):337–49. doi: 10.1016/j.devcel.2016.04.018

71. Vargas JNS, Hamasaki M, Kawabata T, Youle RJ, Yoshimori T. The mechanisms and roles of selective autophagy in mammals. *Nat Rev Mol Cell Biol* (2022) 24(3):167–85. doi: 10.1038/s41580-022-00542-2

72. Towers CG, Wodetzki D, Thorburn A. Autophagy and cancer: modulation of cell death pathways and cancer cell adaptations. *J Cell Biol* (2020) 219(1):e201909033. doi: 10.1083/jcb.201909033

73. Shen HM, Codogno P. Autophagic cell death: loch ness monster or endangered species? *Autophagy* (2011) 7(5):457–65. doi: 10.4161/auto.7.5.14226

74. Yao Z, Zhang P, Guo H, Shi J, Liu S, Liu Y, et al. RIP1 modulates death receptor mediated apoptosis and autophagy in macrophages. *Mol Oncol* (2015) 9(4):806–17. doi: 10.1016/j.molonc.2014.12.004

75. Hou W, Xie Y, Song X, Sun X, Lotze MT, Zeh HJ3rd, et al. Autophagy promotes ferroptosis by degradation of ferritin. *Autophagy.* (2016) 12(8):1425–8. doi: 10.1080/15548627.2016.1187366

76. Yang M, Chen P, Liu J, Zhu S, Kroemer G, Klionsky DJ, et al. Clockophagy is a novel selective autophagy process favoring ferroptosis. *Sci Adv* (2019) 5(7):eaaw2238. doi: 10.1126/sciadv.aaw2238

77. Denton D, Kumar S. Autophagy-dependent cell death. *Cell Death Differ* (2019) 26(4):605–16. doi: 10.1038/s41418-018-0252-y

78. Mizushima N, Levine B. Autophagy in human diseases. *N Engl J Med* (2020) 383(16):1564–76. doi: 10.1056/NEJMra2022774

79. Liu GY, Sabatini DM. mTOR at the nexus of nutrition, growth, ageing and disease. *Nat Rev Mol Cell Biol* (2020) 21(4):183–203. doi: 10.1038/s41580-019-0199-y

80. Kim YM, Jung CH, Seo M, Kim EK, Park JM, Bae SS, et al. mTORC1 phosphorylates UVRAG to negatively regulate autophagosome and endosome maturation. *Mol Cell* (2015) 57(2):207–18. doi: 10.1016/j.molcel.2014.11.013

81. Moscat J, Diaz-Meco MT. p62 at the crossroads of autophagy, apoptosis, and cancer. *Cell.* (2009) 137(6):1001–4. doi: 10.1016/j.cell.2009.05.023

82. Liu J, Liu Y, Wang Y, Li C, Xie Y, Klionsky DJ, et al. TMEM164 is a new determinant of autophagy-dependent ferroptosis. *Autophagy* (2022) 19(3):945–56. doi: 10.1080/15548627.2022.2111635

83. Jiang X, Stockwell BR, Conrad M. Ferroptosis: mechanisms, biology and role in disease. *Nat Rev Mol Cell Biol* (2021) 22(4):266–82. doi: 10.1038/s41580-020-00324-8

84. Cuadrado A, Rojo AI, Wells G, Hayes JD, Cousin SP, Rumsey WL, et al. Therapeutic targeting of the NRF2 and KEAP1 partnership in chronic diseases. *Nat Rev Drug Discovery* (2019) 18(4):295–317. doi: 10.1038/s41573-018-0008-x

85. Sun X, Ou Z, Chen R, Niu X, Chen D, Kang R, et al. Activation of the p62-Keap1-NRF2 pathway protects against ferroptosis in hepatocellular carcinoma cells. *Hepatology.* (2016) 63(1):173–84. doi: 10.1002/hep.28251

86. Zhao Y, Lu J, Mao A, Zhang R, Guan S. Autophagy inhibition plays a protective role in ferroptosis induced by alcohol *via* the p62–Keap1–Nrf2 pathway. *J Agric Food Chem* (2021) 69(33):9671–83. doi: 10.1021/acs.jafc.1c03751

87. Sun Y, He L, Wang T, Hua W, Qin H, Wang J, et al. Activation of p62-Keap1-Nrf2 pathway protects 6-Hydroxydopamine-Induced ferroptosis in dopaminergic cells. *Mol Neurobiol* (2020) 57(11):4628–41. doi: 10.1007/s12035-020-02049-3

88. Li X, Chen J, Yuan S, Zhuang X, Qiao T. Activation of the P62-Keap1-NRF2 pathway protects against ferroptosis in radiation-induced lung injury. *Oxid Med Cell Longev* (2022) 2022:8973509. doi: 10.1155/2022/8973509

89. Xia M, Zhang Q, Zhang Y, Li R, Zhao T, Chen L, et al. Growth differentiation factor 15 regulates oxidative stress-dependent ferroptosis post spinal cord injury by stabilizing the p62-Keap1-Nrf2 signaling pathway. *Front Aging Neurosci* (2022) 14:905115. doi: 10.3389/fnagi.2022.905115

90. Kennedy LB, Salama AKS. A review of cancer immunotherapy toxicity. *CA Cancer J Clin* (2020) 70(2):86–104. doi: 10.3322/caac.21596

91. Zhao H, Wu L, Yan G, Chen Y, Zhou M, Wu Y, et al. Inflammation and tumor progression: signaling pathways and targeted intervention. *Signal Transduct Target Ther* (2021) 6(1):263. doi: 10.1038/s41392-021-00658-5

92. Dong Y, Yang C, Pan F. Post-translational regulations of Foxp3 in treg cells and their therapeutic applications. *Front Immunol* (2021) 12:626172. doi: 10.3389/fimmu.2021.626172

93. Li W, Wang L, Jiang C, Li H, Zhang K, Xu Y, et al. UXT is a novel regulatory factor of regulatory T cells associated with Foxp3. *Eur J Immunol* (2014) 44(2):533–44. doi: 10.1002/eji.201343394

94. Galluzzi L, Vitale I, Warren S, Adjemian S, Agostinis P, Martinez AB, et al. Consensus guidelines for the definition, detection and interpretation of immunogenic cell death. *J Immunother Cancer* (2020) 8(1):e000337. doi: 10.1136/jitc-2019-000337

95. Montico B, Nigro A, Casolaro V, Dal Col J. Immunogenic apoptosis as a novel tool for anticancer vaccine development. *Int J Mol Sci* (2018) 19(2):594. doi: 10.3390/ijms19020594

96. Zappasodi R, Pupa SM, Ghedini GC, Bongarzone I, Magni M, Cabras AD, et al. Improved clinical outcome in indolent b-cell lymphoma patients vaccinated with autologous tumor cells experiencing immunogenic death. *Cancer Res* (2010) 70(22):9062–72. doi: 10.1158/0008-5472.CAN-10-1825

97. Garg AD, More S, Rufo N, Mece O, Sassano ML, Agostinis P, et al. Trial watch: immunogenic cell death induction by anticancer chemotherapeutics. *Oncoimmunology.* (2017) 6(12):e1386829. doi: 10.1080/2162402X.2017.1386829

98. Liang Q, Lan Y, Li Y, Cao Y, Li J, Liu Y. Crizotinib prodrug micelles co-delivered doxorubicin for synergistic immunogenic cell death induction on breast cancer chemo-immunotherapy. *Eur J Pharm Biopharm.* (2022) 177:260–72. doi: 10.1016/j.ejpb.2022.07.006

99. Goliwas KF, Deshane JS, Elmets CA, Athar M. Moving immune therapy forward targeting TME. *Physiol Rev* (2021) 101(2):417–25. doi: 10.1152/physrev.00008.2020

100. Chattopadhyay S, Liu YH, Fang ZS, Lin CL, Lin JC, Yao BY, et al. Synthetic immunogenic cell death mediated by intracellular delivery of STING agonist nanoshells enhances anticancer chemo-immunotherapy. *Nano Lett* (2020) 20(4):2246–56. doi: 10.1021/acs.nanolett.9b04094

101. Wang-Bishop L, Wehbe M, Shae D, James J, Hacker BC, Garland K, et al. Potent STING activation stimulates immunogenic cell death to enhance antitumor immunity in neuroblastoma. *J Immunother Cancer* (2020) 8(1):e000282. doi: 10.1136/jitc-2019-000282

102. Vanpouille-Box C, Alard A, Aryankalayil MJ, Sarfraz Y, Diamond JM, Schneider RJ, et al. DNA Exonuclease Trex1 regulates radiotherapy-induced tumour immunogenicity. *Nat Commun* (2017) 8:15618. doi: 10.1038/ncomms15618

103. Longhi MP, Trumpfheller C, Idoyaga J, Caskey M, Matos I, Kluger C, et al. Dendritic cells require a systemic type I interferon response to mature and induce CD4 + Th1 immunity with poly IC as adjuvant. *J Exp Med* (2009) 206(7):1589–602. doi: 10.1084/jem.20090247

104. Zhao H, Chen C, Yang C, Mo S, Zhao H, Tian Y. Prefoldin and prefoldin-like complex subunits as predictive biomarkers for hepatocellular carcinoma immunotherapy. *Pathol - Res Pract* (2022) 232:153808. doi: 10.1016/j.prp.2022.153808

105. Sakaguchi S, Yamaguchi T, Nomura T, Ono M. Regulatory T cells and immune tolerance. *Cell.* (2008) 133(5):775–87. doi: 10.1016/j.cell.2008.05.009

106. Ormandy LA, Hillemann T, Wedemeyer H, Manns MP, Greten TF, Korangy F. Increased populations of regulatory T cells in peripheral blood of patients with

hepatocellular carcinoma. *Cancer Res* (2005) 65(6):2457–64. doi: 10.1158/0008-5472.CAN-04-3232

107. Nishikawa H, Sakaguchi S. Regulatory T cells in tumor immunity. *Int J Cancer*. (2010) 127(4):759–67. doi: 10.1002/ijc.25429

108. Hiraoka N, Onozato K, Kosuge T, Hirohashi S. Prevalence of FOXP3+ regulatory T cells increases during the progression of pancreatic ductal adenocarcinoma and its premalignant lesions. *Clin Cancer Res* (2006) 12(18):5423–34. doi: 10.1158/1078-0432.CCR-06-0369

109. Kroemer G, Galluzzi L, Kepp O, Zitvogel L. Immunogenic cell death in cancer therapy. *Annu Rev Immunol* (2013) 31:51–72. doi: 10.1146/annurev-immunol-032712-100008

110. Tanaka A, Sakaguchi S. Regulatory T cells in cancer immunotherapy. *Cell Res* (2017) 27(1):109–18. doi: 10.1038/cr.2016.151

111. DuPage M, Chopra G, Quiros J, Rosenthal WL, Morar MM, Holohan D, et al. The chromatin-modifying enzyme Ezh2 is critical for the maintenance of regulatory T cell identity after activation. *Immunity*. (2015) 42(2):227–38. doi: 10.1016/j.immuni.2015.01.007

112. Wang D, Quiros J, Mahuron K, Pai CC, Ranzani V, Young A, et al. Targeting EZH2 reprograms intratumoral regulatory T cells to enhance cancer immunity. *Cell Rep* (2018) 23(11):3262–74. doi: 10.1016/j.celrep.2018.05.050

113. Urata K, Kajihara I, Miyauchi H, Mijiddorj T, Otsuka-Maeda S, Sakamoto R, et al. The warburg effect and tumour immune microenvironment in extramammary paget's disease: overexpression of lactate dehydrogenase a correlates with immune resistance. *J Eur Acad Dermatol Venereol.* (2020) 34(8):1715–21. doi: 10.1111/jdv.16145

114. Matsuo T, Daishaku S, Sadzuka Y. Lactic acid promotes cell survival by blocking autophagy of B16F10 mouse melanoma cells under glucose deprivation and hypoxic conditions. *Biol Pharm Bull* (2019) 42(5):837–9. doi: 10.1248/bpb.b18-00919

115. Romero-Garcia S, Moreno-Altamirano MM, Prado-Garcia H, Sanchez-Garcia FJ. Lactate contribution to the tumor microenvironment: mechanisms, effects on immune cells and therapeutic relevance. *Front Immunol* (2016) 7:52. doi: 10.3389/fimmu.2016.00052

116. Yang J, Ma S, Xu R, Wei Y, Zhang J, Zuo T, et al. Smart biomimetic metal organic frameworks based on ROS-ferroptosis-glycolysis regulation for enhanced tumor chemo-immunotherapy. *J Control Release.* (2021) 334:21–33. doi: 10.1016/j.jconrel.2021.04.013

117. Li Y, Song Z, Han Q, Zhao H, Pan Z, Lei Z, et al. Targeted inhibition of STAT3 induces immunogenic cell death of hepatocellular carcinoma cells *via* glycolysis. *Mol Oncol* (2022) 16(15):2861–80. doi: 10.1002/1878-0261.13263

118. Wang JX, Choi SYC, Niu X, Kang N, Xue H, Killam J, et al. Lactic acid and an acidic tumor microenvironment suppress anticancer immunity. *Int J Mol Sci* (2020) 21(21):8363. doi: 10.3390/ijms21218363

119. Watson MJ, Vignali PDA, Mullett SJ, Overacre-Delgoffe AE, Peralta RM, Grebinoski S, et al. Metabolic support of tumour-infiltrating regulatory T cells by lactic acid. *Nature.* (2021) 591(7851):645–51. doi: 10.1038/s41586-020-03045-2

120. Sprute R, Jergas H, Olmez A, Alawbathani S, Karasoy H, Dafsari HS, et al. Genotype-phenotype correlation in seven motor neuron disease families with novel ALS2 mutations. *Am J Med Genet A*. (2021) 185(2):344–54. doi: 10.1002/ajmg.a.61951

121. Sheerin UM, Schneider SA, Carr L, Deuschl G, Hopfner F, Stamelou M, et al. ALS2 mutations: juvenile amyotrophic lateral sclerosis and generalized dystonia. *Neurology*. (2014) 82(12):1065–7. doi: 10.1212/WNL.0000000000000254

122. Miceli M, Exertier C, Cavaglia M, Gugole E, Boccardo M, Casaluci RR, et al. ALS2-related motor neuron diseases: from symptoms to molecules. *Biol (Basel)* (2022) 11(1):77. doi: 10.3390/biology11010077

123. Millecamps S, Gentil BJ, Gros-Louis F, Rouleau G, Julien JP. Alsin is partially associated with centrosome in human cells. *Biochim Biophys Acta* (2005) 1745(1):84–100. doi: 10.1016/j.bbamcr.2004.12.008

124. Çetin Ozansoy MB, Ozansoy M. Als2 silencing affects the expression of two NF-κB targeted genes *via* UXT in adult mouse primary spinal motor neuron culture. *Medeniyet Med J* (2018) 33(3):227–34. doi: 10.5222/MMJ.2018.46667

125. Enunlu I, Ozansoy M, Basak AN. Alfa-Class prefoldin protein UXT is a novel interacting partner of amyotrophic lateral sclerosis 2 (Als2) protein. *Biochem Biophys Res Commun* (2011) 413(3):471–5. doi: 10.1016/j.bbrc.2011.08.121

126. Kanekura K, Hashimoto Y, Kita Y, Sasabe J, Aiso S, Nishimoto I, et al. A Rac1/phosphatidylinositol 3-kinase/Akt3 anti-apoptotic pathway, triggered by AlsinLF, the product of the ALS2 gene, antagonizes Cu/Zn-superoxide dismutase (SOD1) mutant-induced motoneuronal cell death. *J Biol Chem* (2005) 280(6):4532–43. doi: 10.1074/jbc.M410508200

127. Hadano S, Mitsui S, Pan L, Otomo A, Kubo M, Sato K, et al. Functional links between SQSTM1 and ALS2 in the pathogenesis of ALS: cumulative impact on the protection against mutant SOD1-mediated motor dysfunction in mice. *Hum Mol Genet* (2016) 25(15):3321–40. doi: 10.1093/hmg/ddw180

128. Lattante S, de Calbiac H, Le Ber I, Brice A, Ciura S, Kabashi E. Sqstm1 knock-down causes a locomotor phenotype ameliorated by rapamycin in a zebrafish model of ALS/FTLD. *Hum Mol Genet* (2015) 24(6):1682–90. doi: 10.1093/hmg/ddu580

129. Wang W, Arakawa H, Wang L, Okolo O, Siedlak SL, Jiang Y, et al. Motor-coordinative and cognitive dysfunction caused by mutant TDP-43 could be reversed by inhibiting its mitochondrial localization. *Mol Ther* (2017) 25(1):127–39. doi: 10.1016/j.ymthe.2016.10.013

130. Yu CH, Davidson S, Harapas CR, Hilton JB, Mlodzianoski MJ, Laohamonthonkul P, et al. TDP-43 triggers mitochondrial DNA release *via* mPTP to activate cGAS/STING in ALS. *Cell*. (2020) 183(3):636–49 e18. doi: 10.1016/j.cell.2020.09.020

131. McCauley ME, O'Rourke JG, Yanez A, Markman JL, Ho R, Wang X, et al. C9orf72 in myeloid cells suppresses STING-induced inflammation. *Nature*. (2020) 585(7823):96–101. doi: 10.1038/s41586-020-2625-x

132. Van Damme P, Robberecht W. STING-induced inflammation - a novel therapeutic target in ALS? *N Engl J Med* (2021) 384(8):765–7. doi: 10.1056/NEJMcibr2031048

133. Rentzos M, Evangelopoulos E, Sereti E, Zouvelou V, Marmara S, Alexakis T, et al. Alterations of T cell subsets in ALS: a systemic immune activation? *Acta Neurol Scand* (2012) 125(4):260–4. doi: 10.1111/j.1600-0404.2011.01528.x

134. Sheean RK, McKay FC, Cretney E, Bye CR, Perera ND, Tomas D, et al. Association of regulatory T-cell expansion with progression of amyotrophic lateral sclerosis: a study of humans and a transgenic mouse model. *JAMA Neurol* (2018) 75(6):681–9. doi: 10.1001/jamaneurol.2018.0035

135. Thonhoff JR, Beers DR, Zhao W, Pleitez M, Simpson EP, Berry JD, et al. Expanded autologous regulatory T-lymphocyte infusions in ALS: a phase I, first-in-human study. *Neurol Neuroimmunol Neuroinflamm*. (2018) 5(4):e465. doi: 10.1212/NXI.0000000000000465

136. Thonhoff JR, Berry JD, Macklin EA, Beers DR, Mendoza PA, Zhao W, et al. Combined regulatory T-lymphocyte and IL-2 treatment is safe, tolerable, and biologically active for 1 year in persons with amyotrophic lateral sclerosis. *Neurol Neuroimmunol Neuroinflamm* (2022) 9(6):e200019. doi: 10.1212/NXI.0000000000200019

137. Silveira HC, Sommer CA, Soares-Costa A, Henrique-Silva F. A calcineurin inhibitory protein overexpressed in down's syndrome interacts with the product of a ubiquitously expressed transcript. *Braz J Med Biol Res* (2004) 37(6):785–9. doi: 10.1590/S0100-879X2004000600002

138. Antonarakis SE. Down syndrome and the complexity of genome dosage imbalance. *Nat Rev Genet* (2017) 18(3):147–63. doi: 10.1038/nrg.2016.154

139. Lee SK, Ahnn J. Regulator of calcineurin (RCAN): beyond down syndrome critical region. *Mol Cells* (2020) 43(8):671–85. doi: 10.14348/molcells.2020.0060

frontiers | Frontiers in Immunology

TYPE Original Research
PUBLISHED 04 May 2023
DOI 10.3389/fimmu.2023.1172242

Check for updates

OPEN ACCESS

EDITED BY
Mohammad Azhar Aziz,
Aligarh Muslim University, India

REVIEWED BY
Xing Niu,
China Medical University, China
Haijing Guan,
Capital Medical University, China

*CORRESPONDENCE
Lei Dou
doulei@sdu.edu.cn

†These authors have contributed equally to this work

RECEIVED 23 February 2023
ACCEPTED 17 April 2023
PUBLISHED 04 May 2023

CITATION
Liu S, Jiang N, Dou L and Li S (2023) Cost-effectiveness analysis of serplulimab plus chemotherapy in the first-line treatment for PD-L1-positive esophageal squamous cell carcinoma in China. *Front. Immunol.* 14:1172242. doi: 10.3389/fimmu.2023.1172242

COPYRIGHT
© 2023 Liu, Jiang, Dou and Li. This is an open-access article distributed under the terms of the Creative Commons Attribution License (CC BY). The use, distribution or reproduction in other forums is permitted, provided the original author(s) and the copyright owner(s) are credited and that the original publication in this journal is cited, in accordance with accepted academic practice. No use, distribution or reproduction is permitted which does not comply with these terms.

Cost-effectiveness analysis of serplulimab plus chemotherapy in the first-line treatment for PD-L1-positive esophageal squamous cell carcinoma in China

Shixian Liu[1,2,3†], Nana Jiang[4†], Lei Dou[1,2,3*] and Shunping Li[1,2,3]

[1]Centre for Health Management and Policy Research, School of Public Health, Cheeloo College of Medicine, Shandong University, Jinan, China, [2]NHC Key Laboratory of Health Economics and Policy Research (Shandong University), Jinan, China, [3]Center for Health Preference Research, Shandong University, Jinan, China, [4]Department of Maternal and Child Health, School of Public Health, Cheeloo College of Medicine, Shandong University, Jinan, China

Objective: The ASTRUM-007 trial (NCT03958890) demonstrated that serplulimab plus chemotherapy administered every 2-week significantly improved progression-free and overall survival in patients with previously untreated, programmed death-ligand 1 (PD-L1) positive advanced esophageal squamous-cell carcinoma (ESCC). This study was aimed to investigate the cost-effectiveness of serplulimab plus chemotherapy in the first-line treatment of PD-L1-positive advanced ESCC.

Methods: A partitioned survival model with a 2-week cycle and a 10-year time horizon was constructed from the Chinese healthcare system perspective. The survival data, direct medical costs and utilities were derived from the ASTRUM-007 trial, YAOZHI database and published sources. Total costs, quality-adjusted life-years (QALYs) and incremental cost-effectiveness ratios (ICERs) were calculated. Scenario, one-way and probabilistic sensitivity analyses were performed to assess the uncertainty around model parameters.

Results: Compared with chemotherapy, serplulimab plus chemotherapy provided additional 0.27 QALYs with an incremental cost of $33,460.86, which had an ICER of $124,483.07 per QALY. The subgroup analyses revealed that the ICERs of serplulimab plus chemotherapy were $134,637.42 and $105,589.71 in advanced ESCC patients with $1 \leq CPS < 10$ and $CPS \geq 10$, respectively. The price of serplulimab, patient weight, utility values and discount rate were the most influential parameters on base-case results. At a willingness-to-pay threshold of three times per capita GDP ($40,587.59) in 2022, the probability of serplulimab plus chemotherapy being cost-effective was 0% compared with chemotherapy. When the price of serplulimab decreased by 70%, the probabilities of serplulimab plus chemotherapy being cost-effective were 81.42%, 67.74% and 96.75% in advanced ESCC patients with PD-L1-positive, PD-L1 $1 \leq CPS < 10$ and $CPS \geq 10$, respectively.

Conclusion: Serplulimab plus chemotherapy in the first-line treatment for PD-L1-positive advanced ESCC might not be cost-effective in China.

KEYWORDS

cost-effectiveness, esophageal squamous-cell carcinoma, serplulimab, first-line, immunotherapy

Introduction

Esophageal cancer is the fifth most common malignancy and the fourth leading cause of cancer-related death in China (1, 2). Esophageal squamous cell carcinoma (ESCC) and esophageal adenocarcinoma represent the predominant histological subtype, with the former accounting for approximately 85% of cases (3). Fluoropyrimidine or paclitaxel plus cisplatin-based chemotherapy remains the standard first-line treatment for patients with advanced or metastatic ESCC, which generally carried an extremely poor prognosis with median overall survival (OS) of fewer than 1 year (4, 5). Therefore, there is an unmet need for revolutionary therapeutic strategies to improve survival rates in advanced ESCC patients.

The emergence of immune checkpoint inhibitors targeting programmed death 1 (PD-1) or programmed death-ligand 1 (PD-L1) has drastically altered the landscape of cancer treatment (6). Serplulimab (HLX10), a fully humanized immune-globulin G4 monoclonal antibody against the PD-1 receptor, showed clinical efficacy in multiple malignancies (7, 8). Serplulimab has been approved by the National Medical Products Administration in the treatment of microsatellite instability-high (MSI-H) solid tumors, non-squamous non-small cell lung cancer and extensive-stage small-cell lung cancer in China (9).

Recently, ASTRUM-007, a randomized, double-blind, phase III clinical trial conducted at 70 hospitals in China, assessed the efficacy and safety of serplulimab plus chemotherapy compared with mono-chemotherapy as the first-line treatment of advanced or metastatic ESCC patients with PD-L1 combined positive score (CPS) ≥ 1 (10). The results demonstrated that serplulimab plus chemotherapy significantly prolonged median progression-free survival (PFS) (5.8 months vs. 5.3 months; hazard ratio [HR]: 0.60, 95% confidence interval [CI]: 0.48-0.75) and OS (15.3 months vs. 11.8 months; HR: 0.68, 95% CI: 0.53-0.87) in comparison with placebo plus chemotherapy (10). Compared with PD-L1 CPS < 10 patients, advanced ESCC patients with PD-L1 CPS ≥ 10 achieved better median PFS (7.1 months vs. 5.7 months) and OS (18.6 months vs. 14.2 months) outcomes from serplulimab in combination with chemotherapy. In terms of safety, the incidences of grade 3 or higher treatment-related adverse events (AEs) were 53% and 48% for serplulimab plus chemotherapy and chemotherapy, respectively.

Despite the enthusiasm surrounding serplulimab with superior efficacy, its cost-effectiveness remains unclear but is imperative for health decision-making and clinical practice. Therefore, this study aimed to evaluate the cost-effectiveness of serplulimab plus chemotherapy as the first-line treatment for previously untreated, PD-L1-positive (CPS ≥ 1) advanced ESCC from the perspective of Chinese healthcare system. Such evidence might provide guidance for clinicians and support reimbursement policy to optimize health resource allocation.

Methods

Patients and treatment

This study was reported in accordance with the Consolidated Health Economic Evaluation Reporting Standards 2022 (CHEERS 2022) updated reporting guidelines (Supplementary Table S1) (11). In this institutional review board-exempt economic evaluation, targeted patients were aged 18-75 years with previously untreated, histologically confirmed, inoperable locally advanced or metastatic, PD-L1-positive (CPS ≥ 1) ESCC, with at least one measurable lesion based on central imaging in line with response evaluation criteria in solid tumors v1.1, adequate organ function, and Eastern Cooperative Oncology Group performance status 0-1 (10). Patients who had previously received PD-1 or PD-L1 inhibitors, had central nervous system metastases or presented with active infection or active autoimmune diseases were excluded (10).

Eligible patients received serplulimab (3 mg/kg) or placebo intravenously on day 1 every 2-week cycle for up to 2 years. Chemotherapy was administrated intravenously every 2-week by cisplatin (50 mg/m^2 on day 1 for up to 8-cycle) and 5-fuorouracil (1,200 mg/m^2 on days 1 and 2 of each cycle for up to 12-cycle). Patients would be treated with second-line treatments until disease progression or intolerable toxicities, which mainly included immunotherapy (camrelizumab or tislelizumab), chemotherapy (docetaxel) and best supportive care (Supplementary Materials). In ASTRUM-007 trial, a total of 95 (52%) patients in the chemotherapy group and 139 (38%) in the serplulimab plus chemotherapy group received subsequent anti-cancer treatments (10). The proportion of patients received subsequent therapies in each group was shown in Table 1.

Model construction

A partitioned survival model was constructed with three exclusive health states (PFS, progression-disease [PD], and death)

10.3389/fimmu.2023.1172242

TABLE 1 Model parameters and the range of the sensitivity analysis.

Parameters	Base Case	Range		Distribution	Source
		Minimum	Maximum		
Cost inputs (US $)					
Serplulimab (100 mg)	882.18	705.74	1058.62	Gamma	(12)
Cisplatin (10 mg)	1.47	1.18	1.77	Gamma	(12)
Fluorouracil (250 mg)	8.51	6.81	10.22	Gamma	(12)
Camrelizumab (200 mg)	462.25	369.80	554.69	Gamma	(12)
Tislelizumab (100mg)	228.91	183.13	274.69	Gamma	(12)
Docetaxel (20mg)	13.94	11.15	16.73	Gamma	(12)
BSC	182.23	145.78	218.68	Gamma	(13)
Routine follow-up cost	73.72	58.98	88.47	Gamma	(13)
Laboratory tests and radiological examinations	357.34	285.87	428.81	Gamma	(13)
Hospitalization expense	19.86	15.89	23.83	Gamma	(14)
Cost of AEs per unit					
Anemia	336.63	269.30	403.95	Gamma	(15)
Neutropenia	454.26	363.41	545.11	Gamma	(13)
Leukopenia	454.26	363.41	545.11	Gamma	(13)
Thrombocytopenia	1523.82	1219.06	1828.58	Gamma	(16)
Vomiting	101.15	80.92	121.38	Gamma	(15)
Hyponatraemia	3223.00	2578.40	3867.60	Gamma	(16)
Hypokalemia	3000.00	2400.00	3600.00	Gamma	Assumption
Utility inputs					
Utility of PFS	0.75	0.60	0.90	Beta	(17)
Utility of PD	0.60	0.48	0.72	Beta	(17)
AEs disutility					
Anemia	0.07	0.06	0.09	Beta	(18)
Neutropenia	0.20	0.16	0.24	Beta	(19)
Leukopenia	0.20	0.16	0.24	Beta	(19)
Thrombocytopenia	0.11	0.09	0.13	Beta	(20)
Vomiting	0.13	0.10	0.15	Beta	(19)
Hyponatraemia	0.04	0.03	0.05	Beta	(21)
Hypokalemia	0.04	0.03	0.05	Beta	Assumption
Risk of ≥ grade 3 AEs (%)					
Serplulimab plus chemotherapy					
Anemia	17.54	14.03	21.05	Beta	(10)
Leukopenia	11.26	9.01	13.51	Beta	(10)
Neutropenia	18.59	14.87	22.30	Beta	(10)
Thrombocytopenia	3.93	3.14	4.71	Beta	(10)
Vomiting	3.14	2.51	3.77	Beta	(10)

(Continued)

TABLE 1 Continued

Parameters	Base Case	Range		Distribution	Source
		Minimum	Maximum		
Hyponatremia	4.71	3.77	5.65	Beta	(10)
Hypokalemia	3.66	2.93	4.40	Beta	(10)
Chemotherapy					
Anemia	20.24	16.19	24.29	Beta	(10)
Leukopenia	6.55	5.24	7.86	Beta	(10)
Neutropenia	17.26	13.81	20.71	Beta	(10)
Hypokalemia	3.57	2.86	4.29	Beta	(10)
Proportion of Subsequent treatment (%)					
Chemotherapy					
Immunotherapy	33.33	26.67	40.00	Beta	(10)
Chemotherapy	20.00	16.00	24.00	Beta	(10)
BSC	46.67	37.33	56.00	Beta	(10)
Serplulimab plus chemotherapy					
Immunotherapy	17.39	13.91	20.87	Beta	(10)
Chemotherapy	20.00	16.00	24.00	Beta	(10)
BSC	62.61	50.09	75.13	Beta	(10)
Others					
Discount rate (%)	5.00	0.00	8.00	Beta	(22)
Patient weight (kg)	65.00	52.00	78.00	Gamma	(13)
Body surface area (m^2)	1.72	1.38	2.06	Gamma	(13)

BSC, Best supportive care; AEs, adverse events; PFS, progression-free survival; PD, progressive disease.

to portray disease progression and treatment efficacy (Figure 1). The proportion of progression-free patients derived directly from the PFS curve, while the proportion of patients in the death state as 1 minus the OS curve. With regard to the PD state, its proportion was calculated as the difference between the PFS and OS curves (23).The time horizon of 10 years was adequate to ensure that ESCC patients completely entered the terminal state. The cycle length was 2-week to accommodate the treatment and follow-up regimens. Treatment strategies were compared in terms of overall costs, quality-adjusted life years (QALYs), and incremental cost-effectiveness ratios (ICERs; the incremental cost between two treatments per additional QALY gained). According to China Guidelines for Pharmacoeconomic Evaluations, half-cycle correlation and 5% annual discount rate were applied to costs and health outcomes (22). All costs were adjusted to 2023 prices with the local Consumer Price Index and converted into US dollars (1$=6.33 CNY). As recommended by the World Health Organization (24) and China Guidelines for Pharmacoeconomic Evaluations (22), 3 times per capita gross domestic product (GDP) of China in 2022 ($40,587.59) was implemented as the willingness-to-pay (WTP) threshold to judge the cost-effectiveness of serplulimab plus chemotherapy.

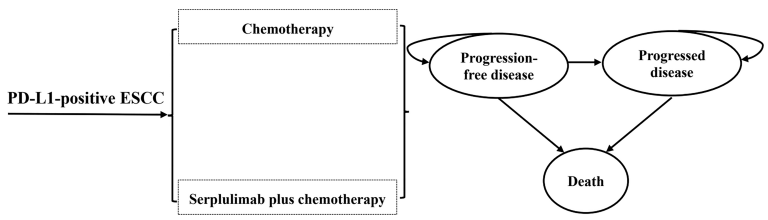


FIGURE 1
The structure of the partitioned survival model.

Clinical inputs

Since individual patient data was unavailable, GetData Graph Digitizer 2.26 (http://www.getdata-graph-digitizer.com/) was applied to extract PFS and OS data points from the Kaplan-Meier curves reported in the ASTRUM-007 trial (Supplementary Tables S2, S3). To optimally extrapolate the lifetime survival outcome, Exponential, Weibull, Log-logistic, Log-normal, and Gompertz distributions were used to fit the individual-level data (25). The selection of optimal parametric distribution was based on clinical plausibility, Akaike Information Criterion, Bayesian Information Criterion and visual examination (26). The estimated shape parameters (γ) and scale parameters (λ) were summarized in Supplementary Table S4. Long-term survival data were presented in Supplementary Table S5, Table S6 and Figure S1.

Cost inputs

Only direct medical costs were considered, including drug costs, subsequent therapy, hospitalization expense, routine follow-up and examinations, and costs for the management of AEs. The prices of serplulimab, camrelizumab and tislelizumab were derived from lowest winning bids. Other drug costs were calculated from the average winning bids in 2023 of the YAOZHI database (https://data.yaozh.com/), which aggregated the latest price data around the country (12). Our prices were accessed on February 2, 2023. To determine the dosage and expenditure of therapeutic agents, the default height of 165 cm and body weight of 65kg, resulting in a body surface area (BSA) of 1.72 m^2 were assumed for the Chinese ESCC patients (13). Other costs were retrieved from previously published literatures, such as best supportive care, routine follow-up, hospitalization, laboratory tests and radiological examinations (13, 14). In both groups, the frequency of laboratory work, computed tomography or magnetic resonance imaging examination were further determined according to Guidelines of Chinese Society of Clinical oncology (27). Grade 3 or above AEs with an incidence of greater than 3% were considered, including anemia, neutropenia, leukopenia, thrombocytopenia, vomiting, hyponatraemia and hypokalemia (13, 15, 16). All cost-related inputs were shown in Table 1.

Health state utility

Each health state was assigned a utility anchored in 0 (death) and 1 (perfect health) in this partitioned survival model. Health state utilities for the PFS and PD health states were estimated from patient-level EQ-5D-3L data from the RAINBOW trial due to the absence of relevant data from the ASTRUM-007 trial (17). The utility values for PFS and PD states associated with advanced ESCC were 0.75 and 0.60, respectively, have been employed in multiple economic evaluations (13, 28, 29). Additionally, utility decrements caused by grade 3 or above treatment-related AEs were considered by multiplying the duration-adjusted disutilities by the incidence of AEs. The disutilities were also extracted from published studies (18–21). All utility-related parameters were shown in Table 1.

Subgroup and scenario and analyses

In subgroup analyses, we analyzed the cost-effectiveness of serplulimab plus chemotherapy in the first-line treatment for advanced ESCC patients with PD-L1 expression level of $1 \leq CPS < 10$, and with PD-L1 $CPS \geq 10$ through the methods of base-case analysis, respectively.

In scenario analyses, the shorter time horizons (2, 5 and 8 years) were used to investigate the impact on the model results. Furthermore, we explored the influence of various price-reduction levels for serplulimab on ICERs. At the same time, we assessed the probability of serplulimab plus chemotherapy being cost-effective by assuming a 70% price reduction of serplulimab, which was comparable to the prices of camrelizumab, sintilimab, tislelizumab and toripalimab.

Sensitivity analyses

One-way and probabilistic sensitivity analyses (PSA) were conducted for all key variables to estimate the robustness of our results. In the one-way sensitivity analyses, the plausible range of each parameter was either based on the reported 95%CI or calculated by assuming a 20% deviation from the base-case value. The range of discount rate was set as 0%-8% in line with China Guidelines for Pharmacoeconomic Evaluations (22). The results were presented in the form of tornado diagrams. For the PSA, 10,000 Monte Carlo simulations were generated by simultaneously sampling all parameters from the pre-specified statistical distributions. Gamma distributions were selected for cost inputs, and beta distributions were used for utility values and probabilities (30). The scatter plot and cost-effectiveness acceptability curves (CEAC) based on the results from 10,000 iterations were plotted to illustrate the probability of serplulimab plus chemotherapy would be considered cost-effective at various WTP thresholds.

Results

Base-case results

The base-case results were shown in Table 2. Compared with chemotherapy, patients received serplulimab plus chemotherapy yielded an additional 0.27 QALY at an incremental cost of $33,460.86. The ICER was $124,483.07 per QALY gained, which was significantly higher than the WTP threshold. When only focused on PFS period, serplulimab plus chemotherapy was associated with 0.19 greater QALYs compared to chemotherapy at an additional cost of $34,204.22, which had an ICER of $176,431.72 per QALY gained.

TABLE 2 Results of base-case analysis and subgroup analysis.

Parameters	All patients		Patients with 1 ≤ CPS < 10		Patients with CPS ≥ 10	
	C	S+C	C	S+C	C	S+C
OS						
Total cost ($)	4,999.71	38,460.57	4,578.46	34,941.82	5,415.47	50,871.24
QALYs	0.83	1.10	0.76	0.98	0.87	1.30
ICER ($/QALY)		124,483.07		134,637.42		105,589.71
Only PFS						
Total cost ($)	2,787.42	36,991.64	2,620.99	33,653.44	3,504.03	49,406.45
QALYs	0.38	0.57	0.36	0.52	0.48	0.77
ICER ($/QALY)		176,431.72		190,015.77		155,496.70

S+C, Serplulimab plus chemotherapy; C, chemotherapy; QALYs, quality-adjusted life years, ICER, incremental cost-effectiveness ratios.

Subgroup and scenario analyses results

In subgroup analyses, the ICERs of serplulimab plus chemotherapy versus chemotherapy were $134,637.42 and $105,589.71 per QALY gained in patients with PD-L1 expression level of 1 ≤ CPS < 10 and CPS ≥ 10, respectively (Table 2). When only focused on PFS period, serplulimab plus chemotherapy compared with chemotherapy resulted in the ICERs of $190,015.77 and $155,496.70 per QALY gained in patients with PD-L1 1 ≤ CPS < 10 and CPS ≥ 10, respectively.

In scenario analyses, as the time horizon lengthened, the ICERs of serplulimab plus chemotherapy gradually decreased, but were consistently higher than the WTP threshold (Supplementary Table S7). When the price of serplulimab was decreased by 66%, 69% and 61%, respectively, the ICERs of serplulimab plus chemotherapy versus chemotherapy were lower than the WTP thresholds for advanced ESCC patients with PD-L1-positive, PD-L1 1 ≤ CPS < 10 and CPS ≥ 10 (Figure 2).

Sensitivity analyses results

One-way sensitivity analyses demonstrated that the price of serplulimab, patient weight, utility of PFS and PD, and discount rate had the most significant impact on the base-case results (Figure 3). The ICERs were consistently higher than the WTP threshold with the alterations in all uncertainty parameters. Results of PSA were shown in Figure 4. According to the scatter plot, compared with chemotherapy, all scatter points were located in the North-East quadrant and above the WTP threshold. At the WTP threshold of 3 times per capita GDP in China, the CEAC revealed that a 0% probability of serplulimab plus chemotherapy being cost-effective in various groups (PD-L1-positive, PD-L1 1 ≤ CPS < 10 and CPS ≥ 10 patients) (Figure 5). When serplulimab was reduced to 30% of the current price ($264.65 per 100mg), the probabilities of serplulimab plus chemotherapy being cost-effective were 81.42%, 67.74% and 96.75% in advanced ESCC patients with PD-L1-positive, PD-L1 1≤CPS<10 and CPS≥10, respectively (Supplementary Figures S2, S3).

Discussion

To our knowledge, this is the first study to appraise the cost-effectiveness of serplulimab plus chemotherapy in the first-line treatment of patients with PD-L1-positive advanced ESCC from the Chinese healthcare system perspective. Compared with chemotherapy, serplulimab plus chemotherapy achieved additional 0.27, 0.23 and 0.43 QALYs with marginal $33,460.86, $30,363.35 and $45,455.77, which resulted in the ICERs of $124,483.07, $134,637.42 and $105,589.71 per QALY gained in advanced ESCC patients with PD-L1-positive, PD-L1 1 ≤ CPS < 10 and CPS ≥ 10, respectively. At the current prices and WTP threshold, serplulimab plus chemotherapy might not be cost-effective compared to chemotherapy. The base-case results were upheld by the subgroup, scenario and sensitivity analyses.

The price of serplulimab, patient weight, utility values and discount rate were the most influential parameters, but alterations in each parameter did not alter the conclusion. The price of serplulimab was extremely expensive compared to other domestic PD-1 inhibitors for the treatment of advanced ESCC patients, which became an essential parameter in dominating cost-effectiveness. Therefore, substantial price reductions or generous patient assistance programs would contribute to increased affordability of patients. Of note, when the price of serplulimab was reduced by 70%, the probability of serplulimab plus chemotherapy being cost-effective increased from 0% to 81.42%, 67.74% and 96.75%, respectively, in advanced ESCC patients with PD-L1-positive, PD-L1 1 ≤ CPS < 10 and CPS ≥ 10. When the price of serplulimab was decreased by 98%, 98% and 99%, respectively, serplulimab plus chemotherapy would be absolutely dominant regimens over chemotherapy (ICER < 0) for advanced ESCC patients with PD-L1-positive, PD-L1 1 ≤ CPS < 10 and CPS ≥ 10. The primary reason was that the higher proportion of patients in the chemotherapy group received second-line immunotherapy compared to the serplulimab plus chemotherapy group. Our results were consistent with previously published studies (13, 31) that patient weight was a significant parameter because serplulimab was administered based on body weight, revealing that serplulimab

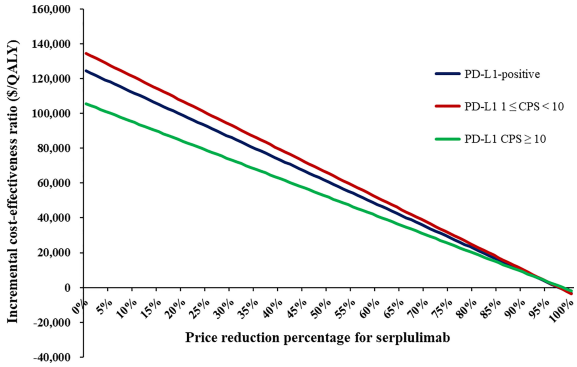


FIGURE 2
The impact of the price reduction of serplulimab on ICERs.

plus chemotherapy would be unfavorable in overweight or obese patients because of more dosages and expenditures required.

Serplulimab received its first approval on 25 March 2022 in China, and the economic evidence was relatively limited (9). Zhu et al. (32) estimated the cost-effectiveness of serplulimab plus chemotherapy as the first-line treatment for extensive-stage small-cell lung cancer (ES-SCLC) from a payer perspective in China based on the ASTRUM-005 trial (7). The results demonstrated that the probability of serplulimab plus chemotherapy being cost-effective was 91.6% compared with mono-chemotherapy at the WTP threshold of 3 times per capita GDP of China in 2021 (32). Another study by Shao et al. (33) showed that serplulimab might be a valuable and cost-effective regime as first-line therapy for ES-SCLC patients in both the United States and China. However, the advantage of cost-effectiveness has not been identified in PD-L1-positive advanced ESCC patients, which primarily attributed to better survival improvements of serplulimab plus chemotherapy in extensive-stage small-cell lung cancers.

PD-L1 expression was enriched in ESCC patients, ranging from 15%-83% in tumor cells and 13%-31% in immune cells, which greatly increased tumor susceptibility in patients receiving immune checkpoint inhibitors (34, 35). Prior economic evidences indicated that PD-1 inhibitors were potentially sensitive to PD-L1-positive ESCC patients, with higher survival benefits and health outcomes compared with the overall population (13, 16, 31, 36, 37). Whether overall or PD-L1-positive advanced ESCC patients, the probability of nivolumab or pembrolizumab plus chemotherapy being cost-effective were 0% compared with chemotherapy (13, 31, 36). Shao et al. demonstrated that the probability of sintilimab plus chemotherapy being cost-effective in PD-L1-positive advanced

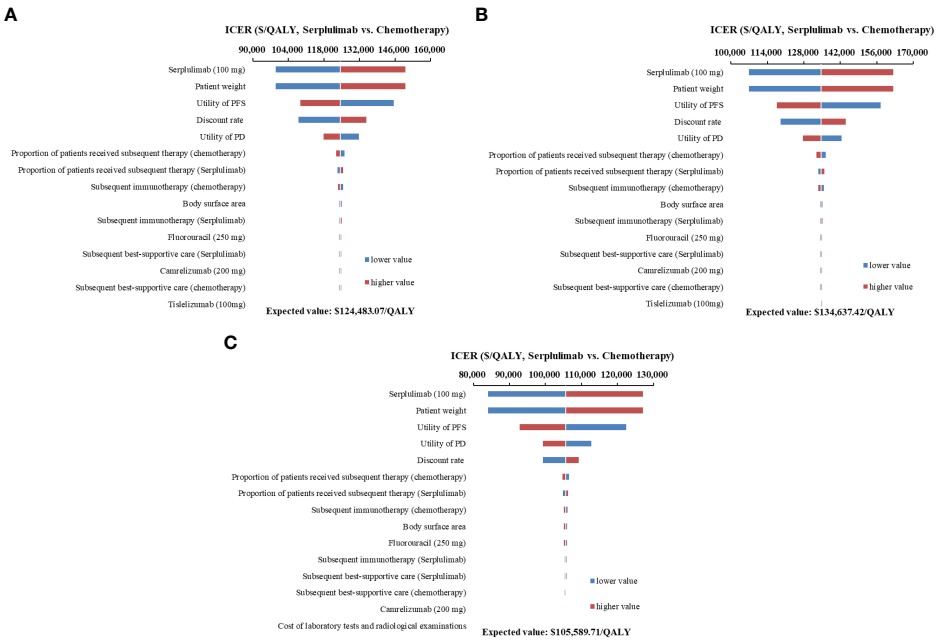


FIGURE 3
Tornado diagrams of one-way sensitivity analyses. **(A)** all PD-L1-positive advanced esophageal squamous cell carcinoma patients; **(B)** Patients with PD-L1 1 ≤ CPS < 10; **(C)** Patients with PD-L1 CPS ≥ 10) ICER, incremental cost-effectiveness ratios; PFS, progression-free survival; PD, progressive disease.

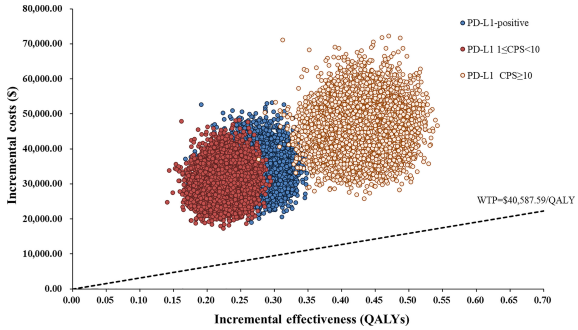


FIGURE 4
Scatter Plot of the ICER between serplulimab plus chemotherapy and chemotherapy. WTP, willingness-to-pay; QALY, quality-adjusted life years.

ESCC patients would be increased by 30% compared to PD-L1-negative patients (16). In this study, we found that higher PD-L1 expression levels were associated with better cost-effectiveness, indicating that patients with advanced ESCC should receive appropriate treatment regimens in accordance with PD-L1 expression levels in clinical management.

Currently, numerous studies are targeted on the economic evaluations of immunotherapies for advanced ESCC patients and warrant discussion. At the current price and WTP threshold, domestic PD-1 inhibitors, such as camrelizumab, sintilimab, tislelizumab and toripalimab, were cost-effective options as first- or second-line treatment for patients with advanced ESCC in China (18, 29, 38–40). The dynamic adjustment mechanism of the national medical insurance catalog has played a predominant role in this situation. Numerous anti-cancer innovative drugs have been substantially reduced in price by approximately 70%, which has greatly improved the accessibility and affordability for patients (41, 42). Intensive concern regarding the affordability of treatment regimens is currently shared by both patients and clinicians (32). Taking cost-effectiveness into considerations in clinical practice and healthcare decisions is crucial for clinicians and policy-makers to address the financial burdens of patients and allocate limited healthcare resources. Serplulimab has not yet successfully undergone national health insurance negotiations, but its significant clinical benefits have emerged as a potential treatment option for health systems and patients (10).

There were several limitations in this study. First, since the sample size of the ASTRUM-007 trial was relatively small and actual survival data were not available, we employed reconstructed and extrapolated individual patient data to construct the partitioned survival model. Further studies based on long-term efficacy data or large samples of real-world evidence would be needed to validate the results. Second, The utilities and disutilities in this analysis primarily derived from the published literature, because of the absence of quality-of-life data in the ASTRUM-007 trial. According to one-way sensitivity analyses, the health state utilities

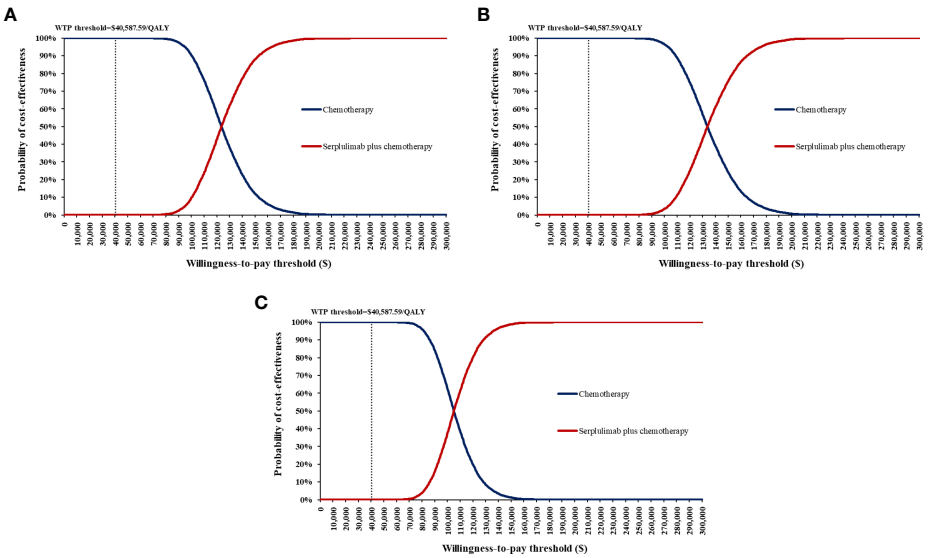


FIGURE 5
Cost-effectiveness acceptability curves for serplulimab plus chemotherapy versus chemotherapy. **(A)** all PD-L1-positive advanced esophageal squamous cell carcinoma patients; **(B)** Patients with PD-L1 1 ≤ CPS < 10; **(C)** Patients with PD-L1 CPS ≥ 10) WTP, willingness-to-pay.

did not influence on the conclusions. Third, subsequent strategies after the progression in the first-line treatment were based on the ASTRUM-007 trial, which might be inconsistent with the actual clinical practice situation. Forth, the costs and disutilities of grade 1-2 treatment-related serious AEs were excluded from this study, which might overestimate the cost-effectiveness of serplulimab plus chemotherapy, although one-way sensitivity analyses performed that only minimal impact on the model results. Fifth, other immunotherapies, such as camrelizumab, nivolumab, pembrolizumab, sintilimab and toripalimab, which had significant survival benefits for overall and PD-L1-positive advanced ESCC patients, were not included in this economic evaluation.

Conclusion

In summary, from the Chinese healthcare system perspective, serplulimab plus chemotherapy might not be considered cost-effective in the first-line treatment for PD-L1-positive advanced ESCC patients despite the extension of PFS and OS. Substantial price reductions could improve cost-effectiveness of serplulimab. When the prices of serplulimab were decreased by 66%, 69% and 61%, respectively, serplulimab plus chemotherapy would be cost-effective in advanced ESCC patients with PD-L1-positive, PD-L1 $1 \leq CPS < 10$ and $CPS \geq 10$.

Data availability statement

The original contributions presented in the study are included in the article/Supplementary Material. Further inquiries can be directed to the corresponding author.

Author contributions

SXL, NJ, and LD were responsible for study design, model building and statistical analysis. SXL and NJ prepared the manuscript. SPL and LD searched literatures and collected data. All authors critically reviewed the model structure, verified results and revised the manuscript. All authors contributed to the article and approved the submitted version.

Conflict of interest

The authors declare that the research was conducted in the absence of any commercial or financial relationships that could be construed as a potential conflict of interest.

Publisher's note

All claims expressed in this article are solely those of the authors and do not necessarily represent those of their affiliated organizations, or those of the publisher, the editors and the reviewers. Any product that may be evaluated in this article, or claim that may be made by its manufacturer, is not guaranteed or endorsed by the publisher.

Supplementary material

The Supplementary Material for this article can be found online at: https://www.frontiersin.org/articles/10.3389/fimmu.2023.1172242/full#supplementary-material

References

1. Zheng R, Zhang S, Zeng H, Wang S, Sun K, Chen R, et al. Cancer incidence and mortality in China, 2016. *J Natl Canc Cent* (2022) 2(1):1–9. doi: 10.1016/j.jncc.2022.02.002

2. Sung H, Ferlay J, Siegel RL, Laversanne M, Soerjomataram I, Jemal A, et al. Global cancer statistics 2020: globocan estimates of incidence and mortality worldwide for 36 cancers in 185 countries. *CA Cancer J Clin* (2021) 71(3):209–49. doi: 10.3322/caac.21660

3. Arnold M, Ferlay J, van Berge Henegouwen MI, Soerjomataram I. Global burden of oesophageal and gastric cancer by histology and subsite in 2018. *Gut* (2020) 69 (9):1564–71. doi: 10.1136/gutjnl-2020-321600

4. Muro K, Lordick F, Tsushima T, Pentheroudakis G, Baba E, Lu Z, et al. Pan-Asian adapted esmo clinical practice guidelines for the management of patients with metastatic oesophageal cancer: a jsmo-esmo initiative endorsed by csco, ksmo, mos, sso and tos. *Ann Oncol* (2019) 30(1):34–43. doi: 10.1093/annonc/mdy498

5. Ajani JA, D'Amico TA, Bentrem DJ, Chao J, Corvera C, Das P, et al. Esophageal and esophagogastric junction cancers, version 2.2019, nccn clinical practice guidelines in oncology. *J Natl Compr Canc Netw* (2019) 17(7):855–83. doi: 10.6004/jnccn.2019.0033

6. Li ZC, Sun YT, Lai MY, Zhou YX, Qiu MZ. Efficacy and safety of pd-1 inhibitors combined with chemotherapy as first-line therapy for advanced esophageal cancer: a systematic review and network meta-analysis. *Int Immunopharmacol* (2022) 109 (8):108790. doi: 10.1016/j.intimp.2022.108790

7. Cheng Y, Han L, Wu L, Chen J, Sun H, Wen G, et al. Effect of first-line serplulimab vs placebo added to chemotherapy on survival in patients with extensive-stage small cell lung cancer: the astrum-005 randomized clinical trial. *Jama* (2022) 328 (12):1223–32. doi: 10.1001/jama.2022.16464

8. Qin S, Li J, Zhong H, Jin C, Chen L, Yuan X, et al. Serplulimab, a novel anti-Pd-1 antibody, in patients with microsatellite instability-high solid tumours: an open-label, single-arm, multicentre, phase ii trial. *Br J Cancer* (2022) 127(12):2241–8. doi: 10.1038/s41416-022-02001-3

9. Lee A. Serplulimab: first approval. *Drugs* (2022) 82(10):1137–41. doi: 10.1007/s40265-022-01740-0

10. Song Y, Zhang B, Xin D, Kou X, Tan Z, Zhang S, et al. First-line serplulimab or placebo plus chemotherapy in pd-L1-Positive esophageal squamous cell carcinoma: a randomized, double-blind phase 3 trial. *Nat Med* (2023) 29(2):473–82. doi: 10.1038/s41591-022-02179-2

11. Husereau D, Drummond M, Augustovski F, de Bekker-Grob E, Briggs AH, Carswell C, et al. Consolidated health economic evaluation reporting standards 2022 (Cheers 2022) statement: updated reporting guidance for health economic evaluations. *Value Health* (2022) 25(1):3–9. doi: 10.1016/j.jval.2021.11.1351

12. Yao ZH. *The big data service platform for china's health industry: information query of drug bid winning* (2023). Available at: https://data.yaozh.com/.

13. Liu S, Dou L, Wang K, Shi Z, Wang R, Zhu X, et al. Cost-effectiveness analysis of nivolumab combination therapy in the first-line treatment for advanced esophageal squamous-cell carcinoma. *Front Oncol* (2022) 12:899966. doi: 10.3389/fonc.2022.899966

14. Shen J, Du Y, Shao R, Jiang R. First-line sintilimab plus chemotherapy in locally advanced or metastatic esophageal squamous cell carcinoma: a cost-effectiveness analysis from China. *Front Pharmacol* (2022) 13:967182. doi: 10.3389/fphar.2022.967182

15. Zhan M, Xu T, Zheng H, He Z. Cost-effectiveness analysis of pembrolizumab in patients with advanced esophageal cancer based on the keynote-181 study. *Front Public Health* (2022) 10:790225. doi: 10.3389/fpubh.2022.790225

16. Shao T, Zhao M, Tang W. Cost-effectiveness analysis of sintilimab vs. placebo in combination with chemotherapy as first-line therapy for local advanced or metastatic oesophageal squamous cell carcinoma. *Front Oncol* (2022) 12:953671. doi: 10.3389/fonc.2022.953671

17. Wilke H, Muro K, Van Cutsem E, Oh SC, Bodoky G, Shimada Y, et al. Ramucirumab plus paclitaxel versus placebo plus paclitaxel in patients with previously treated advanced gastric or gastro-oesophageal junction adenocarcinoma (Rainbow): a double-blind, randomised phase 3 trial. *Lancet Oncol* (2014) 15(11):1224–35. doi: 10.1016/s1470-2045(14)70420-6

18. Cai H, Xu B, Li N, Zheng B, Zheng Z, Liu M. Cost-effectiveness analysis of camrelizumab versus chemotherapy as second-line treatment of advanced or metastatic esophageal squamous cell carcinoma. *Front Pharmacol* (2021) 12:732912. doi: 10.3389/fphar.2021.732912

19. Nafees B, Lloyd AJ, Dewilde S, Rajan N, Lorenzo M. Health state utilities in non-small cell lung cancer: an international study. *Asia Pac J Clin Oncol* (2017) 13(5):e195–203. doi: 10.1111/ajco.12477

20. Tolley K, Goad C, Yi Y, Maroudas P, Haiderali A, Thompson G. Utility elicitation study in the uk general public for late-stage chronic lymphocytic leukaemia. *Eur J Health Econ* (2013) 14(5):749–59. doi: 10.1007/s10198-012-0419-2

21. Wang L, Hong H, Alexander GC, Brawley OW, Paller CJ, Ballreich J. Cost-effectiveness of systemic treatments for metastatic castration-sensitive prostate cancer: an economic evaluation based on network meta-analysis. *Value Health* (2022) 25 (5):796–802. doi: 10.1016/j.jval.2021.10.016

22. Liu G, Hu S, Wu J, Wu J. *China Guidelines for pharmacoeconomic evaluations (2020)*. Beijing: China Market Press (2020).

23. Gye A, Goodall S, De Abreu Lourenco R. Cost-effectiveness analysis of tisagenlecleucel versus blinatumomab in children and young adults with acute lymphoblastic leukemia: partitioned survival model to assess the impact of an outcome-based payment arrangement. *Pharmacoeconomics* (2023) 41(2):175–86. doi: 10.1007/s40273-022-01188-w

24. Marseille E, Larson B, Kazi DS, Kahn JG, Rosen S. Thresholds for the cost-effectiveness of interventions: alternative approaches. *Bull World Health Organ* (2015) 93(2):118–24. doi: 10.2471/blt.14.138206

25. Guyot P, Ades AE, Ouwens MJ, Welton NJ. Enhanced secondary analysis of survival data: reconstructing the data from published Kaplan-Meier survival curves. *BMC Med Res Methodol* (2012) 12(1):9. doi: 10.1186/1471-2288-12-9

26. Latimer NR. Survival analysis for economic evaluations alongside clinical trials–extrapolation with patient-level data: inconsistencies, limitations, and a practical guide. *Med Decis Making* (2013) 33(6):743–54. doi: 10.1177/0272989x12472398

27. CSCO. *Guidelines of Chinese society of clinical Oncologhy(Csco) esophageal cancer*. Beijing: People's Medical Publishing House (2022).

28. Yang F, Fu Y, Kumar A, Chen M, Si L, Rojanasarot S. Cost-effectiveness analysis of camrelizumab in the second-line treatment for advanced or metastatic esophageal squamous cell carcinoma in China. *Ann Transl Med* (2021) 9(15):1226. doi: 10.21037/atm-21-1803

29. Liu S, Dou L, Li S. Cost-effectiveness analysis of pd-1 inhibitors combined with chemotherapy as first-line therapy for advanced esophageal squamous-cell carcinoma in China. *Front Pharmacol* (2023) 14:1055727. doi: 10.3389/fphar.2023.1055727

30. Briggs AH, Weinstein MC, Fenwick EA, Karnon J, Sculpher MJ, Paltiel AD. Model parameter estimation and uncertainty analysis: a report of the ispor-smdm modeling good research practices task force working group-6. *Med Decis Making* (2012) 32(5):722–32. doi: 10.1177/0272989x12458348

31. Cao X, Cai H, Li N, Zheng B, Zheng Z, Liu M. First-line nivolumab plus ipilimumab or chemotherapy versus chemotherapy alone for advanced esophageal cancer: a cost-effectiveness analysis. *Ther Adv Med Oncol* (2022) 14:17588359221122733. doi: 10.1177/17588359221122733

32. Zhu Y, Liu K, Qin Q, Zhu H. Serplulimab plus chemotherapy as first-line treatment for extensive-stage small-cell lung cancer: a cost-effectiveness analysis. *Front Immunol* (2022) 13:1044678. doi: 10.3389/fimmu.2022.1044678

33. Shao T, Zhao M, Liang L, Tang W. Serplulimab plus chemotherapy vs chemotherapy for treatment of us and Chinese patients with extensive-stage small-cell lung cancer: a cost-effectiveness analysis to inform drug pricing. *BioDrugs* (2023). doi: 10.1007/s40259-023-00586-6

34. Kato K, Cho BC, Takahashi M, Okada M, Lin CY, Chin K, et al. Nivolumab versus chemotherapy in patients with advanced oesophageal squamous cell carcinoma refractory or intolerant to previous chemotherapy (Attraction-3): a multicentre, randomised, open-label, phase 3 trial. *Lancet Oncol* (2019) 20(11):1506–17. doi: 10.1016/s1470-2045(19)30626-6

35. Topalian SL, Taube JM, Anders RA, Pardoll DM. Mechanism-driven biomarkers to guide immune checkpoint blockade in cancer therapy. *Nat Rev Cancer* (2016) 16(5):275–87. doi: 10.1038/nrc.2016.36

36. Zhu Y, Liu K, Ding D, Zhou Y, Peng L. Pembrolizumab plus chemotherapy as first-line treatment for advanced esophageal cancer: a cost-effectiveness analysis. *Adv Ther* (2022) 39(6):2614–29. doi: 10.1007/s12325-022-02101-9

37. Ye ZM, Xu Z, Zeng FY, Tang ZQ, Zhou Q. Cost-effectiveness analysis of sintilimab combined with chemotherapy versus chemotherapy alone as the first-line treatment for advanced esophageal cancer. *Front Pharmacol* (2022) 13:934275. doi: 10.3389/fphar.2022.934275

38. Liu L, Wang L, Chen L, Ding Y, Zhang Q, Shu Y. Cost-effectiveness of sintilimab plus chemotherapy versus chemotherapy alone as first-line treatment of locally advanced or metastatic oesophageal squamous cell carcinoma. *Front Immunol* (2023) 14:1092385. doi: 10.3389/fimmu.2023.1092385

39. Fang R, Wang S, Liu Y, Xu J. Cost-effectiveness analysis of toripalimab plus paclitaxel and cisplatin as first-line treatment for advanced or metastatic esophageal squamous cell carcinoma. *Adv Ther* (2023) 40(3):1019–30. doi: 10.1007/s12325-022-02402-z

40. Shi F, He Z, Su H, Wang L, Han S. Economic evaluation of tislelizumab versus chemotherapy as second-line treatment for advanced or metastatic esophageal squamous cell carcinoma in China. *Front Pharmacol* (2022) 13:961347. doi: 10.3389/fphar.2022.961347

41. Zhang Y, Wei Y, Li H, Chen Y, Guo Y, Han S, et al. Prices and clinical benefit of national price-negotiated anticancer medicines in China. *Pharmacoeconomics* (2022) 40(7):715–24. doi: 10.1007/s40273-022-01161-7

42. Zhang Y, Wushouer H, Han S, Fu M, Guan X, Shi L, et al. The impacts of government reimbursement negotiation on targeted anticancer medication price, volume and spending in China. *BMJ Glob Health* (2021) 6(7):e006196. doi: 10.1136/bmjgh-2021-006196

frontiers | Frontiers in Oncology

TYPE Original Research
PUBLISHED 12 May 2023
DOI 10.3389/fonc.2023.1162360

Check for updates

OPEN ACCESS

EDITED BY
Shariq Qayyum,
Harvard Medical School, United States

REVIEWED BY
Suhail Muzaffar,
University of Alabama at Birmingham, United States
Mohd Saad Umar,
Aligarh Muslim University, India

*CORRESPONDENCE
Lingyuan Chen
lingyuanchen@outlook.com

†These authors have contributed equally to this work

RECEIVED 09 February 2023
ACCEPTED 02 May 2023
PUBLISHED 12 May 2023

CITATION
Shi D, Li Y, Liang X and Chen L (2023) Cost-effectiveness of sacituzumab govitecan in hormone receptor-positive/human epidermal growth factor receptor 2-negative metastatic breast cancer. *Front. Oncol.* 13:1162360. doi: 10.3389/fonc.2023.1162360

COPYRIGHT
© 2023 Shi, Li, Liang and Chen. This is an open-access article distributed under the terms of the Creative Commons Attribution License (CC BY). The use, distribution or reproduction in other forums is permitted, provided the original author(s) and the copyright owner(s) are credited and that the original publication in this journal is cited, in accordance with accepted academic practice. No use, distribution or reproduction is permitted which does not comply with these terms.

Cost-effectiveness of sacituzumab govitecan in hormone receptor-positive/human epidermal growth factor receptor 2-negative metastatic breast cancer

Demin Shi[1†], Yan Li[2†], Xueyan Liang[2] and Lingyuan Chen[3*]

[1]Department of Reproductive Medicine, The People's Hospital of Hechi, Hechi, Guangxi, China, [2]Department of Pharmacy, Guangxi Academy of Medical Sciences and the People's Hospital of Guangxi Zhuang Autonomous Region, Nanning, Guangxi, China, [3]Department of Pharmacy, The People's Hospital of Hechi, Hechi, Guangxi, China

Background: The efficiency and safety of sacituzumab govitecan (SG) for the therapy of hormone receptor-positive (HR+)/human epidermal receptor 2-negative (HER2-) metastatic breast cancer (BC) has been demonstrated. The aim of this study is to evaluate its cost-effectiveness on HR+/HER2- metastatic BC from the third-party payer perspective in the United States.

Methods: We performed the cost-effectiveness of SG and chemotherapy using a partitioned survival model. TROPiCS-02 provided clinical patients for this study. We evaluated the robustness of this study by one-way and probabilistic sensitivity analyses. Subgroup analyses were also conducted. The outcomes were costs, life-years, quality-adjusted life years (QALYs), incremental cost-effectiveness ratio (ICER), incremental net health benefit (INHB), and incremental net monetary benefit (INMB).

Results: SG treatment was related to an increase of 0.284 life years and 0.217 QALYs over chemotherapy, as well as a cost increase of $132,689, reaching an ICER of $612,772/QALY. The INHB was -0.668 QALYs, and the INMB was -$100,208. SG was not cost-effective at the willingness to pay (WTP) threshold of $150,000/QALY. The outcomes were sensitive to patient body weight and cost of SG. SG may be cost-effective at the WTP threshold of $150,000/QALY if the price is less than $3.997/mg or the weight of patients is under 19.88 kg. Based on the subgroup analysis, SG did not prove cost-effective in all subgroups at the WTP threshold of $150,000/QALY.

Conclusion: From a third-party payer standpoint in the United States, SG was not cost-effective, even though it had a clinically significant advantage over chemotherapy for the treatment of HR+/HER2- metastatic BC. The cost-effectiveness of SG can be improved if the price is substantially reduced.

KEYWORDS

cost-effectiveness, sacituzumab govitecan, breast cancer, hormone receptor-positive, human epidermal receptor 2-negative, partitioned survival model

Introduction

Globally, breast cancer (BC) surpass lung cancer as the most common malignancy diagnosed in 2020, with 2.3 million new cases (1). BC is common cancer in women (24%) and is the leading cause of cancer-related deaths (15%) worldwide (1). The diagnosis of BC was made in approximately 42% of women in the Asia-Pacific region and 47% in Southeastern Asia, as well as 20% of women in Western countries (2, 3). Molecular subtypes of BC have been defined according to the status of hormone receptors (HR), such as estrogen receptor (ER) and progesterone receptor (PR) and human epidermal growth factor 2 (HER2) (4). Approximately 70% of cases of BC are classified as luminal, a molecular subtype characterized by HR-positive (HR+) and HER2-negative (HER2-). Endocrine therapy (ET), which covers aromatase inhibitors (AIs), selective ER modulators (SERMs), and selective ER down-regulators (SERDs), forms the foundation for the effective treatment of BC (5–8). In the absence of ET resistance, either primary or secondary, subsequent treatment options are limited; there are only a few therapy options available for premenopausal women with HR +/HER2- metastatic BC, and these are mostly derived from trials in which postmenopausal patients were enrolled (9). By combining endocrine therapy with CDK4/6 inhibitors (CDK4/6i), overall survival (OS) for HR+/HER2- metastatic BC can be improved by approximately five years (10–13). In subsequent treatment lines, combination therapy with phosphoinositide 3-kinase inhibitors or mammalian target of rapamycin inhibitors has been shown to be beneficial (8). It is inevitable, however, that endocrine resistance will develop over time. The next therapeutic option is sequential single-agent chemotherapy, but it has declining response rates, diminished disease control, and related to high risk of side effects (8, 14–17).

Sacituzumab govitecan (SG) is a first-in-class antibody-drug conjugate directed at trophoblast cell-surface antigen 2 (Trop-2) consisting of a humanized polyclonal antibody conjugated to the active metabolite SN-38 (18), by a hydrolysable CL2A linker (19, 20). In solid tumors, particularly HR+/HER2- and triple-negative breast cancers (suffering from a prevalence of > 90%), Trop-2 is a transmembrane calcium signal transducer that is associated with tumor progression and prognosis (21, 22). In tumor microenvironments, SN-38 is a membrane-permeable free molecule that may exert antitumor effects on tissues adjacent to those that do not express Trop-2 (bystander effect) (23). As SG was shown to be clinical beneficial and safety in patients with HR +/HER2- metastatic BC who had progressed after completing endocrine therapy and prior chemotherapy in the metastatic setting, the results were encouraging (24, 25). There was, however, a significant increase in the cost of SG treatment, which may limit its availability in some countries (26). SG has not yet been evaluated on an economic basis for its use in treating HR+/HER2- metastatic BC. It is essential for clinicians and policy-makers to consider cost-effectiveness when making healthcare decisions. Herein, cost-effectiveness analysis of SG in comparison with single-agent chemotherapy for HR+/HER2- metastatic BC was conducted from the perspective of third-party payers in the United States.

Methods

Analytical overview

This analysis was conducted on hypothetical patients who had locally recurrent, metastatic HR+/HER2- BC that was endocrine-resistant and treated with chemotherapy, included HR+/HER2- metastatic BC patients from the TROPiCS-02 trial (25). The economic evaluation used a partitioned survival model with three health states to determine whether to use SG or single-agent chemotherapy for the initial treatment decision (27–30). Progression-free survival (PFS), progressed disease (PD), and death are mutually exclusive health states. The area under the OS curve was used to estimate the proportion of patients alive at cycle t (1-week cycle), and the area under the PFS curve was used to estimate the proportion of patients alive with PFS. Based on the difference between the OS and PFS curves, the proportion of patients alive and suffering from PD was estimated. The patients and PFS and OS curve were derived from the TROPiCS-02 trial (25), whose results were validated by comparing modeled PFS and OS to real data. We performed this study following the reporting guideline of Consolidated Health Economic Evaluation Reporting Standards (CHEERS) (31). In view of the fact that this study used a review of publicly available data and modeling techniques, it will not require an institutional review board review or informed consent.

Clinical data inputs

TROPiCS-02 results were obtained to construct PFS and OS for patients in the SG and chemotherapy groups (24) and the data have been extrapolated beyond the follow up time of the model using the statistical methods described by Guyot et al (32). To collect the time-to-survival data points from the PFS and OS curves, we utilized the GetData Graph Digitizer, version 2.26 (33), and the following parametric survival functions were then fitted to these data points: exponential, Weibull, gamma, lognormal, Gompertz, Log-logistic and Generalized gamma models. It was determined that the eligible survival function had the lowest Akaike information criterion and Bayesian information criterion values. SG treatment and chemotherapy treatment final survival functions are illustrated in Table 1, as well as goodness-of-fit results were shown in Supplementary Table 1. PFS and OS proportions were calculated based on the appropriate survival distribution. Model validations are shown in Supplementary Figure 1. A digitized Kaplan-Meier curve was closely reproduced in the virtual patient-level data, which included event and censoring times.

Cost and utility inputs

In this study, we evaluated the costs related to direct medical costs, covering the costs of drugs, the costs associated with terminal care, the costs related to the management of patients, and the costs related to adverse events (AEs) (Table 1). The costs are reported in

TABLE 1 Basic parameters input to the model and the ranges of the sensitivity analyses.

Parameter	Value (95% CI)	Distribution	Source
Clinical input			
Survival model for sacituzumab govitecan			
Log-logistic model for OS[a]	$\gamma = 1.9025$; $\lambda = 0.0162$	ND	(25)
Log-normal model for PFS[a]	$\mu = 3.1013$; $\sigma = 1.0541$	ND	(25)
Survival model for chemotherapy			
Log-logistic model for OS[a]	$\gamma = 1.9082$; $\lambda = 0.0188$	ND	(25)
Log-normal model for PFS[a]	$\mu = 2.7297$; $\sigma = 0.9475$	ND	(25)
Cost input			
Drug costs per 1 mg			
Sacituzumab govitecan	14.88 (11.91 to 17.86)	Gamma	(34)
Eribulin	1266 (1013 to 1520)	Gamma	(35)
Vinorelbine	0.925 (0.740 to 1.110)	Gamma	(35)
Gemcitabine	0.018 (0.014 to 0.021)	Gamma	(35)
Capecitabine	0.004 (0.003 to 0.005)	Gamma	(35)
Cost of terminal care per patient[b]	21,501 (17,201 to 25,801)	Gamma	(36)
Disease management and monitoring costs			
CT scan of chest (per time)	133 (58 to 254)	Gamma	(37)
Best supportive care (per cycle)	472 (377 to 566)	Gamma	(38)
Cost of managing AEs (grade ≥ 3)[c]			
Sacituzumab govitecan	7,309 (5,847 to 8,770)	Gamma	(39–41)
Chemotherapy	5,287 (4,230 to 6,344)	Gamma	(39–41)
Administration cost			
First hour	159 (130 to 206)	Gamma	(37)
Additional hour	34 (28 to 42)	Gamma	(37)
Health utilities			
Disease status utility per year			
PFS	0.830 (0.664 to 0.935)	Beta	(39, 42)
PD	0.443 (0.354 to 0.532)	Beta	(39, 43)
Death	0	NA	
Disutility due to AEs[d]			
Sacituzumab govitecan	0.037 (0.03 to 0.044)	Beta	(39–41)
Chemotherapy	0.023 (0.018 to 0.027)	Beta	(39–41)
Other inputs			
Body surface area, m^2	1.82 (1.44 to 2.16)	Normal	(44)
Body weight, kg	74 (59 to 90)	Normal	(44)

AE, adverse event; NA, not applicable; ND, not determined; OS, overall survival; PD, progressed disease; PFS, progression-free survival.
[a]Only expected values are presented for these survival model parameters.
[b]Overall total cost per patient regardless of treatment duration.
[c]Calculated as the average cost of toxic effects using weighted frequencies of grade ≥ 3 treatment related adverse events for each treatment arm in the TROPiCS-02 trial. Costs of individual toxic effects were derived from the literature and include all care required to manage each toxic effect. References for individual toxic effect costs are summarized in Table 2 in the Supplement.
[d]Calculated as the average disutility of toxic effects using weighted frequencies of grade ≥ 3 treatment-related adverse events for each treatment arm in the TROPiCS-02 trial. Disutilities of individual toxic effects were derived from the literature. References for individual toxic effect disutilities are summarized in Table 2 in the Supplement.

2023 United States dollars and other costs have been inflated using Tom's Inflation Calculator's Medical Care Inflation set (45).

In the TROPiCS-02 trial report (25), patients received SG 10 mg/kg body weight intravenously on days 1 and 8 of every 21 days. The treatment was continued until the disease progressed or the side effects became unacceptable. It is expected that patients assigned to the chemotherapy group received treatment according to locally approved prescribing information or according to National Comprehensive Cancer Network Clinical Practice Guidelines in Oncology (46). Recommended chemotherapy regimens dosage of TROPiCS-02 are following: eribulin, 1.4 mg/m^2 for North American or 1.23 mg/m^2 for European; vinorelbine, 25 mg/m^2; gemcitabine, 200 mg/m^2; and capecitabine 1,000-1,250 mg/m^2 (24).

The prices of SG, eribulin, vinorelbine, gemcitabine and capecitabine were collected from public databases (34, 35). The cost of terminal care was $21,501 per patient with metastatic BC (36). The cost of the CT scans was obtained from the Medicare Clinical Laboratory Fee Schedule (37). The costs of the best supportive care were $472 per cycle (38). This study included the costs of managing grade ≥ 3 AEs, which were obtained from the published literature (Supplementary Table 2) (39–41). To calculate the dosage of SG, eribulin, vinorelbine, gemcitabine and capecitabine, we assumed that the body weight and body surface area of a typical patient in the United States were 74 kg and 1.82 m^2 (44).

Health states were rated on a scale of 0 to 1 according to their utility preference in terms of health. Considering TROPiCS-02 was not provided the results of utility, the utility of metastatic BC was obtained from previously published studies and the PFS and PD states related to metastatic BC were 0.830 and 0.443 respectively (39, 42, 43). The analysis evaluated the disutility values related to grade ≥ 3 AEs (39–41).

Base-case analysis

We calculated the incremental cost-effectiveness ratio (ICER) by comparing the incremental cost per quality-adjusted life year (QALY) gained between the SG group and the chemotherapy group. According to the recommendation, cost-effectiveness was assumed when the ICER was lower than the optional willingness to pay (WTP) threshold ($150,000 per additional QALY gained) (47). Costs and utilities were discounted at an annual rate of 3% (48). We calculated the incremental net health benefit (INHB) and incremental monetary benefit (INMB) using the following formulas: $\mathbf{INHB}(\boldsymbol{\lambda}) = (\mu E_{SG} - \mu E_c) - \frac{\mu C_{SG} - \mu C_C}{\boldsymbol{\lambda}} = \Delta E - \Delta C/\boldsymbol{\lambda}$ and $\mathbf{INMB}(\boldsymbol{\lambda}) = (\mu E_{SG} - \mu E_c) \times \boldsymbol{\lambda} - (\mu C_{SG} - \mu C_C) = \Delta E \times \boldsymbol{\lambda} - \Delta C$, where μC_{SG}, μC_C, and μE_{SG}, μE_C were the cost and QALY of SG or chemotherapy, respectively, and λ was the WTP threshold (49, 50).

Sensitivity and subgroup analyses

Based on the one-way sensitivity analysis and the probabilistic sensitivity analysis, we evaluated the robustness of the model results. Each parameter was subjected to a one-way sensitivity analysis; estimated ranges were based on the reported or estimated 95% confidence intervals in the referenced studies or assumed to change 25% from the base-case value (Table 1). In order to generate a probabilistic sensitivity analysis, the key model variables were simultaneously sampled from prespecified distributions in a Monte Carlo simulation with 10,000 iterations. A gamma distribution was used for the cost variables, and a beta distribution for was used probability and proportion. To calculate the likelihood that SG would consider being cost-effective at different WTP levels, a cost-effectiveness acceptability curve was constructed based on data from 10,000 iterations. Subgroup analyses were conducted by varying the HRs for PFS for the prespecified subgroups reported in TROPiCS-02 in order to investigate the uncertainty arising from the subpopulations. We conducted our statistical analyses in R, version 4.0.5, 2021 (R Foundation for Statistical Computing) using the hesim and heemod packages.

Results

Base-case analysis

By comparison with chemotherapy treatment, SG treatment increased QALYs by 0.217 and overall life-years by 0.284, at an incremental cost of $132,689, which corresponds to a QALY ICER of $612,772. The INHB was -0.668 QALYs, and the INMB was -$100,208 at a WTP threshold of $150,000/QALY (Table 2).

Sensitivity analysis

One-way sensitivity analyses suggested that the HRs for OS, average body weight, HRs for PFS and the costs of SG were related to model results (Supplementary Figure 2). We also estimated the relationship between these key variables and the ICER in the comparison of SG and chemotherapy. When the price of SG was less than $2.821/mg or $3.997/mg, SG was cost-effective at a WTP threshold of $100,000/QALY or $150,000/QALY, respectively (Supplementary Figure 3). On the other hand, when the body weight of patients was less than 19.88 kg, SG was cost-effective at a WTP threshold of $150,000/QALY (Supplementary Figure 3).

The cost-effectiveness acceptability curve was calculated and displayed as a result of the probabilistic sensitivity analysis (Figure 1). When the WTP thresholds are raised, the probability of SG being cost-effective increases. In comparison with chemotherapy, SG had no probability of being considered cost-effective at a WTP threshold of $150,000/QALY.

Subgroup analysis

By varying the HRs for PFS, the subgroup analyses suggested that SG was related to primarily negative INHBs and was not considered cost-effective at a WTP threshold of $150,000/QALY for all subgroups (Table 3).

TABLE 2 Summary of cost and outcome results in the base-case analysis.

Factor	Sacituzumab govitecan	Chemotherapy	Incremental change
Cost, $			
Drug[a]	139,829	13,267	126,562
Nondrug[b]	57,552	51,425	6,127
Overall	197,381	64,692	132,689
Life-years			
Progression-free	0.737	0.451	0.286
Overall	1.766	1.482	0.284
QALYs			
Progression-free	0.592	0.368	0.224
Overall	1.016	0.799	0.217
ICERs, $			
Per life-year	NA	NA	467,013
Per QALY	NA	NA	612,772
INHB, QALY, at WTP threshold 150,000[a]	NA	NA	-0.668
INMB, $, at WTP threshold 150,000[a]	NA	NA	-100,208

ICER, incremental cost-effectiveness ratio; INHB, incremental net health benefit; INMB, incremental net monetary benefit; NA, not applicable; QALYs, quality-adjusted life years.
[a]Compared with chemotherapy.
[b]Nondrug cost includes the costs of adverse event management, subsequent best supportive care per patient, and follow-up care covering physician monitors, drug administration, and terminal care.

Discussion

It is the purpose of this study to satisfy the unmet require for an economic evaluation of SG for the therapy of HR+/HER2- metastatic BC. As a result of this study, it was found that SG was related to an incremental survival of 0.217 QALYs and an incremental cost of $132,689, resulting in ICER of $612,772/QALY, as compared with chemotherapy. The model results were most sensitive to the HRs for OS, average body weight, HRs for PFS, and costs of SG, according to one-way sensitivity analysis. This suggests that the cost-effectiveness of SG can be determined based on these factors compared with chemotherapy. The cost-effectiveness of SG was demonstrated at a WTP threshold of $150,000/QALY when the price of SG was less than $3.997/mg or the weight of patients was less than 19.88 kg. In accordance with one-way sensitivity analysis and probabilistic sensitivity analysis, the results of this model appear to be robust. We found that SG was unfavorable for WTP thresholds less than $612,772/QALY for treatment of HR+/HER2- metastatic BC. Since SG treatment was related to negative INHBs and did not have a probability of cost-effectiveness when compared to chemotherapy at a threshold of $150,000/QALY in all subgroups compared to chemotherapy.

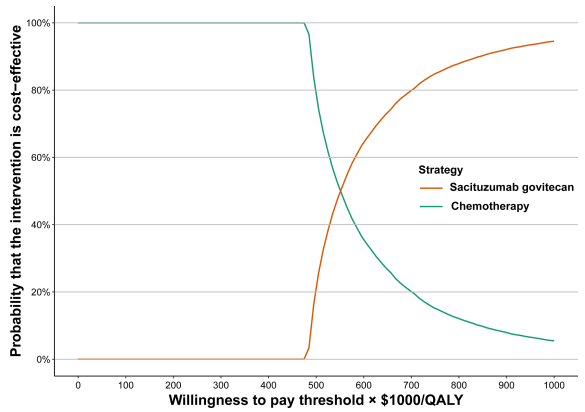


FIGURE 1
Acceptability curves for the choice of sacituzumab govitecan treatment strategies at different WTP thresholds in patients with hormone receptor-positive/human epidermal growth factor receptor 2-negative metastatic breast cancer. WTP, willingness to pay.

Based on the results of the one-way sensitivity analysis, it was suggested that the HR for OS and PFS was the sensitive variable. There was superior clinical efficacy for SG among patients with a favorable prognosis, but no subgroup analysis revealed that SG achieved cost-effectiveness. Thus, the price of SG remains the most sensitive variable and reducing the price of SG was important to increase the feasibility of using SG. In the US, the government announced American Patients First, and aimed to blueprint for cutting drug prices and reducing out-of-pocket payments (51). The availability of innovative treatments requires a significant reduction in price or financial assistance. Because antibody-drug conjugates are expensive to develop, their prices are often high (26, 52, 53). Therefore, it is common to observe that antibody-drug conjugates are not cost-effective, as described in the published literature (54, 55).

TABLE 3 Summary of subgroup analyses obtained by varying the hazard ratios (HRs) for PFS.

Subgroup	Unstratified hazard ratio (95% CI)	Change in cost, $[a]	Change in QALYs[a]	ICER, $/QALY	INHB, QALY, at WTP threshold 150,000
Visceral metastasis					
Yes	0.66 (0.53 to 0.83)	132,689	0.217	612,772	-0.668
No	0.78 (0.25 to 2.40)	131,978	0.182	724,906	-0.698
Endocrine therapy in the metastatic setting ≥ 6 months					
Yes	0.61 (0.48 to 0.78)	133,024	0.230	578,048	-0.657
No	1.13 (0.61 to 2.07)	130,329	0.067	1,938,885	-0.802
Age, years					
<65	0.69 (0.53 to 0.89)	132,500	0.208	636,506	-0.675
≥ 65	0.59 (0.38 to 0.93)	133,167	0.235	565,617	-0.652
Race					
White	0.66 (0.51 to 0.86)	132,689	0.217	612,772	-0.668
Non-white	1.23 (0.55 to 2.75)	129,922	0.031	4,172,372	-0.835
Baseline ECOG performance status scale score					
0	0.61 (0.44 to 0.86)	133,024	0.230	578,048	-0.657
1	0.70 (0.53 to 0.94)	132,439	0.205	644,971	-0.678
Geographic region					
North America	0.72 (0.51 to 1.02)	132,319	0.200	662,817	-0.682
Europe	0.62 (0.46 to 0.82)	132,955	0.227	584,559	-0.659
Prior CDK inhibitor duration					
≤ 12 months	0.59 (0.44 to 0.78)	133,167	0.235	565,617	-0.652
> 12 months	0.77 (0.54 to 1.10)	132,033	0.185	713,553	-0.695
Investigator choice of chemotherapy					
Eribulin	0.71 (0.55 to 0.93)	116,558	0.202	575,610	-0.575
Capecitabine	0.91 (0.53 to 1.57)	144,849	0.142	1,021,786	-0.824
Gemcitabine	0.83 (0.54 to 1.28)	144,964	0.167	868,473	-0.800
Vinorelbine	0.32 (0.22 to 0.47)	144,238	0.301	479,550	-0.661
Early relapse					
Yes	0.10 (0.04 to 0.28)	140,665	0.349	403,091	-0.589
No	0.72 (0.57 to 0.91)	132,319	0.200	662,817	-0.682
No. of prior chemotherapy in metastatic setting					
≤ 2	0.62 (0.45 to 0.85)	132,955	0.227	584,559	-0.659
≥ 3	0.70 (0.52 to 0.95)	132,439	0.205	644,971	-0.678

CDK, cyclin-dependent kinase; ECOG, Eastern Cooperative Oncology Group; HR, hazard ratio; ICER, incremental cost-effectiveness ratio; INHB, incremental net health benefits; PFS, progression-free survival; QALY, quality-adjusted life year; WTP, willingness to pay.
[a]HR for PFS represents the HR of sacituzumab govitecan vs. chemotherapy for PFS; change in cost and change in QALYs represent the results of sacituzumab govitecan minus chemotherapy.

It is critical to highlight the strengths of this study. First, this analysis is the first to synthesize the latest clinical trial in an economic model method in order to evaluate the economic outcomes of SG treatment of HR+/HER2- metastatic BC. Antibody-drug conjugate with an SN-38 payload targeting Trop 2 is a popular option for the therapy of metastatic BC (23, 56). To our knowledge, there is limited data regarding the economic impact of antibody-drug conjugate treatment for metastatic BC. Second, as part of the present study, 22 subgroups defined by the TROPiCS-02 trial were examined in order to determine their economic outcomes. Physicians, patients, and policy makers may benefit from economic information regarding subgroups. The effectiveness of SG treatment needs to be confirmed by further investigation.

Our study has several limitations. First, there are no head-to-head studies for other antibody-drug conjugates, such as trastuzumab-emtansine and trastuzumab-deruxtecan, which have shown benefits for patients with previously treated metastatic BC (57, 58). When head-to-head data becomes available, the current study should be updated. Second, by fitting parametric distributions to the Kaplan-Meier curves, we used the PFS and OS curves reported in the TROPiCS-02 trial, health benefits beyond observation time were assumed. Third, we were unable to take into account the costs associated with follow-up because time series data were not available. Except for the costs of SG, our sensitivity analysis revealed that cost inputs have a limited influence on model outputs. Fourth, the economic results associated with SG may have been overestimated due to the exclusion of costs related to grade 1 or grade 2 AEs. According to the results of the one-way sensitivity analysis, the costs related to AEs were likely to be minor, suggesting that this limitation is not a major concern. It is important to note that the findings of this study are consistent with general clinical practice for the therapy of HR+/HER2- metastatic BC, making them a valuable resource for physicians and policy makers.

Conclusions

For patients with previously treated HR+/HER2- metastatic BC, SG was unlikely to be a cost-effective therapeutic option. The economic outcomes of treatments can be improved by tailoring them based on the characteristics of the individual patient. The reduction of the cost of SG may result in favorable economic outcomes. The findings of this study may assist clinicians in making optimal treatment choices for patients with HR+/HER2- metastatic BC.

Data availability statement

The original contributions presented in the study are included in the article/Supplementary Material. Further inquiries can be directed to the corresponding author.

Author contributions

DS: Conceptualization, data interpretation, methodology, formal analysis, Software. YL: Critical revision of the manuscript, validation, data interpretation, formal analysis. XL: Data curation, revision, validation. LC: Conceptualization, methodology, funding acquisition, supervision. All authors contributed to the article and approved the submitted version.

Funding

This work was supported by the scientific research and technological development projects of Hechi, Guangxi Province of China (Heke B1824–4).

Conflict of interest

The authors declare that the research was conducted in the absence of any commercial or financial relationships that could be construed as a potential conflict of interest.

Publisher's note

All claims expressed in this article are solely those of the authors and do not necessarily represent those of their affiliated organizations, or those of the publisher, the editors and the reviewers. Any product that may be evaluated in this article, or claim that may be made by its manufacturer, is not guaranteed or endorsed by the publisher.

Supplementary material

The Supplementary Material for this article can be found online at: https://www.frontiersin.org/articles/10.3389/fonc.2023.1162360/full#supplementary-material

References

1. Sung H, Ferlay J, Siegel RL, Laversanne M, Soerjomataram I, Jemal A, et al. Global cancer statistics 2020: globocan estimates of incidence and mortality worldwide for 36 cancers in 185 countries. *CA Cancer J Clin* (2021) 71(3):209–49. doi: 10.3322/caac.21660

2. Yap YS, Lu YS, Tamura K, Lee JE, Ko EY, Park YH, et al. Insights into breast cancer in the East vs the West: a review. *JAMA Oncol* (2019) 5(10):1489–96. doi: 10.1001/jamaoncol.2019.0620

3. Youlden DR, Cramb SM, Yip CH, Baade PD. Incidence and mortality of female breast cancer in the Asia-pacific region. *Cancer Biol Med* (2014) 11(2):101–15. doi: 10.7497/j.issn.2095-3941.2014.02.005

4. Perou CM, Sørlie T, Eisen MB, van de Rijn M, Jeffrey SS, Rees CA, et al. Molecular portraits of human breast tumours. *Nature* (2000) 406(6797):747–52. doi: 10.1038/35021093

5. Blows FM, Driver KE, Schmidt MK, Broeks A, van Leeuwen FE, Wesseling J, et al. Subtyping of breast cancer by immunohistochemistry to investigate a relationship between subtype and short and long term survival: a collaborative analysis of data for 10,159 cases from 12 studies. *PloS Med* (2010) 7(5):e1000279. doi: 10.1371/journal.pmed.1000279

6. Khalil S, Hatch L, Price CR, Palakurty SH, Simoneit E, Radisic A, et al. Addressing breast cancer screening disparities among uninsured and insured patients: a student-run free clinic initiative. *J Community Health* (2020) 45(3):501–5. doi: 10.1007/s10900-019-00767-x

7. Clarke CA, Keegan TH, Yang J, Press DJ, Kurian AW, Patel AH, et al. Age-specific incidence of breast cancer subtypes: understanding the black-white crossover. *J Natl Cancer Inst* (2012) 104(14):1094–101. doi: 10.1093/jnci/djs264

8. Rugo HS, Rumble RB, Macrae E, Barton DL, Connolly HK, Dickler MN, et al. Endocrine therapy for hormone receptor-positive metastatic breast cancer: American society of clinical oncology guideline. *J Clin Oncol* (2016) 34(25):3069–103. doi: 10.1200/jco.2016.67.1487

9. Hanker AB, Sudhan DR, Arteaga CL. Overcoming endocrine resistance in breast cancer. *Cancer Cell* (2020) 37(4):496–513. doi: 10.1016/j.ccell.2020.03.009

10. Slamon DJ, Neven P, Chia S, Fasching PA, De Laurentiis M, Im SA, et al. Overall survival with ribociclib plus fulvestrant in advanced breast cancer. *N Engl J Med* (2020) 382(6):514–24. doi: 10.1056/NEJMoa1911149

11. Sledge GWJr., Toi M, Neven P, Sohn J, Inoue K, Pivot X, et al. The effect of abemaciclib plus fulvestrant on overall survival in hormone receptor-positive, Erbb2-negative breast cancer that progressed on endocrine therapy-monarch 2: a randomized clinical trial. *JAMA Oncol* (2020) 6(1):116–24. doi: 10.1001/jamaoncol.2019.4782

12. Gao JJ, Cheng J, Bloomquist E, Sanchez J, Wedam SB, Singh H, et al. Cdk4/6 inhibitor treatment for patients with hormone receptor-positive, Her2-negative, advanced or metastatic breast cancer: a us food and drug administration pooled analysis. *Lancet Oncol* (2020) 21(2):250–60. doi: 10.1016/s1470-2045(19)30804-6

13. Gennari A, André F, Barrios CH, Cortés J, de Azambuja E, DeMichele A, et al. Esmo clinical practice guideline for the diagnosis, staging and treatment of patients with metastatic breast cancer. *Ann Oncol* (2021) 32(12):1475–95. doi: 10.1016/j.annonc.2021.09.019

14. Cazzaniga ME, Pinotti G, Montagna E, Amoroso D, Berardi R, Butera A, et al. Metronomic chemotherapy for advanced breast cancer patients in the real world practice: final results of the victor-6 study. *Breast* (2019) 48:7–16. doi: 10.1016/j.breast.2019.07.006

15. Cortes J, O'Shaughnessy J, Loesch D, Blum JL, Vahdat LT, Petrakova K, et al. Eribulin monotherapy versus treatment of physician's choice in patients with metastatic breast cancer (Embrace): a phase 3 open-label randomised study. *Lancet* (2011) 377(9769):914–23. doi: 10.1016/s0140-6736(11)60070-6

16. Twelves C, Awada A, Cortes J, Yelle L, Velikova G, Olivo MS, et al. Subgroup analyses from a phase 3, open-label, randomized study of eribulin mesylate versus capecitabine in pretreated patients with advanced or metastatic breast cancer. *Breast Cancer (Auckl)* (2016) 10:77–84. doi: 10.4137/bcbcr.S39615

17. Yuan P, Hu X, Sun T, Li W, Zhang Q, Cui S, et al. Eribulin mesilate versus vinorelbine in women with locally recurrent or metastatic breast cancer: a randomised clinical trial. *Eur J Cancer* (2019) 112:57–65. doi: 10.1016/j.ejca.2019.02.002

18. Mathijssen RH, van Alphen RJ, Verweij J, Loos WJ, Nooter K, Stoter G, et al. Clinical pharmacokinetics and metabolism of irinotecan (Cpt-11). *Clin Cancer Res* (2001) 7(8):2182–94.

19. Bardia A. A closer look at sacituzumab govitecan-hziy. *Clin Adv Hematol Oncol* (2020) 18(11):715–7.

20. Starodub AN, Ocean AJ, Shah MA, Guarino MJ, Picozzi VJJr., Vahdat LT, et al. First-in-Human trial of a novel anti-Trop-2 antibody-Sn-38 conjugate, sacituzumab govitecan, for the treatment of diverse metastatic solid tumors. *Clin Cancer Res* (2015) 21(17):3870–8. doi: 10.1158/1078-0432.Ccr-14-3321

21. Bardia A, Tolaney SM, Punie K, Loirat D, Oliveira M, Kalinsky K, et al. Biomarker analyses in the phase iii ascent study of sacituzumab govitecan versus chemotherapy in patients with metastatic triple-negative breast cancer. *Ann Oncol* (2021) 32(9):1148–56. doi: 10.1016/j.annonc.2021.06.002

22. Ambrogi F, Fornili M, Boracchi P, Trerotola M, Relli V, Simeone P, et al. Trop-2 is a determinant of breast cancer survival. *PloS One* (2014) 9(5):e96993. doi: 10.1371/journal.pone.0096993

23. Liu X, Deng J, Yuan Y, Chen W, Sun W, Wang Y, et al. Advances in Trop2-targeted therapy: novel agents and opportunities beyond breast cancer. *Pharmacol Ther* (2022) 239:108296. doi: 10.1016/j.pharmthera.2022.108296

24. Kalinsky K, Diamond JR, Vahdat LT, Tolaney SM, Juric D, O'Shaughnessy J, et al. Sacituzumab govitecan in previously treated hormone receptor-Positive/Her2-Negative metastatic breast cancer: final results from a phase I/Ii, single-arm, basket trial. *Ann Oncol* (2020) 31(12):1709–18. doi: 10.1016/j.annonc.2020.09.004

25. Rugo HS, Bardia A, Marmé F, Cortes J, Schmid P, Loirat D, et al. Sacituzumab govitecan in hormone receptor-Positive/Human epidermal growth factor receptor 2-negative metastatic breast cancer. *J Clin Oncol* (2022) 40(29):3365–76. doi: 10.1200/jco.22.01002

26. Bednova O, Leyton JV. Targeted molecular therapeutics for bladder cancer-a new option beyond the mixed fortunes of immune checkpoint inhibitors? *Int J Mol Sci* (2020) 21(19):7268. doi: 10.3390/ijms21197268

27. Williams C, Lewsey JD, Mackay DF, Briggs AH. Estimation of survival probabilities for use in cost-effectiveness analyses: a comparison of a multi-state modeling survival analysis approach with partitioned survival and Markov decision-analytic modeling. *Med Decis Making* (2017) 37(4):427–39. doi: 10.1177/0272989x16670617

28. Li Y, Liang X, Yang T, Guo S, Chen X. Pembrolizumab vs cemiplimab for the treatment of advanced non-small cell lung cancer with pd-L1 expression levels of at least 50%: a network meta-analysis and cost-effectiveness analysis. *Front Oncol* (2022) 12:878054. doi: 10.3389/fonc.2022.878054

29. Li Y, Liang X, Li H, Chen X. Atezolizumab plus bevacizumab versus nivolumab as first-line treatment for advanced or unresectable hepatocellular carcinoma: a cost-effectiveness analysis. *Cancer* (2022) 128(22):3995–4003. doi: 10.1002/cncr.34457

30. Li Y, Liang X, Li H, Yang T, Guo S, Chen X. Nivolumab versus sorafenib as first-line therapy for advanced hepatocellular carcinoma: a cost-effectiveness analysis. *Front Pharmacol* (2022) 13:906956. doi: 10.3389/fphar.2022.906956

31. Husereau D, Drummond M, Augustovski F, de Bekker-Grob E, Briggs AH, Carswell C, et al. Consolidated health economic evaluation reporting standards 2022 (Cheers 2022) statement: updated reporting guidance for health economic evaluations. *Bmj* (2022) 376:e067975. doi: 10.1136/bmj-2021-067975

32. Guyot P, Ades AE, Ouwens MJ, Welton NJ. Enhanced secondary analysis of survival data: reconstructing the data from published Kaplan-Meier survival curves. *BMC Med Res Methodol* (2012) 12:9. doi: 10.1186/1471-2288-12-9

33. *Getdata graph digitizer* (2023). Available at: http://getdata-graph-digitizer.com (Accessed 12 January 2023).

34. *Lexicomp online* (2023). Wolters Kluwer. Available at: https://www.wolterskluwer.com/en/solutions/lexicomp/lexicomp (Accessed 12 January 2023).

35. Centers for Medicare & Medicaid Services. *Asp drug pricing files* (2023). Available at: https://www.cms.gov/medicare/medicare-part-b-drug-average-sales-price/2023-asp-drug-pricing-files (Accessed 12 January 2023).

36. Bramley T, Antao V, Lunacsek O, Hennenfent K, Masaquel A. The economic burden of end-of-Life care in metastatic breast cancer. *J Med Econ* (2016) 19(11):1075–80. doi: 10.1080/13696998.2016.1197130

37. Centers for Medicare & Medicaid Services. *Physician fee schedule search* (2023). Available at: https://www.cms.gov/medicare/physician-fee-schedule/search (Accessed January 15, 2023).

38. Weng X, Huang X, Li H, Lin S, Rao X, Guo X, et al. First-line treatment with atezolizumab plus nab-paclitaxel for advanced triple-negative breast cancer: a cost-effectiveness analysis. *Am J Clin Oncol* (2020) 43(5):340–8. doi: 10.1097/coc.0000000000000671

39. Jeong E, Wang C, Wilson L, Zhong L. Cost-effectiveness of adding ribociclib to endocrine therapy for patients with hr-positive, Her2-negative advanced breast cancer among premenopausal or perimenopausal women. *Front Oncol* (2021) 11:658054. doi: 10.3389/fonc.2021.658054

40. Wang H, Wang Y, Gong R, Geng Y, Li L. Cost-effectiveness of pertuzumab and trastuzumab as a first-line treatment of Her2-positive metastatic breast cancer in China. *Ann Palliat Med* (2021) 10(11):11382–93. doi: 10.21037/apm-21-2412

41. Diaby V, Adunlin G, Ali AA, Zeichner SB, de Lima Lopes G, Kohn CG, et al. Cost-effectiveness analysis of 1st through 3rd line sequential targeted therapy in Her2-positive metastatic breast cancer in the united states. *Breast Cancer Res Treat* (2016) 160(1):187–96. doi: 10.1007/s10549-016-3978-6

42. Mistry R, May JR, Suri G, Young K, Brixner D, Oderda G, et al. Cost-effectiveness of ribociclib plus letrozole versus palbociclib plus letrozole and letrozole monotherapy in the first-line treatment of postmenopausal women with Hr+/Her2-advanced or metastatic breast cancer: a U.S. payer perspective. *J Manag Care Spec Pharm* (2018) 24(6):514–23. doi: 10.18553/jmcp.2018.24.6.514

43. Lloyd A, Nafees B, Narewska J, Dewilde S, Watkins J. Health state utilities for metastatic breast cancer. *Br J Cancer* (2006) 95(6):683–90. doi: 10.1038/sj.bjc.6603326

44. Le QA, Bae YH, Kang JH. Cost-effectiveness analysis of trastuzumab emtansine (T-Dm1) in human epidermal growth factor receptor 2 (Her2): positive advanced breast cancer. *Breast Cancer Res Treat* (2016) 159(3):565–73. doi: 10.1007/s10549-016-3958-x

45. *Tom's inflation calculator* (2023). Medical-Care Inflation. Available at: https://www.halfhill.com/inflation_js.html (Accessed 16 January 2023).

46. *National comprehensive cancer network clinical practice guidelines: breast cancer, V.4.2022*. Available at: https://www.nccn.org/professionals/physician_gls/pdf/breast.pdf (Accessed 17 January 2023).

47. Grivas P, DerSarkissian M, Shenolikar R, Laliberté F, Doleh Y, Duh MS. Healthcare resource utilization and costs of adverse events among patients with metastatic urothelial cancer in USA. *Future Oncol* (2019) 15(33):3809–18. doi: 10.2217/fon-2019-0434

48. Sanders GD, Neumann PJ, Basu A, Brock DW, Feeny D, Krahn M, et al. Recommendations for conduct, methodological practices, and reporting of cost-effectiveness analyses: second panel on cost-effectiveness in health and medicine. *Jama* (2016) 316(10):1093–103. doi: 10.1001/jama.2016.12195

49. Craig BA, Black MA. Incremental cost-effectiveness ratio and incremental net-health benefit: two sides of the same coin. *Expert Rev Pharmacoecon Outcomes Res* (2001) 1(1):37–46. doi: 10.1586/14737167.1.1.37

50. Stinnett AA, Mullahy J. Net health benefits: a new framework for the analysis of uncertainty in cost-effectiveness analysis. *Med Decis Making* (1998) 18(2 Suppl):S68–80. doi: 10.1177/0272989x98018002s09

51. Burki TK. A new strategy to reduce US drug prices. *Lancet Oncol* (2018) 19(6):732. doi: 10.1016/s1470-2045(18)30374-7

52. McKertish CM, Kayser V. Advances and limitations of antibody drug conjugates for cancer. *Biomedicines* (2021) 9(8):872. doi: 10.3390/biomedicines9080872

53. Nejadmoghaddam MR, Minai-Tehrani A, Ghahremanzadeh R, Mahmoudi M, Dinarvand R, Zarnani AH. Antibody-drug conjugates: possibilities and challenges. *Avicenna J Med Biotechnol* (2019) 11(1):3–23.

54. Lang Y, Wu B, Liu X. Economic evaluation of trastuzumab deruxtecan in previously treated Her2-low advanced breast cancer in the united states. *Breast Cancer (Dove Med Press)* (2022) 14:453–63. doi: 10.2147/bctt.S389696

55. Chen J, Han M, Liu A, Shi B. Economic evaluation of sacituzumab govitecan for the treatment of metastatic triple-negative breast cancer in China and the us. *Front Oncol* (2021) 11:734594. doi: 10.3389/fonc.2021.734594

56. Rassy E, Rached L, Pistilli B. Antibody drug conjugates targeting Her2: clinical development in metastatic breast cancer. *Breast* (2022) 66:217–26. doi: 10.1016/j.breast.2022.10.016

57. Modi S, Jacot W, Yamashita T, Sohn J, Vidal M, Tokunaga E, et al. Trastuzumab deruxtecan in previously treated Her2-low advanced breast cancer. *N Engl J Med* (2022) 387(1):9–20. doi: 10.1056/NEJMoa2203690

58. Cortés J, Kim SB, Chung WP, Im SA, Park YH, Hegg R, et al. Trastuzumab deruxtecan versus trastuzumab emtansine for breast cancer. *N Engl J Med* (2022) 386 (12):1143–54. doi: 10.1056/NEJMoa2115022

frontiers | Frontiers in Oncology

TYPE Original Research
PUBLISHED 30 May 2023
DOI 10.3389/fonc.2023.1198118

Check for updates

OPEN ACCESS

EDITED BY
Subhash Kumar Tripathi,
Seattle Children's Research Institute,
United States

REVIEWED BY
Brahmam Pujala,
Integral BioSciences Pvt. Ltd., India
Deepak Parashar,
Medical College of Wisconsin,
United States

*CORRESPONDENCE
Yong Ma
yma0917@163.com
Longcheng Shang
njushanglc@126.com
Jin Zhou
zhoujin82@njmu.edu.cn

†These authors share first authorship

RECEIVED 31 March 2023
ACCEPTED 15 May 2023
PUBLISHED 30 May 2023

CITATION
Yu C, Zhang X, Wang M, Xu G, Zhao S, Feng Y, Pan C, Yang W, Zhou J, Shang L and Ma Y (2023) Afatinib combined with anti-PD1 enhances immunotherapy of hepatocellular carcinoma *via* ERBB2/STAT3/PD-L1 signaling.
Front. Oncol. 13:1198118.
doi: 10.3389/fonc.2023.1198118

COPYRIGHT
© 2023 Yu, Zhang, Wang, Xu, Zhao, Feng, Pan, Yang, Zhou, Shang and Ma. This is an open-access article distributed under the terms of the Creative Commons Attribution License (CC BY). The use, distribution or reproduction in other forums is permitted, provided the original author(s) and the copyright owner(s) are credited and that the original publication in this journal is cited, in accordance with accepted academic practice. No use, distribution or reproduction is permitted which does not comply with these terms.

Afatinib combined with anti-PD1 enhances immunotherapy of hepatocellular carcinoma *via* ERBB2/STAT3/PD-L1 signaling

Chao Yu†, Xinyi Zhang†, Min Wang†, Gaoxin Xu†, Siqi Zhao, Yongheng Feng, Chao Pan, Weijun Yang, Jin Zhou*, Longcheng Shang* and Yong Ma*

Department of General Surgery, Nanjing First Hospital, Nanjing Medical University, Nanjing, Jiangsu, China

Background: Afatinib is mainly used to treat advanced non-small cell lung cancer, but its therapeutic effect on hepatocellular carcinoma is still unclear.

Methods: Over 800 drugs were screened by CCK8 technology and afatinib was found to have a significant inhibitory effect on liver cancer cells. The expression of PDL1 in tumor cells treated with drugs were detected by qRT-PCR and Weston Blot experiments. The effects of afatinib on the growth, migration and invasion of HCC cells were evaluated using wound healing, Transwell, and cell cloning assays. The in vivo effects of afatinib in combination with anti-PD1 were evaluated in C57/BL6J mice with subcutaneous tumorigenesis. Bioinformatics analysis was performed to explore the specific mechanism of afatinib's inhibition of ERBB2 in improving the expression level of PD-L1, which was subsequently verified through experiments.

Results: Afatinib was found to have a significant inhibitory effect on liver cancer cells, as confirmed by in vitro experiments, which demonstrated that it could significantly suppress the growth, invasion and migration of HCC cells. qRT PCR and Weston Blot experiments also showed that Afatinib can enhance the expression of PD-L1 in tumor cells. In addition, in vitro experiments confirmed that afatinib can significantly enhance the immunotherapeutic effect of hepatocellular carcinoma. Afatinib's ability to increase PD-L1 expression is mediated by STAT3 activation following its action on HCC cells.

Conclusion: Afatinib enhances PD-L1 expression in tumor cells through the STAT3/PD-L1 pathway. The combination of afatinib and anti-PD1 treatment significantly increases the immunotherapeutic effect of HCC.

KEYWORDS

afatinib, hepatocellular carcinoma (HCC), PD-L1, immunotherapy, ERBB2

1 Introduction

Hepatocellular carcinoma (HCC) is the most common type of liver cancer and is the sixth most common cancer worldwide, with the second-highest mortality rate (1). The leading cause of HCC are hepatitis B virus (HBV) or hepatitis C virus (HCV) infection, chronic liver disease caused by alcoholism, and metabolic syndrome (2). Various treatments for HCC, such as liver transplantation, surgical resection, interventional therapy, targeted therapy, and immunotherapy, have been developed. However, surgery remains the only curative treatment option (3). Sorafenib, a multi-tyrosine kinase inhibitor (TKI), has been shown to prolong the survival period of advanced HCC (4). More recently, Lenvatinib, regorafenib and cabozantinib have also been found to significantly prolong the survival of HCC as first-line or second-line drugs (5–7).

In recent years, immune checkpoint inhibitors have emerged as a promising immunotherapy method for HCC treatment. Currently, the FDA has approved four immune checkpoint inhibitors for single or combined use as first-line or second-line treatment for HCC: atilizumab (targeting programmed death ligand 1 (PD-L1)) in combination with bevacizumab (targeting vascular endothelial growth factor (VEGF)), ipilimumab (targeting cytotoxic T lymphocyte-associated antigen 4 (CTLA-4)) in combination with nivolumab (targeting programmed cell death protein 1 (PD1)), and pembrolizumab (PD1) or nivolumab alone. However, the overall response rate of anti-PD1 treatment for HCC is only about 20%, suggesting limited benefits for most HCC patients (8). Hence, more comprehensive research is required to improve the therapeutic outcomes of anti-PD1 treatment for HCC.

The ERBB receptor is a family of receptor tyrosine kinase (RTK) consisting of four members: EGFR (also known as ERBB1), ERBB2 (HER2), ERBB3 (HER3) and ERBB4 (HER4) (9). These receptors are widely expressed in various tissues and play a critical role in regulating cell proliferation, differentiation, survival, and migration. Disorders in ERBB receptor-mediated signal transduction can cause diseases such as developmental disorders and cancer (10). Overexpression or over-activation of ERBB receptor, especially ERBB2, has been found in many types of cancer and has been used as an important drug target for the development of anticancer therapy. However, the role of ERBB2 in HCC immunotherapy is still unclear, and further research is needed.

In conclusion, our study has investigated the effect of ERBB2 on HCC cells and its potential clinical significance, as well as exploring the specific mechanism involved. These findings may offer new insights to guide future clinic practice.

2 Materials and methods

2.1 Drugs

All drugs were purchased from Selleck (USA).

2.2 Cell cultures

The human GC cell lines (HCCLM3 and Hep3B) were provided by the Shanghai Institutes for Biological Sciences in China. The cells were cultured in a DMEM medium (Gibco, Austria) supplemented with 10% fetal bovine serum (Gibco, Austria) and 1%penicillin-streptomycin, and maintained in a humidified incubator at 37°C with 5% CO2.

2.3 Cell counting kit-8 proliferation assay

The inhibitory effect of drugs on cell proliferation was evaluated using the CCK-8 kit (Ribobio, China). For drug screening, HCC cells (2000/well) were seeded in 96 well plates and incubated for 24 hours. The drugs to be tested were added at a concentration of 10 μ M per well. After 24 hours of treatment, cells were further incubated in a humidified incubator at 37° C with 5% CO2. Next, 10 μ l of CCK-8 reagent was added to each well and incubated for an additional 2 hours. The absorbance at 450nm was measured using an enzyme marker.

2.4 Quantitative reverse transcription polymerase reaction

Total RNA was extreated from cells using the centrifugal column method with the total RNA extraction kit (TIANGEN, China). The extracted RNA was reverse transcribed into cDNA using a reverse transcription kit (Vazyme, China), following the manufacturer's instructions. Quantification of PD-L1 mRNA was performed using a SYBR PCR kit (Vazyme, China), and mRNA expression was normalized to GAPDH before calculation.

2.5 Western blot analysis

The anti PD-L1 antibody and anti β-actin antibody were purchased from Proteintech (USA), and total cellular protein was obtained by lysing cells in RIPA lysis buffer (Beyotime, China). A 5% skimmed milk powder solution was used for room temperature blocking for 2h. After incubating with anti GADPH and anti PD-L1 at 4° C for 12 hours, the membrane was incubated with secondary antibody (1:5000) and then detected using an enhanced chemiluminescence kit (NCM Biotech, China). The protein expression level was analyzed using ImageJ software to analyze the western blot image.

2.6 Wound healing assay

After the confluence of HCCLM3 or Hep3B cell lines reaches 90%, use the standard 200 μ l pipette tip to create a scratch quickly, and wash it twice with PBS to remove any floating debris. Then, replace with fresh culture medium containing10 μ M afatinib or dimethyl sulfoxide (DMSO) of the same concentration as a control. The plate is then placed in a humidified incubator at 37° C with 5% CO2. At different time points (0h, 24h, 48h), the wound healing within the scratch line is observed, and representative images of scratch line are taken.

2.7 Transwell assay

When the HCC cell line reached 90% confluency, 10 uM afatinib and an equal concentration of DMSO were added to the treatment and control groups, respectively, and then incubated in a humidified incubator containing 5% CO2 at 37° C for 24 hours. Following the manufacturer's instructions, 4 × 106 HCC cells were added to the upper chamber with 200 μl DMEM medium containing 10uM afatinib, while the lower chamber contained 700 μl DMEM medium containing 10% fetal bovine serum as the chemotactic agent. The control group was treated with DMSO in the same way as the treatment group. After 24 hours, the upper chamber was fixed with formaldehyde and stained with 0.1% crystal violet. Finally, cell migration was observed and counted under the inverted microscope.

2.8 Colony formation assay

HCCLM3 and Hep3B cell lines were seeded into six well plates at a density of 1000 cells/well. The experimental group was treated with 10 uM afatinib, while the control group was treated with DMSO of the same concentration. The six-well plates were incubated in a humidified incubator at 37° C and 5% CO2 for 14 days. The cells were fixed with formaldehyde and stained with 0.1% crystal violet. Colonies were observed and counted under natural light, and representative wells were selected for images. All experiments were performed in triplicate.

2.9 Mice model

Animal experiments were conducted following the guidelines of the Animal Management Committee of Nanjing Medical University, and all animal procedures and management were in compliance with ethical provisions for animal experiments. Prior to the experiment, we randomly divided 20 4-week old male C57/BL6J mice into four groups: afatinib single group, anti-PD1 (BP0273, Biocell, USA) single group, afatinib+anti-PD1 combined group, and PBS group (n=5 for each group). Subcutaneous injection of H22 cells was performed in the mice. In the Afatinib group, we injected Afatinib intraperitoneally every 2 days (10mg/kg) for a total of 28 days. Anti-PD1 (5.5mg/kg) was injected intraperitoneally every 7 days for a total of 28 days. Intraperitoneal injection was performed at the same time and concentration as above in the dual-drug group. After the experiment, the mice were euthanized and the tumors were collected to measure their size and weight for further experiments.

2.10 Immunohistochemistry

Each tissue sample was stained with specific primary antibodies and biotin-conjugated secondary antibodies, followed by incubation with the antibody protein biotin peroxidase complex. The samples were evaluated using the H-score method, which combines the values of the intensity of immune response and the percentage of tumor cells stained. The final immunohistochemical score was obtained by multiplying the percentage of target protein positive cells by the intensity score.

2.11 ERBB2 expression level, clinicopathological analysis, promoter methylation level and pan-cancer analysis

UALCAN (http://ualcan.path.uab.edu/) was used to examine the differential expression of ERBB2 in HCC and normal tissues as well as the difference in promoter methylation level. Kaplan Meier plotter (kmplot.com) was used to determine the correlation between ERBB2 expression and recurrence free survival (RFS) as well as progression-free survival (PFS) in tumor patients. TIMER (cistrome.shinyapps.io/timer) was used to analyze the differential expression of ERBB2 in various tumor tissues.

2.12 Immune-related analysis of ERBB2

TISIDB (cis. hku. hk/TISIDB) is a portal that facilitates the study of the interactions between tumors and the immune system by integrating multiple heterogeneous data types. TISIDB was used to analyze the correlation between the abundance of tumor infiltrating lymphocytes (TIL) and ERBB2.

2.13 ERBB2 location analysis

The human protein atlas can be used to determine the location of ERBB2 in cells. The atlas provides a comprehensive map of the human proteome in various tissues and cell types, including information on protein expression, localization, and function. It also includes data on gene expression in normal and diseased tissues, as well as tools for visualizing and analyzing the data.

2.14 Gene pathway correlation analysis

RNA-sequencing expression (level 3) profiles and corresponding clinical information for LIHC were downloaded from the TCGA dataset (https://portal.gdc.com).The GSVA package in R software was used to perform gene set variation analysis, with the method parameter set to 'ssgsea'. Spearman correlation was used to analyze the correlation between genes and pathway scores. All the analysis methods and R packages were implemented in R version 4.0.3. A p value <0.05 was considered statistically significant.

2.15 Statistical analysis

The continuous data obtained from a single test in the two groups were analyzed using Graphpad Prism 8.0.2 (United States). A p value<0.05 was considered statistically significant.

3 Results

3.1 Afatinib had significant inhibitory effect on liver cancer cells

CCK-8 assay was utilized to investigate the effect of more than 800 drugs on the proliferation of hepatocellular carcinoma cells. The results showed that afatinib significantly inhibited the proliferation of HCC cells (Figure 1A). Additionally, we compared afatinib with other commonly used chemotherapeutic drugs including Ibrutinib, Tivozanib, Pazopanib, and Levatinib, and the results indicated that afatinib exhibited better inhibitory effect on HCC cells than other drugs (Figure 1B). The molecular structure formula of Afatinib is illustrated in Figure 1C. Therefore, we decided to further study the role and mechanism of afatinib in the treatment of HCC.

3.2 Afatinib can significantly inhibit the proliferation, invasion and migration of HCC cells

The inhibitory effect of afatinib on HCC cell migration was confirmed through wound healing assays in HCCLM3 and Hep3B cells at a concentration of 10 μM (Figures 2A, B). The colony formation assay also demonstrated that afatinib inhibited the proliferation of HCC cells (Figures 2C, D). Furthermore, the transwell assay revealed that afatinib significantly reduced the invasive and migratory potential of HCC cells compared to the control group (Figures 2E, F). These findings provide evidence for the potent inhibitory effect of afatinib on HCC cells.

3.3 ERBB2 is implicated in the clinical progress of HCC

To further investigate the impact of ERBB2 inhibitor (afatinib) on the prognosis of HCC, we analyzed the Kaplan-Meier Plotter data and found that HCC patients with high ERBB2 expression had significantly lower recurrence free survival (RFS) and progression-free survival (PFS) than those with low or no expression (Figure 3C). TCGA portal analysis revealed that ERBB2 expression was significantly up-regulated in HCC tumor tissues compared to normal tissues, and the expression levels varied across different tumor grades and stages (Figure 3A). Furthermore, the methylation of the ERBB2 promoter was significantly lower in tumor tissues than in normal tissues (Figure 3B). Timer's pancancer analysis also showed significant difference in ERBB2 expression between various common tumors and normal tissues (Figure 3D).

3.4 Expression of ERBB2 in human HCC tumor tissue

In addition, we analyzed the expression of ERBB2 in various malignant tumors using data from the Human Protein Atlas. Immunofluorescence analysis showed that ERBB2 was clearly

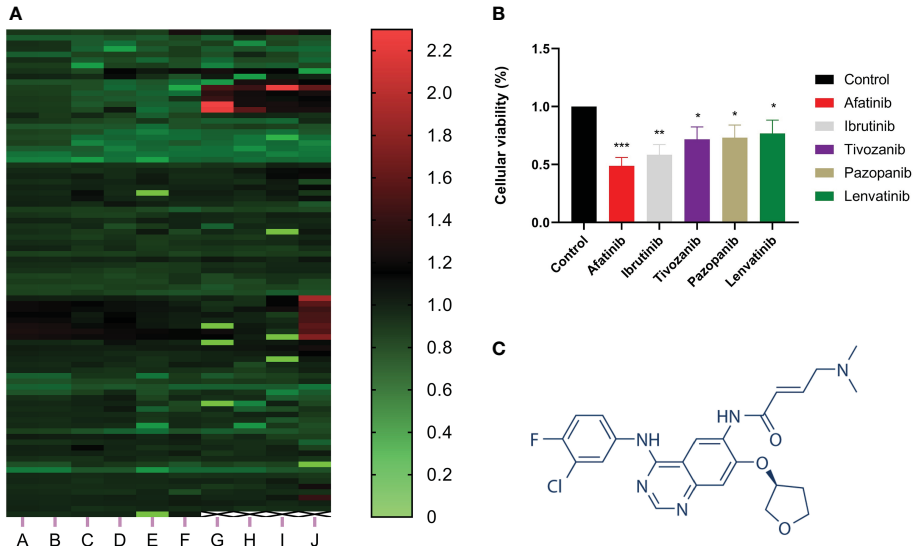


FIGURE 1
Afatinib significantly inhibited the proliferation of liver cancer cells among over 800 drugs. **(A)** Heat map showing the inhibitory effect of more than 800 drugs on the proliferation of liver cancer cells as determined by CCK8 experiment. **(B)** Comparison of the inhibitory effect of afatinib with four other commonly used chemotherapeutic drugs, Ibrutinib, Tivozanib, Pazopanib, and Lenvatinib, on the proliferation of liver cancer cells. **(C)** Chemical structure formula of Afatinib. * $p < 0.05$, ** $p < 0.01$, *** $p < 0.001$.

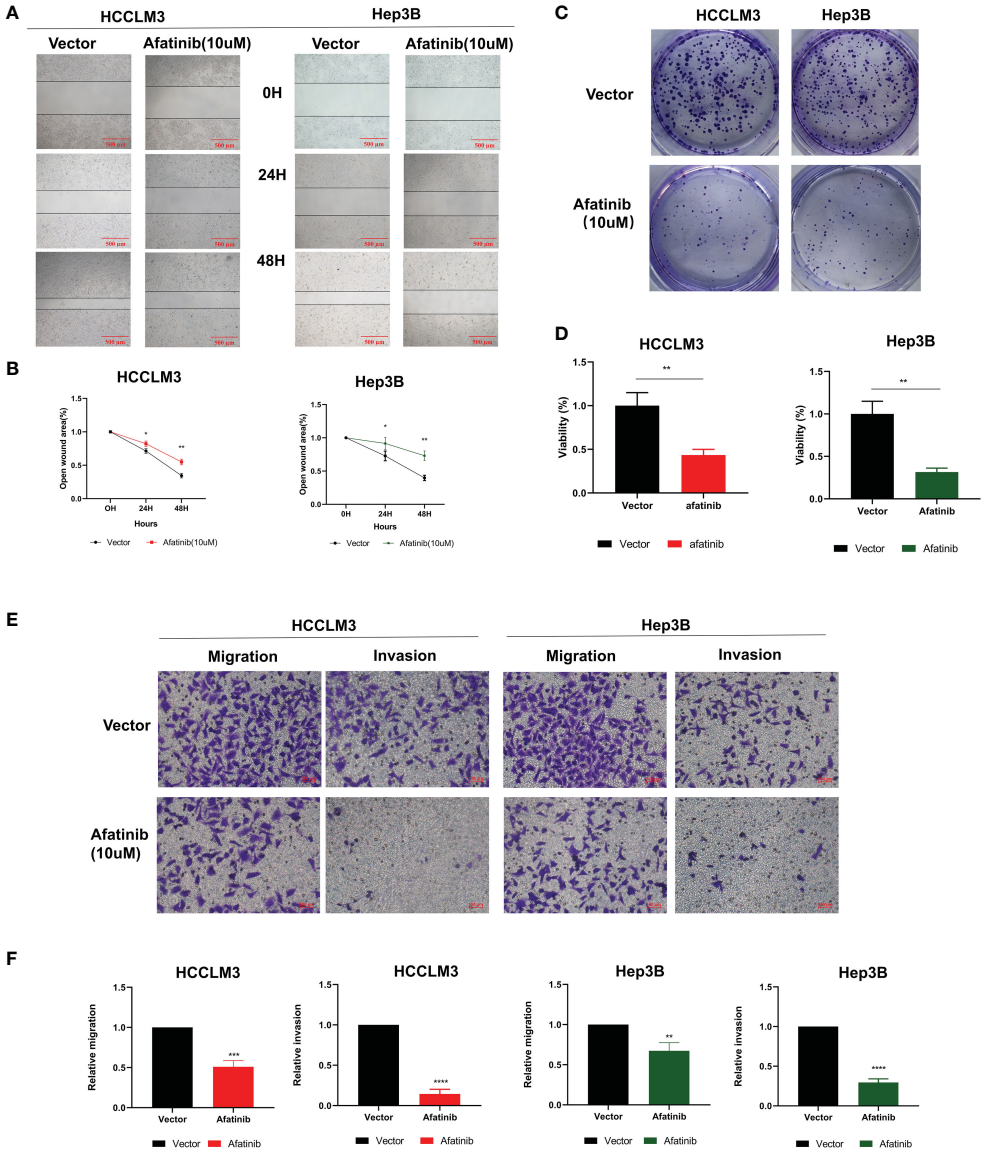


FIGURE 2
The ERBB2 inhibitor afatinib can inhibit the proliferation, invasion, and migration of HCC cells. **(A)** Wound healing assay was performed to assess the migration ability of HCC cells treated with 10 μM Afatinib. **(B)** Quantitation of the wound healing assay results. **(C)** Plate cloning assay was performed to investigate the proliferation ability of HCC cells treated with Afatinib at a concentration of 10 μM. **(D)** Quantitation of the plate cloning assay results. Afatinib can significantly inhibit the migration and invasion ability of HCC cells **(E)**: Transwell assay was used to assess the invasion and migration ability of HCC cells treated with Afatinib (10 μ M). **(F)** Quantitative graph of the results of the Transwell experiment. * $p < 0.05$, ** $p < 0.01$, *** $p < 0.001$, **** $p < 0.0001$.

expressed in the cytoplasm and cell membrane of human epidermal squamous cell carcinoma A-431 cells, human osteosarcoma U2OS cells, and human glioma U251-MG cells, indicating that ERBB2 expression was not limited to specific cell lines (Figure 4D). The Human Protein Atlas showed that ERBB2 staining in the tissues of HCC patients is mostly moderate or mild, and most HCC tissues express this protein, mainly distributed in the cytoplasm and cell membrane (Figure 4E). These findings suggest that ERBB2 is a promising target for the treatment of HCC.

3.5 Afatinib can significantly increase PDL1 expression in HCC tumor cells by up-regulating the STAT3

We examined the expression level of PD-L1 in Hep3B and HCCLM3 hepatoma cell lines using qRT-PCR after treatment with afatinib for 24 hours. We found that the expression of PD-L1 increased in hepatoma cells after the addition of afatinib (Figure 5A). Consistently, the Western blot analysis also demonstrated an increase in PD-L1 protein expression in HCC

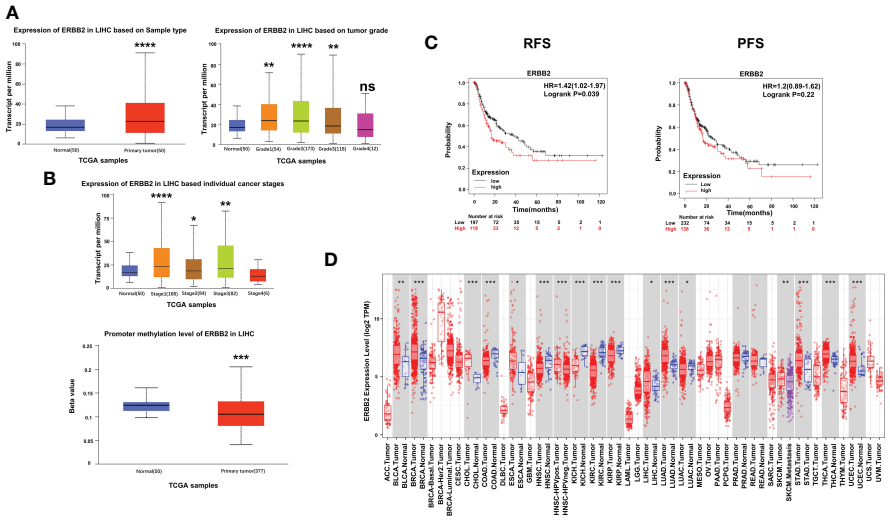


FIGURE 3
Expression of ERBB2 in clinical samples. **(A)** Comparison of ERBB2 expression levels between normal and tumor tissues of HCC; ERBB2 expression levels in different tumor grades; ERBB2 expression levels in different tumor stages. **(B)** Comparison of ERBB2 methylation levels between normal and tumor HCC tissues. **(C)** Kaplan Meier survival curve showed that patients with high ERBB2 expression have significantly worse RFS and PFS than those with low ERBB2 expression. **(D)** Pancancer analysis demonstrated differences in ERBB2 expression levels among different types of tumors. *p < 0.05, **p < 0.01, ***p < 0.001, ****p < 0.0001.

cells treated with Afatinib for 24 hours (Figure 5B). To explore the underlying mechanism of the afatinib-induced increase in PD-L1, we referred to the research by Song et al. on T-cell lymphoma (11) and hypothesized that it could be related to STAT3. Therefore, we assessed the expression of STAT3 and P-STAT3 by Western blot, and as expected, the results showed no significant difference in STAT3 expression but a higher expression of P-STAT3 in the cells treated with afatinib compared to the control group (Figures 5B, C). In conclusion, our findings suggest that the ERBB2 inhibitor afatinib promotes the phosphorylation of STAT3, which in turn induces the increase in PD-L1 expression in HCC.

3.6 Afatinib combined with Anti-PD1 significantly increased the immunotherapeutic effect of HCC in *in vivo* model

We injected H22 cells into the bilateral subcutaneous groin of C57/BL6J mice (5 mice/group, 4 groups in total) at the age of 4 weeks, followed by intraperitoneal injection of PBS, afatinib, anti-PD1, or their combination to analyze the tumor growth size and weight for 28 days. The results showed that compared with the control group, the afatinib group inhibited the growth of HCC, while the anti-PD1 group significantly inhibited the development of HCC. As expected, the combined group of afatinib and anti-PD1 exhibited a better inhibitory effect on tumor growth compared to the single drug group and PBS control group. On day 28, the mice were euthanized, and tumor tissues were weighed and measured (Figure 4C). The tumor weight and volume of the afatinib and anti-pd1 single drug groups were lighter than those of the control group, while the combination of afatinib and anti-PD1 had a more significant tumor inhibition effect. Immunohistochemical analysis of HCC tumors was also performed (Figures 4A, B). The CD8 expression in both the single drug group and combination group was significantly higher than that in the control group, especially in the combination group of Afatinib and Anti-PD-1. In terms of Ki67 expression, both the single drug group and the combination group were able to reduce Ki67 expression, with the combination of Afatinib and Anti-PD1 showing the most significant reduction. Additionally, the results showed that the single drug group and the combination group had varying degrees of inhibitory effects on ERBB2 expression in HCC. The afatinib single drug group slightly increased the expression of PD-1, while the anti-PD1 and afatinib +anti-PD-1 combined group significantly reduced the expression of PD-1. Notably, the expression of PD-L1 was higher in the Afatinib monotherapy group and the combination of afatinib+Anti-PD1 group, highlighting the importance of targeting both ERBB2 and PD-1/PD-L1 pathways for HCC treatment. Overall, these findings suggest that the combination of ERBB2 inhibitor Afatinib and Anti-PD1 therapy is more promising approach for the treatment of HCC compared to traditional monotherapy.

3.7 The correlation between tumor infiltrating lymphocytes abundance and ERBB2 expression

The relative abundance of tumor-infiltrating lymphocytes (TILs) was estimated using gene set variation analysis (GSVA) based on gene expression profiles of HCC (Figure 6A). Based on the immune-related characteristics of 28 TIL types in Charoentong's study, we found that a large number of immune cell types were associated with ERBB2 expression. Specifically, NK/Th17 was significantly positively correlated

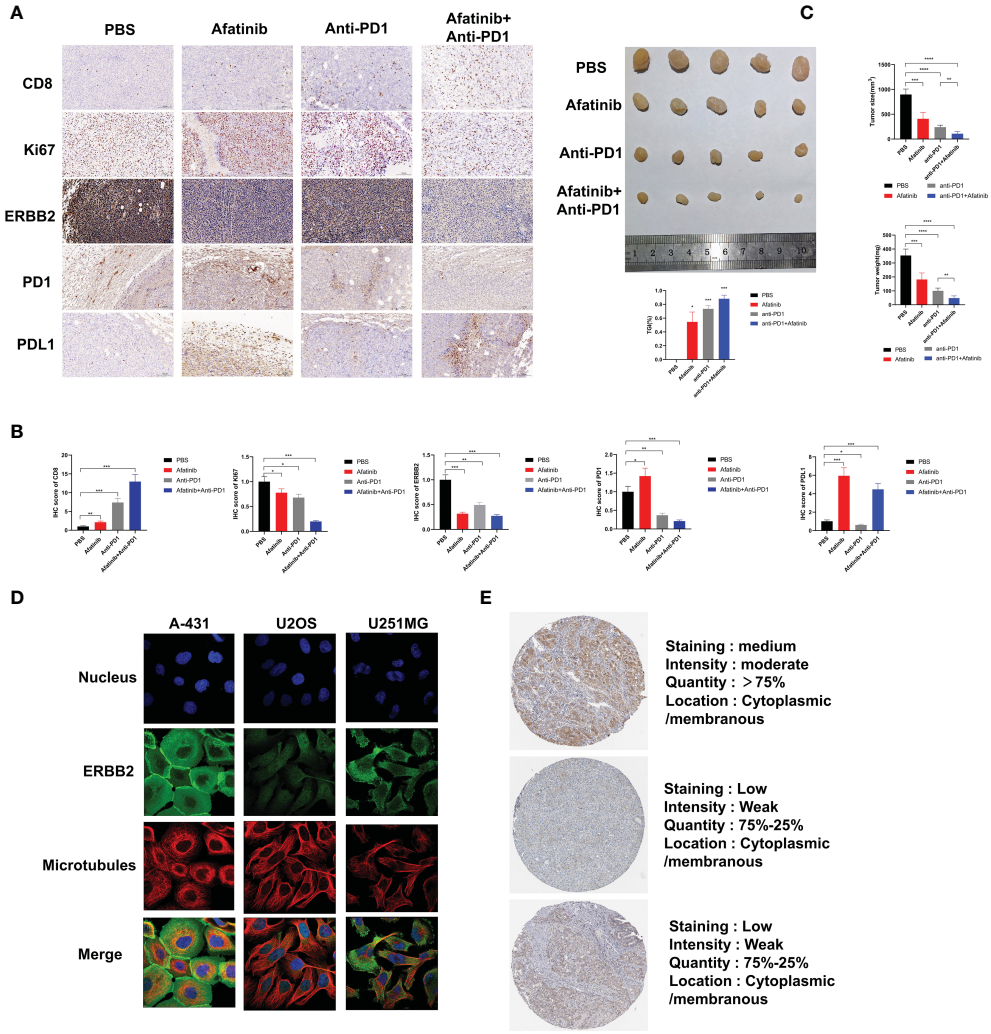


FIGURE 4
In vivo experiments have demonstrated that the ERBB2 inhibitor Afatinib can inhibit the development of HCC and enhance the therapeutic effect of anti-PD1 in HCC. **(A)** Immunohistochemistry was performed to assess the expression of CD8, Ki67, ERBB2, PD1, and PDL1 in PBS group, afatinib group alone, anti PD1 group alone, afatinib and anti-PD1 combined group. **(B)** The quantitative analysis of immunohistochemical results is shown. **(C)** The tumor weight and volume of subcutaneous tumors obtained from C57BL/6 mice were measured on the 28th day. Expression of ERBB2 in various HCC cells and tissues. **(D)** Immunofluorescence staining shows the expression of ERBB2 in human epithelial squamous cell carcinoma A-431 cells, human osteosarcoma U2OS cells, and human glioma U251-MG cells. **(E)** Immunohistochemical staining of ERBB2 in HCC tissue samples. *p < 0.05, **p < 0.01, ***p < 0.001, ****p < 0.0001.

with ERBB2, while CD56bright/Th2 was significantly negatively correlated with ERBB2 expression (Figure 6B). These results provide new clues and ideas for further immunotherapy of HCC.

3.8 ERBB2 participated in multiple metabolic pathways in HCC

Spearman analysis was used to evaluate the correlation between single genes and pathway score in HCC (Figure 6C). The X-axis represents the distribution of gene expression, while the Y-axis represents the distribution of pathway scores. The density curve on the right displays the trend of immune scores of the pathway, and the curve on the top shows the trend of gene expression. The value on top indicates the p value, correlation coefficient, and correlation calculation method. We found that ERBB2 was significantly correlated with several pathways in HCC, including D-glutamine and D-glutamic acid metabolism, ECM degradation, EMT marker gene, p53 pathway, TGFb, mannose O-glycan biosynthesis, collagen formation, glycosylphosphatidylinositol GPI-anchored biosynthesis, cell apoptosis, angiogenesis, drug metabolism other enzymes, and mucin O-glycan biosynthesis.

4 Discussion

HCC is one of the most common malignant tumors worldwide, with approximately 1 million new cases occurring each year.

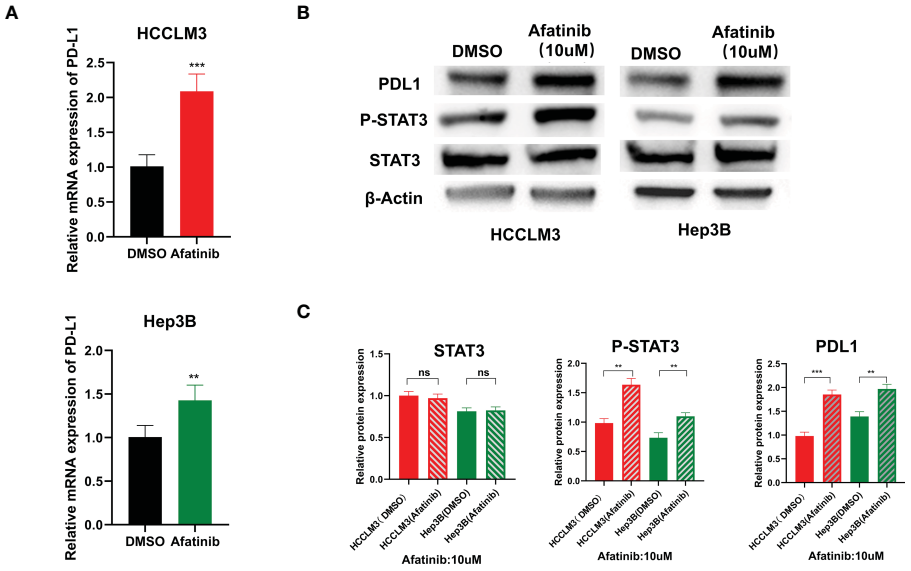


FIGURE 5
ERBB2 inhibitor afatinib upregulates the expression of PDL1 in HCC cells through STAT3. **(A)** qRT-PCR detected an increase in PDL1 expression in HCC cells treated with Afatinib. **(B)** Western blot analysis revealed an increase in PDL1 and p-stat3 expression in afatinib-treated cells. **(C)** Quantitative map of Western blot detection results. * $p < 0.05$, ** $p < 0.01$, *** $p < 0.001$. ns, not statistically.

Although surgical resection and liver transplantation are considered effective methods for treating HCC, but the recurrence rate of HCC remains high. In recent years, with the development of numerous targeted and immunotherapies, there are now more options available for the treatment of HCC.

After screening over 800 small molecule drugs, we identified afatinib, an orally effective and irreversible ERBB2 inhibitor, as having a significant inhibitory effect on HCC cells. Although Afatinib is mostly used in the research of esophageal squamous cell carcinoma (ESCC), non small cell lung cancer (NSCLC), and gastric cancer, its efficacy in treating HCC was not clear. Previous studies suggested that ERBB2 was rarely expressed in HCC, leading to speculation that it may not play a role in HCC (12, 13). Deepak Parashar et al. found that in ovarian cancer, ERBB2 up-regulates ZEB1 in non-attached cells, FOX1 up-regulates ZEB1, and ZEB1 inhibits FOXM1 expression through a negative feedback mechanism. The authors suggest that ZEB1 and FOXM1 are significant in ERBB2 signaling for peritoneal metastasis of ovarian cancer (14). Anjali Geethadevi1 et al. found that in ovarian cancer by RNA seq, Binding of OSM to OSMR caused OSMR-IL6ST dimerization, which is required to produce oncogenic signaling cues for prolonged STAT3 activation (15). Yingqing Deng et al. found that, Single-cell sequencing in high-grade serous ovarian cancer (HGSOC) has shown that ERBB2 is highly expressed in metastatic tumors, and IL6/STAT3 signaling is enriched in fibroblasts and involved in angiogenesis and immune regulation (16). Deepak Parashar et al. found that genomic amplification of 3q26.2 locus leads to the increased expression of microRNA 551b-3p (miR551b-3p) in triple-negative breast cancer (TNBC). MiR551b upregulates the expression of Oncostatin M receptor (OSMR) and interleukin-31 receptor-α (IL31RA) as well as their ligands Oncostatin-M (OSM) and interleukin 31 (IL31) through STAT3 transcription (17). Ling Gao et al. found that in astrocytoma, the inhibition of STAT3 and ERBB2 significantly reduced the survival of glioma cells after radiation and inhibited tumor growth *in vivo*, which they believed was related to the mitochondrial apoptotic pathway (18). However, Shi et al. (19–21) conducted detailed studies that confirmed the expression and function of ERBB2 in HCC, prompting us to explore its specific mechanism. Through wound healing, cloning, and Transwell experiments, we confirmed that the ERBB2 inhibitor afatinib significantly inhibited the migration, proliferation, and invasion of HCC cells. We conducted qRT-PCR and WB experiments, which revealed that treatment of HCC cells with afatinib significantly increased the expression of PDL1. By reviewing previous studies, we found that STAT3 played a role in the expression of PDL1 in HCC. We also confirmed through WB experiments that after afatinib treatment, the expression of phosphorylated STAT3 was upregulated, resulting in an upregulation of PDL1 in HCC. However, the specific mechanism underlying this effect remains to be explored in future studies. To investigate the clinical relevance of ERBB2, we used UALCAN to analyze the expression of ERBB2 in HCC tumor tissues compared to normal tissues. Our results showed that ERBB2 expression was significantly higher in HCC tumor tissues than normal tissues. Furthermore, the expression levels of ERBB2 were higher in grade 1 and grade 2 tumors as well as in stage 1, 2, and 3 tumors when compared to normal tissues. However, the methylation of REBB2 was found to be lower in tumor tissues than in normal tissues. Additionally, Kaplan Meier Plotter analysis confirmed that patients with high ERBB2

10.3389/fonc.2023.1198118

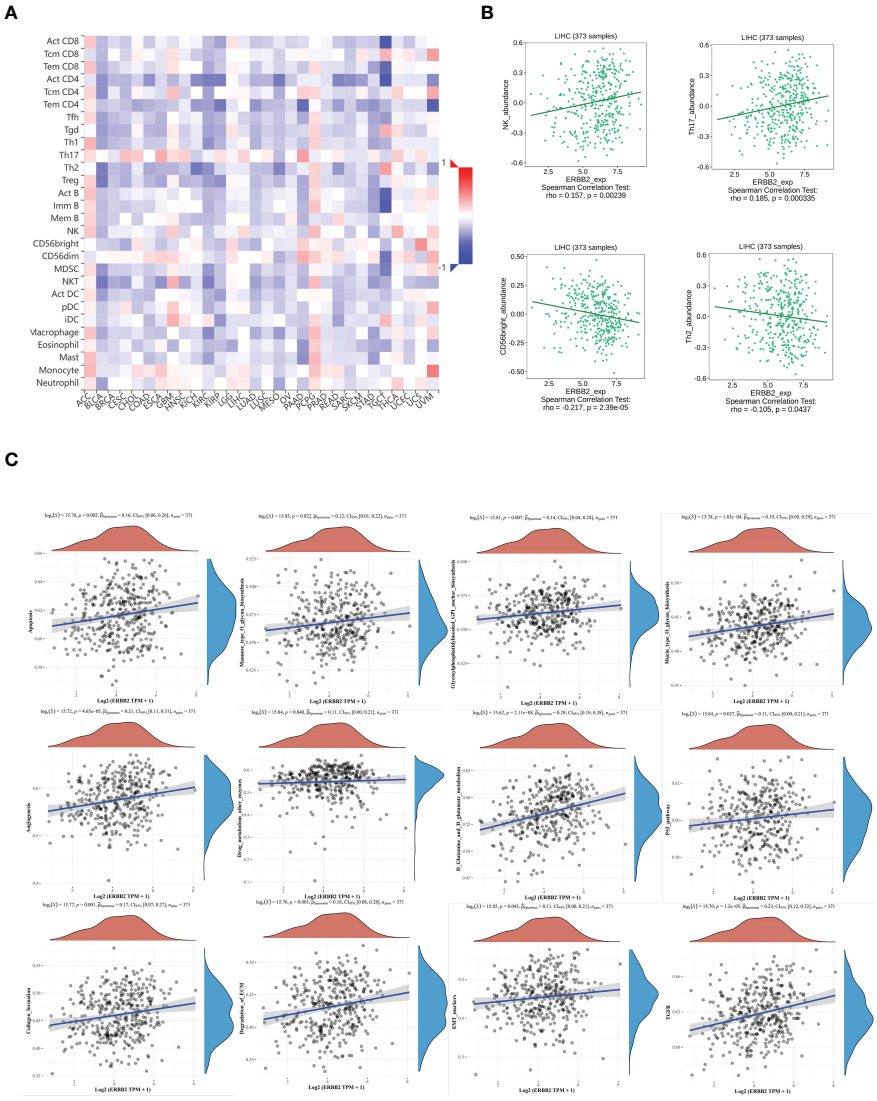


FIGURE 6
The relationship between tumor infiltrating lymphocytes (TIL) and ERBB2 expression in HCC. **(A)** Heatmap representing the infiltration abundance of multiple lymphocyte types in different tumors estimated by GSVA based on gene expression profiles. **(B)** Correlation analysis between ERBB2 expression and the abundance of NK, Th17, CD56bright, and Th2 in HCC. Bioinformatics analysis shows that ERBB2 participates in multiple cellular metabolic pathways of HCC, such as D-glutamine and D-glutamic acid metabolism, ECM degradation, EMT marker gene, p53 pathway, TGFb, mannose O-glycan biosynthesis, collagen formation, glycosylphosphatidylinositol GPI-anchored biosynthesis, cell apoptosis, angiogenesis, drug metabolism other enzymes, and mucin O-glycan biosynthesis **(C)**.

expression had poorer survival and prognosis. Pancancer analysis revealed differential expression of ERBB2 across various tumor tissues. Furthermore, through data mining of The Human Protein Atlas, we observed a relatively fixed distribution of ERBB2 in cells. The immunohistochemical analysis of tumor tissue revealed variable expression of ERBB2 in HCC, and the location of the expressed cells was consistent with the results of immunofluorescence analysis. In order to further validate our conclusion that afatinib enhances HCC immunotherapy by upregulating PDL1, we conducted *in vivo* experiments in mice. Our results demonstrated that the combination of afatinib and anti-PD1 significantly reduced tumor volume and weight compared to the control group and the single drug group. We also confirmed the reliability of our experiments and conclusions through immunohistochemical experiments.

Through bioinformatics analysis, we investigated the association between TIL abundance and ERBB2 expression in HCC and observed a positive correlation between NK/Th17 cells and ERBB2, while a negative correlation was found between CD56bright/Th2 cells and ERBB2 expression. In addition, we analyzed the involvement of ERBB2 in various cellular functional pathways in HCC, which could potentially offer novel avenues for further research in this field.

In summary, while research on ERBB2 in HCC is still relatively limited, our study has found that the combination of ERBB2 inhibitor Afatinib with Anti pd1 can significantly enhance the therapeutic effect of HCC (Figure 7). However, further studies are

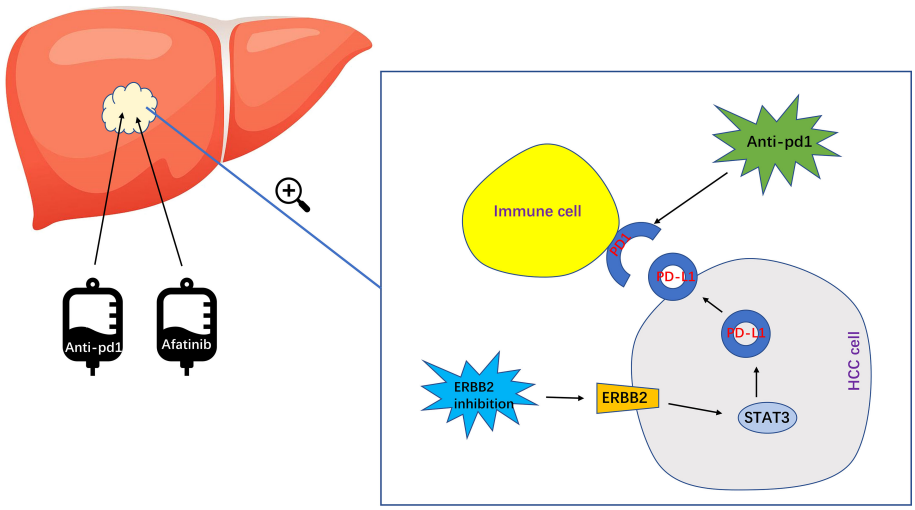


FIGURE 7
The specific mechanism of ERBB2 inhibitor Afatinib combined with anti PD1 to enhance the immunotherapeutic effect of HCC. Afatinib inhibits ERBB2, which leads to the upregulation of activated STAT3 expression. This in turn upregulates the expression of PDL1, ultimately enhancing the immunotherapy of HCC.

needed to elucidate the specific molecular mechanisms involved. With the development of immunotherapy for HCC in recent years, there is great potential for further exploration and advancement in this field.

Data availability statement

The datasets presented in this study can be found in online repositories. The names of the repository/repositories and accession number(s) can be found in the article/Supplementary Material.

Ethics statement

The animal study was reviewed and approved by Ethics Committee of Nanjing Hospital Affiliated to Nanjing Medical University.

Author contributions

There are four first authors in this manuscript, who have made the equal contribution to this project. CY and XZ is responsible for writing the manuscript and experiment. MW and GX are responsible for the experiment. SZ, YF, CP and WY also participated in data collation and chart making. In addition, there are three corresponding authors. YM contributed to the key revisions of the research design and manuscript. JZ and LS are responsible for proofreading manuscripts and data. All authors contributed to the article and approved the submitted version.

Funding

This study was supported by the National Natural Science Foundation (No. 82203762), Chen Xiaoping Foundation for the Development of Science and Technology of Hubei Province (No. CXPJJH12000009-08), and Xinghuo Talent Program of Nanjing First Hospital.

Acknowledgments

We would like to thank Dr. Wubin Zheng and Dr. Guoqiang Sun for their valuable advice on guiding the problems of the experiment. We would also like to thank the Central Laboratory of Nanjing First Hospital for providing an advanced laboratory for our experiments.

Conflict of interest

The authors declare that the research was conducted in the absence of any commercial or financial relationships that could be construed as a potential conflict of interest.

Publisher's note

All claims expressed in this article are solely those of the authors and do not necessarily represent those of their affiliated organizations, or those of the publisher, the editors and the reviewers. Any product that may be evaluated in this article, or claim that may be made by its manufacturer, is not guaranteed or endorsed by the publisher.

Supplementary material

The Supplementary Material for this article can be found online at: https://www.frontiersin.org/articles/10.3389/fonc.2023.1198118/full#supplementary-material

References

1. Ferlay J, Soerjomataram I, Dikshit R, Eser S, Mathers C, Rebelo M, et al. Cancer incidence and mortality worldwide: sources, methods and major patterns in GLOBOCAN 2012. *Int J Cancer* (2015) 136(5):E359–86. doi: 10.1002/ijc.29210

2. Llovet JM, Zucman-Rossi J, Pikarsky E, Sangro B, Schwartz M, Sherman M, et al. Hepatocellular carcinoma. *Nat Rev Dis Primers* (2016) 2:16018. doi: 10.1038/nrdp.2016.18

3. European Association for the Study of the Liver. EASL clinical practice guidelines: management of hepatocellular carcinoma. *J Hepatol* (2018) 69(1):182–236. doi: 10.1016/j.jhep.2018.03.019

4. Llovet JM, Ricci S, Mazzaferro V, Hilgard P, Gane E, Blanc JF, et al. Sorafenib in advanced hepatocellular carcinoma. *N Engl J Med* (2008) 359(4):378–90. doi: 10.1056/NEJMoa0708857

5. Kudo M, Finn RS, Qin S, Han KH, Ikeda K, Piscaglia F, et al. Lenvatinib versus sorafenib in first-line treatment of patients with unresectable hepatocellular carcinoma: a randomised phase 3 non-inferiority trial. *Lancet* (2018) 391(10126):1163–73. doi: 10.1016/S0140-6736(18)30207-1

6. Abou-Alfa GK, Meyer T, Cheng AL, El-Khoueiry AB, Rimassa L, Ryoo BY, et al. Cabozantinib in patients with advanced and progressing hepatocellular carcinoma. *N Engl J Med* (2018) 379(1):54–63. doi: 10.1056/NEJMoa1717002

7. Zhu AX, Kang YK, Yen CJ, Finn RS, Galle PR, Llovet JM, et al. Ramucirumab after sorafenib in patients with advanced hepatocellular carcinoma and increased α-fetoprotein concentrations (REACH-2): a randomised, double-blind, placebo-controlled, phase 3 trial. *Lancet Oncol* (2019) 20(2):282–96. doi: 10.1016/S1470-2045(18)30937-9

8. Girardi DM, Pacífico JPM, Guedes de Amorim FPL, Dos Santos Fernandes G, Teixeira MC, Pereira AAL. Immunotherapy and targeted therapy for hepatocellular carcinoma: a literature review and treatment perspectives. *Pharmaceuticals* (2020) 14 (1):28. doi: 10.3390/ph14010028

9. Yarden Y, Sliwkowski MX. Untangling the ErbB signalling network. *Nat Rev Mol Cell Biol* (2001) 2(2):127–37. doi: 10.1038/35052073

10. Le TL, Galmiche L, Levy J, Suwannarat P, Hellebrekers DM, Morarach K, et al. Dysregulation of the NRG1/ERBB pathway causes a developmental disorder with gastrointestinal dysmotility in humans. *J Clin Invest* (2021) 131(6):e145837. doi: 10.1172/JCI145837

11. Song TL, Nairismägi ML, Laurensia Y, Lim JQ, Tan J, Li ZM, et al. Oncogenic activation of the STAT3 pathway drives PD-L1 expression in natural killer/T-cell lymphoma. *Blood* (2018) 132(11):1146–58. doi: 10.1182/blood-2018-01-829424

12. Potti A, Ganti AK, Tendulkar K, Chitajallu S, Sholes K, Koch M, et al. HER-2/neu and CD117 (C-kit) overexpression in hepatocellular and pancreatic carcinoma. *Anticancer Res* (2003) 23(3B):2671–4.

13. Xian ZH, Zhang SH, Cong WM, Wu WQ, Wu MC. Overexpression/amplification of HER-2/neu is uncommon in hepatocellular carcinoma. *J Clin Pathol* (2005) 58(5):500–3. doi: 10.1136/jcp.2004.023556

14. Parashar D, Nair B, Geethadevi A, George J, Nair A, Tsaih SW, et al. Peritoneal spread of ovarian cancer harbors therapeutic vulnerabilities regulated by FOXM1 and EGFR/ERBB2 signaling. *Cancer Res* (2020) 80(24):5554–68. doi: 10.1158/0008-5472.CAN-19-3717

15. Geethadevi A, Nair A, Parashar D, Ku Z, Xiong W, Deng H, et al. Oncostatin m receptor-targeted antibodies suppress STAT3 signaling and inhibit ovarian cancer growth. *Cancer Res* (2021) 81(20):5336–52. doi: 10.1158/0008-5472.CAN-21-0483

16. Deng Y, Tan Y, Zhou D, Bai Y, Cao T, Zhong C, et al. Single-cell RNA-sequencing atlas reveals the tumor microenvironment of metastatic high-grade serous ovarian carcinoma. *Front Immunol* (2022) 13:923194. doi: 10.3389/fimmu.2022.923194

17. Parashar D, Geethadevi A, Aure MR, Mishra J, George J, Chen C, et al. miRNA551b-3p activates an oncostatin signaling module for the progression of triple-negative breast cancer. *Cell Rep* (2019) 29(13):4389–406. doi: 10.1016/j.celrep.2019.11.085

18. Gao L, Li F, Dong B, Zhang J, Rao Y, Cong Y, et al. Inhibition of STAT3 and ErbB2 suppresses tumor growth, enhances radiosensitivity, and induces mitochondria-dependent apoptosis in glioma cells. *Int J Radiat Oncol Biol Phys* (2010) 77(4):1223–31. doi: 10.1016/j.ijrobp.2009.12.036

19. Zhang C, Peng L, Zhang Y, Liu Z, Li W, Chen S, et al. The identification of key genes and pathways in hepatocellular carcinoma by bioinformatics analysis of high-throughput data. *Med Oncol* (2017) 34(6):101. doi: 10.1007/s12032-017-0963-9

20. Jiang LH, Hao YL, Zhu JW. Expression and prognostic value of HER-2/neu, STAT3 and SOCS3 in hepatocellular carcinoma. *Clin Res Hepatol Gastroenterol* (2019) 43(3):282–91. doi: 10.1016/j.clinre.2018.09.011

21. Shi JH, Guo WZ, Jin Y, Zhang HP, Pang C, Li J, et al. Recognition of HER2 expression in hepatocellular carcinoma and its significance in postoperative tumor recurrence. *Cancer Med* (2019) 8(3):1269–78. doi: 10.1002/cam4.2006

frontiers | Frontiers in Immunology

TYPE Original Research
PUBLISHED 07 June 2023
DOI 10.3389/fimmu.2023.1148317

Check for updates

OPEN ACCESS

EDITED BY
Subhash Kumar Tripathi,
Seattle Children's Research Institute,
United States

REVIEWED BY
Hridayesh Prakash,
Amity University, India
Arpit Mishra,
Benaroya Research Institute, United States
Carlos Rogerio Figueiredo,
University of Turku, Finland

*CORRESPONDENCE
Shweta Joshi
shjoshi@health.ucsd.edu

RECEIVED 19 January 2023
ACCEPTED 02 May 2023
PUBLISHED 07 June 2023

CITATION
Rohila D, Park IH, Pham TV, Jones R, Tapia E, Liu KX, Tamayo P, Yu A, Sharabi AB and Joshi S (2023) Targeting macrophage Syk enhances responses to immune checkpoint blockade and radiotherapy in high-risk neuroblastoma.
Front. Immunol. 14:1148317.
doi: 10.3389/fimmu.2023.1148317

COPYRIGHT
© 2023 Rohila, Park, Pham, Jones, Tapia, Liu, Tamayo, Yu, Sharabi and Joshi. This is an open-access article distributed under the terms of the Creative Commons Attribution License (CC BY). The use, distribution or reproduction in other forums is permitted, provided the original author(s) and the copyright owner(s) are credited and that the original publication in this journal is cited, in accordance with accepted academic practice. No use, distribution or reproduction is permitted which does not comply with these terms.

Targeting macrophage Syk enhances responses to immune checkpoint blockade and radiotherapy in high-risk neuroblastoma

Deepak Rohila[1], In Hwan Park[1], Timothy V. Pham[2], Riley Jones[3], Elisabette Tapia[1], Kevin X. Liu[4], Pablo Tamayo[2], Alice Yu[1,5], Andrew B. Sharabi[3] and Shweta Joshi[1]*

[1]Division of Pediatric Hematology-Oncology, Moores Cancer Center, University of California, San Diego, San Diego, CA, United States, [2]Office of Cancer Genomics, University of California San Diego, San Diego, CA, United States, [3]Department of Radiation Medicine and Applied Sciences, Moores Cancer Center, University of California, San Diego, San Diego, CA, United States, [4]Department of Radiation Oncology, Dana Farber Cancer Institute, Boston, MA, United States, [5]Institute of Stem Cell and Translational Cancer Research, Chang Gung Memorial Hospital at Linkou, Chang Gung University, Taoyuan, Taiwan

Background: Neuroblastoma (NB) is considered an immunologically cold tumor and is usually less responsive to immune checkpoint blockade (ICB). Tumor-associated macrophages (TAMs) are highly infiltrated in NB tumors and promote immune escape and resistance to ICB. Hence therapeutic strategies targeting immunosuppressive TAMs can improve responses to ICB in NB. We recently discovered that spleen tyrosine kinase (Syk) reprograms TAMs toward an immunostimulatory phenotype and enhances T-cell responses in the lung adenocarcinoma model. Here we investigated if Syk is an immune-oncology target in NB and tested whether a novel immunotherapeutic approach utilizing Syk inhibitor together with radiation and ICB could provide a durable anti-tumor immune response in an MYCN amplified murine model of NB.

Methods: Myeloid Syk KO mice and syngeneic MYCN-amplified cell lines were used to elucidate the effect of myeloid Syk on the NB tumor microenvironment (TME). In addition, the effect of Syk inhibitor, R788, on anti-tumor immunity alone or in combination with anti-PDL1 mAb and radiation was also determined in murine NB models. The underlying mechanism of action of this novel therapeutic combination was also investigated.

Results: Herein, we report that Syk is a marker of NB-associated macrophages and plays a crucial role in promoting immunosuppression in the NB TME. We found that the blockade of Syk in NB-bearing mice markedly impairs tumor growth. This effect is facilitated by macrophages that become immunogenic in the absence of Syk, skewing the suppressive TME towards immunostimulation and activating anti-tumor immune responses. Moreover, combining FDA-approved Syk inhibitor, R788 (fostamatinib) along with anti-PDL1 mAb provides a synergistic effect leading to complete tumor regression and durable anti-tumor

immunity in mice bearing small tumors (50 mm^3) but not larger tumors (250 mm^3). However, combining radiation to R788 and anti-PDL1 mAb prolongs the survival of mice bearing large NB9464 tumors.

Conclusion: Collectively, our findings demonstrate the central role of macrophage Syk in NB progression and demonstrate that Syk blockade can "reeducate" TAMs towards immunostimulatory phenotype, leading to enhanced T cell responses. These findings further support the clinical evaluation of fostamatinib alone or with radiation and ICB, as a novel therapeutic intervention in neuroblastoma.

KEYWORDS

macrophage, neuroblastoma, immune suppression, Syk, T cells

Introduction

Neuroblastoma (NB) is the most common pediatric extracranial solid tumor that arises from the sympathetic nervous system (1, 2). Patients with this disease are stratified into low, medium, and high-risk groups based on different molecular and histological parameters among which MYCN amplification is an important determinant of worse prognosis and high-risk disease (3–5). Even after extensive multimodal therapy, chances of long-term survival in the high-risk group are only 40-50% (6–9). Immune checkpoint blockade (ICB) using monoclonal antibodies directed against inhibitory T cell receptor, programmed death 1 (PD1), and its ligand, PDL1, have improved treatment regimens in various solid cancers (10). However, in high-risk NB, the outcome of these therapies is disappointing (11). Hence, novel combination therapies with ICB are needed to improve the outcomes of patients with high-risk disease.

The tumor microenvironment (TME) plays an important role in predicting responses to immunotherapy in solid tumors and our knowledge of the different components of NB TME just started emerging (12). Recently, various groups have utilized computational biology, multiplex immunohistochemistry, and sc-RNA seq approaches to define the immune landscape of NB tumors and have reported the presence of T cells, dendritic cells, B cells, myeloid cells, and natural killer cells (NK) in NB tumors (13–17). These studies have also shown that MYCN amplified (MYCN-A) tumors are immunologically cold with rare infiltration of immune cells. However, immunosuppressive myeloid cells including myeloid derived suppressor cells (MDSCs) and tumor associated macrophages are abundantly infiltrated in the MYCN-A NB tumors and are major mediators of immunosuppression in the tumor microenvironment (TME) of NB (16, 18–20). Among these myeloid cells, TAMs have recently garnered major interest as immunotherapeutic drug targets as they contribute to tumor progression and inhibition of innate and adaptive immune responses that lead to tumor immune escape and resistance to immunotherapies in NB (12, 15, 16, 19–21). Hence, "re-educating" immunosuppressive TAMs into immunogenic phenotype can improve responses to ICB or radiotherapy in high-risk NB (19, 20, 22–26).

Spleen tyrosine kinase (Syk) is a non-receptor tyrosine kinase and is mainly expressed in hematopoietic cells. Syk is an essential regulator of B cell receptor (BCR) and Fc gamma receptor(FcR)-mediated signaling (27–29) and plays a central role in the development of autoimmune diseases and in hematological malignancies such as B cell lymphomas (30). Thus, Syk inhibitors have been tested in several clinical trials for B cell malignancies, mainly chronic lymphoid leukemia (31). R788 (fostamatinib), a prodrug of active metabolite R406, is a specific Syk inhibitor that has shown great efficacy in the preclinical models of chronic lymphocyte leukemia, autoimmune diabetes, rheumatoid arthritis (32–34). R788 was also reported to reduce collagen-induced arthritis in the mouse model (33) that leads to its evaluation in phase 2 clinical trial for patients with rheumatoid arthritis (35). FDA recently approved R788 for the treatment of patients with chronic immune thrombocytopenia (36).

Recent emerging studies have shown that Syk also contributes to tumorigenesis; however, its role in the progression of solid tumors is complex (37–39). A recent report has shown that Syk acts as a tumor promoter in neuroblastoma and Syk inhibitors potentiate the effect of chemotherapeutic drugs on NB cells *in vitro* (40). However, this study did not reveal the presence of Syk in immune cells and the efficacy of Syk inhibitors in suppressing NB growth *in vivo*. Hence, mechanistic details explaining how Syk regulates immune responses in NB need to be further elucidated.

We have recently reported that Syk plays an important role in the immunosuppressive transcriptional programming of macrophages, leading to immune escape in lung adenocarcinoma (41). Herein, our objective was to evaluate the role of Syk in NB growth and anti-tumor immunity. We found that macrophage Syk is a driver of immunosuppression and neuroblastoma growth.

Abbreviations: TME, tumor microenvironment; TAM, tumor-associated macrophage; HIF, hypoxia-inducible factor; TGF beta, transforming growth factor; VEGF, vascular endothelial growth factor; BMDM, bone marrow-derived macrophages; MCSF, macrophage colony-stimulating factor.

Moreover, genetic deletion or pharmacological inhibition of Syk with R788 promotes immunostimulation, increases CD8+ T cells, and decreases tumor progression in a MYCN-driven mouse model of NB. Finally, we demonstrated that R788, in combination with anti-PDL1 mAb treatment, elicit robust anti-tumor effects in mice bearing small (50 mm^3) NB9464 tumors and, when combined with radiation, prolonged survival of mice bearing large NB9464 tumors.

Methods

Human tissues and cell lines

Deidentified human neuroblastoma primary tumor samples were obtained under IRB approval (Protocol 071729) from Rady Children's Hospital, San Diego, California, USA. NB9464 cells were cultured in Dulbecco's modified Eagle's medium (DMEM) containing 10% FBS and M3 base special media as described before (18, 42). Human neuroblastoma cell lines, SKNBE2, IMR32, SKNSH, SH-SY-5Y cells were cultured in DMEM supplemented with 10% FBS, 2 mM L-glutamine, 0.4 mM sodium pyruvate, non-essential amino acids and penicillin/streptomycin as described before (18). All cell lines were routinely tested for mycoplasma.

Immunohistochemistry and immunofluorescence staining

Formalin-fixed paraffin-embedded (FFPE) tissue sections (4μm) of human NB were used for immunohistochemistry (IHC) or immunofluorescence (IF) studies. IHC and IF on paraffin-embedded human samples were performed by the UCSD Histology core facility. For IHC studies, human samples were stained with the following antibodies: anti-CD20 (ab64088, 1:100, Abcam), anti-CD68 (MA5-12407, 1:50, Invitrogen), anti-CD3 (ab16669, 1:500, Abcam) anti-CD4 (ab288724, 1:1000, Abcam), anti-CD8 (70306S, 1:50, Cell Signaling). Antigen retrieval was carried out in citrate buffer (pH 6.0, Vector Laboratories) at 95°C for 30 min. After antigen retrieval, tissue sections were incubated with BLOXALL (Vector Laboratories) for 10 min followed by blocking Blotto (Thermo) for 10 min. Sections were stained with primary antibodies at recommended dilutions in Blotto for 1 hr at room temperature. After washing primary antibodies, the samples were stained with anti-mouse or anti-rabbit secondary antibodies HRP Polymer (Cell IDX for 30 min at RT followed by DAB staining using DAB chromogen (VWR, 95041-478) for 5 min. The images with positive staining were captured using Olympus inverted microscope. The whole area of the tumor was selected as a field of interest, and the area with immunohistochemically positive staining within the field of interest was calculated by the Image J software after setting the thresholds. The results are expressed as the percentage of the positively immunolabelled area within the total area of the tumor. For immunofluorescence staining, antigen retrieval was carried out as described above followed by blocking with Blotto for 10 min. The tissues were then incubated with Syk (clone EP573Y, ab40781, 1:1000, Abcam) and CD68 (MA5-12407, 1:50, Invitrogen) antibodies in Blotto for 1 hr at room temperature. After two washings with 1X TBST buffer, samples were stained with anti-mouse or anti-rabbit HRP polymer-conjugated secondary antibodies (Cell IDX) for 30 min at RT. Tissues were then incubated with Alexa Fluor 488 and Alexa Fluor 594 Tyramide reagents (Thermo) for 10 min. DAPI was used to counterstain the nuclei. The images of fluorescent staining were captured using Keyence BZX-700 fluorescent microscope.

Mouse models and therapeutic treatments

The conditional myeloid Syk knock out mouse strain (Syk^{MC-KO}) and their wild type control (Syk^{MC-WT}) are from the C57BL/6 background and were generated by crossing floxed Syk mice with lysozyme M (LysM) Cre recombinase transgenic mice as described previously (41). 4-6-week-old C57BL/6 mice used in these experiments were obtained from Charles River Laboratories. NB9464 (4 x 10^6) cells were injected subcutaneously into syngeneic 4–6-week-old Syk^{MC-WT} or Syk^{MC-KO} or C57BL/6 mice. For inhibitor experiments, NB9464-bearing mice received 50 mg/kg R788, or 200 μg anti-PDL1 (clone 10F.9G2, Bio-X-cell) or isotype control LTF2 (Bio X cell) or one dose of 10Gy radiation using a SmART radiator.

Macrophage, B cell, and T-cell depletion experiments

For macrophage-depletion experiments, mice bearing NB9464 tumors were treated with 50 mg/kg anti-CSF-1R antibody (clone AFS 98, BioXcell), administered intraperitoneally (ip) every alternate day until tumors were harvested. For B-cell depletion experiments, mice received tail vein injection of 250 μg of ULTRA-LEAF purified anti-mouse CD-20 (clone SA271G2, Bio Legend). For CD8-depletion experiments, mice bearing NB9464 tumors were treated with 200μg of anti-CD8 (clone YTS169.4) from Bio-X-Cell administered ip on day 7, 10 and 13 of tumor inoculation as described before (41).

Single cell preparation and flow cytometric analysis

Single-cell suspensions of NB9464 tumors were prepared for flow cytometry as described before (18). Briefly, NB9464 tumors were isolated, minced, and incubated for 30-45 min at 37°C in a dissociation solution containing Hanks Balanced Salt Solution supplemented with 0.5 mg/ml collagenase IV (Sigma), 0.1 mg/ml hyaluronidase V (Sigma), 0.6 U/ml Dispase II (Roche) and 0.005 MU/ml DNAse I (Sigma). The undigested tissues were removed by

passing through 70 μm nylon mesh and centrifuged at 1500 rpm for 5 min. The red blood cells were lysed using RBC lysis buffer (Pharm Lyse, BD Biosciences, San Jose, CA, USA). Myeloid cells, macrophages, and T cells were enriched using CD11b+, F4/80+, and CD90.2+ microbeads (Miltenyi Biotec, San Diego, CA) on MS columns using manufacturer's instructions. For flow cytometry, single cells isolated from tumors were incubated with a fixable viability stain 510 (BD, Biosciences) followed by incubation with fluorescently labeled antibodies directed against mouse CD45 (30-F11; BD Biosciences), CD11b (M1/70; BD Biosciences), Gr1 (RB6-8C5; BD Biosciences), F4/80 (BM8; BD Biosciences), MHCII (AF6-120.1; BD Biosciences), PDL1 (MIH5, BD Biosciences), CD44 (IM7, BD Biosciences), CD62L (MEL-14, Biolegend), CD3 (145-2C11; eBioscience), CD4 (GK1.5,; eBioscience), CD8 (53-6.7,; eBioscience). Samples were acquired on LSR Fortessa (BD Biosciences) and analyzed withFlowJo 10 (Treestar).

Macrophage adoptive transfer experiments

For macrophage adoptive transfer experiments, $CD11b^{+}$ $F4/80^{+}$ TAMs were isolated from single cell suspensions of NB9464 tumors from $Syk^{MC\text{-}WT}$ or $Syk^{MC\text{-}KO}$ mice by magnetic bead isolation. Purified cells were mixed 1:1 with NB9464 tumor cells, and 2 x 10^{6} total tumor cells were injected into naïve $Syk^{MC\text{-}WT}$ or $Syk^{MC\text{-}KO}$ mice.

Isolation of BMDMs and hypoxia experiments

Bone marrow derived macrophages (BMDMs) were generated from 6-8 week old C57BL/6 mice as described before (43). Briefly, the bone marrow derived cells were collected by flushing the femurs and tibias of the mice with PBS using a 30-gauge needle. Following treatment with red cell lysis buffer, purified cells were cultured in RPMI + 10% FBS + 50 ng/ml MCSF (Peprotech) for 5-7 days before use. For hypoxia experiments, BMDMs were placed in a modulator incubator chamber (Billups-Rothenberg) under 1% O_2 conditions as previously described (41, 43).

Preparation of conditioned media and co-culture experiments

Tumor conditioned media (TCM) was prepared from confluent NB9464 cells. For this, cells were grown to 80% confluence, washed with PBS and media changed to DMEM without FBS for another 48 hrs. TCM was collected after 48 hrs. and used for co-culture experiments. BMDMs from C57BL/6 WT mice were incubated with TCM from NB9464 cells, followed by treatment with R788 for 24 hours and RNA isolation. For some experiments, BMDMs incubated with TCM from NB9464 were given hypoxia for six hrs. in the presence of 500 nM R788, followed by the preparation of nuclear extracts.

Cell viability assays

Cell viability assay was performed on R788-treated NB9464, SKNBE2, and IMR32 cells using AlamarBlue® (Roche) reagent according to manufacturer's protocol. Briefly, 1x 10^{4} cells were seeded in 96 well plates and different concentrations of R788 were added to the culture. After 48 hours, AlamarBlue® was added and plates were incubated at 37°C in 5% CO_2 for 6 hours. Fluorescence signals were read as emission at 590 nm after excitation at 560 nm.

Immunoblotting

CD45- tumor cells, CD45+ immune cells, CD11b+F4/80+ TAMs from NB9464 tumors, BMDMs, CD90.2 + T cells, CD19+ B cells isolated from splenocytes of NB9464-bearing mice and *in vitro* cultured SKNBE2, IMR32, SKNBE2, SH-SY-5Y and NB9464 cells were solubilized in RIPA buffer containing protease and phosphatase inhibitors. Proteins were run on SDS-PAGE gels, electro transferred to nitrocellulose membranes and were immunoblotted with antibodies from Syk (Santa Cruz), β-actin (Santa Cruz).

qPCR analysis

Total RNA was isolated from BMDMs or TAMs from NB9464 tumors or bulk NB9464 tumors using the Qiagen RNAeasy kit (Qiagen, Hilden, Germany), and cDNA was synthesized using iscript cDNA synthesis kit (Bio-Rad, Hercules, CA) according to manufacturer's instructions. SYBR green-based qPCR was performed using murine primers to immune-responsive genes as described earlier (41). The data were quantified with the comparative Ct method for relative gene expression. GAPDH was used as the housekeeping gene.

RNA-sequencing

RNA was harvested from WT BMDMs incubated with NB9464 TCM and TAMs isolated from $Syk^{MC\text{-}WT}$ and $Syk^{MC\text{-}KO}$ mice bearing NB9464 tumors, and R788-treated NB9464 tumors using Qiagen RNAeasy kit (Qiagen, Hilden, Germany). RNA libraries were prepared and sequenced using standard Illumina protocols. RNA sequencing was performed by Novagene Corporation Inc (Sacremento, CA). mRNA profiles were generated by single read deep sequencing, in triplicate, using Illumina HiSeq2000. FASTQ files from sequencing experiments were mapped to mouse genome build mm10 using STAR (44) with default parameters, with reads quantified by Salmon (45) in a standard BCBio RNAseq pipeline. Differential expression analysis was then performed using the DESeq2 R package (46). Apeglm was used for empirical shrinkage effect size estimation (47). P-values were multiple hypothesis corrected using the Benjamini-Hochberg method in the python stats models package (48). All heatmaps showing relative expression

of selected genes were created using the seaborn python package (49) on the Z-scores of the TPM-normalized expression.

Sc-RNA-seq data acquisition, integration, and analyses

Single cell RNA-seq data from TH-MYCN murine tumors (n = 3) were downloaded from accession GSE180101 and analyzed in the R package Seurat. First, anchor genes were used to integrate and normalize all cells across all mice into a single data set that could be clustered and visualized as a UMAP, using default settings. Next, the CIPR package, combined with canonical marker genes in cases where the cluster identity was ambiguous, was used to assign cluster identities with the mmrnaseq reference. All clusters identified as non-immune cells were grouped together as "Tumor" for clarity. Finally, a violin plot of Syk expression across different cell types was generated.

Statistical analysis

Data is represented as mean ± SEM. Differences in survival were determined using Kaplan-Meier method and using the log-rank test. Statistical significance was determined by parametric or nonparametric student's t-test when only two groups were compared or by one-way ANOVA with Tukey's *post-hoc* testing for multiple pairwise testing with more than two groups. In all cases, * $p < 0.05$, ** $p < 0.01$ *** $p < 0.001$, **** $p < 0.0001$, ns = not significant. Statistical analysis was performed using GraphPad Prism V.9 software.

Results

High-risk MYCN-amplified tumors are 'immunologically cold' tumors with abundant infiltration of immunosuppressive macrophages

The immune microenvironment of NB plays an important role in disease progression and predicting responses to immunotherapy (12, 50). However, limited studies are available which exemplify the presence of immune cells in NB tumors (13, 15, 16). To delineate the immune composition of NB tumors, we performed IHC on 18 human patient samples {n = 5, early-stage NB; n = 7, non-MYCN amplified (MYCN-NA) late-stage NB, n = 6, MYCN amplified (MYCN-A) late-stage NB} collected under IRB protocol (071729) (Supplementary Table S1). IHC on human NB patient samples reveals the higher infiltration of CD20+ B cells, CD3+ T cells, CD4+ T cells, and CD8+ T cells in early-stage tumors, followed by decreased or rare infiltration of these cells in late-stage MYCN-NA tumors and MYCN-A tumors respectively (Figures 1A, B). Interestingly, we found increased infiltration of CD68+ macrophages in late-stage MYCN-A tumors compared to early-stage NB and late-stage MYCN-NA tumors (Figures 1A, B).

We implanted murine MYCN-A (NB9464) cells in C57BL/6 mice to further study these dynamics using *in vivo* models. To evaluate the immune composition of these tumors, we used early-stage tumors (tumor volume = 100-200 mm^3) and late-stage tumors (tumor volume = 800-1000mm^3) and evaluated the immune infiltrates using flow cytometry. Like human tumors, late-stage murine MYCN-A tumors also showed decreased infiltration of CD3+ T cells, and CD8+ T cells (Figures 1C, S1, S2). Interestingly, we found higher infiltration of CD11b+ Gr1+ granulocytes and CD19+ B cells in late-stage tumors with no changes in the infiltration of $CD11b^+Gr1^-F4/80^+$ TAMs (Figures 1C, S2). Considering the results from both human and murine tumors, we found that late-stage MYCN-A tumors showed high infiltration of macrophages and B cells. Hence, we investigated if the deletion of either of these cell types can impede NB tumor progression. For this, NB9464 cells were subcutaneously implanted into C57BL/6 mice and were treated with macrophage-depleting anti-CSF1R antibodies (clone AFS98) or B-cell depleting ULTRA-LEAF^{TM} purified anti-CD20 mAb (SA271G2, Biolegend). We found that administration of anti-mouse CSF1R depleted macrophages from the treated mice and suppressed tumor growth in mice implanted with NB9464 tumors (Figures S3A–C). However, administration of ULTRA-LEAF^{TM} purified mAb depleted B cells, but did not suppress NB9464 tumor growth (Figures S3A–C). Taken together, these results suggest that macrophages and not B cells play an important role in the progression of NB, and these results were also validated by other groups (19, 51).

Several studies have shown that macrophages promote tumor growth by facilitating immunosuppression in NB (52, 53). Verhoeven et al, have recently shown that macrophages with an immunosuppressive 'M2' phenotype significantly correlated with decreased survival, while monocytes and macrophages with an immunostimulatory 'M1' phenotype significantly correlated with increased survival (15). Similarly we found that TAMs isolated from late stage murine MYCN-A NB tumors exhibited decreased expression of proinflammatory genes like *Il12*, *Ifng*, and *Tnfa* and increased expression of immunosuppressive genes like *Il1*, *Il10*, and *Arg* (Figures 1D, E). Altogether, these results suggest that immunosuppressive macrophages predominate in late-stage MYCN-A NB tumors, and approaches that aim to polarize macrophages into immunostimulatory phenotype can be used as an effective strategy to treat high-risk NB.

Macrophage Syk fosters neuroblastoma growth

We have recently shown that Syk, a macrophage key kinase, promotes immunosuppression and tumor growth in different syngeneic murine tumor models (41). As macrophages predominate in the NB TME, we asked if Syk is expressed in the NB tumors. To study the accumulation of Syk-positive macrophages in NB, we immunostained human NB patient tissues with SYK and macrophage marker CD68. Immunofluorescence microscopy revealed the presence of SYK+ cells in the tissue sections of both

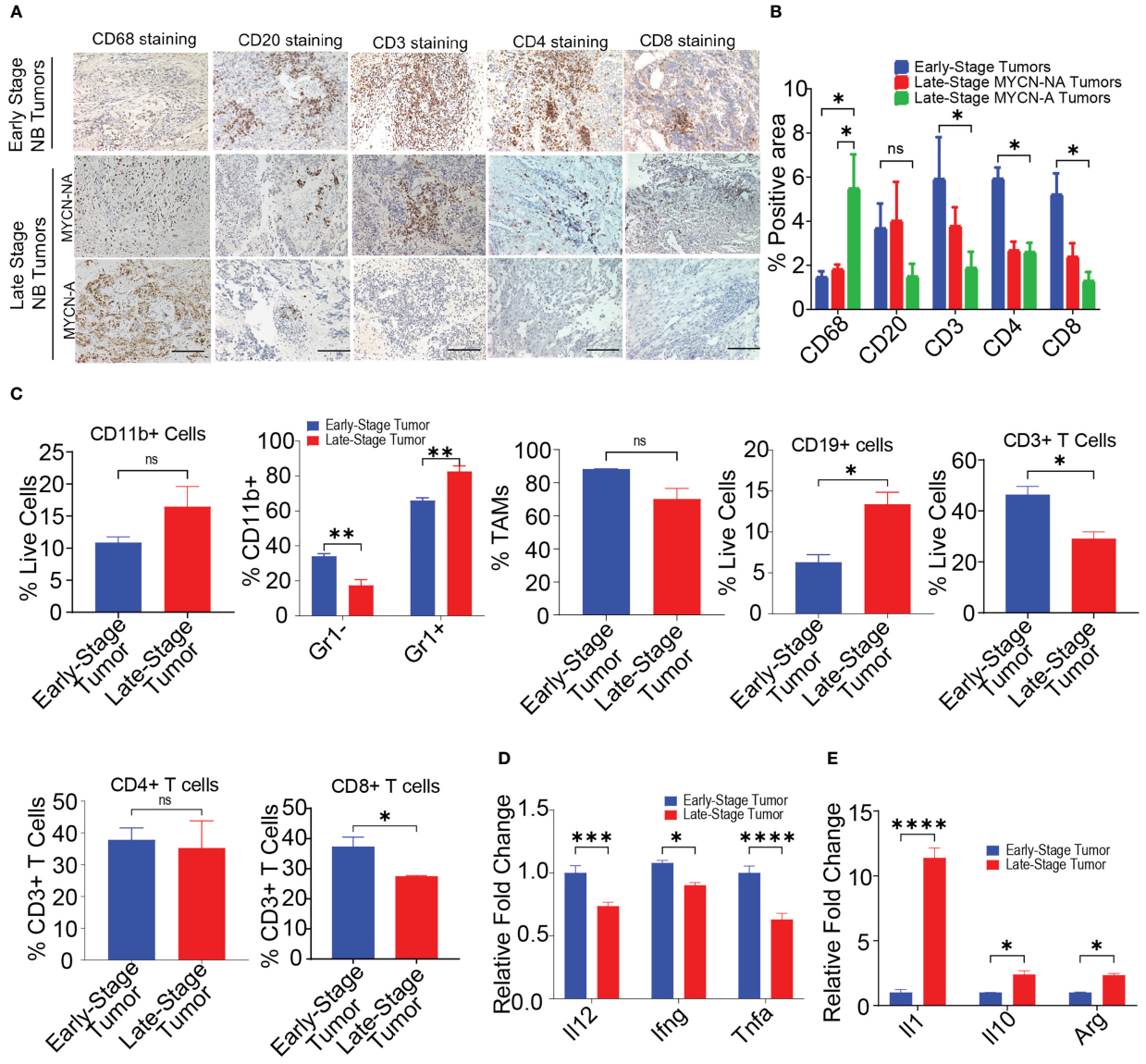


FIGURE 1
MYCN amplified tumors are abundantly infiltrated with immunosuppressive macrophages. **(A, B)** Representative images **(A)** and quantification of positive IHC staining **(B)** for CD68, CD20, CD3, CD4, and CD8 in tissue sections from early-stage MYCN-NA (n = 5), late-stage MYCN-NA (n= 7) and MYCN-A (n = 6) human NB; scale bar = 50μm. **(C)** The percentages of intratumoral CD11b+ myeloid cells, CD11b+Gr1- monocytes and CD11b+Gr1+ granulocytes, CD3+ T cells, CD4+ T cells, and CD8+ T cells in early-stage and late-stage murine NB9464 tumors (n = 4). **(D, E)** Relative mRNA expression of immunostimulatory **(D)** and immunosuppressive genes **(E)** in TAMs isolated from early-stage and late-stage NB9464 tumors (n =3). * $p < 0.05$, ** $p < 0.01$ *** $p < 0.001$, **** $p < 0.0001$, ns, not significant.

MYCN-A and MYCN-NA NB human specimens and immunoreactivity of SYK in CD68+ TAMs (Figure 2A). A recent study has shown that Syk is abundantly present in both MYCN-A and MYCN-NA human NB tumors, but it is expressed explicitly in human MYCN-NA NB cell lines (40). Hence, we evaluated the protein expression of Syk in MYCN-A (SKNBE2, IMR 32) and MYCN-NA (SH-SY-5Y, SKNSH) human NB cell lines and immune cells isolated from the mice bearing NB9464 (MYCN-A) tumors. Contrary to a previous report (40), we did not find the expression of Syk in MYCN-A or MYCN-NA human NB cell lines or murine NB9464 cells (Figure 2B). We found that Syk is specifically expressed in the CD45 + immune cells isolated from the murine NB9464 (MYCN-A) tumors and not in CD45-tumor cells (Figure 2B). Most notably, we found that Syk is specifically expressed in CD11b+F4/80+ TAMs isolated from NB9464 tumors; BMDMs and CD19+ B cells isolated from splenocytes of mice bearing NB9464 tumors (Figure 2B). We found minimal expression of Syk in CD90.2+ T cells isolated from splenocytes of mice bearing NB9464 tumors (Figure 2B). We next analyzed the Syk expression in tumor cells and different immune cells in spontaneous TH-MYCN murine tumors, using the publicly available single cell RNAseq data set (GSE180101). We found that Syk is maximally expressed in macrophages, followed by granulocytes and lymphoid cells, but not in tumor cells and CD8+T cells (Figure 2C). Most notably, SYK expression is also positively correlated with expression of macrophage marker CD68 in a publicly available GEO dataset (GSE62564) (Figure 2D).

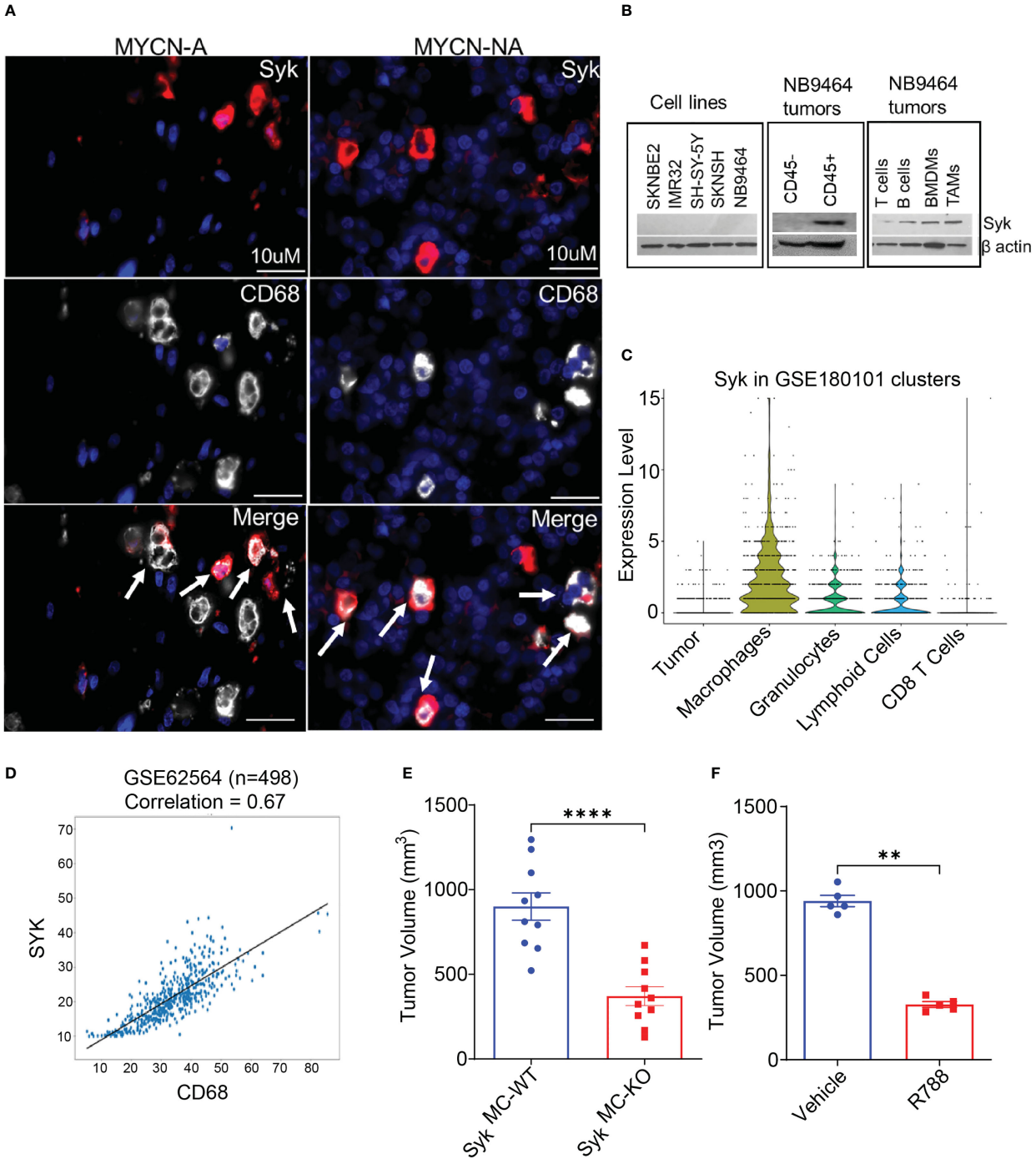


FIGURE 2
Macrophage Syk promotes neuroblastoma growth. **(A)** Figure shows IF staining of SYK and CD68 in human MYCN-A and MYCN-NA NB tissue sections. The tissue sections were stained with DAPI to detect nuclei. The cells stained positive for SYK, and CD68 are shown in the merged figure; scale bar = 10µm. **(B)** Protein expression of Syk in human NB cell lines: SKNBE2, IMR32, SH-SY-5Y and SKN-SH; murine NB9464 cells, CD45- tumor cells, CD45+ immune cells, CD11b+F4/80+ TAMs isolated from NB9464 tumors, and CD19+ B cells, CD90.2+ T cells, BMDMs isolated from splenocytes of NB9464-bearing mice. **(C)** Syk expression in tumor cells and different immune cells in spontaneous TH-MYCN murine tumors, using the publicly available single cell RNAseq data set (GSE180101). **(D)** Correlation between SYK and CD68 was analyzed using a dataset containing 498 NB samples (Cohort SEQC, GSE62564). **(E)** Tumor volume of NB9464 tumors implanted in $Syk^{MC\text{-}WT}$ and $Syk^{MC\text{-}KO}$ mice (n=10), ****p≤ 0.0001. **(F)** Tumor volume of NB9464 tumors treated with 50mg/kg R788 (five times a week) (n = 5), **p≤ 0.01.

As Syk is present in both B cells and macrophages, and deletion of B cells has no impact on NB growth (Figure S3A), we hypothesized that Syk is a marker of neuroblastoma-associated macrophages and might have a functional role in NB growth. To study the contribution of macrophage Syk on immunosuppression and NB tumorigenesis, we studied the growth of subcutaneous NB9464 tumors in conditional myeloid Syk KO mice model, generated as described before (41). We

observed that tumor growth of NB9464 was reproducibly and significantly reduced in $Syk^{MC\text{-}KO}$ animals as compared to that in $Syk^{MC\text{-}WT}$ animals (Figure 2E). We next asked if pharmacological inhibition of Syk can reduce NB growth. Like genetic deletion, pharmacological inhibition of Syk with FDA approved Syk inhibitor, Fostamatinib or R788 also reduced tumor growth in WT mice implanted with NB9464 tumors (Figure 2F). Most notably, we found that Syk inhibition didn't directly affect the survival of MYCN-A NB cells *in vitro* (Figure S4).

Syk blockade can overcome NB-related immunosuppression and enhances T cell activation *in situ*

Since inhibition of myeloid Syk was protective against NB, we asked if blockade of Syk can overcome NB-induced immunosuppression. To explore how Syk blockade affected the immune responses in the tumor- bearing $Syk^{MC\text{-}WT}$ and $Syk^{MC\text{-}KO}$ mice, we analyzed immune response genes in these mice. We found elevated expression levels of proinflammatory mRNAs like *Il12*, *Ifng*, *Tnfa* in the tumors isolated from $Syk^{MC\text{-}KO}$ mice as compared to $Syk^{MC\text{-}WT}$ mice (Figure 3A). As Syk deletion, enhanced immune stimulation in the TME, we next analyzed if Syk blockade has any impact on the infiltration and activation of T cells. We found that Syk blockade stimulated T cell recruitment into NB tumors as CD3+ and CD8+ T cell content was significantly increased in the tumors implanted in $Syk^{MC\text{-}KO}$ mice and in NB9464 tumors treated with R788 (Figures 3B–E). We found a significant decrease in the relative infiltration of CD4+ T cells in the R788-treated tumors (Figure 3E). Hence, we analyzed if R788 has any impact on Treg population in the NB tumors. We did not find any changes in the $CD4^+CD25^+FoxP3^+$ Tregs in the vehicle and R788-treated tumors (Figure 3F). However, in addition to an increase in CD8 T cell frequency, NB-infiltrating CD8+ T cells were markedly activated with a $CD44^+CD62L^-$ effector CD8+ T cells are highly infiltrated in R788-treated tumors (Figure 3G). Moreover, we also found high expression of the T_H1 cytokine *Ifng*, and decreased expression of immunosuppressive cytokines, *Il10* and *Tgfb* in CD90.2+ T cells isolated from R788 treated tumors (Figure 3H). Interestingly, consistent with a cytotoxic effector phenotype, the expression of *Gzm* and *Prf* was also upregulated in the T cells isolated from the R788-treated tumors (Figure 3H). Remarkably, Syk inhibition did not directly activate T cells as neither Syk deletion nor treatment of T cells with R788 affected T cell proliferation *ex vivo* (Figures S5A, B). Collectively these data suggest that targeting Syk can overcome NB-related immunosuppression and enhances cytotoxic CD8+ T cell responses in NB.

Syk inhibition induces immunostimulatory reprogramming of intratumoral macrophages

Since Syk deletion promoted recruitment and activation of T cells in NB tumors with no impact on T cell proliferation *ex vivo* (Figure S5), we hypothesized that myeloid Syk deletion reprograms macrophages to promote immunostimulatory responses *in vivo*. We observed no changes in the infiltration of $CD11b^+Gr1^-$ monocytes, $CD11b^+Gr1^+$ granulocytes, and $CD11b^+Gr1^-F4/80^+$ TAMs in $Syk^{MC\text{-}WT}$ and $Syk^{MC\text{-}KO}$ tumors (Figures 4A, B). Whereas genetic deletion of Syk didn't alter the accumulation of TAMs in the tumors, it enhanced the expression of MHCII+ TAMs in $Syk^{MC\text{-}KO}$ tumors (Figure 4C). In addition, Syk enhanced the expression of immunosuppressive cytokines like *Arg*, *Tgfb*, *Il1*, *Mmp9*, and *Vegf* in TAMs and inhibited expression of pro-inflammatory genes, *Il12*, *Ifng*, and *Nos2* (Figure 4D). These results were also validated by RNA-seq on TAMs from NB9464 tumors which also revealed high expression of genes related to antigen presentation and immune stimulation in $Syk^{MC\text{-}KO}$ mice (Figure 4E). These results indicate that Syk skews the macrophages towards an immunosuppressive phenotype in NB tumors.

To confirm that macrophage Syk controls tumor growth and inhibits adaptive immune responses in NB, TAMs isolated from $Syk^{MC\text{-}WT}$ and $Syk^{MC\text{-}KO}$ were mixed in a 1:1 ratio with NB9464 tumor cells and were adoptively transferred into different $Syk^{MC\text{-}WT}$ and $Syk^{MC\text{-}KO}$ mice (Figure 4F). The adoptive transfer of WT macrophages into $Syk^{MC\text{-}KO}$ mice showed an increase in tumor growth. In contrast, the transfer of Syk KO macrophages suppressed tumor growth in $Syk^{MC\text{-}WT}$ mice (Figure 4F). Similarly, treatment of mice bearing NB9464 tumors with R788 or macrophage depleting anti-CSF1R antibody showed that anti-CSF1R ab or R788 treatment alone significantly blocked tumor growth, but together did not show additive effects on tumor regression (Figure 4G). Most notably, we found that Syk inhibition did not reduce tumor growth in CD8-depleted mice suggesting that Syk inhibition reduces tumor growth by promoting immunostimulatory transcriptional programming in macrophages leading to the recruitment and activation of CD8+ T cells (Figure 4H). These results implicate that Syk blockade remodels immune microenvironment towards immunostimulation, leading to enhanced CD8+ T cell responses in NB.

Syk signaling promotes stabilization of HIF1 alpha to control macrophage polarization

Since Syk induces polarization of macrophages into immunosuppressive phenotype *in vivo*, we investigated if Syk promotes transcriptional programming of macrophages *in vitro*. For this, we incubated BMDMs derived from $Syk^{MC\text{-}WT}$ and $Syk^{MC\text{-}KO}$ or C57BL6 WT mice with tumor-conditioned media (TCM) from NB9464 cells as shown in the schema (Figure 5A). We found that stimulation of $Syk^{MC\text{-}WT}$ and $Syk^{MC\text{-}WT}$ BMDMs with NB9464 TCM increases polarization of macrophages in immunosuppressive phenotype only in $Syk^{MC\text{-}WT}$ BMDMs (Figure 5B). RNA-seq data revealed that incubation of WT BMDMs with NB9464 TCM enhanced the expression of immunosuppressive genes like *Ido1*, *Arg1*, *Il1b*, *Mmp9*, *Il10*, and treatment with R788 significantly decreased the expression of these genes (Figure 5C).

Next, we investigated the mechanism by which Syk regulates macrophage immune responses in neuroblastoma tumors. We have previously shown that Syk controls the stabilization of HIF1α to promote tumor growth and immunosuppression (41). We found

10.3389/fimmu.2023.1148317

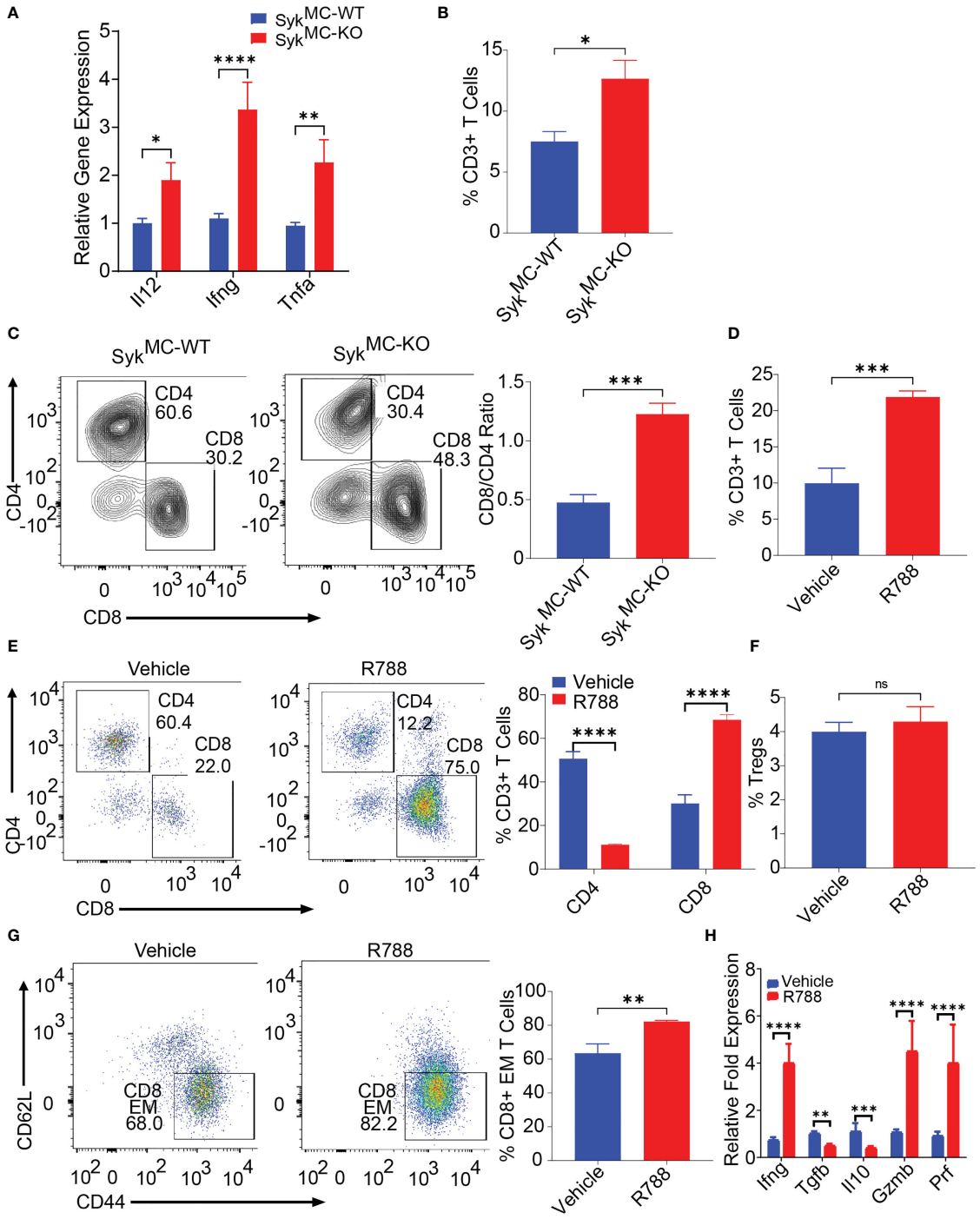


FIGURE 3
Syk blockade can overcome NB-related immunosuppression and enhances T cell infiltration and activation *in situ*. **(A)** mRNA expression of *Il12*, *Ifng*, *Tnfa* in Syk$^{MC\text{-}WT}$ and Syk$^{MC\text{-}KO}$ NB9464 tumors. **(B, C)** The percentages of intratumoral CD3+ T cells **(B)** and CD4+ T cells and CD8+ T cells **(C**, left panel shows FACS plots and right panel shows CD8/CD4 ratio) in Syk$^{MC\text{-}WT}$ and Syk$^{MC\text{-}KO}$ NB9464 tumors. **(D–G)** FACS quantification of CD3+ T cells **(D)** CD4+, and CD8+ T cells **(E**, left panel shows FACS plots and right panel shows quantification), CD4+CD25+FOXP3+ T regs (gated on CD4+ T cells) **(F)**, and CD44+CD62L- effector T cells (gated on CD8+ T cells (**G**, left panel shows FACS plots and right panel shows quantification) in R788 treated NB9464 tumors). **(H)** Relative mRNA expression of *Ifng*, *Il10*, *Tgfb*, *Gzm* and *Prf* in R788-treated NB9464 tumors. ns, not significant. *p < 0.05, ** p < 0.01 *** p < 0.001, **** p < 0.0001.

that BMDMs from Syk$^{MC\text{-}WT}$ mice, when exposed to NB9464 TCM and hypoxic conditions (1% O_2) showed higher stabilization of HIF1α in Syk$^{MC\text{-}WT}$ BMDMs only and not in Syk$^{MC\text{-}KO}$ BMDMs (Figure 5D). Similarly, WT BMDMs incubated with NB9464 TCM and exposed to hypoxia showed higher stabilization of HIF1α and R788 destabilized HIF1α in these BMDMs (Figure 5E). Hence, these results suggest that Syk controls stabilization of HIF1α in macrophages to promote immunosuppression in MYCN-A tumors.

10.3389/fimmu.2023.1148317

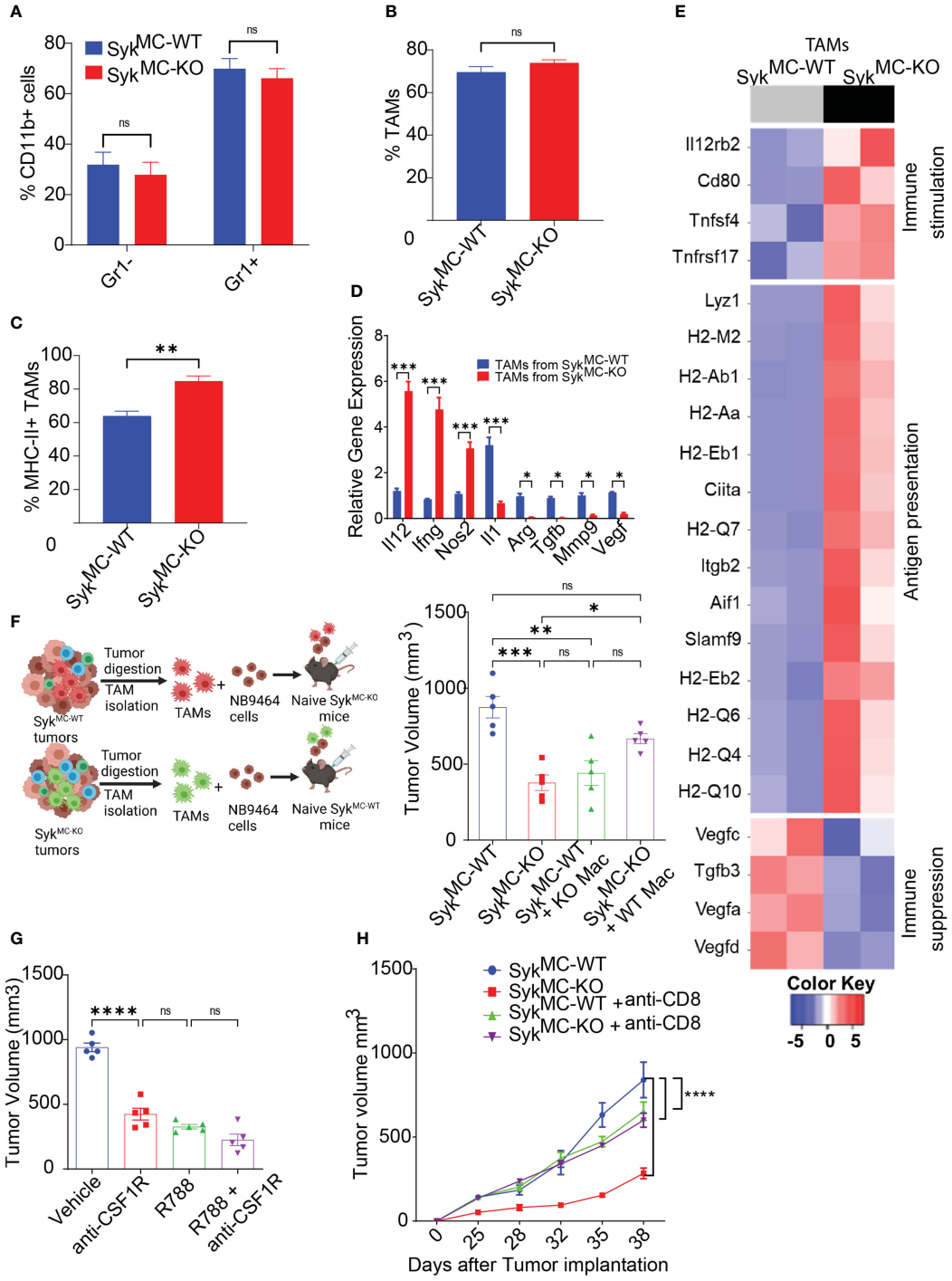


FIGURE 4
Syk inhibition induces immunostimulatory reprogramming of intratumoral macrophages. **(A–C)** The percentages of intratumoral CD11b+Gr1-, CD11b+Gr1+ cells **(A)**, TAMs **(B)**, and MHCII+ TAMs **(C)** in Syk^{MC-WT} and Syk^{MC-KO} NB9464 tumors. **(D)** Relative mRNA expression of immune response genes in TAMs isolated from Syk^{MC-WT} and Syk^{MC-KO} NB9464 tumors. **(E)** Relative mRNA expression of immune response genes in TAMs isolated from Syk^{MC-WT} (grey) and Syk^{MC-KO} (black) NB9464 tumors as determined by RNA sequencing. **(F)** Left panel shows schema of adoptive transfer experiments. Right panel shows tumor volumes of Syk^{MC-WT} and Syk^{MC-KO} NB9464 tumors adoptively transferred with Syk^{MC-WT} and Syk^{MC-KO} TAMs. **(G)** NB9464 tumor volumes of C57BL/6 mice treated with anti-CSF1R mAb and/or R788. **(H)**. NB9464 tumor volumes from Syk^{MC-WT} and Syk^{MC-KO} mice treated with anti-CD8 or isotype control antibodies (n = 5). ns, not significant. * $p < 0.05$, ** $p < 0.01$ *** $p < 0.001$, **** $p < 0.0001$.

Syk inhibition with immune checkpoint blockade is effective in small NB9464 tumors

Unlike some adult cancers, most pediatric cancers are immunologically cold and resistant to ICB. As Syk inhibition has remodeled the TME towards immunostimulation, we next determined if Syk inhibition combined with ICB can improve survival outcomes in NB. In line with previous report (54), we found that CD45- tumor cells exhibited low expression of PDL1 (Figures 6A, S6). Interestingly, we found that PDL1 was expressed on CD11b+F4/80+ TAMs isolated from NB9464 tumors and the expression of PDL1 further increased on R788 treatment (Figure 6A). Hence, we hypothesized that combining anti-PDL1 mAb with R788 can improve anti-tumor immune responses in neuroblastoma. We found that the combination of R788 and anti-PDL1 blockade provided complete tumor regression in 50% (4/8) of the mice (Figures 6B, C) and exhibited disease-free survival past 80 days (Figure 6D). None of the control untreated mice survived after day 45 (Figure 6D). Four mice which were disease-free after treatment were rechallenged with NB9464 tumors after three months following the completion of the last dose of treatment, and 100% (4/4) of mice rejected the tumor growth, and none of these mice developed tumor growth (Figures 6E, F). In contrast, all 6/6 naïve mice challenged in parallel with NB9464 cells showed progressive tumor growth (Figure 6F). These results suggest that Syk inhibitor sensitized NB tumors to ICB and cured the mice bearing small NB9464 tumors.

Radiation combined with Syk inhibition and checkpoint blockade is effective in big NB9464 tumors

Our results showed that R788, together with anti-PDL1 mAb, cured mice bearing small NB9464 tumors (Figure 6). Since, most of the neuroblastoma patients had metastatic disease at the time of diagnosis, we investigated if R788 and anti-PDL1 mAb could cure mice when treatment was initiated at later stage when the tumor volume reached 250 mm^3. This treatment regimen was ineffective at a later-stage, and none of the treated mice was tumor-free (Figures 7A–C). Since, radiation therapy is an important modality in frontline treatment of high-risk NB (55) and previous studies have shown that radiation can enhance the efficacy of ICB in solid tumors (56, 57) by enhancing T cell infiltration in the TME and boosting IFN-gamma mediated immune responses (58–60), we evaluated if combined treatment of R788 along with radiation and anti-PDL1 can provide complete regression in large NB9464 tumors. We found that radiation together with anti-PDL1 or R788 was effective in regressing tumor growth, but the combination of R788 together with anti-PDL1 and radiation significantly decreased tumor burden and prolonged overall survival of mice bearing big NB tumors (Figures 7B, C). The median survival time of different treatment groups were: vehicle mice: 37 days, R788 + anti-PDL1 mAb: 44 days, Rad + R788: 57.5 days, Rad + PDL1: 58 days, and Rad + R788 + anti-PDL1: 84 days (Figures 7B, C). RNA-seq data also shows that Rad + R788 + anti-PDL1 treated NB9464 tumors showed increased expression of genes related to antigen presentation, T cell activation, immune stimulation, IFN gamma activation and decreased expression of immunosuppressive genes as compared to Vehicle, R788 + anti-PDL1 mAb treated tumors (Figure 7D). Taken together, these results suggest that R788 has a capacity to remodel the immune "cold" tumors into immune "hot" tumors by reprogramming the macrophages and together with anti-PDL1mAb and radiation it can regress tumor growth in high-risk MYCN-A NB (Figure 7E).

Discussion

Tumor associated macrophages (TAMs) are abundantly infiltrated in human and murine NB tumors and play an instrumental role in NB progression and impeding responses to ICB (15, 19, 20). Based on our previous findings that macrophage Syk promotes immunosuppression in lung adenocarcinoma (41), herein, we investigated the functional significance of macrophage Syk in neuroblastoma tumorigenesis. We demonstrated that genetic deletion or pharmacological inhibition of Syk using R788, skews macrophages in a pro-inflammatory state that leads to further changes in the TME by recruitment of CD8+ T cells and increased cytotoxicity against neuroblastoma tumor cells. Furthermore, combination treatment of R788 and anti-PDL1 mAb leads to complete tumor regression in 50% mice with durable anti-tumor immunity in small NB9464 tumors but not larger NB9464 tumors. However, combining radiation with R788 and anti-PDL1 mAb extended the survival of mice bearing large NB9464 tumors. Taken together, these data support Syk inhibition alone and in concert with anti-PDL1 mAb and radiation as a novel therapeutic strategy in neuroblastoma.

Our present analysis of the TME in human patient samples and murine NB models revealed an immunosuppressive TME with decreased infiltration of CD8+ T cells and increased infiltration of immunosuppressive TAMs in late-stage tumors. This data is in line with recent sc-RNA seq analysis performed on human NB patient samples which shows that Mono 2 (monocytes with high expression of genes related to antigen presentation and immunostimulation) was associated with better survival in high-risk neuroblastoma (15). However, Macro 1 (macrophages with immunosuppressive M2 gene signature) was significantly correlated with decreased survival. Furthermore, previous studies have shown that targeting immunosuppressive macrophages by using anti-CSF1R antibodies (19, 25) or stimulating the effector macrophages by using anti-CD40 antibodies (23, 24) have significantly decreased neuroblastoma growth in MYCN driven NB mouse models, suggesting that "re-educating" TAMs into immunostimulatory phenotype can be an effective strategy to improve responses to immunotherapy in NB.

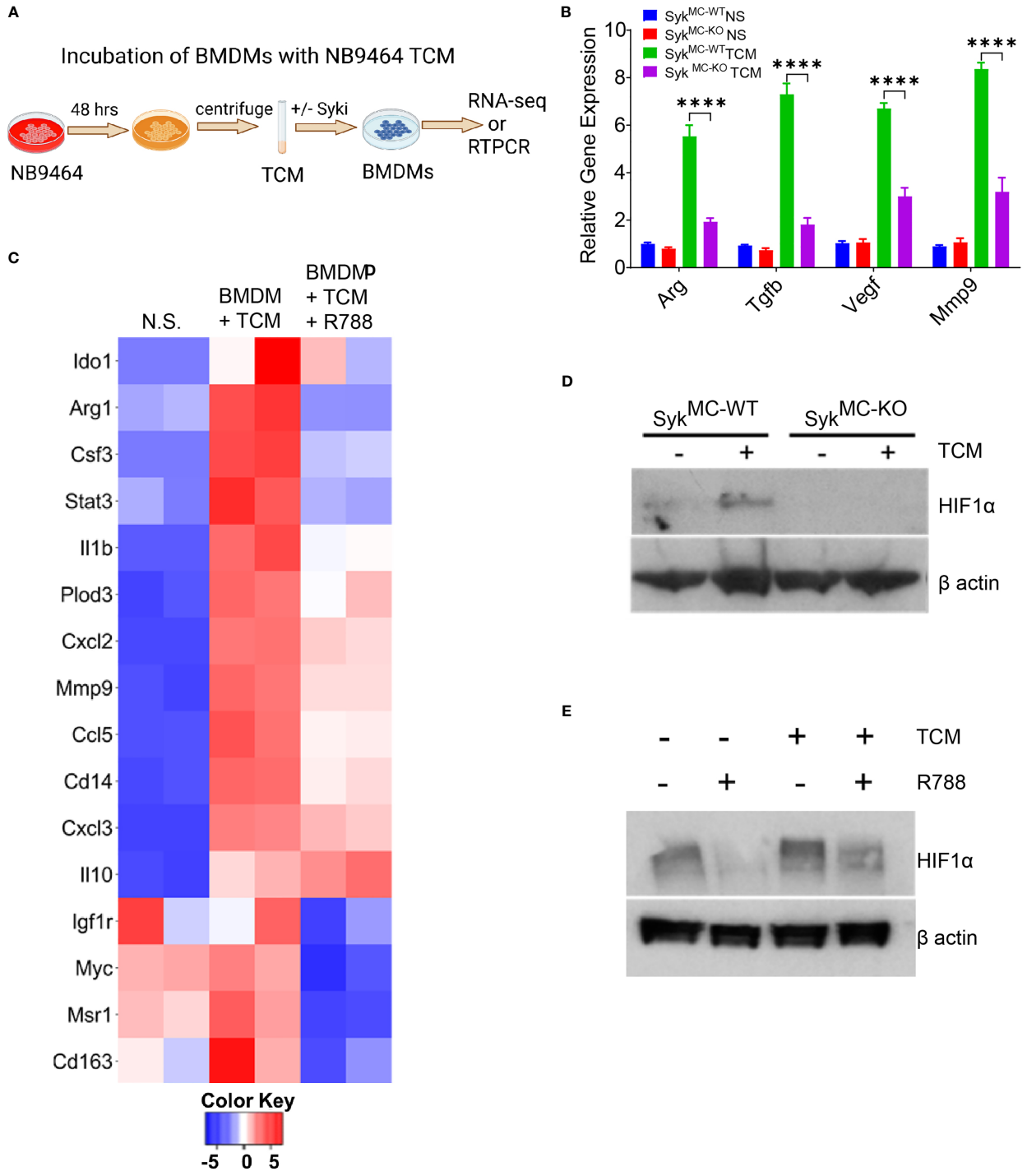


FIGURE 5
Syk signaling promotes stabilization of HIF1 alpha to control macrophage polarization. **(A)** Schema showing TCM experimental details. **(B)** mRNA expression of immunosuppressive genes in BMDMs incubated with NB9464 TCM. **** p< 0.0001. **(C)** Relative mRNA expression of genes related to immune suppression in BMDMs incubated with NB9464 TCM and treated with 500 nM R788 as determined by RNA sequencing. **(D, E)** Western blot analysis of nuclear extracts for HIF1α from Syk^{MC-WT} and Syk^{MC-KO} BMDMs incubated with NB9464 TCM **(D)** or WT BMDMs incubated with NB9464 TCM and treated with 500 nM R788 **(E)** and exposed to hypoxic conditions (1% O_2).

A recent study found that Syk inhibition decreases cell viability of NB tumor cells that express Syk and potentiates cytotoxicity of chemotherapy drugs *in vitro* (40). In contrast to this study, we found that Syk is not expressed by human and murine NB cell lines, and Syk inhibition has no or modest effect on the viability of these cells. We found that macrophage-Syk is sufficient to promote NB growth and immunosuppression.

Syk is also reported to be present in dendritic cells and has a role in priming cytotoxic T-cell responses (61, 62). While, we have not tested the impact of Syk inhibition on DC's capacity to generate CD8+ T cell

10.3389/fimmu.2023.1148317

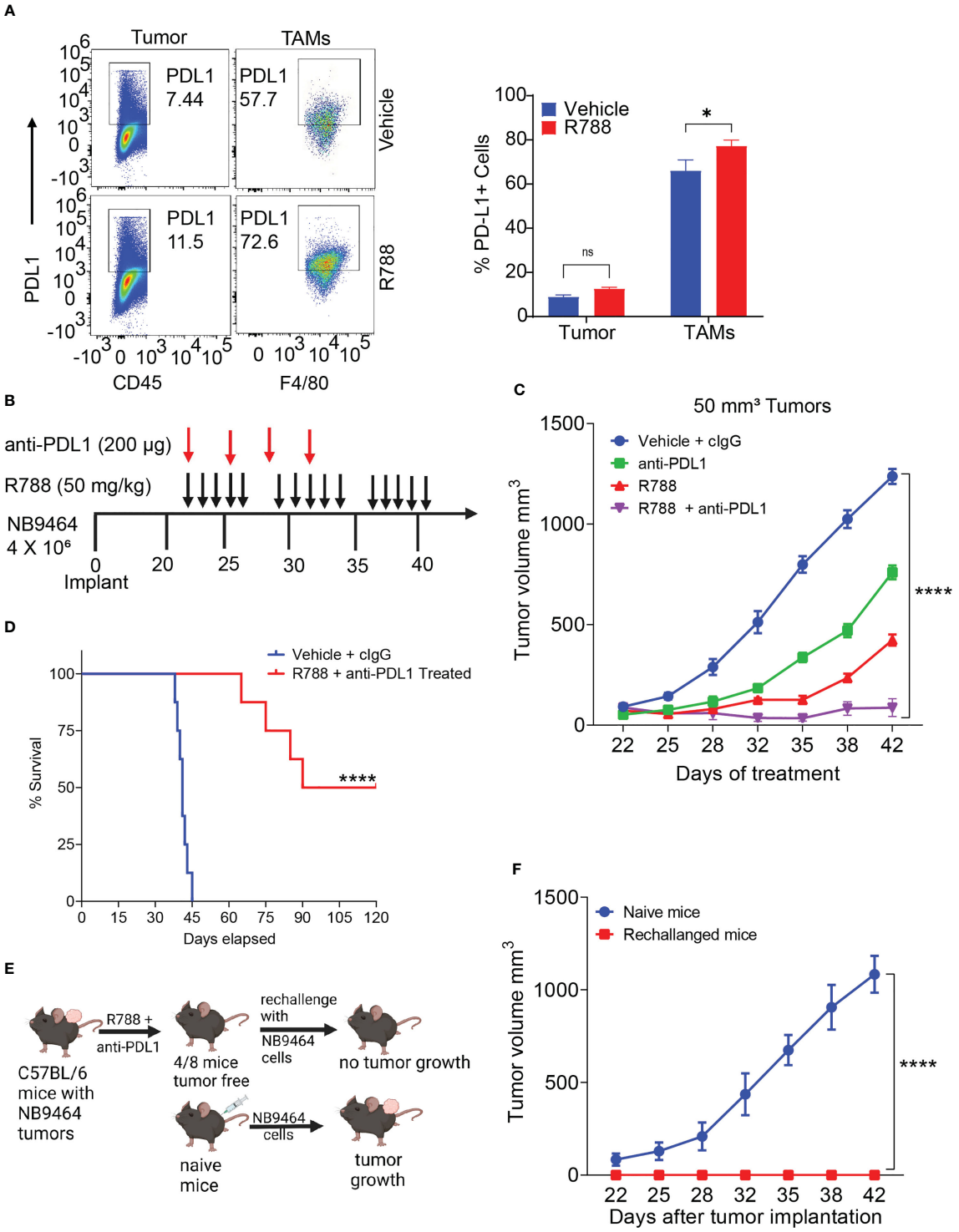


FIGURE 6
Syk inhibition synergizes with checkpoint blockade to enhance anti-tumor immune responses in small neuroblastoma tumors. **(A)** Select pseudo-color plots (left panel) and quantification (right panel) of PDL1 in CD45- tumor cells and CD11b+F4/80+ TAMs from vehicle and R788-treated NB9464 tumors. ns, not significant. *$p < 0.05$. **(B)** NB9464 tumors were implanted into C57 BL/6 mice and treated with different inhibitors according to the depicted schema. **(C)** Tumor volume of NB9464 tumors implanted in C57BL/6 WT mice treated with either R788 or PDL1 or in combination, as shown in **(B)**. **(D)** Kaplan Meir survival curves of mice treated with R788 and anti-PDL1 mAb. **(E)** Schema showing the strategy to rechallenge the cured mice. **(F)** Tumor volume of NB9464 tumors implanted in naïve C57BL/6 mice (n = 6) and cured mice (n = 4) from Figure **(C)** **** $p < 0.0001$.

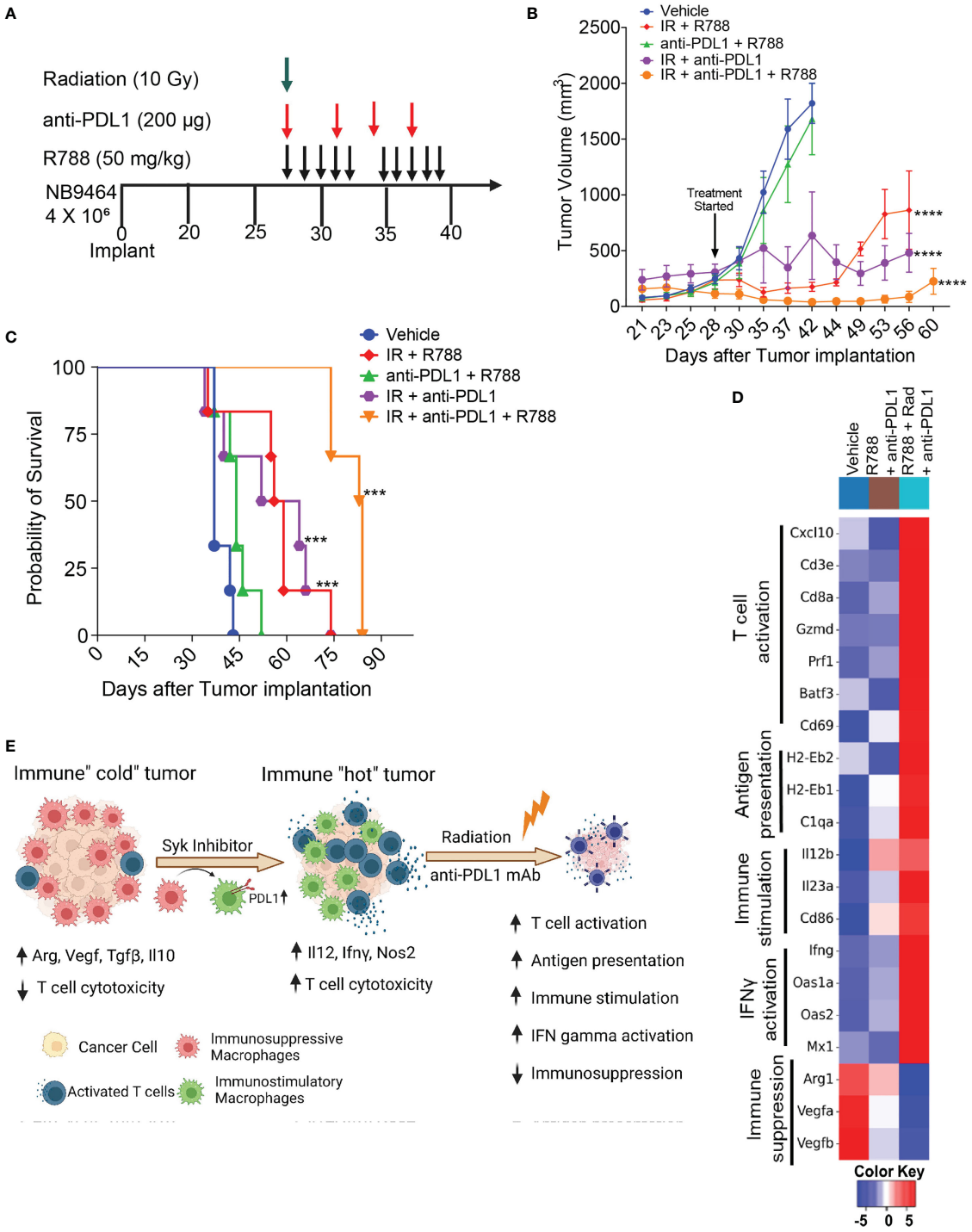


FIGURE 7
Radiation combined with R788 and anti-PDL1 mAb improved survival in mice bearing large NB9464 tumors. **(A)** NB9464 tumors implanted in C57BL/6 mice and treated according to the depicted schema. **(B)** Tumor volume of NB9464 tumors treated as mentioned in **(A)**, **** $p < 0.0001$. **(C)** Kaplan Meir survival curves of mice treated with the combination of R788 or anti-PDL1 mAb or radiation. *** $p < 0.001$. **(D)** Heat map of immune-related mRNA expression in bulk NB9464 tumors treated with R788, anti-PDL1 mAb and radiation. **(E)** Graphical abstract showing that R788 can turn immune "cold" tumors into "hot" inflamed tumors, thus enhancing the efficacy of anti-PDL1 blockade and radiation in high-risk NB.

responses, we found the predominant role of macrophage Syk in controlling tumor growth and inhibition of adaptive immune responses in the neuroblastoma model. We further confirm that macrophage Syk controls HIF1α stabilization to promote tumor growth and immunosuppression. HIF1α is previously reported to be involved in immunosuppressive macrophage differentiation and suppression of T cell function (63). Hence, studies combining R788 with VEGF inhibitors are warranted in the near future.

While immune checkpoint inhibitors, such as PD1 or PDL1, have been shown to improve outcomes in various adult tumors,

their efficacy in pediatric tumors has thus far been limited (11, 64). Several studies have shown that PDL1 is expressed in NB tumors and correlates with worse outcomes (65, 66). Interestingly, a recent study has shown that chemotherapy significantly increased expression of PDL1 in NB tumors and specifically increased the expression of PDL1 in TAMs (54). We also found that TAMs from NB9464 tumors highly express PDL1 and R788 treatment further increased the expression of PDL1 in TAMs.

Studies have also found that treatment with anti-PDL1 and/or PD-1 antibodies in concert with anti-CD4 antibody, anti-CTLA4 mAb, anti-GD2 antibody, or a CSF-R1 inhibitor can significantly decrease tumor growth compared to monotherapy alone in neuroblastoma models *in vivo* (19, 54, 67, 68). We found that combination treatment with R788 and anti-PDL1 antibody results in complete tumor regression with durable anti-tumor immunity with rechallenge experiments *in vivo*. However, this treatment regimen was ineffective in mice bearing large NB9464 tumors. In support of this data, a recent study has shown that treatment of small NB9464-GD2 tumors (50 mm^3) with extensive treatment regimen including radiation, hu14.18-IL2 immunocytokine (IC), anti-CD40, CpG, anti-CTLA-4 cured the mice but the treatment of large tumors (100 mm^3) with this regimen only prolonged the survival with no mice cured (22, 26). However, we found that using R788 with radiation and anti-PDL1 mAb was effective in prolonging the survival of mice bearing NB9464 tumors even when started treatment at a later stage. Radiation may be functioning here to cytoreduce tumor volume as well as modulate the residual TME. Future studies will aim to identify other immunotherapeutic combinations that can cure mice with large tumors.

In conclusion, our results provide evidence that Syk is a marker of NB-associated macrophages, and therapeutic targeting of Syk with R788 reshapes the TME and sensitizes NB tumors to anti-PDL1 mAb. The data presented in this manuscript suggest that FDA-approved Syk inhibitor, fostamatinib, in combination with anti-PDL1 mAb and radiation, may be an effective strategy for NB and should be further explored in clinical investigations.

Data availability statement

Data are available on reasonable request. The sequencing data and processed expression matrix have been deposited at the Gene Expression Omnibus with access number GSE224020, GSE224021, GSE224024, GSE224025. The code is avaialble on GitHub and can be accessed at: https://github.com/tpham2654/Neuroblastoma-SYK-RNAseq. The full list of differentially expressed genes for each experiment is available in Supplementary Table S2.

Ethics statement

The use of human tissues was approved under the auspices of UCSD Institutional Review (Protocol 071729). Informed consent was obtained from all the patients. The deidentified biological samples were used under "exempt category 4" for research. All procedures involving animals were approved by the Institutional Animal Care and Use Committee of the University of California San Diego (Protocol S09398).

Author contributions

SJ and DR conceived the idea and designed the study. DR, IP, TP, ET, and RJ performed experiments, analyzed, and interpreted data. IP and ET assisted in animal studies, including drug administration and tumor measurements. TP and PT assisted with RNA-seq data analysis and statistical analyses. RJ and AS assisted in designing radiation experiments. SJ, AS, AY, KL, and PT participated in the discussion of the data and contributed to the writing of the manuscript. All authors approved the final manuscript. SJ supervised the entire study and is the guarantor of this publication. All authors contributed to the article and approved the submitted version.

Funding

This work was supported by NIH grants K22 CA229594, R01NS122835 to SJ and Pediatric Padres Pedal award to SJ and AS. KL is funded by the National Institutes of Health Loan Repayment Program L40 CA264321. This work was also supported by NIH grants: R01CA154480, R01CA121941, R01CA247551, U01CA176058, R01DE026870, U24CA220341, U24CA248457, R01CA226803, U01CA217885 and R01CA109467, a State of California Initiative to Advance Precision Medicine award (OPR18112) to PT and the GCBSR shared resources at the UCSD Moores Cancer center P30CA023100.

Acknowledgments

The authors thank Dr. Paul Sondel (University of Wisconsin, Madison) for NB9464 cells. Cartoon figures were created with the Bio Render online platform (BioRender.com).

Conflict of interest

AS reports being a paid consultant/advisory board member for AstraZeneca, Primmune, Merck, and Jounce Therapeutics; reports receiving commercial research grants from Varian Medical Systems and Pfizer; holds ownership interest in Toragen Inc. outside of submitted work.

The remaining authors declare that the research was conducted in the absence of any commercial or financial relationships that could be construed as a potential conflict of interest.

Publisher's note

All claims expressed in this article are solely those of the authors and do not necessarily represent those of their affiliated organizations, or those of the publisher, the editors and the reviewers. Any product that may be evaluated in this article, or claim that may be made by its manufacturer, is not guaranteed or endorsed by the publisher.

Supplementary material

The Supplementary Material for this article can be found online at: https://www.frontiersin.org/articles/10.3389/fimmu.2023.1148317/full#supplementary-material

References

1. Matthay KK, Maris JM, Schleiermacher G, Nakagawara A, Mackall CL, Diller L, et al. Neuroblastoma. *Nat Rev Dis Primers* (2016) 2:16078. doi: 10.1038/nrdp.2016.78

2. Brodeur GM. Neuroblastoma: biological insights into a clinical enigma. *Nat Rev Cancer* (2003) 3:203–16. doi: 10.1038/nrc1014

3. Sokol E, Desai AV. The evolution of risk classification for neuroblastoma. *Children (Basel)* (2019) 6. doi: 10.3390/children6020027

4. Pinto NR, Applebaum MA, Volchenboum SL, Matthay KK, London WB, Ambros PF, et al. Advances in risk classification and treatment strategies for neuroblastoma. *J Clin Oncol* (2015) 33:3008–17. doi: 10.1200/JCO.2014.59.4648

5. Seeger RC, Brodeur GM, Sather H, Dalton A, Siegel SE, Wong KY, et al. Association of multiple copies of the n-myc oncogene with rapid progression of neuroblastomas. *N Engl J Med* (1985) 313:1111–6. doi: 10.1056/NEJM198510313131802

6. Campbell K, Gastier-Foster JM, Mann M, Naranjo AH, Van Ryn C, Bagatell R, et al. Association of MYCN copy number with clinical features, tumor biology, and outcomes in neuroblastoma: a report from the children's oncology group. *Cancer* (2017) 123:4224–35. doi: 10.1002/cncr.30873

7. Park JR, Kreissman SG, London WB, Naranjo A, Cohn SL, Hogarty MD, et al. Effect of tandem autologous stem cell transplant vs single transplant on event-free survival in patients with high-risk neuroblastoma: a randomized clinical trial. *JAMA* (2019) 322:746–55. doi: 10.1001/jama.2019.11642

8. Mallepalli S, Gupta MK, Vadde R. Neuroblastoma: an updated review on biology and treatment. *Curr Drug Metab* (2019) 20:1014–22. doi: 10.2174/1389200221666191226102231

9. MacFarland S, Bagatell R. Advances in neuroblastoma therapy. *Curr Opin Pediatr* (2019) 31:14–20. doi: 10.1097/MOP.0000000000000711

10. Joshi S, Durden DL. Combinatorial approach to improve cancer immunotherapy: rational drug design strategy to simultaneously hit multiple targets to kill tumor cells and to activate the immune system. *J Oncol* (2019) 2019:5245034. doi: 10.1155/2019/5245034

11. Kabir TF, Chauhan A, Anthony L, Hildebrandt GC. Immune checkpoint inhibitors in pediatric solid tumors: status in 2018. *Ochsner J* (2018) 18:370–6. doi: 10.31486/toj.18.0055

12. Joshi S. Targeting the tumor microenvironment in neuroblastoma: recent advances and future directions. *Cancers (Basel)* (2020) 12. doi: 10.3390/cancers12082057

13. Wienke J, Dierselhuis MP, Tytgat GAM, Kunkele A, Nierkens S, Molenaar JJ. The immune landscape of neuroblastoma: challenges and opportunities for novel therapeutic strategies in pediatric oncology. *Eur J Cancer* (2021) 144:123–50. doi: 10.1016/j.ejca.2020.11.014

14. Melaiu O, Chierici M, Lucarini V, Jurman G, Conti LA, De Vito R, et al. Cellular and gene signatures of tumor-infiltrating dendritic cells and natural-killer cells predict prognosis of neuroblastoma. *Nat Commun* (2020) 11:5992. doi: 10.1038/s41467-020-19781-y

15. Verhoeven BM, Mei S, Olsen TK, Gustafsson K, Valind A, Lindstrom A, et al. The immune cell atlas of human neuroblastoma. *Cell Rep Med* (2022) 3:100657. doi: 10.1016/j.xcrm.2022.100657

16. Costa A, Thirant C, Kramdi A, Pierre-Eugene C, Louis-Brennetot C, Blanchard O, et al. Single-cell transcriptomics reveals shared immunosuppressive landscapes of mouse and human neuroblastoma. *J Immunother Cancer* (2022) 10. doi: 10.1136/jitc-2022-004807

17. Masih KE, Wei JS, Milewski D, Khan J. Exploring and targeting the tumor immune microenvironment of neuroblastoma. *J Cell Immunol* (2021) 3:305–16.

18. Ishfaq M, Pham T, Beaman C, Tamayo P, Yu AL, Joshi S. BTK inhibition reverses mdsc-mediated immunosuppression and enhances response to anti-pdl1 therapy in neuroblastoma. *Cancers (Basel)* (2021) 13. doi: 10.3390/cancers13040817

19. Mao Y, Eissler N, Blanc KL, Johnsen JI, Kogner P, Kiessling R. Targeting suppressive myeloid cells potentiates checkpoint inhibitors to control spontaneous neuroblastoma. *Clin Cancer Res* (2016) 22:3849–59. doi: 10.1158/1078-0432.CCR-15-1912

20. Liu KX, Joshi S. "Re-educating" tumor associated macrophages as a novel immunotherapy strategy for neuroblastoma. *Front Immunol* (2020) 11:1947.

21. Hadjidaniel MD, Muthugounder S, Hung LT, Sheard MA, Shirinbak S, Chan RY, et al. Tumor-associated macrophages promote neuroblastoma *via* STAT3 phosphorylation and up-regulation of c-MYC. *Oncotarget* (2017) 8:91516–29. doi: 10.18632/oncotarget.21066

22. Voeller J, Erbe AK, Slowinski J, Rasmussen K, Carlson PM, Hoefges A, et al. Combined innate and adaptive immunotherapy overcomes resistance of immunologically cold syngeneic murine neuroblastoma to checkpoint inhibition. *J Immunother Cancer* (2019) 7:344. doi: 10.1186/s40425-019-0823-6

23. Buhtoiarov IN, Sondel PM, Wigginton JM, Buhtoiarova TN, Yanke EM, Mahvi DA, et al. Anti-tumour synergy of cytotoxic chemotherapy and anti-CD40 plus CpG-ODN immunotherapy through repolarization of tumour-associated macrophages. *Immunology* (2011) 132:226–39. doi: 10.1111/j.1365-2567.2010.03357.x

24. Lum HD, Buhtoiarov IN, Schmidt BE, Berke G, Paulnock DM, Sondel PM, et al. *In vivo* CD40 ligation can induce T-cell-independent antitumor effects that involve macrophages. *J Leukoc Biol* (2006) 79:1181–92. doi: 10.1189/jlb.0405191

25. Webb MW, Sun J, Sheard MA, Liu WY, Wu HW, Jackson JR, et al. Colony stimulating factor 1 receptor blockade improves the efficacy of chemotherapy against human neuroblastoma in the absence of T lymphocytes. *Int J Cancer* (2018) 143:1483–93. doi: 10.1002/ijc.31532

26. Aiken TJ, Erbe AK, Zebertavage L, Komjathy D, Feils AS, Rodriguez M, et al. Mechanism of effective combination radio-immunotherapy against 9464D-GD2, an immunologically cold murine neuroblastoma. *J Immunother Cancer* (2022) 10. doi: 10.1136/jitc-2022-004834

27. Berton G, Mocsai A, Lowell CA. Src and syk kinases: key regulators of phagocytic cell activation. *Trends Immunol* (2005) 26:208–14. doi: 10.1016/j.it.2005.02.002

28. Pradip D, Peng X, Durden DL. Rac2 specificity in macrophage integrin signaling: potential role for syk kinase. *J Biol Chem* (2003) 278:41661–9. doi: 10.1074/jbc.M306491200

29. Mocsai A, Ruland J, Tybulewicz VL. The SYK tyrosine kinase: a crucial player in diverse biological functions. *Nat Rev Immunol* (2010) 10:387–402. doi: 10.1038/nri2765

30. Geahlen RL. Getting syk: spleen tyrosine kinase as a therapeutic target. *Trends Pharmacol Sci* (2014) 35:414–22. doi: 10.1016/j.tips.2014.05.007

31. Liu D, Mamorska-Dyga A. Syk inhibitors in clinical development for hematological malignancies. *J Hematol Oncol* (2017) 10:145. doi: 10.1186/s13045-017-0512-1

32. Suljagic M, Longo PG, Bennardo S, Perlas E, Leone G, Laurenti L, et al. The syk inhibitor fostamatinib disodium (R788) inhibits tumor growth in the emu- TCL1 transgenic mouse model of CLL by blocking antigen-dependent b-cell receptor signaling. *Blood* (2010) 116:4894–905. doi: 10.1182/blood-2010-03-275180

33. Pine PR, Chang B, Schoettler N, Banquerigo ML, Wang S, Lau A, et al. Inflammation and bone erosion are suppressed in models of rheumatoid arthritis following treatment with a novel syk inhibitor. *Clin Immunol* (2007) 124:244–57. doi: 10.1016/j.clim.2007.03.543

34. Colonna L, Catalano G, Chew C, D'Agati V, Thomas JW, Wong FS, et al. Therapeutic targeting of syk in autoimmune diabetes. *J Immunol* (2010) 185:1532–43. doi: 10.4049/jimmunol.1000983

35. Weinblatt ME, Kavanaugh A, Genovese MC, Musser TK, Grossbard EB, Magilavy DB. An oral spleen tyrosine kinase (Syk) inhibitor for rheumatoid arthritis. *N Engl J Med* (2010) 363:1303–12. doi: 10.1056/NEJMoa1000500

36. Connell NT, Berliner N. Fostamatinib for the treatment of chronic immune thrombocytopenia. *Blood* (2019) 133:2027–30. doi: 10.1182/blood-2018-11-852491

37. Luangdilok S, Box C, Patterson L, Court W, Harrington K, Pitkin L, et al. Syk tyrosine kinase is linked to cell motility and progression in squamous cell carcinomas of the head and neck. *Cancer Res* (2007) 67:7907–16. doi: 10.1158/0008-5472.CAN-07-0331

38. Ghotra VP, He S, van der Horst G, Nijhoff S, de Bont H, Lekkerkerker A, et al. SYK is a candidate kinase target for the treatment of advanced prostate cancer. *Cancer Res* (2015) 75:230–40. doi: 10.1158/0008-5472.CAN-14-0629

39. Krisenko MO, Geahlen RL. Calling in SYK: SYK's dual role as a tumor promoter and tumor suppressor in cancer. *Biochim Biophys Acta* (2015) 1853:254–63. doi: 10.1016/j.bbamcr.2014.10.022

40. Tummler C, Dumitriu G, Wickstrom M, Coopman P, Valkov A, Kogner P, et al. SYK inhibition potentiates the effect of chemotherapeutic drugs on neuroblastoma cells in vitro. *Cancers (Basel)* (2019) 11. doi: 10.3390/cancers11020202

41. Joshi S, Liu KX, Zulcic M, Singh AR, Skola D, Glass CK, et al. Macrophage syk-PI3Kgamma inhibits antitumor immunity: SRX3207, a novel dual syk-PI3K inhibitory chemotype relieves tumor immunosuppression. *Mol Cancer Ther* (2020) 19:755–64. doi: 10.1158/1535-7163.MCT-19-0947

42. Joshi S, Singh AR, Zulcic M, Bao L, Messer K, Ideker T, et al. Rac2 controls tumor growth, metastasis and M1-M2 macrophage differentiation in vivo. *PloS One* (2014) 9:e95893. doi: 10.1371/journal.pone.0095893

43. Joshi S, Singh AR, Zulcic M, Durden DL. A macrophage-dominant PI3K isoform controls hypoxia-induced HIF1alpha and HIF2alpha stability and tumor growth, angiogenesis, and metastasis. *Mol Cancer Res* (2014) 12:1520–31. doi: 10.1158/1541-7786.MCR-13-0682

44. Dobin A, Davis CA, Schlesinger F, Drenkow J, Zaleski C, Jha S, et al. STAR: ultrafast universal RNA-seq aligner. *Bioinformatics* (2013) 29:15–21. doi: 10.1093/bioinformatics/bts635

45. Patro R, Duggal G, Love MI, Irizarry RA, Kingsford C. Salmon provides fast and bias-aware quantification of transcript expression. *Nat Methods* (2017) 14:417–9. doi: 10.1038/nmeth.4197

46. Love MI, Huber W, Anders S. Moderated estimation of fold change and dispersion for RNA-seq data with DESeq2. *Genome Biol* (2014) 15:550. doi: 10.1186/s13059-014-0550-8

47. Anqi Zhu JGI, Love MI. Heavy-tailed prior distributions for sequence count data: removing the noise and preserving large differences. *Bioinformatics* (2019) 35:2084–92. doi: 10.1093/bioinformatics/bty895

48. Perktold J, Seabold S. Statsmodels: econometric and statistical modeling with Python, in: *PROC. OF THE 9th PYTHON IN SCIENCE CONF. (SCIPY 2010)*, .

49. Waskom ML. Seaborn: statistical data visualization. *J Open Source software* (2021). doi: 10.21105/joss.03021

50. Blavier L, Yang RM, DeClerck YA. The tumor microenvironment in neuroblastoma: new players, new mechanisms of interaction and new perspectives. *Cancers (Basel) 12* (2020). doi: 10.3390/cancers12102912

51. Weissenborn C, von Lenthe S, Hinz N, Langwisch S, Busse M, Schumacher A, et al. Depletion of Foxp3+ regulatory T cells but not the absence of CD19+IL-10+ regulatory b cells hinders tumor growth in a para-orthotopic neuroblastoma mouse model. *Int J Cancer* (2022) 151:2031–42. doi: 10.1002/ijc.34262

52. Van de Velde LA, Allen EK, Crawford JC, Wilson TL, Guy CS, Russier M, et al. Neuroblastoma formation requires unconventional CD4 T cells and arginase-1-Dependent myeloid cells. *Cancer Res* (2021) 81:5047–59. doi: 10.1158/0008-5472.CAN-21-0691

53. Larsson K, Kock A, Idborg H, Arsenian Henriksson M, Martinsson T, Johnsen JI, et al. COX/mPGES-1/PGE2 pathway depicts an inflammatory-dependent high-risk neuroblastoma subset. *Proc Natl Acad Sci USA* (2015) 112:8070–5.

54. Shirinbak S, Chan RY, Shahani S, Muthugounder S, Kennedy R, Hung LT, et al. Combined immune checkpoint blockade increases CD8+CD28+PD-1+ effector T cells and provides a therapeutic strategy for patients with neuroblastoma. *Oncoimmunology* (2021) 10:1838140. doi: 10.1080/2162402X.2020.1838140

55. Liu KX, Naranjo A, Zhang FF, DuBois SG, Braunstein SE, Voss SD, et al. Prospective evaluation of radiation dose escalation in patients with high-risk neuroblastoma and gross residual disease after surgery: a report from the children's oncology group ANBL0532 study. *J Clin Oncol* (2020) 38:2741–52. doi: 10.1200/JCO.19.03316

56. Gong X, Li X, Jiang T, Xie H, Zhu Z, Zhou F, et al. Combined radiotherapy and anti-PD-L1 antibody synergistically enhances antitumor effect in non-small cell lung cancer. *J Thorac Oncol* (2017) 12:1085–97. doi: 10.1016/j.jtho.2017.04.014

57. Dovedi SJ, Adlard AL, Lipowska-Bhalla G, McKenna C, Jones S, Cheadle EJ, et al. Acquired resistance to fractionated radiotherapy can be overcome by concurrent PD-L1 blockade. *Cancer Res* (2014) 74:5458–68. doi: 10.1158/0008-5472.CAN-14-1258

58. Lugade AA, Sorensen EW, Gerber SA, Moran JP, Frelinger JG, Lord EM. Radiation-induced IFN-gamma production within the tumor microenvironment influences antitumor immunity. *J Immunol* (2008) 180:3132–9. doi: 10.4049/jimmunol.180.5.3132

59. Zhang F, Manna S, Pop LM, Chen ZJ, Fu YX, Hannan R. Type I interferon response in radiation-induced anti-tumor immunity. *Semin Radiat Oncol* (2020) 30:129–38. doi: 10.1016/j.semradonc.2019.12.009

60. Chow J, Hoffend NC, Abrams SI, Schwaab T, Singh AK, Muhitch JB. Radiation induces dynamic changes to the T cell repertoire in renal cell carcinoma patients. *Proc Natl Acad Sci U.S.A.* (2020) 117:23721–9.

61. Leibundgut-Landmann S, Osorio F, Brown GD, Reis e Sousa C. Stimulation of dendritic cells *via* the dectin-1/Syk pathway allows priming of cytotoxic T-cell responses. *Blood* (2008) 112:4971–80. doi: 10.1182/blood-2008-05-158469

62. Chen X, Kunda PE, Lin J, Zhou M, Huang J, Zhang H, et al. SYK-targeted dendritic cell-mediated cytotoxic T lymphocytes enhance the effect of immunotherapy on retinoblastoma. *J Cancer Res Clin Oncol* (2018) 144:675–84. doi: 10.1007/s00432-018-2584-x

63. Doedens AL, Stockmann C, Rubinstein MP, Liao D, Zhang N, DeNardo DG, et al. Macrophage expression of hypoxia-inducible factor-1 alpha suppresses T-cell function and promotes tumor progression. *Cancer Res* (2010) 70:7465–75. doi: 10.1158/0008-5472.CAN-10-1439

64. Majzner RG, Heitzeneder S, Mackall CL. Harnessing the immunotherapy revolution for the treatment of childhood cancers. *Cancer Cell* (2017) 31:476–85. doi: 10.1016/j.ccell.2017.03.002

65. Melaiu O, Mina M, Chierici M, Boldrini R, Jurman G, Romania P, et al. PD-L1 is a therapeutic target of the bromodomain inhibitor JQ1 and, combined with HLA class I, a promising prognostic biomarker in neuroblastoma. *Clin Cancer Res* (2017) 23:4462–72. doi: 10.1158/1078-0432.CCR-16-2601

66. Ferdousi Chowdhury SD. Simon Mitchell,Toby Mellows,Margaret Ashton-key &Juliet c Gray, PD-L1 and CD8+PD1+ lymphocytes exist as targets in the pediatric tumor microenvironment for immunomodulatory therapy. *OncoImmunology* (2015) 4. doi: 10.1080/2162402X.2015.1029701

67. Rigo V, Emionite L, Daga A, Astigiano S, Corrias MV, Quintarelli C, et al. Combined immunotherapy with anti-PDL-1/PD-1 and anti-CD4 antibodies cures syngeneic disseminated neuroblastoma. *Sci Rep* (2017) 7:14049. doi: 10.1038/s41598-017-14417-6

68. Siebert N, Zumpe M, Juttner M, Troschke-Meurer S, Lode HN. PD-1 blockade augments anti-neuroblastoma immune response induced by anti-GD2 antibody ch14.*18/CHO. Oncoimmunology* (2017) 6:e1343775.

frontiers | Frontiers in Immunology

TYPE Mini Review
PUBLISHED 26 June 2023
DOI 10.3389/fimmu.2023.1212209

Check for updates

OPEN ACCESS

EDITED BY
Subhash Kumar Tripathi,
Seattle Children's Research Institute, United States

REVIEWED BY
Santosh Bhosale,
Cedars Sinai Medical Center, United States
Ranjan Nanda,
International Centre for Genetic Engineering and Biotechnology, India

*CORRESPONDENCE
Yan Cui
ycui@augusta.edu

†These authors have contributed equally to this work

RECEIVED 25 April 2023
ACCEPTED 31 May 2023
PUBLISHED 26 June 2023

CITATION
Kurago Z, Guo G, Shi H, Bollag RJ, Groves MW, Byrd JK and Cui Y (2023) Inhibitors of the CD73-adenosinergic checkpoint as promising combinatory agents for conventional and advanced cancer immunotherapy.
Front. Immunol. 14:1212209.
doi: 10.3389/fimmu.2023.1212209

COPYRIGHT
© 2023 Kurago, Guo, Shi, Bollag, Groves, Byrd and Cui. This is an open-access article distributed under the terms of the Creative Commons Attribution License (CC BY). The use, distribution or reproduction in other forums is permitted, provided the original author(s) and the copyright owner(s) are credited and that the original publication in this journal is cited, in accordance with accepted academic practice. No use, distribution or reproduction is permitted which does not comply with these terms.

Inhibitors of the CD73-adenosinergic checkpoint as promising combinatory agents for conventional and advanced cancer immunotherapy

Zoya Kurago[1†], Gang Guo[2,3†], Huidong Shi[2,3], Roni J. Bollag[3,4], Michael W. Groves[3,5], J. Kenneth Byrd[3,5] and Yan Cui[2,3*]

[1]Department of Oral Biology and Diagnostic Sciences, Dental College of Georgia at Augusta University, Medical College of Georgia, Augusta University, Augusta, GA, United States, [2]Department of Biochemistry and Molecular Biology, Medical College of Georgia, Augusta University, Augusta, GA, United States, [3]Georgia Cancer Center, Medical College of Georgia, Augusta University, Augusta, GA, United States, [4]Department of Pathology, Medical College of Georgia, Augusta University, Augusta, GA, United States, [5]Department of Otolaryngology, Medical College of Georgia, Augusta University, Augusta, GA, United States

The cell surface enzyme CD73 is increasingly appreciated as a pivotal non-redundant immune checkpoint (IC) in addition to PD-1/PD-L1 and CTLA-4. CD73 produces extracellular adenosine (eADO), which not only inhibits antitumor T cell activity via the adenosine receptor (AR) $A_{2A}R$, but also enhances the immune inhibitory function of cancer-associated fibroblasts and myeloid cells via $A_{2B}R$. Preclinical studies show that inhibition of the CD73-adenosinergic pathway in experimental models of many solid tumors either as a monotherapy or, more effectively, in combination with PD-1/PD-L1 or CTLA-4 IC blockades, improves antitumor immunity and tumor control. Consequently, approximately 50 ongoing phase I/II clinical trials targeting the CD73-adenosinergic IC are currently listed on https://clinicaltrials.gov. Most of the listed trials employ CD73 inhibitors or anti-CD73 antibodies alone, in combination with $A_{2A}R$ antagonists, and/or with PD-1/PD-L1 blockade. Recent evidence suggests that the distribution of CD73, $A_{2A}R$ and $A_{2B}R$ in tumor microenvironments (TME) is heterogeneous, and this distribution affects CD73-adenosinergic IC function. The new insights have implications for the optimally effective, carefully tailored approaches to therapeutic targeting of this essential IC. In the mini-review, we briefly discuss the cellular and molecular mechanisms of CD73/eADO-mediated immunosuppression during tumor progression and therapy in the spatial context of the TME. We include preclinical data regarding therapeutic CD73-eADO blockade in tumor models as well as available clinical data from completed trials that targeted CD73-adenosinergic IC with or without PD-1/PD-L1 inhibitors and discuss factors that are potentially important for optimal therapeutic outcomes in cancer patients.

KEYWORDS

CD73, NT5E, CD39, adenosine, $A_{2A}R$, $A_{2B}R$, immune checkpoint inhibitor, combination therapy

1 Introduction

CD73 is a type I transmembrane glycoprotein widely expressed on cell surfaces of smooth muscle, epithelium, endothelium, fibroblasts, neurons, and the immune system (1–3). Functionally, CD73 is a rate-limiting ecto-5'-nucleotidase (NT5E), which together with other cell surface ectonucleoside triphosphate diphosphohydrolases, such as CD39 (ENTPDase 1), dephosphorylate ATP released from stressed/damaged cells and produce extracellular adenosine (eADO) (1–3). CD73 plays a critical role in tissue homeostasis under physiological and pathological conditions, including epithelial and endothelial barrier function, neuronal function, as well as immunity and inflammation (4–6). The roles of CD73 in modulating tumorigenesis, angiogenesis, and metastasis are increasingly appreciated (7–9) such that it is now recognized as a critical cancer immune checkpoint (IC) non-redundant to PD-1/PD-L1 and CTLA-4 (10–14). Preclinical studies and early clinical trials reveal important breakthroughs as well as challenges. Here, we briefly describe the cellular and molecular events associated with the CD73-adenosinergic pathway, discuss the current status of therapeutic interventions that target the CD73-ADO axis, and propose potential ways to enhance cancer treatment outcomes.

2 The CD73-adenosinergic pathway in the tumor microenvironment

Hypoxia is a hallmark of the TME (15–17). Hypoxia and therapy-induced cell death potentiate ATP release into the extracellular space, which is rapidly metabolized by the CD39/CD73 enzyme-pair to ADO (Figure 1A). ADO acts on specific adenosine receptors (AR), A_1R, $A_{2A}R$, $A_{2B}R$, and A_3R. Stimulatory A_1R and A_3R are coupled with G_i or G_o proteins, whose activation suppresses cAMP with downstream immune-stimulatory effects. In contrast, $A_{2A}R$ and $A_{2B}R$ are coupled with G_s and/or G_{olf} or G_q proteins, which promote cAMP signaling and thus inhibit anti-tumor immune responses (Figure 1B) (4, 18, 19).

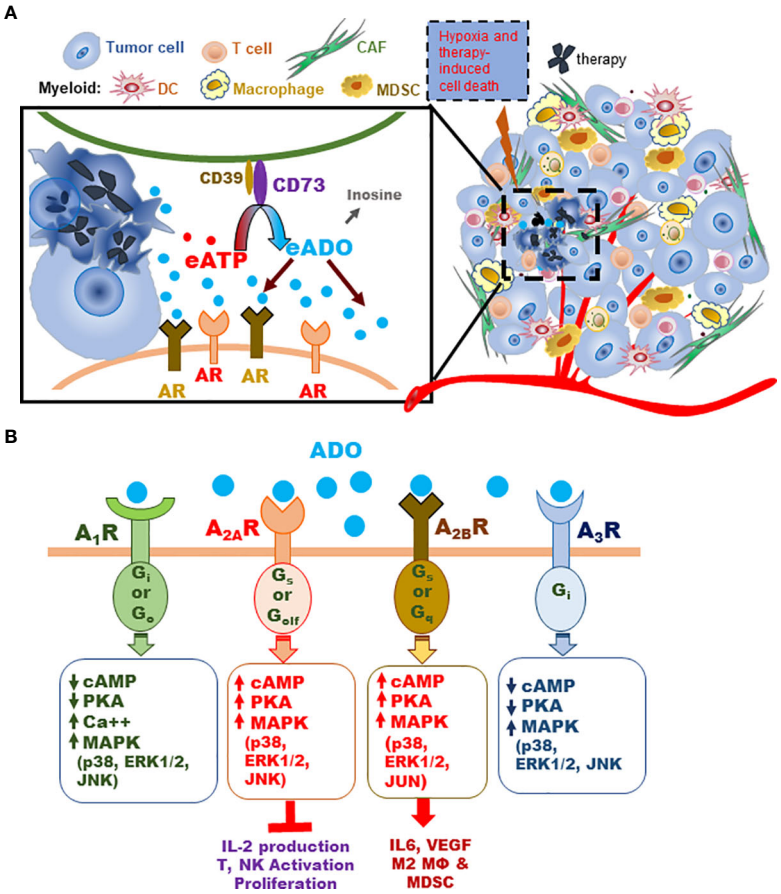


FIGURE 1
Schematic illustration of the CD73-adenosinergic pathway activity in the TME during tumor progression and treatment. **(A)** The CD39/CD73 enzyme pair converts ATP released by dying or stressed cells to immunosuppressive ADO, which inhibits antitumor immunity primarily by engaging $A_{2A}R$ and $A_{2B}R$ on various TME cells. **(B)** Schematic illustration of major AR signals activated by ADO. All four AR activate MAPK (p38, ERK1/2 and JNK or JUN) phosphorylation. Stimulatory A_1R and A_3R share several signaling events, including: A_1R or A_3R stimulation decreases adenylate cyclase activity and cAMP, inhibits protein kinase A (PKA), activates phospholipase C (PLCβ), and closes Ca^{++} channels. Stimulation of $A_{2A}R$ or $A_{2B}R$ produces opposite effects on adenylate cyclase, cAMP, and PKA (i.e. stimulates them) (4, 18, 19). Key functional impact of $A_{2A}R$ activity in TME effector T and NK cells are inhibition of activation, IL-2 production, and proliferation. The impact of ADO on $A_{2B}R$-expressing myeloid and non-immune TME cells causes skewed pro-tumor phenotypes and activities that affect the TME and T/NK effector functions (4, 18, 19).

Preclinical and clinical studies show that in the TME, ADO mainly mediates immunosuppression via $A_{2A}R$ and $A_{2B}R$ due to hypoxia, inflammation and typically high ADO levels (4, 10, 13, 20). In particular, $A_{2A}R$ is highly expressed on T and NK cells and when activated, suppresses cell proliferation and effector function (13, 21–26). High $A_{2B}R$ levels on other TME cells potentiate immune suppressors including regulatory dendritic cells (DC), myeloid-derived suppressor cells (MDSC), tumor-associated macrophages (TAM) (13, 27–31), and cancer associated fibroblasts (CAF) (32). Moreover, $A_{2B}R$ augments CD73 expression on CAF via a CD73-$A_{2B}R$-CD73 positive feedback loop, further exacerbating immunosuppression (13, 27–32).

3 CD73-adenosinergic pathway as a critical IC

3.1 Preclinical models

Preclinical studies targeting CD73 via genetic inactivation, neutralization, or small molecule inhibitors in numerous tumor models were reviewed extensively elsewhere (8–10, 13, 33). These studies reveal that the efficacy of anti-CD73 alone has limitations, in part because ADO can be generated by additional, though less prominent, pathways besides CD39/CD73. Similarly, clinical trials show that CD73 monotherapy is well-tolerated with moderate benefit in subsets of patients (9, 13, 34, 35). Treatment efficacy can be enhanced when CD73 targeting is combined with strategies to inhibit down-stream ADO signaling, among other methods. Here, we mainly focus on how these treatments impact specific AR-mediated cellular and molecular events that modulate the TME immune landscape.

3.1.1 $A_{2A}R$ activity on T and NK cells

The critical inhibitory role of $A_{2A}R$ in T cell activation and antitumor immunity was first revealed by Ohta et al. in 2006 (22). This seminal study demonstrated that genetic inactivation of $A_{2A}R$ enhanced CD8 T cell-dependent antitumor immunity leading to the rejection of immunogenic tumors in ~60% of hosts without affecting the progression of non-immunogenic tumors (22). Subsequent studies revealed that ADO-induced $A_{2A}R$ signaling suppressed TCR-induced T cell activation including decreased production of IL-2, IFN-γ and TNF-α, which subsequently disrupted T cell proliferation and CD4 differentiation to Th1 and Th17 effectors (24, 36). Instead, $A_{2A}R$ activation promoted the generation of $FoxP3^+$ and $Lag\text{-}3^+$ regulatory T cells (Treg) and persistent T cell unresponsiveness to subsequent stimuli (24). $A_{2A}R$ signaling in CD8 T cells also interfered with Notch-1 upregulation and granzyme B production following TCR stimuli (23).

Early studies suggested that NK cell-dependent cytotoxicity was inhibited by $CD73^+$ tumors leading to enhanced tumor metastasis (37, 38). Subsequent research revealed that CD73-$A_{2A}R$ activity suppressed NK cell maturation (39) and inhibited IL-15-induced NK cytotoxicity (40). Moreover, $CD73^+$ NK cells within large tumors possessed immune-regulatory function via STAT3-induced IL-10, which suppressed CD4 T cell proliferation and IFN-γ production (41).

The immunosuppressive role of $A_{2A}R$ in T and NK cells was validated in preclinical murine tumor models. Genetic inactivation as well as $A_{2a}R$ antagonists alleviated T and NK cell unresponsiveness and enhanced antitumor immunity (37, 39, 42–45). A recent study employed the CRISPR/Cas9-mediated *$A_{2A}R$* knockout in engineered human chimeric antigen receptor (CAR)-T cells, which made them resistant to ADO (46) and enhanced effector function and antitumor immunity *in vivo* in a preclinical model (46). These exciting results warrant clinical application of targeted $A_{2A}R$ inhibition/inactivation in T and NK cells to improve antitumor immunity and treatment outcomes.

3.1.2 $A_{2B}R$ activity

Less is known about $A_{2B}R$ expression and function in various cell subsets and its relationship to CD73 in the TME. Unlike $A_{2A}R$, $A_{2B}R$ has low affinity for ADO and is only activated by high ADO concentrations found under pathological conditions, which in the TME include hypoxia and therapy-induced cell stress or death (4, 5, 10, 47, 48). Notably, the expression of $A_{2B}R$ is markedly upregulated in response to hypoxia or inflammation (4, 20, 49). In the TME, $A_{2B}R$ is expressed in immune and non-immune cells, including myeloid cells, CAF, endothelium, and tumor cells (4, 18, 20, 32, 47). High levels of $A_{2B}R$ on some tumor cell types apparently promotes tumor proliferation, angiogenesis and metastasis (12, 47, 50, 51), which may be independent of immune regulation. In a glioblastoma model, a CD73-$A_{2B}R$-CD73 positive feedback loop enhanced tumor chemoresistance (52).

So far, only myeloid cells, CAF and endothelium have been shown to exert ADO-$A_{2B}R$-mediated immunosuppression. Moreover, a hypoxia-induced CD73-$A_{2B}R$-CD73 positive feedback loop augmented CD73 and $A_{2B}R$ expression on endothelial cells (49). Much of this knowledge comes from *in vitro* studies and investigations of tissue damage in the absence of cancer (28, 48, 53), partly validated in the TME (27, 29, 47, 54). Activated $A_{2B}R$ in myeloid precursors promotes the immunosuppressive function of MDSC, differentiation of macrophages towards M2 phenotype, and induction of regulatory DC (27, 48, 54–57). These myeloid cells in turn inhibit antitumor T cell activity and promote angiogenesis and tumor metastasis potentially by reducing production of TNF-α and IL-12 while increasing IL-10, IL-6 and VEGF secretion (27, 58, 59).

Overall, these observations suggest an important immunosuppressive role for TME-associated $A_{2B}R$ and suggest that the CD73-$A_{2B}R$-CD73 amplification loop may be a plausible therapeutic target.

3.1.3 Combinatory targeting of $A_{2A}R$ and/or $A_{2B}R$ together with other IC

Preclinical evidence showed that while targeting individual $A_{2A}R$- or $A_{2B}R$-axis each positively impacted antitumor immunity and generally delayed tumor progression (60–62), we found that combined anti-CD73, $A_{2A}R$- and $A_{2B}R$-axis blockade markedly improved anti-tumor immunity with tumor regression (32). The

specific reasons for the observed additive/synergistic effects are incompletely understood. Evidence does suggest that the effectiveness of anti-IC strategies depends upon the tumor type and TME conditions (13, 32). Furthermore, combinatory regimens that inhibit various CD73-AR axes and PD-1/PD-L1 are more effective, substantiating the non-redundant roles of CD73-AR IC and the advantage of targeting multiple IC (32, 61, 63).

3.2 Clinical observations

A large body of clinical evidence supports the negative impact of TME CD73 on cancer patient outcomes. Markedly elevated CD73 levels found in numerous tumors, including colorectal cancer (CRC), triple negative breast cancer (TNBC), head and neck cancer (HNC) and ovarian cancer (OC), have been linked to poor patient survival (64–70). Moreover, cancer therapies, including PD-1 ICB (71, 72), upregulated CD73-expression and ADO-AR signaling in the TME, potentially amplifying the role of this IC in patient outcomes (70, 73–76).

Several clinical studies have suggested that high blood levels of soluble (s)CD73, potentially generated by shedding, MMP-mediated clipping, or exome secretion, may prognosticate poor clinical outcome (77–79). However, a positive correlation between sCD73 and CD73 levels in the TME has not been established (77). While sCD73 has enzymatic activity in circulation, its' impact on T cell-mediated antitumor immunity in the TME might be limited due to the spatial impact (addressed in the discussion). A mechanistic insight concerning sCD73 production and distribution in the TME is needed in order to fully understand its impact on antitumor immunity.

The specific roles of $A_{2A}R$ or $A_{2B}R$ and their relationship to CD73 expression in patient outcomes are less clear and possibly depend upon specific-tumor type, immunogenicity, and the TME landscape. On one hand, recent reports suggest that in non-small cell lung cancer (NSCLC), high $A_{2A}R$ expression in the TME independently predicted better patient overall survival (OS), while high CD73 levels were associated with poor OS (69). Similarly, high $A_{2A}R$ expression on CD8 T cells within OC nests correlated with durable clinical benefit/response (CBR) during a clinical trial of PD-1 ICB and an epigenetic modifier (80). On the other hand, the negative impact of $A_{2A}R$ on anti-tumor immunity was shown in a combined trial of PD-L1 and $A_{2A}R$ inhibitors in renal cell carcinoma (RCC), demonstrating better clinical responses to $A_{2A}R$ inhibitors when tumors exhibited high adenosine signature profiles (81). Additional studies are necessary to dissect the relationships of various CD73-AR axes and application to treatments.

4 Clinical trials targeting the CD73-adenosinergic pathway

So far, approximately 50 active phase I/II cancer immunotherapy trials targeting the CD73-AR IC are listed on https://clinicaltrials.gov. Among these, more than 60% were designed to target CD73 by monoclonal antibodies or small molecule inhibitors, some of which were combined with PD-1/PD-L1 ICB regimens. The other 30-40% have employed small molecule inhibitors targeting $A_{2A}R$ alone or together with anti-CD73 and/or $A_{2B}R$ inhibitors (8, 61, 83–86). In addition to the safety (severity of adverse event, AE) and pharmacokinetic assessment of the therapeutic agents, a secondary objective was to collect data on clinical benefit rate (CBR), consisting of complete response (CR), partial response (PR) and stable disease (SD). Also, progression-free survival (PFS), objective response (OR), overall response rates (ORR) and overall survival (OS) were assessed based on standardized Response Evaluation Criteria in Solid Tumors version 1.1 (82) (for details, see legend to Table 1).

4.1 Clinical trials targeting CD73

4.1.1 Anti-CD73 antibodies

In approximately 20 trials in a variety of solid tumors, anti-CD73 monoclonal antibodies have been employed alone or more often, in combination with anti-PD-L1 or anti-PD-1. These antibodies are listed as Oleclumab, MEDI9447, AK119, HLX23, IPH5301, Sym042, CPI-0006, IBI325, PT199, JAB-BX102, TJ004309, NZV930, INCA00186 and BMS-986179. Most of the trials were/are phase I/Ib for safety assessment with limited preliminary reports of clinical outcomes in publications, abstracts, or oral presentations at international conferences, briefly described below.

In general, anti-CD73 caused low-grade AE classified as manageable or acceptable tolerability (NCT02503774, NCT03381274, NCT03616886, NCT03611556 and NCT03334617). Early reported outcomes have been mixed, as some showed promising signs of disease control, while others lacked solid evidence of clinical benefits. For instance, the NCT02503774 phase I trial of anti-CD73 with or without anti-PD-L1 enrolled 77 patients with CRC, 73 with pancreatic adenocarcinoma (PDAC) and 42 with NSCLC positive for EGFR mutation (EGFRm). Among those with evaluable outcomes, one CRC, two PDAC and four EGFRm NSCLC patients had OR, while nine CRC, eight PDAC and nine EGFRm NSCLC patients had SD. Overall, the antitumor activity was promising in EGFRm NSCLC patients receiving anti-CD73/anti-PD-L1 therapy, whereas the effectiveness in CRC and PDAC is yet to be verified (34).

The NCT03381274 phase Ib/II study evaluated the effects of anti-CD73 combined with third-generation tyrosine kinase inhibitors (TKI) in advanced EGFRm NSCLC in previously treated patients and reported acceptable tolerability. Clinical observations up to July 2021 were published in 2023 for patients with T790M-negative EGFRm NSCLC and showed CBR of 75% and OR of 25% in five patients receiving 1500 mg anti-CD73 antibody; CBR of 82.4% and OR of 11.8% were noted in 21 patients administered 3000 mg anti-CD73 antibody (35). For patients on the higher dose of anti-CD73, the median PFS was 7.4 months as compared with PFS of 2.8 months without anti-CD73 (35).

Similar studies include NCT03616886 phase I/II trial testing anti-CD73, anti-PD-L1 and chemotherapy in subjects with advanced TNBC (87), NCT03611556 phase Ib/II trial testing anti-

TABLE 1 List of registered clinical trials that target various aspects of CD73-adenosinergic axis.

anti-CD73 (mAb or small molecule inhibitor) +1- chemotherapy (w/anti-A2AR yellow)		anti-CD73 + anti-PDI/PDLI ICB +1- CTLA4 +1- A2aR inhibitor +/- chemotherapy (w/A2aR inhibitor – yellow)	
NCT03381274	Oleclumab (MED19447); AZD4635, Osimertinib	NCT02503774	Oleclumab MED19447 - MED14736
NCT03954704**	Dalutrafusp alfa; mFOLFOX6 Regimen	NCT02740985	Oleclumab, AZD4635; Durvalumab, Abiraterone Acetate; Enzalutamide; Docetaxel
NCT04797468	HLX23	NCT02754141	BMS-986179 - Nivolumab- rHuPH20
NCT05001347	TJ004309	NCT03267589	Oleclumab (MED19447); Durvalumab; Tremelilumab- MEDI 0562
NCT05143970	IPH5301; Trastuzumab	NCT03334617	Oleclumab (MED19447); Durvalumab
NCT05173792	AK119	NCT03454451	CPI-006; CPI-444; pembrolizumab
NCT05227144	ORIC-533	NCT03549000	NZV930 PDR00I- NIR178
$A_{2A}R$ antagonist		NCT03611556	Oleclumab (MED19d47); Durvalumab; Gemcitabine; Nab-paclitaxel
NCT02403193***	PBF-509; PDR00I	NCT03616886	Oleclumab (MED19447); MED14736; Paciitaxel; Carboplatin
NCT03207867***	NIR178, PDR00I	NCT03835949	TJ004309, Atezolizumab
NCT04895748***	MRI 78, PDR00I; DFF332; RADOOI	NCT03875573	Oleclumab (MED19447); Durvalumab; Radiatiom Stereotactic Body Radiotherapy
NCT05501054$	Ciforadenant; Nivolumab; Ipilimumab,	NCT04104672	AB680; Zimberelimab; Nab-paclitaxel; Gemcitabine
$A_{2B}R$ antagonist		NCT04148937	LY3475070 (CD73 inhibitor); Pembrolizumab
NCT03274479	PBF-1129	NCT04262388	Oleclumab MED19447; Durvalumab
NCT05234307****	PBF-1129; Nivolumab	NCT04381832*	Quemliclustat (AB680); Etrumadenant (AB928); Zimberelimab; Enzalutamide; Docetaxel; SG
NCT05272709	TT-702	NCT04572152	AK119; AK104
$A_{2A}R$ and $A_{2B}R$ antagonist		NCT04660812*	AB680; etrumadenant; zimberelimab, mFOLFOX-6 regimen; bevacizumab; regorafenib
NCT05024097***	Etrumadenant (AB928); Zimberelimab (AB122); Radiation therapy; FOLFOX	NCT04668300	Oleclumab (MED19447); Durvalumab
NCT05177770	Etrumadenant (AB928); Zimberelimab- SRF617	NCT04672434	Sym024; Sym021
NCT05198349	M1069	NCT04869501	TJ004309 Atezolizumab
A3R antagonist		NCT04989387	INCA00186; Retifanlimab; INCB106385
NCT00790218	CF-102 (CI-IB-MECA)	NCT05119998	IB1325; sintilimab
		NCT05174585	JAB-BX102; mbrolizumab
		NCT05246995	IB1325; sintilimab
		NCT05329766	Quemliclustat; Zimberelimab; Domvanalimab; Fluorouracil; Leucovorin; Oxaliplatin
		NCT05431270	PT199; Q3W
		NCT05559541	AK119; AK104
		NCT05632328**	AGEN1423; Balstilimab; Gemcitabine; Nabpaclitaxel

*w/A2AR/A2BR inhibitor;
**dual anti-CD73/anti-TGF-beta;
***w/anti-PD1;
****w/anti-CD39/anti-PD1;
$w/anti-PD1/anti-CTLA4.

Not listed in the table are >20 trials using non-selective inhibitors of multiple AR. Clinical trials record a variety of outcomes, according to standardized Response Evaluation Criteria in Solid Tumors (RECIST) version 1.1. Complete response (CR) = disappearance of all target lesions; partial response (PR) = at least a 30% decrease in the sum of diameters of target lesions; progressive disease (PD) = at least a 20% increase in the sum of diameters of target lesions, taking as reference the smallest sum on study; stable disease (SD) = neither sufficient shrinkage to qualify for PR nor sufficient increase to qualify for PD; objective response rates (OR) = overall response rates (ORR) = percentage of patients with partial or complete response; progression-free survival (PFS) = the length of survival without disease progression; overall survival (OS) = the length of survival time from either the date of diagnosis or the start of treatment. Adverse events (AE) are graded 1-5: Grade 1 - mild; asymptomatic or mild symptoms; Grade 2 - moderate; minimal, local or noninvasive intervention indicated; Grade 3 - severe or medically significant but not immediately life-threatening; Grade 4 - life-threatening consequences; urgent intervention indicated. Grade 5 - death related to AE.

CD73 alone or combination with gemcitabine chemotherapy and anti-PD-L1 in 212 patients with metastatic PDAC, and NCT03334617 HUDSON Platform multi-arm phase II trial for NSCLC patients who previously failed anti-PD(L)1 immunotherapy. These trials have yet to report the results (NCT03611556), or else had limited patient numbers (87) (NCT03616886) or short treatment duration (NCT03334617) (88) insufficient to assess clinical benefits.

The NCT03954704 phase I trial initiated in 2019 differs from others by testing a bi-functional antibody against CD73 and TGFβ (known as GS-1423 and AGEN1423) in patients with advanced solid tumors (89). Because TGF-β is an immunosuppressive cytokine that enhances ADO-mediated CD73 upregulation (76, 90–92), it is expected to improve treatment efficacy. Early assessment in 21 patients showed AE ranging from mild to severe, including death (89). In patients administered a high dose (20-45 mg/Kg), the circulating bi-functional antibody was durable and effectively bound to B cell CD73. Among the 17 patients who reached the first response assessment, 4.8% had a PR, 33.3% had SD, and 42.9% showed progressive disease (PD) (89).

4.1.2 CD73 small molecule inhibitors

Besides anti-CD73 antibody, small molecule inhibitors specific for CD73, AB680, ORIC-533 and LY3475070, have been employed. The NCT04104672 phase I/Ib trial was designed to evaluate safety and tolerability of AB680 with chemotherapy (paclitaxel and gemcitabine) and anti-PD-1 for treatment-naive patients with metastatic mPDAC (93). Preliminary observations in 13 patients receiving various doses of AB680 showed a manageable safety profile with AE up to grades 3-4. Early clinical responses among nine evaluable patients included three PR and five SD (93).

4.2 Trials targeting $A_{2A}R$ or $A_{2B}R$

The $A_{2A}R$ antagonists AZD4635, NIR178 and Ciforadenant (CPI-444) were developed to block the $A_{2A}R$-mediated inhibition of T and NK activity. The $A_{2B}R$ antagonists PBF-1129 and TT-702 as well as the dual $A_{2A}R/A_{2B}R$ antagonists Etrumadenant (AB928) and M1069 were developed to target the myeloid, stromal and potential tumor cell-mediated immunosuppression for additive/synergistic effects of dual CD73-AR axes blockade.

Fong et al. reported the results of $A_{2A}R$ inhibitor CPI-444 phase I trial NCT03454451 in 68 patients with RCC (81), 33 of which received CPI-444 alone and 35 received both CPI-444 and anti-PD-L1. *In both groups*, the regimens were safe and improved overall survival with durable clinical benefit associated with increased $CD8^+$ T cell recruitment into the tumors and broadened circulating T-cell repertoires (81). Remarkably, better clinical response was associated with enriched adenosine-related gene-expression profile in pre-treatment RCC specimens (81), supporting the hypothesis that elevated CD73-AR signaling is a targetable non-redundant IC, and its blockade may enhance antitumor immunity. Moreover, adenosine-regulated gene signature may be a useful marker to predict clinical prognosis (69, 80).

Early results of the NCT02740985 phase Ia/b trials using $A_{2A}R$ inhibitor AZD4635 alone or in combination with anti-PD-L1 antibody in 250 PD-1/PD-L1 inhibitor-naive patients with advanced solid tumors, including metastatic castration-resistant prostate cancer (mCRPC), CRC or NSCLC were reported recently (94). Both monotherapy and combination therapy were well tolerated with an overall <20% above grade 3 AE. ORR was observed in ~5% of the 39 mCRPC patients on AZD4635 monotherapy and ~16.2% of 37 patients on combination therapy (94). This trial also revealed a positive correlation between high adenosine signature in the blood and better clinical response, as 24-week PFS was noted in 48.9% of high adenosine-signature patients versus 20.8% of low adenosine-signature patients (94).

Clinical trials that target the $A_{2B}R$ are limited. The NCT04381832 phase Ib/II trial to evaluate the $A_{2A}R/A_{2B}R$ dual antagonist AB928 with or without anti-PD-1 and chemotherapy in patients with mCRPC reported a manageable safety profile in 17 enrolled patients (95). Among 16 patients that continued with AB928 treatment, the composite ORR was 43% (95).

5 Discussion and future perspectives

5.1 Combinatory regimens of CD73-ICB with other therapies

The early clinical observations of CD73-AR ICB trials have demonstrated feasibility, manageable toxicity and promising potential for tumor control. The benefits of anti-CD73 monotherapy appear modest, but markedly improved when combined with PD-1/PD-L1 ICB and/or other cancer therapies. As CD73-IC is continuously activated and exacerbated by hypoxia and therapy-induced cell death (32, 80, 81, 94), targeting multiple CD73-AR axes in the context of conventional or advanced therapies will improve therapeutic benefits. In particular, CD73-ICB before and during cell death induced by therapy will promote eATP-mediated antitumor immunity (96, 97). While current CD73-AR ICB trials include chemotherapy-treated patients, future trials designed to target CD73-IC aspects specific to the patient and the TME may significantly improve outcomes.

5.2 Targeting strategies based on spatial context of CD73-AR axes

Productive antitumor immunity relies on direct interactions between effector and tumor cells. Recent studies have illustrated that close effector-target cell proximity in the TME directly affects clinical outcomes (98, 99). As eADO stability and diffusion are limited, the expression levels, distribution and proximity of CD73, A2AR and A2BR in the TME will determine the activity of specific CD73-AR axes and the mechanisms of ADO-mediated immunosuppression. For example, in the TME with few T and NK cells, CD73-A2AR axis might be insignificant despite high prevalence of CD73. Yet, in the absence of the spatial distribution mapping, it is unclear which aspects of ADO-mediated

immunosuppression, and at what stage of treatment, would be most relevant. We propose that spatial distribution maps of these receptors, combined with the knowledge of relevant cellular compartments, could be important tools to identify key pathways of ADO-mediated immunosuppression operating in various TME over time and inform the design of CD73-IC targeting strategies.

In conclusion, tremendous advances have occurred in the area of CD73-AR ICB in the past decade. Combined ICB strategies targeting CD73-AR and PD-1/PD-L1 with conventional or advanced therapies remain a promising and exciting area of research. Further advances will be made possible through better understanding of the tumor-specific and treatment-specific TME, including the spatial distribution of CD73, $A_{2A}R$ and $A_{2B}R$.

Author contributions

ZK, GG and YC reviewed the literature and wrote the manuscript. HS, RB, MG, and KB participated in the discussion and revision. All authors contributed to the article and approved the submitted version.

Funding

This work was supported in part by 1R21DE028716 from the NIH/NIDCR and funds from AU-Georgia Cancer Center, Augusta University to YC.

Conflict of interest

The authors declare that the research was conducted in the absence of any commercial or financial relationships that could be construed as a potential conflict of interest.

Publisher's note

All claims expressed in this article are solely those of the authors and do not necessarily represent those of their affiliated organizations, or those of the publisher, the editors and the reviewers. Any product that may be evaluated in this article, or claim that may be made by its manufacturer, is not guaranteed or endorsed by the publisher.

References

1. Alcedo KP, Bowser JL, Snider NT. The elegant complexity of mammalian ecto-5'-nucleotidase (CD73). *Trends Cell Biol* (2021) 31(10):829–42. doi: 10.1016/j.tcb.2021.05.008

2. Borea PA, Gessi S, Merighi S, Varani K. Adenosine as a multi-signalling guardian angel in human diseases: when, where and how does it exert its protective effects? *Trends Pharmacol Sci* (2016) 37(6):419–34. doi: 10.1016/j.tips.2016.02.006

3. Colgan SP, Eltzschig HK, Eckle T, Thompson LF. Physiological roles for ecto-5'-nucleotidase (CD73). *Purinergic Signal* (2006) 2(2):351–60. doi: 10.1007/s11302-005-5302-5

4. Cekic C, Linden J. Purinergic regulation of the immune system. *Nat Rev Immunol* (2016) 16(3):177–92. doi: 10.1038/nri.2016.4

5. Di Virgilio F, Sarti AC, Falzoni S, De Marchi E, Adinolfi E. Extracellular ATP and P2 purinergic signalling in the tumour microenvironment. *Nat Rev Cancer* (2018) 18 (10):601–18. doi: 10.1038/s41568-018-0037-0

6. Yuan X, Ferrari D, Mills T, Wang Y, Czopik A, Doursout MF, et al. Editorial: purinergic signaling and inflammation. *Front Immunol* (2021) 12:699069. doi: 10.3389/fimmu.2021.699069

7. Boison D, Yegutkin GG. Adenosine metabolism: emerging concepts for cancer therapy. *Cancer Cell* (2019) 36(6):582–96. doi: 10.1016/j.ccell.2019.10.007

8. Antonioli L, Novitskiy SV, Sachsenmeier KF, Fornai M, Blandizzi C, Hasko G. Switching off CD73: a way to boost the activity of conventional and targeted antineoplastic therapies. *Drug Discovery Today* (2017) 22(11):1686–96. doi: 10.1016/j.drudis.2017.06.005

9. Chen S, Wainwright DA, Wu JD, Wan Y, Matei DE, Zhang Y, et al. CD73: an emerging checkpoint for cancer immunotherapy. *Immunotherapy* (2019) 11(11):983–97. doi: 10.2217/imt-2018-0200

10. Allard B, Allard D, Buisseret L, Stagg J. The adenosine pathway in immuno-oncology. *Nat Rev Clin Oncol* (2020) 17(10):611–29. doi: 10.1038/s41571-020-0382-2

11. Chiarella AM, Ryu YK, Manji GA, Rustgi AK. Extracellular ATP and adenosine in cancer pathogenesis and treatment. *Trends Cancer* (2021) 7(8):731–50. doi: 10.1016/j.trecan.2021.04.008

12. Jacobson KA, Gao ZG. Adenosine receptors as therapeutic targets. *Nat Rev Drug Discovery* (2006) 5(3):247–64. doi: 10.1038/nrd1983

13. Thompson EA, Powell JD. Inhibition of the adenosine pathway to potentiate cancer immunotherapy: potential for combinatorial approaches. *Annu Rev Med* (2021) 72(1):331–48. doi: 10.1146/annurev-med-060619-023155

14. Vijayan D, Young A, Teng MWL, Smyth MJ. Targeting immunosuppressive adenosine in cancer. *Nat Rev Cancer* (2017) 17(12):765–. doi: 10.1038/nrc.2017.110

15. Hanahan D. Hallmarks of cancer: new dimensions. *Cancer Discovery* (2022) 12 (1):31–46. doi: 10.1158/2159-8290.CD-21-1059

16. Hanahan D, Weinberg RA. The hallmarks of cancer. *Cell* (2000) 100(1):57–70. doi: 10.1016/S0092-8674(00)81683-9

17. Turley SJ, Cremasco V, Astarita JL. Immunological hallmarks of stromal cells in the tumour microenvironment. *Nat Rev Immunol* (2015) 15(11):669–82. doi: 10.1038/nri3902

18. Antonioli L, Blandizzi C, Pacher P, Hasko G. Immunity, inflammation and cancer: a leading role for adenosine. *Nat Rev Cancer* (2013) 13(12):842–57. doi: 10.1038/nrc3613

19. Borea PA, Gessi S, Merighi S, Vincenzi F, Varani K. Pharmacology of adenosine receptors: the state of the art. *Physiol Rev* (2018) 98(3):1591–625. doi: 10.1152/physrev.00049.2017

20. Linden J, Koch-Nolte F, Dahl G. Purine release, metabolism, and signaling in the inflammatory response. *Annu Rev Immunol* (2019) 37:325–47. doi: 10.1146/annurev-immunol-051116-052406

21. Cekic C, Linden J. Adenosine A2A receptors intrinsically regulate CD8+ T cells in the tumor microenvironment. *Cancer Res* (2014) 74(24):7239–49. doi: 10.1158/0008-5472.CAN-13-3581

22. Ohta A, Gorelik E, Prasad SJ, Ronchese F, Lukashev D, Wong MK, et al. A2A adenosine receptor protects tumors from antitumor T cells. *Proc Natl Acad Sci U S A* (2006) 103(35):13132–7. doi: 10.1073/pnas.0605251103

23. Sorrentino C, Hossain F, Rodriguez PC, Sierra RA, Pannuti A, Osborne BA, et al. Adenosine A2A receptor stimulation inhibits TCR-induced Notch1 activation in CD8+T-cells. *Front Immunol* (2019) 10:162. doi: 10.3389/fimmu.2019.00162

24. Zarek PE, Huang CT, Lutz ER, Kowalski J, Horton MR, Linden J, et al. A2A receptor signaling promotes peripheral tolerance by inducing T-cell anergy and the generation of adaptive regulatory T cells. *Blood* (2008) 111(1):251–9. doi: 10.1182/blood-2007-03-081646

25. Cekic C, Day YJ, Sag D, Linden J. Myeloid expression of adenosine A2A receptor suppresses T and NK cell responses in the solid tumor microenvironment. *Cancer Res* (2014) 74(24):7250–9. doi: 10.1158/0008-5472.CAN-13-3583

26. Chambers AM, Matosevic S. Immunometabolic dysfunction of natural killer cells mediated by the hypoxia-CD73 axis in solid tumors. *Front Mol Biosci* (2019) 6:60. doi: 10.3389/fmolb.2019.00060

27. Chen S, Akdemir I, Fan J, Linden J, Zhang B, Cekic C. The expression of adenosine A2B receptor on antigen-presenting cells suppresses CD8+ T-cell responses and promotes tumor growth. *Cancer Immunol Res* (2020) 8(8):1064–74. doi: 10.1158/2326-6066.CIR-19-0833

28. Csóka B, Selmeczy Z, Koscsó B, Németh ZH, Pacher P, Murray PJ, et al. Adenosine promotes alternative macrophage activation via A2A and A2B receptors. *FASEB J* (2012) 26(1):376–86. doi: 10.1096/fj.11-190934

29. Sorrentino C, Miele L, Porta A, Pinto A, Morello S. Activation of the A2B adenosine receptor in B16 melanomas induces CXCL12 expression in FAP-positive

tumor stromal cells, enhancing tumor progression. *Oncotarget* (2016) 7(39):64274–88. doi: 10.18632/oncotarget.11729

30. Ryzhov S, Novitskiy SV, Goldstein AE, Biktasova A, Blackburn MR, Biaggioni I, et al. Adenosinergic regulation of the expansion and immunosuppressive activity of CD11b+Gr1+ cells. *J Immunol* (2011) 187(11):6120–9. doi: 10.4049/jimmunol.1101225

31. Sorrentino C, Morello S. Role of adenosine in tumor progression: focus on A2B receptor as potential therapeutic target. *J Cancer Metastasis Treat* (2017) 3:127–38. doi: 10.20517/2394-4722.2017.29

32. Yu M, Guo G, Huang L, Deng L, Chang CS, Achyut BR, et al. CD73 on cancer-associated fibroblasts enhanced by the A2B-mediated feedforward circuit enforces an immune checkpoint. *Nat Commun* (2020) 11(1):515. doi: 10.1038/s41467-019-14060-x

33. Azambuja JH, Ludwig N, Braganhol E, Whiteside TL. Inhibition of the adenosinergic pathway in cancer rejuvenates innate and adaptive immunity. *Int J Mol Sci* (2019) 20(22):5698. doi: 10.3390/ijms20225698

34. Bendell JC, LoRusso P, Overman MJ, Noonan AM, Kim D-W, Strickler J, et al. Safety and efficacy of the anti-CD73 monoclonal antibody (mAb) oleclumab ± durvalumab in patients (pts) with advanced colorectal cancer (CRC), pancreatic ductal adenocarcinoma (PDAC), or EGFR-mutant non-small cell lung cancer (EGFRm NSCLC). *J Clin Oncol* (2021) 39(15_suppl):9047. doi: 10.1200/JCO.2021.39.15_suppl.9047

35. Kim D-W, Kim S-W, Camidge DR, Shu CA, Marrone KA, Le X, et al. CD73 inhibitor oleclumab plus osimertinib in previously treated patients with advanced T790M-negative EGFR-mutated NSCLC: a brief report. *J Thorac Oncol* (2023) 18 (5):650–56. doi: 10.1016/j.jtho.2022.12.021

36. Lappas CM, Rieger JM, Linden J. A2A adenosine receptor induction inhibits IFN-gamma production in murine CD4+ T cells. *J Immunol* (2005) 174(2):1073–80. doi: 10.4049/jimmunol.174.2.1073

37. Beavis PA, Divisekera U, Paget C, Chow MT, John LB, Devaud C, et al. Blockade of A2A receptors potently suppresses the metastasis of CD73+ tumors. *Proc Natl Acad Sci U S A* (2013) 110(36):14711–6. doi: 10.1073/pnas.1308209110

38. Qin L, Thompson LF, Kuzel TM, Zhang B. Requirement of NK cells for selective A2A receptor blockade to suppress CD73+ tumor metastasis. *Immunotherapy* (2014) 6 (1):19–21. doi: 10.2217/imt.13.154

39. Young A, Ngiow SF, Gao Y, Patch AM, Barkauskas DS, Messaoudene M, et al. A2AR adenosine signaling suppresses natural killer cell maturation in the tumor microenvironment. *Cancer Res* (2018) 78(4):1003–16. doi: 10.1158/0008-5472.CAN-17-2826

40. Kang G, Zhao X, Sun J, Cheng C, Wang C, Tao L, et al. A2AR limits IL-15-induced generation of CD39(+) NK cells with high cytotoxicity. *Int Immunopharmacol* (2023) 114:109567. doi: 10.1016/j.intimp.2022.109567

41. Neo SY, Yang Y, Record J, Ma R, Chen X, Chen Z, et al. CD73 immune checkpoint defines regulatory NK cells within the tumor microenvironment. *J Clin Invest* (2020) 130(3):1185–98. doi: 10.1172/JCI128895

42. Hatfield SM, Sitkovsky M. A2A adenosine receptor antagonists to weaken the hypoxia-HIF-1α driven immunosuppression and improve immunotherapies of cancer. *Curr Opin Pharmacol* (2016) 29:90–6. doi: 10.1016/j.coph.2016.06.009

43. Leone RD, Sun IM, Oh MH, Sun IH, Wen J, Englert J, et al. Inhibition of the adenosine A2a receptor modulates expression of T cell coinhibitory receptors and improves effector function for enhanced checkpoint blockade and ACT in murine cancer models. *Cancer Immunol Immunother* (2018) 67(8):1271–84. doi: 10.1007/s00262-018-2186-0

44. Waickman AT, Alme A, Senaldi L, Zarek PE, Horton M, Powell JD. Enhancement of tumor immunotherapy by deletion of the A2A adenosine receptor. *Cancer Immunol Immunother* (2012) 61(6):917–26. doi: 10.1007/s00262-011-1155-7

45. Mediavilla-Varela M, Castro J, Chiappori A, Noyes D, Hernandez DC, Allard B, et al. A novel antagonist of the immune checkpoint protein adenosine A2a receptor restores tumor-infiltrating lymphocyte activity in the context of the tumor microenvironment. *Neoplasia* (2017) 19(7):530–6. doi: 10.1016/j.neo.2017.02.004

46. Giuffrida L, Sek K, Henderson MA, Lai J, Chen AXY, Meyran D, et al. CRISPR/Cas9 mediated deletion of the adenosine A2A receptor enhances CAR T cell efficacy. *Nat Commun* (2021) 12(1):3236. doi: 10.1038/s41467-021-23331-5

47. Gao Z-G, Jacobson KA. A2B adenosine receptor and cancer. *Int J Mol Sci* (2019) 20(20):5139. doi: 10.3390/ijms20205139

48. Haskó G, Csóka B, Németh ZH, Vizi ES, Pacher P. A(2B) adenosine receptors in immunity and inflammation. *Trends Immunol* (2009) 30(6):263–70. doi: 10.1016/j.it.2009.04.001

49. Eltzschig HK, Ibla JC, Furuta GT, Leonard MO, Jacobson KA, Enjyoji K, et al. Coordinated adenine nucleotide phosphohydrolysis and nucleoside signaling in posthypoxic endothelium: role of ectonucleotidases and adenosine A2B receptors. *J Exp Med* (2003) 198(5):783–96. doi: 10.1084/jem.20030891

50. Mittal D, Sinha D, Barkauskas D, Young A, Kalimutho M, Stannard K, et al. Adenosine 2B receptor expression on cancer cells promotes metastasis. *Cancer Res* (2016) 76(15):4372–82. doi: 10.1158/0008-5472.CAN-16-0544

51. Desmet CJ, Gallenne T, Prieur A, Reyal F, Visser NL, Wittner BS, et al. Identification of a pharmacologically tractable fra-1/ADORA2B axis promoting breast cancer metastasis. *Proc Natl Acad Sci* (2013) 110(13):5139–44. doi: 10.1073/pnas.1222085110

52. Yan A, Joachims ML, Thompson LF, Miller AD, Canoll PD, Bynoe MS. CD73 promotes glioblastoma pathogenesis and enhances its chemoresistance via A(2B) adenosine receptor signaling. *J Neurosci* (2019) 39(22):4387–402. doi: 10.1523/JNEUROSCI.1118-18.2019

53. El-Naccache DW, Chen F, Palma MJ, Lemenze A, Fischer MA, Wu W, et al. Adenosine metabolized from extracellular ATP promotes type 2 immunity through triggering A2BAR signaling in intestinal epithelial cells. *Cell Rep* (2022) 40(5):111150. doi: 10.1016/j.celrep.2022.111150

54. Iannone R, Miele L, Maiolino P, Pinto A, Morello S. Blockade of A2b adenosine receptor reduces tumor growth and immune suppression mediated by myeloid-derived suppressor cells in a mouse model of melanoma. *Neoplasia* (2013) 15(12):1400–9. doi: 10.1593/neo.131748

55. Novitskiy SV, Ryzhov S, Zaynagetdinov R, Goldstein AE, Huang Y, Tikhomirov OY, et al. Adenosine receptors in regulation of dendritic cell differentiation and function. *Blood* (2008) 112(5):1822–31. doi: 10.1182/blood-2008-02-136325

56. Xaus J, Mirabet M, Lloberas J, Soler C, Lluis C, Franco R, et al. IFN-gamma up-regulates the A2B adenosine receptor expression in macrophages: a mechanism of macrophage deactivation. *J Immunol* (1999) 162(6):3607–14. doi: 10.4049/jimmunol.162.6.3607

57. Belikoff BG, Hatfield S, Georgiev P, Ohta A, Lukashev D, Buras JA, et al. A2B adenosine receptor blockade enhances macrophage-mediated bacterial phagocytosis and improves polymicrobial sepsis survival in mice. *J Immunol* (2011) 186(4):2444–53. doi: 10.4049/jimmunol.1001567

58. Németh ZH, Lutz CS, Csóka B, Deitch EA, Leibovich SJ, Gause WC, et al. Adenosine augments IL-10 production by macrophages through an A2B receptor-mediated posttranscriptional mechanism. *J Immunol* (2005) 175(12):8260–70. doi: 10.4049/jimmunol.175.12.8260

59. Wilson JM, Ross WG, Agbai ON, Frazier R, Figler RA, Rieger J, et al. The A2B adenosine receptor impairs the maturation and immunogenicity of dendritic cells. *J Immunol* (2009) 182(8):4616–23. doi: 10.4049/jimmunol.0801279

60. Sequeira I, Neves JF, Carrero D, Peng Q, Palasz N, Liakath-Ali K, et al. Immunomodulatory role of keratin 76 in oral and gastric cancer. *Nat Commun* (2018) 9(1):3437. doi: 10.1038/s41467-018-05872-4

61. Young A, Ngiow SF, Barkauskas DS, Sult E, Hay C, Blake SJ, et al. Co-Inhibition of CD73 and A2AR adenosine signaling improves anti-tumor immune responses. *Cancer Cell* (2016) 30(3):391–403. doi: 10.1016/j.ccell.2016.06.025

62. Dziedzic K, Węgrzyn P, Gałęzowski M, Bońkowska M, Grycuk K, Satała G, et al. Release of adenosine-induced immunosuppression: comprehensive characterization of dual A(2A)/A(2B) receptor antagonist. *Int Immunopharmacol* (2021) 96:107645. doi: 10.1016/j.intimp.2021.107645

63. Willingham SB, Ho PY, Hotson A, Hill C, Piccione EC, Hsieh J, et al. A2AR antagonism with CPI-444 induces antitumor responses and augments efficacy to anti-PD-(L)1 and anti-CTLA-4 in preclinical models. *Cancer Immunol Res* (2018) 6 (10):1136–49. doi: 10.1158/2326-6066.CIR-18-0056

64. Leclerc BG, Charlebois R, Chouinard G, Allard B, Pommey S, Saad F, et al. CD73 expression is an independent prognostic factor in prostate cancer. *Clin Cancer Res* (2016) 22(1):158–66. doi: 10.1158/1078-0432.CCR-15-1181

65. Liu N, Fang XD, Vadis Q. CD73 as a novel prognostic biomarker for human colorectal cancer. *J Surg Oncol* (2012) 106(7):918–9; author reply 20. doi: 10.1002/jso.23159

66. Ren ZH, Lin CZ, Cao W, Yang R, Lu W, Liu ZQ, et al. CD73 is associated with poor prognosis in HNSCC. *Oncotarget* (2016) 7(38):61690–702. doi: 10.18632/oncotarget.11435

67. Turcotte M, Spring K, Pommey S, Chouinard G, Cousineau I, George J, et al. CD73 is associated with poor prognosis in high-grade serous ovarian cancer. *Cancer Res* (2015) 75(21):4494–503. doi: 10.1158/0008-5472.CAN-14-3569

68. Sidders B, Zhang P, Goodwin K, O'Connor G, Russell DL, Borodovsky A, et al. Adenosine signalling is prognostic for cancer outcome and has predictive utility for immunotherapeutic response. *Clin Cancer Res* (2020) 26(9):2176–87. doi: 10.1158/1078-0432.Ccr-19-2183

69. Inoue Y, Yoshimura K, Kurabe N, Kahyo T, Kawase A, Tanahashi M, et al. Prognostic impact of CD73 and A2A adenosine receptor expression in non-small-cell lung cancer. *Oncotarget* (2017) 8(5):8738–51. doi: 10.18632/oncotarget.14434

70. Buisseret L, Pommey S, Allard B, Garaud S, Bergeron M, Cousineau I, et al. Clinical significance of CD73 in triple-negative breast cancer: multiplex analysis of a phase III clinical trial. *Ann Oncol* (2018) 29(4):1056–62. doi: 10.1093/annonc/mdx730

71. Allard B, Pommey S, Smyth MJ, Stagg J. Targeting CD73 enhances the antitumor activity of anti-PD-1 and anti-CTLA-4 mAbs. *Clin Cancer Res* (2013) 19 (20):5626–35. doi: 10.1158/1078-0432.CCR-13-0545

72. Beavis PA, Slaney CY, Milenkovski N, Henderson MA, Loi S, Stagg J, et al. CD73: a potential biomarker for anti-PD-1 therapy. *OncoImmunology* (2015) 4(11): e1046675. doi: 10.1080/2162402X.2015.1046675

73. Goswami S, Walle T, Cornish AE, Basu S, Anandhan S, Fernandez I, et al. Immune profiling of human tumors identifies CD73 as a combinatorial target in glioblastoma. *Nat Med* (2020) 26(1):39–+. doi: 10.1038/s41591-019-0694-x

74. Rocha P, Salazar R, Zhang J, Ledesma D, Solorzano JL, Mino B, et al. CD73 expression defines immune, molecular, and clinicopathological subgroups of lung adenocarcinoma. *Cancer Immunol Immunother* (2021) 70(7):1965–76. doi: 10.1007/s00262-020-02820-4

75. Ott M, Tomaszowski K-H, Marisetty A, Kong L-Y, Wei J, Duna M, et al. Profiling of patients with glioma reveals the dominant immunosuppressive axis is refractory to immune function restoration. *JCI Insight* (2020) 5(17). doi: 10.1172/jci.insight.134386

76. Sidders B, Zhang P, Goodwin K, O'Connor G, Russell DL, Borodovsky A, et al. Adenosine signaling is prognostic for cancer outcome and has predictive utility for immunotherapeutic response. *Clin Cancer Res* (2020) 26(9):2176–87. doi: 10.1158/1078-0432.CCR-19-2183

77. Messaoudi N, Cousineau I, Arslanian E, Henault D, Stephen D, Vandenbroucke-Menu F, et al. Prognostic value of CD73 expression in resected colorectal cancer liver metastasis. *Oncoimmunology* (2020) 9(1):1746138. doi: 10.1080/2162402X.2020.1746138

78. Morello S, Capone M, Sorrentino C, Giannarelli D, Madonna G, Mallardo D, et al. Soluble CD73 as biomarker in patients with metastatic melanoma patients treated with nivolumab. *J Trans Med* (2017) 15(1):244. doi: 10.1186/s12967-017-1348-8

79. Turiello R, Capone M, Giannarelli D, Morretta E, Monti MC, Madonna G, et al. Serum CD73 is a prognostic factor in patients with metastatic melanoma and is associated with response to anti-PD-1 therapy. *J Immunother Cancer* (2020) 8(2): e001689. doi: 10.1136/jitc-2020-001689

80. Chen S, Xie P, Cowan M, Huang H, Cardenas H, Keathley R, et al. Epigenetic priming enhances antitumor immunity in platinum-resistant ovarian cancer. *J Clin Invest* (2022) 132(14). doi: 10.1172/JCI158800

81. Fong L, Hotson A, Powderly JD, Sznol M, Heist RS, Choueiri TK, et al. Adenosine 2A receptor blockade as an immunotherapy for treatment-refractory renal cell cancer. *Cancer Discovery* (2020) 10(1):40–53. doi: 10.1158/2159-8290.CD-19-0980

82. Eisenhauer EA, Therasse P, Bogaerts J, Schwartz LH, Sargent D, Ford R, et al. New response evaluation criteria in solid tumours: revised RECIST guideline (version 1.1). *Eur J Cancer* (2009) 45(2):228–47. doi: 10.1016/j.ejca.2008.10.026

83. Allard B, Longhi MS, Robson SC, Stagg J. The ectonucleotidases CD39 and CD73: novel checkpoint inhibitor targets. *Immunol Rev* (2017) 276(1):121–44. doi: 10.1111/imr.12528

84. Antonioli L, Yegutkin GG, Pacher P, Blandizzi C, Hasko G. Anti-CD73 in cancer immunotherapy: awakening new opportunities. *Trends Cancer* (2016) 2(2):95–109. doi: 10.1016/j.trecan.2016.01.003

85. Willingham SB, Ho PY, Hotson A, Hill C, Piccione EC, Hsieh J, et al. A2AR antagonism with CPI-444 induces antitumor responses and augments efficacy to anti–PD-(L)1 and anti–CTLA-4 in preclinical models. *Cancer Immunol Res* (2018) 6 (10):1136–49. doi: 10.1158/2326-6066.CIR-18-0056

86. Vijayan D, Young A, Teng MWL, Smyth MJ. Targeting immunosuppressive adenosine in cancer. *Nat Rev Cancer* (2017) 17(12):709–24. doi: 10.1038/nrc.2017.86

87. Eiger D, Maurer C, Brandao M, Aftimos PG, Punie K, Taylor D, et al. 348P first findings from SYNERGY, a phase I/II trial testing the addition of the anti-CD73 oleclumab (O) to the anti-PD-L1 durvalumab (D) and chemotherapy (ChT) as first line therapy for patients (pts) with metastatic triple-negative breast cancer (mTNBC). *Ann Oncol* (2020) 31:S386–S7. doi: 10.1016/j.annonc.2020.08.450

88. Besse B, Awad M, Forde P, Thomas M, Park K, Goss G, et al. OA07.08 HUDSON: an open-label, multi-drug, biomarker-directed, phase II platform study in patients with NSCLC, who progressed on anti-PD(L)1 therapy. *J Thorac Oncol* (2021) 16(3, Supplement):S118–S9. doi: 10.1016/j.jtho.2021.01.299

89. Tolcher AW, Gordon M, Mahoney KM, Seto A, Zavodovskaya M, Hsueh C-H, et al. Phase 1 first-in-human study of dalutrafusp alfa, an anti–CD73-TGF-β-trap bifunctional antibody, in patients with advanced solid tumors. *J Immunother Cancer* (2023) 11(2):e005267. doi: 10.1136/jitc-2022-005267

90. Chen S, Fan J, Zhang M, Qin L, Dominguez D, Long A, et al. CD73 expression on effector T cells sustained by TGF-beta facilitates tumor resistance to anti-4-1BB/CD137 therapy. *Nat Commun* (2019) 10(1):150. doi: 10.1038/s41467-018-08123-8

91. Ryzhov SV, Pickup MW, Chytil A, Gorska AE, Zhang Q, Owens P, et al. Role of TGF-beta signaling in generation of CD39+CD73+ myeloid cells in tumors. *J Immunol* (2014) 193(6):3155–64. doi: 10.4049/jimmunol.1400578

92. Tauriello DVF, Palomo-Ponce S, Stork D, Berenguer-Llergo A, Badia-Ramentol J, Iglesias M, et al. TGFβ drives immune evasion in genetically reconstituted colon cancer metastasis. *Nature* (2018) 554(7693):538–43. doi: 10.1038/nature25492

93. Manji GA, Wainberg ZA, Krishnan K, Giafis N, Udyavar A, Quah CS, et al. ARC-8: phase I/Ib study to evaluate safety and tolerability of AB680 + chemotherapy + zimberelimab (AB122) in patients with treatment-naive metastatic pancreatic adenocarcinoma (mPDAC). *J Clin Oncol* (2021) 39(3_suppl):404. doi: 10.1200/JCO.2021.39.3_suppl.404

94. Lim EA, Bendell JC, Falchook GS, Bauer TM, Drake CG, Choe JH, et al. Phase ia/b, open-label, multicenter study of AZD4635 (an adenosine A2A receptor antagonist) as monotherapy or combined with durvalumab, in patients with solid tumors. *Clin Cancer Res* (2022) 28(22):4871–84. doi: 10.1158/1078-0432.CCR-22-0612

95. Subudhi SK, Bendell JC, Carducci MA, Kopp LM, Scott J, Grady MM, et al. ARC-6: a phase 1b/2, open-label, randomized platform study to evaluate efficacy and safety of etrumadenant (AB928)-based treatment combinations in patients with metastatic castrate-resistant prostate cancer (mCRPC). *J Clin Oncol* (2021) 39 (15_suppl):5039. doi: 10.1200/JCO.2021.39.15_suppl.5039

96. Wennerberg E, Spada S, Rudqvist NP, Lhuillier C, Gruber S, Chen Q, et al. CD73 blockade promotes dendritic cell infiltration of irradiated tumors and tumor rejection. *Cancer Immunol Res* (2020) 8(4):465–78. doi: 10.1158/2326-6066.CIR-19-0449

97. McLaughlin M, Patin EC, Pedersen M, Wilkins A, Dillon MT, Melcher AA, et al. Inflammatory microenvironment remodelling by tumour cells after radiotherapy. *Nat Rev Cancer* (2020) 20(4):203–17. doi: 10.1038/s41568-020-0246-1

98. Phillips D, Matusiak M, Gutierrez BR, Bhate SS, Barlow GL, Jiang S, et al. Immune cell topography predicts response to PD-1 blockade in cutaneous T cell lymphoma. *Nat Commun* (2021) 12(1):6726. doi: 10.1038/s41467-021-26974-6

99. Oliveira G, Wu CJ. Dynamics and specificities of T cells in cancer immunotherapy. *Nat Rev Cancer* (2023) 23:295–316. doi: 10.1038/s41568-023-00560-y

Frontiers in Immunology

Explores novel approaches and diagnoses to treat immune disorders.

The official journal of the International Union of Immunological Societies (IUIS) and the most cited in its field, leading the way for research across basic, translational and clinical immunology.

Discover the latest Research Topics

See more →



Frontiers

Avenue du Tribunal-Fédéral 34
1005 Lausanne, Switzerland
frontiersin.org

Contact us

+41 (0)21 510 17 00
frontiersin.org/about/contact